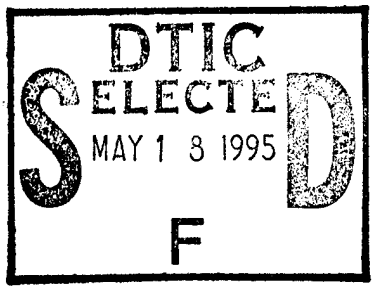
95-00210

RR Lyrae Variable Stars in the CCD/Transit Instrument Survey



By

Charles J. Wetterer

B.S., Physics and Astronomy, University of Maryland, 1986

M.S., Physics, University of New Mexico, 1990

This document has been approved for public release and sale; its distribution is unlimited.

DISSERTATION

Submitted in Partial Fulfillment of the
Requirements for the Degree of
Doctor of Philosophy in Physics

The University of New Mexico
Albuquerque, New Mexico

July, 1995

19950517 101

REPORT DOCUMENTATION PAGE

Form Approved
OMB No. 0704-0188

Public reporting burden for this collection of information is estimated to average 1 hour per response, including the time for reviewing instructions, searching existing data sources, gathering and maintaining the data needed, and completing and reviewing the collection of information. Send comments regarding this burden estimate or any other aspect of this collection of information, including suggestions for reducing this burden, to Washington Headquarters Services, Directorate for information Operations and Reports, 1215 Jefferson Davis Highway, Suite 1204, Arlington, VA 22202-4302, and to the Office of Management and Budget, Paperwork Reduction Project (0704-0188), Washington, DC 20503.

1. AGENCY USE ONLY (Leave blank)	2. REPORT DATE	3. REPORT TYPE AND DATES COVERED
	Jul 95	

4. TITLE AND SUBTITLE
RR Lyrae Variable Stars in the Early Transit Instrument Survey

5. FUNDING NUMBERS

6. AUTHOR(S)
Charles J Wetterer

7. PERFORMING ORGANIZATION NAME(S) AND ADDRESS(ES)
AFIT Students Attending:
Univ of New Mexico

8. PERFORMING ORGANIZATION REPORT NUMBER
AFIT/CI/CIA
95-002D

9. SPONSORING/MONITORING AGENCY NAME(S) AND ADDRESS(ES)
DEPARTNEMT OF THE AIR FORCE
AFIT/CI
2950 P STREET, BDLG 125
WRIGHT-PATTERSON AFB OH 45433-7765

10. SPONSORING/MONITORING AGENCY REPORT NUMBER

11. SUPPLEMENTARY NOTES

12a. DISTRIBUTION/AVAILABILITY STATEMENT
Approved for Public Release IAW AFR 190-1
Distribution Unlimited
BRIAN D. GAUTHIER, MSgt, USAF
Chief Administration

12b. DISTRIBUTION CODE

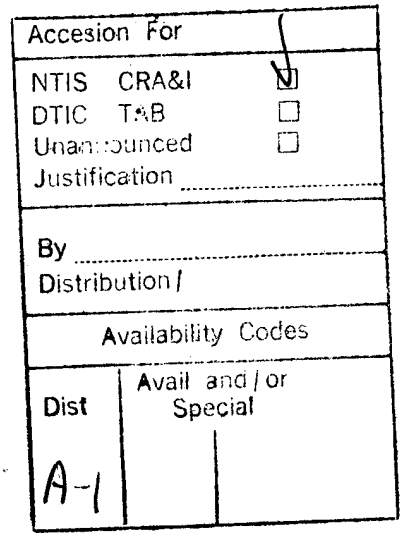
13. ABSTRACT *(Maximum 200 words)*

DTIC QUALITY INSPECTED 5

14. SUBJECT TERMS	15. NUMBER OF PAGES 343
	16. PRICE CODE

17. SECURITY CLASSIFICATION OF REPORT	18. SECURITY CLASSIFICATION OF THIS PAGE	19. SECURITY CLASSIFICATION OF ABSTRACT	20. LIMITATION OF ABSTRACT

© 1995, Charles J. Wetterer



ACKNOWLEDGEMENTS

I would like to thank the members of my dissertation committee, primarily John T. McGraw, for their salient comments and guidance during this work. I would also like to thank Thomas R. Hess for his work with the CTI databases and programing, Randy Grashuis for many nights of observing at Capilla Peak observatory, Fritz Benedict for his help with the CTI astrometry, and Jim Kunkle for many useful conversations and insights. Thanks also to Kirsten Boudreau, Heather Vogel, and Alex Collins for help throughout this endeavor.

This dissertation builds on the work of many who worked on CTI in the past. In addition to John T. McGraw and Thomas R. Hess, the CTI group at Arizona included J.R.P. Angel, T.A. Sargent, M.G.M Cawson, M.J. Keane, and J.D. Kirkpatrick.

RR Lyrae Variable Stars in the CCD/Transit Instrument Survey

By

Charles J. Wetterer

ABSTRACT OF DISSERTATION

Submitted in Partial Fulfillment of the
Requirements for the Degree of

Doctor of Philosophy in Physics

The University of New Mexico
Albuquerque, New Mexico

July, 1995

RR LYRAE VARIABLE STARS IN THE CCD/TRANSIT INSTRUMENT SURVEY

by

Charles J. Wetterer

BS, Physics and Astronomy, University of Maryland, 1986

MS, Physics, University of New Mexico, 1990

PhD, Physics, University of New Mexico, 1995

ABSTRACT

RR Lyrae variable stars have long been recognized as important tools in probing the mass, chemical distribution and kinematics of the Galaxy from the inner recesses of the nuclear bulge to the outer environs of the distant Galactic halo. This dissertation chronicles an RR Lyrae variable star survey from a thorough description of the initial observations with the CCD/Transit Instrument (CTI), to an examination of RR Lyrae space density and the Galactic mass using the discovered RR Lyrae stars.

The RR Lyrae space density as a function of Galactocentric distance is shown to be a power-law function ($R^{-3 \text{ to } -3.5}$) and consistant with an ellipsoidal distribution in the nuclear bulge and more spherically symmetric distribution in the Galactic halo. The unique area of the CTI survey and comparison to other RR Lyrae surveys verifies this function is valid throughout the Galactic halo and over the range of Galactocentric distances sampled ($0.6 < R < 40$ kpc). Local

underdensities and overdensities of RR Lyrae stars are discussed, including a possible resonance with the Magallenic Clouds ($R \approx 50$ kpc).

The Galactic mass estimated using radial velocities of RR Lyrae stars discovered in the CTI survey does not support the existence of a massive dark Galactic halo. This result is compared to the mass as determined from the radial velocities of other halo objects. Depending on the type of orbits assumed, the radial velocities of RR Lyrae stars, globular clusters, and dwarf elliptical galaxies can be used to support the notion that a massive dark halo exists (i.e. the mass-to-light ratio increases for increasing Galactocentric distance), or that no excessive dark matter exists in the Galactic halo (i.e. the mass-to-light ratio remains constant for increasing Galactocentric distance).

Table of Contents

List of Figures xi

List of Tables xiv

Chapter 1: Introduction 1

Chapter 2: The CCD/Transit Instrument (CTI) . . . 3

2.1 CTI Description 4

2.2 CTI Survey Area Description 11

Chapter 3: CTI Data Reduction and Calibration . . 15

3.1 Initial Entry of Data 18

3.2 Removal of Instrumental Signature . . 19

3.3 Background Fitting and Cosmic Ray Removal 24

3.4 Analyzing and Filtering 26

3.5 Calibration 30

3.5.1 Positional Calibration 30

3.5.2 Photometric Calibration . . . 34

3.6 Merging and Updating Databases . . . 48

Chapter 4: Variable Stars in the CTI Survey . . . 52

4.1 Variable Stars 53

4.2 Finding Variable Stars in the CTI Survey 58

4.2.1 Spurious Variables 59

4.2.2 Blind Spots (Completeness) . . 73

4.3 CTI Variable Star Index Description . 77

Chapter 5: RR Lyrae Variable Stars in the CTI Survey 81

5.1 RR Lyrae Variable Stars 82

Table of Contents (continued)

5.2 Search Technique 87

5.3 Completeness 96

5.4 Alias Breaking Observations at Capilla Peak 102

5.4.1 Capilla Peak Telescope and CCD Description . . 102

5.4.2 Capilla Peak Image Reduction . . 104

5.4.3 Combining CTI and Capilla Peak data 112

5.4.4 Summary of Observations . . . 113

5.5 CTI RR Lyrae Survey Statistics . . . 120

Chapter 6: RR Lyrae Variable Star Space Densities . 125

6.1 Calculating RR Lyrae Space Densities . 129

6.2 Other RR Lyrae Space Density Surveys . 137

6.2.1 Lick RR Lyrae Star Survey . . 139

6.2.2 Palomar-Groningen Variable Star Survey . . 140

6.2.3 Saha's RR Lyrae Survey . . . 142

6.2.4 Hawkins' RR Lyrae Survey . . . 144

6.2.5 Baade's Window RR Lyrae Survey . 145

6.2.6 Local RR Lyrae Space Density . 147

6.2.7 Miscellaneous Surveys 149

6.3 RR Lyrae Space Densities 151

Chapter 7: Mass Distribution in the Milky Way . . 159

7.1 RR Lyrae Astrometry 161

7.2 RR Lyrae Spectroscopy 167

Table of Contents (continued)

7.3 Galactic Mass versus Radial Distance . 171

Appendix 1 - Tables 182

Appendix 2 - CTI Database Descriptions 222

Appendix 3 - CTI RR Lyrae Survey Photometry, Light Curves, and Finding Charts . . 233

References 327

List of Figures

1.1 - Schematic outline of dissertation 1

2.1 - CTI optical design 4

2.2 - CTI structural design 5

2.3 - CCD sidereal rate Time Delay and Integrate mode 8

2.4 - CTI survey strip in equatorial coordinates . . 11

2.5 - CTI survey strip in Galactic coordinates . . . 12

3.1 - Schematic flow chart representation of CTI analysis process 16

3.2 - Contrast filter 28

3.3 - V magnitude offset versus CTI dayno 38

3.4 - Adjusted V magnitude offset versus CTI dayno . 39

3.5 - Magnitude offsets, background intensity, and number of stars versus right ascension . . 41

3.6 - Number of objects versus right ascension . . . 42

3.7 - Magnitude offset versus seeing for various confusions 43

3.8 - Relationship between magnitude offset, seeing, and confusino explained 44

3.9 - Number of V and B observations versus right ascension 50

4.1 - Positions of variable star types on Hertzsprung-Russell (H-R) diagram 55

4.2 - Variable fraction of objects versus mean instrumental V magnitude 62

4.3 - Peak luminosity versus mean luminosity . . . 66

4.4 - Variable fraction of objects versus number of V observations 69

4.5 - Variable fraction of objects versus right ascension 71

List of Figures (continued)

4.6 - Variable fraction of objects versus mean instrumental V magnitude (19.4^h - 19.8^h) . . . 72

4.7 - Average V magnitude random and total error versus average instrumental V magnitude . . . 74

4.8 - Percent detectability versus period. 75

4.9 - Light curves of different variable stars . . . 79

5.1 - Light curves of different RR Lyrae Bailey types. 84

5.2 - E(B-V) versus right ascension for CTI strip . . 88

5.3 - CTI RR Lyrae survey area (declination versus right ascension 89

5.4 - Fraction of survey area not masked by bright stars versus right ascension 89

5.5 - Detectable fraction versus period 97

5.6 - Detectable fraction versus # V observations . . 98

5.7 - Detectable fraction versus right ascension . . 99

5.8 - RR Lyrae stars as a function of amplitude . . 101

5.9 - Detectable fraction versus average V magnitude . 101

5.10- V_{min} - <V> versus ΔV 120

5.11- $(B-V)_{min}$ versus period 122

5.12- Distribution in period and amplitude of RR Lyraes in CTI survey and Palomar-Groningen survey . . 124

6.1 - Galactocentric coordinates 126

6.2 - Fraction of total volume surveyed as function of Galactocentric radial distance 131

6.3 - Fraction of total volume surveyed versus Galactocentric radial distance for CTI survey . . . 133

6.4 - Cumulative number of RRab type variables versus Galactocentric Radial Distance for CTI Survey . 134

List of Figures (continued)

6.5 - RR Lyrae Space Density versus Galactocentric Radial Distance and Semi-Major Axis Distance for CTI survey 135

6.6 - Location of other RR Lyrae survey fields in right ascension versus declination . . . 138

6.7 - Fraction of volume surveyed and cumulative number of RRab type variables versus Galactocentric radial distance for Lick survey 139

6.8 - Fraction of volume surveyed and cumulative number of RRab type variables versus Galactocentric radial radial distance for Palomar-Groningen survey . 141

6.9 - Fraction of volume surveyed and cumulative number of RRab type variables versus Galactocentric radial distance for Saha's survey . . 143

6.10- Fraction of volume surveyed and cumulative number of RRab type variables versus Galactocentric radial distance for Hawkins' survey . . 144

6.11- Fraction of volume surveyed and cumulative number of RRab type variables versus Galactocentric radial distance for Baade's Window survey 146

6.12- RR Lyrae space density versus heliocentric distance using Bright RR Lyrae Stars in GCVS . 148

6.13- RR Lyrae space density versus Galactocentric radial distance for all fields 152

6.14- RR Lyrae space density versus Galactocentric semi-major axis distance for all fields . . 153

7.1 - Positional error versus instrumental luminosity for CTI 162

7.2 - Velocity components in Galactocentric cylindrical coordinate system 164

7.3 - Flux versus wavelength for RR Lyrae star . . . 168

7.4 - Interior Galactic mass versus Galactocentric radial distance (previous measurements) . . . 175

7.5 - Interior Galactic mass versus Galactocentric radial distance 177

List of Tables

2.1 - CTI Optical Design 5

2.2 - CTI Filter Set 6

2.3 - CCD Operational Parameters 7

2.4 - Constellation Boundaries in CTI Survey . . . 13

3.1 - Possible Contamination of CTI Survey Strip by Mars and Jupiter during 1987 - 1992 46

5.1 - RR Lyrae final candidate list 94

5.2 - GCVS name for stars in final candidate list . . 95

5.3 - Photometry results for RR Lyrae survey stars . 116

5.4 - Standard magnitudes for RR Lyrae survey stars . 118

6.1 - CTI RR Lyrae Galactocentric Coordinates . . . 128

6.2 - RR Lyrae Space Density Surveys 137

7.1 - McDonald Observatory Operating Parameters . . 167

7.2 - Center-of-mass velocity measurements 170

A1.1 - CTI Observing Log 182

A1.2 - Bright Stars in CTI Survey 197

A1.3 - SAO Stars in CTI Survey 198

A1.4 - Previously Known Variable Stars in CTI Survey . 205

A1.5 - Bright Galaxies in CTI Survey 206

A1.6 - Variable Star Types 208

A1.7 - Bright Star Masks 213

A1.8 - Sample signal to noise calculations for Capilla 214

A1.9 - Capilla Peak Observing Log 217

A1.10- Capilla Peak Observers Log 219

A1.11- Capilla Peak Image Log 219

A1.12- RR Lyrae Variable Stars with V<11.5 in GCVS . 220

Chapter 1 Introduction

RR Lyrae variable stars have long been recognized as important tools in probing the mass, chemical distribution and kinematics of the Galaxy from the inner recesses of the nuclear bulge to the outer environs of the distant Galactic halo. Questions concerning dark matter, the age of the Galaxy, and the size of the universe can all be addressed using information obtained from the study of RR Lyrae stars.

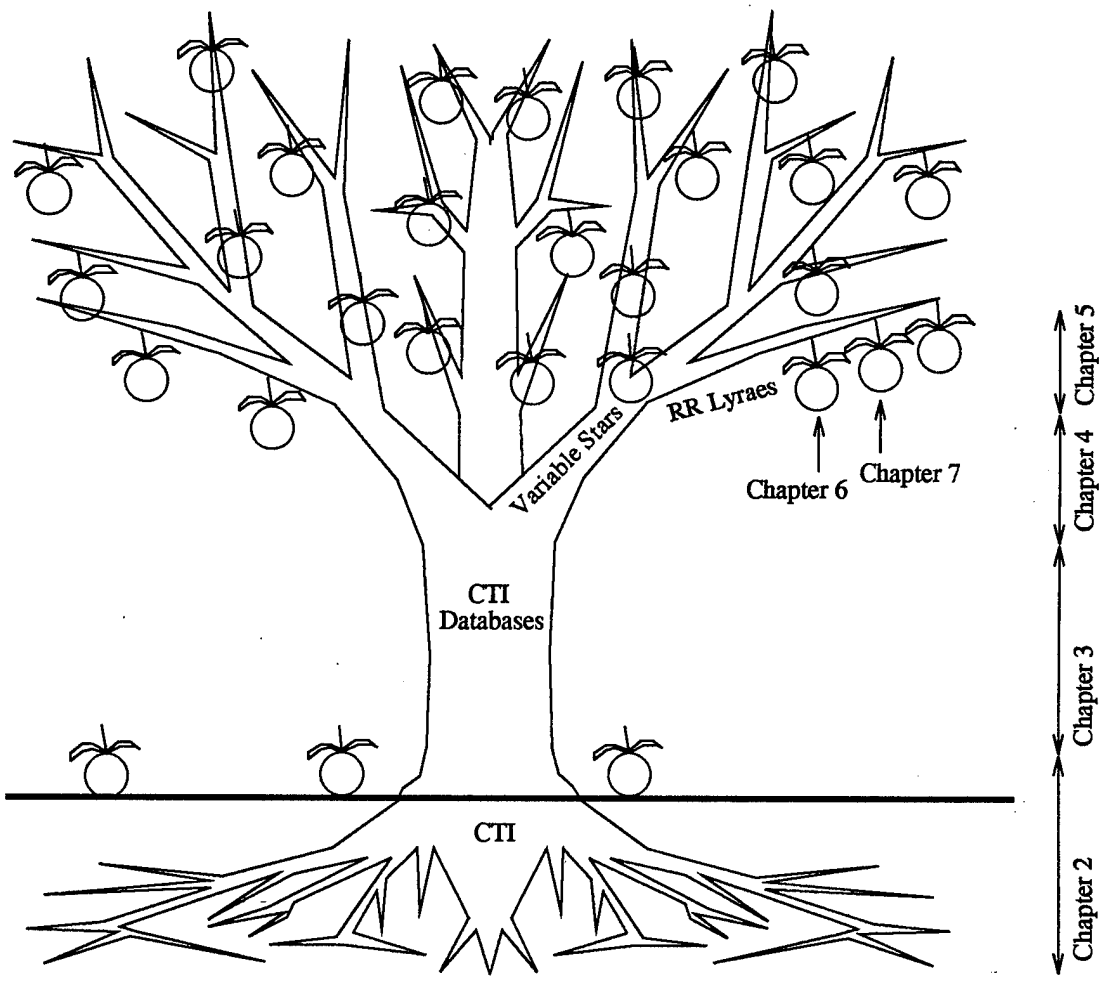


Figure 1.1 - Schematic outline of dissertation. (Not all "branches" and "fruit" shown.)

This dissertation chronicles an RR Lyrae variable star survey from its roots, in the observations of the CCD/Transit Instrument (CTI), to its fruits, in results of astrophysical significance. The outline is shown schematically in Figure 1.1. Two chapters are devoted to describing CTI and are intended to serve as a starting point for those wishing to explore other branches of the tree in Figure 1.1. Chapter 2 describes the CTI in detail as well as the portion of the sky contained in the resulting survey and Chapter 3 describes the reduction and calibration of the CTI data and contents of the survey databases. The next two chapters use the CTI survey databases to identify particular types of objects. Chapter 4 discusses the search for variable stars in the CTI survey, while Chapter 5 narrows the search to a particular type of variable star, namely RR Lyraes. Both of these chapters contain information relavent to those interested in conducting similar searches in the CTI databases. The final two chapters use the RR Lyraes discovered in the CTI survey to examine the distribution of RR Lyraes in the Galactic halo (Chapter 6) and the total mass as a function of Galactocentric radial distance of the Milky Way (Chapter 7).

Chapter 2 The CCD/Transit Instrument

The CCD/Transit Instrument (CTI) is a stationary, meridian pointing optical telescope that images a narrow strip of the sky at all right ascensions. The telescope is rigidly mounted to point at a single declination and relies on the Earth's rotation to bring different parts of the sky into view. The databases resulting from the survey contain over 500,000 objects observed during the seven years the telescope operated on Kitt Peak. This chapter describes in detail the CTI's design and the portion of the sky CTI surveys.

2.1 CTI Description

CTI is a 1.8 meter, f/2.2 telescope operated on Kitt Peak in Arizona (31° 57' 41.9" north latitude, 111° 36' 00.5" west longitude, 2080 m elevation) from 1984 to 1992 (McGraw et al. 1980, 1983, 1986 and McGraw 1992a). A schematic of the optical design is shown in Figure 2.1 with optical characteristics of each element given in Table 2.1. The paraboloidal primary reflects light first to a 0.76 meter secondary, then to a 0.76 meter tertiary located just above the primary, and finally to the detectors located near the center of the structure. The secondary and tertiary are figured as a Paul-Baker two mirror corrector (Paul 1935, Baker 1969), providing achromatic correction of the primary's coma aberration and an almost diffraction limited field of view of over one degree at the focal plane. Originally designed for the Hale 5-meter telescope, this type of corrector has never been used

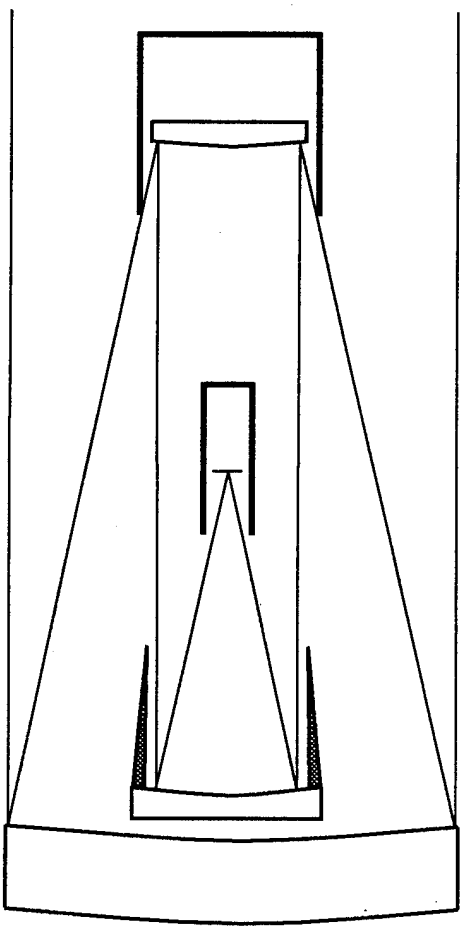


Figure 2.1 - CTI Optical Design

Table 2.1 - CTI Optical Design (dimensions in cm)

Surface	Diameter	Radius of Curvature	Aspheric Coefs K	A6	Distance to next surface
primary	180	-308.0399	-1	0	105.1778
secondary	76	97.80481	0	-3.15795E-11	97.2942
tertiary	76	-97.19998	0	0	48.5404

before because it places the focal plane in an inconvenient position for conventional telescopes, high in the structure midway between the secondary and tertiary mirrors. Since CTI uses electronic detectors and is a dedicated transit instrument rigidly mounted in its own building to point at a single declination, it does not suffer from this limitation.

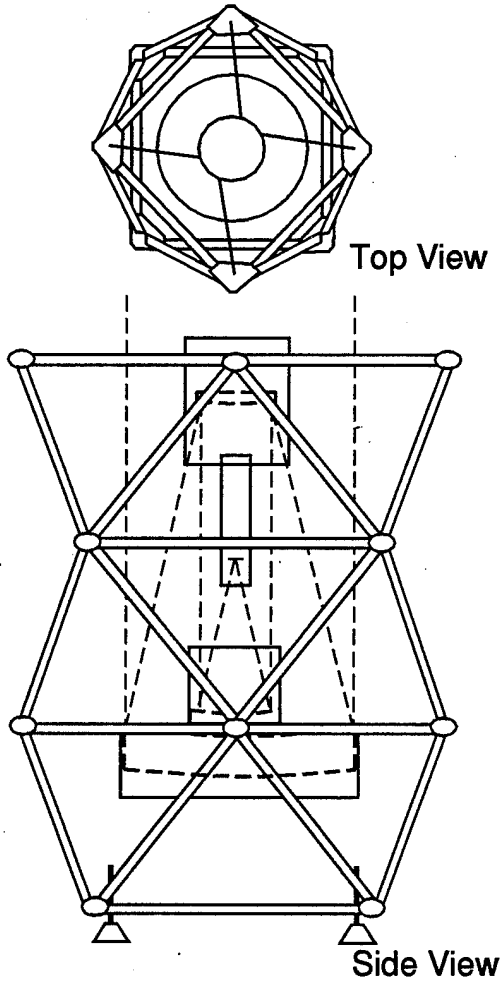


Figure 2.2 CTI Structural Design

The optics are mounted in a thermally compensating structure in which the vertically diagonal sections are made of stainless steel with a lower linear expansion coefficient than the aluminum horizontal sections. A schematic of the structure is shown in Figure 2.2. The angles at the joints were

chosen such that expansion and contraction due to temperature changes in both metals have no effect in the vertical dimension. This enables the telescope to maintain its focus throughout the night, independent of changes in temperature.

The large field of view enables the telescope to simultaneously use two side-by-side RCA charge-coupled devices (CCDs). Typically, one of the CCDs observed through a V filter while the other cycled through the B, R, and I filters. For several nights, however, an ultraviolet transparent clear filter (C) for faint galaxy and supernova detection and narrow

Table 2.2 - CTI Filter Set

B	BG-12 (1 mm) + BG-18 (1 mm) + GG-385 (1 mm)
V	BG-18 (1 mm) + GG-495 (2 mm)
R	OG-570 (1 mm) + KG-3 (2 mm)
I	RG-9 (3 mm)
C	UV-28 (2.5 mm)
A	H-alpha 658 nm - on (>3 mm)
O	H-alpha 663 nm - off (>3 mm)

band H-alpha filters were used. A summary of the CCD filter set for CTI, made up of Schott and Hoya glass filters and H_α interference filters, is given in Table 2.2. The CTI observing log, listing the filter combination and observational conditions of every night of operation of CTI on Kitt Peak, is summarized in Table A1.1 of Appendix 1 of this dissertation.

The RCA CCDs have 320 x 512 x 30 μm square pixels with the construction of the CCD camera and controllers following

Table 2.3 - CCD Operational Parameters

CCD0	72 electron readout noise
	9.18 electrons/ADU
CCD1	40 electron readout noise
	10.78 electrons/ADU
CCDs have no cosmetic blemishes	

a design first used by Kitt Peak National Observatory (Marcus et al. 1979). The CCD operational parameters are given in Table 2.3. The field scale for the telescope is 52 arcsec/mm with each pixel subtending 1.55 arcseconds. The CCDs are aligned with their columns in the east-west direction and are operated in the time-delay and integrate (TDI) mode at the apparent sidereal rate. Thus, for the stationary telescope pointed at a particular declination on the meridian, images of objects in the sky drift across the CCDs at the same rate as the electronic image is read off. This is illustrated in Figure 2.3. The effective exposure time for an object is 1 minute.

Images of the sky 8.26 arcminutes wide (320 pixels) in the north-south direction and arcminutes to more than a hundred degrees long in the east-west direction (depending on the length of the night) are obtained each night of observation. Due to interruptions by clouds or problems with the telescope's control computer, a single night's observation is not necessarily continuous, and may be segmented into several "sweeps", the term William Herschel applied to his observations made in a similar manner about 200 years ago.

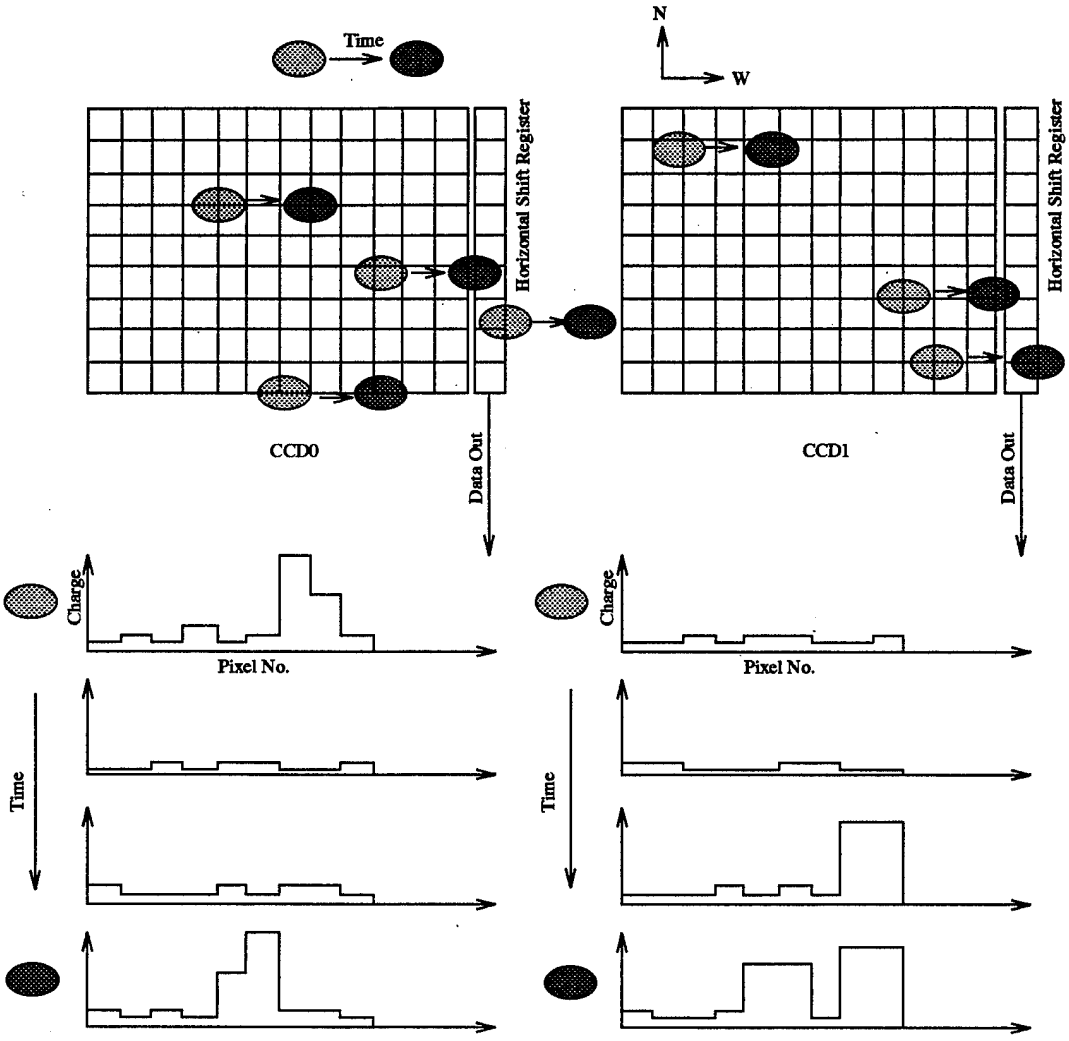


Figure 2.3 - CCD sidereal rate Time Delay and Integrate (TDI) mode. Due to the Earth's rotation, images of stars drift across the CCDs at a calculable rate. The electronic image forming in the pixels of the CCD is read out at the same rate, creating an unsmeared digitized image of the stars. The shaded dots represent stars, with the darker shade corresponding to the same stars some time later.

Additionally, due to precession and slight shifts in telescope pointing, each night's observation doesn't exactly overlap in declination, making the effective width of the CTI survey 9.5 arcminutes. The total area surveyed by CTI is approximately

50 square degrees, corresponding to 0.065% of the total sky. The CCDs saturate for stars brighter than V ≈ 12 and the nightly limiting magnitude is V ≈ 20. The resulting raw images are not unlike an image obtained from a CCD operating in its standard staring mode.

The data from the telescope goes through many steps of processing before information is merged into an object master list and history lists. A detailed description of this analysis and calibration process is given in Chapter 3. The history lists contain a day-by-day record of the time, calibrated instrumental luminosity, error in luminosity, calibrated position and size of every object observed for each filter. The history lists also reference the master list, which contains averaged positional and photometric information as well as various measures of each object's characteristics. These lists are the primary databases produced by CTI for use in scientific study, although several other intermediate databases which contain interesting information as well are produced throughout the reduction process.

CTI offers unique advantages over other types of telescopes. The stability and simplicity of the design lends itself to automation. Indeed, this telescope is the Earth-based model for the proposed Lunar Ultraviolet Telescope Experiment (LUTE) (McGraw 1992b, 1993). Additionally, by its very nature, CTI observes everything in the survey strip equally well, providing an unbiased sample of a particular

type of object. Finally, and perhaps most importantly, because CTI is a dedicated instrument, a complete, astrometrically and photometrically precise survey of all types of stars and other astronomical objects over an extended period of time is obtained. Ongoing projects include the search for and study of quasars (McGraw et al. 1988), white dwarf stars (Kirkpatrick and McGraw 1988), red dwarf stars (Kirkpatrick et al. 1990, 1994, Kirkpatrick 1992, 1994), extragalactic supernovae, high proper motion stars (Benedict et al. 1989, 1991), standard stars (McGraw et al. 1994) and all types of variable stars (McGraw 1992a, Wetterer et al. 1994, and this dissertation). Other telescopes and large surveys using techniques pioneered by CTI include the Sloan Digital Sky Survey (Kent et al. 1994, Kron 1994, Stoughton et al. 1994), new liquid mirror telescopes (Borra et al. 1989, 1992, Content et al. 1989), and standard telescopes employing the TDI mode of CCD operation (for example, Kent et al. 1993).

2.2 CTI Survey Area Description

CTI observed at a declination centered at +28°02' (1987.5 epoch, J2000 equinox), four degrees from the zenith at Kitt Peak. This declination was chosen to pass within a degree of the north galactic pole ($12^h\ 50^m$), and intersects the heart of the Coma cluster of galaxies. The CTI survey strip also passes within a degree of the galactic anti-center ($5^h\ 45^m$), and within two degrees of the direction of solar motion ($18^h\ 09^m$). Figures 2.4 and 2.5 illustrate the sky coverage in

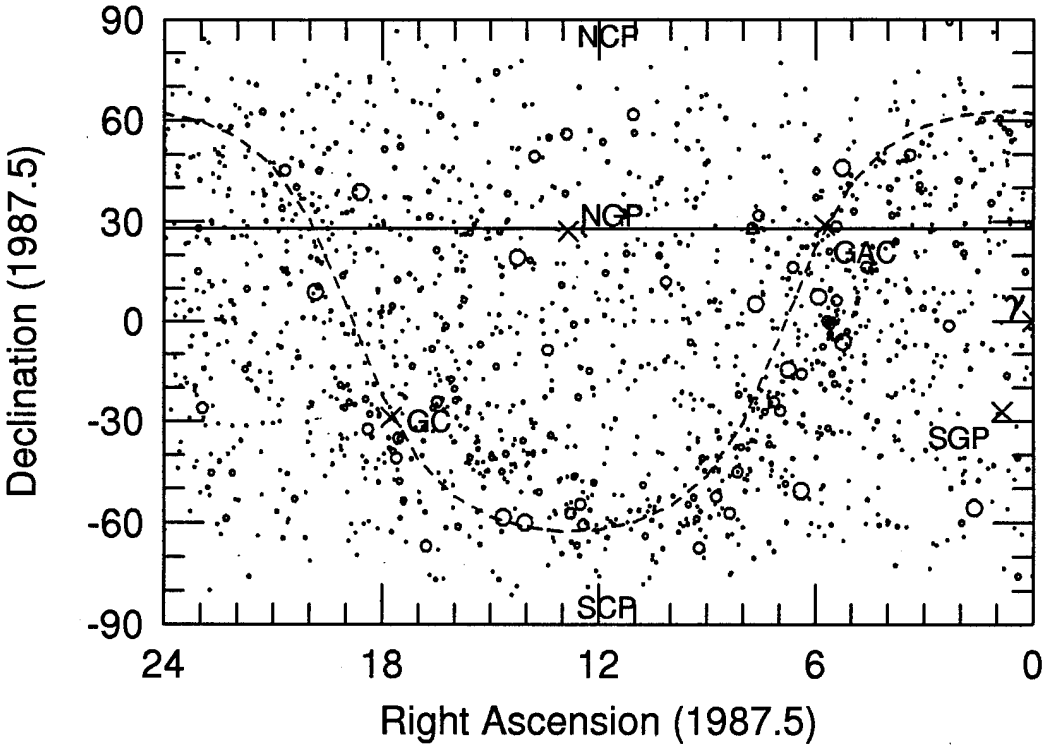


Figure 2.4 - CTI survey strip in equatorial coordinates. SAO stars brighter than 5th magnitude plotted with increasing symbol size corresponding to brighter stars. CTI survey strip (solid line) and Galactic Plane (dashed line), Galactic poles (NGP and SGP), Galactic center (GC) and anti-center (GAC), celestial poles (NCP and SCP) and first point of Aries (γ) are also marked.

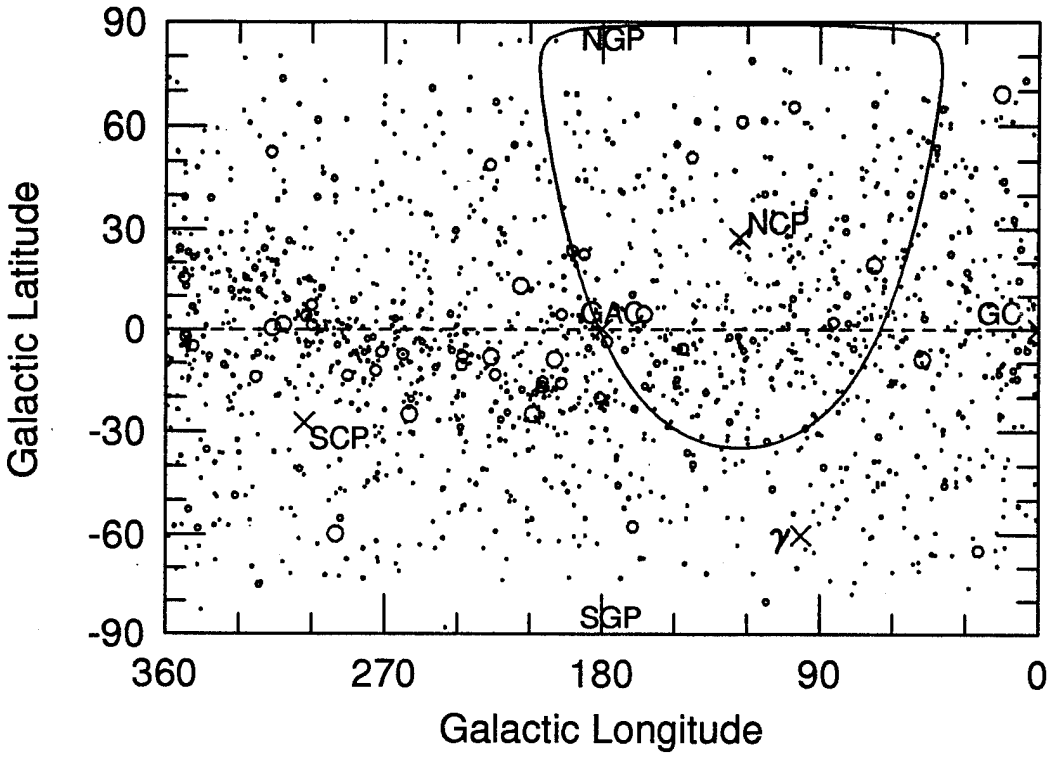


Figure 2.5 - CTI survey strip in galactic coordinates. SAO stars brighter than 5th magnitude plotted with increasing symbol size corresponding to brighter stars. CTI survey strip (solid line) and Galactic Plane (dashed line), Galactic poles (NGP and SGP), Galactic center (GC) and anti-center (GAC), celestial poles (NCP and SCP) and first point of Aries (γ) are also marked.

both equatorial and galactic coordinates. The constellation boundaries transversed by the CTI survey strip are listed in Table 2.4 (Delporte 1930). A nearly complete representation of the CTI survey strip can be found in The CCD/Transit Instrument Atlas and Database Guide (Wetterer 1995), written as a supplement to this dissertation.

The machine-readable versions of several different catalogs distributed by the Astronomical Data Center (ADC) were used to identify named objects within the CTI survey. All right ascensions and declinations were precessed to the

Table 2.4 - Constellation Boundaries in CTI Survey

Constellation	Start RA (1987.5)	End RA
Pegasus	$21^h\ 29^m\ 57^s$	$00^h\ 09^m\ 48^s$
Andromeda	00 09 48	00 49 02
Pisces	00 49 02	01 46 20
Triangulum	01 46 20	02 31 34
Aries	02 31 34	03 28 48
Taurus	03 28 48	06 00 06
Gemini	06 00 06	06 15 08
Auriga	06 00 06	06 39 05
Gemini	06 39 05	08 02 25
Cancer	08 02 25	09 21 38
Leo	09 21 38	10 36 16
Leo Minor	10 36 16	11 06 06
Leo	11 06 06	11 57 48
Coma Berenices	11 57 48	13 35 14
Bootes	13 35 14	15 15 46
Corona Borealis	15 15 46	16 24 33
Hercules	16 24 33	18 26 26
Lyra	18 26 26	19 20 01
Cygnus	19 20 01	19 44 34
Vulpecula	19 44 34	21 29 57

CTI epoch of 1987.5.

The 5th revised edition of the Bright Star Catalogue (BSC) (Hoffleit 1982) was used to identify all stars brighter than 6.5 magnitude whose effects are noticeable in the atlas. Stars with a V magnitude brighter than 12 will start saturating pixels in the CCDs. Diffraction effects of brighter stars in the BSC can be seen even if they lie well outside the strip. Table A1.2 in Appendix 1 lists each star's name, right ascension, declination, and visual magnitude. A total of 20 stars were identified. The Smithsonian Astrophysical Observatory (SAO) catalog (SAO Staff 1966) was used to identify other bright stars within the survey. These 311 stars, including the 20 BSC stars, are listed in Table

A1.3 in Appendix 1.

The 4th edition of the General Catalogue of Variable Stars (GCVS) (Kholopov et al. 1985-88) was used to identify known variable stars in the atlas. The papers containing the original finders for each star were also consulted to verify the identifications when needed (see references). Table A1.4 in Appendix 1 lists each star's name, right ascension, declination, magnitude range and type. A total of 35 previously known variable stars were identified.

The Revised New General Catalogue of Nonstellar Astronomical Objects (RNGC) (Sulentic and Tifft 1973), and the galaxy portion of the Catalogue of Galaxies and Clusters of Galaxies (CGCG) (Zwicky et al. 1961-68) were used to identify a selection of bright galaxies in the atlas. The Palomar Sky Survey with overlays (Dixon et al. 1981) and Volume 5 of the Webb Society Deep-Sky Observer's Handbook (Jones 1981) were consulted to verify most of the identifications, and the Catalogue of Quasars and Active Galactic Nuclei (Veron-Cetty and Veron 1989) was used to identify a bright quasar (GQ Com) and a galaxy with an active galactic nucleus (NGC 4504) falling within the boundaries of the CTI survey strip. Table A1.5 in Appendix 1 lists the name, right ascension, declination and magnitude for each of the 86 objects identified.

Chapter 3 CTI Data Reduction and Calibration

The raw pixel data from the CTI goes through many steps of processing before it can be used in a scientific project (Cawson et al. 1986a, 1986b, McGraw et al. 1989, and McGraw 1992a). Each night of CTI observation potentially yields over 460 Mbytes of data (2 CCDs of 320 pixels per row read out every 0.12 seconds at 16 bits per pixel giving 10.67 kbytes/s). Because of the large amount of data being processed, a nearly automated data handling procedure was developed. A schematic representation of this is shown in Figure 3.1, and will be described in six steps: initial entry of night's data, removal of instrumental signature, background fitting and cosmic-ray removal, analyzing and filtering, positional and photometric calibration, and merging with the master and history databases. During each step of the analysis, one or more databases (labelled with unique two or three letter extensions) are produced for use later in the analysis, for scientific study, or for diagnostic purposes. The extension specifies the format and content of each database in the reduction system. These databases are shown as ovals in Figure 3.1.

In addition to the reduction and analysis products, one database and two text files record output from all computer routines. The *trace* file contains diagnostic information related to a single sweep (in early work this text file has a *ls* extension), while the *log* file lists the reduction and

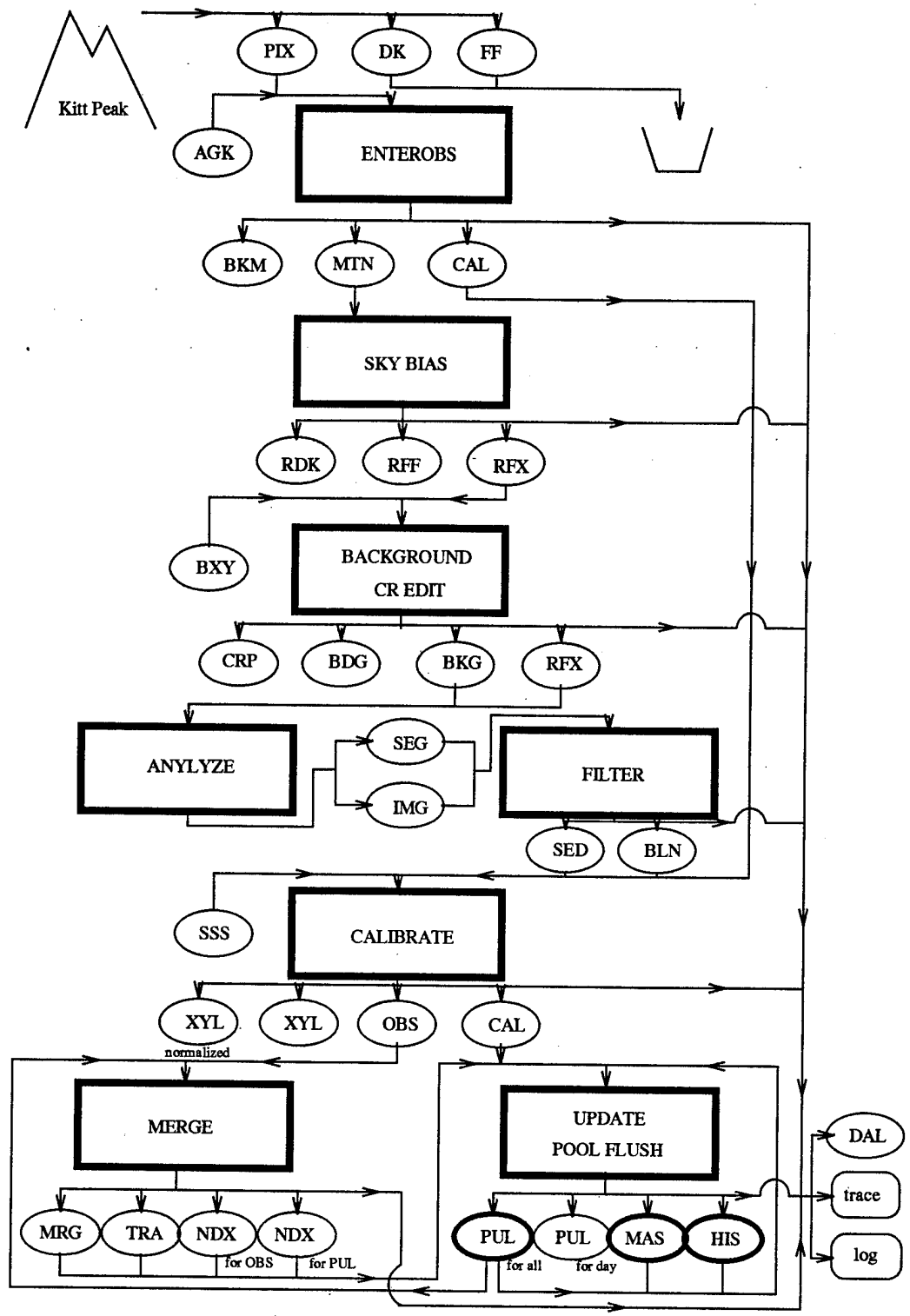


Figure 3.1 - Schematic flow chart representation of the CTI analysis process. Rectangles represent computer routines, ovals represent databases, and rounded rectangles represent text files.

analysis steps completed for all sweeps during a particular automated reduction run. These two text files are shown as rounded rectangles in Figure 3.1. The daily analysis log (**.DAL** database) records the completion of each stage of the reduction and analysis process for every sweep, and can be used to determine the sweep's present status. A complete description of the contents of each type of database can be found in The CCD/Transit Instrument Atlas and Database Guide (Wetterer 1995), written as a supplement to this dissertation.

This chapter describes the current status of the CTI data reduction and analysis process, as well as areas requiring further work. These areas include: testing and implementing a new method for determining the bias and flat field functions (see Sections 3.2 and 4.2.1), testing the cosmic ray removal algorithm under various seeing conditions and resetting the thresholds (see Sections 3.3 and 4.2.1), modifying object position determination (see Section 7.1), automating discovery and rejection of data contaminated by rapid background changes due to clouds or stray light from planets (see Sections 3.5.2 and 4.2.1), and inclusion of aperture and curve-of-growth photometry to combat difficulties with photometry of galaxies and in the Galactic plane (see Sections 3.5.2 and 4.2.1).

3.1 Initial Entry of Night's Data

A night's data is transferred from the CTI on magnetic tape in the format of a **.PIX** database. Each row of data contains 8 underscan pixels, 320 data pixels, and 8 overscan pixels. Using the computer routine ENTEROBS, the data are examined and several stars from the AGK-3 catalog (Dieckvoss et al. 1975) at the beginning of each sweep are identified. This is done interactively with CTI personnel verifying and choosing the centroid of stars selected by the computer from an **.AGK** database. From this information, a rough calibration of the initial right ascension and declination, the right ascension and declination scaling, and precessional coefficients are determined and written to the header of a **.CAL** database. (This **.CAL** database will later be refined during the calibration phase of the analysis.) Additionally, a **.BKM** database recording the median background value over the course of the night is created to enable a quick check of observing conditions if desired. Finally, the **.PIX** database is converted into a **.MTN** database in preparation for the next step of the analysis. A **.MTN** database contains 320 image pixels and the mean and variance of the overscan and underscan for each row of data.

3.2 Removal of Instrumental Signature

In the CTI CCD image, instrumental additive effects, such as the readout voltage offset (bias), and instrumental multiplicative effects, such as the pixel-to-pixel response to light (flat field), of the CCD must be removed. Because the TDI procedure requires that an image of a particular object utilize every row, the nonuniformities of the CCDs are averaged over one dimension leaving only a "simple" additive and multiplicative function to be corrected in the other dimension. Determining the correct *multiplicative* function is essential if accurate photometry is desired.

For each night of observation, the CCDs were operated under dark conditions to produce the one-dimensional "dark bias" (additive function with **.DK** extension), and while observing a uniformly illuminated screen in the telescope dome to create the "flat field" (multiplicative function with **.FF** extension) for each filter. These functions, however, proved to be inadequate in removing the CCDs instrumental signature to obtain photometry precise to our goal of 1%. The dark bias functions appear to be corrupted by a light leak or reflection off the dark slide inserted over the CCDs before acquisition and no provision was made to map out the deferred charge structure of the CCDs. The flat field functions suffered from related problems.

It was necessary to develop a new method for determining the additive and multiplicative functions for CTI's CCDs. For

the initial versions of the master and history lists, a new dark bias function was constructed (using the computer routine FIXUP) by adjusting the original dark bias function to eliminate streaks in the data created by the deferred charge structure. The flat field function was left unchanged. Unfortunately, the flat field function from the mountain is not perfect and introduces systematic errors in the photometry of up to ≈0.02 magnitudes in V and ≈0.1 magnitudes in B.

Another method, where both the dark bias and flat field functions are obtained directly from the data, was needed. This is possible because during a night's observation, the CCDs are primarily measuring the background light level, which is recording the structure of the additive and multiplicative functions. In order for the method to work, however, the background light level must be *flat* in declination. This means that nights when the moon is above the horizon or when the strip is crossing the Galactic plane must be handled very carefully. The second condition, which seems almost incompatible with the first, is that there must be a change in the background light level over the course of the night. If the additive and multiplicative functions remain stable, however, several night's worth of data could be used to accomplish the necessary background change. Finally, the overall bias level can't be determined and thus a guess must be made to start the process. These last two points will be explained below.

For CTI's CCDs, a pixel value can be calculated using the equation

$$p_{ij}=a_i+m_i\times k_j, \tag{3.1}$$

where a_i is the additive terms (bias, deferred charge, self illumination), m_i are the multiplicative terms (flat field), k_j is the background light level (stars having been removed), and i and j are declination and right ascension respectively. It has been assumed that k is a function of right ascension only to meet the first condition stated in the above paragraph. The background light level can be determined by taking the mean of Equation 3.1 over all columns (declination) and solving for k_j, remembering that m_i is normalized ($\sum m_i = n_{col}$),

$$k_j=\frac{\sum_{i=1}^{n_{col}} p_{ij}-\sum_{i=1}^{n_{col}} a_i}{n_{col}}. \tag{3.2}$$

If a guess of the additive function is made, the multiplicative function can be calculated by combining Equations 3.1 and 3.2,

$$m_{i(j)}=\frac{n_{col}(p_{ij}-a_i)}{\sum_i p_{ij}-\sum_i a_i}. \tag{3.3}$$

As the background light level (or equivalently p_{ij}) changes, m_i should remain the same if the correct values for the a_i's relative to $\sum a_i$ were used. If a slope exists when comparing the calculated $m_{i(j)}$ for a particular column against the

background light level, the a_i for that column is incorrect. A positive slope indicates a_i is too low while a negative slope indicates a_i is too high. All a_i's can thus be adjusted to minimize these slopes for all columns to approach the correct solution. As stated earlier, however, the background light level must change to give leverage in determining the slopes, and the changes in the a_i's are made relative to the average bias level ($\sum a_i$).

Stars, truncation noise (the fact that the p_{ij}'s are integerized), random error (including readout noise), low background levels, and a small background change over the night will all reduce the quality of the resulting additive and multiplicative functions. In addition, most nights had the original **.DK** and **.FF** applied, and then were *reintegerized*, resulting in additional systematic errors above the original truncation noise.

This entire process is accomplished by several programs managed by the computer routine SKY_BIAS. The resulting additive function is written to a **.RDK** database while the multiplicative function is written to a **.RFF** database, both recorded as real (i.e. non-integer) numbers. Currently, however, the resulting dark bias and flat field functions using this method are inadequate in improving the existing calibration.

For the next incarnation of CTI, the method used to determine the additive and multiplicative functions will be

crucial in improving CTI's photometry. The best alternative might be to start acquiring data during astronomical twilight. As the twilight deepens, the changing background starting from a high initial value would give the factors necessary in making the method described above to work optimally. Because all the CTI raw data are recorded on magnetic tape, regenerating all databases from the current data is possible, though time consuming.

These functions (**.RFF** and **.RDK**), however determined, are applied to the pixel information in the **.MTN** database to remove the CCD's instrumental signature, with the result entered into a new **.RFX** database made up of real numbers. (Reductions using FIXUP, described earlier, reintegerized the data and saved it to a **.FIX** database.)

3.3 Background Fitting and Cosmic Ray Removal

The next step involves fitting the background sky brightness in the **.RFX** database. Accurate photometry depends on being able to fit the background well. This is accomplished with the computer routine BACKGROUND. The background fitting algorithm divides the strip into five overlapping sub-strips of 106 columns each and calculates the modal pixel value (in initial reductions, the biased median pixel value was calculated) for each sub-strip in a particular row. A **.BXY** database is accessed to identify regions of the strip where possible problems might occur. The resulting median values are entered into a least squared regression of the form

$$Back=A+Bx+Cy+Dx^2 \qquad (3.4)$$

where x is the column number (declination), and y is the row number (right ascension). In the fit, the five modal values of each sub-strip are weighted by the inverse of the difference between the median (50-percentile point) and the 80-percentile point of that particular substrip. The larger the difference, the more stars present in the region, and the less weight that region's value is given in the regression. For each row (y), these coefficients (A,B,C, and D) are saved to a **.BKG** database. Additionally, a **.BDG** database containing the modal values and weights used in the regression for each row of data is produced.

Next, cosmic rays are detected and removed by the

computer routine CR_EDIT. The technique is based on the fact that the ionization trails deposited in the detectors by charged particles are basically single (or few) pixel events. This signature has a contrast much higher than the point spread function and can be isolated by simply selecting pixels greater than a certain pre-set value above the background level while requiring the mean of the surrounding eight pixels be below another lower pre-set value, (both these thresholds are listed in the header of the **.CRP** database for that particular sweep). A cosmic ray pixel in the **.RFX** database is assigned the mean value of the surrounding eight pixels, with the result of all pixel substitutions sent to the **.CRP** database. All cosmic ray events are thus fully recoverable.

The search for variable stars in the CTI survey strip turned up photometry anomalies related to cosmic ray removal. For a few nights entered into the current databases, the CR_EDIT algorithm removed the peak pixel of several faint stars resulting in either non-detections or anomalously low luminosity values for these stars on those nights. For the purposes of finding RR Lyrae type variable stars, these nights were easy to remove from the data (see Section 4.2.1). It will be necessary, however, to test the cosmic ray removal algorithm under various seeing conditions and reset the thresholds to distinguish between the actual short lived dimming of a star (e.g. Algol type variable stars) and a false dimming or non-detection created by cosmic ray removal.

3.4 Analyzing and Filtering

The pixel data in the **.RFX** database can now be background subtracted (using the **.BKG** database) and partitioned into images (group of pixels above some threshold) and segments (individual peaks within an image). This is accomplished by the computer routine ANALYZE. The pixel information is transformed into attributes associated with each segment's position, luminosity, shape and blending with other segments.

First, all pixels below a pre-set isophotal threshold (listed in the header of the **.IMG** database for the particular sweep) are ignored, with the pixels above the threshold forming groups, connected either adjacently or diagonally. All pixels in each group are considered part of the same "image." The luminosity, centroid, radius of gyration, ellipticity, and position angle of each image are calculated from the first and second moments of the group of pixels from which it is composed. For images above a preset luminosity threshold (listed in the header of the **.IMG** database), this information is output to the **.IMG** database.

Next, all pixels are grouped, connecting either adjacently or diagonally, to their nearest local peak. All pixels in each group formed are now considered part of the same "segment." Segments can be thought of as individual peaks in a mountain range, where the mountain range itself is an image. The properties of each segment are calculated in the same way as an image and output to a **.SEG** database.

Again, because the way segments are found guarantees to produce a segment from noise for about one pixel in nine over the entire background, segments below a preset luminosity threshold (listed in the header of the **.SEG** database) are not considered. The **.IMG** and **.SEG** databases also contain information specifying which segments refer to each image.

The **.IMG** and **.SEG** databases are then processed by the computer routine FILTER to produce a final list of recognized detections for that particular night's data. Segments representing real detections must be separated from the remaining noise-produced segments with the use of a contrast filter. If the log of the peak luminosity is plotted against the log of the mean luminosity for each segment, as in Figure 3.2(a), noise-produced segments lie close to the y=x line representing the case where the peak and mean luminosity are equal. Additionally, noise segments lie closer to the y=x line for segments with higher mean luminosities. If the axes in Figure 3.2(a) are rotated by 45°, an empirically determined division between the noise segments and potentially "real" segments can be set, represented by an exponential asymptote to the new x-axis, which is simply the y=x line in Figure 3.2(a). Figure 3.2(b) shows this plot, with the log of the y-axis used to display the exponential asymptote division between noise and real segments as a straight line. This division is also plotted in Figure 3.2(a).

The y-axis of Figure 3.2(b) is defined as the contrast,

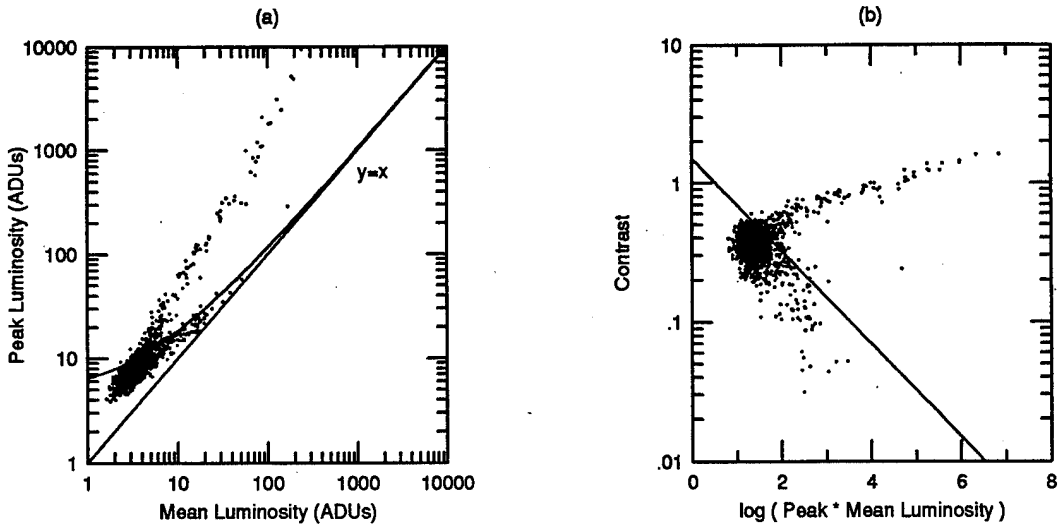


Figure 3.2 (a) peak luminosity versus mean luminosity for a single night's data, (b) log of the contrast versus log(peak luminosity × mean luminosity) for a single night's data. Empirically determined division between noise and real segments shown as solid line.

and can be represented by the simple equation

$$contrast = \log\left(\frac{peak}{mean}\right), \tag{3.5}$$

where *peak* and *mean* are the peak and mean luminosity respectively. The x-axis is now log(peak×mean), which is related to the brightness of the segment. All segments below the empirically defined division are thrown out, while an unnormalized probability of reality value is assigned to each real segment determined using the distance of the segment above the empirically defined division.

All information about each real segment, as well as its

unnormalized probability value, are output to the **.SED** database. Additionally, the information regarding what segments in the **.SED** database make up a particular image is entered into a **.BLN** database. For the rest of the analysis, only segments entered into the **.SED** database are considered, although the parent images are trace-recoverable by using the **.BLN** database.

3.5. Calibration

Each segment must now be fixed in a positional and photometric standard calibration to prepare the night's data for merging with other nights. This calibration is critical in determining the usefulness of the CTI data. We must be confident that each night has been calibrated such that changes in luminosity for an object over time or between two different objects anywhere in the CTI survey strip are actual differences in the brightness of the object or between the objects. The instrumental calibration is achieved by several programs managed by the CTI routine AUTO_CALIBRATE.

3.5.1. Positional Calibration

A rough positional calibration was carried out at the start of the analysis with the identification of bright stars from the AGK-3 catalog at the beginning of each sweep. This is improved by using a set of secondary positional standard stars selected from the Space Telescope Guide Star Catalog (Lasker et al. 1990). These secondary standard stars are contained in a database with a **.SSS** extension. The observed positions of each segment are first converted to the CTI epoch of 1987.5, taking into account proper motion, parallax, precession, nutation, aberration of starlight due to the Earth's revolution around the sun, and diurnal aberration due to the Earth's rotation. The resulting positions are compared with the list of the expected positions for the positional

standards within the list of secondary standard stars. Typically a 2 x 2 pixel window centered on the expected star position is used to determine a positive identification. The matching routine, however, is not rigid and will follow uniform smooth deviations greater than 2 pixels over the course of the sweep to accommodate possible shifts in telescope pointing. Each standard star identified, as well as the x and y displacements (in pixels) for each, are annotated in a newly created **.XYL** database.

The standard star identifications in the **.XYL** database are then used to produce a minute-by-minute (temporal) positional calibration to be contained in the **.CAL** database for the sweep. This is achieved by taking the median of the x and y displacements for every standard within a three minute window about each minute of observation to determine the global displacements to be used for that minute. Interpolations between two of these global displacements in the **.CAL** database will then be applied to all stars during the sweep. The **.CAL** database contains this, as well as the nine parameter conversion of the observed coordinates for the sweep's epoch to the CTI's 1987.5 epoch.

During this phase of the analysis, a problem was discovered that necessitated additional processing of each star's position. It was found that standard stars of similar right ascension had systematic x and y displacements dependent on their declination. The standard stars appeared closer

together than they should in declination, while there appeared to be a shearing present in right ascension. For example, a situation existed where standard stars on the north edge of the strip required a positive displacement of two pixels in right ascension to put the observed position of the star to where it was expected, while stars on the south edge required a negative displacement of two pixels, and stars in the center of the strip required no displacement at all. The resulting median displacement written to the **.CAL** database would thus be zero and only be valid for stars near the center of the strip, resulting in an incorrect positional determination for stars on each edge. Because the severity of this effect was different for the two CCDs and changed from night to night, double images of stars near the edges were formed in the master list producing spurious variable stars that appeared to blink on and off.

The severity was very different in magnitude for the two CCDs, and positively correlated between the two as the severity of the problem changed. Errors in any of the astrometric routines could not explain what was observed. The problem was eventually diagnosed as coming from two different causes. The first involves a misalignment of CCD0's columns from the east-west direction. This has the effect of elongating images in the north-south direction, and also creates most of the shearing effect observed. Indeed, it is with this CCD that the problem is most evident. The second

and more subtle cause involves an astigmatism in CTI's optics caused by a misalignment of either the secondary mirror, the tertiary mirror, or both. The astigmatism effects the declination scale as well as producing additional shearing in right ascension, and also elongates the images along the axis of the astigmatism, all of which are observed in the data.

To combat the misalignment and astigmatism, the positional displacements versus declination are analyzed for each sweep. The calculated slopes (x and y displacement versus declination) and intercepts were then used to remove the dependence from the data. An iterative process was necessary to entirely correct the data with the final slopes and intercepts used for each sweep saved in the header of the **.CAL** database. Additionally, a second normalized **.XYL** database is produced which is simply the original displacements in the previous **.XYL** database with the global corrections from the **.CAL** database applied. This database is used to check the quality of the global corrections. Currently, no correction has been made to the shapes of the objects. As a result, virtually every object observed with CCD0 (primarily through the B, R, and I filters) will be elongated north-south with a non-zero ellipticity, while objects observed with CCD1 (primarily through the V filter) will also be elongated, but along the axis of the astigmatism, and also have a non-zero, but smaller, ellipticity.

Early work with CTI data included the program STANDARDS,

which was used to modify the expected position for the standard stars in the **.SSS** database. It compared positions in the **.SSS** database with positions in a sweep's **.XYL** database, and output relevant information regarding changes to a **.RES** database. The program was used both before and after the positional calibration. It was eventually decided to discontinue using this program because any changes to a standard's position must be accompanied by a recalibration of the history and master lists in order to reflect those changes, and this was considered impractical.

3.5.2 Photometric Calibration

Concurrently with the positional calibration, a photometric calibration is also carried out. Certain secondary standard stars appear constant and thus have expected luminosities. For each of these standard stars, the **.XYL** database contains the multiplicative luminosity factor needed to match the expected luminosity with the observed. For example, if the observed luminosity was half that expected, the luminosity factor would be 0.5. As with positional displacements, the median of all luminosity factors is taken for standard stars within a three minute window to produce a minute-by-minute luminosity calibration for the **.CAL** database. It is an interpolation between two of these global luminosity factors that will be used to adjust the luminosities of all stars within the sweep.

Because the quality of the photometric calibration depends entirely on the accuracy of the expected luminosities in the standard star list, the method developed to compile and test this list once the difficulties with the dark bias and flat field functions are solved will be described in detail. It was found early on that the luminosities in the Space Telescope Guide Star Catalog were not accurate enough for CTI's calibration, making it necessary for the expected luminosities to be determined from the CTI data itself.

Several night's observations under photometric conditions were linked together over the full CTI survey strip to produce an initial estimate for the expected luminosities. The resulting closure error was 0.02 magnitudes in V, possibly related to the systematic error introduced by the incorrect flat field function. Currently, the master and history lists use this calibration to derive all instrumental magnitudes. This can be improved by processing all the nights and examining the luminosity factors of each standard star for every night the star was observed. A systematic offset indicates the star's initial estimate for the expected luminosity was incorrect. These offsets can be calculated for each standard, and the expected luminosity adjusted to eliminate them. Before this calculation can be done, however, the effects of dimming caused by dust settling on the optics, dimming caused by background overestimation during poor seeing in confused regions of the sky, dimming caused by clouds, and

inaccurate photometry caused by background fitting or other problems must be eliminated from the data. Each of these will be addressed in turn.

For a particular night of observation, there will be a mean luminosity factor related to the amount of dust on the optics. Essentially, the more dust on the optics, the dimmer stars will appear, and the lower the luminosity factor. Using the **.XYL** or **.CAL** databases for a large number of V observations, these luminosity offsets as a function of time can be examined.

The effective reflecting (or refracting) area of a telescope, and thus the flux from a standard source, will slowly decrease over time as dust settles onto the optics. For example, if the initial reflecting area of a mirror is A_o, a given time interval later, the effective area will be $A_1 = A_o - [nA_o]A_d = A_o\ (1 - nA_d)$, where n is the number of dust particles deposited per unit area in the given time interval and A_d is the effective obscuration area of one dust particle. After another time interval, $A_2 = A_1 - [nA_1]A_d = A_o\ (1 - nA_d)^2$. Given that the rate at which dust settles onto the optics is constant and the time interval between calculations is short enough, the flux reflecting from this mirror as a function of time can be represented by the equation

$$F(t) = F_o(1-nA_d)^{t/T}, \qquad (3.6)$$

where F_o is some arbitrary initial flux, and T is the time interval over which n was calculated. Notice that the

relationship between flux and time is not linear because dust particles that land on other dust particles do not degrade the performance of the mirror. Equation 3.6 can be manipulated to express the above relationship in magnitudes as a function of time. The resulting equation is

$$\Delta m = [(-2.5/T)\log(1-nA_d)]\,t. \qquad (3.7)$$

Here, the equation is linear in time. The constants in square brakets of Equation 3.7 are independent of the size of the mirror, so for telescopes with several reflective (or refractive) surfaces, each surface contributes an identical term. The "constant" n, of course, will be different for each surface. If the constants in square brakets and contributions from all surfaces are lumped together into a single constant, we obtain the simple result

$$\Delta m = K \times t. \qquad (3.8)$$

where K is in units of magnitudes per unit time.

For several photometric V nights of observation with CTI, the average magnitude offset was calculated from the luminosity offset (dm = -2.5*log(dl)). Figure 3.3 plots this magnitude offset versus time. Notice that there are four distinct breaks in an otherwise linear trend. By looking back in the CTI logs, these breaks were found to correspond to times when the telescope mirrors were washed. (1988 Sep 13, 1989 Apr 25, assumed washing during summer of 1989, and 1991 Apr 22). The slope of the line for each interval was

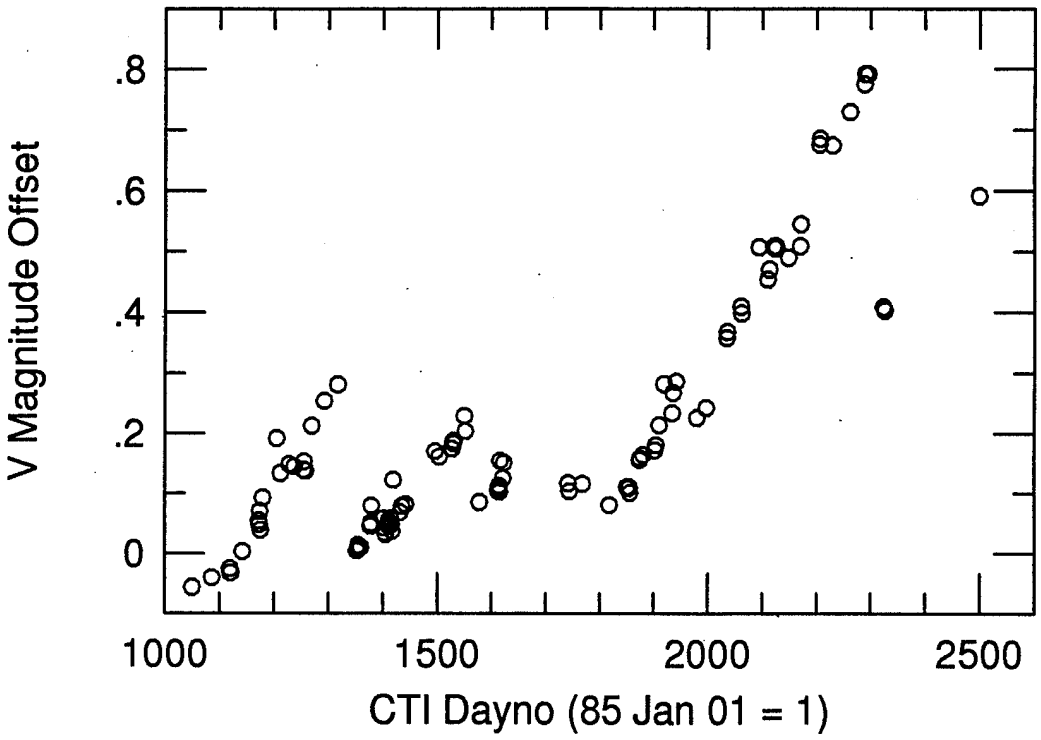


Figure 3.3 - V magnitude offset versus CTI dayno

calculated and the data adjusted such that the best fit lines for each segment yield the same value at the midpoint between them. The resulting plot of magnitude offset versus time is shown in Figure 3.4. The best fit to this scaled data is also plotted. The slope of this line is 0.001239 +/- 0.000010 mags/day which corresponds to 0.452 +/- 0.004 mags/year. This means that the CTI is only 65% as sensitive to light after only one year of observing without any cleaning! Generally, K appears to remain fairly constant over the four years of observing represented. Slight variations in the slope, however, indicate the presence of seasonal variations.

A similar calculation using Capilla Peak data acquired

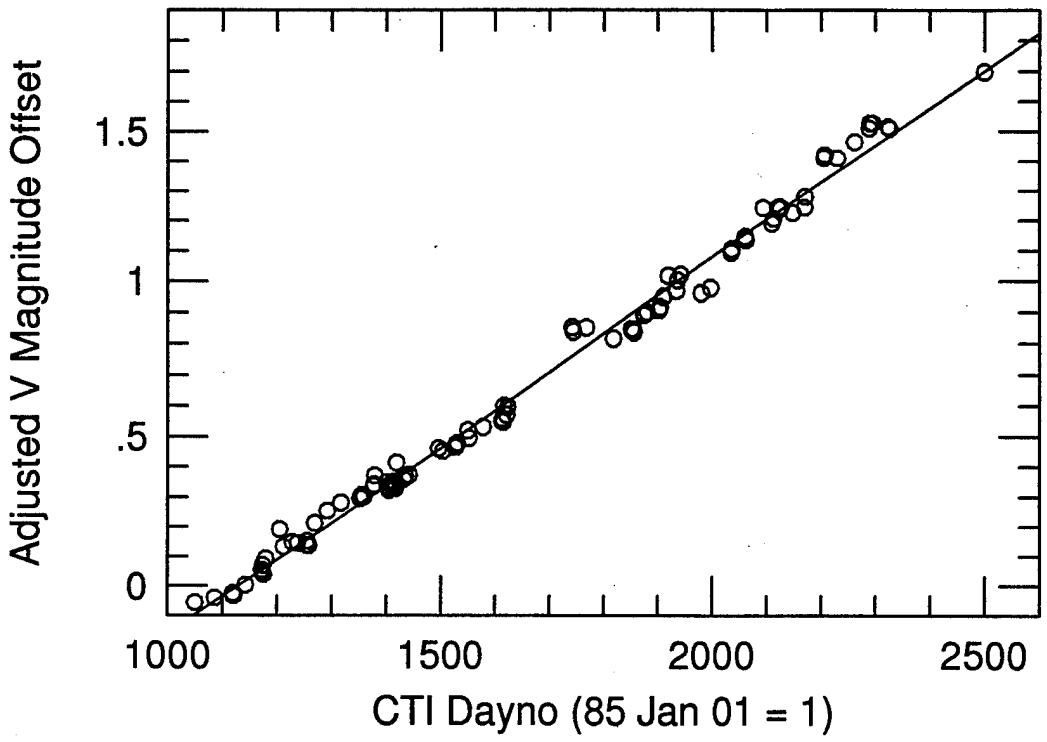


Figure 3.4 - Adjusted V magnitude offset versus CTI dayno.

over one year for three separate variable star fields gives K = 0.101 +/- 0.011 mags/year. The fact that CTI has three reflective surfaces collecting dust and that the primary and tertiary mirror are always horizontal while Capilla Peak's telescope is stored with the primary vertical probably accounts for most of the difference.

The effect of dust settling on the optics can thus be eliminated by scaling each night's observation to the mode (to eliminate the effects of clouds) of all luminosity offsets for that particular night. This is exactly what is done in calculating the normalizing factor used in adjusting each star's dl in the normalized **.XYL** database.

Next, the effect of dimming caused by background overestimation during poor seeing in regions of high confusion must be dealt with. In examining the **.CAL** databases for several nights of observation in the V bandpass, there appear systematic variations in magnitude offset at certain right ascensions. Figure 3.5(a) plots the magnitude offset versus right ascension for a number of nights for right ascensions between 18^h and 22^h. An individual night's magnitude offset as a function of right ascension has been normalized to zero to eliminate the effect of dust settling on the optics. Figure 3.5(b) plots the average background intensity in V (as contained in the **.CAL** database) versus right ascension for several observation nights over the same right ascension interval. The summer galactic plane at approximately 19^h40^m is clearly visible. The increase in background intensity at the galactic plane indicates that stars are included in the background estimate. This suggests a possible link between the magnitude offset calculated for a particular star and the concentration of background stars.

The "confusion," proportional to the concentration of background stars, was calculated to compare with the magnitude offset (determined from the luminosity factor) and seeing for several night's observations as contained in **.CAL** databases. To calculate the confusion, a histogram of all objects with two or more observations in the declination slice from +28°00' to +28°03' (1987.5 epoch) contained in the CTI master list was

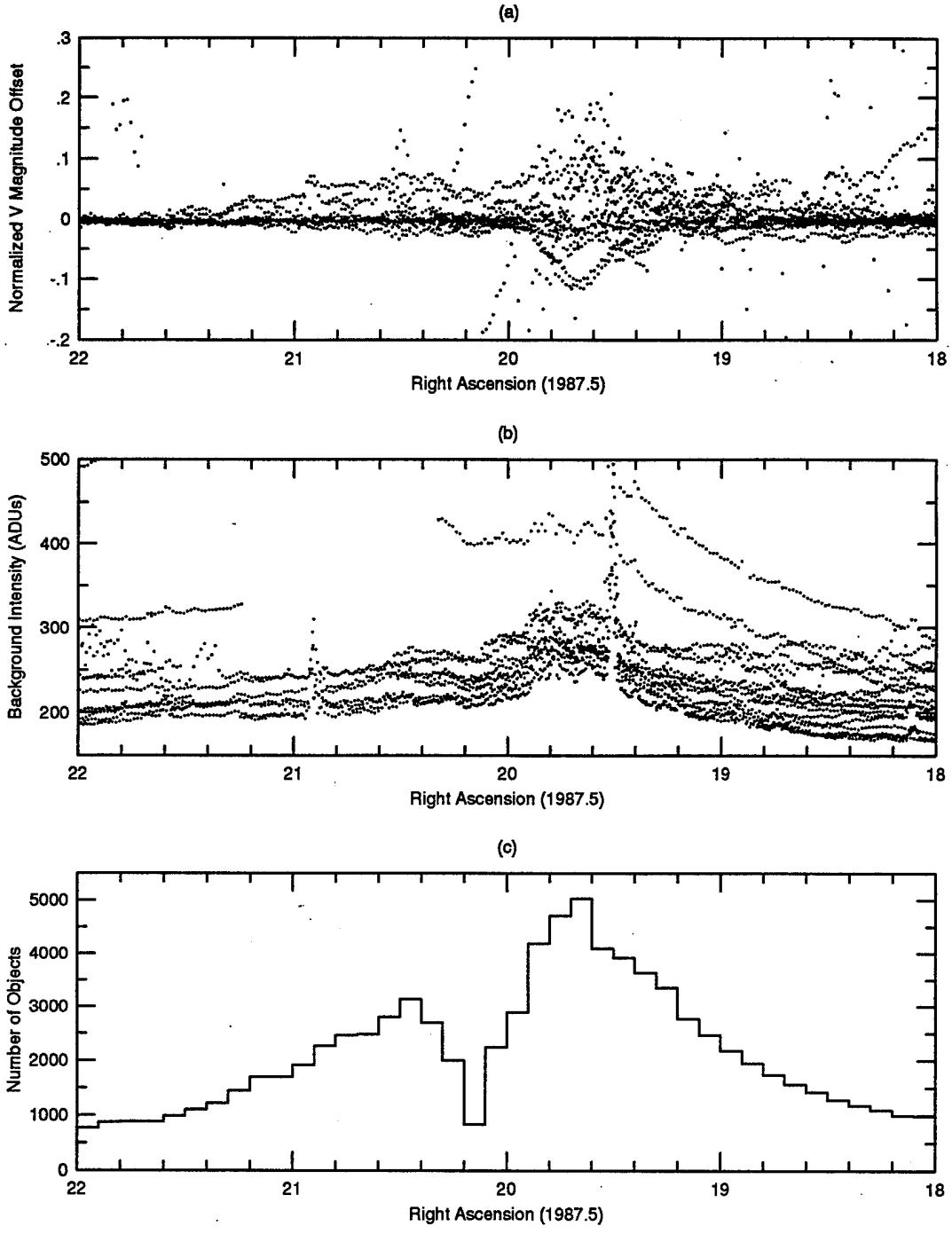


Figure 3.5 - (a) Normalized magnitude offsets versus right ascension, (b) Background intensity versus right ascension, (c) Number of stars per 3 arcminutes declination by 6^m right ascension versus right ascension for several nights crossing the summer Galactic plane.

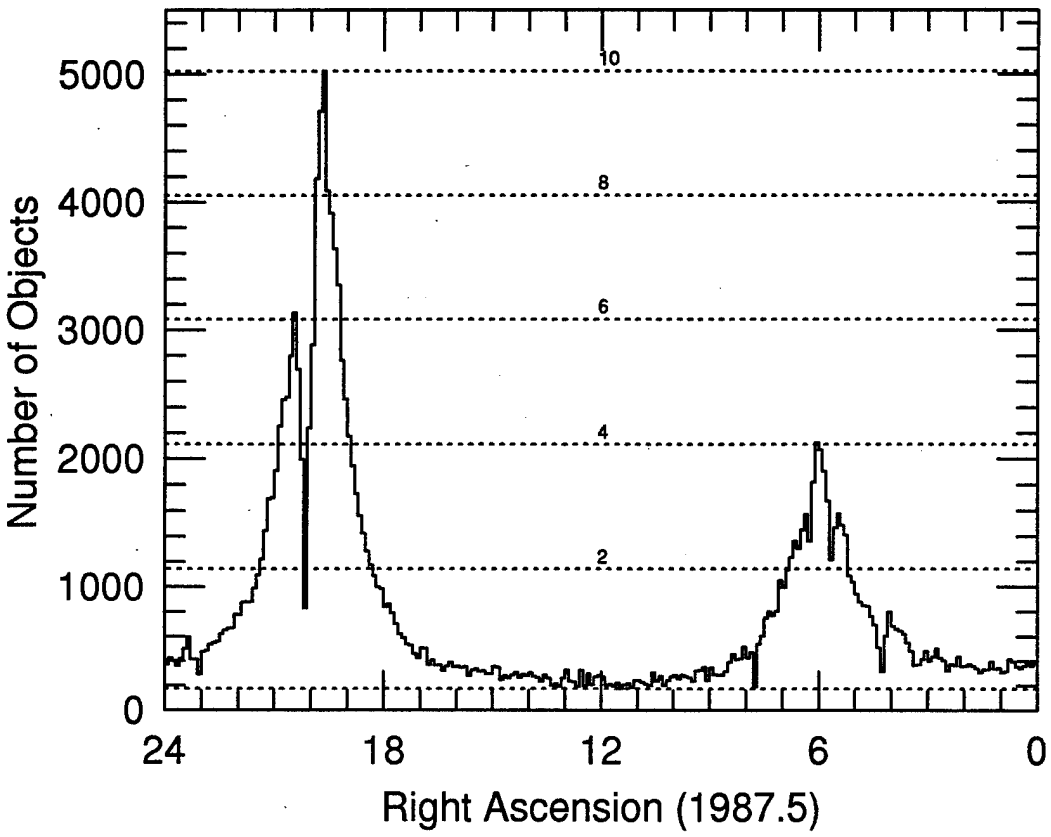


Figure 3.6 - Histogram in right ascension of the number of objects in CTI survey strip between 28°00' and 28°03' declination. Each bin corresponds to 6^m right ascension. Even confusion levels shown as horizontal dashed lines.

taken with respect to right ascension. Figure 3.6 shows this histogram, with every bin corresponding to 6^m of right ascension. The confusion was defined as a real number between 0 and 10 directly proportional to the concentration of stars, with confusion equal to zero for the minimum concentration, and confusion equal to ten for the maximum concentration.

Figures 3.7(a) through (c) display the magnitude offset versus seeing for increasing confusion. For each plot there

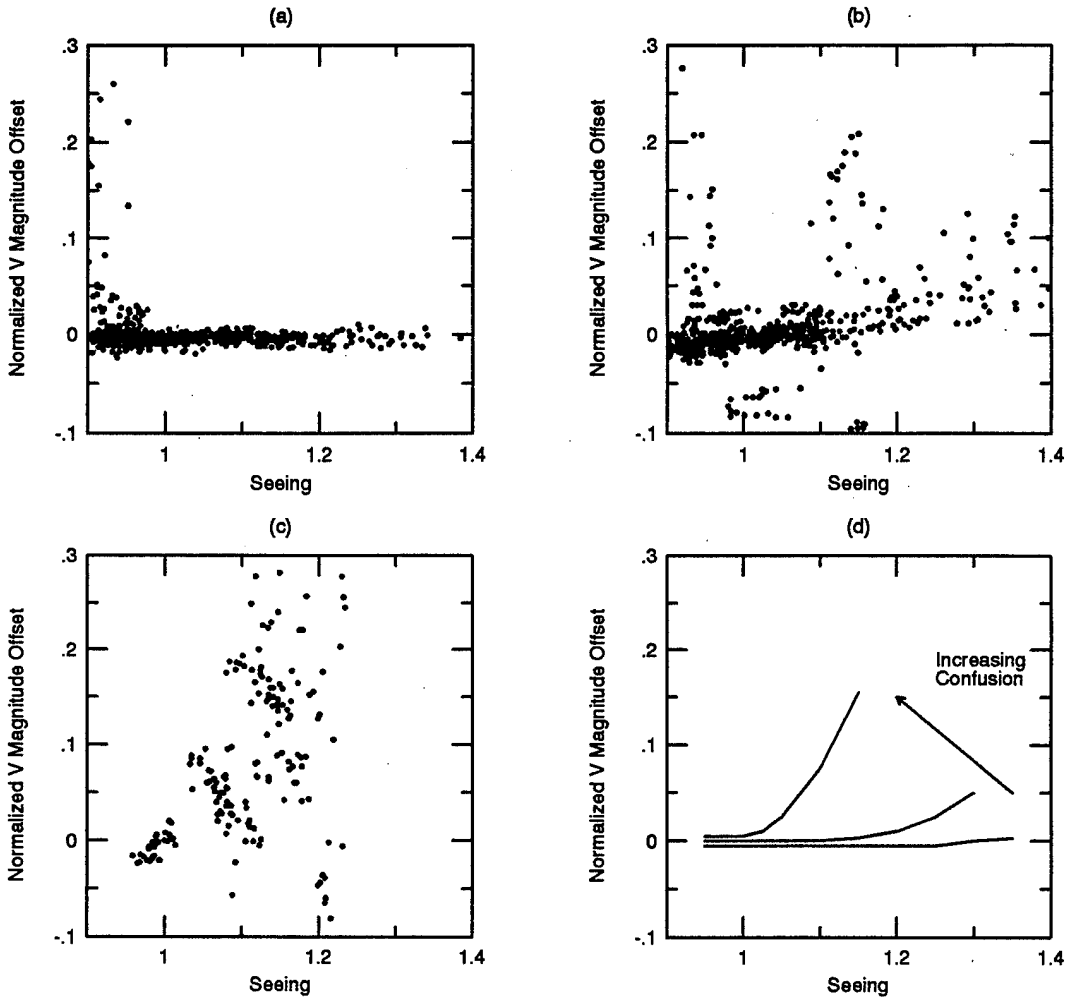


Figure 3.7 - Normalized magnitude offset versus seeing for (a) confusion < 1 in region near the north Galactic pole, (b) 3 < confusion < 4 in winter Galactic plane, (c) confusion > 9 in summer Galactic plane, and (d) trend summarized.

is a value of seeing above which the magnitude offset begins to increase. As the confusion increases, this value of seeing decreases. The trend is summarized schematically in Figure 3.7(d). Points far from the given standard trend for a particular confusion level most likely represent clouds.

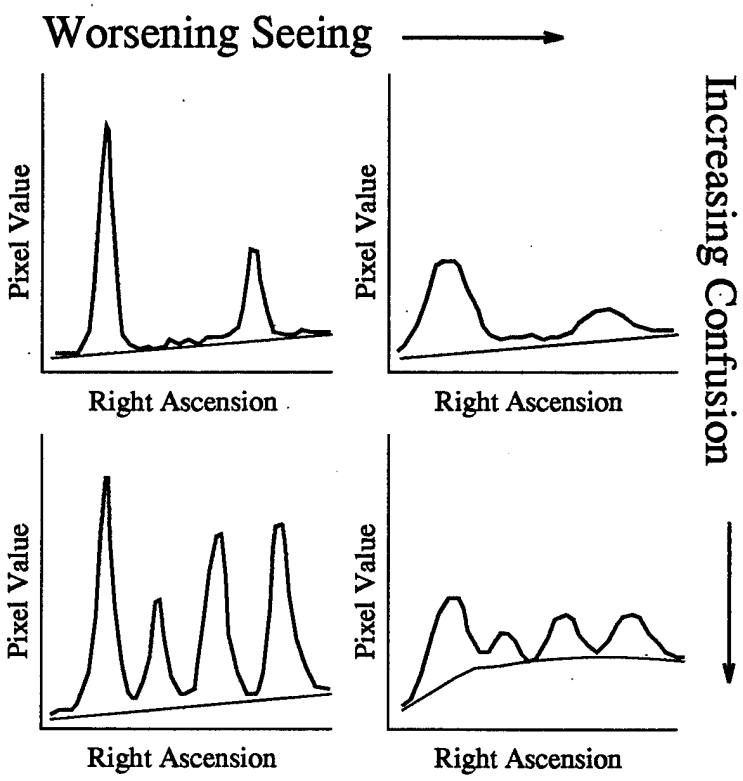


Figure 3.8 - Relationship between confusion, seeing, and magnitude offset explained. Worsening seeing is to the right. Increasing confusion is towards the bottom.

The explanation for why there is a relationship between magnitude offset and seeing for a given confusion level lies in how the background is determined. Figure 3.8 illustrates in one-dimension how the background level is affected for variable seeing and confusion conditions. Low confusion is on top with high confusion on bottom, and good seeing is to the left with bad seeing to the right. Changes in seeing have little or no effect in areas of low confusion because there are still large areas of sky that essentially remain unperturbed. The background can thus follow the true sky

brightness to determine the level consistently. In areas of high confusion, however, as seeing gets worse, stars begin to merge. There is no longer any sky for the background to trace. In effect, the background level rises because it begins to trace the very stars for which we wish to estimate magnitudes. The stars thus appear dimmer, and the magnitude offset increases in order to compensate for the elevated background.

In order for the systematic variations caused by incorrect standard star luminosities to be examined and corrected, the data from the **.XYL** databases must first be cleaned of all seeing/confusion effects. This can be done using the above definition for confusion and setting seeing limits as determined from a process analogous to that described by Figure 3.7.

The only other effects to be addressed are clouds, photometry anomolies such as those created by CR_EDIT (see Section 3.3) and inaccurate photometry due to incorrect background determinations. An example of the latter would be photometry in a portion of the sky contaminated by diffracted or reflected light where the background fitting algorithm was unable to follow the background changes. Most of the these effects occur near bright stars, and thus the region of the CTI survey strip contaminated by their effects can be easily eliminated (see Section 4.2.1). One notable exception, however, is a diffraction effect or reflection from a bright

Table 3.1 - Possible Contamination of CTI Survey Strip by Mars and Jupiter during 1987-1992.

Date of Opposition	Planet	RA (1987.5)	Dec
1987 Oct 25	Jupiter	$1^h\ 31^m$	+8°
1988 Nov 29	Jupiter	$3^h\ 52^m$	+19°
1990 Jan 06	Jupiter	$6^h\ 19^m$	+23°
1990 Dec 05	Mars	$3^h\ 59^m$	+22°
1991 Feb 11	Jupiter	$8^h\ 38^m$	+20°
1992 Mar 13	Jupiter	$10^h\ 40^m$	+10°

planet. The effect of Jupiter, for instance, is clearly evident in data taken during the fall and winter of 1988 at right ascensions about 3^h, although other regions of the CTI survey strip passing close to the ecliptic can be affected in much the same way by other planets or the Moon. Table 3.1 lists possible occurances for contamination from Mars and Jupiter during the period from 1987 to 1992. The planet Saturn was never in a position to affect the CTI survey strip during this period.

Assuming that most observations of a particular standard star are free from clouds, photometry anomolies and the effects of solar system objects, by simply taking the mode instead of the mean to find systematic offsets, the effect of these outliers are eliminated.

The final result of the calibration process is an **.OBS** database, identical in form to the **.SED** database, but containing the *calibrated* position, luminosity, and second moments of every object observed in the particular sweep.

As a side note, if the expected luminosities in the **.SSS**

database were correct, the **.RDK** and **.RFF** databases could be determined by simply examining the **.XYL** or **.CAL** databases for systematic trends in standard star luminosities as a function of declination, and adjusting them accordingly to eliminate those trends. Unfortunately, at this stage we can't be sure if the trends in declination are caused by an incorrect flat field application or incorrect standard star luminosities. This could be remedied by obtaining luminosities to the desired precision for all standard stars located in a small section of the CTI survey strip using another telescope. These expected luminosities could be used to correct the flat-field function for a single night's data, thus obtaining correct expected luminosities for many more standards. Other overlapping nights of data could then be corrected until the entire set of CTI standard star luminosities are free from systematic errors created by incorrect flat-field application.

3.6. Merging Data into Master and History Databases

The day's data can now be merged into the history list of the particular color filter and the master list using the computer routines AUTO_MERGE, AUTO_UPDATE and AUTO_FLUSH.

AUTO_MERGE compares the existing **.PUL** database (containing a right ascension-sorted record of every object observed) with the **.OBS** database of a particular day and matches the records of objects found in both. A **.MRG** database containing the data for each match, and two **.NDX** databases containing a pointer to the record of any unmatched records in the **.PUL** and **.OBS** databases are produced. Additionally, a **.TRA** database containing information relevant to all matches to trace possible mismatches is produced.

Next, AUTO_UPDATE uses the **.MRG** database to refine the information on existing objects in the **.PUL**, **.MAS**, and **.HIS** databases, and uses the **.OBS** combined with the **.NDX** pointer to add new objects. Only objects with a probability value of 0.5 or above are added to the **.MAS** and **.HIS** databases while all new objects, regardless of the probability value, are listed in a newly created **.PUL** database. Including all objects in the **.PUL** database retains the possibility of a very faint object building on its probability value with subsequent detections to eventually be inculded in the **.MAS** and **.HIS** databases. The **.HIS** database contains the day-to-day record of the time, calibrated instrumental luminosity, and error in luminosity of every object observed. The **.HIS** databases also

reference the **.MAS** database, which contains variance-weighted average positional and photometric information as well as various measures of the object's shape and blending. The **.PUL** database contains information similar to the **.MAS** database, but retains all detections regardless of the probability value of detection and is sorted by right ascension for ease in comparing the next day's data. The **.MAS** and **.HIS** databases are not sorted by right ascension, with new detections being added to the end.

Finally, AUTO_FLUSH combines the existing **.PUL** file with the new objects contained in the day's **.PUL** file. The probability value of all non-detections are adjusted downward, and the entire database is sorted by right ascension in preparation for the next day's data.

Currently, data from 77 V nights, 8 B nights, 8 R nights, and 8 I nights have been entered into the **.MAS** and **.HIS** databases. The solid lines in Figure 3.9 displays the distribution of the V and B observations in right ascension for the **.MAS** and **.HIS** databases. The lack of observations about 21^h corresponds to the summer observing season where clear nights were hard to come by. An additional 68 V nights, 26 B nights, 39 R nights, and 23 I nights have been analyzed but not yet merged into these databases.

A second analysis of all 145 V nights and 34 B nights was made for this dissertation with the output entered into new versions of the master and history databases (**.NML** and **.NHL**

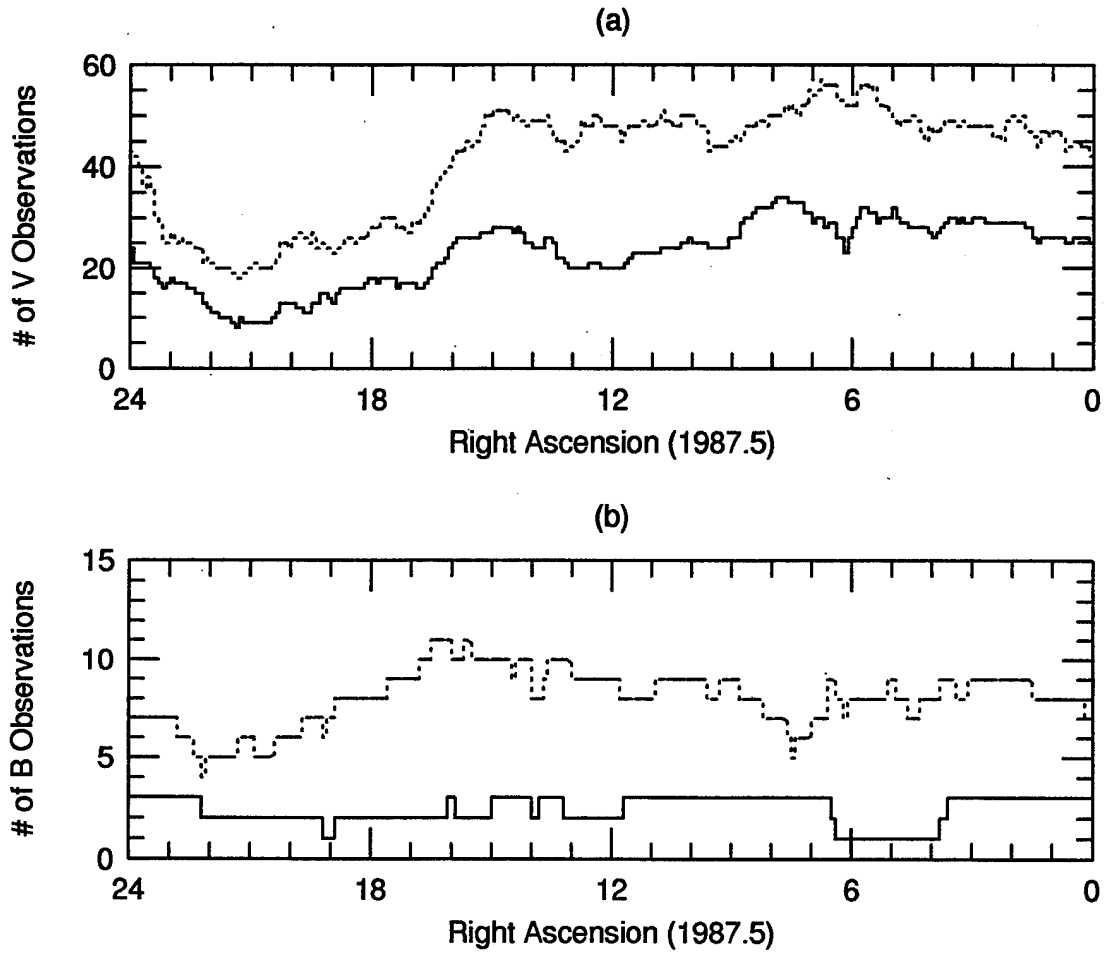


Figure 3.9 - (a) Number of V observations and (b) number of B observations as a function of right ascension. Solid line represents those days merged into the current **.MAS** and **.HIS** databases. Dashed line represents those days merged into the current **.NML** and **.NHL** databases.

respectively). The primary difference between these new databases and the old versions is that the **.NHL** database now contains a day-to-day record of the position of every object in addition to its luminosity. Also, the positional calibration of the data used to create these new databases employed the misalignment and astigmatism correction procedure (see Section 3.5.1) not used previously. The dashed line in

Figure 3.9 displays the distribution of the V and B observations versus right ascension for the **.NML** and **.NHL** databases.

We are now ready to query the information contained in the master (**.MAS** or **.NML**), pool (**.PUL**), and history (**.HIS** or **.NHL**) databases, or any of the other databases produced during the analysis process. This is accomplished using the computer program PSI, which was specifically developed for use with the CTI survey. A user's guide to this and other CTI database programs can be found in The CCD/Transit Instrument Atlas and Database Guide (Wetterer 1995), written as a supplement to this dissertation.

Chapter 4 Variable stars in the CTI survey

The CTI observes over 500,000 objects, many of which vary in luminosity as a function of time. This chapter describes the discovery of variable stars in the CTI survey. First, a short history of the study of variable stars is given. Next, the method for finding variable stars and the completeness of the variable star list is presented with the issues of spurious variables and blind spots discussed. Finally, a description of the resulting variable star index database is presented.

4.1 Variable Stars

A variable star refers to a star where one or more of its physical properties change with time. Typically it is the star's luminosity in a certain wavelength range that is examined to determine variability, although it may be another property, such as spectral type (or color), radial velocity, or details within the spectra that vary with or without a luminosity variation. The simple fact that stars have finite lifetimes make all stars variable at some level. Over time, certain stars become variable due to evolutionary changes. Helium core burning RR Lyrae variable stars were quiet members of the main-sequence earlier in life. Even if time restraints are specified, small scale variability, such as the Sun's 11-year sunspot cycle, are probably present in most stars. In the following discussion, however, I will restrict the definition of a variable star to those for which luminosity in visible light (V bandpass) changes appreciably over a time interval detectable by CTI (a few minutes to a few years).

The history of the study of variable stars spans nearly four centuries (see, for instance, Campbell and Jacchia 1941). Although many novae and supernovae had been detected beforehand, such as the supernova leading to the Crab Nebula in Taurus recorded by the Chinese in 1054 AD, the first star to be classified as a periodic variable was a star in the constellation Cetus. The star was designated o Ceti by Bayer in 1603, who was unaware of its variability, and later also

named Mira. Fabricius first noted its presence and disappearance in August 1596 and February 1609, although it was not until 1638 that Holwarda noted the star was periodic in its brightening and dimming (Allen 1963). By the end of the 18th century, sixteen stars were classified as variables. There were four Mira variables, two eclipsing variables (the star Algol being the prototype), two Cepheid variables (named after one of the two, δ Cephei), five novae, and three others stars that exhibited their own unique variations (α Herculis with a small and irregular variation, R Scuti with a semi-regular periodicity, and R Coronae Borealis with erratic and large variations). By the end of the 19th century, the number of identified variable stars had grown to over 1000. With improvements in photography, the discovery rate of variable stars greatly increased. By the middle of the 20th century, 10000 variables had been identified, and as we near the 21st century, nearly 30000 are known and cataloged in the Milky Way (Kholopov et al. 1985-88) with many more variable stars identified in other nearby galaxies (see, for example, Saha et al. 1990). As with the advent of photographic surveys, in the coming years, CCD surveys such as the CTI survey will undoubtedly continue the dramatic increase in the number of detected variable stars.

Because of similarities between variable stars, astronomers have continually attempted to group them into

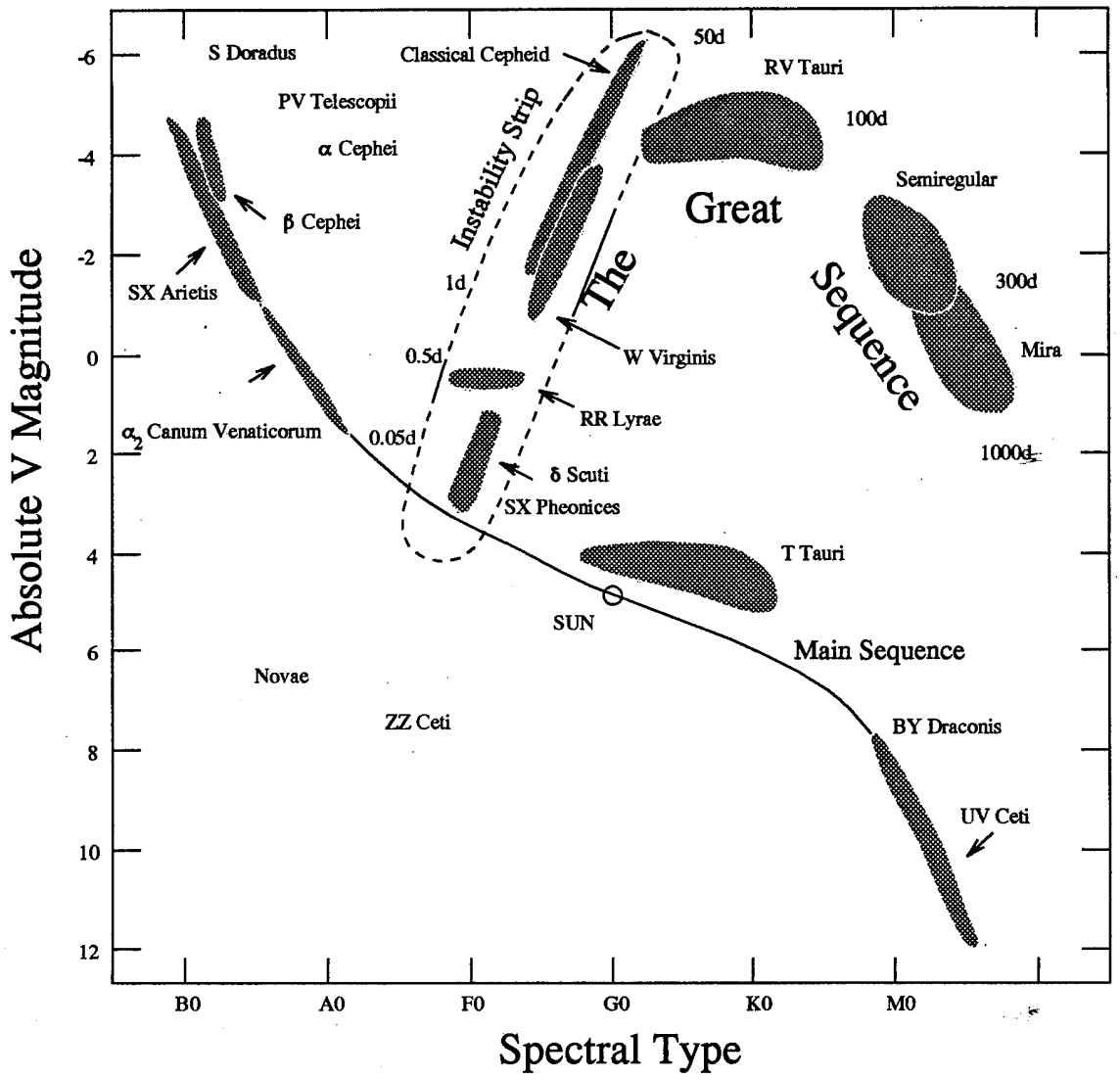


Figure 4.1 - Positions of variable star types on Hertzsprung-Russell (H-R) diagram, (Adapted from Cox 1980). Variable stars in the "Instability Strip" are radially pulsating stars and share a common mechanism that drives their pulsations. Variable stars in "The Great Sequence" (SX Pheonices to Mira) are pulsational variables of decreasing density and increasing size and period (typical periods shown in days).

different categories and types. Whereas the number of recognized variable star types in 1800 were 7, there are currently nearly 50. The first division used in the

classifications of the General Catalog of Variable Stars (GCVS) (Kholopov et al. 1985-88) are between *cataclysmic* (thermonuclear burst processes deep in star's interiors, in surface layers, or in surrounding space), *eruptive* (violent processes and flares occurring in the chromosphere or corona), *pulsating* (periodic radial or nonradial contractions and expansions of surface layers), *rotating* (nonuniform surface brightness and/or ellipsoidal shapes), and *eclipsing* (close binary geometric effects) variables. Other broad distinctions can be made between *intrinsic* variables where the variability is the result of changes within the star itself, and *extrinsic* variables where the variability is a result of an interaction with another star or interstellar medium. Also, light curve morphology is often used to make distinctions between variables. Confusing matters still further, several stars exhibit variability from more than one source, presenting the possibility of multiple classifications. Table A1.6 in Appendix 1 (adapted from the GCVS and Petit 1987) attempts to summarize all the types represented in the GCVS detectable by the CTI. Many of these variables occupy specific parts of the Hertzsprung-Russell (H-R) diagram, as shown in Figure 4.1 (adapted from Cox 1980).

Variable stars are stars in certain phases of their evolution, or undergoing rapid changes. The study of variable stars has improved our understanding of stellar structure and evolution. Perhaps the most important result to come from the

study of variable stars, however, involves using certain types of variable stars as "standard candles" or distance indicators. The famous period-luminosity relationship of classical Cepheid variable stars allows their distance to be accurately calculated given knowledge of their period and apparent magnitude (see, for example, Madore and Freedman 1991, Jacoby et al. 1992). With absolute magnitudes of M_V = -2 to -7, Cepheid variable stars can be detected in galaxies out to 10 Mpc. Most other types of pulsating variable stars also exhibit a similar relationship. One of these types, RR Lyrae stars, are abudent in the old population of the Galaxy, enabling astronomers to probe the properties of the Milky Way's halo as well as the properties of globular clusters. The study of RR Lyrae variable stars, and subsequent search for this type of star within the CTI survey, is discussed in more detail in the next chapter.

4.2 Finding variable stars in CTI survey

The obvious CTI database to use in order to start our search for variable stars in the CTI survey is the V filter's history list (**.HIS** or **.NHL** database). The history list contains the time, luminosity (*lum*) and luminosity error (σ_{lum}) for every observation with the V filter of each object in the survey. The scatter in luminosity measurements is approximated well by a Gaussian distribution, and thus a simple test can determine if the observed variability of the luminosity is statistically significant (Chapter 10, Bevington 1969).

The error estimates should follow a χ^2 distribution. The reduced χ^2 is given by

$$\chi_{\upsilon}^2=\sum_{i=1}^{n} \frac{(lum-\langle lum\rangle)^2}{\upsilon\sigma_{lum}^2}, \qquad (4.1)$$

where $\langle lum\rangle$ is the mean luminosity, n is the number of observations and ν = n-1. It is evident that for a given number of observations, the larger χ_ν^2, the more probable the object's variability is a result of an actual change in its luminosity rather than from random errors. This probability can be calculated using the equation

$$P_\chi(\chi_{\upsilon}^2)=\int_{\chi_{\upsilon}^2}^{\infty} P(x^2,\nu)\,dx^2, \qquad (4.2)$$

where

$$P(x^2,\nu) = \frac{(x^2)^{1/2(\nu-2)} e^{-x^2/2}}{2^{\nu/2}\Gamma(\nu/2)} \qquad (4.3)$$

is the probability distribution function for χ_ν^2. In the search for variable stars in the CTI survey, only those objects were selected for which this probability of the observed distribution being a product of the calculated random error is less than 1%.

Due to photometry errors, if this test is applied to objects in the current **.HIS** or **.NHL** databases, approximately 60% pass the test and are considered variable. It is thus necessary to screen the photometry data before testing for variability to eliminate sources of spurious variables.

4.2.1 Spurious Variables

There are several sources of systematic error that affect the photometry of objects in the CTI survey. Before the above test for variability can be conducted, the data contaminated by these photometry errors must be eliminated.

Stars surrounding a bright star may all appear variable as the amount of contamination from the diffraction spikes of the bright star varies. These night-to-night variations are caused by different observing conditions, such as seeing, transparency, and estimated background level. To reduce this problem, a region surrounding each bright star was removed from the survey corresponding to the area visually

contaminated by false objects produced by the star's diffraction spikes and charge bleeding. The biggest offenders are Pollux, Scheat, and Alberio for which it was necessary to remove 0.24%, 0.17% and 0.07% of the CTI survey area respectively. Another 308 stars contained in the SAO catalog (see Table A1.5 in Appendix 1), and 2060 stars determined to be brighter that V = 12 from CTI's **.MAS** database were also removed. The CTI selected stars were carefully screened to exclude bright objects in the database created by meteor or satellite trails. The size of the regions masked around each star varied as a function of the magnitude of the star. The formulas used in calculating the size and shape of the mask were determined empirically using a small selection of representative stars and are given in Table A1.7 of Appendix 1. The total area removed because of bright star contamination was approximately 1.0 square degree, or 1.93% of the CTI survey area. The remaining CTI survey area contains 532,878 objects with four or more V observations.

The luminosity data of an object may also be contaminated by isolated events, such as meteor trails, systematic errors caused by photometry in regions where the background was not accurately calculated (see Chapter 3.5.2), and accidental non-detections caused by the cosmic ray removal algorithm (see Chapter 3.3). For a nonvariable star, these effects will create anomalously bright or faint data in an otherwise constant luminosity light curve. As a first cut, the minimum

and maximum luminosity for a particular star is not considered. Next, luminosity measurements which deviate more than 3σ above the mean luminosity and 2σ below the mean luminosity for each object, (σ being the standard deviation of the luminosity from the mean not considering the minimum and maximum luminosities) were removed from consideration. Finally, σ and the mean were recalculated, with any more extreme luminosity data removed as in the first pass. The limits used in this prescreening were chosen empirically to remove the bulk of the spurious variables created. This prescreening of the luminosity data does bias the resulting variable object list against stars that vary by exhibiting an occasional short-lived brightening (e.g. some eruptive-type variables) or dimming (e.g. Algol type eclipsing variables). This bias, however, does not affect the detection of RR Lyrae variable stars with good phase coverage, which was the primary goal of the present search. A total of 39,334 objects (7.4%) pass the variability test after employing the above prescreening.

Figure 4.2 plots the variable fraction of the total number of objects as a function of mean instrumental V magnitude (solid line labeled σ = 0%) after prescreening. Also plotted in Figure 4.2 is the total number of objects as a function of mean V magnitude (dashed line). Only objects outside the Galactic plane with 9 or more V observations were used in making this plot to reduce the effects of other

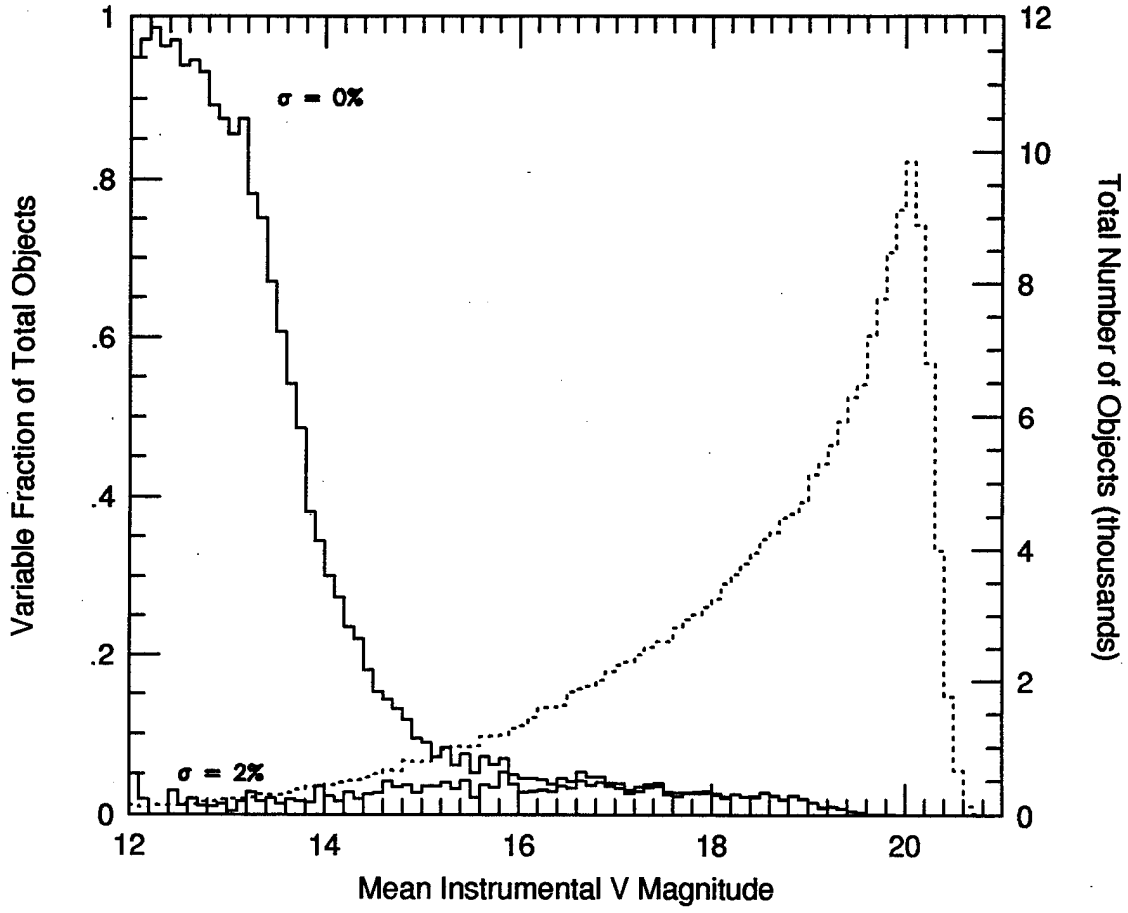


Figure 4.2 - Variable fraction of objects outside Galactic plane with 9 or more V observations versus mean instrumental V magnitude for additional systematic errors of 0.00 and 0.02 times the luminosity (solid lines). Total number of objects outside the Galactic Plane with 9 or more V observations versus mean instrumental V magnitude also shown as dashed line and using scale on right.

sources of spurious variables. The most striking feature in Figure 4.2 is the dramatic increase of the variable fraction of objects for stars with V < 15. For brighter stars, the error in luminosity relative to the luminosity decreases, making the variability test more sensitive to lower amplitudes of variation in magnitudes. The increase in the fraction of

variable objects for V < 15 could simply be an actual detection of more variables due to the increased sensitivity. An additional luminosity-dependent error not accounted for in the calculated luminosity error, however, would produce the same effect. A possible source for this type of error is incorrect flat-field application (see Chapter 3.2). An error in the flat-field would directly manifest itself as a systematic error in the calculated luminosity of an object. The calculated error in the luminosity for the object, however, is not affected. If the position and magnitude of these flat-field errors vary from night-to-night, the induced systematic errors for a particular object would be similar to increasing the random error in luminosity. The variable fraction of the total number of objects as a function of mean instrumental V magnitude after adding in quadrature an additional error of 2% the object's luminosity to the existing random error (solid line labeled σ = 2%) is also plotted in Figure 4.2. The variable fraction of objects is now virtually independent of magnitude. Unfortunately increasing the error in the luminosities to remove spurious variables created by flat-field application (or from another source of a luminosity dependent error) undoubtedly removes true variables as well, just as using the existing error undoubtedly includes spurious variables. The former represents a conservative estimate of what objects are variable, while the latter a liberal estimate.

If the additional error as described above is applied, an effective lower limit in amplitude of about $\Delta V \approx 0.1$ magnitudes for detecting variables is set. For fainter magnitudes, the increasing random error requires ever greater amplitude variations to be detected as a variable star. This sets a faint limit to the detection of variable stars and will be discussed in more detail in the next section. A total of 25,325 objects (4.7%) pass the variability test after employing the prescreening and additional error.

Another source of spurious variables are stars that are very close together or segments of extended objects such as galaxies. These objects might appear variable because the photometry splits the light between them differently under different conditions. Thus, sometimes one star appears dimmer while the other brighter, while at other times the reverse is true. Both stars appear variable when in fact they are not. For all stars passing the variability test using the prescreening and additional error, and with 9 or more V observations, the linear correlation coefficient was calculated between the star's luminosity and the luminosity of its nearest variable neighbor (Chapter 7, Bevington 1969)

$$r \equiv \frac{N\Sigma x_i y_i - \Sigma x_i \Sigma y_i}{\sqrt{N\Sigma x_i^2 - (\Sigma x_i)^2}\sqrt{N\Sigma y_i^2 - (\Sigma y_i)^2}}, \qquad (4.4)$$

where x_i is the star's luminosity, y_i is the neighboring star's luminosity, and N is the number of observation dates common to

both. The light curves of the two stars are inversely correlated for $r < 0$. The probability that a random sample of N uncorrelated experimental data points would yield an experimental linear-correlation coefficient $|r|$ as large as or larger than the observed value was calculated with

$$P_c(r,N) = 2\int_{|r|}^{1} P_r(\rho,\nu)\,d\rho, \qquad (4.5)$$

where

$$P_r(r,\nu) = \frac{1}{\sqrt{\pi}}\,\frac{\Gamma[(\nu+1)/2]}{\Gamma(\nu/2)}\,(1-r^2)^{(\nu-2)/2}, \qquad (4.6)$$

$\nu = N - 2$, and Γ is the Gamma function. If $r < 0$ and $P_c(r,N)$ less than 1%, the two stars in question were not considered variable. A total of 19,412 (4.3%) stars pass the variability test after employing the prescreening, additional error, and correlation test.

Galaxies may still appear variable due to a dependence of the photometry on the seeing or the throughput of the telescope (see, for instance, Hawkins 1984 and Stobie et al. 1986). For example, as dust settles on the mirror reducing the throughput of the telescope, the contribution of a galaxy's faint outer structure may slowly be lost in the noise of the surrounding background. Because the luminosity calibration is determined by stars, a spurious long period variable could thus be created from the photometry of a galaxy. An indication that this may indeed be happening is

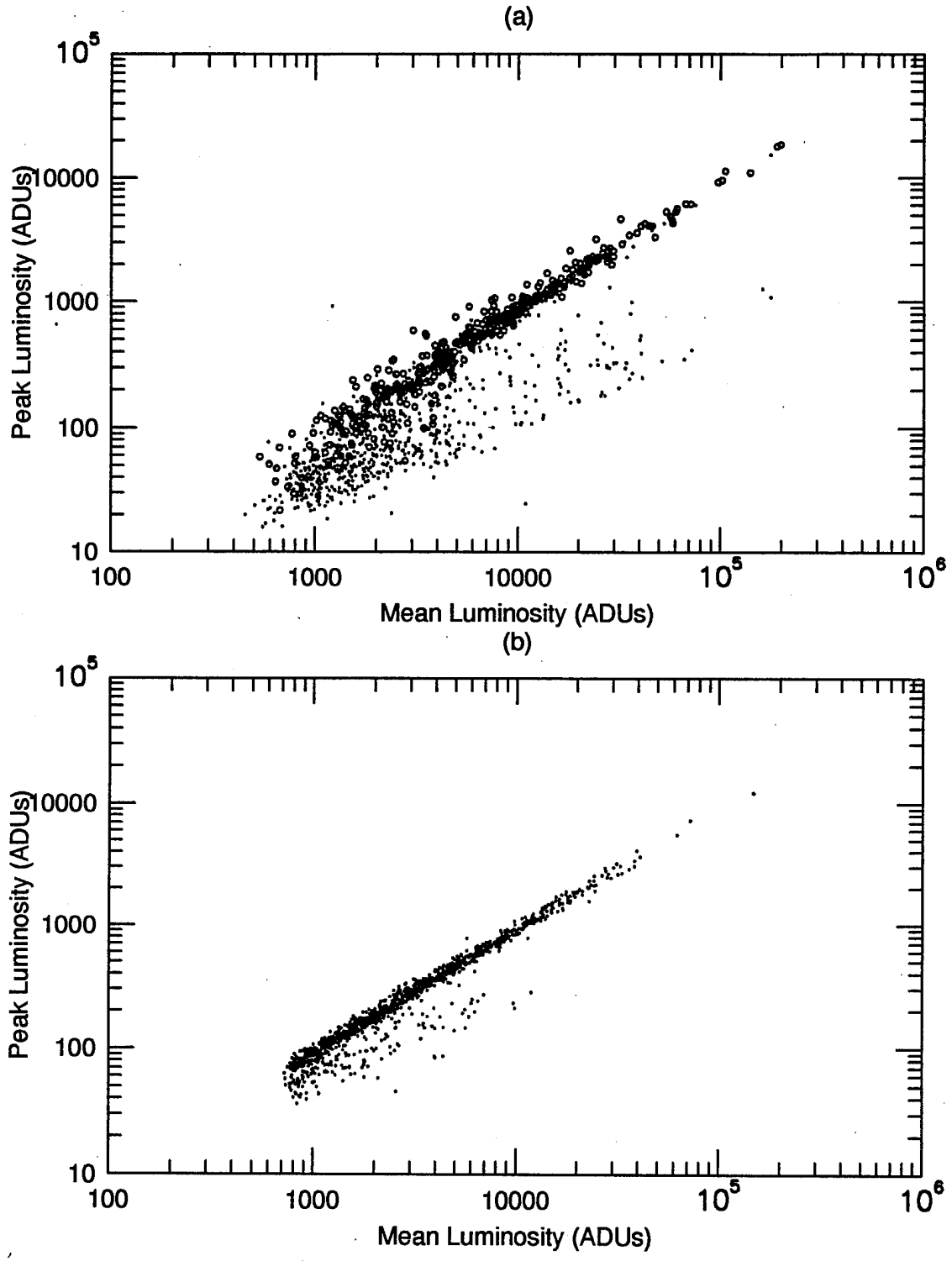


Figure 4.3 - Peak luminosity versus mean luminosity for (a) variable objects with 9 or more V observations and a right ascension between 7^h and 18^h, and, (b) non-variable objects with 9 or more V observations and a right ascension between 7^h and 18^h. Circles in (a) are for objects with V_COMB = 0.

illustrated in Figure 4.3. The peak luminosity is plotted versus the mean luminosity for (a) variable objects and (b) the same number of non-variable objects. Only objects with 9 or more V observations and a right ascensions between 7^h and 18^h are plotted to reduce the effect of other sources of spurious variables. All stars have the same point spread function and thus fall on a straight line in these plots. Extended objects such as galaxies will have a lower peak luminosity as compared to the same mean luminosity for a star, and will thus fall below the line tracing stars. As seen when comparing Figure 4.3(a) to 4.3(b), it is clear there is a higher percentage of galaxies that are variable.

A useful CTI database attribute that can be used to eliminate galaxies as well as other blended stars and artifacts surrounding bright stars not previously masked is V_COMB. V_COMB is related to possible matching errors, with a non-zero V_COMB indicating that at some time the automated matching accomplished during AUTO_MERGE (see Chapter 3.6) had trouble matching the observed object(s) with the records contained in the **.PUL** database. The more complicated the matching problem (corresponding to greater values of V_COMB), the greater fraction of these objects are detected as variable. The circles plotted in Figure 4.3(a) are variable objects with V_COMB = 0 (i.e. no matching problem), with nearly all falling close to the line representing stars. Requiring V_COMB to equal zero appears to eliminate galaxies,

but is also reducing the effective CTI survey area by eliminating stars from consideration. A total of 13,547 (3.5%) stars pass the variability test after employing the prescreening, additional error, correlation test, and requiring V_COMB = 0. The last condition also reduces the total number of observed stars to 387,998.

Figure 4.4 plots the variable fraction of objects as a function of the number of V observations using (a) all the screening described above except the restriction on V_COMB, and (b) all the screening described above including V_COMB = 0 (solid line). Only objects outside the Galactic plane between right ascensions 1^h and 15^h, corresponding to regions of the CTI survey strip with approximately the same maximum number of V observations, were used in making this plot to reduce the effects of other sources of spurious variables. The total number of objects as a function of the number of V observations for this region is also plotted (dashed line). The increase in the fraction of variables for objects with less than 15 detections in Figure 4.4(a) can be explained by comparing this to Figure 4.4(b). The majority of these objects with less than 15 detections and variable have also experienced a matching problem (V_COMB $\neq$ 0). It is likely that most of these objects are segments of extended objects or noise segments in the diffraction halos of bright stars not previously masked. Since changing observing conditions will change the positions of these false objects, many such objects

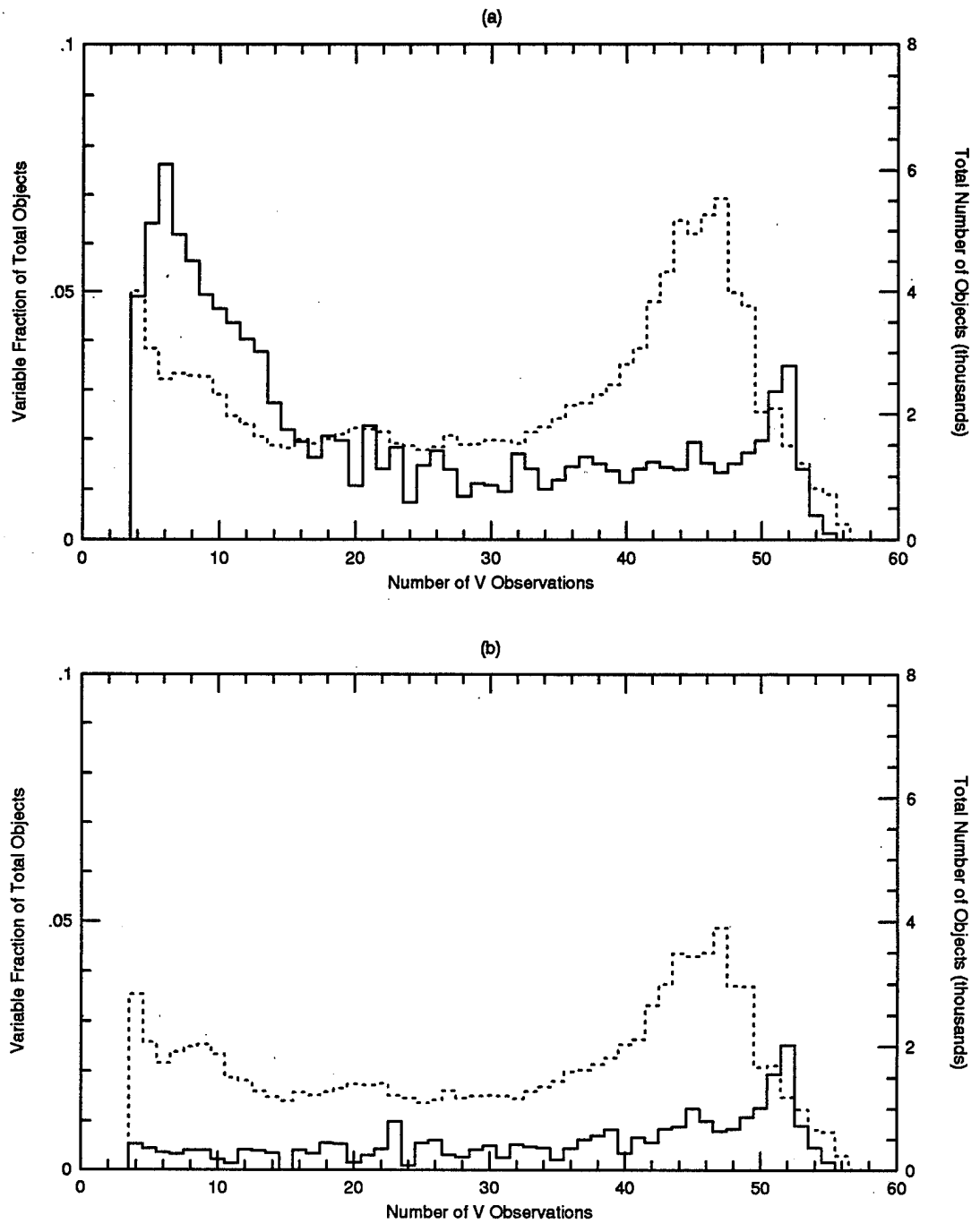


Figure 4.4 - Variable fraction of objects outside Galactic plane between right ascensions 1^h - 15^h versus number of V observations (a) no restriction on V_COMB and (b) V_COMB = 0 shown as solid line. Total number of objects outside the Galactic plane between right ascensions 1^h to 15^h versus number of V observations also shown as dashed line and using scale on right.

are created, with a particular object being "observed" only on a fraction of the total number of nights. The rise in the variable fraction of objects when the number of V observations is above 50 is related to confusion near the Galactic plane.

Figure 4.5 plots the variable fraction of objects as a function of right ascension using (a) all the screening described above except the restriction on V_COMB, and (b) all the screening described above including V_COMB = 0 (solid line). Only objects with 9 or more V observations were used in making the plot. Also plotted is the total number of objects as a function of right ascension (dashed line). In general, the fraction of variable objects remains reasonably constant, except in the Galactic plane where there is a sharp rise directly correlated to the density of objects (i.e. confusion), and in highly localized regions outside the Galactic plane. The first effect is most probably a result of photometry errors created by the link between background estimation and observing conditions in regions of high confusion (see Chapter 3.5.2). Figure 4.6 plots the fraction of variable objects as a function of V magnitude for objects in the heart of the summer Galactic plane. The photometry errors resulting from the background estimation clearly increase the scatter in the luminosity data such that nearly all bright stars pass the variability test because this error is not reflected in the luminosity error. The increased fraction of variables in highly localized regions outside the

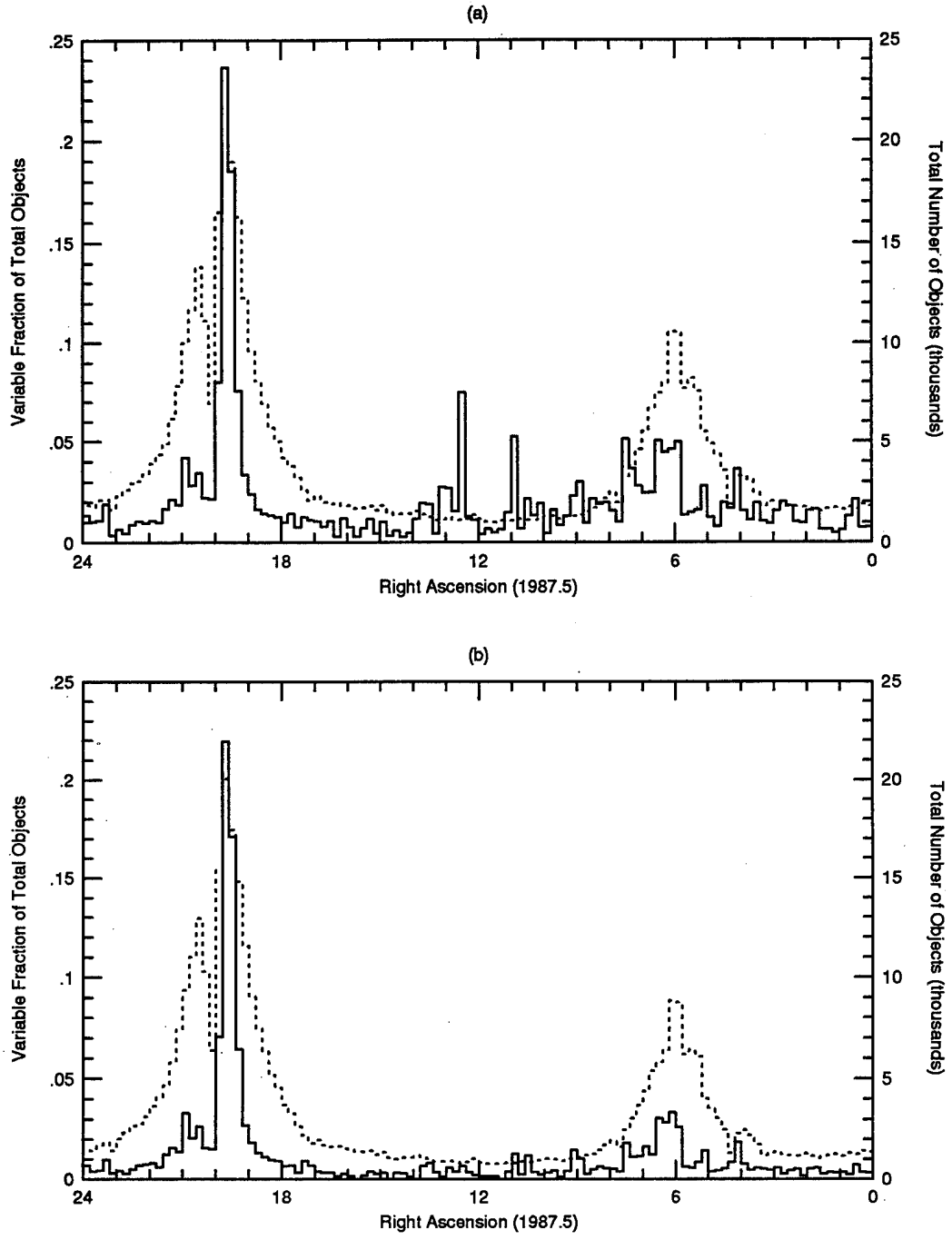


Figure 4.5 - Variable fraction of objects with 9 or more V observations versus right ascension (a) no restriction on V_COMB and (b) V_COMB = 0 shown as solid line. Total number of objects with 9 or more V observations versus right ascension also shown as dashed line and using scale on right.

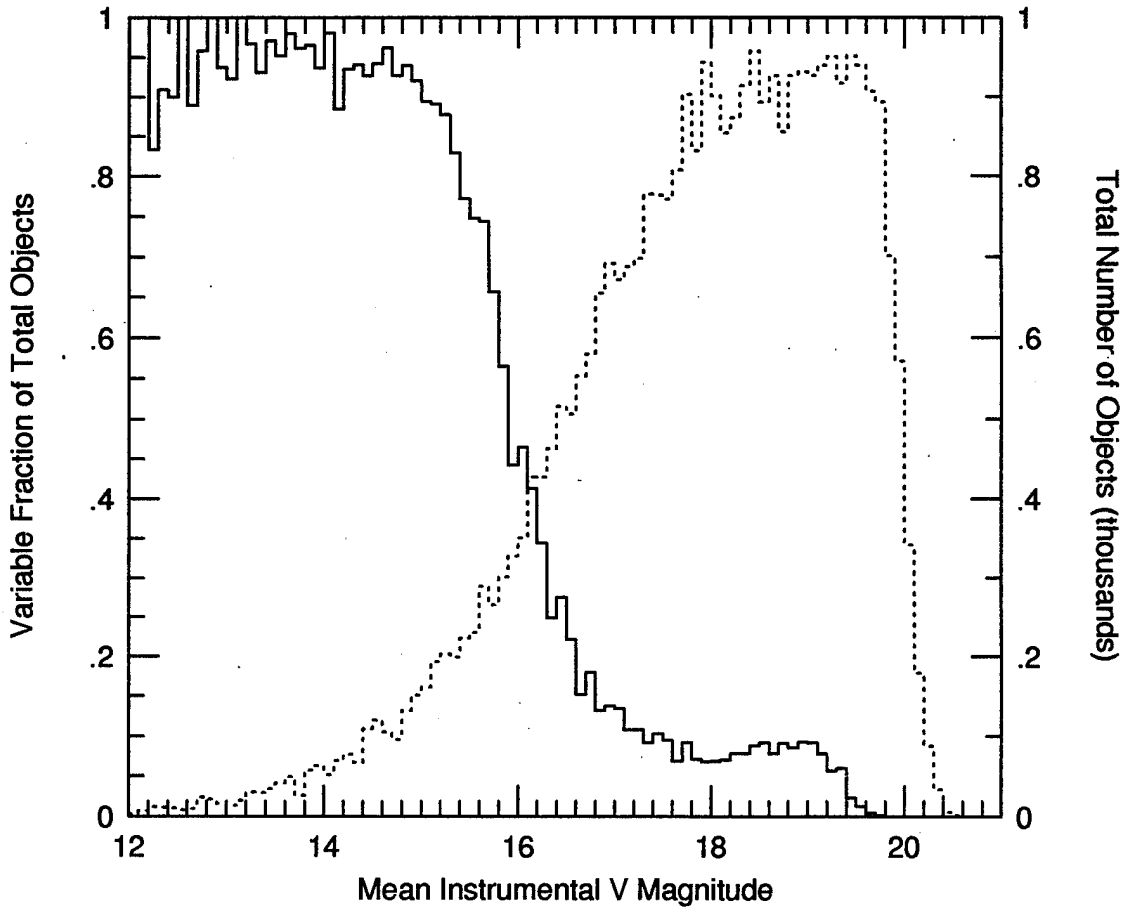


Figure 4.6 - Variable fraction of objects in Galactic plane (right ascensions 19.4h to 19.8h) with 9 or more V observations versus mean instrumental V magnitude shown as solid line. Total number of objects in this region versus mean instrumental V magnitude also shown as dashed line and using scale on right.

Galactic plane are possibly due to spurious variables created by extended objects or bright stars. This is supported by the fact that these high variable fraction regions are eliminated by requiring V_COMB = 0, as shown in Figure 4.5(b).

In summary, searching for variable stars in the CTI

databases also exposes sources of photometry errors that create spurious variables. Indeed, many of the sources discussed above were discovered due to clues left in the "light curves" of the spurious variables created. Each solution employed to eliminate spurious variables has unfortunately eliminated true variables as well, and depending on the type of variable star being sought, will effect the completeness of the resulting sample.

4.2.2 Blind Spots (Completeness)

There are certain variable stars that CTI will not be able to detect. As stated above, with the addition of a systematic error to account for flat-fielding problems, variable stars with changes in luminosity less than ≈0.1 magnitudes will not be detected. For fainter stars, this minimum detectable magnitude difference increases as the observational error increases. This is illustrated in Figure 4.7 which plots the average random error (solid line) and average adjusted error (including the 2% systematic error discussed in previous section, dashed line) in the instrumental V magnitude versus the average instrumental V magnitude. It is clear that the fainter the object, the greater the average error, and thus the greater amplitude in variability needed for detection. This is evident in Figure 4.2 as a decline in the variable fraction of objects for V > 19. Using synthesized sinusoidal light curves, the minimum

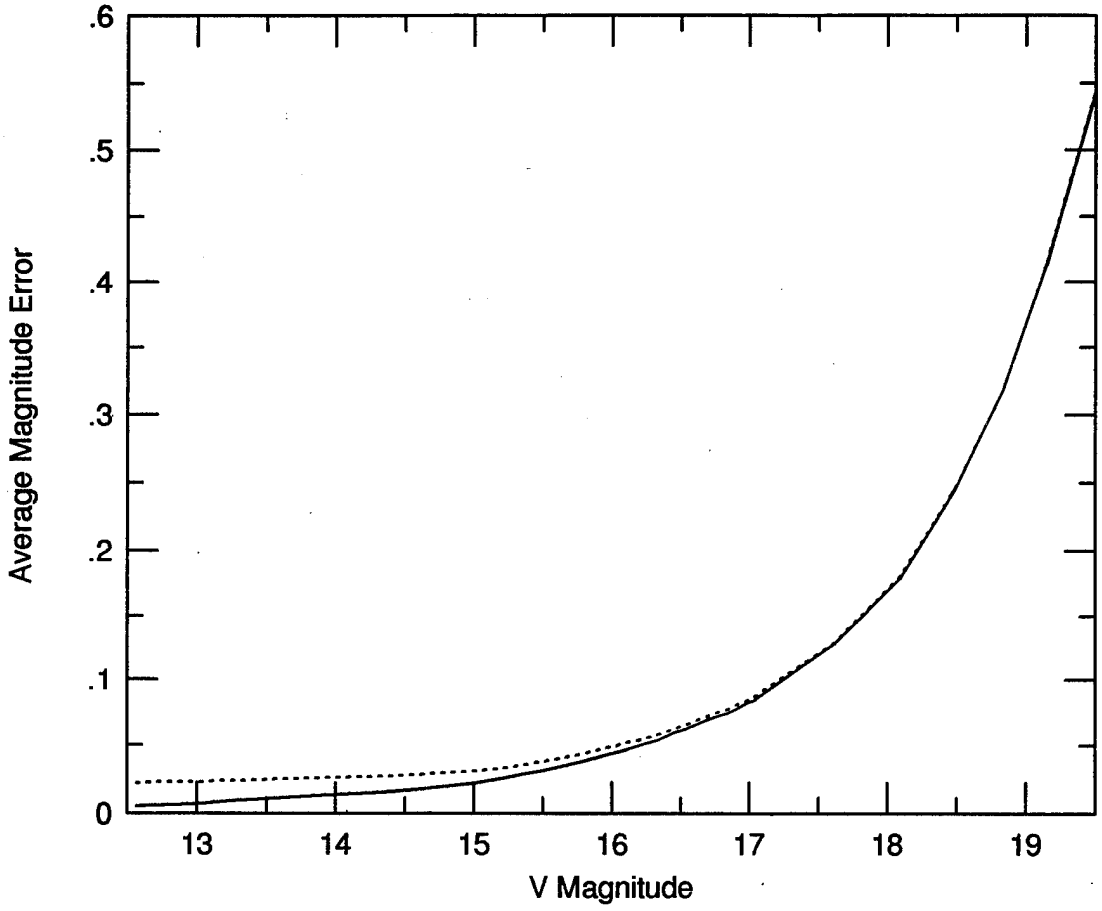


Figure 4.7 - Average V magnitude random error (solid line) and total error (dashed line) as a function of average instrumental V magnitude.

amplitude limit as a function of magnitude was determined to be between 3 and 4 times the total error.

Another blind spot involves variable stars of specific periods. As an obvious example, a variable star with a period of exactly one sidereal day will appear constant due to the fact that CTI *observes* with exactly a one sidereal day period. Depending on the type of variability, variable stars with

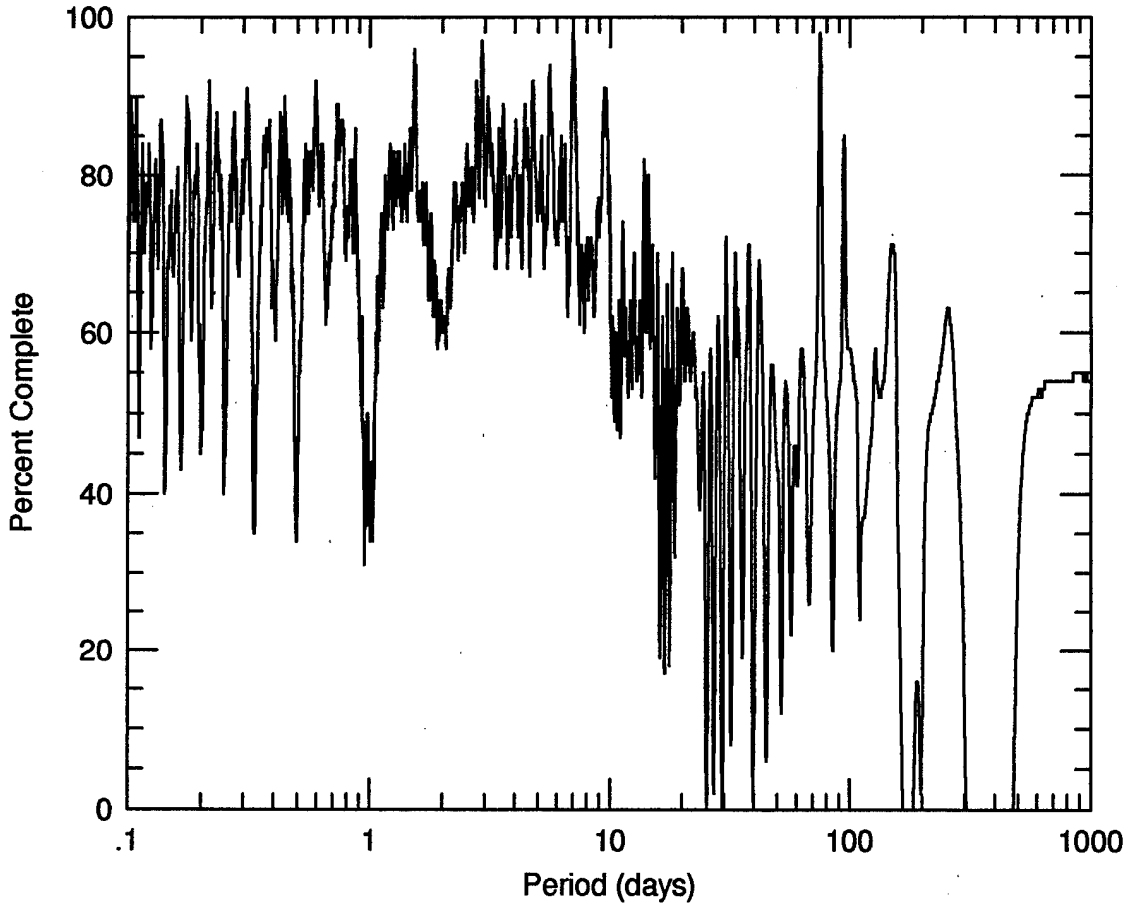


Figure 4.8 - Percent detectability as a function of period as calculated from the observation times of a typical star with 19 observations.

periods close to fractions or multiples of a sidereal day will also not be detected. These period-specific blind spots can be identified and an estimate of the completeness of detecting a certain type of variable star can be made.

Figure 4.8 maps out these blind spots for periods between a tenth of a day to 1000 days. This graph was produced using a typical list of observation times and assuming a sinusoidal

light curve with an amplitude four times that of the observational error. The observation times were first converted to heliocentric observation times to account for varying arrival times of the light from stars during different times of the year. Given the heliocentric observation times and period, the phase distribution of observations was calculated. Given some initial phase, luminosities were calculated and the resulting data was tested for variability using the same test as described above. For each period, the detections were averaged over all initial phases to determine the detection rate for that period. Fractions and multiples of the sidereal day and the tropical year are clearly visible. Any serious completeness estimate, however, should take into account minimum and maximum periods, light curve shape, and minimum and maximum amplitude of the particular variable in question.

4.3 CTI Variable Star Index Description

All entries in the CTI survey's **.NML** database with at least one V observation are listed in the CTI variable star index (**.VNX** database). This database can be used to produce index listings for the **.NML** or **.NHL** databases of potential variable stars by setting limits on the various other attributes. The following is a description of the information contained in the **.VNX** database.

The first two attributes are pointers to the **.NML** database (MLINK) and the B and V **.NHL** databases (HLINK). Positional information is contained in the next two attributes, YCTI (right ascension in centipixels) and XCTI (declination in centipixels). These values are given using CTI's epoch of 1987.5, and can be easily converted to hours of right ascension and degrees of declination using

$$RA = \frac{YCTI}{3.0 \times 10^6} \qquad (4.7)$$

and

$$Dec = 28.0 + \cos(28.0) \times \frac{XCTI}{2.0 \times 10^5}. \qquad (4.8)$$

When referring to a listing, the object name is "CTI" plus the right ascension (HHMMSS.S) and declination (+DDMMSS.S) (e.g. CTI025001.4+280123.3). The **.VNX** database is sorted by increasing YCTI.

The next attribute, NDET, refers to the number of V observations, including those observations that might suffer

from photometry errors. The next two attributes were calculated for all objects using the data prescreening procedure described in Section 4.2.1. V refers to the average instrumental V magnitude and AMP refers to the amplitude of variation in V magnitude. In both cases, the minimum and maximum luminosities were considered if they fell within the specified luminosity limits determined by the prescreening procedure.

Finally, the last attribute, FLAG, contains information pertaining to the search for variable stars. The first number in the array corresponds to whether the object passed the variability test or not. There are four possible values: 0 refers to a star that has never passed, 100 refers to stars that only pass with no prescreening of the data (must have at least 2 V observations), 110 refers to stars that pass with prescreening of the data but no additional error (must have at least 4 V observations), and 111 refer to stars that pass with prescreening and additional error (must have at least 4 V observations). The second number in the array corresponds to whether the object is close to a bright star (value equal to 1) or not (value equal to 0). The third number in the array is simply V_COMB as contained in the **.NML** database. Finally, the fourth number in the array corresponds to whether the luminosity data of the object is anti-correlated with the luminosity data of it's nearest variable neighbor (value equal to 1) or not (value equal to 0).

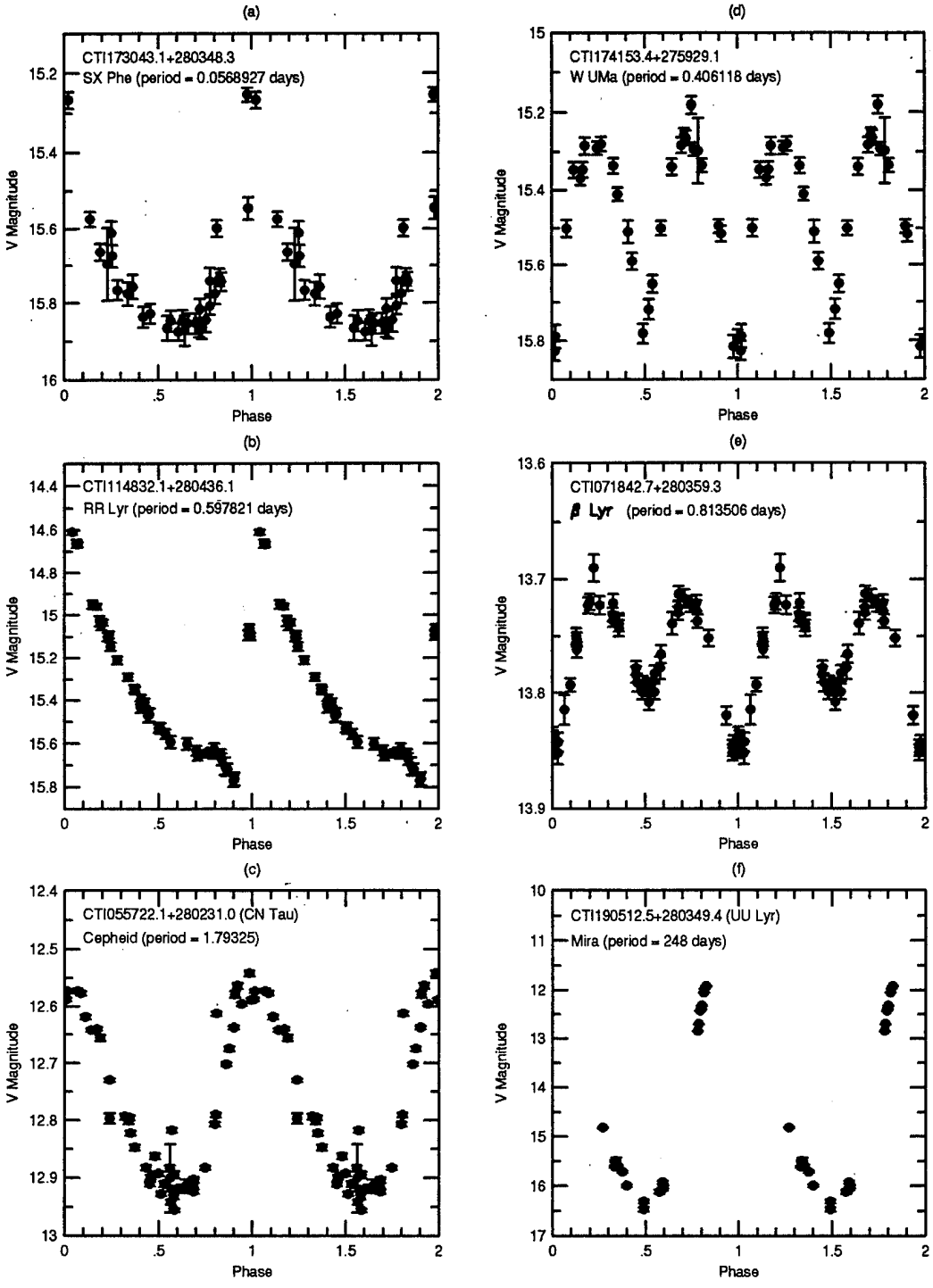


Figure 4.9 - Light curves of different types of variable stars found in CTI survey. Periods for (a) - (c) determined using additional observations at Capilla Peak (not shown). Periods for (d) and (e) potentially aliased. Period for (f) from GCVS.

The CTI survey can provide samples of many different types of variable stars (see Figure 4.9). An index created using the **.VNX** database is just the starting point in discovering examples of a particular type of variable star. In addition to V_COMB, the size and shape information in the **.NML** database can be used to eliminate or select galaxies. The **.NHL** databases can be used to find periodicity, calculate colors, and ultimately classify stars as a particular type of variable. The completeness of a given sample can then be estimated using information provided in this chapter and details concerning the limits used in the search. This is done for RR Lyrae type variable stars in the next chapter.

Chapter 5 RR Lyrae Variable Stars in CTI Survey

This chapter describes the search for and identification of RR Lyrae variable stars contained in the CTI survey. First, a short history of the study of RR Lyraes is presented. Next, a description of the search for RR Lyraes through the CTI survey databases is given with a discussion of the completeness of the resulting RR Lyrae variable star list. Confirmation and alias-breaking observations at Capilla Peak observatory of the RR Lyrae variable star candidates are also described. Finally, the characteristics of the resulting list of RR Lyrae variable stars is compared to those contained in other surveys of field RR Lyrae variables.

5.1 RR Lyrae Variable Stars

In 1895, Bailey discovered several short period Cepheid-like variables in the globular cluster ω Cen (Tsesevich 1975). He divided the variables into three subclasses corresponding to differences primarily in the rise time from minimum to maximum light as compared to the total period. The subclasses also showed differences, however, in their amplitude of variation and period of variation. These variable stars were found to be common in globular clusters, occupying the intersection of the horizontal branch and the instability strip of the H-R diagram.

It was soon discovered that these "cluster Cepheids" were not limited to globular clusters. In 1899, Fleming discovered a star in the constellation Lyra that exhibited the same characteristics as the cluster Cepheids but was unassociated with a cluster. This star was designated RR Lyrae, with this name eventually referring to all stars of this type.

Horizontal branch stars are highly evolved Population II stars, having already passed through their giant phase, and are burning helium in their core (Mihalas and Binney 1981). These stars have masses less than half the solar mass and radii 4-5 times greater than the Sun. RR Lyrae stars also reside in the instability strip of the H-R diagram, as do classical Cepheids, W Virginis, δ Scuti, and SX Phoenices type variable stars (see Figure 4.1). Gravity and pressure provide the counteracting forces for radial oscillations. The

resulting oscillations would be damped and disappear, however, if it were not for a driving mechanism. The second ionization layer of helium for stars within this region of the H-R diagram is at the correct depth such that changes in temperature of this layer changes the opacity in such a way as to drive the radial oscillations. Specifically, when He^{+} first begins to ionize, its opacity increases with increasing temperature. When the star contracts and the temperature increases, the opacity increases. The He^{+} -> He^{++} layer traps radiation, building up a reservoir of extra thermal energy. The radiative pressure outward slows the contraction and eventually reverses it. As the star expands, the extra energy stored in the thermal reservoir is released, accelerating the gas to a higher velocity than would have been realized without the trapped energy. The expansion overshoots the equilibrium radius of the star. The opacity of the layer decreases as the temperature decreases, and at maximum expansion, the radiative pressure is not enough to support the star. The star begins to contract once more. For hotter stars, the ionization layer is too far out in the star's atmosphere, and for cooler stars, the ionization layer is too deep within the star for the oscillations to be sustained.

The resulting light curves range from a rapid increase to maximum light followed by a slower decline (RRa type) to a nearly sinusoidal light curve (RRc type), as shown in Figure 5.1. Bailey types a and b (commonly lumped together as type

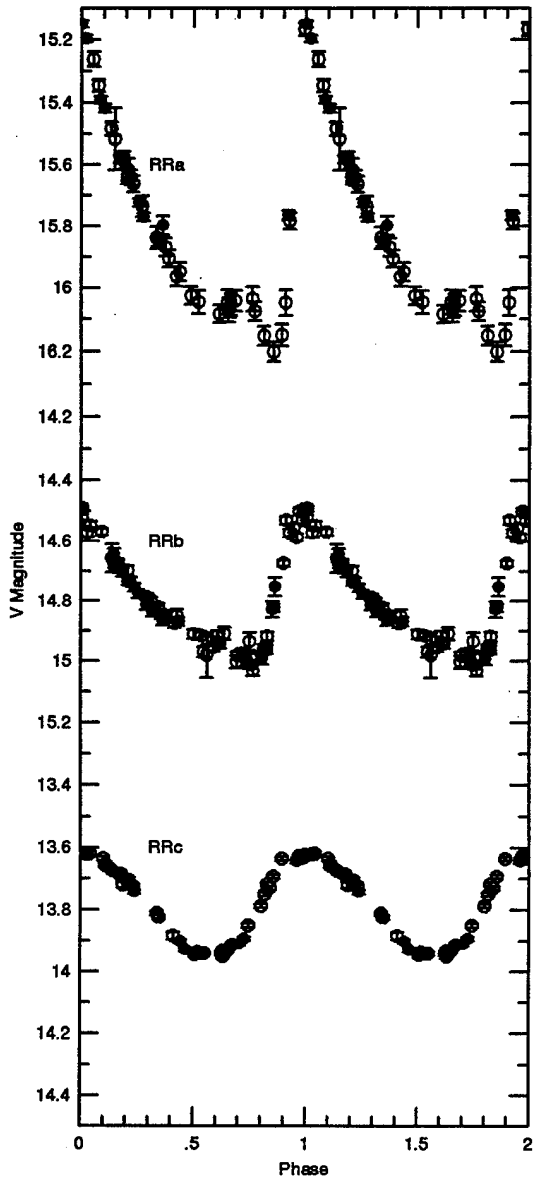


Figure 5.1 - RR Lyrae variable star light curves (combined CTI and Capilla Peak data).

ab) correspond to stars oscillating in the fundamental mode, while Bailey type c correspond to stars oscillating in the first harmonic. The mode of oscillation a star will attain depends on the depth of the He^+ layer in the star. Some RR Lyrae variable stars oscillate in both modes simultaneously, resulting in what is known as the Blazhko effect where the light curve shape and amplitude vary periodically (Tsesevich 1975). Approximately 15 - 30% of all RR Lyrae variables exhibit the Blazhko effect to some degree, with the fraction increasing for stars with decreasing metal abundance. Additionally, some RR Lyrae variable stars exhibit gradual or sudden period changes probably due to evolution. When very short period (< 0.1 days) Cepheid-like variables were discovered, they were originally designated as RRs type

variables. These variables have since been renamed δ Scuti or SX Phoenices type stars (depending on the star's Population type) although the RRs reference still shows up in the literature.

The radial velocity curve of an RR Lyrae variable star has a shape similar to the light curve (positive velocity corresponding to expansion). Maximum light occurs when the expansion velocity is maximum. The hydrogen absorption lines observed in the spectra occur higher in the star's atmosphere where higher radial velocities are observed resulting in a larger amplitude of variation than the metal lines. In addition, hydrogen line emission and line splitting can occur during the ascending part of the light curve when a shock is produced as the old contracting hydrogen layer meets a new expanding layer. Maximum light also corresponds to the time when the star exhibits its earliest spectral type (about A2). The RR Lyrae star's latest spectral type (about F2) occurs at minimum light. The maximum radius of the star occurs after maximum light, during the descending part of the light curve, while minimum radius is obtained during the ascending part of the light curve.

RR Lyrae variable stars exhibit a relationship similar to the famous period-luminosity relationship of classical Cepheids. The RR Lyrae relationship takes many forms, from a simple constant absolute magnitude (Hawley et al. 1986, Barnes and Hawley 1986, Layden et al. 1994), to a dependence on

metallicity (Carney et al. 1992), to a more complex period-luminosity-amplitude relationship (Sandage 1981a, 1981b, 1982a, 1982b, Sandage et al. 1981) or period-luminosity-metallicity relationship (Nemec et al. 1994). Using these relationships, RR Lyrae variable stars have been used extensively as standard candles to determine the distance to globular clusters as well as probe the mass distribution of the galactic halo (see Chapters 6 and 7). With the improvement of imaging technology, RR Lyraes have now been observed in nearby galaxies and can be used as yet another yardstick of extragalactic distances (see, for instance, Saha 1990). Due to advances in theoretical modeling of stellar evolution tracks, RR Lyrae variable stars can also now be used to help determine the age of globular clusters (Carney et al. 1992, Lee 1992 and references therein) and help answer questions regarding the formation of the Galaxy.

5.2 Search for RR Lyrae Variable Stars

After prescreening the data for photometric outliers and application of an additional error of amplitude 2% times the luminosity, all objects passing the variability test were considered. Additionally, objects near bright stars, with light curves correlated with their nearest variable neighbor, within the Galactic plane (defined below), with average V magnitudes > 18.5, or with less than 9 V observations were removed. Finally, only objects with V_COMB ≤ 20 (related to blending with other objects) were retained. A combined B and V history list (**.BVH** database) was created for these variables, and conditions were placed on various attributes of each object to discover the RR Lyrae variable stars contained in the list.

The first such condition was on average color. RR Lyrae variable stars are of spectral type A2-F2, with <B> - <V> ≈ 0.26 for RRab type stars (Hawley et al. 1986). The reddest an RRab type star will appear, however, is at minimum light, and can be calculated using (McDonald 1977)

$$B_{min}-V_{min}=0.40+0.25\times(P-0.5) \qquad (5.1)$$

This gives a maximum B-V of approximately 0.5 for RRab type stars. Due to the limited number of B observations, it is possible that many of the RR Lyraes were observed at or near minimum light, and thus this upper limit must be used. RRc type variables are bluer than RRab types, so this color limit will apply to them as well.

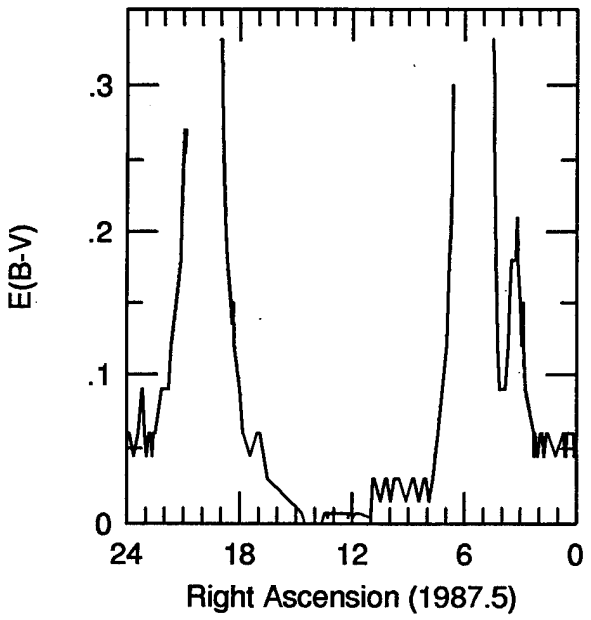


Figure 5.2 - E(B-V) versus right ascension for CTI survey strip.

Because of reddening by dust in the Galactic disk, the <B-V> of each star must first be corrected using the Galactic HI maps of Burstein and Heiles (1982). The E(B-V) as determined from these maps as a function of right ascension on the CTI survey strip is shown in Figure 5.2. No reddening information is given for galactic latitudes less than 10°. The Galactic plane, corresponding to the region excluded from this search, was defined as the region where E(B-V) > 0.24 (right ascensions 4.4^h to 6.7^h and 18.8^h to 21.1^h). The resulting RR Lyrae survey area is shown in Figure 5.3. The declination boundaries are determined by the requirement that the star have 9 or more V observations and at least one B observation. The search for RR Lyrae variable stars was conducted using two different compilations of the CTI databases: the current **.MAS** and **.HIS** databases (hereafter, referred to as list 1, with boundaries shown as solid lines in Figure 5.3), and the recently compiled **.NML** and **.NHL** databases (list 2, dashed lines in Figure 5.3). Due to bright star masking, the percentage coverage as a function of right ascension varies. This percentage, smoothed to intervals of

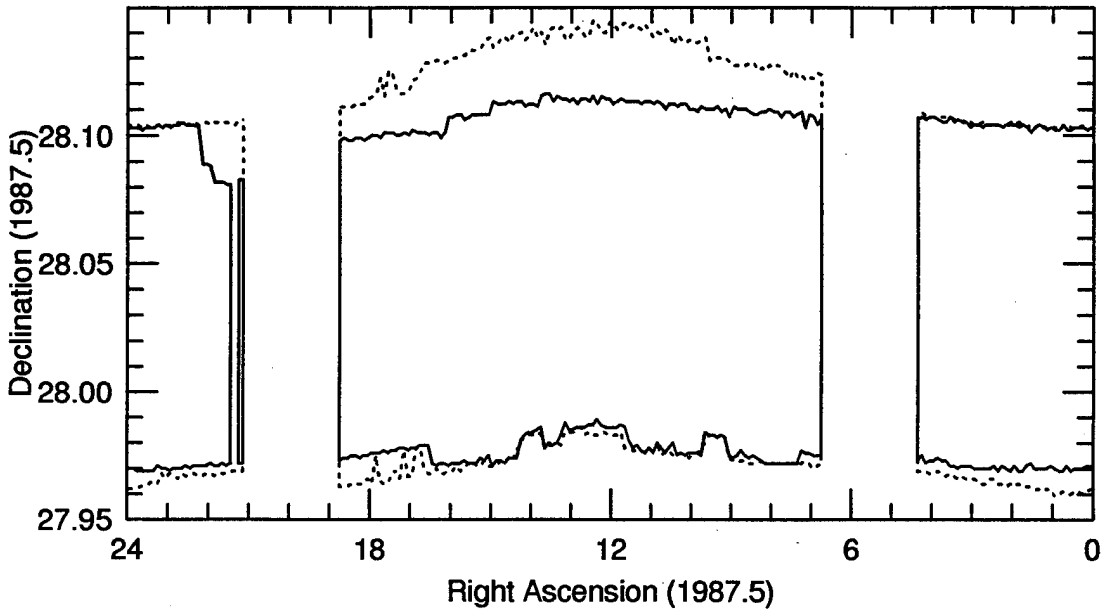


Figure 5.3 - CTI RR Lyrae survey area. Solid line for list 1 and dashed line for list 2.

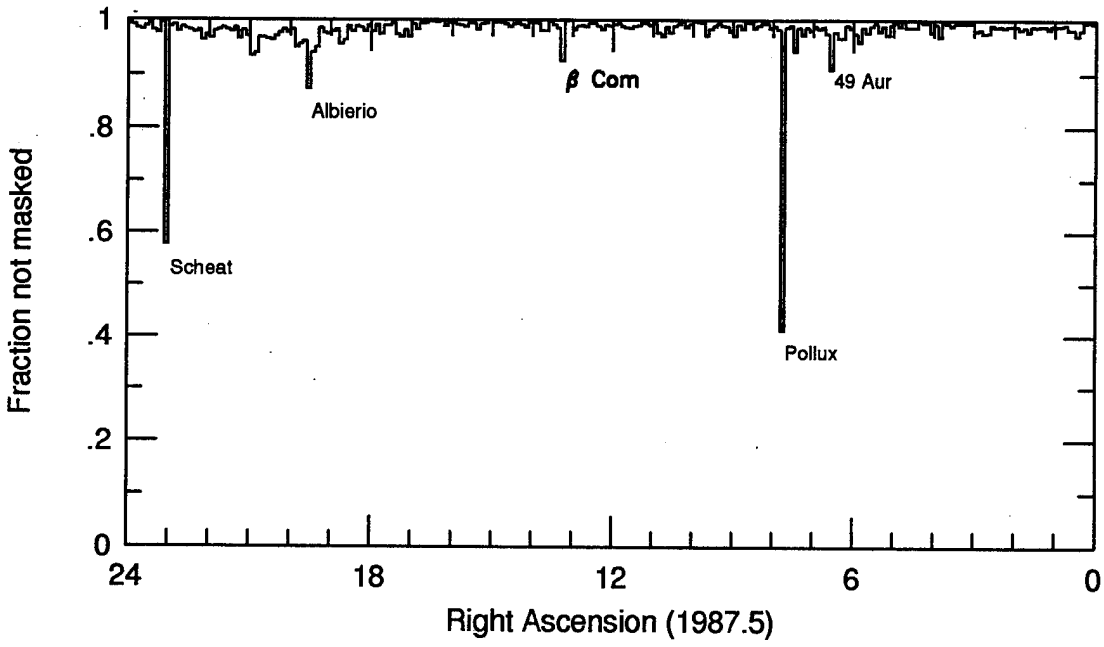


Figure 5.4 - Fraction of survey area masked by bright stars as a function of right ascension. Smoothed to 6m intervals. Five stars masking the greatest area are labeled.

6^m in right ascension, is shown in Figure 5.4.

Next, a limit on the amplitude of variation was set. Several searches were conducted. For both lists, the first search used a color limit of <B-V> < 0.6 and an amplitude limit of $\Delta V > 0.2$. A total of 5 variables listed as RR Lyrae variable stars in the GCVS have amplitudes less than 0.2, corresponding to less than 0.08%, and these stars are probably misclassified anyway. Due to possible systematic errors created by the flat field (see Chapter 3.2) of up to 0.2 magnitudes for the B magnitude, another search using a limit of <B-V> < 0.7 and an amplitude limit of $\Delta V > 0.6$ was made. No new confirmed RR Lyrae type stars were found with this search using both list 1 and list 2. A final search, only conducted on list 1, used a color limit of <B-V> < 0.8 and an amplitude limit of $\Delta V > 0.2$. Again, no new confirmed RR Lyrae type stars were found.

The best period for each object passing the above criteria within the range of 0.2 to 1.2 days was determined using a standard period finding algorithm (see Lafler and Kinman 1965 or Stellingwerf 1978) and the light curve shape was examined. This period range ensures that for an RR Lyrae variable star, the best period found corresponds to the actual period or an alias to the actual period. Objects with sinusoidal (RRc) to sawtooth (RRab) light curves were included in the final candidate list.

The sidereal day alias inherent to the CTI data has

several unfortunate consequences pertaining to period selection and light curve shape. Noisy RRab-like light curves with periods close to 1/2 or 1/3 a sidereal day can be created for many variables. This occurs for most "long period" variables displaying systematic shifts in their mean magnitude from one year to the next. The source of this group of variables is unknown, although it's possible they're spurious and related to the photometry of galaxies (see Chapter 4.2.1). Another group of variables with bimodal magnitude distributions will often produce noisy RRc-like light curves at fractional sidereal day periods. Again, the nature of these variables is unknown and it's possible they are also spurious. Considering the fact it is unlikely a large population of RR Lyrae variable stars exist at these specific fractional sidereal day periods, noisy RR Lyrae-like light curves with these periods were not selected duing the search for candidates. Another problem related to the sidereal day alias in the CTI data occurs for variables with only a few V observations. These variables display a multitude of periods and a wide range of light curve shapes can be found. This problem becomes so severe that for variables with less than ≈9 observations, a period search yields no useful information relative to classification by light curve shape.

The resulting final RR Lyrae candidate lists contain 52 objects each (list1 and list2), with 39 candidates in common. Thirteen candidates in list 1 were not in list 2. Seven of

these are W UMa type variables rejected due to the improved phase coverage offered by the additional observations contained in the **.NHL** database, four of these are non-RR Lyrae type variables not contained in list 2 due to color considerations, and two are RR Lyrae type variables whose light curves degraded with the additional observations, possibly due to a changing period or the Blazhko effect. Thirteen candidates in list 2 were not in list 1, all of which either had poor phase coverage or were near the edge of the CTI survey area and had less than 9 V observations in the **.HIS** database. Eight of these are confirmed RR Lyrae variable stars, three are possible RR Lyrae variable stars, and two are probable W UMa variable stars.

Six of the final candidates are previously known RR Lyrae variable stars listed in the GCVS (GR Com, GS Com, DV Com, EZ Com, V385 Her and V532 Her). All previously known RR Lyrae variable stars within the RR Lyrae search area were found. Another previously known variable star (V375 Her), classified as a semiregular type variable star in the GCVS, is also on both final candidate lists. In addition to those candidates found in the above searches, four other previously known variable stars outside the RR Lyrae search area but within the CTI survey strip were included in the final combined RR Lyrae candidate list for a total of 69 objects. CN Tau, V427 Lyr and V926 Cyg are designated as RR Lyrae stars in the GCVS, and GS Lyr is listed as an irregular variable in the GCVS, but has

an RR Lyrae shape light curve for a particular period using the data contained in the **.HIS** database. Table 5.1 lists each object's right ascension, declination, number of B and V observations (from list 2), E(B-V) as determined from Burstein and Heiles (1982), average B-V as initially determined from CTI data (from list 2), master list number for list 1 (**.MAS** database) and list 2 (**.NML** database), and variable type as determined from subsequent observations at Capilla Peak observatory (see Chapter 5.4). The list 1 and 2 mlink columns also indicate whether or not the star was found during that particular search. Table 5.2 identifies all previously known variable stars.

Table 5.1 - RR Lyrae final candidate list

#	RA (1987.5 epoch)	Dec	# B	# V	E(B-V)	<B-V>	list 1 mlink	list 2 mlink	Type
1	00 21 01.3	28 05 18.0	8	39	0.060	0.672	1770*	1770	W UMa
2	01 13 58.1	28 02 47.1	8	46	0.049	0.519	5890*	5890*	W UMa
3	01 26 59.2	28 03 54.3	7	44	0.057	0.835	6829+	6829	W UMa
4	01 58 55.9	27 58 09.5	5	48	0.055	0.466	9134	9134*	RRab
5	02 01 50.4	28 04 22.6	7	46	0.050	0.260	9353*	9353*	RRab(B)
6	02 31 40.3	27 59 47.3	9	45	0.076	0.789	11615+	11615	W UMa
7	03 46 21.7	28 01 24.7	6	46	0.101	-0.226	18722	18722*	RRab
8	04 02 57.9	28 01 30.5	7	46	0.090	0.607	21446*	21446	W UMa
9	05 57 22.1	28 02 31.0	7	50	INDEF	0.879	48925	48925	Cδs
10	06 49 46.1	28 04 59.5	6	54	0.181	0.862	105847*	112136	W UMa
11	07 53 50.3	28 01 58.2	7	49	0.016	0.385	117092*	122309*	RRab
12	08 46 51.7	28 02 45.3	8	45	0.030	0.299	122995*	130077*	RRab(B)
13	09 01 17.7	28 01 31.3	9	45	0.020	0.261	140537*	143625*	RRab(B)
14	09 56 59.1	28 02 02.6	8	49	0.016	0.126	152725*	164491*	RRc
15	10 26 04.7	28 02 51.5	8	44	0.018	0.290	153914*	165680*	RRab
16	10 36 17.2	27 59 07.7	3	14	0.020	0.211	154337*	166103*	RRab
17	10 57 41.6	28 02 46.0	7	48	0.012	0.165	155137*	166905*	RRc
18	11 48 32.1	28 04 36.1	8	45	0.007	0.318	163979*	174580*	RRab
19	12 04 40.4	28 01 08.5	9	48	0.007	0.244	164643*	175244*	RRab
20	12 05 25.4	28 03 28.8	9	47	0.007	0.340	164674	175275*	RRab
21	12 24 18.6	28 03 17.4	9	50	0.007	0.382	165395*	175996*	RRab
22	12 43 17.6	28 05 21.7	9	45	0.007	0.372	166086*	176687*	RRab
23	13 14 03.3	28 00 26.7	7	35	0.007	0.105	167332*	177933*	RRc
24	13 17 32.5	28 01 39.4	9	45	0.007	0.299	167472*	178073*	RRab
25	13 23 46.7	28 06 32.5	7	37	0.007	0.708	167695+	178296	Galaxy
26	14 33 13.2	28 01 17.0	8	49	0.014	0.174	178400*	194872*	RRab
27	14 54 39.0	28 05 32.8	10	51	0.010	0.354	179503*	195975*	RRab
28	15 16 28.1	28 00 41.6	6	47	0.014	0.137	187650	203872*	RRab
29	16 23 17.6	27 58 28.9	3	13	0.028	0.568	196711	212616*	W UMa
30	16 50 08.8	27 59 55.0	6	29	0.053	0.346	203356*	221010*	RRab
31	16 58 30.7	28 06 00.7	6	20	0.060	0.297	204123	221777*	RRc?
32	17 13 10.9	28 00 10.3	6	27	0.055	0.388	205617*	223271*	RRab
33	17 15 23.9	28 00 43.0	6	27	0.053	0.234	205868*	223522*	RRab
34	17 15 57.0	28 06 44.6	3	15	0.053	0.609	433757	556381*	RRab
35	17 19 06.6	28 06 28.2	3	17	0.051	0.645	433799	556429*	RRab?
36	17 20 58.6	28 01 15.2	8	27	0.049	0.141	206532*	224186*	RRc
37	17 30 43.1	28 03 48.3	8	30	0.047	0.268	207769*	225423*	SX Phe
38	17 41 51.5	28 03 53.2	7	30	0.055	0.311	209299*	226953*	RRab
39	17 42 40.2	28 04 44.7	7	30	0.055	0.275	209407*	227060*	RRab
40	17 44 19.7	28 01 21.6	7	30	0.056	0.266	209648*	227302	RRc?
41	17 50 17.0	28 01 00.0	7	25	0.061	0.412	216980*	234109*	W UMa
42	18 11 01.2	27 59 27.4	6	26	0.108	0.374	221799*	238926*	RRab
43	18 11 26.7	28 03 45.4	8	25	0.109	0.436	221928*	239057*	RRab
44	18 36 06.3	28 03 21.6	7	25	0.170	0.416	229745*	246872*	RRab
45	18 39 18.3	28 04 16.6	7	25	0.178	0.453	230978*	248106*	RRab
46	18 40 18.8	28 00 54.1	8	25	0.181	0.571	231410+	248537	W UMa
47	18 43 15.3	28 01 14.7	8	24	0.196	0.644	232642	249768*	W UMa?
48	18 44 20.6	27 59 36.6	6	24	0.202	0.549	233103+	250230*	W UMa?
49	18 47 46.9	28 04 47.0	4	24	0.223	0.556	234619*	251747*	RRab(B)
50	19 03 50.4	28 00 44.9	7	23	INDEF	1.757	252097	269174	L
51	19 13 11.8	28 00 51.5	6	24	INDEF	0.733	259179	276256	RRab
52	19 38 06.6	27 59 09.9	7	25	INDEF	0.653	318729	336159	RRc
53	21 07 16.1	28 02 29.2	6	19	0.206	0.531	385417*	415882	W UMa
54	21 20 11.2	28 06 09.3	2	13	0.154	0.611	505079	477321*	RRc?
55	21 21 10.2	28 05 56.5	2	13	0.152	0.176	468466	477369*	RRc
56	21 34 29.8	28 01 56.9	5	18	0.127	0.687	403397*	431575	W UMa
57	21 46 11.6	28 00 57.2	4	20	0.093	0.382	405697*	433874*	RRab

Table 5.1 - RR Lyrae final candidate list (continued)

#	RA (1987.5 epoch)	Dec	# B	# V	E(B-V)	<B-V>	list 1 mlink	list 2 mlink	Type
58	21 57 35.4	28 02 37.5	3	20	0.090	0.472	407892*	436069*	RRab
59	21 58 55.9	27 58 09.5	5	20	0.090	0.240	407995	436173*	RRab
60	22 00 54.8	28 00 20.1	5	21	0.090	0.471	408475*	436652*	RRab
61	22 02 44.8	27 59 04.0	5	21	0.090	0.888	408775+	436953	W UMa
62	22 10 22.8	28 04 16.2	3	20	0.088	0.314	410030	438208*	RRab B
63	22 20 36.4	27 59 39.2	5	23	0.072	0.478	60633*	60635*	W UMa
64	22 36 18.9	27 58 38.4	5	24	0.056	0.526	63071*	63069	RRab
65	22 47 34.7	28 01 20.8	6	24	0.060	0.504	64566*	64569*	W UMa
66	23 05 19.7	28 05 44.1	3	21	0.068	0.206	67062*	66402*	RRab
67	23 21 38.0	28 01 25.6	2	21	0.063	0.535	68710*	68049	W UMa
68	23 32 06.7	28 02 10.9	5	37	0.051	0.477	80409*	89389*	RRab
69	23 52 26.0	28 01 18.9	7	40	0.060	0.447	82132*	91112*	RRab

Notes to Table 5.1
In list 1 and list 2 mlink column:
* = discovered in RR Lyrae search
+ = discovered in extended color (<B-V> < 0.8) RR Lyrae search of list 1
In Type column:
RRab - type ab RR Lyrae
RRc - type c RR Lyrae
RRab(B) - type ab RR Lyrae exhibiting Blazhko effect
SX Phe - SX Phoenices type variable star
Cδs - short period classical Cepheid
W UMa - W Ursa Majoris
L - Irregular

Table 5.2 - GCVS name for stars in RR Lyrae candidate list

#	GCVS name
9	CN Tau
19	GR Com
21	GS Com
22	DV Com
24	EZ Com
27	NSV 06854*
32	V375 Her
34	V385 Her
43	V532 Her
50	GS Lyr
51	V427 Lyr
52	V926 Cyg

Notes to Table 5.2
* - from New Catalogue of Suspected Variable Stars (Kukarkin et al. 1982)

5.3 - Completeness

In estimating the completeness of the resulting RR Lyrae variable star list, each step in the search must be examined to determine how it affects the discovery of RR Lyraes. The final result will be estimated functions for completeness versus position and completeness versus magnitude.

During the initial testing for variability, stars with poor phase coverage due to having a small number of observations and a period close to 1/2 or 1/3 a sidereal day may not even pass the variability test. More likely, however, is that the resulting light curve for the star will not be recognized as an RR Lyrae during the final selection. The completeness as a function of position was estimated by first calculating the detectable fraction of variable stars as a function of period. Typical observation times were used to calculate the phase (ϕ) of all observations for all periods (0.0005 day bins) cycled through all initial phases. If at least two observations fell during maximum light (ϕ = 0.0 - 0.2), at least two observations during the descending part of the light curve (ϕ = 0.2 - 0.5), at least two observations at minimum light (ϕ = 0.5 - 0.9), and at least one more observation during minimum or the ascending part of the light curve (ϕ = 0.5 - 1.0), it was considered detectable. This ensures a well distributed sample in phase and requires that the full amplitude of the variable is observed. Figure 5.5 plots the resulting detectable fraction of RR Lyraes as a

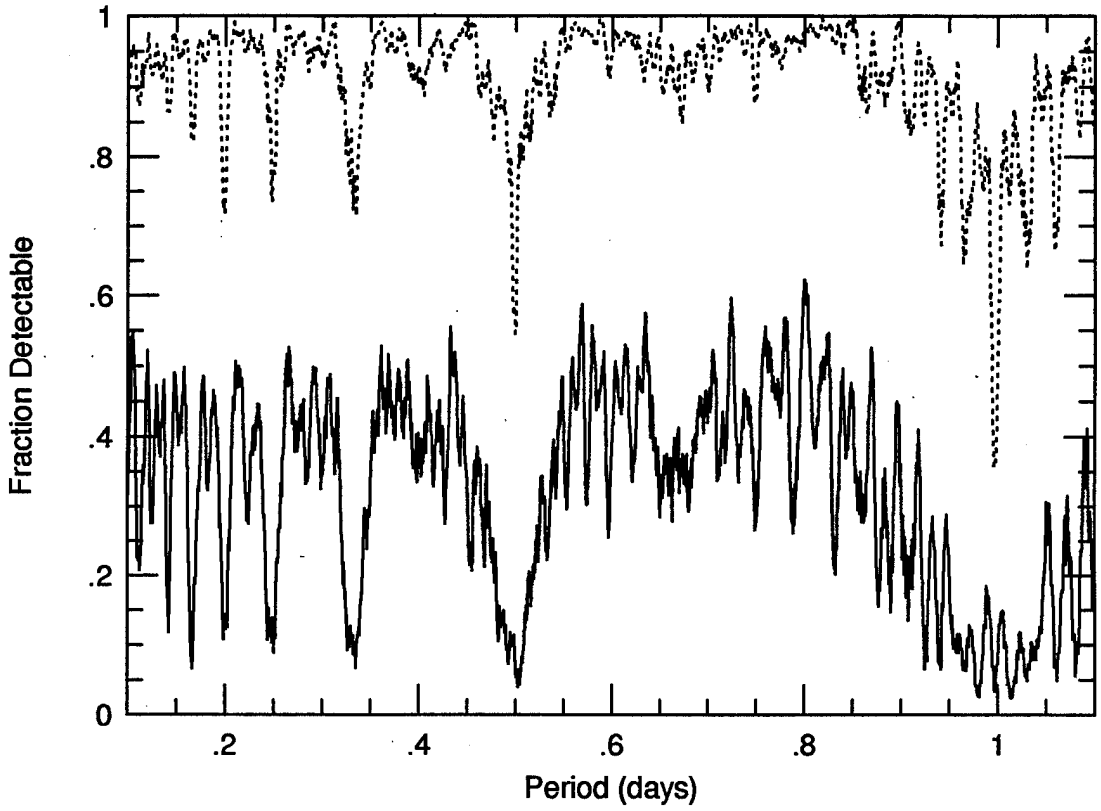


Figure 5.5 - Detectable fraction of RR Lyrae variable stars versus period for 9 observations (solid line) and 20 observations (dashed line). Original bins 0.0005 days, smoothed to 0.005 days.

function of period for 9 and 20 V observations. For RRab type variables, the average percentage in the interval from 0.4 to 0.7 days was then calculated for a number of cases with the number of V observations ranging from 9 to 60. The resulting detectable percentage as a function of the number of V observations is shown in Figure 5.6. The same calculation for RRc type variables with periods ranging from 0.25 to 0.4 days yields an almost identical curve. Using the information from Figure 5.6, as well as the maximum number of V observations as

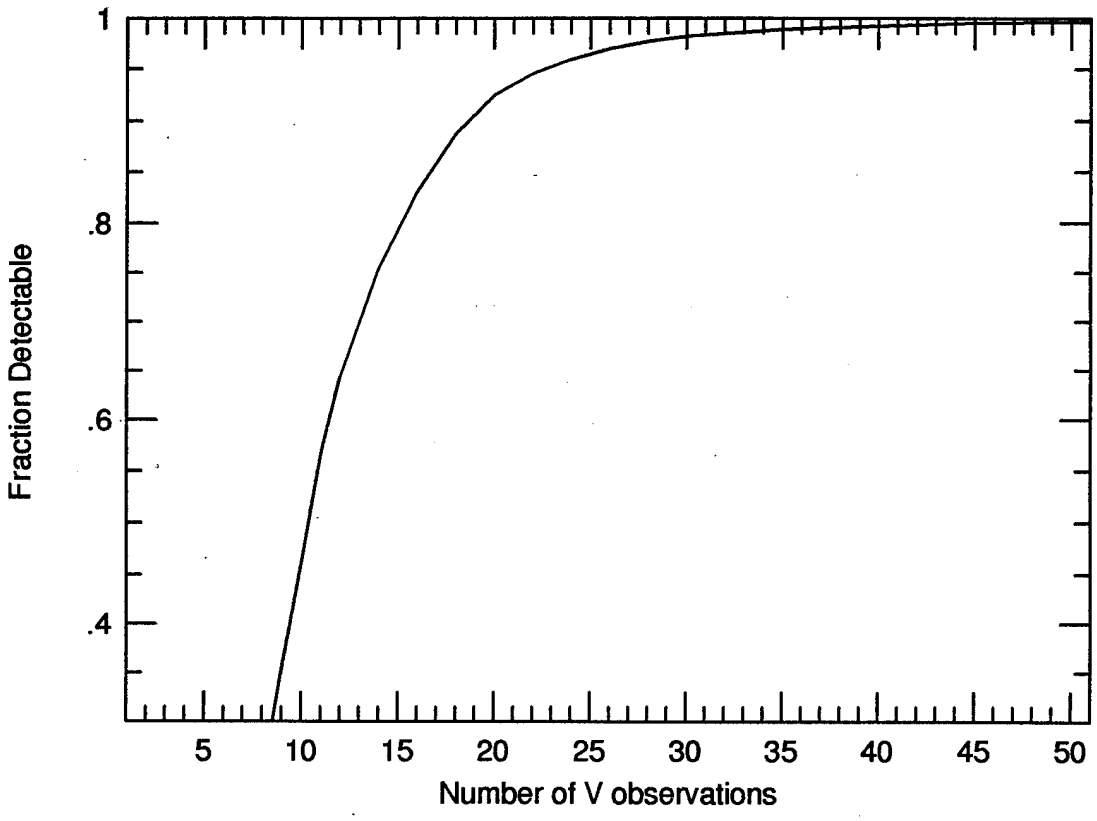


Figure 5.6 - Detectable fraction of RR Lyrae variable stars as a function of the number of V observations.

a function of right ascension (see Figure 3.7) and the number of objects as a function of the number of V observations and right ascension (see, for example, Figure 4.4), the completeness of the CTI RR Lyrae Survey as a function of position was calculated and is shown in Figure 5.7. The solid and dashed lines represent the completeness of list 1 and list 2 respectively.

The completeness as a function of magnitude was calculated considering the fact that the amplitude of variability needs to be four times the average error for a

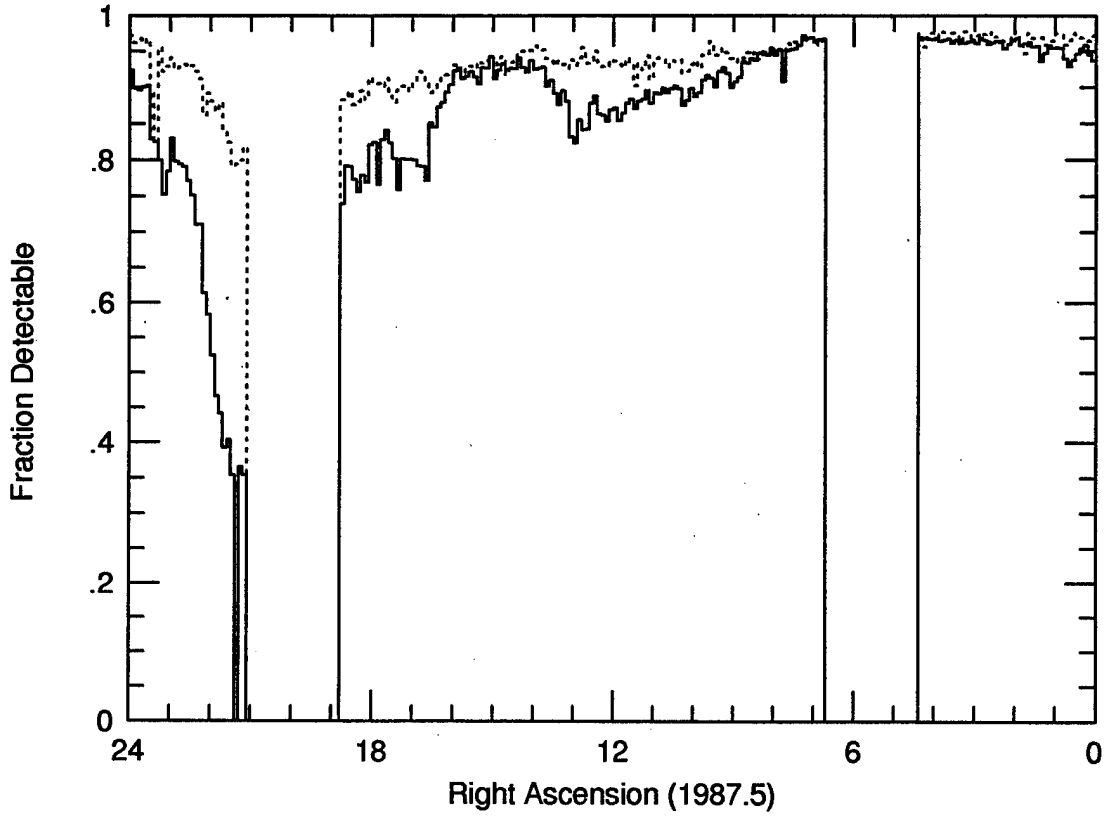


Figure 5.7 - Detectable fraction of RR Lyrae variables as a function of right ascension for list 1 (solid line) and list 2 (dashed line).

positive detection (see Chapter 4.2.2). This can be accomplished by using the information from the plot of average error versus mean instrumental magnitude (Figure 4.6), and knowing the distribution of RR Lyrae stars as a function of amplitude. The Palomar-Groningen Variable Star survey provides a large homogeneous sample of RR Lyrae variable stars to estimate this last function.

It was first necessary to convert each star's amplitude in B (ΔB) as listed in the Palomar-Groningen survey to a corresponding amplitude in V (ΔV) to compare to the CTI RR

Lyrae survey. For RRab type stars, this was done by combining Equation 5.1 (B_{min}-V_{min} as a function of period where B_{min} and V_{min} are magnitudes at minimum light), <B>-<V> ≈ 0.26 (Hawley et al. 1986), and the empirical equation (from Barnes and Hawley 1986)

$$<V>=V_{min}-0.375\times\Delta V-0.04. \qquad (5.2)$$

Using these equations, and assuming a similar relation for <B> as in Equation 5.2, the color at maximum light can be calculated using

$$B_{max}-V_{max}=0.03-0.42\times(P-0.5), \qquad (5.3)$$

and the amplitude in V can be calculated using

$$\Delta V=\Delta B-0.37-0.67\times(P-0.5). \qquad (5.4)$$

For RRc type variable stars, the V and B observations of RRc type variable stars in the CTI survey were examined yielding the relationship, $\Delta V \approx \Delta B - 0.115$.

The resulting histogram of V amplitude for RR Lyrae stars in the Palomar-Groningen Variable Star survey is shown in Figure 5.8. The distribution of RRab and RRc type variables are shown with a solid and dashed line respectively. The completeness as a function of average instrumental V magnitude is shown in Figure 5.9 for RRab (solid line) and RRc (dashed line) type variable stars in the CTI RR Lyrae survey.

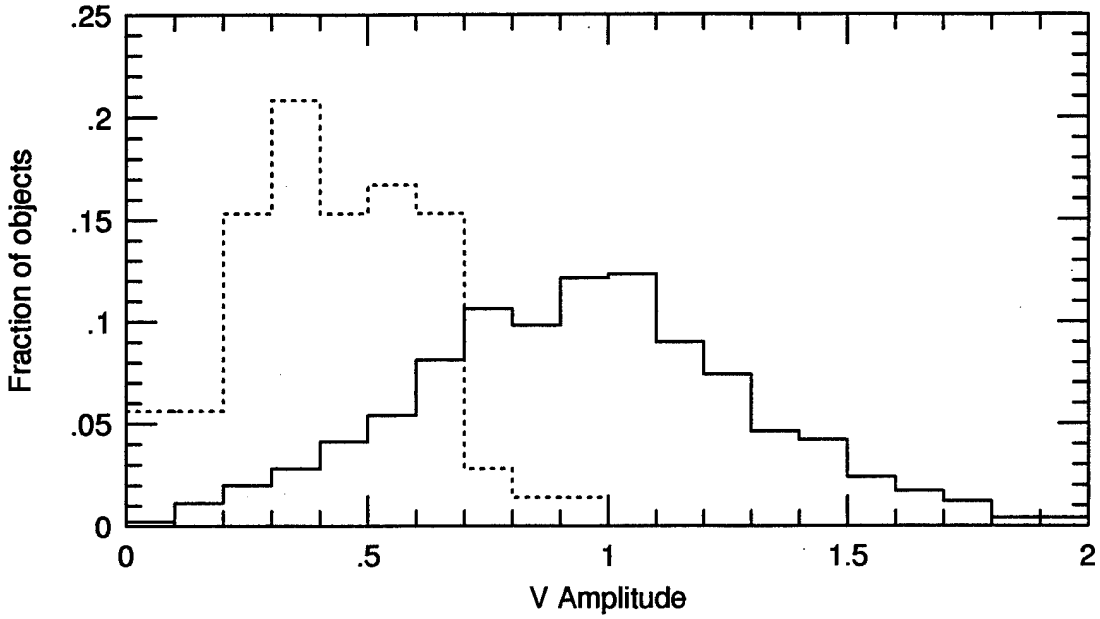


Figure 5.8 - Percentage of RR Lyrae variable stars in Palomar-Groningen Variable Star survey (regions 1, 2, and 3) as a function of amplitude of variation in V (using Equation 5.4). RRab type (solid line) and RRc type (dashed line).

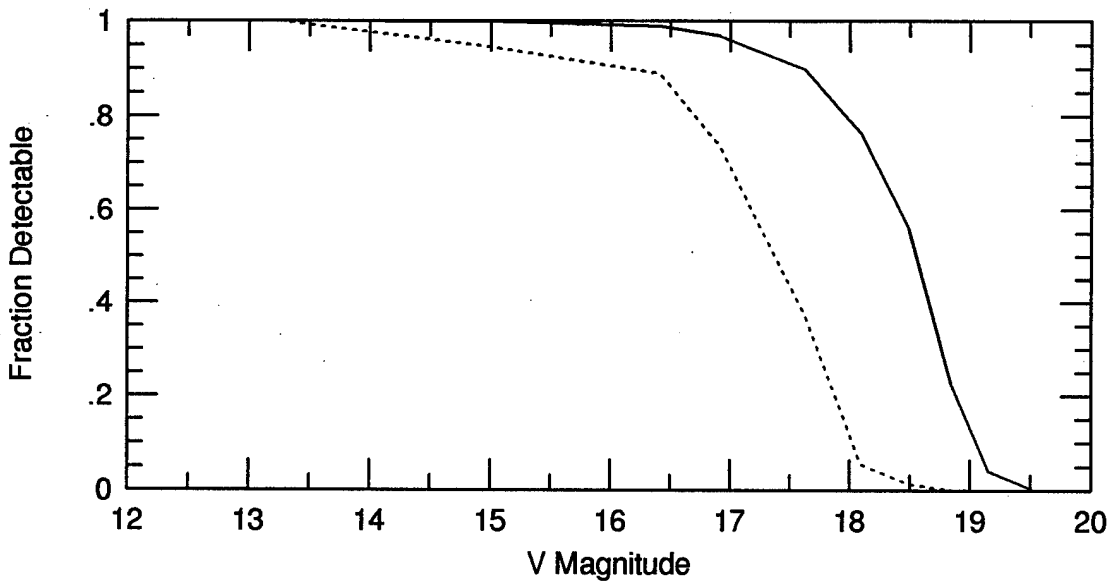


Figure 5.9 - Detectable fraction of RR Lyrae variable stars as a function of average V magnitude for RRab type variables (solid line) and RRc type variables (dashed line).

5.4 Alias Breaking Observations at Capilla Peak

Complementary observations of the candidate RR Lyrae stars are necessary to determine their correct pulsational period. This is due to CTI's built in frequency of observation, the sidereal day, and the fact that RR Lyrae variable star periods are typically less than a sidereal day. Thus, for each variable with a true period P, many aliased periods exist, given by

$$P_{alias} = \left| \frac{1}{\frac{1}{P} + n f_{sd}} \right| \qquad (5.5)$$

where f_{sd} = 1.002740 day^{-1} is the sidereal day frequency and n is a positive or negative integer.

The telescope at Capilla Peak Observatory was used to make alias breaking observations. What follows is a short description of the telescope and CCD at Capilla Peak and a description of the image reduction process, which is also intended to serve as a guide to future users of Capilla Peak. Finally, the method used in combining CTI and Capilla Peak data is described.

5.4.1 Capilla Peak Telescope/CCD Description

Operated by the Institute for Astrophysics at the University of New Mexico, Capilla Peak is a small observatory located in the Manzano Mountains, 30 miles south of Albuquerque, New Mexico. The observatory is located at latitude 34° 41' 53" and longitude 106° 24' 13", and elevation

of 2842 meters. It is the 15th highest observatory in the world as listed in the The Astronomical Almanac for the year 1993.

Located at the observatory is a single 61-cm Boller and Chivens telescope equipped with a RCA 320 x 512 x 30 μm SID50EX CCD (Laubscher et al. 1988). With a system f/# of 15.2, the image field scale is 0.67 arcsecs/pixel which produces an image size of 3.57' x 5.72'. The CCD operates with a gain of 15.6 electrons/ADU, 14-bit digitization, and has a readout noise of 57 electrons. The current filter set includes H_α filters centered at 657, 665 and 673 nm, an OIII filter (manufactured by Barr Associates), polarization filters, and BVRI filters (described in Beckert and Newberry 1989). The telescope is also equipped with an additional CCD camera with a microchannel plate amplifier used for real-time guiding on off-axis stars during lengthy exposures.

The telescope operates year round as a research and instructional instrument. Published scientific papers using data collected at Capilla Peak include studies of variable stars (Zeilik et al. 1994 and references therein, Wetterer et al. 1994 and this dissertation), standard stars (Odewahn et al. 1992), brown dwarfs (Bryja and Lawrence 1991, Bryja et al. 1992), galaxies (Gregory et al. 1990, Odewahn 1991, Hayes et al. 1993, Laubscher and Gregory 1993, Taylor et al. 1995, and others), extragalactic supernova (Schmidt et al. 1993, 1994), and the SL-9 impact on Jupiter (Gisler et al. 1994).

5.4.2 Capilla Peak Image Reduction

CCD images obtained at Capilla Peak must go through several reduction steps before useful photometry can be done (Newberry 1991, Tyson 1990). These steps include bias subtraction, removal of the deferred charge structure, preflash subtraction (if used), dark current subtraction (if desired), division by a flat-field frame, and cosmic ray removal. Several steps require that additional CCD images be acquired at the time of observation. What follows is a discussion of each step, which includes both the observational and reduction procedures required.

Every image has a device-specific baseline level, known as the bias, created by the CCD camera's electronics. The bias level does not represent charge contained in individual pixels, but is rather a baseline voltage added to the image as the image is being read out of the CCD array. A bias frame, simply a zero second exposure, can be taken and examined at the telescope by using the *bias* command. Ideally, the bias level should be constant and uniform over the entire CCD frame. The CCD at Capilla Peak has a nearly constant bias structure, but a bias level that changes during the course of the night. The bias level has short-term fluctuations of about 8 electrons, and can have a drift greater than 90 electrons during the night. The bias structure also changes with changing bias level, primarily in the first 50 columns. These changes are probably due to changes in the ambient

temperature of the CCD camera's electronics located in the observatory dome. To accurately subtract the bias requires that the bias structure and level be tracked and recorded during observations. This can be accomplished in two ways. If the preflash is used, the bias and preflash are recorded in the same frames and can be subtracted from other images together. This will be described later. Otherwise, "superbias" frames can be made between observations to track the structure and bias level. A superbias is simply the average of several bias frames and can be made at the telescope using the *addup* command. Averaging is done in order to reduce the effect of readout noise in the final product. Two or more of these superbias frames bracketing your observations can then be used to create the final reduction bias. The bias level immediately before each image can also be recorded in the image header by using the *bobs* command at the telescope instead of *obs*. The noise added to all other images by bias subtraction is

$$RB=\sqrt{\frac{\frac{R^2}{n_b}+T^2}{n_{sb}}+BL^2} \qquad (5.6)$$

where R = 57 electrons is the readout noise, n_b (typically 25) is the number of bias frames used in creating a superbias, T = 4.5 electrons is the truncation noise as determined from the gain, n_{sb} (typically 2) is the number of superbias frames used in creating the final reduction bias, and BL = 8 electrons is

the empirically determined short term bias level uncertainty.

Next, the horizontal band structure created by deferred charge within the horizontal shift register must be eliminated. This is accomplished by mapping out the structure with the preflash or a low light level sky flat (approximately 100 ADUs or 1560 electrons) known as a skim flat. If the latter method is used, only a single skim flat is required and can be taken through any filter during astronomical twilight. To create the final frame used in reducing all other images, a high light level sky flat (approximately 8000 ADUs) taken through the same filter and scaled to the level of the skim flat must first be subtracted off the skim flat in order to remove the CCD's response to light. The remaining feature is simply the deferred charge structure. Exposure times for the skim flat and sky flat should either be identical or greater than 3 seconds in order to eliminate the effect of the shutter speed on the final images. To reduce noise, the skim flat is sliced into 512 one-dimensional rows, all containing the deferred charge structure. These rows are averaged column by column, and 512 of the resulting average slice are then stacked back together to create the final "superskim". The noise added to all other images by deferred charge subtraction is

$$RS=\sqrt{\frac{R^2+T^2+L_{skim}(1+RK^2\times L_{skim})+RB^2}{512}} \qquad (5.7)$$

where L_{skim} is the skim flat light level in electrons, and RK

is the superskyflat error, to be discussed later. Two aspects of using a superskim frame for deferred charge subtraction should be noted. First, in order for the deferred charge structure to be accurately eliminated by using a superskim, the background sky level must be greater than the maximum deferred charge structure. Although this corresponds to about 10 ADUs, in practice the background sky level must be greater than about 50 ADUs for the superskim to work. Also, since a sky flat (containing the deferred charge structure) is used to make the superskim, a residual deferred charge structure on the order of 1% will remain. This can be remedied by creating the superskim in an iterative manner, or by using the preflash on the sky flats in order to eliminate the deferred charge structure beforehand. The deferred charge structure remains nearly constant, and thus a superskim frame from one night was typically used for several months of data.

Bias subtraction and correction of deferred charge structure can be accomplished in a single step if the preflash is used. A preflash is simply the addition of a specific number of electrons to each pixel in the CCD prior to an exposure. At Capilla Peak, the preflash consists of 6 light emitting diodes (LEDs) located inside the shutter and arranged to uniformly illuminate the CCD array. This is currently manually applied. To examine the preflash, a preflashed dark exposure can be taken at the telescope by using the *dark* command. A dark exposure is an exposure of a certain length

without opening the shutter. A 2 to 5 second exposure is necessary to accurately record the preflash. The resulting image will show the deferred charge structure superimposed on the bias and preflash structure. As with creating a superbias, several of these frames are averaged together to reduce noise. This is accomplished by taking several preflashbias frames and storing each in one of the eight different caches (using *ci* command to move between caches) of the CCD control computer memory, and then averaging them together using the *median* command. Because of bias and preflash level changes during the night, these superpreflashbias frames should be taken throughout the night to track the changes. Two or more superpreflashbiases bracketing your observations can be used later to create the final reduction preflashbias. The noise added to an object frame by preflashbias subtraction is

$$RP=\sqrt{\frac{R^2+L_{preflash}}{\frac{n_p}{n_{sp}}}+T^2+BL^2+PL^2} \qquad (5.8)$$

where $L_{preflash}$ is the preflash light level (about 50 - 100 ADUs = 780 - 1560 electrons), n_p (up to 7) is the number of preflashbias frames used in making the superpreflashbias, n_{sp} (typically 2) is the the number of superpreflashbias frames used in making the final reduction preflashbias, and PL = 16 electrons is the empirically determined preflash level uncertainty.

The final additive term in the reduction process is the dark current of the CCD. Several dark frames as long as or longer than all other image frames must be taken. A pixel-by-pixel median of these dark frames, after bias and deferred charge subtraction, must then be taken to eliminate the effect of pixels contaminated by cosmic rays. The resulting superdark can now be scaled to the exposure length of the remaining images, and subtracted. The noise per second of observation added to all other frames by dark current subtraction is

$$SD=\frac{\sqrt{\frac{R^2+T^2+P^2}{n_d}}}{t_d} \qquad (5.9)$$

where P = RP for preflashbias subtracted dark frames or P = $(RB^2 + RS^2)^{1/2}$ for bias and skim flat subtracted dark frames, n_d (3 or greater) is the number of dark frames used in creating the superdark, and t_d is the exposure length of the dark frames. The dark current for nearly the entire CCD is less than the bias level uncertainty and can thus not be determined accurately. The dark current is thus ignored in further calculations.

Next, the response of the CCD to light must be estimated. This requires images of a uniform background in order to map out the pixel-to-pixel response. Typically, sky flats are taken during evening or morning twilight. The resulting images, specific to the particular filter used, are combined

and normalized, and then used to divide out the response of the CCD from all the remaining images. The sky flats must first be bias and skim flat subtracted, (or preflashbias subtracted), before the final superskyflat can be produced. Additionally, as with the skim flat, the exposure time for a sky flat must be greater than 3 seconds to reduce the residual shutter structure to a tolerable level. Also, sky flats show up to 1% variations depending on the pointing of the telescope. This is probably due to flexing of the telescope as it is moved. If feasible, sky flats should thus be taken at different telescope pointings with the resulting superskyflats used for images of similar hour angle, and the filters and CCD window should be cleaned regularly. The noise contained in the superskyflat frame is

$$RK=\frac{\sqrt{\frac{R^2+T^2+P^2+L_{flat}}{n_k}}}{L_{flat}} \qquad (5.10)$$

where L_{flat} is the sky flat light level (typically 10,000 ADUs or 156,000 electrons), and n_k (3 or greater) is the number of sky flats used to create superskyflat.

Finally, corrupted pixels from cosmic rays or decay events in the radioactive glass used in the construction of the CCD must be removed. A cosmic ray or decay event impinging on the CCD during an exposure will corrupt the pixel value where it passes through the array. An average of 18 pixels per minute of observation are effected in this way.

Typically, only a single pixel is effected per event. Because of this unique signature, each CCD image can be examined for these cosmic ray pixels, with the pixel value of the resulting cosmic ray detections replaced with the average of the surrounding pixel values. This works well for cosmic rays located in areas of the CCD that measure background sky. If a cosmic ray happens to coincide with your object of interest, however, the image is essentially useless for accurate photometry.

Using equations 5.6 to 5.10, the total noise in a reduced image is

$$N=\sqrt{n(R^2+T^2+P^2)+L\times(1+RK^2L)} \qquad (5.11)$$

where $L = L_{object} + nL_{sky}$, L_{object} is the total signal level of the object of interest in electrons, L_{sky} is the background sky level per pixel in electrons, and n is the number of pixels used in the photometry (depends on the seeing during the night of observation). L_{object} can be calculated in electrons for the V filter using

$$L_{object}=15.6\times10^{((V_{limit}-V)/2.5)}\times t \qquad (5.12)$$

where V_{limit} = (19.224 ± 0.018) - (0.101 ± 0.011) × (years since last cleaning), V is the object's V magnitude, and t is the exposure length in seconds. For moonless nights, L_{sky} is approximately 0.87 x t electrons per pixel in V. This corresponds to a sky brightness of 22.3 magnitudes in V. A moonlit sky will have a L_{sky} value approximately 5 times

greater, corresponding to a sky brightness of 20.5 magnitudes in V. Table A1.8 of Appendix 1 gives sample signal to noise calculations using Equation 5.8 for various magnitude stars, exposure lengths, and conditions.

5.4.3 Combining CTI and Capilla Peak Data

The next step in determining an accurate period for a candidate RR Lyrae star is to combine the Capilla Peak data with the CTI data. Within arcminutes of every candidate variable, the CTI database also contains information on stars determined to be nonvariable from CTI light curves. Several stars of similar magnitude and color to the variable and close enough to the variable to fit within a Capilla Peak image are picked to be used as standard comparison stars. Differential Capilla Peak instrumental magnitudes ($\Delta V_{Capilla}$) are found for all standard pairs and between each standard and the variable using the photometry package in IRAF. Using the standard stars, differential CTI instrumental magnitudes (ΔV_{CTI}) are used to create a Capilla Peak to CTI conversion factor ($K_V = |\Delta V_{CTI}/\Delta V_{Capilla}|$), with the resulting CTI instrumental magnitude for the variable calculated by

$$V_{CTI}(var) = V_{CTI}(std) + K_V \times \Delta V_{Capilla}(var\text{-}std) . \qquad (5.13)$$

Due to the similarity of the CTI and Capilla Peak's V filter and CCD, the value K_V is essentially equal to 1. This was verified using several standard star pairs and calculating K_V directly. A similar calculation can be done for each of the

other filters.

By selecting standard stars of similar color and magnitude, effects created by extinction in the Earth's atmosphere are practically eliminated. Where suitable standard stars do not exist for a particular variable, care was taken to observe only at low airmasses.

5.4.4 Summary of Observations

Each variable star required an average of two nights of observing to accurately determine its period with two to four variable stars observed per night. Several cloudy nights were also used to test the CCD system and aspects of the reduction and analysis process. Table A1.9 in Appendix 1 lists each night of observation at Capilla Peak used in this dissertation. The date, CTI dayno (1 = 85 Jan 01), percentage of the night used, observers, and cumulative percentage of nights observed are given. Tables A1.10 and A1.11 summarize all the images obtained and reduced.

Table 5.2 summarizes the results for all stars listed on the final RR Lyrae candidate list. The number of CTI and Capilla observations through the V filter, the maximum, minimum, flux averaged instrumental V magnitudes, and error in the flux averaged instrumental V magnitude, amplitude of variation in V, (M-m)/P (rise time in fraction of the period), period (in days), heliocentric epoch of maximum light (for RR Lyrae) or primary minimum light (for eclipsing), and type of

each variable star is given. The flux averaged instrumental magnitude was calculated using

$$\langle V\rangle = -2.5\times\log\sum_{i=1}^{N} 0.5\,(\phi_{i+1}-\phi_{i-1})\,10^{\frac{V_i}{-2.5}} \qquad (5.14)$$

where ϕ_i is the phase of the ith observation in order of increasing ϕ, $\phi_0 = \phi_N$ and $\phi_{N+1} = \phi_1$. Photometry, finder charts, and light curves for each variable is supplied in Appendix 3.

Individual standard V magnitudes were determined using

$$V_{std} = V_{inst} + 0.084\times(B-V)_{std} - 0.054 \qquad (5.15)$$

and

$$(B-V)_{std} = 1.007\times(B-V)_{inst} + 0.089, \qquad (5.16)$$

where the subscript *std* is for the standard Johnson system and *inst* is for instrumental magnitudes (McGraw et al. 1989). The $(B-V)_{std}$ as a function of phase for each RR Lyrae star was calculated by first determining the minimum B-V and the B magnitude amplitude of variation (ΔB) using the CTI B observations. The B-V at any phase can then be calculated using

$$B-V = (B-V)_{min} - \frac{(\Delta B-\Delta V)}{\Delta V}\times(V-V_{min}). \qquad (5.17)$$

Equation 5.4 was used for stars where the number of B observations or the distribution in phase of the B observations was insufficient to determine ΔB. The error in $(B-V)_{min}$ ranges from 0.03 to 0.2 magnitudes, while the error in

ΔB ranges from 0.1 to 0.4 magnitudes. At most, this results in an additional systematic error of <0.02 magnitudes for the amplitude, minimum and mean magnitudes, and <0.04 magnitudes for the maximum magnitude. The (B-V) of all eclipsing variable stars was assumed to be constant. Table 5.4 summarizes the results for all stars listed on the final RR Lyrae candidate list. The instrumental B-V at minimum light, amplitude in instrumental V and B magnitudes, standard B-V at minimum light, the minimum, maximum, and flux averaged standard V magnitudes, and the amplitude in standard V magnitudes are listed.

Table 5.3 - Photometry results for RR Lyrae survey stars

			<-Instrumental magnitudes ->								
#	CTI	CAP	Max	Min	Mean	Err	Amp	m-M	Period	Epoch	Type
1	39	10	16.67	17.09	16.837	0.0090	0.42	0.50	0.276682	3539.373	W UMa
2	45	16	16.23	16.73	16.415	0.0091	0.50	0.50	0.383472	3539.565	W UMa
3	43	10	16.43	16.73	16.580	0.0076	0.30	0.50	0.349120	3546.520	W UMa
4	48	29	16.33	17.59	17.081	0.0094	1.26	0.20	0.497854	3641.220	RRab
5	46	51	16.71	18.00	17.517	0.0088	1.29	0.20	0.461291	3559.380	RRab B
6	44	10	13.83	14.06	13.947	0.0015	0.23	0.50	0.265461	3539.429	W UMa
7	46	20	17.29	18.41	17.905	0.0219	1.12	0.15	0.561891	3685.125	RRab
8	46	19	17.40	18.13	17.711	0.0185	0.73	0.50	0.319400	3546.455	W UMa
9	50	32	12.56	12.91	12.739	0.0008	0.35	0.25	1.79325	3299.884	Cδs
10	51	17	18.02	18.81	18.267	0.0228	0.79	0.50	0.269392	3622.235	W UMa
11	48	20	15.80	16.29	16.085	0.0058	0.49	0.20	0.632536	3308.300	RRab
12	45	28	15.55	16.74	16.344	0.0053	1.19	0.10	0.552704	3307.320	RRab B
13	45	23	15.44	16.73	16.255	0.0048	1.29	0.20	0.513581	3331.312	RRab B
14	49	15	16.32	16.88	16.571	0.0074	0.56	0.35	0.286813	3342.322	RRc
15	44	28	17.75	18.70	18.250	0.0167	0.95	0.20	0.552801	3666.438	RRab
16	13	32	17.50	18.44	18.037	0.0140	0.94	0.15	0.707095	3641.348	RRab
17	47	16	16.47	17.04	16.740	0.0064	0.57	0.30	0.327640	3363.304	RRc
18	43	16	14.56	15.80	15.305	0.0029	1.24	0.10	0.597821	3356.253	RRab
19	48	12	15.61	16.79	16.364	0.0065	1.18	0.10	0.521823	3361.121	RRab
20	47	16	14.97	16.19	15.737	0.0078	1.22	0.10	0.508702	3683.373	RRab
21	50	10	15.76	16.91	16.470	0.0068	1.15	0.10	0.529449	3361.268	RRab
22	45	10	14.22	15.24	14.820	0.0022	1.02	0.10	0.540837	3361.347	RRab
23	34	10	13.67	14.00	13.825	0.0012	0.33	0.40	0.314639	3361.432	RRc
24	45	12	16.44	17.09	16.770	0.0090	0.65	0.25	0.568389	3468.281	RRab
25	36	11	16.75	17.41	17.056	0.0240	0.66	----	--------	--------	Galaxy
26	49	20	17.63	18.34	17.995	0.0271	0.71	0.20	0.437536	3481.155	RRab
27	50	17	14.52	15.06	14.810	0.0028	0.54	0.20	0.622135	3112.203	RRab
28	46	7	17.52	18.24	17.897	0.0218	0.72	0.15	0.571900	3685.029	RRab
29	13	4	15.13	15.36	15.234	0.0055	0.23	0.50	0.343670	3685.451	W UMa
30	28	20	14.77	15.76	15.368	0.0035	0.99	0.15	0.570831	3113.209	RRab
31	20	5	14.64	15.15	14.884	0.0042	0.51	0.50	0.272711	3685.586	RRc?
32	27	19	15.54	16.62	16.202	0.0064	1.08	0.15	0.531433	3481.184	RRab
33	27	20	17.28	18.59	17.998	0.0187	1.31	0.05	0.516250	3474.160	RRab
34	15	16	14.67	15.42	15.090	0.0034	0.75	0.25	0.528145	3385.207	RRab
35	17	0	17.22	17.99	17.637	0.0304	0.77	0.10	0.47259	3385.248	RRab?
36	26	25	14.60	14.94	14.768	0.0031	0.34	0.40	0.295405	3469.480	RRc
37	30	27	15.28	15.91	15.686	0.0044	0.63	0.20	0.0568927	3385.429	SX Phe
38	30	13	15.18	16.23	15.807	0.0052	1.05	0.10	0.566966	3113.194	RRab
39	30	33	16.08	16.98	16.642	0.0074	0.90	0.20	0.526354	3186.109	RRab
40	30	16	15.46	15.87	15.666	0.0041	0.41	0.40	0.377069	3487.309	RRc?
41	25	20	13.15	13.37	13.244	0.0014	0.22	0.50	0.695000	3474.190	W UMa
42	26	27	16.36	17.50	17.072	0.0224	1.14	0.20	0.454185	3181.102	RRab
43	25	16	15.19	15.98	15.610	0.0047	0.79	0.15	0.541466	3169.122	RRab
44	25	22	15.84	17.06	16.621	0.0074	1.22	0.10	0.484114	3175.196	RRab
45	25	19	16.30	17.07	16.698	0.0114	0.77	0.15	0.709921	3516.300	RRab
46	25	12	14.21	14.75	14.427	0.0023	0.54	0.50	0.366912	3473.422	W UMa
47	24	0	16.19	16.60	16.373	0.0101	0.41	0.50	0.656278	3473.717	W UMa?
48	24	10	16.90	17.38	17.103	0.0133	0.48	0.50	0.345930	3481.409	W UMa?
49	24	44	16.85	17.52	17.175	0.0081	0.67	0.25	0.764461	3488.260	RRab B
50	23	94	12.47	13.41	12.976	0.0058	0.94	----	--------	(3174)	L
51	24	21	15.74	16.83	16.359	0.0064	1.09	0.20	0.424599	3474.433	RRab
52	25	22	14.93	15.43	15.131	0.0043	0.50	0.45	0.306999	3488.337	RRc
53	18	17	12.73	13.17	12.894	0.0014	0.44	0.50	0.438854	3517.448	W UMa
54	13	0	16.34	16.66	16.493	0.0150	0.32	0.20	0.448676	3517.381	RRc?
55	13	0	15.18	15.61	15.423	0.0075	0.43	0.30	0.325160	3517.511	RRc
56	18	17	16.69	17.27	16.892	0.0104	0.58	0.50	0.333247	3516.360	W UMa
57	20	18	14.79	15.47	15.233	0.0038	0.68	0.20	0.592806	3517.220	RRab

Figure 5.3 - Photometry Results (continued)

			<-Instrumental Magnitudes ->								
#	CTI	CAP	Min	Max	Mean	Err	Amp	m-M	Period	Epoch	Type
58	20	26	16.33	17.77	17.137	0.0104	1.44	0.05	0.464627	3234.243	RRab
59	21	13	14.62	15.63	15.192	0.0049	1.01	0.25	0.525361	3660.060	RRab
60	21	29	15.01	16.02	15.630	0.0037	1.01	0.10	0.529309	3517.108	RRab
61	21	8	13.81	14.07	13.927	0.0016	0.26	0.50	0.279144	3478.351	W UMa
62	20	19	15.92	16.85	16.566	0.0089	0.93	0.05	0.554907	3673.098	RRab B
63	23	17	15.05	15.35	15.185	0.0032	0.30	0.50	0.426090	3517.356	W UMa
64	24	32	16.44	16.88	16.693	0.0069	0.44	0.10	0.611901	3622.260	RRab
65	24	8	13.40	13.68	13.525	0.0016	0.28	0.50	0.379380	3480.338	W UMa
66	21	21	16.28	17.51	17.064	0.0094	1.23	0.15	0.522284	3174.327	RRab
67	27	24	16.24	16.72	16.411	0.0055	0.48	0.50	0.394387	3545.638	W UMa
68	37	24	16.69	17.67	17.265	0.0113	0.98	0.10	0.692859	3187.329	RRab
69	40	28	17.10	17.90	17.565	0.0141	0.80	0.15	0.589192	3545.372	RRab

Notes to Table 5.3

1 - Other short periods possible.
3 - Other short periods possible.
5 - A period of 0.461300 days fits CTI data well, while a period of 0.461877 days fits Capilla data well. Possible example of period changing with time.
9 - CN Tau previously classified as RRab with period of 0.642062 days.
24 - EZ Com period listed as 0.568404 days in GCVS.
25 - Systematic shifts in mean magnitude from one year to the next possibly indicate this galaxy is a spurious variable (see Chapter 4.2.1 and 5.2), although an actual variability can't be ruled out.
28 - Other aliased periods possible.
29 - Other short periods possible.
31 - Other aliased periods possible. Possibly W UMa.
32 - V375 Her previously classified as SR with period of 84.1 days.
35 - Not observed at Capilla Peak. Many aliased periods possible. B-V color redder than other RR Lyraes.
40 - CTI data from 1990 and 1991 does not agree well with chosen period. No good periods were found with this data included, and so it did not pass the search for RR Lyraes in list 2. Color consistent with RRc classification. Possibly changing period with time.
43 - V532 Her had no period listed in GCVS.
47 - Not observed at Capilla Peak. Many aliased periods possible. B-V color redder than other RR Lyraes, but possibly RRc.
48 - Short period so not classified RRc although asymmetry possibly present. Other short periods possible.
51 - V427 Lyr combined with other fainter stars in photometry (see finder chart in Appendix 3).
52 - V926 Cyg period given as 0.30697965 days in GCVS. Combined with other fainter stars in photometry (see finder chart in Appendix 3).
54 - Not observed at Capilla Peak. Many aliased periods possible. Asymmetric light curve, possibly RRc.
55 - Not observed at Capilla Peak. Many aliased periods possible. Asymmetric light curve and color consistent with RRc type.
61 - Some CTI data does not agree well with chosen period. Other short periods possible.
64 - Combined with other star of equal brightness in photometry (see finder chart in Appendix 3).

Figure 5.4 - Standard Magnitudes for RR Lyrae survey stars

#	(B-V)	Vamp	Bamp	|<- (B-V)	Standard magnitudes Max	Min	Mean	Vamp ->|
1	0.60	0.42	0.42	0.69	16.67	17.09	16.841	0.42
2	0.47	0.50	0.50	0.56	16.22	16.72	16.408	0.50
3	0.80	0.30	0.30	0.89	16.45	16.75	16.601	0.30
4	0.20	1.26	1.45	0.29	16.29	17.56	17.045	1.27
5	0.40	1.29	1.60	0.49	16.67	18.00	17.495	1.33
6	0.78	0.23	0.23	0.87	13.85	14.08	13.966	0.23
7	0.45	1.12	1.30	0.54	17.27	18.40	17.889	1.13
8	0.60	0.73	0.73	0.69	17.40	18.13	17.715	0.73
9	0.80	0.35	0.50	0.89	12.56	12.92	12.755	0.36
10	0.75	0.79	0.79	0.84	18.04	18.83	18.284	0.79
11	0.33	0.49	0.60	0.42	15.77	16.30	16.063	0.53
12	0.21	1.19	1.40	0.30	15.51	16.71	16.310	1.20
13	0.30	1.29	1.60	0.39	15.40	16.71	16.226	1.31
14	0.07	0.56	0.69	0.16	16.27	16.84	16.525	0.57
15	0.32	0.95	1.10	0.41	17.71	18.68	18.224	0.97
16	0.24	0.94	1.20	0.33	17.46	18.42	18.003	0.96
17	0.12	0.57	0.65	0.21	16.42	17.00	16.700	0.58
18	0.36	1.24	1.62	0.45	14.52	15.78	15.278	1.26
19	0.20	1.18	1.25	0.29	15.58	16.77	16.332	1.19
20	0.32	1.18	1.50	0.41	14.92	16.17	15.705	1.25
21	0.33	1.15	1.50	0.42	15.72	16.89	16.442	1.17
22	0.35	1.02	1.29	0.44	14.19	15.23	14.794	1.04
23	0.05	0.33	0.43	0.14	13.62	13.95	13.779	0.33
24	0.35	0.65	1.00	0.44	16.40	17.07	16.743	0.67
25	0.60	0.66	0.66	0.69	16.75	17.41	17.060	0.66
26	0.40	0.71	1.05	0.49	17.60	18.32	17.972	0.72
27	0.36	0.54	0.75	0.45	14.49	15.04	14.787	0.55
28	0.30	0.72	1.10	0.39	17.47	18.22	17.860	0.75
29	0.47	0.23	0.23	0.56	15.12	15.35	15.227	0.23
30	0.33	0.99	1.25	0.42	14.73	15.74	15.341	1.01
31	0.30	0.51	0.80	0.39	14.59	15.13	14.850	0.54
32	0.30	1.08	1.50	0.39	15.49	16.60	16.170	1.11
33	0.35	1.31	1.55	0.44	17.25	18.57	17.972	1.32
34	0.45	0.75	1.20	0.54	14.64	15.41	15.071	0.77
35	0.60	0.77	0.77	0.69	17.22	17.99	17.641	0.77
36	0.15	0.34	0.48	0.24	14.56	14.91	14.730	0.35
37	0.15	0.63	0.75	0.24	15.23	15.88	15.649	0.65
38	0.30	1.05	1.30	0.39	15.14	16.21	15.779	1.07
39	0.30	0.90	1.25	0.39	16.04	16.96	16.612	0.92
40	0.22	0.41	0.50	0.31	15.43	15.84	15.634	0.41
41	0.28	0.22	0.22	0.37	13.13	13.35	13.221	0.22
42	0.38	1.14	1.30	0.47	16.33	17.48	17.052	1.15
43	0.43	0.79	0.90	0.52	15.18	15.97	15.595	0.79
44	0.49	1.22	1.70	0.58	15.80	17.05	16.604	1.25
45	0.55	0.77	1.00	0.64	16.29	17.07	16.690	0.78
46	0.52	0.54	0.54	0.61	14.21	14.75	14.424	0.54
47	0.66	0.41	0.41	0.75	16.20	16.61	16.382	0.41
48	0.45	0.48	0.48	0.54	16.89	17.37	17.095	0.48
49	0.65	0.67	1.00	0.74	16.84	17.53	17.174	0.69
50	1.75	0.94	0.94	1.85	12.57	13.51	13.078	0.94
51	0.60	1.09	1.50	0.69	15.90	17.44	16.694	1.54
52	0.60	0.50	0.70	0.69	15.03	15.63	15.258	0.60
53	0.42	0.44	0.44	0.51	12.72	13.16	12.883	0.44
54	0.43	0.32	0.32	0.52	16.33	16.65	16.483	0.32
55	0.25	0.43	0.55	0.34	15.15	15.58	15.394	0.43
56	0.70	0.58	0.58	0.79	16.70	17.28	16.905	0.58
57	0.45	0.68	1.00	0.54	14.76	15.46	15.214	0.70
58	0.38	1.44	1.78	0.47	16.29	17.76	17.107	1.47

Figure 5.4 - Standard Magnitudes (continued)

				|<- Standard Magnitudes			->|
#	(B-V)	Vamp	Bamp	(B-V)	Max	Min	Mean	Vamp
59	0.35	1.01	1.31	0.44	14.58	15.61	15.162	1.03
60	0.38	1.01	1.50	0.47	14.96	16.01	15.597	1.05
61	0.79	0.26	0.26	0.88	13.83	14.09	13.947	0.26
62	0.30	0.93	1.10	0.39	15.88	16.83	16.540	0.95
63	0.35	0.30	0.30	0.44	15.03	15.33	15.168	0.30
64	0.45	0.44	0.60	0.54	16.84	17.54	17.245	0.70
65	0.40	0.28	0.28	0.49	13.39	13.67	13.512	0.28
66	0.30	1.23	1.60	0.39	16.23	17.48	17.030	1.25
67	0.40	0.48	0.48	0.49	16.23	16.71	16.398	0.48
68	0.44	0.98	1.25	0.53	16.65	17.66	17.241	1.01
69	0.48	0.80	1.00	0.57	17.08	17.89	17.549	0.81

Notes to Table 5.4

35 - Particularly poor B observations.

51 - Luminosity of blended stars (V = 18.008 ± 0.056 and V = 19.497 ± 0.133 as determined by Capilla Peak photometry) removed. Random error in standard magnitude 0.0092.

52 - Luminosity of blended stars (V = 18.273 ± 0.040 and V = 18.093 ± 0.025 as determined by Capilla Peak photometry) removed. Random error in standard magnitude 0.0048.

64 - Luminosity of blended star (V = 17.718 ± 0.035 as determined by Capilla Peak photometry) removed. Random error in standard magnitude 0.0115.

5.5 CTI RR Lyrae Survey Statistics

Equation 5.2 (from Barnes and Hawley 1986), which empirically accounts for changing light curve shape with increasing amplitude when comparing the mean, minimum, and maximum magnitudes, will be used in Chapter 6 to calculate mean magnitudes for RR Lyrae stars in surveys where only the minimum and maximum magnitudes are listed. Equation 5.2 can be checked using the CTI data. Figure 5.10 plots (V_{min} - <V>) versus ΔV for the twenty-five brightest RR Lyrae variable

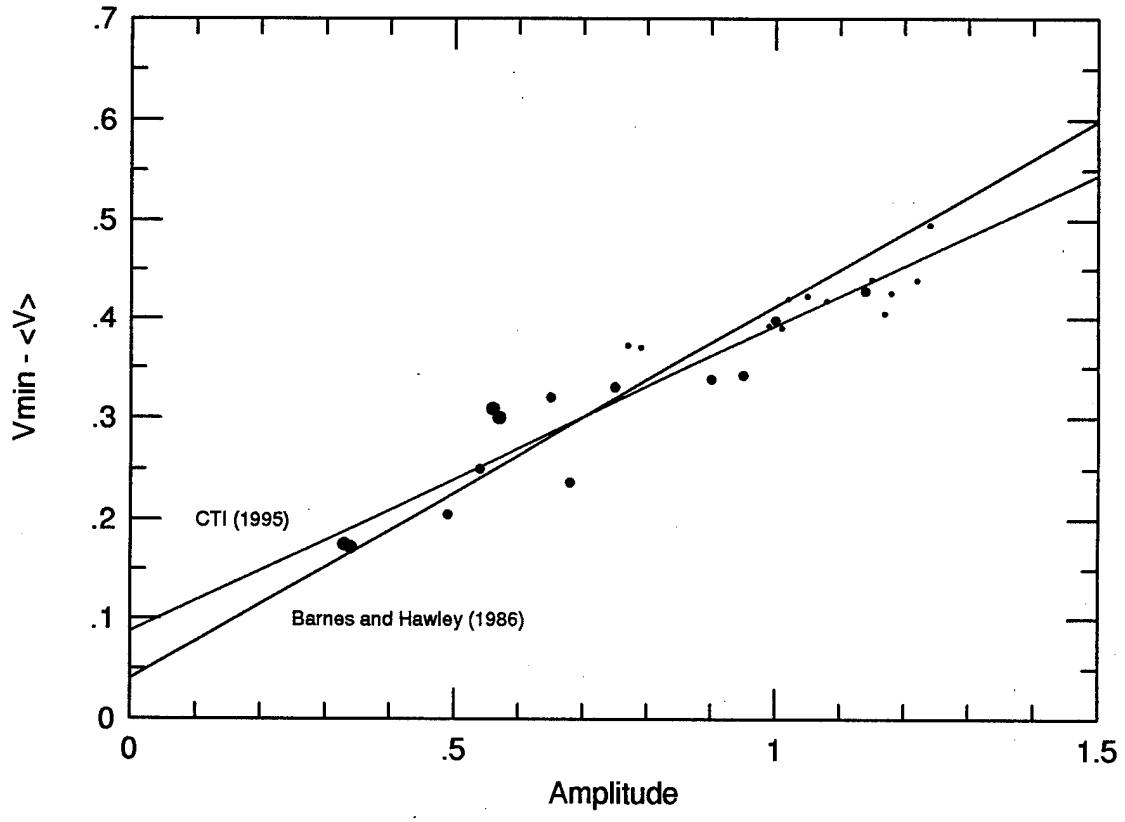


Figure 5.10 - Vmin - <V> versus ΔV for bright RR Lyrae variable stars in CTI survey. Increasing symbol size corresponds to increasing (m-M)/P. Barnes and Hawley 1986 relation and CTI regression fit also plotted.

stars in the CTI survey with increasing symbol size corresponding to increasing (m-M)/P (a measure of light curve shape). The Barnes and Hawley 1986 relation (V_{min} - <V> = 0.04 + 0.375×ΔV) and the regression fit to the CTI data (V_{min} - <V> = (0.087 ± 0.030) + (0.305 ± 0.021)×ΔV) are also plotted. For stars of identical light curve shape, the intercept of V_{min} - <V> versus ΔV must be equal to zero. This is the case for RRc type variables (represented by the largest symbols in Figure 5.10), where the resulting slope is close to 0.5 (as would be expected for a sinusoidal light curve). For the more asymmetric light curves of RRab type stars, a slope between 0.35 and 0.45 fits the data best with zero intercept. The fact that increasing asymmetry is correlated with amplitude makes it possible for a relation like Equation 5.2 to be calculated using all types of RR Lyraes. The slight difference in slope and intercept between the Barnes and Hawley 1986 and CTI best fit lines are comparable to the scatter of the CTI data from the best fit lines. The CTI best fit line, however, was calculated using over three times the number of stars, and is thus more representative of the actual relationship.

Equation 5.1 (McDonald 1977), an empirical relation between B-V at minimum light and period for RRab type variable stars, was used earlier to establish a color limit in selecting RR Lyrae variables. This relation can also be checked using CTI data. Figure 5.11 plots the B-V at minimum

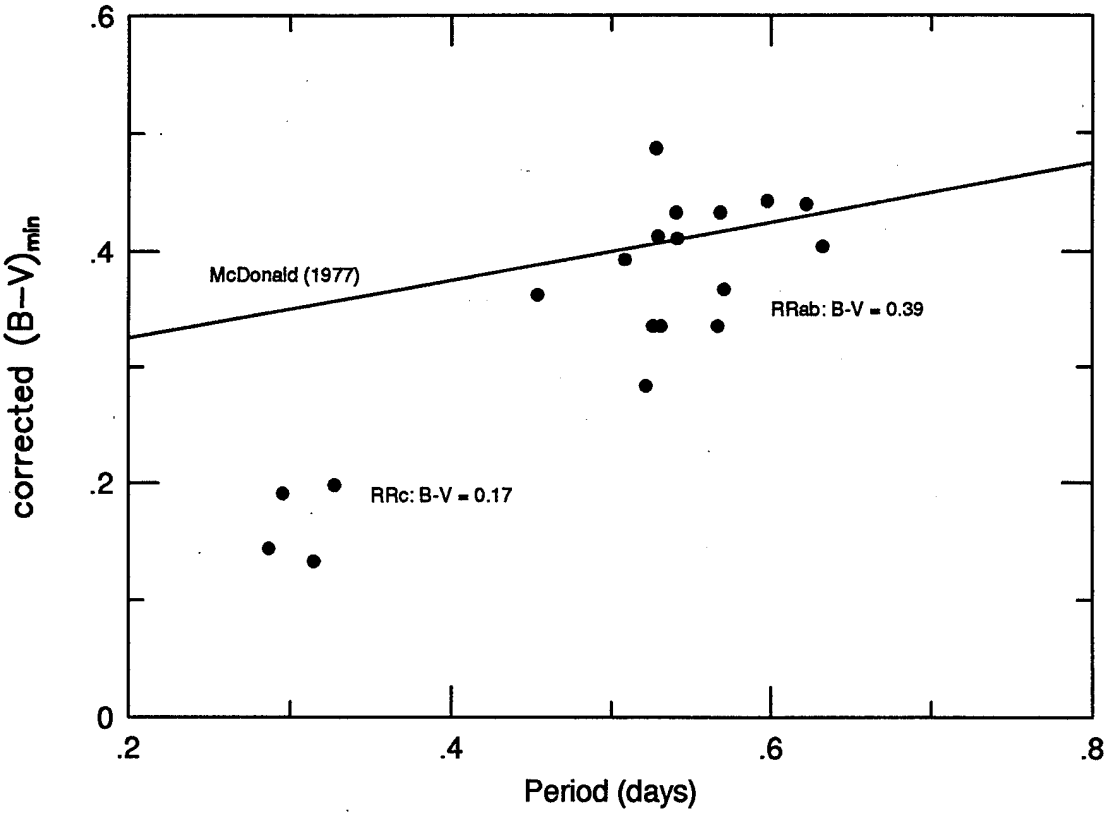


Figure 5.11 - B-V at minimum light (corrected for Galactic reddening) versus period for bright RR Lyrae variable stars in CTI survey. McDonald 1977 relation also plotted.

light versus period for nineteen of the brightest RR Lyrae stars with more than 5 B observations and little Galactic reddening. The reddening corrected mean B-V at minimum light of the RRab type variables is 0.39 ± 0.05. There is only the slightest hint of a dependence on period, although this dependence might manifest itself more clearly if the sample included RRab type stars with a larger range of periods. If the four RRc type variables are included (having a mean B-V at minimum light of 0.17 ± 0.03), Figure 5.11 clearly displays

the trend of redder colors for longer periods.

Finally, Figure 5.12 compares the period and amplitude distribution of the CTI RR Lyrae variable stars to that of the RR Lyrae variable stars contained in the Palomar-Groningen Variable Star survey. Despite the fact that the CTI survey covers a large range of Galactic latitude and longitude as compared to the Palomar-Groningen survey, there are no significant deviations between the period and amplitude distributions for these surveys and thus it can be assumed they are subsets of the same parent population.

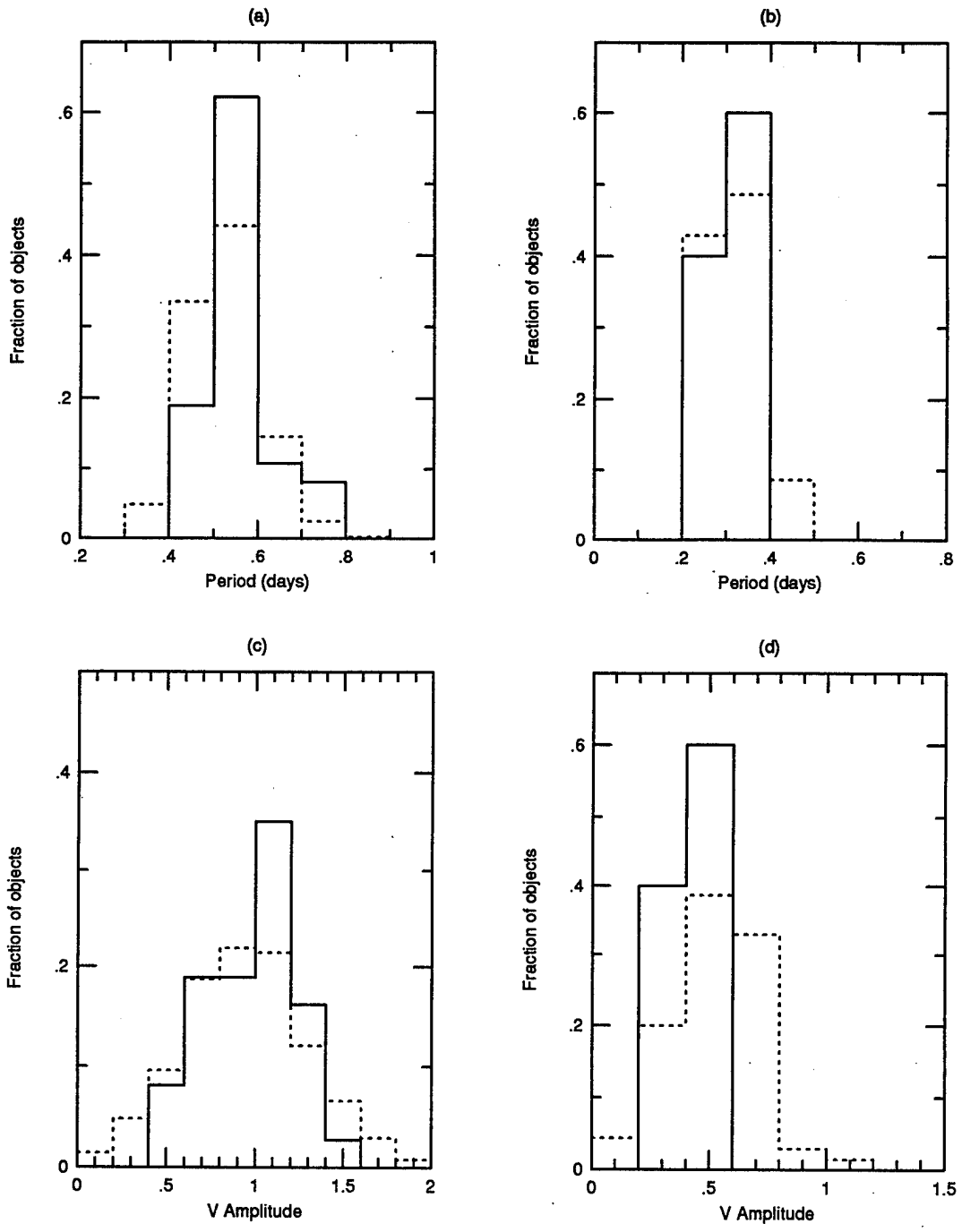


Figure 5.12 - Distribution in (a),(b) period and (c),(d) amplitude for the CTI RR Lyrae stars (solid lines) and the RR Lyrae stars contained in the Palomar-Groningen Variable Star survey (dashed lines). RRab type stars are shown in (a) and (c) while RRc type stars are shown in (b) and (d).

Chapter 6 RR Lyrae Variable Star Space Densities

The space density of RR Lyrae variable stars in the Galactic halo can now be examined. RR Lyrae variable stars exhibit a period-luminosity relationship similar to the period-luminosity relationship of Classical Cepheids. Knowing the absolute magnitude (M_V, M_B), Galactic absorption ($A_V = 3 \times E(B-V)$, $A_B = 4 \times E(B-V)$), and apparent magnitude (<V>, <B>), the heliocentric distance (r) to the RR Lyrae star can be readily calculated using

$$r = 10^{\frac{\langle V \rangle - M_V + 5 - A_V}{5}} \qquad (6.1)$$

In this chapter the simplest luminosity function, namely that all RR Lyraes have an absolute magnitude of $M_V = 0.74 \pm 0.12$ (Layden et al. 1994) will be used. This is necessary because metallicity measurements have not been made for all the RR Lyrae stars in the CTI survey, nor in most of the other surveys with which the calculated CTI RR Lyrae space densities will be compared. Given that <B> - <V> ≈ 0.26 (Hawley et al. 1986), $M_B = 1.00$.

Knowing the Galactic latitude (b), Galactic longitude (l) and heliocentric distance (r) leads directly to a calculation of the Galactocentric coordinates ((x,y,z) or (R,θ,ϕ)). Figure 6.1 displays this coordinate system with R_0 the distance from the Sun (S) to the Galactic center (O) defined to be along the positive x-axis, and P marking an arbitrary position for an RR Lyrae Star.

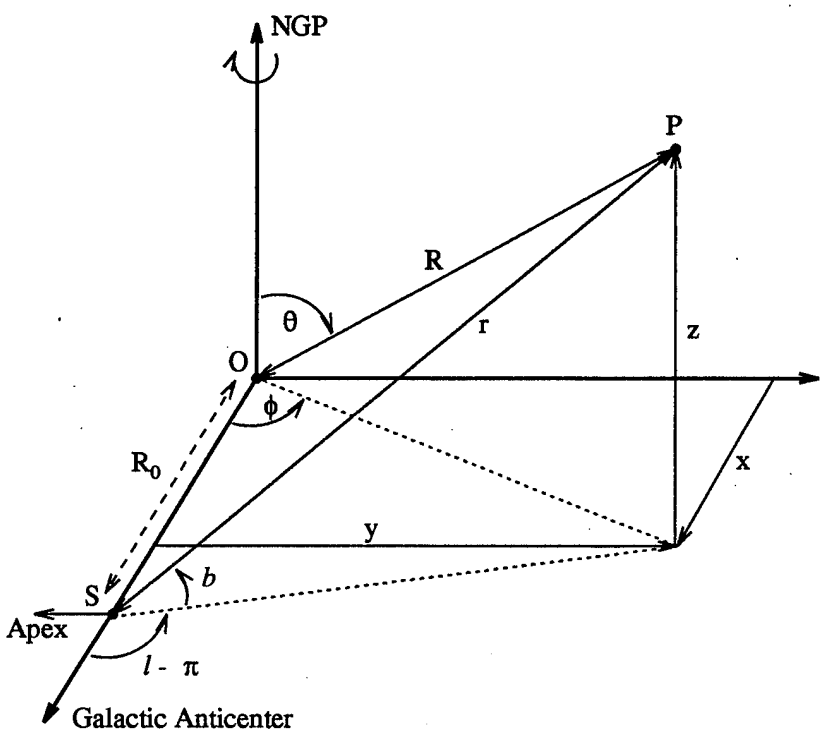


Figure 6.1 - Galactocentric coordinates. O is the Galactic center, S is the Sun's position, NGP is the north Galactic pole.

Oort and Plaut (1975) calculated R_0 with the RR Lyrae space density data from the Palomar-Groningen variable star survey and Baade's Window. Their value of $R_0 = 8.7 \pm 0.6$ kpc, however, was calculated assuming $M_{pg} = 0.7$ (or equivalently, $M_V = 0.44$). If this distance is recalculated using $M_V = 0.74$, $R_0 = 7.6 \pm 0.5$ kpc. This value of R_0 will be used when calculating distances in this chapter and agrees well with recent calculations using the rotation curve of HI in the solar neighborhood ($R_0 = 7.9 \pm 0.8$ kpc, Merrifield 1992), and an analysis based on the weighted average of several methods ($R_0 = 7.7 \pm 0.7$ kpc, Reid 1989).

Table 6.1 lists <V>, $\sigma_{<V>}$, E(B-V), the heliocentric coordinates (r, b, and l), the Galactocentric coordinates (x, y, z, R, θ, and ϕ) and the error in the Galactocentric radial distance (σ_R) for all confirmed RRab type stars in the CTI Survey. This last value was calculated using

$$\sigma_R^2 = (1+KR_0^2)\, r^2 \ln(10)^2 (\sigma_{<V>}^2 + \sigma_{M_V}^2 + \sigma_{A_V}^2) + (1+Kr^2)\, \sigma_{R_0}^2, \qquad (6.2)$$

where $K = (\cos(b)\cos(l) - 1)/R^2$ and $\sigma_{AV} \geq 0.03$ (Burstein and Heiles 1982). Due to the different completeness estimates for RRab and RRc type variables in the CTI as well as all other RR Lyrae surveys, the contribution to the space density from RRc type variables will not be considered.

Using the Galactocentric radial distances for the RRab type variable stars in the CTI survey, the RR Lyrae space density as a function of distance can be calculated. Due to the unique shape of the CTI survey field, covering a large range of both Galactic latitude and longitude, a method for determining the RR Lyrae space density must first be developed. The RR Lyrae space density will be calculated for the CTI survey and then compared to several other surveys of RR Lyrae variable stars.

Table 6.1 - CTI RR Lyrae Galactocentric coordinates

#	<V>	$\sigma_{<V>}$	E(B-V)	r	l	b	x	y	z	R	σ_R	θ	ϕ
4	17.045	0.0094	0.055	16904.4	140.8	-32.5	18652.4	9014.8	-9074.0	22616.7	4454.4	113.7	25.8
5	17.495	0.0088	0.050	20941.1	141.5	-32.2	21469.6	11040.2	-11148.0	26591.5	5683.1	114.8	27.2
7	17.889	0.0219	0.101	23399.1	163.8	-20.6	28634.5	6127.6	-8217.2	30413.9	6497.5	105.7	12.1
11	16.063	0.0058	0.016	11350.1	193.0	25.3	17595.8	-2306.1	4857.1	18398.9	2740.1	74.7	352.5
12	16.310	0.0053	0.030	12473.8	196.9	36.6	17189.5	-2906.6	7429.0	18950.4	3085.3	66.9	350.4
13	16.226	0.0048	0.020	12167.5	197.9	39.6	16518.3	-2873.8	7762.3	18476.1	2991.9	65.2	350.1
15	18.224	0.0167	0.018	30619.6	202.9	58.0	22532.5	-6296.9	25979.4	34961.4	8671.6	42.0	344.4
16	18.003	0.0140	0.020	27580.4	203.5	60.3	20140.9	-5454.8	23950.9	31765.7	7736.6	41.1	344.8
18	15.278	0.0029	0.007	8005.7	205.7	76.2	9322.7	-828.7	7774.1	12167.0	1726.0	50.3	354.9
19	16.332	0.0065	0.007	13007.7	205.7	79.7	9686.8	-1003.5	12799.9	16083.5	3274.5	37.3	354.1
20	15.705	0.0078	0.007	9745.4	205.4	79.9	9142.0	-733.1	9594.7	13272.9	2260.6	43.7	355.4
21	16.442	0.0068	0.007	13683.6	203.1	84.1	8901.5	-555.2	13610.2	16272.2	3490.1	33.2	356.4
22	14.794	0.0022	0.007	6406.2	184.4	88.1	7811.0	-16.1	6402.7	10099.8	1261.6	50.7	359.9
24	16.743	0.0090	0.007	15718.1	42.5	84.0	6393.4	1105.1	15632.7	16925.7	4146.6	22.5	9.8
26	17.972	0.0271	0.014	27415.7	41.0	67.3	-369.3	6929.6	25300.1	26234.5	7923.0	15.3	93.1
27	14.787	0.0028	0.010	6359.2	42.1	62.6	5431.3	1959.4	5647.7	8076.8	1256.0	45.6	19.8
28	17.860	0.0218	0.014	26037.6	43.0	57.8	-2532.7	9453.1	22043.7	24118.4	7463.2	23.9	105.0
30	15.341	0.0035	0.053	7733.9	48.7	37.5	3549.2	4604.6	4711.9	7483.4	1645.2	51.0	52.4
32	16.170	0.0064	0.055	11298.0	50.3	32.6	1519.0	7318.5	6091.3	9642.2	2798.8	50.8	78.3
33	17.972	0.0187	0.053	25977.7	50.4	32.2	-6404.6	16956.7	13826.7	22797.5	7456.7	52.7	110.7
34	15.071	0.0034	0.053	6829.7	50.6	32.1	3926.5	4472.2	3626.1	6969.0	1386.5	58.6	48.7
38	15.779	0.0052	0.055	9436.3	52.5	26.6	2460.8	6692.3	4224.3	8287.7	2184.3	59.4	69.8
39	16.612	0.0074	0.055	13848.4	52.6	26.4	60.3	9845.8	6163.7	11616.1	3637.2	58.0	89.6
42	17.052	0.0224	0.108	15761.6	54.7	20.5	-922.7	12054.7	5520.3	13290.7	4342.5	65.5	94.4
43	15.595	0.0047	0.109	8046.4	54.8	20.4	3258.8	6164.6	2810.0	7517.9	1756.3	68.1	62.1
44	16.604	0.0074	0.170	11770.6	57.0	15.4	1413.8	9514.4	3123.4	10113.2	3217.0	72.0	81.5
45	16.690	0.0114	0.178	12111.6	57.3	14.7	1267.1	9853.0	3082.5	10401.4	3383.6	72.8	82.7
49	17.174	0.0081	0.223	14223.3	58.1	13.0	267.6	11757.8	3208.2	12190.5	4427.9	74.7	88.7
57	15.214	0.0038	0.093	6902.4	80.5	-19.2	6529.5	6429.1	-2272.4	9441.0	1402.7	103.9	44.6
58	17.107	0.0104	0.090	16573.0	82.6	-20.9	5595.7	15354.7	-5905.8	17376.9	4423.0	109.9	70.0
59	15.162	0.0049	0.090	6767.1	82.6	-21.0	6790.2	6264.1	-2428.5	9552.2	1364.5	104.7	42.7
60	15.597	0.0037	0.090	8268.0	83.1	-21.4	6679.7	7643.7	-3014.3	10589.2	1806.0	106.5	48.9
62	16.540	0.0089	0.088	12799.7	84.9	-22.7	6554.8	11765.9	-4929.8	14342.4	3229.9	110.1	60.9
64	17.245	0.0069	0.056	18509.7	90.0	-26.1	7587.4	16625.0	-8137.6	20004.5	4998.2	114.0	65.5
66	17.030	0.0094	0.068	16489.2	96.3	-29.2	9173.5	14308.8	-8042.2	18803.5	4368.2	115.3	57.3
68	17.241	0.0113	0.051	18603.7	102.5	-31.6	11033.4	15464.0	-9755.7	21355.2	5017.9	117.2	54.5
69	17.549	0.0141	0.060	21173.9	107.6	-33.0	12955.3	16924.4	-11542.0	24238.3	5811.4	118.4	52.6

6.1 Calculating RR Lyrae Space Densities

In most previous RR Lyrae surveys, space densities were calculated by determining the volume of space occupied by a certain number of stars of increasing *heliocentric* distance (based on Kinman et al. 1965). The space density at particular Galactocentric distances are then obtained by converting a given heliocentric distance to its corresponding Galactocentric distance. This method works fine for surveys covering a small solid angle at a fixed Galactic latitude and longitude where a given heliocentric distance corresponds to a single Galactocentric distance. This method will not work, however, with the CTI survey because of the unique shape of the CTI survey area.

Saha (1985) proposed a similar method for calculating space densities using the relationship

$$N=\int \omega \rho(r) r^2 dr \qquad (6.2)$$

where N is the total number of RR Lyrae stars found in a solid angle ω along a given direction, r is the heliocentric distance, and ρ is the RR Lyrae space density. Equation 6.2 can be solved for ρ giving

$$\rho(r)=\frac{1}{\omega r^2}\frac{dN}{dr} \qquad (6.3)$$

By using a plot of N versus r, dN/dr can be estimated as a function of r, and Equation 6.3 used to calculate the RR Lyrae space density as a function of heliocentric distance. As

before, the space density as a function of Galactocentric distance is found by converting heliocentric distances to Galactocentric distances. Again, because of the unique shape of CTI's survey area, this method will not work for the CTI survey. A variation on this method, however, can be used. An equivalent expression to Equation 6.2 is

$$N=\int f(R)\,\rho(R)\,4\pi R^2 dR \qquad (6.4)$$

where f(R) is the fraction of the volume of space at Galactocentric distance R the survey samples, and ρ is now measured as a function of Galactocentric distance. The function 4πf(R) is analogous to ω in Equation 6.3, but whereas ω is constant with increasing heliocentric distance, f(R) varies with increasing Galactocentric distance and must be calculated numerically knowing the magnitude limits and borders of the survey area. Equation 6.4 can be solved for ρ giving

$$\rho(R)=\frac{1}{f(R)\,4\pi R^2}\frac{dN}{dR} \qquad (6.5)$$

By using a plot of N versus R, the RR Lyrae space density as a function of Galactocentric distance can be calculated directly (assuming a spherically symmetric distribution).

A similar derivation can be done for any type of distribution. For a distribution where the density is constant on ellipsoids with a semi-major axis of *a* in the plane of the Galaxy, and a semi-minor axis of *c* perpendicular

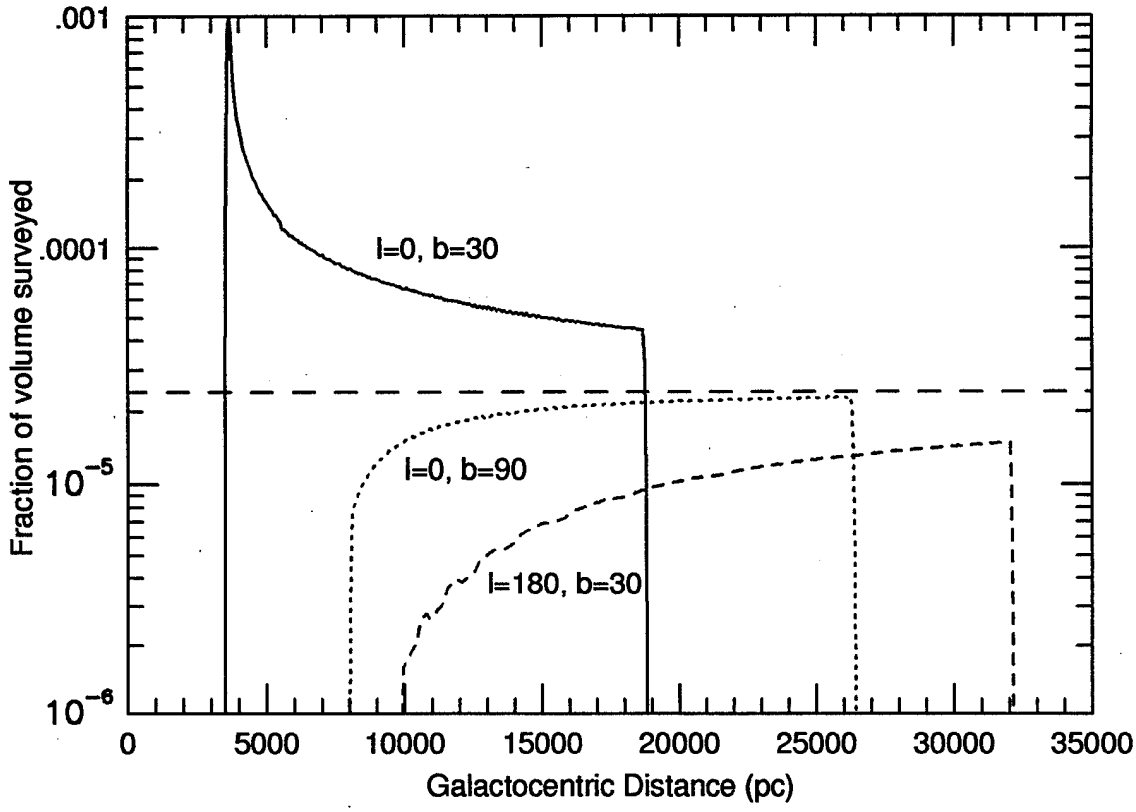


Figure 6.2 - Fraction of total volume as function of Galactocentric distance surveyed for three different 1 square degree pointings for <B> = 14 - 18: solid line for l=0° and b=30°, dotted line for l=0° and b=90°, and short dashed line for l=180° and b=30°. Long dashed line is asymptotic limit.

to the plane of the Galaxy, the resulting equation for space density is

$$\rho(a) = \frac{1}{f(a) \times \frac{C}{a}(a) \times 4\pi a^2} \frac{dN}{da} \qquad (6.6)$$

where f(a) is the fraction of the volume of space at Galactocentric semi-major axis distance a sampled by the survey.

In order to determine RR Lyrae space densities, the

functions f(R) and f(a) in Equations 6.5 and 6.6 respectively must be calculated. This was done by numerically integrating over the volume of space surveyed. Figure 6.2 plots f(R) as a function of Galactocentric distance for three 1 square degree pointings with magnitude limits B = 14 to 18 and assuming no Galactic reddening. All three pointings asymptotically approach the value of (solid angle of 1 square degree)/4π representing the case where $R_0 = 0$.

Due to the different completeness estimates for RRab and RRc type variables as a function of magnitude, only RRab type variables are considered. The ellipsoidal distribution described in Preston et al. 1991, namely

$$\frac{c}{a}(a) = \begin{matrix} (\frac{c}{a})_0 + [1-(\frac{c}{a})_0](\frac{a}{a_u}), a<a_u \\ 1, a>a_u \end{matrix} \qquad (6.7)$$

where $(c/a)_0 = 0.5$ and $a_u = 20$ kpc, was used.

The result for the CTI survey and a spherically symmetric distribution are shown in Figure 6.3. The survey area used in the calculations is that for list 2 shown in Figure 5.4, as modified by Figure 5.3 (bright star masking) and Figure 5.7 (completeness as a function of right ascension), and requiring E(B-V) (Figure 5.2) to be less than 0.15. The magnitude limits used were <V> = 13.0 to 18.5. This faint magnitude limit corresponds to the point where the CTI survey becomes 50% complete (see Figure 5.9).

The values (dN/dR) and (dN/da) as functions of

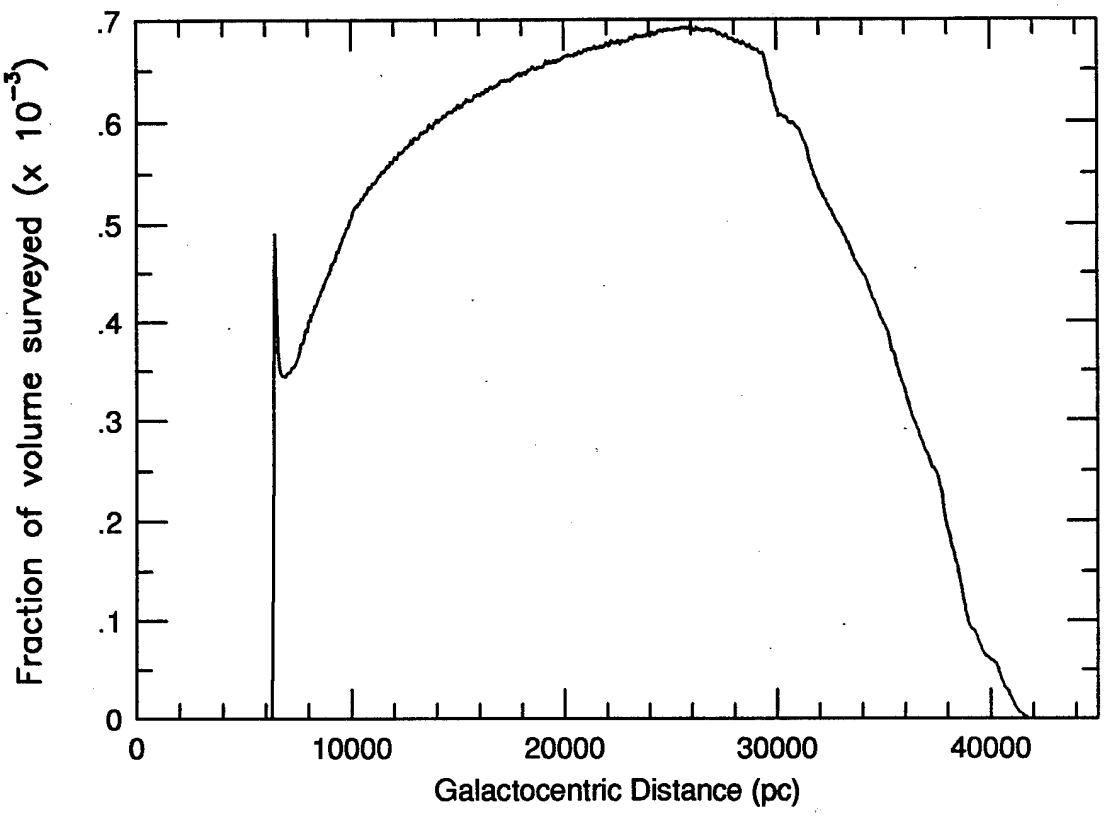


Figure 6.3 - Fraction of total volume surveyed by CTI RR Lyrae survey (× 10^{-5}) as a function of Galactocentric distance.

Galactocentric distance and semi-major axis distance respectively must also be calculated. Figure 6.4 plots the number of RR Lyrae stars out to a certain Galactocentric distance (N) versus the Galactocentric distance (R). The value (dN/dR) for each RR Lyrae was estimated by calculating the slope of five consecutive points, two on either side of the point in question. For the two most distant and two closest to the Galactic center, only three or four points were used to calculate the slope. Similar calculations were done to determine (dN/da) as a function of the semi-major axis distance.

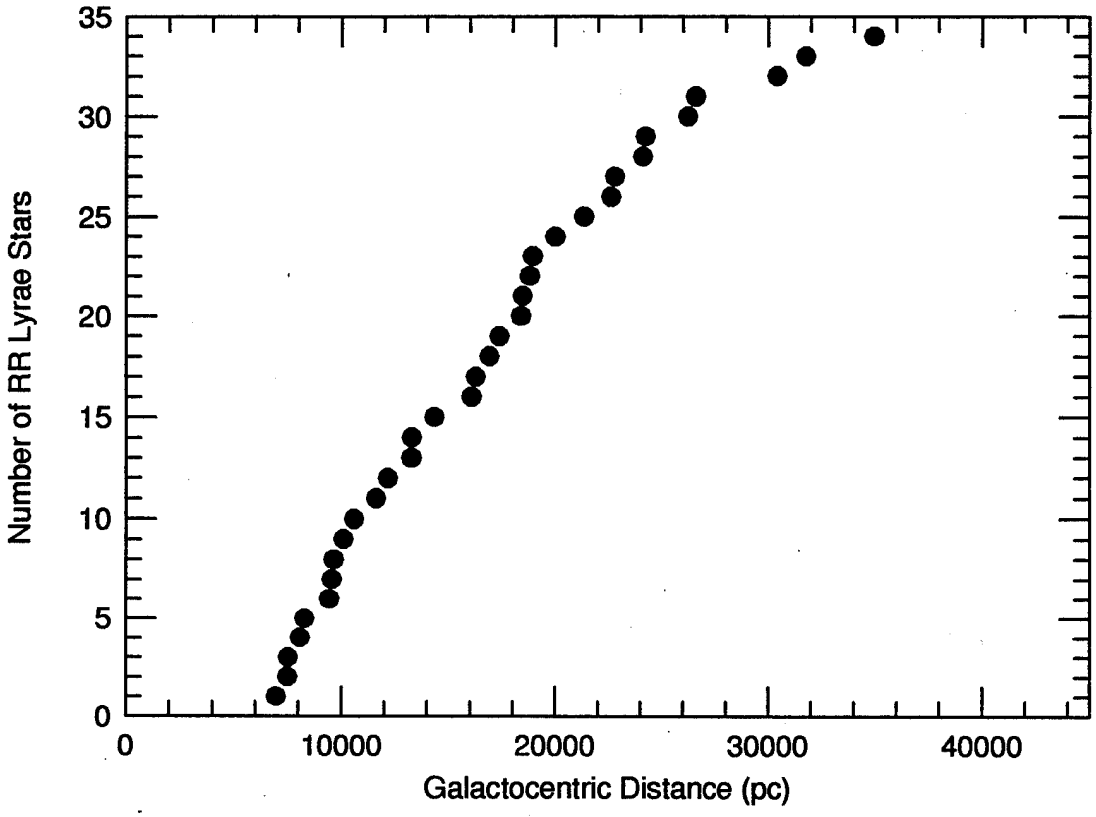


Figure 6.4 - Cumulative number of RRab type stars in the CTI RR Lyrae survey as a function of Galactocentric distance.

The method described above for calculating space densities was tested using generated N versus R plots for different spherically symmetric power-law distributions and the f(R) function appropriate for the CTI RR Lyrae survey. The resulting calculated functions matched the input functions to within the calculated errors.

The space density was calculated at the position of every RRab type star using Equations 6.5 and 6.6. The errors in R and *a* were taken to be the standard deviation of the individual distances going into the calculation. The error in

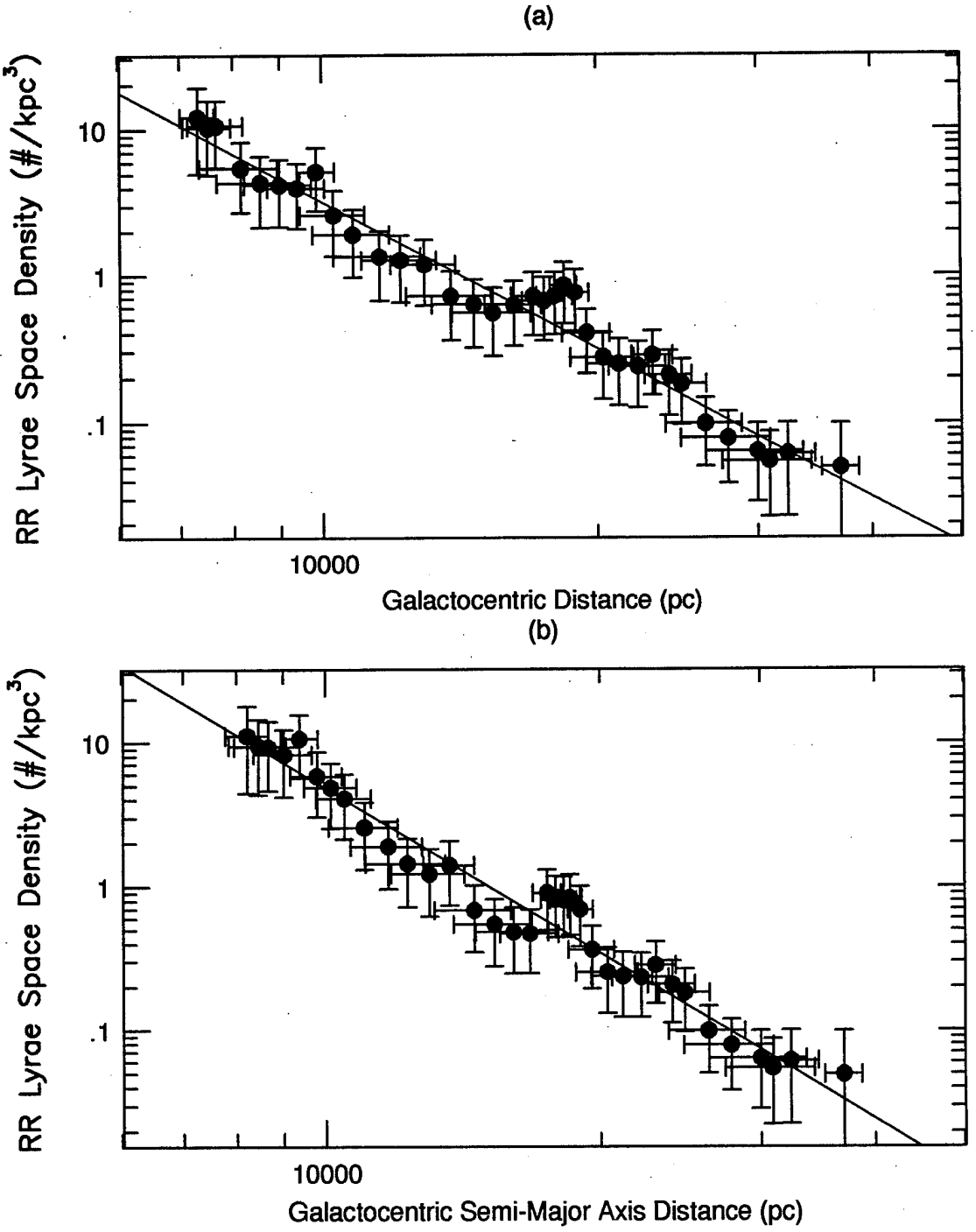


Figure 6.5 - RR Lyrae Space Density in #/kpc^3 versus (a) Galactocentric radial distance and (b) Galactocentric semi-major axis distance for the CTI RR Lyrae survey. Solid lines correspond to best-fit linear regression.

ρ was calculated from the errors in R or *a*, the error in f (taken to be the standard deviation of the values of f for the stars used in calculating (dN/dR) or (dN/da)), and in (dN/dR) or (dN/da) (taken to be 100%/sqrt(# of points)). Figure 6.5 plots the calculated space densities as a function of Galactocentric radial distance and Galactocentric semi-major axis distance for RRab type variables in the CTI survey.

The most distant data points in Figure 6.5 correspond to an estimated most probable value given the faint limiting magnitude of the CTI survey. In other words, what must the space density be for no RR Lyrae stars to have been observed to the faint limiting magnitude. This space density was calculated by taking one over the volume of space surveyed beyond a distance midway between the two faintest RR Lyrae stars observed. The error in this space density is assumed to be 100%.

The solid lines in Figure 6.5 correspond to the best fit linear regression to the data, and are $\log(\rho) = (13.861 \pm 0.471) - (3.336 \pm 0.112) \times \log(R)$ and $\log(\rho) = (15.705 \pm 0.557) - (3.757 \pm 0.132) \times \log(a)$ for Figure 6.5(a) and (b) respectively. These results are commensurate with other RR Lyrae surveys (see Chapter 6.3), and because of the wide range of Galactic latitude and longitude covered by the CTI survey, demonstrates the large scale homogeneity of the Galactic halo.

6.2 Other RR Lyrae Variable Star Surveys

Several other variable star surveys have calculated RR Lyrae space densities. These include the Lick RR Lyrae Survey (Kinman et al. 1965a, Lafler and Kinman 1965, Kinman et al. 1965b, 1966, 1982, 1984, hereafter papers L1 - L6), the Palomar-Groningen Variable Star Survey (Plaut 1966, 1968a, 1968b, 1970, 1971, 1973a, and Oort and Plaut 1975, papers P-G1 - P-G7), surveys of Baade's Window (Blanco 1984 and references therein), an RR Lyrae survey by Saha (Saha 1984, Saha and Oke 1985, Saha 1985, Papers S1 - S3), and an RR Lyrae survey by Hawkins (Hawkins 1984 and references therein). Table 6.2 lists the area in square degrees, the central right ascension

Table 6.2 - RR Lyrae Space Density Surveys

Survey/Field	Area sq deg	RA	Dec	l	b	Paper
Lick						
RR1 (MWF 361)	29.2	$16^h\ 22^m$	-3° 30'	11.0	+29.4	L3, L6
RR2	29.2	$12^h\ 26^m$	+31° 16'	172.7	+84.3	L4
RR3	22.2	$12^h\ 47^m$	+28° 35'	121.1	+89.1	L4
RR4	29.2	$13^h\ 04^m$	+29° 55'	64.8	+85.9	L4
RR5	29.2	$02^h\ 26^m$	+40° 35'	142.6	-18.0	L5
RR6	29.2	$07^h\ 38^m$	+39° 49'	180.0	+26.5	L5
RR7	29.2	$08^h\ 30^m$	+39° 46'	182.4	+36.4	L5
Palomar-Groningen						
PG1	42.3	$16^h\ 04^m$	-12° 15'	359.0	+28.5	P-G1
PG2	33.6	$17^h\ 07^m$	-19° 25'	3.5	+12.5	P-G2. P-G3
PG3	19.1	$18^h\ 24^m$	-34° 00'	0.0	-10.0	P-G4. P-G5
Saha						
SII	43.6	$07^h\ 29^m$	+39° 00'	180.0	+24.1	S1-3
SIII	43.6	$07^h\ 58^m$	+40° 17'	180.2	+30.0	S1-3
SIV	43.6	$23^h\ 56^m$	+32° 06'	110.2	-29.2	S1-3
Hawkins (H)	16.0	$21^h\ 28^m$	-45° 00'	355.0	-47.0	
Baade's Window (BW)	0.14	$18^h\ 00^m$	-30° 02'	1.0	-3.9	
CTI	35.6	$12^h\ 00^m$	+28° 01'	-	-	

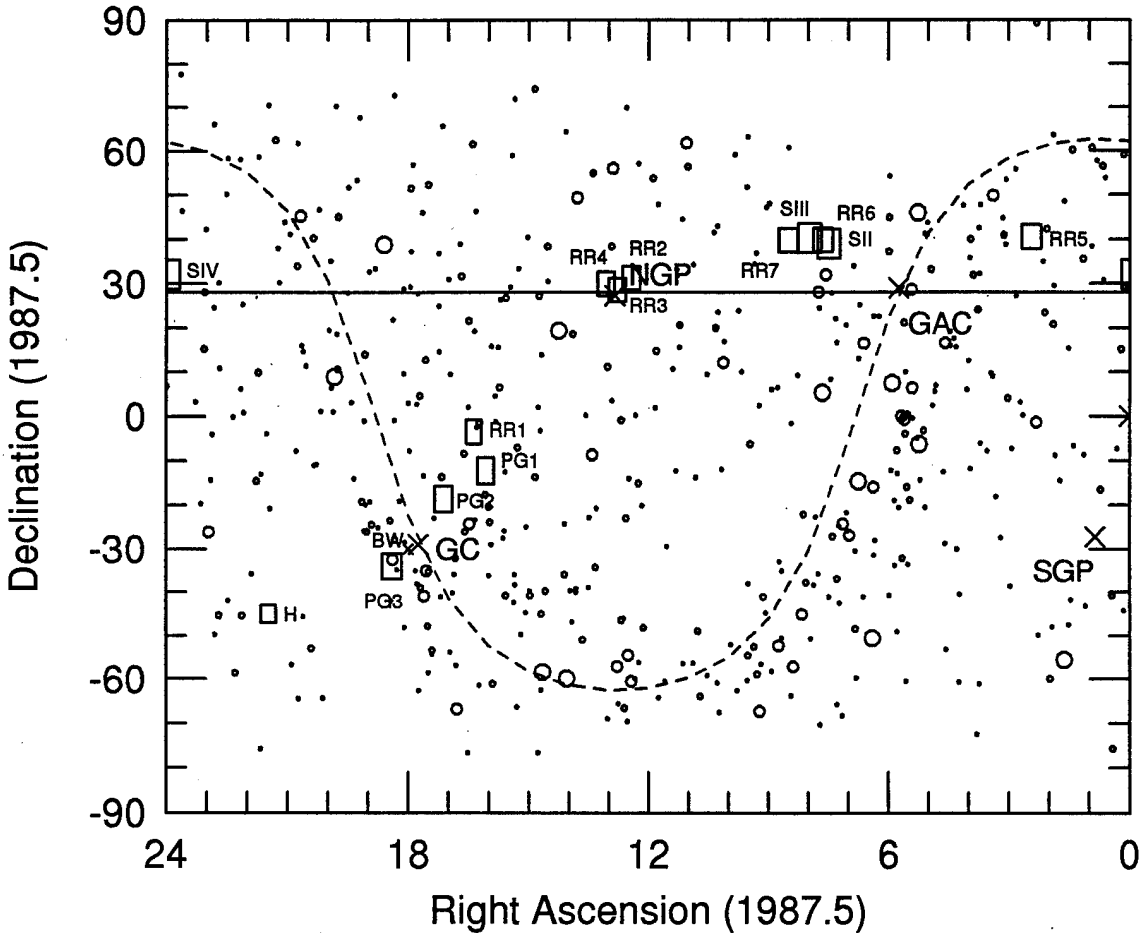


Figure 6.6 - Location of all fields listed in Table 6.2 in right ascension and declination. CTI survey strip (solid line), Galactic plane (dashed line), Galactic poles (NGP and SGP), Galactic center (GC) and Galactic anti-center (GAC) also marked.

and declination (1950 epoch), and the central Galactic longitude and latitude for each field in these surveys.

Figure 6.6 plots the position of all fields in the above surveys in right ascension and declination. Fields RR3 and RR4 in the Lick survey are slightly overlapped, thus reducing the overall area of field RR3. As done with the CTI survey, the E(B-V) maps of Burstein and Heiles (1982) were used to estimate the Galactic reddening for all fields except Baade's

Window. As a result, it was necessary to exclude from consideration portions of fields PG2 and PG3 in the Palomar-Groningen survey closer than 10° to the Galactic plane.

6.2.1 Lick RR Lyrae Star Survey

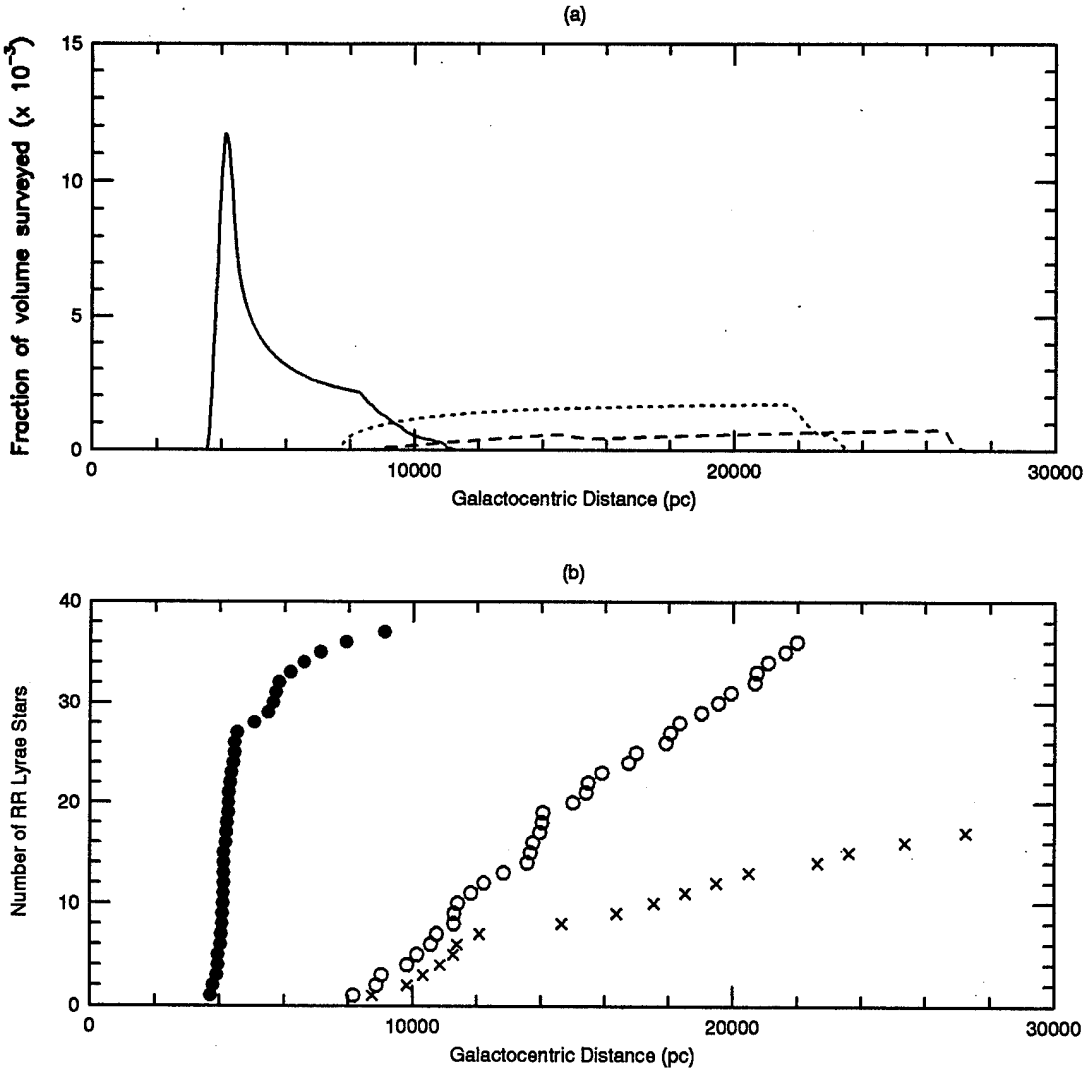


Figure 6.7 - (a) Fraction volume surveyed and (b) cumulative number of RRab stars versus Galactocentric radial distance. RR1 (solid, filled), RR2+RR3+RR4 (dotted, open) and RR5+RR6+RR7 (dashed, x's)

The Lick RR Lyrae Star Survey used the 20-inch Carnegie Astrograph at Lick Observatory and 14 x 14-inch plates to cover an area of the sky 5° 26' square for each field. The seven Lick fields listed in Table 6.2 will be considered in three separate groups corresponding to Papers L3 and L6 (RR1), Paper L4 (RR2+RR3+RR4), and Paper L5 (RR5+RR6+RR7).

Completeness as a function of magnitude for the Lick survey is described in detail in Paper L1. For RRab type variables with amplitudes greater than 0.75, the survey is 100% complete to $\langle m_{pg} \rangle$ = 17.0 and reduces to 50% complete at $\langle m_{pg} \rangle$ = 17.7. By not considering variables with amplitudes less than 0.75, the overall completeness for each field is 92% when compared to the Palomar-Groningen survey (taken to be the standard, as done with the CTI survey). Additionally, from the discussion in Paper L1, photographic magnitudes ($\langle m_{pg} \rangle$) will be considered identical to <B>.

Figure 6.7 plots (a) the fraction of space surveyed and (b) the cumulative number of RRab type variable stars as a function of Galactocentric radial distance for RR1 (solid line and filled circles), RR2+RR3+RR4 (dotted line and open circles), and RR5+RR6+RR7 (dashed line and x's).

6.2.2 Palomar-Groningen Variable Star Survey

The plates for the Palomar-Groningen Variable Star Survey were all taken with the 48" Palomar Schmidt telescope. The three survey fields listed in Table 6.2 will be considered

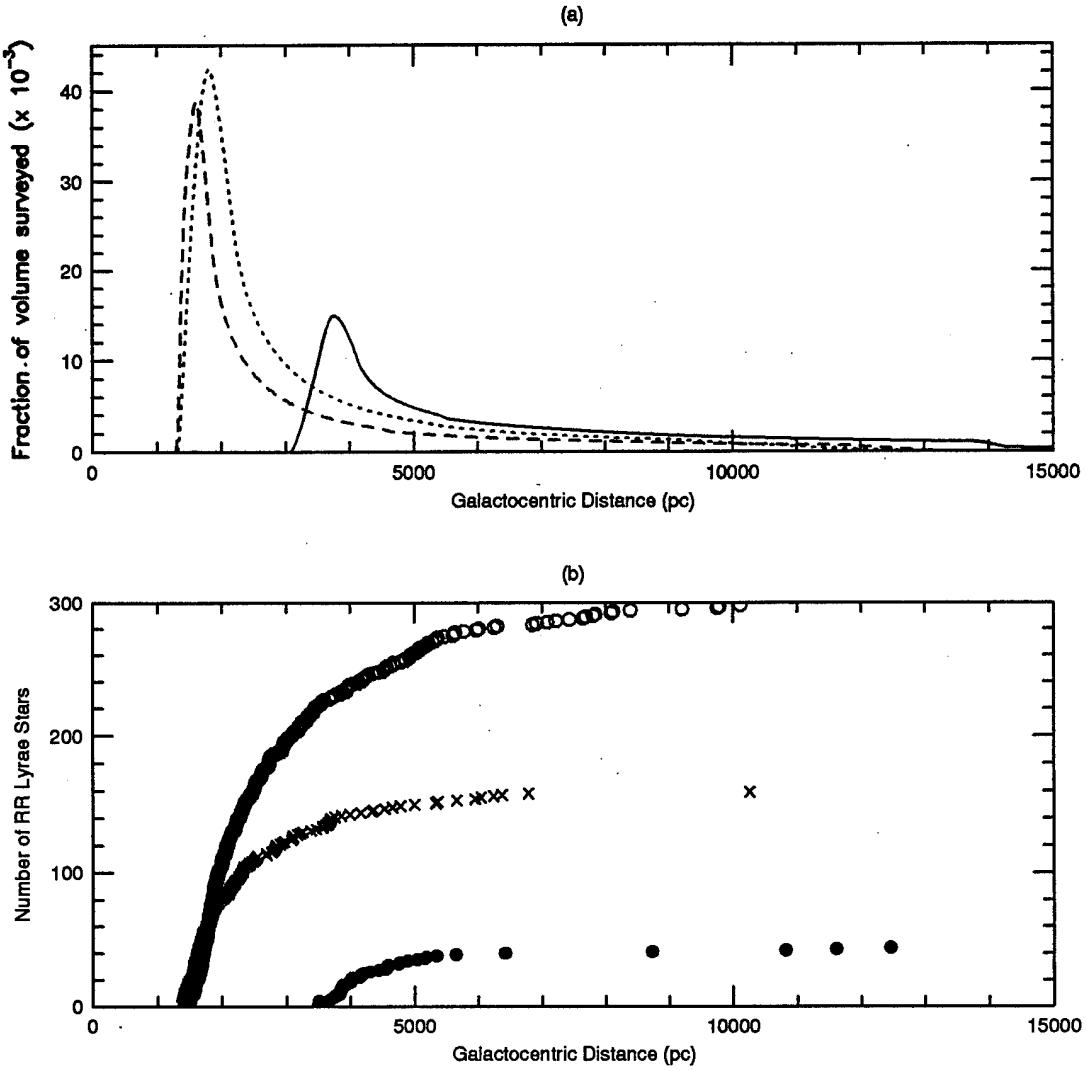


Figure 6.8 - (a) Fraction volume surveyed and (b) cumulative number of RRab stars versus Galactocentric radial distance. PG1 (solid, filled), PG2 (dotted, open) and PG3 (dashed, x's).

separately. The boundaries of fields PG2 and PG3 were modified to eliminate the region with $|b| < 10°$.

In Papers P-G1 and P-G7, the completeness as a function of amplitude and magnitude are discussed in detail. Table 3 of Paper P-G7 summarizes the results. The completeness as a

function of magnitude as outlined in Table 3 of Paper P-G7 will be used. The magnitude limits of $<m_{pg}>$ = 14 - 18.5 for fields PG1 and PG2, and $<m_{pg}>$ = 14 - 18.0 for field PG3, as detailed in the same paper, will also be used. As with the Lick survey, photographic magnitudes will be considered identical to <B>.

Only the minimum and maximum photographic magnitudes were listed for each star, and so Equation 5.2 (using the CTI values detailed in Chapter 5.5) was used to calculate a mean magnitude for each RRab type variable star.

Figure 6.8 plots (a) the fraction of space surveyed and (b) the cumulative number of RRab type variable stars as a function of Galactocentric radial distance for field 1 (solid line and filled circles), field 2 (dotted line and open circles), and field 3 (dashed line and x's).

6.2.3 Saha's RR Lyrae Survey

The 1.2-m Schmidt telescope at Palomar with 14 x 14-inch photographic plates was used to observe each field in Saha's RR Lyrae survey. The resulting fields covered an area of sky 6° 36' square. All three of Saha's fields will be considered together.

Saha describes completeness calculations in detail with the final results of completeness as a function of period shown in Figure 2 of Paper S1 (similar to Figure 5.5 of this dissertation). Using this figure for periods 0.4 to 0.7 days

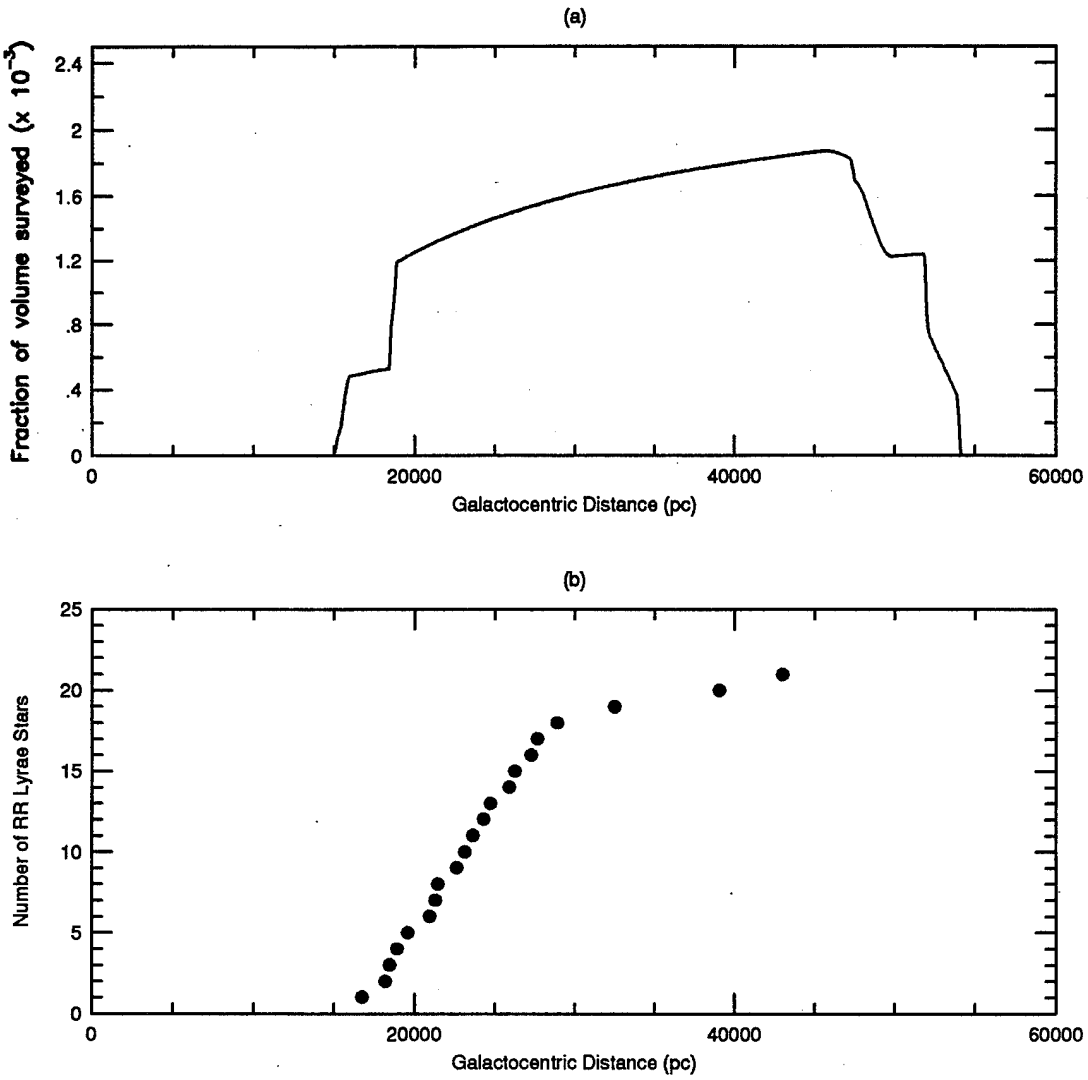


Figure 6.9 - (a) Fraction volume surveyed and (b) cumulative number of RRab stars versus Galactocentric radial distance for Saha's survey.

(as done with the CTI survey), Fields SII, SIII, and SIV are estimated to be 85%, 78%, and 73% complete respectively. The magnitude limits for all three fields are <B> = 16.5 - 19.5.

Figure 6.9 plots (a) the fraction of space surveyed and

(b) the cumulative number of RRab type variable stars as a function of Galactocentric radial distance for all of Saha's fields.

6.2.4 Hawkins' RR Lyrae Survey

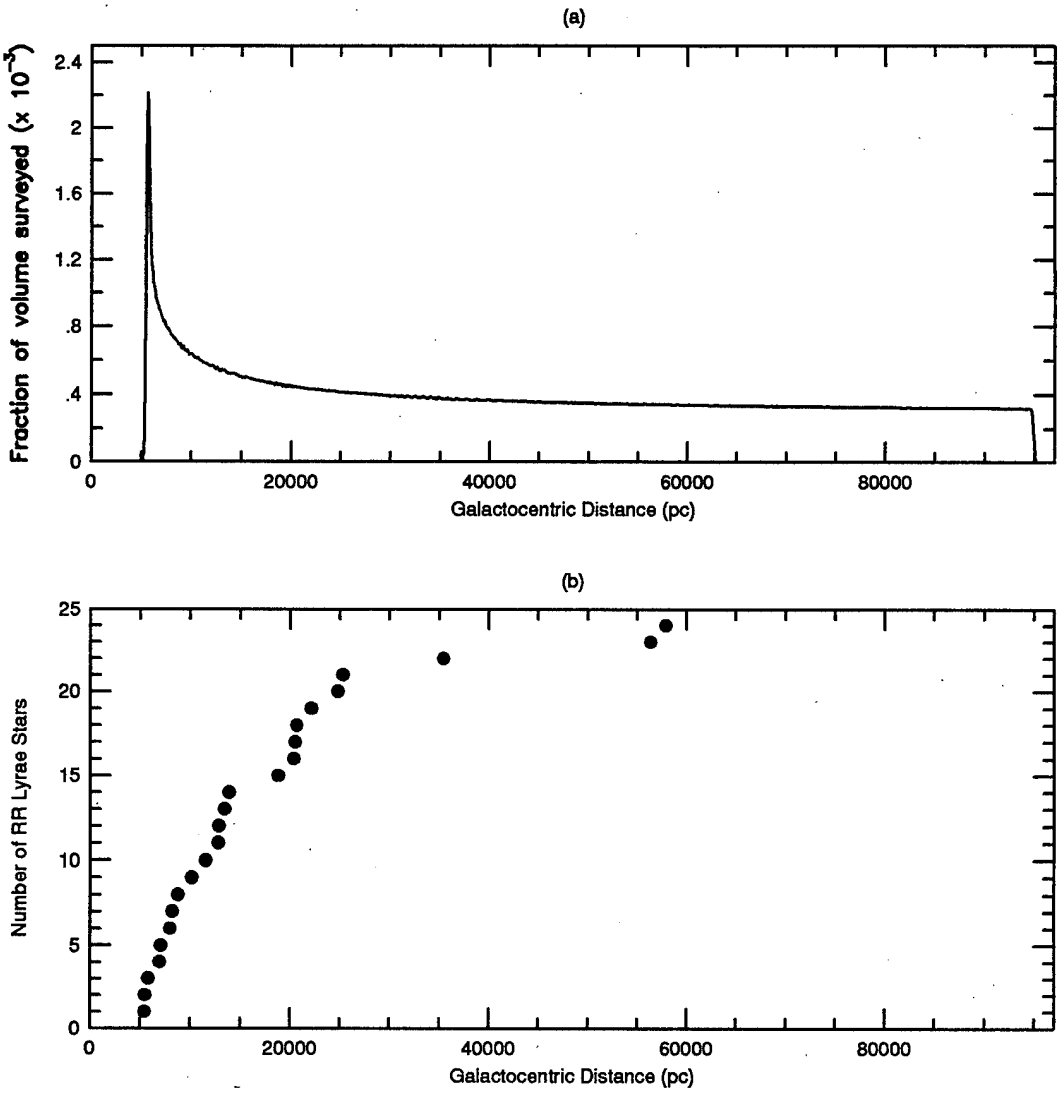


Figure 6.10 - (a) Fraction volume surveyed and (b) cumulative number of RRab stars versus Galactocentric radial distance for Hawkins' survey.

Photographic plates taken with the UK 1.2-m Schmidt telescope in Australia and scanned with the COSMOS measuring machine were used by Hawkins to detect RR Lyrae variable stars (Hawkins 1984). The magnitude limits of his survey are <B> = 14.0 - 21.0, but no discussion of completeness is given.

To estimate the completeness, the detectable fraction of RR Lyrae stars as a function of period for different amplitudes of variation was first calculated. This was done using a synthetic RRab type variable star of a particular amplitude observed at the times listed in Table 1 of Hawkins 1984, and requiring the rms variation in magnitude with the extreme data point removed to be greater than 0.2 (Hawkins' selection criteria as described in Hawkins 1984). Using the distribution of RRab type variables as a function of amplitude of variation from the RR Lyraes in the Palomar-Groningen survey as representing the true distribution (as done with the CTI survey), the completeness of Hawkins' survey is 74%.

Figure 6.10 plots (a) the fraction of space surveyed and (b) the cumulative number of RRab type variable stars as a function of Galactocentric radial distance for Hawkins' survey field.

6.2.5 Baade's Window RR Lyrae Survey

Baade's Window is a region of relatively small Galactic absorption centered on the globular cluster NGC 6522 approximately 4° from the Galactic center. Baade's original

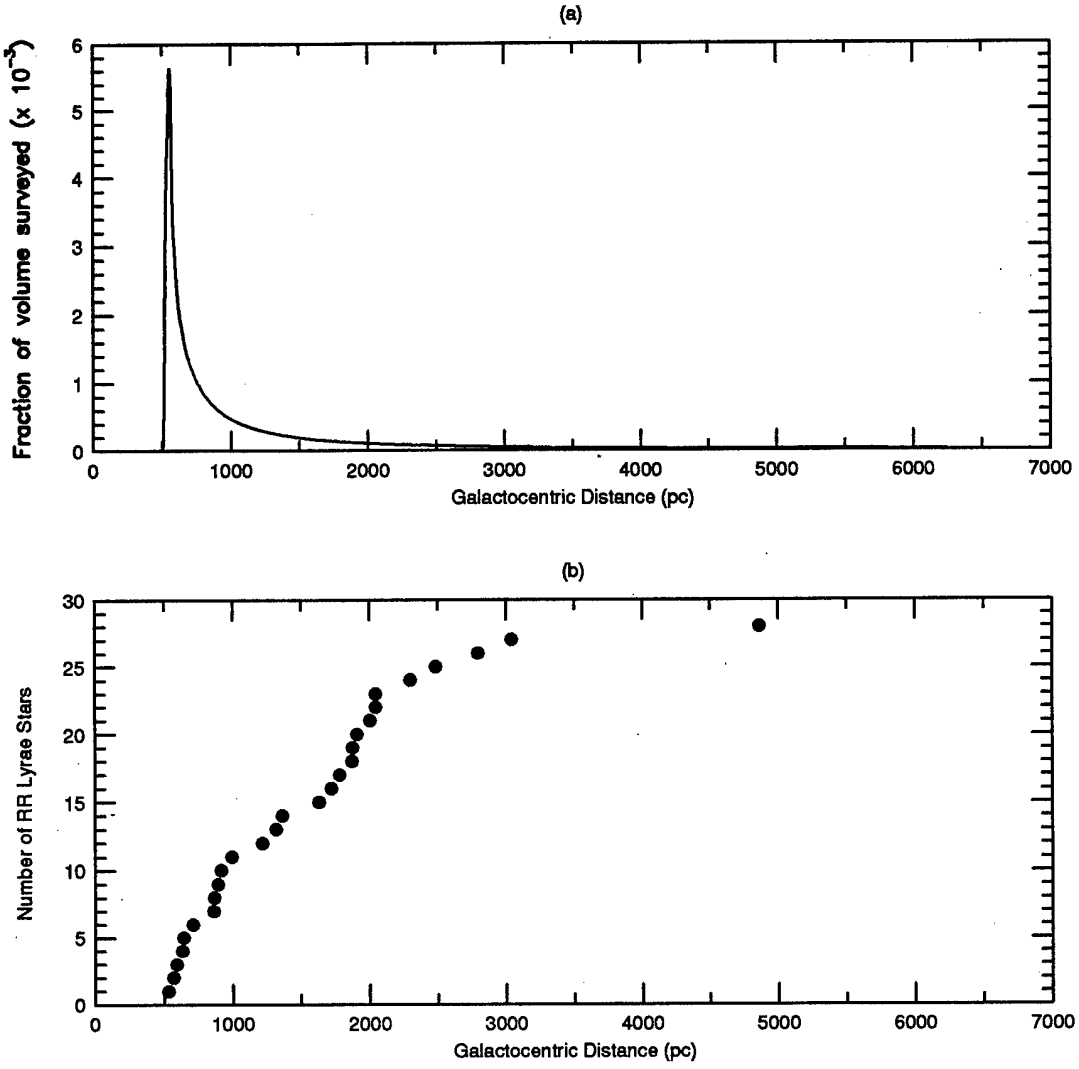


Figure 6.11 - (a) Fraction volume surveyed and (b) cumulative number of RRab stars versus Galactocentric radial distance for region W of Blanco's survey of Baade's window.

survey for RR Lyrae variable stars was from Mt. Wilson Observatory and suffered from incorrect period determinations due to period aliasing to the sidereal day. Many investigators have accomplished subsequent observations in order to redetermine the RR Lyrae periods (Blanco 1984 and

references therein). Blanco's survey was accomplished using photographic plates with the CTIO's 1.5-m telescope.

The Galactic reddening of the globular cluster NGC 6522 has been estimated at 0.45 ± 0.03 (van den Bergh 1971). Because of a possible east-west absorption gradient (van den Bergh 1971), only region W in Figure 1 of Blanco (1984), corresponding to the NGC 6522 field, is considered. Blanco (1984) gives a faint magnitude limit of <B> = 18.5, and argues that the completeness is ≈100% in light of the great deal of attention given to discovering RR Lyrae stars in this region.

Figure 6.11 plots (a) the fraction of space surveyed and (b) the cumulative number of RRab type variable stars as a function of Galactocentric radial distance for region W of Blanco's survey.

6.2.6 Local RR Lyrae Space Density

The local RR Lyrae space density, (or at least a lower limit to the local space density due to possible incompleteness), can be calculated and compared to the results obtained from the other surveys by using RR Lyrae data contained in the General Catalog of Variable Stars (GCVS) (Kholopov 1985-88). First, a list of all RR Lyrae stars in the GCVS with a minimum apparent magnitude brighter than 11.5 and greater than 10° from the Galactic plane was made. After calculating the average apparent magnitude with Equation 5.2 and estimating the Galactic reddening of each star from the

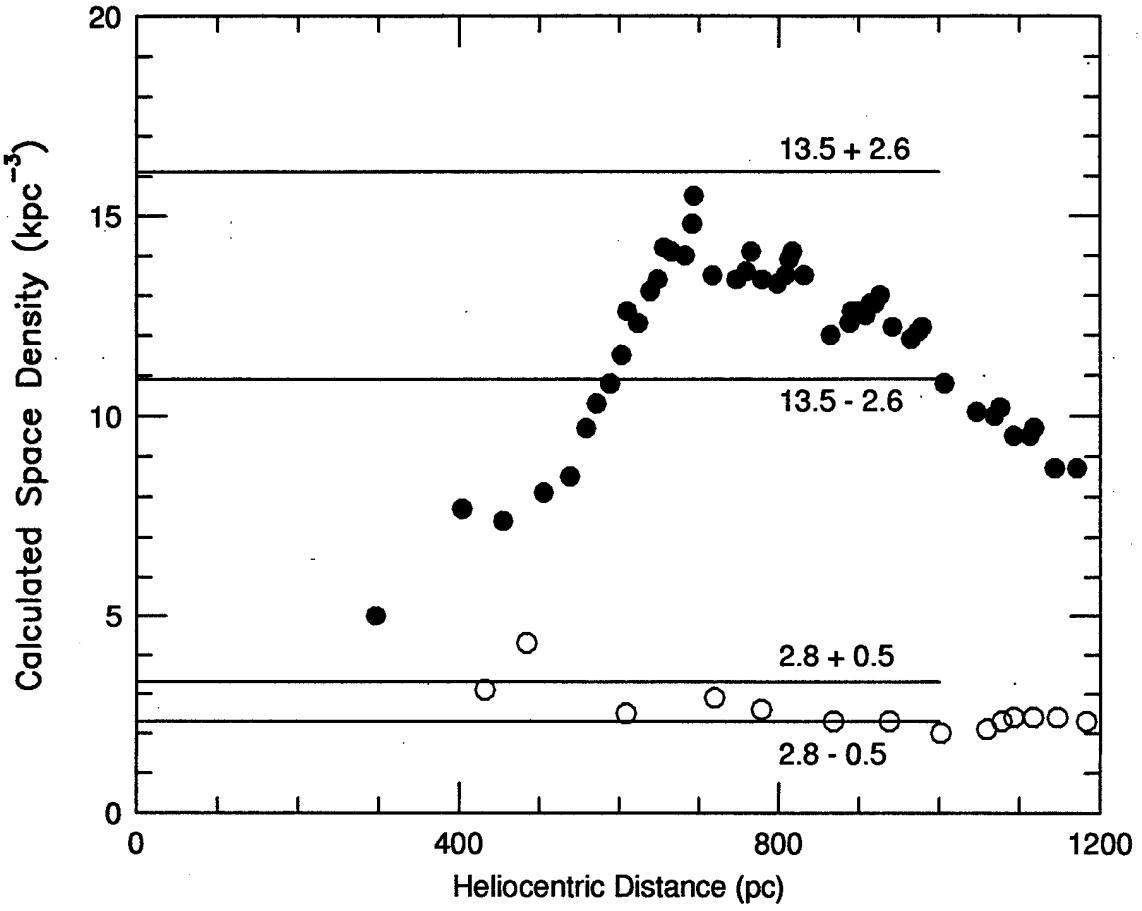


Figure 6.12 - RR Lyrae space density in kpc^{-3} versus heliocentric distance for bright RRab type variables (filled circles) and bright RRc type variables (open circles) in GCVS.

E(B-V) maps of Burstein and Heiles (1982), a heliocentric distance was calculated to each. Since the magnitudes of all these stars are listed as visual estimates in the GCVS, an absolute magnitude of $\langle M_V \rangle = 0.74$ was assumed. For each RR Lyrae, the space density was determined by dividing the number of stars interior to the RR Lyrae's heliocentric distance by the volume enclosed by the star. This was done for RRab and RRc type variables seperately. The variable star name, right

ascension, declination, type, minimum, maximum and mean magnitude, Galactic absorption, and heliocentric distance are listed in Table A1.12 of Appendix 1.

Figure 6.12 plots the calculated space density versus heliocentric distance for these bright RRab type variables (filled circles) and RRc type variables (open circles). The decreasing space density for the RRab type variables with heliocentric distances greater than 800 pc is probably due to incompleteness of the GCVS for fainter magnitudes. The local RR Lyrae space density was estimated by simply taking the number of RR Lyrae stars within 800 pc divided by the volume enclosed, resulting in 13.5 +/- 2.6 kpc^{-3} for RRab type variables, and 2.8 +/- 0.5 kpc^{-3} for RRc type variables. The error in these values was taken to be 100%/sqrt(# of stars). These values include both halo and potential "thick disk" (Zinn 1985, Suntzeff et al. 1991) RR Lyrae stars (see Chapter 6.3), and are commensurate with similar calculations in Paper L3 (10.8 kpc^{-3} for RRab using M_B = 1.0 with $\Delta B > 0.75$) and by Preston et al. 1991 (10-13 kpc^{-3} for all RR Lyrae stars using M_V = 0.6 and [Fe/H] < -1.0).

6.2.7 Miscellaneous Surveys

A few RR Lyrae surveys were not considered due to a lack of information in the corresponding paper necessary to calculate the completeness of the survey. These are a survey centered on the globular cluster NGC 6304 at l=356°, b=+5°

(Hartwick et al. 1981), a survey centered on a Galactic bulge window at l=1°, b=-6° (Blanco 1992), and a survey centered on the south Galactic cap (Stobie et al. 1986). The second survey listed also does not currently have any information concerning the Galactic reddening in the field.

6.3 RR Lyrae Space Densities

Calculations identical to those described in Section 6.1 for the CTI survey can be carried out for all the other surveys listed in Table 6.2. The different completeness of each survey was accounted for when calculating the functions f(R) and f(a) of Equations 6.5 and 6.6 respectively. The most distant space density in the Saha and Hawkins surveys correspond to most probable values determined in the same way as for the CTI survey.

To lessen the confusion, data from individual stars in each survey were divided into bins equally spaced in log(R) (or log(a)) and averaged. Figure 6.13 plots the RR Lyrae space density as a function of Galactocentric radial distance for RRab type variables in the CTI survey (open circles), Lick survey (open squares), Palomar-Groningen survey (filled triangles), Saha's survey (open triangles), Hawkins' survey (x's), Baade's Window survey (filled circles) and the local space density (filled square). The best-fit least squares linear regression for the data is

$$\log(\rho) = 12.237(0.299) - 3.024(0.077) \times \log(R) \qquad (6.8)$$

where the calculated error for the intercept and slope is given in parentheses.

Figure 6.14 plots the same data as a function of Galactocentric semi-major axis distance. Clearly, using an ellipsoidal distribution for smaller Galactocentric distances yields greater agreement among surveys. This is most

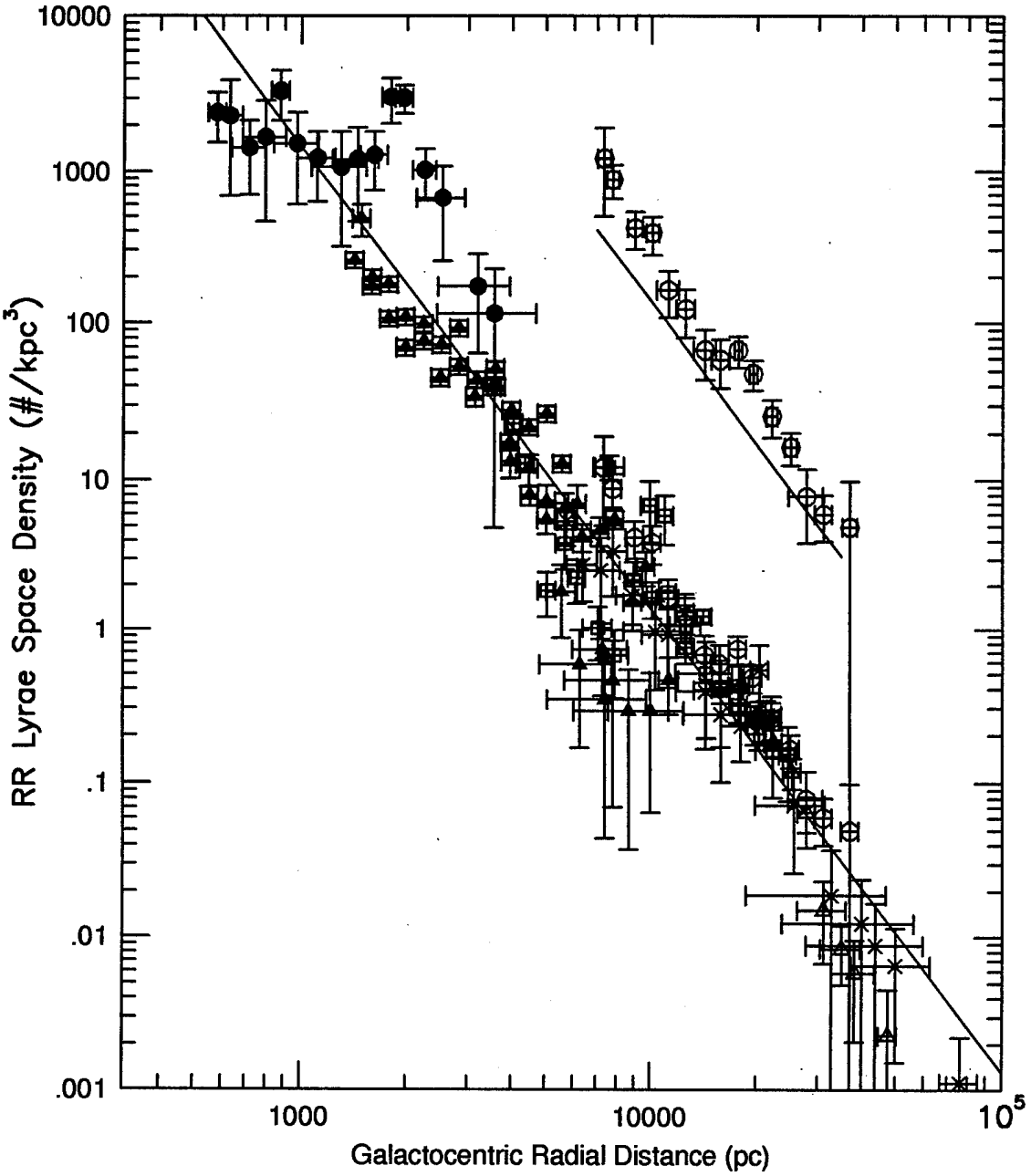


Figure 6.13 - RR Lyrae space density in #/kpc^3 versus Galactocentric radial distance for CTI survey (open circles), Lick survey (open squares), Palomar-Groningen survey (closed triangles), Saha's survey (open triangles), Hawkins' survey (x's), Baade's Window survey (closed circles) and the local space density as determined from the GCVS (open square). Solid line corresponds to best-fit linear regression. A second set of CTI survey points two orders of magnitude above actual value are also plotted for clarity.

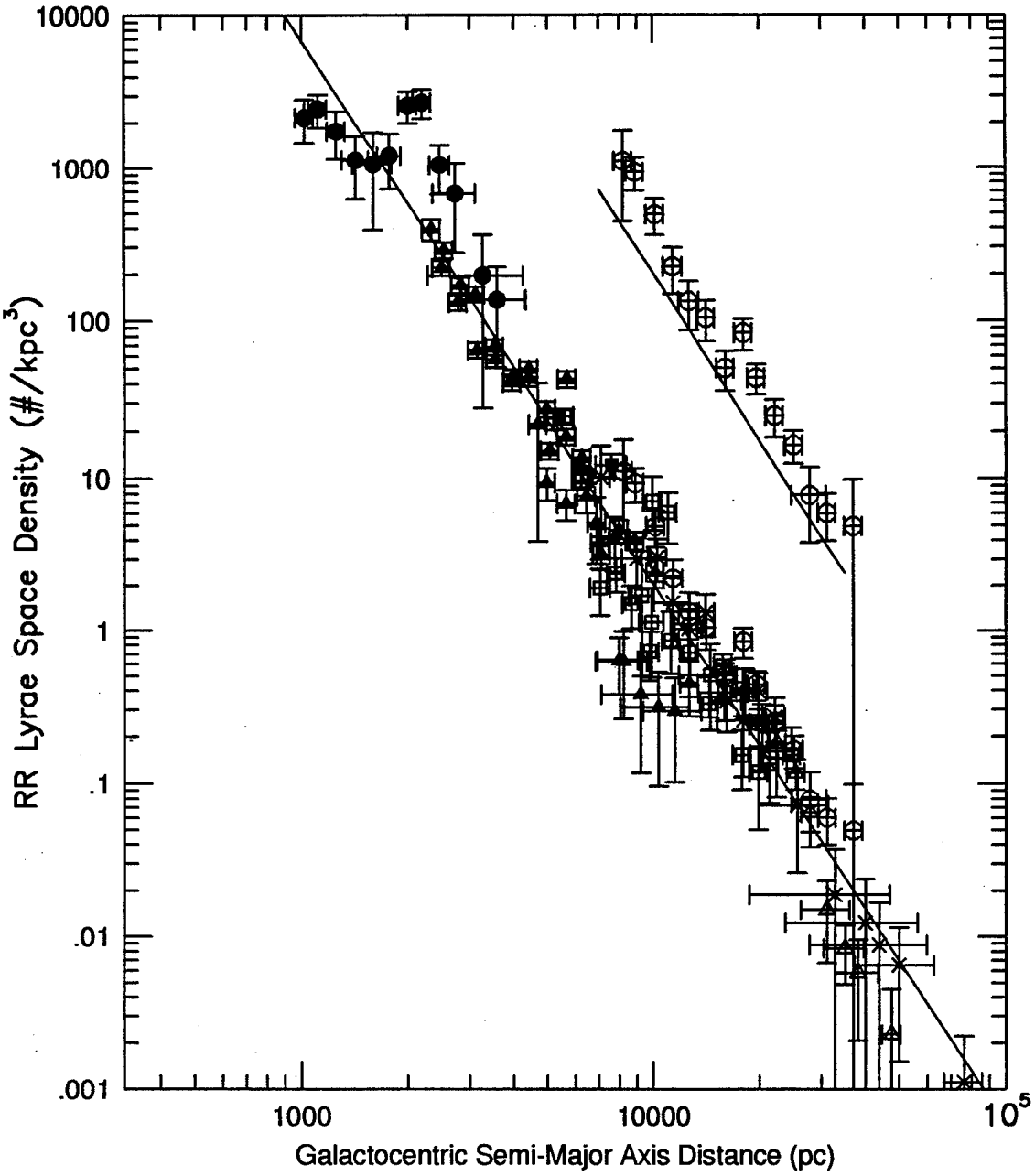


Figure 6.14 - RR Lyrae space density in #/kpc^3 versus Galactocentric semi-major axis distance for CTI survey (open circles), Lick survey (open squares), Palomar-Groningen survey (closed triangles), Saha's survey (open triangles), Hawkins' survey (x's), Baade's Window survey (closed circles) and the local space density as determined from the GCVS (open square). Solid line corresponds to best-fit linear regression. A second set of CTI survey points two orders of magnitude above actual value are also plotted for clarity.

evident between the Baade's Window and Palomar-Groningen surveys (~1-3 kpc). The best fit linear regression for this

$$\log(\rho) = 14.425(0.307) - 3.530(0.077) \times \log(a) \qquad (6.9)$$

data is

where again the calculated error is given in parentheses.

Although it is clear the mean RR Lyrae space density falls off with a power law distribution, the RR Lyrae space density does vary locally. Kinman noticed in field RR5 of the Lick survey (Paper L5), that all the RR Lyrae variable stars were concentrated on one half of the field. All the survey fields display systematic deviations from the best-fit linear regression at certain distances, suggesting a halo distribution that is clumpy, with locally overdense and underdense regions of RR Lyraes, but retaining an overall power law decrease with increasing distance.

The space densities at the Sun's Galactocentric distance (7.6 kpc) is of particular interest, spanning nearly two orders of magnitude. The local space density as calculated from the GCVS is 4.2 and 2.5 times above that expected for the spherically symmetric (Equation 6.8) and ellipsoidal (Equation 6.9) distributions respectively. If the local RR Lyrae stars are divided into halo and "thick disk" (defined as [Fe/H] > -0.8 with z < 1.5 kpc) components (Suntzeff et al. 1991), the space density of the halo RR Lyrae stars is still 3.0 or 1.8 times that expected. To explain this anomalously high value,

it has been suggested there exists a new population of metal-poor ([Fe/H] < -0.8) RR Lyrae stars with very low scale height from the Galactic disk (Preston et al. 1991). The CTI survey space density at R = 7.6 kpc (z > 4 kpc and well outside the thick disk), however, agrees well with the GCVS value, indicating that the local space density of RR Lyrae stars is not as anomalous as once thought. The space density at 7.6 kpc as calculated from Hawkins' survey and field PG2 of the Palomar-Groningen survey agree well with Equations 6.8 and 6.9, while the space densities for field RR1 of the Lick survey and fields PG1 and PG3 of the Palomar-Groningen survey are about 1/10th that expected. Because this distance roughly corresponds to the faint magnitude limits of the Lick and Palomar-Groningen fields, it's possible the measured underdensities are an artifact of incorrectly estimating the completeness as a function of magnitude. The other fields of the Lick survey and field PG2 of the Palomar-Groningen survey, however, do not show a commensurate underdensity at their faint magnitude limit. It's also possible the underdensities are caused by difficulties in discovering faint RR Lyraes in a crowded field, although again, field PG2 is very crowded and does not show an underdensity. The space density as calculated from field PG1 of the Palomar-Groningen survey even displays a flattening out and increase near its faint magnitude limit that would possibly bring it back to the best-fit line if the survey was extended to fainter magnitudes.

Although it's not possible from the present data to know for certain, the evidence suggests these deviations may indeed be real.

Another example of a significant underdensity can be found in Saha's survey beyond 25 kpc where the calculated space densities are systematically lower than the best fit power law. It is possible this underdensity is similar in origin to the underdensities found at 10 kpc, although as Saha suggested, the distribution beyond 25 kpc may be expressed by a different power law than that of the inner halo. Indeed at some distance, the space density would be expected to fall off precipitously as the effects of other galaxies begin to strip the Milky Way of its most distant members. The Large and Small Magellanic Clouds (LMC and SMC) are suggestively only twice the distance from the Galactic center as the distance where Saha's RR Lyrae space density begins to drop. The globular cluster distribution displays a similar underdensity starting at ≈20 kpc, with no globular clusters in the region 33 kpc < R < 60 kpc, again corresponding to the LMC and SMC Galactocentric distance. The globular clusters beyond 60 kpc, however, display space densities consistent with the $R^{-3.5}$ densities calculated for clusters at 4 < R < 20 kpc (Harris 1976, Zinn 1985). Due to this underdensity as well as chemical and structural differences between the distant and nearby globular clusters, Harris (1976) has even suggested that the Milky Way's globular cluster system ends at R ≈ 40

kpc and that the more distant clusters constitute a separate group perhaps related to the dwarf elliptical galaxies at similar distances. Although it's conceivable the underdensity of globular clusters and possible underdensity of RR Lyrae stars at the LMC and SMC's Galactocentric distance is the result of chance, it is equally plausible the underdensity is the direct result of a dynamical interaction. If the latter is correct, the underdensity could simply be the 1:1 resonance gap created by the Magellanic Clouds. The RR Lyrae space density as calculated from Hawkins' survey and the CTI survey do not fully support the conclusion of an RR Lyrae underdensity beyond 25 kpc. Due to the small number of RR Lyraes discovered at these distances (nine with R > 30 kpc in these surveys), however, clearly other deep surveys for RR Lyraes are needed.

Indeed, deep surveys can clear up many of the questions addressed above. Of particular interest would be extending the search for RR Lyrae variable stars in and near the RR1 field of the Lick survey and field PG1 of the Palomar-Groningen survey to see if the calculated space densities indeed return to the calculated best fit power law, or if more RR Lyraes are found to fill in the underdensity if it is indeed caused by incompleteness. As stated in the last paragraph, deeper surveys will also add to the number of stars past 25 kpc to better define the space densities at these distances. Perhaps the most promising survey would be one at

-30° declination using a CTI-like telescope. This survey would pass over Baade's Window, close to the Galactic center and Galactic south pole, providing consistent photometry and completeness over a much larger range of Galactocentric radial distances than provided by any previous survey field.

Chapter 7 Mass Distribution of the Milky Way

In the previous chapter, the Galactocentric position of each RR Lyrae variable star in the CTI RR Lyrae survey was calculated. If in addition to this positional information, the star's velocity is determined for all three dimensions, an estimation of the mass interior to the star's orbit can be accomplished.

The total energy of a star in orbit about the center of the Milky Way is simply

$$E=\frac{1}{2}mv^2-\frac{GM(R)m}{R}, \qquad (7.1)$$

where m is the star's mass, v is the star's velocity, and M(R) is the Milky Way's mass at Galactocentric distance R. If for a given star's orbit the Milky Way's mass can be approximated as being concentrated at the Galactic center, Equation 7.1 and the energy of a Keplerian orbit of given eccentricity ($E = -GMm(1 - e^2)/2R$, where e is the eccentricity of the star's orbit) can be combined and solved for M(R) giving,

$$M(R)=\frac{Rv^2}{(1+e^2)G}. \qquad (7.2)$$

With a precise knowledge of R and v, the mass of the Milky Way at the Galactocentric distance R can be calculated to within a factor of two, assuming the star is in a bound orbit with a value of e between e = 0 (circular orbit) and e = 1 (parabolic orbit).

The calculation of R from the magnitude and position of

each star was accomplished in the previous chapter. In this chapter, preliminary results calculating the space velocity for RR Lyrae variable stars will be presented. First, the possibility of using astrometry to determine the proper motion of the RR Lyrae stars relative to the local standard of rest is examined. Next, radial velocity measurements of CTI RR Lyrae stars are presented. Finally, the mass of the Milky Way as a function of Galactocentric distance as calculated using Equations 7.2 is given.

7.1 - RR Lyrae Astrometry

In addition to the photometric information compiled in the CTI databases for each star in the CTI survey strip, there exists astrometric information as well. Seasonal variance-weighted positions for a given object can be calculated using the nightly luminosity weighted positions (YCTI and XCTI), second moments (XX and YY), and calibrated luminosity and luminosity error (LUM and LUMERR), all contained in the CTI **.NHL** database.

The variance of the position in right ascension (YCTI) or declination (XCTI), however, is the second moment (XX or YY respectively) divided by the *uncalibrated* total luminosity. It was necessary to calculate the uncalibrated total luminosity from the calibrated luminosity and luminosity error. The uncalibrated luminosity and error (L and σ_L) and the calibrated luminosity and error (C and σ_C) are related through the luminosity scaling factor (dl, contained in the **.CAL** database on a minute-by-minute basis, see Chapter 3.5.2), namely, $C = dl \times L$ and $\sigma_C = dl \times \sigma_L$. Using $\sigma_L^2 \propto L$, this leads to $L \propto C^2/\sigma_C^2$, resulting in a positional variance of $\sigma_{XCTI}^2 \propto (XX \times \sigma_C^2)/C^2$. The error in the seasonal position was calculated by taking the standard deviation of the individual measurements from the calculated weighted mean added in quadrature to a measurement error of 0.5 centipixels.

Figure 7.1 plots the total positional error $(\sigma_{XCTI}^2 + \sigma_{YCTI}^2)^{1/2}$ of the seasonal position in centipixels versus

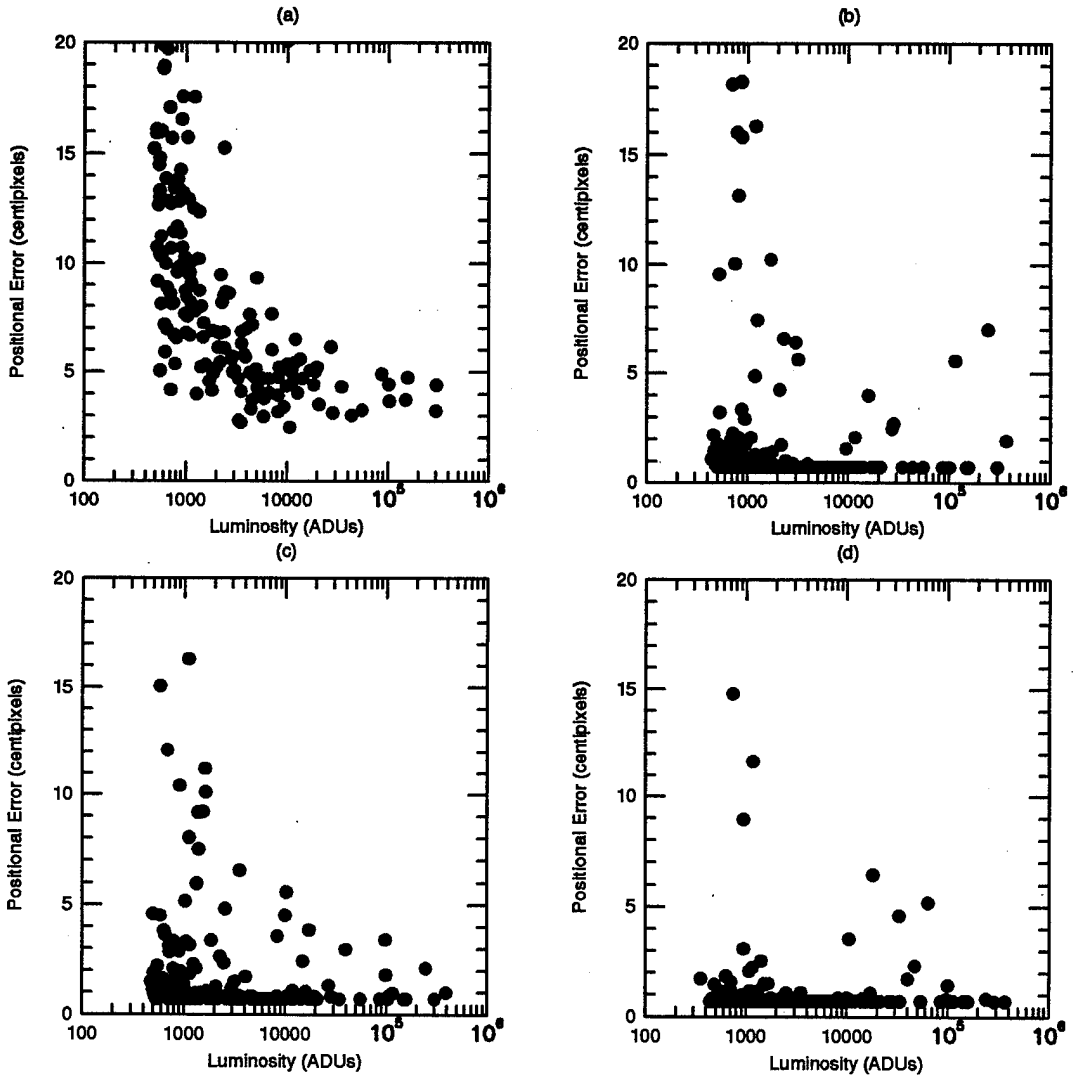


Figure 7.1 - Positional error in centipixels versus instrumental luminosity in ADUs for field near north Galactic pole. (a) 1987-1988 observing season, (b) 1988-1989 observing season, (c) 1989-1990 observing season, (d) 1990-1991 observing season.

instrumental luminosity (in ADUs) for several objects with more than one observation in a sample field for (a) the 1987-1988 observing season, through (d) the 1990-1991 observing season. As expected, the error in position decreases for

increasing luminosity. Previous astrometry with CTI (Benedict et al. 1991), using early uncalibrated CTI data reported errors commensurate with those seen in Figure 7.1(a). It is not clear why the positional calibration improved after the first full year of operation, as seen in Figures 7.1(b) through (d). A number of stars in these seasons actually show no scatter in position. Either the scatter is sub-centipixel, or the position has somehow been quantized during data reduction. An in-depth analysis of positions throughout the reduction process is required to examine this question, although is not necessary for the present purposes.

The positions of objects in the CTI Survey strip for all four seasons of CTI operation can be compared to positions obtained from the Palomar Observatory-National Geographic Sky Survey (POSS). The copies of the E and O POSS plates at the University of Texas at Austin were scanned with the McDonald Observatory PDS Microdensiomter Automated Inventory System (Benedict and Shelus 1978). The scanned image was then ported into IRAF to measure the centroids of all the stars. These measurements were kindly carried out by Dr. G. F. Benedict and associates.

The process of overlapping the CTI and POSS positional data is described in detail in Benedict et al. 1991. The program GAUSSFIT (Jeffreys et al. 1989) is used to determine simultaneously the least-squares fit of all plate parameters (scale, offset and rotation) and relative proper motions for

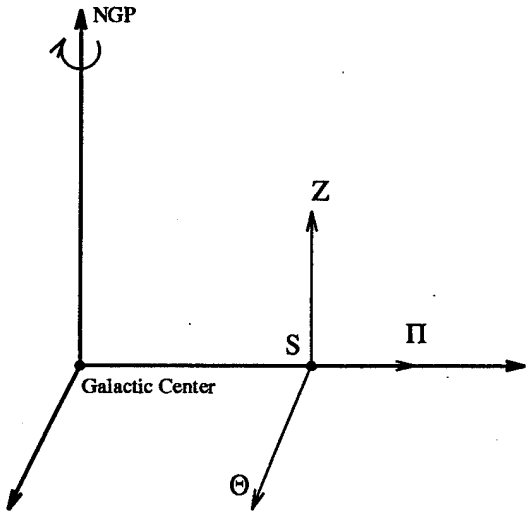


Figure 7.2 - Definition of velocity components in Galactocentric cylindrical coordinate system

all stars, where the "plates" are the four CTI positions and the two POSS positions (from the E and O POSS plates separately).

The measured relative proper motions are relative to the mean motion of the sample of stars within the field used in the calculations. If this sample is dominated by nearby disk stars, the resulting sample's space motion can be approximated by the motion of the local standard of rest (LSR). A cylindrical coordinate system centered at the Galactic center (R, θ, z), with Π, Θ, and Z the respective velocities, will be used, as shown in Figure 7.2. The LSR velocity at a given radius is defined as the velocity of a circular orbit ($\Pi = 0$, $Z = 0$, $\Theta = \Theta_0$) for an axisymmetric time-independent Galactic mass distribution (resulting in only a constant radial gravitational force). Peculiar velocities are defined as the velocities relative to the LSR ($u = \Pi - \Pi_{LSR}$, $v = \Theta - \Theta_{LSR}$, and $w = Z - Z_{LSR}$). It is the tangential component of these peculiar velocities of the RR Lyrae stars (as measured against the Sun's local standard of rest) combined with the peculiar velocity of the Sun with respect to the LSR that is measured astrometrically for each

star. It is necessary to transform to the rest frame of the Galactic center using knowledge of the space velocity of the LSR and the Sun's peculiar velocity. Many studies have been done using measured radial velocities of objects in the Galactic halo as well as external galaxies, yielding an LSR space velocity of Θ_0 = 250 ± 25 km/s (Mihalas and Binney 1981). The Sun's peculiar motion (as calculated against the most commonly measured velocities for stars in the solar neighborhood) is u = -9 km/s, v = 11 km/s and w = 6 km/s (Mihalas and Binney 1981).

The CTI field surrounding the RR Lyrae star DV Com was used to test the astrometric accuracy and precision of combined CTI and POSS data. This star was chosen because it is the brightest RR Lyrae variable star near the north Galactic pole, and a halo star near the Galactic poles represents the best chance of measuring a RR Lyrae proper motion relative to the LSR. For a Θ_{LSR} = 250 km/s, r = 6.36 kpc and assuming Θ_{halo} = 0 km/s, DV Com's relative proper motion should be ≈8 mas/year (milliarcseconds per year) directed away from b = 0°, l = 90°.

No significant relative proper motion was measured for DV Com. The standard deviation in all relative proper motions for the DV Com field was 9 mas/year (as compared to Benedict et al.'s 5 mas/year calculation). This higher value may be a result of actual relative proper motions within the field. Disk stars with peculiar velocities comparable to the Sun's

would have relative proper motions of up to 7 mas/year at 500 pc and up to 33 mas/year at 100 pc. Taking Benedict et al.'s value of 5 mas/year as the obtainable accuracy and precision for combined CTI and POSS data, the error in a space velocity measurement as a function of heliocentric distance would be $\sigma = (0.023 \times r)$ km/s where r is measured in parsecs. This corresponds to a 150 km/s error for the closest RR Lyrae in the CTI survey strip. In light of this, and the further research necessary regarding CTI position measurements, space velocity measurements from relative proper motions will not be pursued for the CTI RR Lyrae stars in this dissertation.

7.2 - RR Lyrae Spectroscopy

Several RR Lyrae stars discovered in the CTI survey were observed with McDonald Observatory's 2.7-m (f/18) telescope using the Large Cass Spectrometer (LCS) on UT 94 Oct 7 - 10 to measure radial velocities. RR Lyrae metallicity standards, (Liu and Janes 1989, Layden 1994) SW And, XX And, DX Del, RR Cet, and RR Gem were observed for future calculation of the metallicity index ΔS, and will also serve as RR Lyrae velocity standards. All RR Lyraes were observed at a phase near minimum light. The velocity standards HR-458 and HR-2047 and flux standard G191-B2B were also observed.

Because of the low throughput of the LCS, it was necessary to use a low dispersion grating (300 l/mm). Details of the instrumentation and resulting coverage of the spectra are given in Table 7.1. Every object spectra (RR Lyraes and standards) were bracketed by argon comparison lamp spectra.

The data were reduced using IRAF with the final spectra

Table 7.1 - McDonald Observatory Operating Parameters

Telescope: McDonald Observatory's 2.7-m
f/18
Instrument: Large Cass Spectrometer
Detector: TI1V5C
800 x 800 x 15 μm pixels
15 e^- readout noise
Grating: #40 (1st order)
300 l/mm
420 nm blaze
Wavelength coverage: 320 - 600 nm
Dispersion: 0.3379 nm/pixel
Slit width: 1 arcsecond

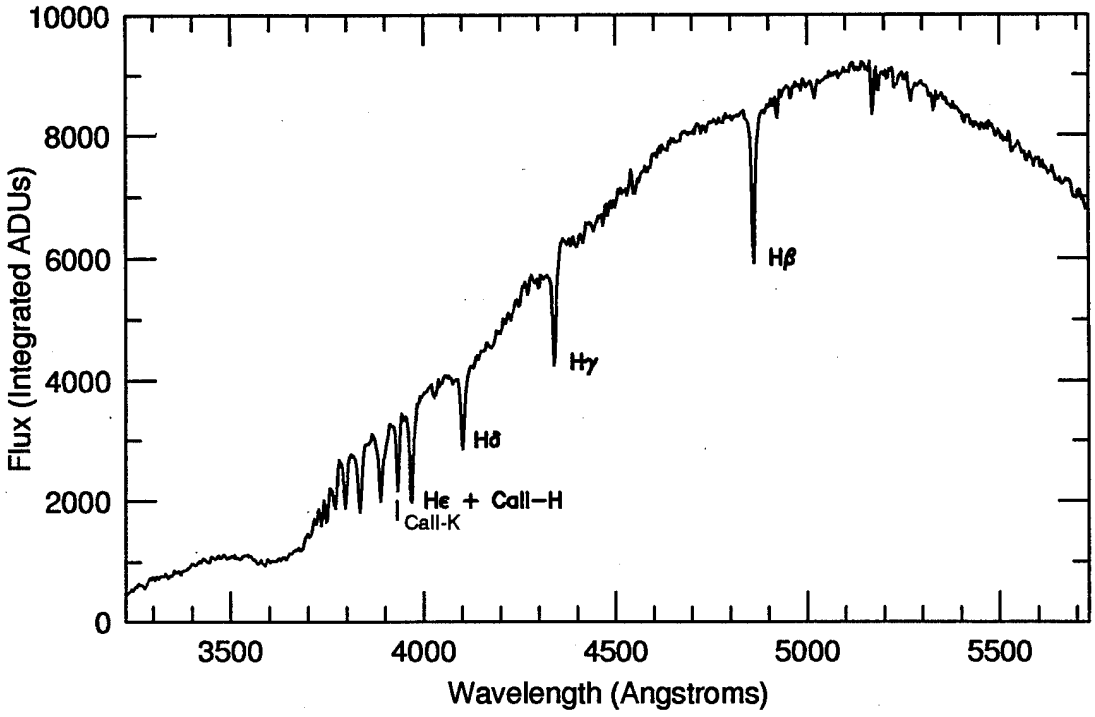


Figure 7.3 - Flux (arbitrary units) versus wavelength for RR Lyrae metallicity standard star XX And.

collapsed to one dimension. The reduction process included bias subtraction, application of flat field, distortion correction and wavelength calibration using the argon comparison lamp spectra, and sky subtraction. Figure 7.3 gives an example of an RR Lyrae spectrum (not corrected for atmospheric extinction and not flux calibrated).

The radial velocities of the RR Lyrae stars from these low resolution spectra can be determined by finding the wavelength centers of the hydrogen and CaII K lines. However, because the hydrogen and metal lines originate from different altitudes in the star's atmosphere, only the hydrogen lines

were used. The regions surrounding Hβ, Hγ, and Hδ of each spectrum were cross-correlated with the spectra of SW And, RR Cet and DX Del, producing relative velocity measurements between each star's spectrum and the templates. For all RRab type variable stars, the center-of-mass velocity (v_{cm}) and heliocentric velocity at a particular phase ($v(\phi)$) can be determined from one another if $v(\phi)$ is measured in the phase interval ≈0.15 - 0.85 (Saha and Oke 1984). By examining the radial velocity curves for X Ari (Oke, Giver, and Searle 1962) and SU Dra (Oke 1966), the center-of-mass velocity can be calculated using

$$v_{cm}=v(\varphi)+b\times(\varphi-a) \qquad (7.3)$$

where b and a are empirically determined constants. For the Hγ spectral line in the above two radial velocity curves, a = 0.44 ± 0.03 and b = -104 ± 4 km/s. Published values of v_{cm} for SW And, RR Cet and DX Del (Layden 1994) and the observation times were used to calculate $v(\phi)$ for the template spectra. The measured relative velocities for all other stars were then converted to heliocentric velocities and averaged, and using Equation 7.3, the center-of-mass velocities were determined. The error in the heliocentric velocities was taken to be the standard deviation of the calculated values. Table 7.2 lists the heliocentric radial velocity, radial velocity error and phase, and the resulting center-of-mass radial velocity and error for the observed stars. The SW And, RR Cet and DX Del spectra were not cross-correlated with themselves, so the

listed center-of-mass velocity is that determined from cross-correlation with the other two. The values listed for SW And and DX Del also represent the average of two spectra.

Table 7.2 - Center-of-mass velocity measurements

#/name	v_{hel}	σ_v	ϕ	v_{cm}	σ_v
5	-62	27	0.59	-77	27
11	61	27	0.45	60	28
36	-368	25	0.31	-354	25
39	-358	30	0.56	-371	30
42	-265	25	0.56	-277	25
51	-200	23	0.58	-215	23
57	-288	28	0.51	-295	28
58	-246	27	0.27	-229	27
66	-368	30	0.29	-352	30
68	-299	29	0.55	-311	29
69	-110	28	0.38	-103	29
SW And	60	9	0.81	21	10
RR Cet	-118	25	0.35	-108	25
DX Del	-30	29	0.59	-45	30

The metallicity standards XX And and RR Gem were also observed, but due to an error in predicting the phase of observation, these stars were observed during the ascending part of their light curve or at maximum light (phase between 0.9 to 0.1). The measured velocities for SW And, RR Cet, DX Del, and HR 458 agree reasonably well with the published values, with the differences consistant with σ = 32 km/s. The measured velocity for HR 2047, however, is 60 km/s off.

7.3 Galactic Mass versus Radial Distance

With only radial velocity measurements, the Galaxy's mass interior to a particular orbit can't be determined on a star-by-star basis. The radial velocities of a collection of stars at a particular Galactocentric radial distance must be used to make this estimate. Equation 7.2 thus becomes

$$M(R) = \frac{R\langle v^2 \rangle}{G(1+\langle e^2 \rangle)}. \qquad (7.4)$$

Certain assumptions must be made about the types of orbits in order to calculate the total space velocity from the observed heliocentric radial velocity.

The kinematics of a collection of halo RR Lyrae stars can be described by systemic motion in each dimension (V_R, V_θ, and V_ϕ for R, θ and ϕ in Figure 6.1) and the average square of the peculiar motion in each dimension ($\langle v_R^2 \rangle$, $\langle v_\theta^2 \rangle$, and $\langle v_\phi^2 \rangle$). The systemic velocities can be measured directly by taking the average radial velocity for a number of RR Lyrae stars at particular Galactic coordinates. For example, V_R can be calculated using heliocentic radial velocities for stars towards the Galactic anticenter (see Saha 1985). Currently, however, the detected systemic motion of halo RR Lyrae variable stars has been of the order of or less than the error in the measurement. It will thus be assumed that $V_R = V_\theta = V_\phi = 0$. If the RR Lyrae orbits are distributed isotropically, then the average of the three peculiar velocity components squared are equal ($\langle v_R^2 \rangle = \langle v_\theta^2 \rangle = \langle v_\phi^2 \rangle$). In this situation,

the measurement of one component of the space velocity, on average, would equal the space velocity divided by the square root of 3. Since the averaging is over the velocity squared, the high velocity RR Lyrae stars at a given distance have the largest leverage in determining the mass. Errors in these velocities could dramatically increase the mass estimate. To allow for velocity errors, the average of $(v+\sigma)(v-\sigma)$ will be used instead of v^2 (Lynden-Bell et al. 1983). The average total space velocity squared for N RR Lyrae stars is then

$$\langle v^2 \rangle = \frac{3}{N} \sum_{i=1}^{N} (v_r^2 - \sigma_v^2)_i \qquad (7.5)$$

where v_r is the heliocentric radial velocity corrected for the Sun's motion about the Galactic center and σ_v is the corresponding error. For isotropic orbits, all eccentricities are equally probable, so $\langle e^2 \rangle$ will be taken to be

$$\langle e^2 \rangle = \int_0^1 e^2 de = \frac{1}{3} \qquad (7.6)$$

If the RR Lyrae stars instead have radial orbits ($\langle v_R^2 \rangle >> \langle v_\theta^2 \rangle \approx \langle v_\phi^2 \rangle$), $\langle v_R^2 \rangle$ (and thus $\langle v^2 \rangle$) can be easily calculated from the heliocentric radial velocity measurements and knowledge of each star's Galactocentric position (see Figure 6.1) using

$$\langle v^2 \rangle = \frac{1}{N} \sum_{i=1}^{N} \frac{(v_r^2 - \sigma_v^2)_i}{\cos^2 \beta_i}, \qquad (7.7)$$

where β is the angle subtended by the Sun and the Galactic

center as seen from the RR Lyrae star. The average eccentricity squared will be taken to be $\langle e^2 \rangle = 1$ for radial orbits. For both cases, Equation 7.4 can now be used to estimate the Galaxy's mass interior to the average Galactocentric radial distance. It is interesting to note that for large Galactocentric distances, $\cos(\beta)$ approaches 1 resulting in $\langle v^2 \rangle_{isotropic} = 3 \times \langle v^2 \rangle_{radial}$ and $M(R)_{isotropic} = 4.5 \times M(R)_{radial}$.

Other methods for determining the mass of the Galaxy from the dynamics of halo objects are similar to the one described above, but not identical. Hartwick and Sargent (1978) approximated globular clusters as a collisionless spherically symmetric system of mass points and used the collisionless Boltzmann equation to derive the mass. The resulting equation is

$$M(R) = \frac{R\langle v_r^2 \rangle}{G} \left[-\frac{d\ln\rho(R)}{d\ln R} - \frac{d\ln\langle v_r^2 \rangle}{d\ln R} + (\lambda - 2) + \frac{V_\varphi^2}{\langle v_r^2 \rangle} \right], \quad (7.8)$$

where $\rho(R)$ is the globular cluster space density, $\lambda = (\langle v_\theta^2 \rangle + \langle v_\phi^2 \rangle)/\langle v_R^2 \rangle$ ($\lambda = 0$ for radial orbits and $\lambda = 2$ for isotropic orbits), and V_ϕ is the systemic rotation. Saha (1985) used a similar equation for a sample of RR Lyrae variable stars. Lynden-Bell et al. (1983) derived a mass formula to use with globular cluster radial velocities by time averaging the radial distance times the square of the radial velocity observed from the focus over one orbit. The Galaxy's mass interior to the orbit was approximated as a point mass. The

resulting equation is

$$M(R) = \frac{2\langle R(v_r^2 - \sigma_v^2)\rangle}{G\langle e^2\rangle}, \qquad (7.9)$$

where it is implicitly assumed that the average heliocentric radial velocity corrected for the Sun's motion is a good approximation to the average radial velocity measured from the focus of the orbit. Other investigators of globular cluster and dwarf elliptical galaxy dynamics (Peterson 1985, Olszewski et al. 1986) have also used Equation 7.9 to estimate the mass of the Galaxy. Little and Tremaine (1987) devised an entirely different method employing Bayes' theorem with an assumed point potential, later used by Zaritsky et al. (1989). Mass estimates using this method are nearly identical to those using Equations 7.8 or 7.9. Finally, Kulessa and Lynden-Bell (1992) employed a maximum likelihood method with results indicating a massive dark halo. The Galactic mass estimates for the dynamical studies described above are shown in Figure 7.4. Open and closed symbols indicate masses calculated assuming isotropic and radial orbits respectively. All studies, including Frenk and White's (1980) study testing kinematical models of the globular clusters in the inner and outer Galactic halo against observational data, have concluded a massive dark halo exists in the Milky Way.

The radial velocity measurements for the CTI RR Lyrae stars were divided into two groups corresponding to Galactocentric radial distance. This was also done for those

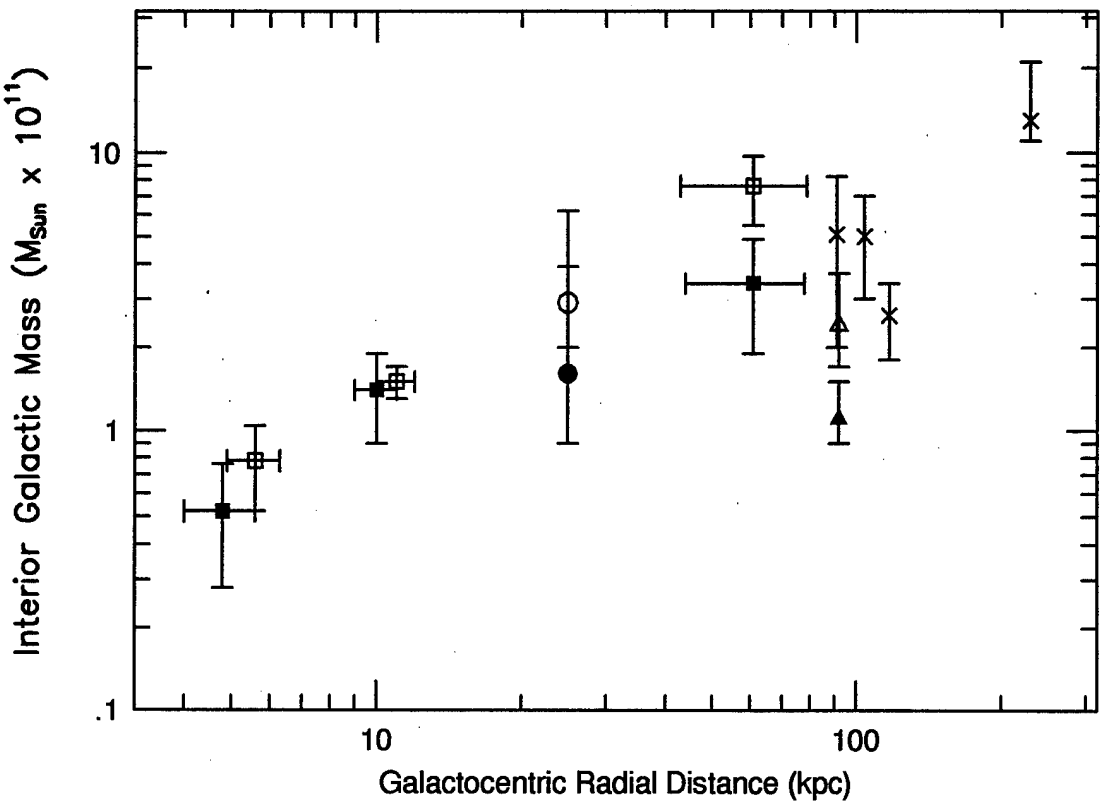


Figure 7.4 - Interior Galactic mass versus Galactocentric radial distance. Hartwick and Sargent 1978 (squares), Lynden-Bell et al. 1983 (x at 120 kpc), Peterson 1985 (x at 90 kpc) Saha 1985 (circles), Olszweski et al. 1986 (x at 100 kpc), Little and Tremaine 1987 (triangles), Zaritsky et al. 1989 (diamonds), and Kulessa and Lynden-Bell (x at 230 kpc).

stars with radial velocity measurements in Saha's (Saha and Oke 1985, Saha 1985) and Hawkins' (Hawkins 1984) RR Lyrae surveys. The two most distant stars in Hawkins' survey were not included due to their isolation from the rest. One of these stars is reported to have a very large radial velocity, and if it is assumed this star is bound to the Galaxy, requires a Galactic mass at 60 kpc of over 1.5 × 10^{12} M_{Sun}

(Hawkins 1983). The bright RRab-type stars in the GCVS with velocity measurements (Layden 1994) were used to calculate the mass interior to the Sun's orbit. Additionally, radial velocities for 38 distant globular clusters in four distance ranges and 9 distant dwarf elliptical galaxies in two distance ranges were used to calculate the mass of the Galaxy using the identical method as for RR Lyrae stars. The velocity and distance data for the globular clusters and dwarf elliptical galaxies are those listed in Table 1 of Kulessa and Lynden-Bell's (1992) study, except for Pal 15 (Peterson and Latham 1989) and Eridanus, Pal 14, Leo I, and Leo II (Zaritsky et al. 1989). The velocity errors for the other objects were obtained from the original papers (Webbink 1981, Lynden-Bell et al. 1983, Peterson 1985, Hesser et al. 1986, Armandroff and DaCosta 1986, Olszewski et al. 1986). Figure 7.5 plots the calculated mass versus Galactocentric radial distance assuming (a) isotropic orbits and (b) radial orbits. The error in the average radial distance is the standard deviation of the distances of the individual RR Lyrae stars, globular clusters, or dwarf elliptical galaxies. The error in the calculated average space velocity was calculated using 100% / sqrt (# of objects). The upper and lower error bars for the mass were calculated using $(\sqrt{\langle v^2 \rangle} + \sigma_v)^2$ and $(\sqrt{\langle v^2 \rangle} - \sigma_v)^2$ in Equation 7.4 respectively. Also plotted is the expected mass as a function of distance if the mass is proportional to the space density of RR Lyrae stars (Equation 6.8), pinned to a mass derived at

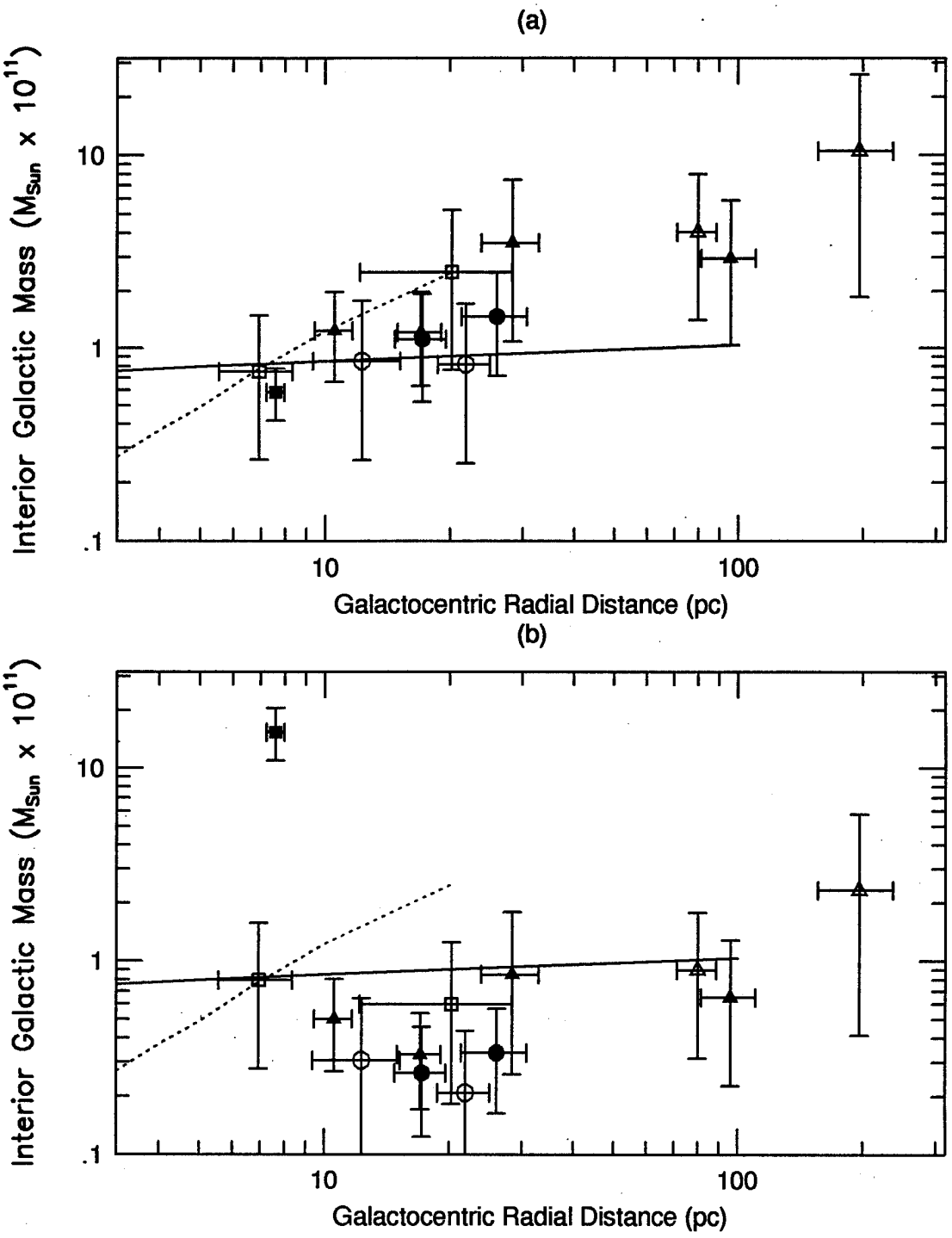


Figure 7.5 - Interior Galactic mass versus Galactocentric radial distance for (a) isotropic orbits and (b) radial orbits. CTI (open circles), Saha (filled circles), Hawkins (open squares), GCVS (filled square), globular clusters (filled triangles), dwarf elliptical galaxies (open triangles) data shown. Expected mass as derived from Equation 6.8 shown as solid line. Expected mass as derived from HI rotation curve shown as dashed line.

the Sun's distance using Θ_{LSR} = 250 km/s (solid line), and the mass as calculated from the HI rotation curve of the Milky Way assuming circular orbits (dashed line, Merrifield 1992). The solid line in Figure 7.5 assumes the mass of the entire Galaxy (both halo and disk) is described by a single power law distribution. This of course may become a very poor approximation for decreasing Galactocentric distances.

The large error bars are due to the fact that the radial velocities of 3 (farthest dwarf elliptical point) to 15 (closest globular cluster point) objects were used to calculate all of these masses except the GCVS point. For isotropic orbits, all the RR Lyrae data and the nearby globular clusters (R < 25 kpc), are consistent with a mass distribution traced by the RR Lyrae distribution in the outer halo (i.e. no dark matter necessary). The more distant globular clusters, the dwarf elliptical galaxies, and the HI rotation curve, however, are consistent with a mass distribution requiring a massive dark halo. This of course assumes these distant globular clusters and dwarf elliptical galaxies are bound to the Milky Way, and the mass of the Galaxy can be calculated from the HI rotation curve by assuming circular orbits. For radial orbits, the distant globular clusters and dwarf elliptical galaxies are now more consistent with a near constant interior mass. The calculated masses from the RR Lyrae radial velocities are also approximately one-fourth that calculated assuming isotropic

orbits, except for the GCVS data point. The large mass calculated for this point indicates that radial orbits are not appropriate for these stars. The low mass for the Galaxy (less than the mass interior to the Sun's orbit) determined for the other RR Lyrae stars and the inner globular clusters indicate that radial orbits are probably not appropriate for these objects as well.

Depending on the type of orbits assumed, the radial velocity data for RR Lyrae stars, globular clusters, and dwarf elliptical galaxies can be used to support the notion that a massive dark halo exists (i.e. the mass-to-light ratio increases for increasing Galactocentric distance), or that no excessive dark matter exists at all in the Galaxy (i.e. the mass-to-light ratio is constant). The latter argument requires that the orbits for objects with $R < 25$ kpc are isotropic while the orbits for objects with $R > 25$ kpc are predominantly radial. Additionally, some other explanation for the HI rotation curve would need to be found.

Some have claimed that the orbits of globular clusters and dwarf elliptical galaxies in the distant Galactic halo are actually more circular (Lynden-Bell et al. 1983). They argue that globular clusters and dwarf elliptical galaxies with central densities typical with these systems and on highly eccentric orbits do not survive their perigalactic encounter due to tidal disruption, leaving intact the systems in the outer halo with near circular orbits. This would support a

massive dark halo if these objects were indeed bound to the Milky Way. As discussed in the previous chapter, however, these distant globular clusters and dwarf elliptical galaxies might constitute a distinct population (R > 40 kpc) completely separate from the Milky Way's globular clusters (Harris 1976). This population, although perhaps bound to the Local Group, may not be bound to the Milky Way at all. Indeed, the dynamics of this group may be described well by radial orbits as the objects fall into the Milky Way's gravitational potential, perhaps for the first time.

Whereas the number of globular clusters available to make mass estimates of the Milky Way is nearly complete, a large number of known and yet to be found RR Lyrae stars exist in the distant Galactic halo. By combining radial velocity data from many surveys and increasing the number of RR Lyrae stars with radial velocity measurements, the error in the mass for all distances in Figure 7.5 can be decreased. In addition to discovering and observing spectroscopically more distant RR Lyrae variable stars to extend the mass estimates to larger radial distances, RR Lyrae variables in the inner halo and nuclear bulge could be sampled as well. The mass function, independent of the HI rotation curve, could then be calculated for a large range of Galactocentric distances.

This dissertation has used a unique sample of RR Lyrae stars to estimate their space density and to derive a mass for the Milky Way. Our dynamical results do not require a massive

dark halo. It is clear that additional work is necessary on several fronts, including the dynamics of Galactic stars and stellar systems, the Galactic HI rotation curve, and the distribution of stellar populations, to arrive at a robust, rationalized estimate of the mass distribution of the Milky Way.

Appendix 1 - Tables

Table A1.1 - CTI Observing Log

Key
  filters:
    B - Johnson B
    V - Johnson V
    R - Johnson R
    I - Johnson I
    C - UV transparent clear
    A - H-alpha on
    O - H-alpha off
  codes:
    * - Merged into current .**NML** and .**NHL** databases (B and V filters), calibrated, but not merged (R and I filters)
    ** - Merged into current .**MAS** and .**HIS** databases, and .**NML** and .**NHL** databases

Date	Dayno	CCD0	CCD1	Comments
84dec09	-23	I	V	test of sky
84dec10	-22	I	V	Cirrus at start, marginal night
85jan04	4	R	V	
85jan17	17	R	V	
85feb06	37	I	V	mostly clear with light cirrus to NW
85feb07	38	R	V	Clear with cirrus to NW at sunset
85feb13	44	B	V	
85mar18	77	-	V	light cirrus at sunset, CCD0 in for repair
85mar19	78	-	V	Closed due to high winds
85may18	138	?	?	some clouds
85may19	139	?	?	
85may20	140	?	?	moderate cirrus, extremely marginal
85may21	141	?	?	
85may22	142	?	?	
85may26	146	?	?	
85jun18	169	?	?	worked on dewar rotation
85jun19	170	?	?	light clouds at sunset, clouds later
85jun20	171	?	?	
85jun21	172	?	?	light cirrus to SW at sunset, marginal data
85jun27	178	?	?	Clear
85jun28	179	?	?	light cirrus throughout night
85aug14	226	R	V	poor seeing
85aug15	227	R	V	
85aug16	228	?	?	

Table A1.1 - CTI Observing Log (continued)

Date	Dayno	CCD0	CCD1	Comment
85aug23	235	?	?	Close to photometric
85sep05	248	?	?	Very windy, rest of mountain closed, high variable background
85sep13	256	?	?	Clear and calm
85sep22	265	?	?	Cirrus early, bad seeing, clear later
85sep23	266	?	?	Clear, beautiful night
86mar01	425	?	?	Clouds, close early due to clouds
86mar06	430	?	?	Clear, late start, calm
86mar08	432	?	?	much cirrus
86mar09	433	?	?	Very cloudy, no data acquired
86mar20	444	?	?	photometric
86mar21	445	?	?	photometric, high background
86apr04	459	?	?	Clear and calm, some dust
86apr05	460	?	?	Clear, photometric, may have cirrus in early A.M.
86apr10	465	?	?	Clear,photometric, some cirrus in west
86apr17	472	?	?	windy, cleared late, photometric
86apr18	473	?	?	photometric, thick clouds
86apr20	475	?	?	Clear
86may10	495	?	?	photometric, clear and calm
86jun10	526	?	?	Clear photometric, try to realign telescope
86jun11	527	?	?	photometric
86jun14	530	?	?	Clear and calm
87may20	870	?	?	TROUBLE
87may23	873	?	?	flashlight at start, data screwed up
87may24	874	V	R	photometric
87may25	875	?	?	Cirrus, close early due to clouds
87may27	877	?	?	
87may28	878	?	?	photometric
87jun08	889	?	?	Clear, possibly photometric
87jun17	898	?	?	Clear
87jun19	900	B	V	photometric
87jun27	908	?	?	warm night
87jun28	909	?	?	photometric
87jun29	910	?	?	windy and photometric
87jun30	911	?	?	photometric
87jul03	914	?	?	
87jul07	918	?	?	warm, fans on all night
87jul09	920	?	?	telescope moved
87jul14	925	?	?	Clouds on horizon, clear overhead, close early due to clouds
87sep28	1001	I	V	dewar pumped, filters cleaned, variable clouds all night
87sep29	1002	I	V	Clear at start, some clouds in morning

Table A1.1 - CTI Observing Log (continued)

Date	Dayno	CCD0	CCD1	Comment
87oct17	1020	R**	V**	Clear
87oct04	1007	O	A	Clear and photometric all night, refocused for H-alpha filters
87oct05	1008	O	A	Clear
87oct06	1009	O	A	Clear, large gradients in data, closed early due to WWVB error
87oct12	1015	I	V	light cirrus throughout night
87oct15	1018	I	V	Clear all night, power supply on DMC crapped out
87oct16	1019	R	V	partly cloudy all night, use with caution
87oct18	1021	R**	V	Clear
87oct20	1023	B**	V**	photometric
87oct21	1024	B	V	Clear, clouds in morning
87nov09	1043	I	V	Clear, no data
87nov10	1044	I	V	Clear, maybe problem with data due to computer
87nov11	1045	I	V	light cirrus, first use of MgFe coating on filters
87nov12	1046	I	V	light cirrus,
87nov13	1047	I	V	Clear, occasional light cirrus
87nov15	1049	R	V	Clear
87nov16	1050	R*	V**	Clear
87nov17	1051	R	V	Clear, no good data
87nov20	1054	R	V**	Clear, windy, poor seeing
87nov21	1055	R*	V**	Clear, cirrus in morning
87nov22	1056	B	V*	Clear, technical problems
87nov23	1057	B	V	technical problems
87nov25	1059	B	V	Clear
87dec09	1073	A	O	Clear
87dec11	1075	O	A	photometric, changed focus
87dec12	1076	O	A	Clear
87dec22	1086	B*	V**	Clear, maybe photometric
87dec23	1087	B	V*	Clear, windy
87dec28	1092	R	V	Clear, clouded out at end
87dec29	1093	R	V	Cirrus
88jan07	1102	I	V	Clear, cirrus at end, telescope turned off incorrectly
88jan10	1105	I	V	Clear, maybe photometric
88jan11	1106	I	V	Clear, maybe photometric
88jan22	1117	B	V	Clear, technical problems
88jan24	1119	B**	V**	Clear, maybe photometric, use caution
88jan25	1120	B	V**	Clear
88jan26	1121	R*	V**	Clear, light cirrus
88feb01	1127	R	V	Clear,
88feb08	1134	R	V	Clear, technical problems, no data
88feb15	1141	B	V	Clear, maybe photometric

Table A1.1 - CTI Observing Log (continued)

Date	Dayno	CCD0	CCD1	Comment
88feb16	1142	B**	V**	Clear, maybe photometric
88feb17	1143	B	V	Clear, slight wind
88feb18	1144	R**	V**	Clear
88feb21	1147	B	V	Clear, cirrus at morning
88mar11	1166	I	V	Clear, then cloudy
88mar12	1167	I	V	Clear, maybe photometric, slight wind
88mar13	1168	R	V	Cirrus
88mar14	1169	B	V	Clear, cloudy later
88mar15	1170	B	V	Clear
88mar16	1171	R	V	Clear, very windy
88mar17	1172	R**	V**	Clear, windy
88mar18	1173	I*	V**	Clear
88mar19	1174	B*	V**	Clear maybe photometric
88mar20	1175	B	V**	Clear, windy
88mar21	1176	R	V	Cirrus
88mar22	1177	R	V	slight clouds
88mar24	1179	B	V**	Clear, maybe high dust
88mar25	1180	R	V	Clear, near photometric
88mar26	1181	I	V	Clear, bright moon
88mar27	1182	I	V	Clouded out, no data
88mar29	1184	I	V	Clear, windy
88mar30	1185	O	A	Clear, refocused
88apr08	1194	O	A	Clear
88apr09	1195	I	V	Clear
88apr10	1196	R	V	light cirrus
88apr19	1205	B	V**	Clear
88apr20	1206	R	V	Clear, scattered cirrus, wind gusts
88apr22	1208	I	V	Clear
88apr24	1210	R	V	scattered clouds. wind gusts, dusty
88apr25	1211	B	V	Clear, data out of focus, something is amiss
88apr26	1212	R*	V**	Clear, maybe photometric
88apr27	1213	I	V	Clear.
88may05	1221	I	V	Clear, windy, gusts, no data
88may06	1222	I	V	Cloudy
88may11	1227	R	V	no information on conditions, possible computer trouble
88may12	1228	B**	V**	Clear
88may13	1229	B	V	Clear, slight clouds
88may21	1237	B**	V**	Clear, photometric, slight wind
88may24	1240	R	V	Cloudy
88may25	1241	I	V	slight haze

Table A1.1 - CTI Observing Log (continued)

Date	Dayno	CCD0	CCD1	Comment
88may26	1242	R	V	Clear
88may27	1243	I	V	slight cirrus, questionable data
88may28	1244	I	V	slight cirrus
88jun07	1254	I*	V**	Clear
88jun08	1255	R*	V**	Clear
88jun09	1256	I	V	Clear, occasional cirrus
88jun10	1257	I	V*	Clear, maybe photometric
88jun11	1258	R*	V**	Clear
88jun12	1259	R	V	Clear
88jun13	1260	R	V	Clear, windy
88jun14	1261	R*	V	Clear, some cirrus
88jun15	1262	I*	V	Clear, slight haze, maybe photometric
88jun16	1263	I	V*	Clear, some cirrus
88jun17	1264	B	V	Clear, scattered clouds
88jun20	1267	B	V	scattered clouds
88jun21	1268	B*	V	scattered clouds, cleared latter, flashlights around 2:00am
88jun22	1269	R*	V**	Clear
88jun23	1270	R	V	Cloudy, windy
88jun24	1271	R	V	Cloudy
88jun26	1273	I	V	Clear, scattered clouds, poor data
88jun27	1274	I	V	scattered clouds
88jun28	1275	R	V	Clear
88jul05	1282	I	V	(dewar pumped Jul 03) scattered clouds, 4 july fireworks, no data
88jul06	1283	V	R	Cloudy, only 1/2 hour of data
88jul12	1289	R	V	scattered clouds
88jul13	1290	B	V	no information on conditions
88jul15	1292	B	V**	slight clouds
88jul16	1293	R*	V	Clear
88jul17	1294	R	V	scattered clouds
88aug09	1317	R**	V**	Clear
88sep13	1352	I*	V**	Clear, maybe photometric, mirrors washed since last data
88sep14	1353	B	V	Clear, probably photometric, focusing procedures
88sep15	1354	B**	V**	Clear, probably photometric
88sep16	1355	B**	V**	Clear
88sep17	1356	R**	V	Clear, probably photometric
88sep18	1357	R	V	Clear, KPNO "fun-night" (problems with car lights)
88sep19	1358	R	V	Clear, data doesn't look that good
88sep20	1359	I*	V**	Clear, dust in atmosphere?, stayed closed due to high winds
88sep24	1363	O	A	Clear, probably photometric
88sep26	1365	O	A	Clear, data looks good

Table A1.1 - CTI Observing Log (continued)

Date	Dayno	CCD0	CCD1	Comment
88nov04	1404	I	V**	Clear, data looks O.K.
88sep27	1366	O	A	scattered clouds
88sep28	1367	O	A	Clear, slightly hazy, data quality poor
88oct02	1371	O	A	Clear
88oct03	1372	O	A	Clear, poor seeing
88oct04	1373	I	V	Cloudy, no data
88oct08	1377	I	V**	Clear, probably photometric
88oct09	1378	I	V**	Clear, cirrus visible at sunset
88oct10	1379	I	V**	Cloudy to east, clear overhead
88oct18	1387	B	V	Clear after afternoon thunderstorms, no data recorded
88oct19	1388	R	V	low cirrus, thunderstorms in area, not photometric
88oct23	1392	I	V	Clear, very bright moon, high background
88oct24	1393	I	V	Clear, very bright moon, data quality much better than yesterday
88nov01	1401	I*	V**	Clear, probably photometric, high moon background at end
88nov02	1402	I	V	scattered clouds, good seeing
88nov03	1403	I	V**	Clouds on horizon, not photometric
88nov05	1405	I	V**	Clear, definitely photometric
88nov06	1406	R	V	patchy cirrus and hazy
88nov07	1407	B	V	some cirrus, hazy and very windy, data quality questionable
88nov08	1408	R	V	Cirrus all over
88nov10	1410	B	V**	Clear, clouds by morning
88nov11	1411	B	V**	Clear, clouds in morning, data looks good
88nov12	1412	B*	V**	possibly photometric
88nov13	1413	B	V**	Clear, photometric at start, images elongated by wind at times
88nov14	1414	R	V**	Clear
88nov16	1416	R	V**	Clear, data looks good
88nov17	1417	R	V**	high cirrus
88nov18	1418	R	V*	Clear but very foggy in early morning
88nov19	1419	R	V**	Intermittent cloudiness, data useless and not recorded
88nov20	1420	R	V	high cirrus very bad
88dec02	1432	I	V**	Clear, data looks good
88dec04	1434	R	V	scattered cirrus, images fuzzy but cleared up later
88dec05	1435	R	V**	scattered cirrus and hazy, data looks O.K.
88dec06	1436	R	V**	Clear with cirrus in west at sunset
88dec07	1437	R	V	Cirrus overcast with brief openings, no data taken
88dec12	1442	B	V**	Very clear, data looks O.K.
88dec13	1443	B	V	Clear, possibly photometric, clouds in east at sunrise
88dec14	1444	B	V	Clear, data looks good
89jan06	1467	B	V	not photometric, closed by clouds
89jan09	1470	I	V	Clear, probably photometric, dewar problems

Table A1.1 - CTI Observing Log (continued)

Date	Dayno	CCD0	CCD1	Comment
89jan11	1472	R	V	Clear, elongated images because of strong winds
89jan12	1473	R	V	hazy with cirrus to north, high humidity
89jan14	1475	R	V	Clear
89jan15	1476	I	V	Cirrus, not photometric
89jan16	1477	I	V	scattered cirrus and hazy, high background at start
89jan17	1478	R*	V	Clear with some haze, high background
89jan31	1492	I*	V	Clear overhead,clouds to south, closed by heavy cloud cover later
89feb03	1495	R	V	Clear, possibly photometric, images elongated due to wind
89feb04	1496	R	V**	Clear with clouds on horizon, cirrus at sunrise, data looks good
89feb12	1504	B*	V**	Clear, data looks O.K.
89feb13	1505	R	V	some cirrus
89feb14	1506	I	V	Cirrus at sunset, closed early due to clouds
89feb16	1508	I	V	Clear
89mar02	1522	I	V	scattered cirrus and very hazy, complete cloud cover at end
89mar05	1525	I	V	Cirrus all night, no data recorded
89mar06	1526	I	V**	Clear
89mar07	1527	I*	V**	Clear, data looks good
89mar08	1528	B**	V**	Clear
89mar09	1529	B	V**	Clear, data looks O.K.
89mar10	1530	R*	V**	scattered cirrus on horizons all night
89mar11	1531	R	V**	Clear
89mar12	1532	R	V	light cirrus, look carefully at data
89mar13	1533	R*	V	some cirrus at sunset, mostly clear
89mar15	1535	R	V	Cirrus throughout night
89mar16	1536	I	V	some scattered cirrus, cleared somewhat during night
89mar30	1550	R*	V*	Clear, data looks good
89apr01	1552	I*	V*	Clear, data looks good
89apr02	1553	I	V	Clear, data looks good despite wind, some clouds in morning
89apr03	1554	?	?	moderate cirrus at sunset, wind causing severe data smearing
89apr05	1556	R	C	Clear, probably photometric, r data out of focus
89apr06	1557	I	C	Clear, data looks good
89apr07	1558	I	C	Clear, probably photometric, good sweep!
89apr08	1559	R	C	Clear, data looks O.K.
89apr09	1560	R	C	Clear, data looks O.K.
89apr10	1561	R	C	no information on conditions
89apr11	1562	R	C	Clear, probably photometric
89apr25	1576	R	V	(mirrors washed Apr 24) clear, pumped dewar
89apr26	1577	R	V	Clear, closed early due to wind
89apr27	1578	I	V**	Clear, data looks O.K.
89apr28	1579	R	V	Clear

Table A1.1 - CTI Observing Log (continued)

Date	Dayno	CCD0	CCD1	Comment
89apr29	1580	I	V	some scattered cirrus, data looks O.K. with some coma
89may03	1584	B	V	Cirrus but good seeing, coma present at end of data
89may04	1585	I	V	some scattered cirrus
89may09	1590	B*	V*	Clear at start, data looks reasonable, closed early due to clouds
89may11	1592	B	V	partly cloudy, ragged images perhaps due to wind, coma present
89may12	1593	R	V**	Cirrus on horizon at sunset, clear overhead, images look good
89may13	1594	R	V	Clear, data looks good at start, ghost images later
89may14	1595	R	V	Clear, data looks good at start, ghost images later
89may15	1596	I	V	Clear with some cirrus to north, high wind and bad seeing
89may30	1611	B	V	Cirrus to west, not transparent, images elongated by wind
89may31	1612	B	V**	Clear, images look fairly good
89jun01	1613	R**	V**	Clear all night
89jun02	1614	R*	V**	scattered cirrus and slightly hazy
89jun03	1615	I*	V**	Clear, data looks O.K.
89jun04	1616	I*	V**	Clear, data looks good
89jun05	1617	B	V*	scattered cirrus, not photometric, windy
89jun06	1618	I	V	Cirrus at start
89jun07	1619	B	V	scattered clouds
89jun08	1620	B*	V**	Clear, bright moon, data looks good
89jun09	1621	R	V**	Clear, data looks quite good!
89jun11	1623	R	V**	Clear, data looks pretty good
89jun13	1625	I	V	no go
89jun26	1638	I	V	Cloudy, pumped dewar
89jun27	1639	I	V	partly cloudy, questionable data because of clouds
89jul01	1643	B	V	Clear but slightly hazy, stars out of focus
89jul02	1644	B	V	scattered cirrus, data reasonable but focus still a problem
89jul03	1645	B*	V	Clear, stars still out of focus, coma also exists
89jul04	1646	B*	V	Clear with slight haze, continued focus problems
89jul06	1648	B	V	thunderclouds and lightning, did not open
89oct08	1742	I	V**	Clear, possibly photometric, ran well and images look good
89oct09	1743	R*	V*	Clear, probably photometric, data looks good
89oct10	1744	I	V**	Clear, probably photometric, moved telescope closer to strip
89oct11	1745	R	V	Clear, scattered cirrus by morning, data looks O.K.
89oct18	1752	R	V	Clear, stars slightly out of focus
89oct19	1753	I	V	slight haziness, cirrus in morning, stars slightly unfocused
89oct20	1754	I	V	Clouds to east and south, closed early due to increasing clouds
89oct24	1758	R*	V**	Clear, data looks O.K.
89oct25	1759	I	V	scattered cirrus, data looks O.K.
89oct28	1762	B	V	Clear, data looks good, power outage
89oct29	1763	B	V	Clear

Table A1.1 - CTI Observing Log (continued)

Date	Dayno	CCD0	CCD1	Comment
89oct30	1764	B	V	Cirrus to south, windy, data pretty good
89nov03	1768	I*	V*	Clear, probably photometric, moved telescope
89nov04	1769	I	V	Clear, data very good
89nov05	1770	R*	V	Clear, data pretty good
89nov23	1788	I	V	scattered cirrus, closed early due to clouds
89nov24	1789	I	V	scattered cirrus, hazy, very windy, cloud cover in morning
89nov25	1790	I	V	Variable high clouds, elongated images due to wind, closed early clouds
89nov28	1793	B	V	Cloudy at start, cleared later, power failure during night
89dec01	1796	B	V	Clear with haze on horizon, data good
89dec02	1797	I	V	Clear, early shutdown due to high winds
89dec03	1798	R	V	Clear, did not open due to high winds
89dec04	1799	R	V	Clear, data good
89dec05	1800	I	V	Clear, still trying to fix A/D problems
89dec06	1801	R	V	Clear with patches of cirrus, data O.K.
89dec07	1802	R	V	Clear
89dec09	1804	R	V	some scattered cirrus, data is acceptable
89dec21	1816	I*	V**	(fixed computer hard disk Dec 11) clear, data good
89dec23	1818	I*	V**	Clear, data promising
89dec24	1819	B	V	scattered cirrus, heavy cirrus in morning, data is acceptable
90jan05	1831	R	V	Clear, problems with WWVB signal, cannot open telescope
90jan06	1832	R*	V**	Clear, data O.K.
90jan21	1847	B	V	scattered cirrus, hazy, data good, moderate cloud cover in morning
90jan22	1848	B	V	scattered cirrus, very hazy, data acceptable, closed early due to clouds
90jan24	1850	B*	V**	Clear, data good, images slightly out of focus, power failure
90jan25	1851	B*	V**	Clear, very windy, data does not look too bad
90jan26	1852	R	V**	Clear, data good, slightly hazy with cirrus in morning
90jan28	1854	R*	V**	scattered cirrus, data looks O.K., stars slightly unfocused
90jan29	1855	R*	V*	Clear, data very good
90jan30	1856	I*	V*	Clear, data very good
90feb04	1861	I	V	Clear, data O.K., partly cloudy in morning
90feb17	1874	I*	V*	Clear, data good
90feb18	1875	I*	V*	Clear with some clouds to north, data good
90feb21	1878	I	V	Clear with clouds on horizon, same in morning, may be a good night
90feb22	1879	R*	V*	Clear with clouds on horizon, clear in morning, data fairly good
90feb23	1880	R*	V*	Clear with cirrus to north, data good, clear all night
90feb24	1881	B	V	Clear with cirrus to west, telescope refused to open
90mar01	1886	B*	V*	Clear with cumulus to east, data O.K., clear throughout night
90mar08	1893	R	V	widely scattered cirrus throughout night
90mar17	1902	R*	V*	widely scattered cirrus, closed early due to clouds and moon

Table A1.1 - CTI Observing Log (continued)

Date	Dayno	CCD0	CCD1	Comment
90mar19	1904	R*	V*	Clear, data looks good, excellent night, closed early due to moon
90mar20	1905	I	V	Clear, clouds to west, closed early due to moon, lots of cirrus in morning
90mar23	1908	I	V	scattered cirrus and hazy throughout night, data looks O.K.
90mar24	1909	B	V	Clear with cirrus on horizon, data looks good, lots of cirrus in morning
90mar25	1910	B*	V*	Clear all night, data looks good
90apr03	1919	I*	V*	Clear, data looks O.K.
90apr14	1930	I	V	Cirrus throughout night, data looks acceptable
90apr16	1932	I	V*	Very clear early but also windy, closed due to moon
90apr18	1934	I	V*	windy, closed early due to fog and moon
90apr19	1935	I	V*	good night, clear and calm
90apr20	1936	R	V*	good night
90apr21	1937	R	V	Cirrus, humid, breezy, Grinnell problem
90apr26	1942	R	V*	Clear, good night
90apr27	1943	B	V	Breezy, clouds on horizon, low moon
90apr29	1945	B	V	Very windy, distortion, early shutdown for wind, possible Grinnell problem
90apr30	1946	B	V	windy, 35deg moon, distortion
90may15	1961	R	V	Breezy, early shutdown for moon
90may16	1962	R	V	windy, clear, early shutdown for moon
90may17	1963	I	V	Cloudy, poor seeing, diagnostic data only
90may22	1968	B	V	Cloudy, diagnostic data, cleared up later
90may24	1970	B	V	diagnostic data only
90may25	1971	B*	V	windy, distorted
90may27	1973	B*	V	Clear, calm
90may28	1974	B	V	Cirrus, setting moon, data fair
90may30	1976	I	V	moon 30deg, cirrus, SEVERE data shearing
90may31	1977	R	V	moon 30deg, slight cirrus, possible data smearing
90jun01	1978	I*	V	gusty wind, 30deg moon, good data
90jun02	1979	I	V	40deg moon, very good night
90jun03	1980	R**	V*	40deg moon, clear, calm
90jun05	1982	I	V	late open for moon, wind, dewar drift
90jun20	1997	I*	V*	(pumped dewar Jun 18) clear, slight breeze, good data
90jun21	1998	I	V	Clear, calm, but dewar failed during night
90jun22	1999	R	V	Bad dewar, no data, power supply check
90jun26	2003	B	V	system fixed, some clouds, got data
90jun28	2005	R	V*	Clear after midnight
90jul28	2035	R*	V*	15deg moon, clear, very good data
90jul29	2036	I*	V*	Calm, clear, moon and lightning on horizon, good data
90aug19	2057	R	V*	Calm, clear with morning cirrus, high humid, good data
90aug20	2058	I	V	Clear, light wind, humid 37%, Grinnell problem, close early for clouds
90aug21	2059	I	V	slight breeze, good data in spite of tape drive failure

Table A1.1 - CTI Observing Log (continued)

Date	Dayno	CCD0	CCD1	Comment
90aug22	2060	B	V	good night, good data
90aug23	2061	B	V*	Clear,calm , good data
90aug24	2062	I*	V*	Clear, windy, good data
90aug25	2063	R	V*	Clear, windy, good data
90aug26	2064	I	V	Clear, windy, Grinnell problem in middle, good data
90sep13	2082	R*	V*	Breezy, close early for storm, very good data in spite of tape drive failure
90sep20	2089	I*	V*	Clouds on horizon, close early for clouds, good data
90sep22	2091	I	V	Clear, windy, early close for clouds, good data
90sep25	2094	I	V*	some clouds, low moon, data problems
90sep26	2095	R	V	hazy, cirrus, fair data
90sep27	2096	R*	V*	Clear, calm, 25deg moon, good data
90sep28	2097	R	V	scattered cirrus, windy, good data
90oct11	2110	I	V*	Breezy, hazy, close early for moon, good data (long flat)
90oct12	2111	I	V	Clear, close early for moon, good data
90oct13	2112	I	V	data problems
90oct14	2113	R	V*	Clear, calm good data
90oct15	2114	R	V	Clear, Grinnell problem, close early for humid, good data
90oct16	2115	B	V	good data
90oct18	2117	B	V	Clear calm, becoming windy, data fuzzy and distorted
90oct19	2118	B	V	Clear, breezy to windy, humid
90oct21	2120	B	V	Clear, breezy, data problems
90oct22	2121	I	V*	Clear, calm good data
90oct23	2122	I	V	Beautiful night, good data
90oct24	2123	R*	V*	Clear, calm, data problems
90oct25	2124	R*	V*	Clear, breezy, good data
90oct26	2125	R*	V*	Clear, calm, 10deg moon, good data
90oct27	2126	I	V*	Clear, good seeing, good data
90nov10	2140	I	V	Clear, windy, focus fuzzy, good data, power supply problem
90nov11	2141	I	V	Bad power supply, no data
90nov15	2145	I	V	Clear, breezy, good data
90nov16	2146	I	V	Cirrus, calm, fair data
90nov17	2147	B*	V*	Clear, humid good data
90nov18	2148	B	V*	Cloudy, fair data
90nov19	2149	B	V	Clear with cirrus later, good data
90nov22	2152	I	V	some cirrus, good data
90nov23	2153	I	V	Clear, breezy to windy, stuck filter, fair data
90dec10	2170	R	V*	Clear, breeze, good data
90dec11	2171	R*	V*	Clear, breeze, good data
90dec18	2178	B	V*	Clear, windy, bad focus, good data
90dec19	2179	B	V	Clear, windy, bad focus, Grinnell problem, needs realignment

Table A1.1 - CTI Observing Log (continued)

Date	Dayno	CCD0	CCD1	Comment
91jan08	2199	I	V*	cirrus, closed-moon, O.K data
91jan11	2202	I	V*	Clear, O.K. data
91jan13	2204	I	V	cirrus, good data
91jan14	2205	B	V	partly cloudy, good data
91jan15	2206	B*	V*	Clear, clouds, O.K. data
91jan16	2207	B	V*	Clear, breeze, good data
91jan19	2210	I	V	Clear, good data
91jan24	2215	R	V	Cirrus early, hazy at start
91jan25	2216	R*	V*	Clear, haze
91feb07	2229	R	V	Clear, windy, hazy, closed-clouds, good data
91feb08	2230	R*	V*	Clear, clouds in East, calm, closed-moon, O.K. data
91feb09	2231	I	V	cirrus, breezy, closed-cirrus, data marginal
91feb15	2237	B	V*	cirrus, breeze, closed-clouds, good data
91feb20	2242	I	V	Clear, very windy, monitor blank in A.M., good data
91feb21	2243	I*	V*	Clear, cold, breezy, images not focused
91mar09	2259	V	I	Clear, ccd and dewar temp high, stop early
91mar12	2262	I*	V*	Clear, clouds in East, slight breeze, images not focused, data acceptable
91mar13	2263	R	V*	Clear, breeze, scattered cirrus in A.M., data good
91apr08	2289	R*	V*	Clear, very windy, closed-moon, calm, data O.K.
91apr09	2290	I*	V*	Clear, breezy, closed-moon, data O.K.
91apr10	2291	B	V	Clear, Grinnell problem, data good
91apr13	2294	I	V	(changed ccd voltages Apr 11) clear, breeze, data O.K.
91apr14	2295	B*	V*	Clear, good data
91apr15	2296	B	V	Clear, data O.K.
91apr16	2297	I	V	hazy, thin cirrus, closed-wind and clouds, data mediocre
91apr20	2301	R	V	thin cirrus, slight wind, data O.K.
91apr21	2302	I	V	Clear, very windy, closed-winds, images distorted
91apr22	2303	I	V	mirrors washed, Grinnell re-installed, clear, cirrus, data good
91apr24	2305	R	V*	Clear, calm, good data
91may07	2318	I*	V*	Clear, breeze, closed-moon, data good
91may08	2319	R	V	cirrus, breeze, closed-moon, data acceptable
91may09	2320	R	V	Cloudy, windy, closed-clouds and wind, data fair
91may10	2321	I	V	Clear, windy, distorted images, closed-wind
91may11	2322	I	V	Clear, windy, haze, data acceptable
91may12	2323	B*	V*	Clear, data good
91may14	2325	R	V	Clear, windy, distorted images, closed-wind
91may15	2326	I	V*	Clear, data good
91may16	2327	B	V	Clear, data good
91may17	2328	I	V	Clear, wind later, data good
91may18	2329	R	V	Clear, windy, data O.K.

Table A1.1 - CTI Observing Log (continued)

Date	Dayno	CCD0	CCD1	Comment
91may19	2330	I	V	Clear and breezy, good data
91jun05	2347	B	V	(adjusted current ccd0 May 30, ccd tests Jun 03) clear and breezy, data good
91jun06	2348	V	I	Clear, close early
91jun07	2349	R	V	Clear and calm, data looks good, close early due to moon
91jun08	2350	I	V	Clear, slight breeze, data looks good, close early due to moon
91jun15	2357	I	V	(test dewar hold time Jun 09) clear and slight breeze, data looks good
91jun16	2358	B	V	Clear and calm, data looks O.K.
91jun17	2359	R	V	Clear, slight breeze, Grinnell problem early
91jun18	2360	I	V	Clear, clouds in horizon, hazy in A.M., data looks O.K.
91jun20	2362	R	V	Clear, data looks O.K.
91jun21	2363	I	V	Clear and breezy, data looks O.K.
91jun22	2364	R	V	Clear and breezy, calm in A.M.
91jul09	2381	I	V	thick clouds, clearing, lightning in South, close early due to clouds
91jul10	2382	B	V	Install two new tape drives, clear
91jul13	2385	B	V	Clear and slight breeze
91aug06	2409	I	V	Clear, clouds in East, breezy, data looks good
91aug07	2410	R	V	Clear and breezy, data looks good, close early due to moon
91aug08	2411	R	V	Clear, data looks good, close early due to clouds and moon
91aug13	2416	B	V	(dewar pumped Aug 11) clear but hazy, data looks good
91aug14	2417	B	V	patchy clouds, lightning in SE
91aug18	2421	I	V	hazy, scattered cirrus, clearing, data marginally O.K.
91aug19	2422	R	V	hazy, close early due to clouds
91oct06	2470	C	R	down past months due to lightning strike, clear and calm, no data
91oct07	2471	C	R*	Clear and slightly breezy, data very good, close early
91oct08	2472	C	R*	Clear and calm, data very good, close early
91oct09	2473	C	B	scattered cirrus, breezy, close early due to clouds, data questionable
91oct10	2474	C	B*	scattered cirrus, slight breeze, close early, data looks good
91oct11	2475	C	B	Clear and windy, data looks good
91oct14	2478	C	B*	Clear and breezy, data good
91oct15	2479	C	I*	Clear and slight breeze, data looks good
91oct16	2480	C	I	Clear and calm, data looks good
91oct17	2481	C	I	Clear and breezy, data looks good
91oct18	2482	C	I	Clear and calm
91oct29	2493	C	I	Clear, slight breeze, data looks good, close early due to moon
91oct31	2495	C	I	Clear, data O.K., close early due to humidity
91nov01	2496	C	R*	Clear, slight breeze, data looks good, stars slightly out-of-focus
91nov02	2497	C	R*	Clear and calm, data looks good
91nov03	2498	C	R*	scattered cirrus, calm, data looks good
91nov04	2499	C	B*	Clear, occasional breeze, gusts, data good
91nov05	2500	C	V*	Clear and calm, mirror focused, data looks good

Table A1.1 - CTI Observing Log (continued)

Date	Dayno	CCD0	CCD1	Comment
91nov07	2502	C	B	Clear and calm, data very good
91nov08	2503	C	V	Clear and calm, data looks good
91nov09	2504	C	V	Clear and calm, data looks good, close early due to clouds
91nov12	2507	C	B	Clear, data has many horizontal streaks, close early
91nov13	2508	C	R*	scattered cirrus, calm, data good, close early due to clouds and rain
91nov26	2521	C	R	scattered cirrus, data looks good, close early due to moon, Grinnell problems
91nov27	2522	C	I	Clear and calm, software problem, close early due to moon
91nov30	2525	C	I	Clear but very windy, no data acquired
91dec03	2528	C	I	Clear, slight breeze, data looks good, close early due to winds
91dec04	2529	C	V*	scattered cirrus, windy, data looks O.K.
91dec07	2532	C	B*	Clear and calm, lightning in South, data looks good
91dec08	2533	C	I	Clear and windy, data looks O.K.
91dec14	2539	C	R*	Clear and windy, data looks O.K., close early due to wind
91dec15	2540	C	I	Clear and windy, data looks O.K., moonlight strong
91dec16	2541	C	V	Cloudy, close early due to clouds, data poor
92jan02	2558	C	I	Clear and breezy, Grinnell problem, close early due to clouds
92jan09	2565	C	I*	scattered cirrus and windy, no data acquired
92jan10	2566	C	V*	Clear and breezy, data good
92jan13	2569	C	I*	Clear and breezy, data looks good
92jan14	2570	C	I*	Clear and calm, strong moonlight, data looks good
92jan15	2571	C	R*	Clear and breezy, data looks good
92jan25	2581	C	I	scattered cirrus, windy, data probably O.K.
92jan26	2582	C	V	thin cirrus, calm, data looks good
92jan27	2583	C	V	thin cirrus, calm, data looks good
92jan28	2584	C	V	Clear and breezy, data good
92jan29	2585	C	I*	Clear and breezy, data good
92jan30	2586	C	I	Clear and very breezy, images slightly distorted, data O.K.
92jan31	2587	C	B*	Clear and calm
92feb01	2588	C	V	partial clouds, high humidity, no data acquired
92feb10	2597	C	I	Clear and breezy, data looks O.K., close early due to moon
92feb24	2611	C	R	Clear and breezy, data very good, close early due to moon
92feb25	2612	C	V	Clear and breezy, data looks good
92feb26	2613	C	V	Clear and windy, data O.K.,
92feb27	2614	C	B	Clear and breezy, A/D problems, data O.K.
92feb28	2615	C	B	A/D converters test, clear and breezy, data looks good, thick cirrus later
92feb29	2616	C	B	(voltage test Mar 04) clear and calm, horizontal bars in data, data marginal
92mar06	2622	C	V	Clear and calm, 100% humidity, no data acquired
92mar11	2627	C	R	Clear and breezy, no data on screen
92mar12	2628	C	I	Clear and calm, data looks good, close early due to moon
92mar25	2640	C		

Table A1.1 - CTI Observing Log (continued)

Date	Dayno	CCD0	CCD1	Comment
92mar26	2641	C	I	scattered cirrus, calm, data marginal, close early due to clouds
92apr06	2652	C	V	Clear and slight breeze, data looks good
92apr07	2653	C	B	Clear and calm, data looks good
92apr08	2654	C	I	scattered cirrus, calm, data O.K., close early due to clouds
92apr09	2656	C	V	Clear and calm, data looks good
92apr10	2657	C	I	Clear and calm, data looks good
92apr11	2658	C	I	Cirrus everywhere, calm
92apr25	2672	C	R	traces of cirrus, data looks very good
92apr26	2673	C	I	scattered cirrus at start, data looks good
92apr27	2674	C	V	Clear with slight cirrus, data looks very good
92apr28	2675	C	V	Clear overhead, data looks good
92apr29	2676	C	V	Clear but very windy, data looks good
92apr30	2677	C	B	scattered cirrus throughout night, data looks O.K.
92may02	2679	C	B	some cirrus, heavier in morning, data looks O.K.
92may03	2680	C	B	thin cirrus with heavy clouds to east, data looks O.K.
92may07	2684	C	V	Clear overhead with clouds on horizon, data looks very good
92may08	2685	C	R	Clear overhead, clouds to east, data looks good, early closing due to clouds

Table A1.2 - Bright Stars in CTI Survey

name	RA (1987.5)	Dec	visual mag
SAO 76990	$05^h\ 08^m\ 57.8^s$	$28^\circ\ 00'\ 57.6''$	6.01
SAO 77121	05 20 12.2	27 56 44.3	6.33
SAO 77625	05 50 10.8	27 57 53.4	5.56
49 Aur	06 34 24.8	28 01 58.7	5.27
ι Gem	07 24 57.4	27 49 28.4	3.79
64 Gem	07 28 33.9	28 08 43.8	5.05
65 Gem	07 29 02.2	27 56 34.6	5.01
β Gem (Pollux)	07 44 34.9	28 03 27.3	1.14
ψ_1 Cnc	08 25 42.3	27 56 11.3	5.57
ρ_2 Cnc	08 54 54.9	27 58 33.8	5.22
67 Cnc	09 01 04.4	27 57 11.8	6.07
44 LMi	10 49 12.6	28 02 23.4	6.04
β Com	13 11 19.7	27 55 55.5	4.26
SAO 82944	13 40 04.7	28 07 41.1	6.23
SAO 84015	15 48 03.4	28 11 40.9	5.85
SAO 87165	19 23 52.3	28 03 46.0	6.53
β_1 Cyg (Albireo-A)	19 30 13.0	27 55 58.5	3.08
β_2 Cyg (Albireo-B)	19 30 15.1	27 56 18.8	5.11
32 Vul	20 54 01.6	28 00 34.9	5.01
β Peg (Scheat)	23 03 09.4	28 00 48.4	2.42

Table A1.3 - SAO stars in CTI Survey

SAO #/ name	RA (1987.5)	Dec	visual mag
73878	$00^h\ 17^m\ 27.1^s$	$28^\circ\ 06'\ 12.5"$	9.4
73901	00 19 44.7	28 05 04.7	9.1
73920	00 20 47.2	28 06 20.0	9.4
73923	00 20 59.7	28 00 53.7	9.0
73965	00 24 31.5	28 00 29.8	8.6
74015	00 27 09.0	28 06 18.1	8.0
74022	00 27 37.2	27 59 29.4	8.0
74045	00 29 47.9	28 00 15.6	8.2
74053	00 30 09.2	28 02 33.8	9.0
74075	00 31 39.3	28 02 54.0	9.1
74124	00 34 58.7	28 05 38.0	9.2
74198	00 40 45.3	27 58 27.5	8.2
74337	00 52 43.2	28 00 07.8	9.3
74380	00 55 54.4	28 00 44.8	9.0
74403	00 57 43.9	28 04 16.5	9.0
74528	01 09 26.4	27 58 37.8	8.9
74555	01 11 53.4	27 59 43.1	9.0
74584	01 13 55.9	28 00 33.3	8.3
74711	01 25 07.7	28 01 13.1	8.9
74733	01 26 39.5	28 01 58.8	9.2
74794	01 33 03.4	27 57 53.8	9.5
74835	01 37 02.7	28 05 53.9	9.3
74857	01 38 51.9	28 02 45.8	7.9
74876	01 41 07.3	28 03 46.5	8.6
74891	01 42 33.9	27 59 47.9	9.1
74937	01 47 05.0	28 00 23.0	9.1
74998	01 52 28.8	27 57 39.0	8.3
75027	01 54 58.8	27 59 10.9	9.0
75105	02 01 54.8	28 02 57.5	9.0
75137	02 05 11.5	28 02 31.5	9.0
75206	02 12 13.5	27 57 36.1	9.3
75230	02 14 39.5	28 00 38.7	9.0
75301	02 20 36.4	28 00 51.8	8.9
75328	02 22 35.7	28 05 06.3	8.6
75365	02 25 57.8	27 59 35.3	8.8
75402	02 28 51.3	27 59 08.9	9.0
75475	02 36 54.1	27 57 43.9	9.0
75484	02 37 17.0	27 59 37.8	8.6
75520	02 40 49.2	27 59 35.1	8.8
75538	02 43 04.8	28 05 31.2	8.9
75543	02 43 45.6	27 57 46.6	7.9
75561	02 45 41.8	28 00 19.1	9.0
75617	02 52 07.3	28 01 33.3	8.6
75640	02 54 40.9	28 05 43.9	8.2
75678	02 59 16.9	27 57 59.7	9.4
76223	03 48 10.5	28 01 36.1	9.0
76278	03 51 13.8	27 58 39.9	8.8
76288	03 51 41.5	28 05 49.5	8.6

Table A1.3 (continued) - SAO stars in CTI Survey

SAO #/ name	RA (1987.5)	Dec	visual mag
76298	03 52 33.4	27 59 44.2	8.5
76304	03 52 51.3	28 06 42.5	7.8
76354	03 56 52.8	28 03 48.6	9.2
76403	04 01 28.7	28 05 33.2	7.5
76418 (RW Tau)	04 03 08.1	28 05 32.6	8.0
76540	04 17 40.8	28 04 23.9	8.7
76634	04 29 32.9	28 06 17.1	6.6
76659	04 34 07.1	28 02 23.8	9.0
76673	04 36 15.8	27 59 11.2	9.3
76690	04 38 45.5	27 59 52.5	8.8
76781	04 49 35.5	28 05 04.6	8.9
76805	04 52 13.7	28 05 15.6	8.2
76918	05 02 06.7	28 01 20.3	9.8
76990	05 08 57.8	28 00 57.6	6.0
76991	05 08 58.2	28 01 07.8	8.1
77093	05 17 55.1	28 04 41.8	8.4
77114	05 19 47.5	28 03 20.3	9.0
77121	05 20 12.2	27 56 44.3	6.3
77130	05 21 47.5	28 05 26.3	8.8
77268	05 33 51.8	28 02 35.9	8.1
77346	05 37 56.0	28 00 27.2	9.3
77351	05 38 19.9	27 59 41.2	9.0
77401	05 40 59.0	28 06 40.1	9.1
77625	05 50 10.8	27 57 53.4	5.6
77638	05 50 45.6	28 05 22.4	8.0
77662	05 52 08.3	27 59 45.5	9.0
77728	05 55 05.9	27 58 28.7	9.2
77818	05 59 17.6	28 07 33.0	7.0
78126	06 13 35.8	28 01 57.9	8.7
78185	06 16 54.9	28 04 33.5	9.1
78191	06 17 12.6	28 00 44.0	7.4
78206	06 17 59.9	28 03 39.7	8.0
78240	06 19 34.1	28 04 59.6	8.6
78291	06 22 00.6	27 59 36.9	7.5
78334	06 24 12.1	28 02 22.7	7.7
78483	06 32 17.7	28 05 33.6	7.6
78488	06 32 32.1	28 05 44.4	8.7
78496	06 32 54.2	27 59 25.3	7.8
78524 (49 Aur)	06 34 24.8	28 01 58.7	5.0
78533	06 34 57.3	28 02 58.4	9.3
78553	06 36 34.3	27 59 14.2	8.9
79050	07 05 19.9	28 00 58.7	8.9
79112	07 08 29.4	28 04 25.2	8.4
79184	07 12 59.2	27 59 18.9	8.8
79270	07 17 55.7	28 00 55.2	9.0
79283	07 18 41.0	27 59 31.8	9.3
79374 (ι Gem)	07 24 57.4	27 49 28.4	3.9
79390	07 26 17.8	28 03 18.0	9.0
79427 (64 Gem)	07 28 33.8	28 08 43.0	5.0

Table A1.3 (continued) - SAO stars in CTI Survey

SAO #/ name	RA (1987.5)	Dec	visual mag
79434 (65 Gem)	07 29 02.2	27 56 34.6	5.1
79457	07 30 22.6	28 01 42.5	9.0
79602	07 40 03.3	27 58 30.1	8.7
79666 (β Gem)	07 44 34.9	28 03 27.3	1.2
79772	07 52 34.7	28 05 07.0	6.7
79807	07 55 31.2	28 05 31.8	9.4
79891	08 02 26.1	27 58 02.1	8.2
80118	08 20 21.1	28 07 40.9	9.0
80181 (ψ_1 Cnc)	08 25 42.3	27 56 11.3	5.8
80183	08 25 55.3	28 06 17.9	8.5
80214	08 29 24.5	28 07 26.1	8.7
80430	08 47 09.1	28 01 38.4	8.4
80464	08 51 00.8	28 04 08.4	9.0
80511 (ρ_2 Cnc)	08 54 54.9	27 58 33.8	5.3
80584	09 01 00.2	27 58 37.1	9.0
80585 (67 Cnc)	09 01 04.4	27 57 11.8	6.0
80646	09 06 55.0	28 03 23.8	8.3
80854	09 28 23.2	27 59 18.0	8.9
80911	09 34 25.1	27 59 23.4	8.2
80922	09 35 52.3	28 01 17.1	8.9
80926	09 36 07.0	28 01 50.4	8.9
80941	09 37 44.0	28 03 45.4	7.9
80969	09 40 52.8	28 00 47.2	8.6
81194	10 06 51.0	28 06 38.1	8.8
81209	10 08 43.4	28 02 39.7	8.7
81272	10 16 41.1	28 07 51.4	9.1
81308	10 20 44.3	28 04 00.3	9.2
81395	10 30 52.4	28 06 21.5	9.0
81423	10 34 07.8	28 01 39.7	6.9
81429	10 34 47.1	28 01 58.4	9.2
81461	10 39 32.1	28 04 54.6	8.9
81462	10 39 39.5	28 04 36.1	8.9
81503	10 45 00.9	28 01 52.4	8.5
81542 (44 LMi)	10 49 12.6	28 02 23.4	6.1
81663	11 04 55.0	28 05 21.7	9.0
81666	11 05 32.0	28 07 05.9	9.1
81695	11 08 15.9	28 03 18.3	8.3
81814	11 24 40.0	28 00 43.1	8.8
81892	11 35 23.8	27 58 20.3	8.2
81932	11 39 31.7	27 58 32.8	9.1
81955	11 42 43.7	28 07 27.3	7.3
82041	11 53 23.4	28 01 58.4	8.7
82100	12 00 26.7	28 01 55.8	8.6
82121	12 03 26.9	28 07 48.9	8.4
82149	12 07 47.0	28 03 11.3	8.9
82208	12 15 24.8	28 07 05.1	8.2
82236	12 18 23.9	28 07 08.3	9.0
82241	12 18 43.3	27 59 39.6	9.2

Table A1.3 (continued) - SAO stars in CTI Survey

SAO #/ name	RA (1987.5)	Dec	visual mag
82359	12 31 12.1	28 02 52.1	9.2
82430	12 39 30.0	27 58 43.4	9.3
82445	12 41 46.1	28 00 51.2	9.3
82465	12 43 43.9	28 03 00.8	7.8
82560	12 54 14.1	27 58 51.3	9.3
82561	12 54 20.5	28 03 37.7	8.9
82595	12 58 56.6	28 07 58.6	7.1
82706 (β Com)	13 11 19.7	27 55 55.5	4.3
82763	13 17 23.0	28 07 51.6	9.0
82793	13 20 08.4	28 02 37.9	9.3
82826	13 24 31.7	28 02 41.0	8.3
82904	13 36 19.5	28 01 41.8	7.9
82944	13 40 04.7	28 07 41.1	6.4
82983	13 44 32.8	28 07 25.7	9.1
82992	13 46 00.2	28 00 17.6	8.1
83009	13 48 25.3	28 01 29.7	9.4
83142	14 02 39.0	28 03 50.3	9.0
83209	14 10 37.9	28 03 54.1	9.1
83213	14 11 00.2	28 05 39.4	8.3
83218	14 11 52.5	28 06 55.4	9.3
83237	14 13 34.6	27 59 29.6	9.0
83386	14 30 30.6	28 03 52.9	9.0
83439	14 36 29.2	28 03 12.6	8.5
83519	14 46 46.3	28 07 16.1	9.0
83791	15 21 23.0	28 05 07.4	9.0
83797	15 22 14.4	28 06 04.2	7.5
83855	15 29 39.7	28 05 53.8	9.0
83860	15 30 15.9	28 07 21.7	9.1
83949	15 41 05.1	28 02 05.0	8.0
83967	15 43 02.5	28 07 07.8	9.0
84015	15 48 03.4	28 11 40.9	5.8
84050	15 51 47.1	28 07 37.1	8.9
84215	16 08 42.8	28 05 12.5	8.7
84648	16 50 57.4	28 08 31.6	6.9
84810	17 04 15.9	28 06 27.9	7.2
84822	17 05 00.6	28 06 16.2	8.6
84857	17 06 58.8	28 08 13.1	8.0
84859	17 07 01.6	28 03 28.1	9.0
84870	17 07 53.0	28 03 13.5	9.0
84920	17 11 56.6	28 00 51.6	9.0
84946	17 13 46.8	28 00 14.6	8.9
84949	17 14 12.1	27 59 19.7	8.4
85006	17 18 54.1	28 02 18.5	7.1
85011	17 19 09.4	28 05 47.9	9.0
85056	17 22 52.9	28 03 15.1	9.0
85059	17 23 08.1	28 02 39.0	9.4
85173	17 30 41.8	28 08 43.6	8.6
85220	17 34 08.1	27 59 50.4	8.8
85378	17 44 28.5	28 00 40.4	8.7

Table A1.3 (continued) - SAO stars in CTI Survey

SAO #/ name	RA (1987.5)	Dec	visual mag
85405	17 46 12.7	27 59 13.6	8.7
85407	17 46 24.0	28 05 55.2	8.0
85581	17 57 05.1	27 59 36.7	8.5
85598	17 57 50.4	27 59 23.7	8.4
85803	18 10 19.4	27 58 30.5	8.5
85830	18 12 26.7	28 03 11.4	9.1
85981	18 22 02.7	28 06 47.4	9.1
86027	18 24 50.7	28 04 30.7	8.0
86269	18 37 52.5	28 00 21.4	8.9
86301	18 39 25.6	28 04 58.9	9.1
86306	18 39 39.1	28 00 01.0	9.1
86340	18 41 54.4	28 06 44.0	7.5
86376	18 43 11.7	28 05 53.7	8.7
86388	18 43 51.6	28 05 17.4	7.3
86402	18 44 50.8	28 00 41.3	9.2
86410	18 45 12.8	27 59 44.1	9.4
86718	19 01 13.0	28 05 53.3	8.3
87059	19 18 29.1	28 01 57.8	9.0
87108	19 20 46.5	28 02 32.4	9.0
87165	19 23 52.3	28 03 46.0	6.4
87229	19 26 47.4	27 59 45.2	9.0
87301 (β_1 Cyg)	19 30 13.0	27 55 58.5	3.2
87302 (β_2 Cyg)	19 30 15.1	27 56 18.8	5.4
87500	19 38 16.0	28 03 24.4	9.3
87503	19 38 22.4	28 03 00.2	9.2
87520	19 39 02.5	28 07 01.7	8.5
87590	19 41 31.1	28 04 29.6	8.9
87614	19 42 21.8	28 01 30.8	8.7
87651	19 43 59.9	28 03 20.0	9.3
87716	19 46 27.8	28 00 50.4	8.6
87769	19 48 47.5	28 04 34.5	9.4
87842	19 51 33.7	28 04 08.3	8.5
87877	19 52 45.3	28 03 59.9	7.8
87890	19 53 08.3	28 03 48.5	9.3
87931	19 54 48.5	28 04 58.2	9.2
88180	20 05 17.2	28 05 43.9	7.7
88197	20 05 37.1	28 05 23.2	8.3
88265	20 08 56.7	28 02 05.7	8.5
88357	20 12 12.0	28 02 11.0	8.9
88474	20 17 01.8	28 02 37.1	9.4
88475	20 17 03.9	28 04 21.2	9.0
88537	20 19 50.0	28 02 30.3	9.0
88563	20 20 44.3	28 04 08.5	8.5
88568	20 21 02.2	28 07 02.7	8.5
88627	20 23 36.9	28 04 26.4	9.3
88634	20 23 53.6	27 59 03.6	9.0
88684	20 26 15.0	28 01 34.4	8.8
88702	20 27 01.7	28 00 57.6	8.6

Table A1.3 (continued) - SAO stars in CTI Survey

SAO #/ name	RA (1987.5)	Dec	visual mag
88760	20 29 13.1	27 58 09.7	8.7
88854	20 33 50.6	27 59 45.3	9.4
88857	20 34 03.1	28 03 16.0	8.5
88948	20 38 01.1	27 58 01.7	9.2
88970	20 38 58.2	28 02 39.7	8.0
89100	20 44 58.3	28 05 59.0	9.2
89102	20 45 01.8	28 01 35.9	9.2
89108	20 45 19.1	28 01 18.8	9.2
89118	20 46 17.3	28 04 54.0	8.3
89125	20 46 31.7	28 05 54.6	9.2
89160	20 48 24.5	28 06 32.6	9.2
89169	20 48 55.5	28 03 16.2	9.1
89262	20 53 44.5	28 04 35.6	9.0
89272 (32 Vul)	20 54 01.6	28 00 34.9	5.2
89276	20 54 09.0	28 00 49.9	9.2
89278	20 54 29.9	28 02 36.4	8.0
89279	20 54 32.8	28 05 06.0	9.3
89359	20 59 44.5	28 01 48.3	9.2
89378	21 01 09.4	28 03 08.8	7.6
89433	21 04 06.6	28 04 52.1	9.1
89455	21 05 31.9	27 58 13.5	9.3
89534	21 12 26.7	28 06 14.0	8.1
89558	21 14 01.6	28 06 09.6	8.4
89562	21 14 35.7	28 05 10.0	9.0
89567	21 14 49.2	28 05 34.4	9.0
89569	21 15 04.0	27 57 26.4	8.1
89717	21 26 52.4	27 57 44.3	9.0
89816	21 34 47.5	27 57 51.4	8.8
89900	21 40 20.9	28 00 41.8	8.8
89996	21 46 45.5	28 02 01.3	8.4
90063	21 51 53.1	27 59 56.1	9.0
90152	21 59 02.8	28 04 50.0	8.5
90168	22 00 17.6	27 59 14.6	8.2
90172	22 00 48.8	27 58 22.9	9.3
90221	22 05 21.0	27 58 52.4	9.2
90253	22 07 14.0	28 04 19.2	9.3
90261	22 07 47.6	27 59 02.7	9.0
90264	22 08 02.4	28 05 06.4	8.6
90268	22 08 23.8	28 01 24.9	9.2
90272	22 08 42.0	28 01 01.6	9.0
90286	22 09 48.3	28 05 16.1	8.5
90369	22 15 21.6	28 04 22.4	9.2
90394	22 16 46.3	28 02 42.0	8.8
90464	22 23 05.0	27 57 31.1	9.5
90479	22 23 55.7	28 01 21.1	9.0
90534	22 27 58.1	28 04 48.9	9.0
90561	22 30 08.5	28 05 08.6	8.5
90617	22 34 20.2	28 01 27.2	9.0
90675	22 38 25.9	28 06 14.7	9.0

Table A1.3 (continued) - SAO stars in CTI Survey

SAO #/ name	RA (1987.5)	Dec	visual mag
90715	22 41 06.4	27 59 34.0	8.6
90732 (BD Peg)	22 42 23.3	28 05 30.2	8.9
90762	22 44 52.2	28 02 06.0	8.7
90799	22 47 54.2	28 03 22.2	8.1
90905	22 57 32.6	28 00 36.1	9.1
90929	22 59 21.8	28 04 15.9	9.0
90981 (β Peg)	23 03 09.4	28 00 48.4	2.6
91118	23 14 21.1	28 00 10.4	7.0
91153	23 17 14.0	27 57 31.8	8.5
91193	23 20 17.3	27 59 56.7	8.8
91214	23 21 43.8	28 03 20.9	8.5
91224	23 22 20.5	27 58 58.0	9.0
91252	23 24 43.2	28 07 23.7	8.6
91363	23 34 51.4	27 57 06.2	8.7
91406	23 39 02.8	27 57 19.4	9.1
91421	23 41 05.7	27 58 38.6	9.3
91472	23 45 10.8	28 06 29.5	7.9
91505	23 48 03.4	27 58 41.7	9.1

Table A1.4 - Previously known variable stars in CTI Survey

name	RA (1987.5)	Dec	mag range	Type
RW Tri	$02^h\ 24^m\ 52.4^s$	$28^\circ\ 02'\ 30.0''$	12.5 - 12.61	Algol
EP Tau	03 29 18.6	28 04 20.5	11 - >13	SR
RW Tau	04 03 08	28 05 37	7.98 - 11.59	Algol
AB Tau	05 40 14	28 06 06	10.4 - 12.0	SR
SV Tau	05 51 20	28 06 36	9.68 - 10.78	Algol
CN Tau	05 57 22.1	28 02 23.1	13.1 - 13.7	RR Lyr
AH Aur	06 25 17	28 00 26	10.2 - 10.70	W UMa
IR Gem	06 46 52	28 05 34	10.7 - >14.5	U Gem
GR Com	12 04 40.4	28 01 08.6	15.4 - 16.7	RR Lyr
GS Com	12 24 18.6	28 03 17.2	15.9 - 16.9	RR Lyr
DV Com	12 43 18.6	28 05 21.5	14.2 - 15.5	RR Lyr
EZ Com	13 17 32.6	28 01 39.6	16.5 - 17.5	RR Lyr
V375 Her	17 13 11.0	28 00 10.2	15.8 - 17.2	SR
V385 Her	17 15 57.0	28 06 44.6	14.9 - 15.9	RR Lyr
V532 Her	18 11 26.7	28 03 45.4	14.8 - 16.0	RR Lyr
CE Lyr	18 36 22.8	28 03 39.5	11.7 - 14.5	Mira
CV Lyr	18 50 06.0	28 05 59.7	10.8 - 13.1	SR
DF Lyr	18 53 04.5	28 03 22.6	13.1 - 13.5	W UMa
GS Lyr	19 03 50.3	28 00 44.9	14.4 - 14.8	L
UU Lyr	19 05 12.5	28 03 49.3	11.5 - >16.1	Mira
TY Lyr	19 09 17.7	28 03 04.6	9.0 - 14.6	Mira
V427 Lyr	19 13 11.8	28 00 51.6	15.3 - 17.3	RR Lyr
PP Lyr	19 17 13.8	28 06 06.6	13.3 - >15.6	Mira
V1129 Cyg	19 33 21.9	28 03 16.9	15.3 - >17	Mira
V911 Cyg	19 35 24.5	27 57 20.9	14.4 - 16.5	Algol
EH Cyg	19 36 18.5	28 06 00.1	11.8 - 16.5	Mira
V926 Cyg	19 38 06.6	27 59 09.9	15.2 - 15.9	RR Lyr
V1140 Cyg	19 39 16.7	28 03 26.4	15.3 - >20	Mira
AI Vul	19 46 17	28 05 55	13.2 - >17.5	Mira
EQ Vul	19 57 52.6	27 59 05.2	11.8 - 12.5	Algol
KW Vul	20 20 34.3	27 57 35.0	15 - >19	Mira
BY Peg	21 38 18.9	28 02 21.6	12.9 - 13.6	W UMa
CW Peg	21 47 54.0	28 02 59.1	11.8 - 16.1	Algol
BD Peg	22 42 23	28 05 28	9.4 - 10.3	SR
β Peg	23 03 09	28 00 43	2.31 - 2.74	Slow Irg

Table A1.5 - Bright galaxies in CTI Survey

name		RA (1987.5)	Dec	mag
Z 499020		00^h 09.3^m	28° 06'	15.7
Z 501011		00 46.4	28 00	15.4
Z 504093		02 28.3	28 05	15.7
Z 505003	(NGC 962)	02 32.0	28 01	14.2
Z 505052		02 45.2	27 58	15.6
Z 144002		06 19.8	27 59	15.6
Z 148026		07 47.3	28 03	15.6
Z 148028		07 47.5	28 03	15.5
Z 148056		07 53.1	28 04	15.6
Z 148116		08 07.9	28 06	15.4
Z 148117		08 08.4	28 02	15.3
Z 149014		08 18.2	28 03	15.6
Z 149026		08 27.5	28 07	15.2
Z 150004		08 35.5	28 06	14.9
Z 151008		09 03.7	28 00	14.4
Z 151044		09 16.1	28 07	15.7
Z 151054		09 18.0	28 01	15.7
Z 152042		09 37.4	28 07	14.8
Z 152071		09 49.3	28 05	15.3
Z 153027		10 09.7	28 01	14.6
Z 154004		10 20.6	27 59	15.2
Z 154008	(NGC 3232)	10 23.6	28 05	15.4
Z 154010	(NGC 3235)	10 24.2	28 05	14.7
Z 154039		10 41.7	28 05	15.5
Z 155004		10 44.5	28 03	15.7
Z 155020		10 48.5	27 59	15.3
Z 155029	(NGC 3414)	10 50.6	28 02	12.0
Z 155049	(NGC 3504)	11 02.6	28 03	11.5
Z 155051	(NGC 3512)	11 03.4	28 06	12.9
Z 156021		11 11.8	28 06	15.7
Z 156022		11 12.1	20 08	15.7
Z 156024		11 12.2	28 03	15.5
Z 156098		11 31.7	28 07	15.0
GQ Com		12 04.1	27 58	14.7-16.1
Z 158021		12 05.7	28 01	15.7
Z 158022		12 05.9	28 00	15.4
Z 158076		12 19.4	28 03	14.9
Z 158079		12 19.7	28 00	15.7
Z 159024	(NGC 4559)	12 35.3	28 02	10.7
Z 159051		12 40.3	28 03	15.4
NGC 4828		12 56.1	28 05	15.5
NGC 4850		12 57.4	28 02	15.5
NGC 4864		12 58.6	28 03	15.0
NGC 4867		12 58.7	28 04	15.5
NGC 4871		12 58.9	28 02	15.0
NGC 4872		12 59.0	28 01	15.5
NGC 4873		12 58.9	28 03	15.5
NGC 4874		12 59.0	28 02	13.5

Table A1.5 (continued) - Bright galaxies in CTI Survey

name		RA (1987.5)	Dec	mag
NGC 4883		12 59.3	28 06	15.0
NGC 4886		12 59.5	28 03	15.0
NGC 4889		12 59.5	28 03	12.5
NGC 4894		12 59.7	28 02	15.5
NGC 4898		12 59.7	28 01	14.5
NGC 4906		13 00.1	28 00	15.0
NGC 4908		13 00.2	28 07	15.0
NGC 4927		13 01.4	28 04	15.0
Z 160113	(NGC 4929)	13 02.1	28 06	14.9
Z 160118	(NGC 4931)	13 02.4	28 06	14.4
Z 160120	(NGC 4934)	13 02.7	28 05	15.0
Z 160123		13 03.3	28 03	15.4
Z 160141		13 06.6	28 06	15.5
Z 160149		13 08.4	28 06	15.6
Z 161065		13 28.6	28 06	15.7
Z 161092		13 57.1	28 04	15.7
Z 162039		13 58.5	28 05	15.6
Z 162040		13 58.5	28 07	15.6
Z 162041		13 58.6	28 02	15.7
Z 162044		13 59.0	28 08	15.3
Z 162053		14 02.4	28 05	14.7
Z 163055		14 27.5	28 00	15.7
Z 163079		14 33.0	28 06	15.3
Z 163081		14 33.5	28 00	15.2
Z 165021		15 07.4	28 01	15.5
Z 165024		15 08.7	28 02	15.7
Z 166036		15 40.9	28 02	15.2
Z 166052		15 45.1	28 08	14.9
Z 167021		16 04.2	28 08	15.6
Z 167030		16 09.1	28 05	14.7
Z 167048	(NGC 6092)	16 12.2	28 00	15.0
Z 169013	(NGC 6261)	16 56.0	28 01	15.2
Z 170028		17 24.3	28 05	15.7
Z 171030		17 56.3	28 05	15.6
Z 496043	(NGC 7487)	23 08.3	28 07	15.0
Z 498037		23 51.5	28 01	15.7
Z 499102		23 58.1	28 02	15.7

Table A1.6 - Variable star types (adapted from GCVS)

Cataclysmic (Characterized by thermonuclear processes in the interior of a star, the surface layers of star, or the surrounding space volume.)

Nova	Close binary system with one component a hot dwarf star. Mass transfer from cooler component excites a thermonuclear burst in dwarf's surface layers. Brightness increases of 7 to 19 magnitudes in V. Distinctions made between fast (fading of 3 magnitudes in V in < 100 days), slow (fading of 3 magnitudes in V in > 150 days), very slow (also called pseudonova, fading takes place over 10 years or longer) and recurrent (two or more outbursts observed) nova.
Supernova	Thermonuclear burst of entire star triggered by collapse of core. Brightness increases by 20 magnitudes or more in V. Distinctions made between Type I (no hydrogen lines present in spectra) and Type II (hydrogen lines present in spectra) supernova.
U Geminorum	(Also called dwarf nova.) Close binary with one component a white dwarf star surrounded by an accretion disk. Mass transfer excites periodic bursts in space surrounding white dwarf. Brightness increases from 2 to 6 magnitudes in V. Distinctions made between SS Cygni-type (cyclic), SU Ursae Majoris-type (cyclic with occasional larger outbursts), and Z Camelopardalis-type (cyclic with occasional variations in maximum and minimum brightness) variables.
Z Andromedae	Close binary of hot and late-type star with extended envelope excited by hot star's radiation. Irregular variations of up to 4 magnitudes in V.

Eruptive (Characterized by violent processes or flares in the star's chromosphere and coronae.)

Orion	Stars connected with diffuse nebulae and probably evolving to the zero-age main sequence. Variations of up to 6 magnitudes caused by star's interaction with surrounding circumstellar material. Irregular or cyclic variations observed. Distinctions made between early spectral types, intermediate and late spectral types, T Tauri-type (spectral type Fe-Me), YY Orionis-type (infall of matter observed in spectra), FU Orionis-type (large and sustained outburst), and flaring (identical to UV Ceti and related to nebulosity).
Rapid irregular	Similar to Orion variables, but with no apparent connection with diffuse nebulae. Brightness variations between 0.5 and 1.0 magnitudes in V. Distinctions made between early, intermediate, and late-type stars.

Table A1.6 (continued) - Variable star types (adapted from GCVS)

S Doradus	High luminosity stars connected with diffuse nebula and surrounded by expanding envelopes. Irregular, (although sometimes cyclic), brightness increases of 1 to 7 magnitudes in V.
G Cassiopeiae	Rapidly rotating stars with mass outflow from equatorial zone. Brightness variations of up to 1.5 magnitudes in V. Equatorial rings and disks often present.
Wolf-Rayet	Irregular brightness changes of up to 0.1 magnitudes in V probably caused by nonstable mass outflow from their atmospheres (stellar wind). Broadband emission features present.
UV Ceti	K-M stars displaying flare activity with brightness increases of tenths to 6 magnitudes in V. Flares peak rapidly and last from minutes to hours.
R Coronae Borealis	Hydrogen-poor, carbon- and helium-rich, high luminosity stars showing slow nonperiodic fading (1 to 9 magnitudes in V) and cyclic pulsations (tenths of magnitudes over 30-100 days).

Pulsating (Characterized by periodic radial or nonradial contractions and expansions of surface layers. Those variables within the "instability strip" of the H-R diagram are thought to all owe their pulsation to a variable opacity of the second ionization state of helium. Many types of pulsating variables also form the "Great Sequence" on the H-R diagram.)

δ Scuti	Both radial and non-radial pulsations of amplitudes from 0.003 to 0.9 magnitudes in V over periods of 0.01 to 0.2 days. Stars are of Population I with spectral types A0-F5, and are contained in the "instability strip" of the H-R diagram near the Main Sequence.
SX Pheonices	(Previously called dwarf Cepheid or RRs.) Similar to δ Scuti variables except stars are of Population II.
RR Lyrae	Radially pulsating giant (A2-F2) helium core burning stars of amplitudes from 0.2 to 2 magnitudes in V over periods of 0.3 to 1.2 days. Stars are of Population II and are in the "instability strip" of the H-R diagram. Distinctions made between ab-type (steep ascending branch), c-type (nearly symmetric with shorter periods and smaller light amplitudes), and stars with more than one pulsational mode present.
Classical Cepheids	(Also known as δ Cephei-type variables.) Population I, massive, high luminosity stars that have left the main sequence and evolved into the "instability strip" of the H-R diagram. Radial pulsations produce brightness variations of hundredths to 2 magnitudes in V

Table A1.6 (continued) - Variable star types (adapted from GCVS)

	over periods of 1 to 135 days. Exhibits relation between period and absolute luminosity. Distinctions made between stars with single and multiple pulsation modes.
W Virginis	Similar to Classical Cepheids, except stars are of Population II. Radial pulsations produce brightness variations of 0.3 to 1.2 magnitudes in V over periods of 0.8 to 35 days.
RV Tauri	Radially pulsating supergiant exhibiting two pulsations of unequal maxima and minima. Occasional shifts between primary and secondary minima observed. Periods between two primary minima range form 30 to 150 days with a brightness variation of up to 4 magnitudes in V. Distinctions made between stars whose mean magnitude also changes over periods of 600 to 1500 days and those that do not change.
Semi-regular	Giants and supergiants of intermediate to late spectral types showing noticeable periodicity accompanied by various irregularities. Shape of light curve is also variable. Brightness amplitudes range from hundredths to several magnitudes over periods of 20 to over 2000 days. Distinctions made between late-type giants, late-type giants with poor periodicity, late-type supergiants, and earlier-type giants and supergiants.
Slow Irregular	Late-type giants or supergiants showing no evidence of periodicity.
Mira	Giants with late-type emission spectra. Brightness amplitudes from 2.5 to 11 magnitudes in V over periods from 80 to 1000 days. Periodicity well pronounced.
α Cygni	Nonradially pulsating supergiant (B-A spectral type) with brightness variations of approximately 0.1 magnitudes in V. Superposition of many oscillations with close periods and cycles from several days to several weeks.
β Cephei	(Also known as β Canis Majoris variables.) Radially pulsating stars of spectral type O8-B6 with brightness variations of 0.01 to 0.3 magnitudes in V over periods from 0.1 to 0.6 days. Many of these stars exhibit multiple periods and nonradial pulsations.
PV Telescopium	B spectral type supergiant with weak hydrogen lines and enhanced helium and carbon lines. Brightness variations of up to 0.1 mags in V over periods from 0.1 to 1 day.

Table A1.6 (continued) - Variable star types (adapted from GCVS)

ZZ Ceti	Nonradially pulsating white dwarfs with brightness variations of 0.001 to 0.2 in V over periods of 30 seconds to 25 minutes. Many close oscillation modes are present. Distinctions made between those having hydrogen absorption lines and those having helium absorption lines.

Rotating (Characterized by stars with nonuniform surface brightness or ellipsoidal shapes. Variability caused by star's rotation.)

α_2 Canum Venaticorum	Main sequence B8-A7 stars having strong variable magnetic fields. Brightness variations of 0.01 to 0.1 magnitudes in V over periods from 0.5 to >160 days. Distinction made between those also displaying nonradial pulsations of about 0.01 magnitudes in V over 0.004 to 0.01 days and those that do not.
RS Canum Venaticorum	CaII H and K emission line of stars in close binary system showing nonuniform surface brightness (star spots) and chromospheric activity. Brightness variations on the order of 0.2 magnitudes in V.
BY Draconis	CaII H and K emission line dwarfs of K-M spectral type showing nonuniform surface brightness (star spots) and chromospheric activity. Brightness variations of hundredths to 0.5 magnitudes in V over periods from hours to 120 days. Some stars also exhibit flares, and are simultaneously classified as UV Ceti stars. Similar to RS Canum Venaticorum variable stars.
FK Comae Bernices	Giants of G-K spectral type with broad H and K CaII emission. Brightness variations of tenths of magnitudes in V over periods up to several days. Possibly related to W Ursa Majoris eclipsing variables.
SX Arietis	Main sequence B0-B9 stars with variable spectral features and magnetic fields. Brightness variations of about 0.1 magnitudes in V over periods of about 1 day. Similar to α_2 Canum Venaticorum type variables.
ellipsoidal	Close binary system with ellipsoidal components. Brightness variations caused by varying projection of stars as seen by observer. No eclipses are present.
pulsars	Rapidly rotating neutron stars with strong magnetic fields emitting narrow beams of synchrotron radiation (radio, visible, X-ray). Brightness variations of up to 0.8 magnitudes in V over periods from 0.004 to 4 seconds.

Table A1.6 (continued) - Variable Star Types (adapted from GCVS)

Eclipsing (Characterized by close binary systems where variation is primarily caused by eclipses of one star by the other.)

Algol	Spherical or near spherical components where it is possible to specify the beginning and end of the eclipses. Spectral types of components and degree of filling of inner Roche lobes are also often specified in classification. (This is true for β Lyrae-type and W Ursae Majoris-type variables as well.)
β Lyrae	Ellipsoidal components where it is impossible to specify the beginning and end of the eclipses. Depth of secondary minimum is considerably smaller than primary minimum.
W Ursae Majoris	Ellipsoidal components almost in contact with each other where it is impossible to specify the beginning and end of the eclipses. Depths of primary and secondary minima are almost equal.

Table A1.7 - Bright Star Masks

SAO stars with V < 5 (individually masked)	
ι Gem	$7^h\ 24^m\ 50^s$ - $7^h\ 25^m\ 00^s$ (south of 28° 03' 00")
Pollux	$7^h\ 42^m\ 45^s$ - $7^h\ 46^m\ 15^s$
β Com	$13^h\ 10^m\ 45^s$ - $13^h\ 12^m\ 00^s$ (south of 28° 25' 12")
Albireo	$19^h\ 29^m\ 30^s$ - $19^h\ 31^m\ 00^s$ (south of 28° 03' 36")
Scheat	$23^h\ 02^m\ 00^s$ - $23^h\ 04^m\ 30^s$
SAO stars with 5 < V < 7.6	
radius	$43 + (4.037 \times 10^{-7}) \times 10^{((25.75-V)/2.5)}$ pixels
centered	on star
additionally	10 pixel wide region in RA for all declinations
additionally	10 pixel wide region in declination, 1.6 times mask radius to east if radius > 60
SAO stars with V > 7.6	
radius	$27 + (1.287 \times 10^{-6}) \times 10^{((25.75-V)/2.5)}$ pixels
centered	on star
additionally	10 pixel wide region in RA for all northern declinations
additionally	10 pixel wide region in RA, 1.5 times mask radius for southern declinations if radius > 35
CTI stars with V < 12	
radius	22 pixels (V < 11), or 22 - 10 × (V - 11) pixels (V > 11)
centered	10 × (12 - V) pixels north and east of star

Table A1.8 - Sample S/N Calculations for Capilla Peak

I. Signal to Noise Calculation Parameters

gain = 15.6 electrons/ADU
Readout Noise = 57.0 electrons
Truncation Noise = 4.5 electrons
Bias level Noise = 8.0 electrons
Preflash level Noise = 16.0 electrons

photometry area = 380.12 (11 pixel radius)
3 flat field frames at 10000 ADU level
flat field noise = 0.001478 electrons per pixel per ADU

OPTION #1: superbias and superskim subtracted frames
2 superbiases with 25 bias frames per superbias
3 skimflats at 100 ADU level
Baseline Noise = **58.49** electrons

OPTION #2: superpreflashbias subtracted frames
2 superpreflashbiases with 7 preflashbiases per superpreflashbias, preflash at 100 ADU level
Baseline Noise = **74.25** electrons

OPTION #3: superpreflashbias subtracted frames
1 superpreflashbias made up of 2 preflashbiases
preflash at 100 ADU level
Baseline Noise = **82.43** electrons

Table A1.8 - Sample S/N Calculations (continued)

II. Moonless night
sky brightness = 0.87 #electrons per pixel per second
= 22.3 V mag

OPTION #1 Signal to Noise

	time (seconds)									
V	30	60	120	180	300	600	900	1200	1500	1800
12	258.1	402.0								
13	117.7	214.4	348.5	428.1						
14	49.0	94.7	175.0	240.3	334.0					
15	19.8	39.1	75.6	109.2	167.8	269.2	327.7	363.0		
16	7.9	15.7	30.9	45.5	72.8	129.1	170.3	200.1	221.9	238.1
17	3.2	6.3	12.4	18.4	29.9	55.2	75.8	92.2	105.2	115.6
18	1.3	2.5	5.0	7.4	12.0	22.6	31.5	38.9	45.1	50.1
19		1.0	2.0	2.9	4.8	9.1	12.8	15.9	18.5	20.7
20			0.8	1.2	1.9	3.6	5.1	6.4	7.4	8.3
21					0.8	1.4	2.0	2.5	3.0	3.3
22								1.0	1.2	1.3

OPTION #2 Signal to Noise:

	time (seconds)									
V	30	60	120	180	300	600	900	1200	1500	1800
12	218.0	360.5								
13	95.2	178.8	306.9	391.8						
14	39.0	76.4	144.8	204.2	296.6					
15	15.7	31.1	60.9	89.1	140.5	238.4	301.5	342.3		
16	6.3	12.5	24.7	36.6	59.3	109.1	148.9	179.7	203.5	222.0
17	2.5	5.0	9.9	14.7	24.1	45.7	64.4	80.2	93.5	104.5
18	1.0	2.0	3.9	5.9	9.7	18.5	26.4	33.4	39.4	44.6
19		0.8	1.6	2.3	3.9	7.4	10.7	13.5	16.0	18.2
20				0.9	1.5	3.0	4.3	5.4	6.4	7.3
21					0.6	1.2	1.7	2.2	2.6	2.9
22								0.9	1.0	1.2

OPTION #3 Signal to Noise:

	time (seconds)									
V	30	60	120	180	300	600	900	1200	1500	1800
12	201.1	340.6								
13	86.5	164.1	287.8	373.7						
14	35.3	69.3	132.6	188.7	279.1					
15	14.2	28.1	55.2	81.2	129.1	224.1	288.3	331.2		
16	5.7	11.3	22.3	33.1	54.0	100.7	139.2	170.0	194.3	213.6
17	2.3	4.5	8.9	13.3	21.9	41.8	59.5	74.9	88.0	99.1
18	0.9	1.8	3.6	5.3	8.8	16.9	24.3	31.0	36.8	42.0
19		0.7	1.4	2.1	3.5	6.8	9.8	12.5	14.9	17.1
20				0.8	1.4	2.7	3.9	5.0	6.0	6.9
21					0.6	1.1	1.6	2.0	2.4	2.7
22								0.8	1.0	1.1

Table A1.8 - Sample S/N Calculations (continued)

III. Bright Moon night
sky brightness = 4.33 #electrons per pixel per second
= 20.5 V mag

OPTION #1 Signal to Noise

	time (seconds)									
V	30	60	120	180	300	600	900	1200	1500	1800
12	251.4	382.0								
13	115.1	203.5	313.9	372.4						
14	48.1	90.5	157.7	204.8	260.7					
15	19.5	37.5	68.8	93.8	128.7	169.3	185.3	193.3		
16	7.8	15.2	28.4	39.5	56.2	78.0	87.4	92.3	95.2	97.1
17	3.1	6.1	11.4	16.1	23.2	33.1	37.5	39.9	41.3	42.2
18	1.2	2.4	4.6	6.4	9.4	13.5	15.4	16.4	17.0	17.4
19		1.0	1.8	2.6	3.8	5.4	6.2	6.6	6.9	7.1
20			0.7	1.0	1.5	2.2	2.5	2.7	2.8	2.8
21					0.6	0.9	1.0	1.1	1.1	1.1
22								0.4	0.4	0.4

OPTION #2 Signal to Noise:

	time (seconds)									
V	30	60	120	180	300	600	900	1200	1500	1800
12	213.9	345.8								
13	93.8	172.3	282.5	347.8						
14	38.5	74.1	134.6	181.0	241.7					
15	15.5	30.3	57.2	80.1	115.1	160.8	180.2	189.9		
16	6.2	12.2	23.3	33.2	49.2	72.9	84.1	90.0	93.6	95.9
17	2.5	4.9	9.4	13.4	20.2	30.6	35.9	38.7	40.5	41.6
18	1.0	1.9	3.7	5.4	8.1	12.5	14.7	15.9	16.7	17.2
19		0.8	1.5	2.1	3.2	5.0	5.9	6.4	6.7	6.9
20				0.9	1.3	2.0	2.4	2.6	2.7	2.8
21					0.5	0.8	0.9	1.0	1.1	1.1
22								0.4	0.4	0.4

OPTION #3 Signal to Noise:

	time (seconds)									
V	30	60	120	180	300	600	900	1200	1500	1800
12	197.8	328.2								
13	85.5	159.1	267.4	334.9						
14	34.9	67.6	124.6	170.0	232.0					
15	14.0	27.5	52.4	74.2	108.6	156.2	177.2	188.0		
16	5.6	11.0	21.3	30.6	46.1	70.2	82.2	88.7	92.6	95.2
17	2.2	4.4	8.5	12.3	18.8	29.4	35.0	38.1	40.0	41.2
18	0.9	1.8	3.4	4.9	7.6	11.9	14.3	15.6	16.5	17.0
19		0.7	1.4	2.0	3.0	4.8	5.8	6.3	6.6	6.9
20				0.8	1.2	1.9	2.3	2.5	2.7	2.8
21					0.5	0.8	0.9	1.0	1.1	1.1
22								0.4	0.4	0.4

Table A1.9 - Capilla Peak Observation Dates

date	dayno	%used	observers	nights
93Jun20	3093	5%	Wetterer, Boudreau	0.05
93Jun24	3097	70%	Boudreau	0.75
93Jun26	3099	55%	McGraw, Kunkle, Boudreau, Vogel	1.30
93Jul06	3109	45%	Grashuis, Boudreau	1.75
93Jul09	3112	50%	Wetterer, Grashuis	2.25
93Jul10	3113	85%	Grashuis	3.10
93Jul23	3126	50%	Wetterer, Kunkle	3.60
93Jul25	3128	100%	Wetterer, Grashuis	4.60
93Jul26	3129	100%	Grashuis	5.60
93Jul27	3130	30%	Grashuis, Kunkle	5.90
93Sep04	3169	50%	Grashuis	6.40
93Sep09	3174	100%	Wetterer, Grashuis, Weichman	7.40
93Sep10	3175	70%	Grashuis	8.10
93sep15	3180	100%	Wetterer, Grashuis	9.10
93Sep16	3181	100%	Grashuis	10.10
93Sep21	3186	60%	Grashuis	10.70
93Sep22	3187	60%	Grashuis, Adams	11.30
93Sep24	3189	40%	Grashuis, Kunkle, Vogel, Collette	11.70
93Sep29	3194	40%	Grashuis	12.10
93Sep30	3195	40%	Grashuis	12.50
93Oct06	3201	5%	Grashuis	12.55
93Oct08	3203	5%	Grashuis	12.60
93Oct09	3204	15%	Grashuis, Boudreau	12.75
93Oct10	3205	45%	Grashuis, Boudreau	13.20
93Oct11	3206	10%	Grashuis, Adams	13.30
93Oct14	3209	20%	Boudreau	13.50
93Oct15	3210	0%	Boudreau (Sky flats only)	13.50
93Oct16	3211	20%	Boudreau	13.70
93Oct22	3217	10%	Grashuis, Fairweather, Malahkov	13.80
93Oct23	3218	5%	Grashuis, Fairweather, Gregory, +	13.85
93Oct28	3223	5%	Grashuis	13.90
93Nov05	3231	40%	Grashuis	14.30
93Nov06	3232	25%	Grashuis, McGraw, McGraw's class	14.55
93Nov08	3234	100%	Wetterer, Grashuis	15.55
93Nov19	3245	30%	Grashuis, Boudreau	15.85
93Nov20	3246	25%	Grashuis, Kunkle	16.10
93Nov21	3247	12%	Boudreau, Fairweather, Kraybill	16.22
93Dec06	3262	5%	Grashuis, Adams	16.27
93Dec09	3265	0%	Wetterer, Grashuis, Miller (tests)	16.27
93Dec17	3273	25%	Grashuis, Adams	16.52
94Jan10	3297	0%	Wetterer, Grashuis (CCD tests)	16.52
94Jan11	3298	100%	Wetterer, Grashuis	17.52
94Jan14	3301	0%	Grashuis, Adams (CCD tests)	17.52
94Jan20	3307	40%	Grashuis	17.92
94Jan21	3308	60%	Grashuis	18.52
94Feb13	3331	80%	Grashuis, Boudreau	19.32
94Feb17	3335	0%	Grashuis (CCD tests)	19.32
94Feb24	3342	90%	Grashuis, Adams	20.22
94Mar05	3355	30%	Boudreau	20.52

Table A1.9 - Capilla Peak Observation Dates (continued)

date	dayno	%used	observers	nights
94Mar06	3356	5%	Boudreau	20.57
94Mar10	3360	75%	Grashuis, Adams	21.32
94Mar11	3361	10%	Grashuis	21.42
94Mar15	3365	100%	Grashuis	22.42
94Mar17	3367	90%	Grashuis	23.32
94Apr07	3384	2%	Wetterer	23.34
94Apr08	3385	90%	Wetterer, Grashuis	24.24
94Jun15	3453	100%	Wetterer, Grashuis	25.24
94Jun16	3454	100%	Wetterer, Grashuis	26.24
94Jun25	3463	35%	Boudreau, Chavot, Lopshire, Rivers	26.59
94Jun26	3464	16%	Boudreau	27.75
94Jun27	3465	35%	Boudreau	28.10
94Jun30	3468	100%	Grashuis, Boudreau	29.10
94Jul01	3469	60%	Grashuis, Boudreau	29.70
94Jul05	3473	60%	Wetterer, Kunkle	30.30
94Jul06	3474	100%	Wetterer, Grashuis	31.30
94Jul10	3478	60%	Boudreau	31.90
94Jul12	3480	60%	Grashuis, Kunkle	32.50
94Jul13	3481	95%	Wetterer, Grashuis	33.45
94Jul16	3484	20%	Boudreau	33.65
94Jul19	3487	50%	Grashuis	34.15
94Jul20	3488	60%	Grashuis	34.75
94Aug04	3503	20%	Boudreau, Kunkle, Rivers	34.95
94Aug13	3512	80%	Wetterer, Kraybill	35.75
94Aug17	3516	90%	Wetterer, Rivers	36.65
94Aug18	3517	100%	Wetterer, Oetiker	37.65
94Sep09	3539	100%	Grashuis	38.65
94Sep10	3540	65%	Grashuis	39.30
94Sep15	3545	100%	Wetterer, Grashuis	40.30
94Sep16	3546	65%	Wetterer, Grashuis	40.95
94Sep29	3559	30%	Grashuis	41.25
94Oct03	3563	40%	Wetterer, Grashuis	41.55
94Oct09	3569	100%	Grashuis, Boudreau	42.55
94Nov15	3606	15%	Grashuis	42.70
94Nov16	3607	30%	Grashuis	43.00
94Dec01	3622	100%	Wetterer, Grashuis	44.00
94Dec20	3641	90%	Wetterer, Grashuis	44.90
95Jan08	3660	20%	Wetterer, Grashuis	45.10
95Jan14	3666	90%	Grashuis	46.00
95Jan15	3667	15%	Grashuis	46.15
95Jan21	3673	2%	Grashuis, Adams	46.17
95Jan29	3681	33%	Grahsuis, Adams	46.50
95Jan31	3683	15%	Grashuis	46.65
95Feb02	3685	95%	Wetterer, Grashuis	47.60

Table A1.10 - Capilla Peak Observer Log Summary

observer	# V images
Grashuis	1227
Wetterer	644
Boudreau	266
Kunkle	104
Adams	53
Rivers	45
Oetiker	41
Vogel	33
Weichman	30
Kraybill	25
McGraw	23
Collette	10
Chavot	10
Lopshire	10
Fairweather	10
Malahkov	6
Gregory	2
Anderson	2
TOTAL	1465

Table A1.11 - Capilla Peak Image Log

images	description
1465	images through V filter (RR Lyr candidates)
35	images through V filter (Mira variables)
44	images through V filter (calibration)
83	images through V filter (CCD tests)
33	images through B filter (RR Lyr candidates)
360	bias or superbias images
615	V and B sky flats
46	V skim flats
367	preflash darks
18	superpreflashbias-7s
13	darks
1	pretty picture
3036	TOTAL

Table A1.12 - Bright RR Lyrae stars in GCVS

RRab

	Name	RA			Dec		Type	Max	Min	Mean	Av	r(pc)
1	RR Lyr	19	23	52	42	41.2	RRAB	7.06	8.12	7.68	0.36	207
2	FW Lup	15	19	07	-40	44.9	RR	8.82	9.22	9.03	0.36	385
3	X Ari	03	05	48	10	15.4	RRAB	8.97	9.95	9.54	0.68	422
4	UV Oct	16	20	24	-83	47.5	RRAB	8.70	9.97	9.45	0.27	488
5	XZ Cyg	19	31	27	56	16.8	RRAB	8.90	10.16	9.65	0.32	523
6	ST Pic	06	13	30	-61	27.3	RR	9.29	9.77	9.55	0.09	555
7	XZ Cet	01	57	53	-16	35.3	RRAB	9.24	9.71	9.49	0.00	563
8	SW And	00	21	06	29	07.5	RRAB	9.14	10.09	9.69	0.14	580
9	RX Eri	04	47	29	-15	49.6	RRAB	9.17	10.10	9.71	0.09	597
10	RR Cet	01	29	34	01	05.1	RRAB	9.10	10.10	9.69	0.02	609
11	DX Del	20	45	06	12	16.7	RRAB	9.52	10.26	9.94	0.27	612
12	SV Eri	03	09	28	-11	32.6	RRAB	9.56	10.23	9.94	0.18	636
13	SU Dra	11	35	07	67	36.4	RRAB	9.18	10.27	9.82	0.05	642
14	TU UMa	11	27	10	30	20.6	RRAB	9.26	10.24	9.83	0.01	655
15	TT Lyn	08	59	49	44	47.1	RRAB	9.42	10.21	9.87	0.05	657
16	V Ind	21	08	11	-45	16.7	RRAB	9.12	10.48	9.93	0.05	675
17	IK Hya	12	02	14	-27	23.9	RR	9.96	10.42	10.21	0.27	691
18	XZ Dra	19	09	24	64	46.6	RRAB	9.59	10.65	10.21	0.27	693
19	V440 Sgr	19	29	20	-23	57.6	RRAB	9.60	10.80	10.31	0.36	695
20	VY Ser	15	28	30	01	51.2	RRAB	9.73	10.46	10.15	0.06	740
21	SS For	02	05	36	-27	06.1	RRAB	9.45	10.60	10.13	0.00	755
22	S Ara	17	55	19	-49	25.8	RRAB	9.96	11.20	10.70	0.54	764
23	RU Scl	00	00	14	-25	13.4	RRAB	9.35	10.75	10.19	0.02	767
24	SV Hya	12	27	53	-25	46.3	RRAB	9.78	11.00	10.50	0.27	792
25	BH Peg	22	50	32	15	30.8	RRAB	9.99	10.79	10.45	0.18	805
26	AT And	23	40	02	42	44.3	RRAB	10.42	10.92	10.69	0.41	812
27	V413 CrA	18	44	34	-37	47.6	RRAB	10.23	10.90	10.61	0.32	814
28	AV Peg	21	49	47	22	19.3	RRAB	9.88	10.92	10.49	0.18	820
29	RS Boo	14	31	25	31	58.4	RRAB	9.69	10.84	10.37	0.00	843
30	SW Dra	12	15	26	69	47.3	RRAB	9.94	10.94	10.53	0.05	887
31	V445 Oph	16	22	00	-06	25.3	RRAB	10.53	11.39	11.03	0.54	890
32	VX Her	16	28	28	18	28.1	RRAB	9.89	11.21	10.68	0.18	893
33	V341 Aql	20	29	58	00	24.9	RRAB	10.13	11.39	10.88	0.36	903
34	XX And	01	14	36	38	41.3	RRAB	10.08	11.13	10.70	0.15	915
35	U Lep	04	54	09	-21	17.6	RRAB	9.84	11.11	10.59	0.05	916
36	W CVn	14	04	21	38	04.0	RRAB	10.03	10.96	10.57	0.00	925
37	UU Vir	12	06	01	00	12.5	RRAB	9.89	11.07	10.59	0.01	928
38	WY Ant	10	13	48	-29	28.2	RRAB	10.27	11.22	10.82	0.18	957
39	WZ Hya	10	10	59	-12	53.6	RRAB	10.27	11.28	10.86	0.18	973
40	RR Leo	10	04	56	24	14.2	RRAB	9.94	11.27	10.73	0.05	976
41	RV UMa	13	31	21	54	14.7	RRAB	9.81	11.30	10.70	0.00	982
42	RV Cet	02	12	49	-11	02.0	RRAB	10.35	11.22	10.85	0.05	1031
43	KX Lyr	18	31	45	40	08.0	RRAB	10.38	11.47	11.02	0.15	1062
44	UY Boo	13	56	20	13	11.7	RRAB	10.25	11.35	10.90	0.00	1075
45	RY Col	05	13	33	-41	41.1	RRAB	10.44	11.24	10.90	0.00	1076
46	AN Ser	15	51	11	13	07.1	RRAB	10.40	11.44	11.01	0.05	1109
47	ST Boo	15	28	44	35	57.3	RRAB	10.49	11.41	11.03	0.05	1117
48	VW Scl	01	15	59	-39	28.6	RRAB	10.40	11.40	10.99	0.00	1119
49	SX For	03	28	26	-36	13.3	RRAB	10.68	11.38	11.08	0.00	1168
50	BB Vir	13	49	11	06	40.7	RRAB	10.70	11.42	11.11	0.02	1174

RRc

1	MT Tel	18	58	31	-46	43.5	RRC	8.68	9.28	8.98	0.18	409
2	CS Eri	02	35	11	-43	10.8	RRC	8.75	9.31	9.03	0.00	455
3	DH Peg	22	12	55	06	34.4	RRC	9.15	9.80	9.48	0.18	514
4	T Sex	09	50	53	02	17.6	RRC	9.81	10.32	10.07	0.09	703
5	RU Psc	01	11	42	24	09.1	RRC	9.93	10.40	10.17	0.09	736

Table A1.12 (continued) - Bright RR Lyrae stars in GCVS

	Name	RA	Dec	Type	Max	Min	Mean	Av	r(pc)
6	BB CMi	07 48 46	05 02.8	RRC	10.00	10.80	10.40	0.09	820
7	XZ Gru	22 44 43	-39 19.8	RRC	10.40	10.70	10.55	0.00	916
8	AE Boo	14 45 15	17 03.3	RRC	10.44	10.88	10.66	0.01	959
9	SS Psc	01 18 10	21 28.5	RRC	10.73	11.21	10.97	0.14	1045
10	SX UMa	13 24 17	56 31.0	RRC	10.58	11.21	10.90	0.00	1074
11	LS Her	15 59 49	17 37.2	RRC	10.79	11.12	10.96	0.05	1081
12	BV Aqr	22 00 07	-21 46.1	RRC	10.80	11.20	11.00	0.05	1104
13	TV Boo	14 14 37	42 35.5	RRC	10.71	11.30	11.01	0.00	1130
14	AP Ser	15 11 37	10 10.0	RRC	10.85	11.38	11.12	0.05	1164
15	AO Tuc	00 01 34	-59 45.8	RRC	10.88	11.40	11.14	0.00	1202
	RR Lyrae stars within 10° of Galactic plane								
	V1719Cyg	21 02 56	50 35.1	RRC	7.95	8.33	8.23		
	RZ Cep	22 37 28	64 35.7	RRC	9.11	9.75	9.55		
	V675 Sgr	18 10 16	-34 19.9	RRAB	9.80	10.76	10.36		
	AR Per	04 13 38	47 16.7	RRAB	9.92	10.83	10.45		
	V363 Cas	00 12 33	60 03.8	RRAB	10.29	10.73	10.53		
	CZ Lac	22 17 33	51 13.2	RRAB	10.77	11.26	11.04		
	BN Vul	19 25 50	24 14.7	RRAB	10.63	11.40	11.07		
	UY Cyg	20 54 22	30 14.1	RRAB	10.59	11.46	11.09		
	Possible additional RR Lyrae variable stars								
	S Eri	04 57 36	-12 36.6	RRC	4.77	4.80			
	V819 Cen	13 16 12	-57 55.9	RR	9.00	9.07			
	AW Mic	21 16 02	-34 07.8	RRC	9.04	9.13			
	V429 Ori	04 53 44	-03 36.5	RRAB	10.00	11.00			
	V753 Cen	11 48 44	-55 31.3	RRC	10.24	10.64			
	V1356Aql	19 44 23	-02 11.5	RRC	10.30	10.50			
	IV Pav	20 29 23	-72 47.2	RR	10.40	10.80			

Appendix 2 - Database Descriptions

Descriptions for those databases created specifically for this dissertation and used frequently are listed in this appendix. Descriptions for CTI data reduction and analysis databases can be found in The CCD/Transit Instrument Atlas and Database Guide (Wetterer 1995). Descriptions for other user defined databases must be found elsewhere. The contents of all databases and all attribute titles are available by using the CTI program DBDESC. The database descriptions in this appendix are listed in alphabetical order. Each listing contains the database extension, date and time of creation, database title, listing of header attributes and main attributes with attribute type (e.g. integer) and array size (e.g. scalar), and a short description of each main attribute. If the internal and external type differ or there exists a mapping, this is listed as well. All databases with headers have essentially the same attributes in their header. The descriptions for these header attributes are:

NRECS - number of records contained in the database
DATE - date file was produced (yy/mm/dd)
PROGNAME- program used to create database
ORIGIN - description of database's origin
PARM - Twenty three to eighty three parameters. Described for particular database type if appropriate. (For example, the parameters for the .CAL database are defined in CALPARMS.INC, and the parameters for all other databases in the pipeline are defined in PCP.INC.)

Database: .BSA Version: (94/02/11|09:08:03)
Description: bright star mask areas

Header attributes...

NRECS	type: INTEGER	(scalar)
DATE	type: STRING* 8	(scalar)
PROGNAME	type: STRING*12	(scalar)
ORIGIN	type: STRING*44	(scalar)
PARM	type: REAL	(23)

Record attributes...

YCTI	ext: DOUBLE int: INTEGER map: LINEAR	(scalar)
P_AREA	type: REAL	(scalar)

YCTI - right ascension of bright star in centipixels
P_AREA - Area in square pixels masked by star

Database: .BSM Version: (93/11/29|10:28:39)
Description: bright star masks

Header attributes...

NRECS	type: INTEGER	(scalar)
DATE	type: STRING* 8	(scalar)
PROGNAME	type: STRING*12	(scalar)
ORIGIN	type: STRING*44	(scalar)
PARM	type: REAL	(23)

Record attributes...

XCTI	ext: DOUBLE int: INTEGER map: LINEAR	(scalar)
YCTI	ext: DOUBLE int: INTEGER map: LINEAR	(scalar)
RMASK	type: INTEGER	(scalar)
CATID	type: INTEGER	(scalar)

XCTI - Declination of bright star in centipixels
YCTI - Right ascension of bright star in centipixels
RMASK - Radius of mask in pixels
CATID - Identification of bright star (SAO number or mlink)

Database: .BVH Version: (94/01/28|14:13:15)
Description: B and V history list

Header attributes...

NRECS	type: INTEGER	(scalar)
DATE	type: STRING* 8	(scalar)
PROGNAME	type: STRING*12	(scalar)
ORIGIN	type: STRING*44	(scalar)
PARM	type: REAL	(23)

Record attributes...

MLINK	ext: POINT int: INTEGER	(scalar)
HLINK	ext: POINT int: INTEGER	(2)
YCTI	ext: DOUBLE int: INTEGER map: LINEAR	(scalar)
XCTI	ext: DOUBLE int: INTEGER map: LINEAR	(scalar)
BDAYVAL	type: INTEGER	(21)
BLUM	type: REAL	(21)
BLUMERR	type: REAL	(21)
VDAYVAL	type: INTEGER	(63)
VLUM	type: REAL	(63)
VLUMERR	type: REAL	(63)

MLINK - Pointer to master list (**.NML** database)
HLINK - Pointers to B and V history lists (**.NHL** databases)
YCTI - Right Ascension in centipixels
XCTI - Declination in centipixels
BDAYVAL - B Observation times in CTI dayno × 10^5
BLUM - B Luminosities in ADUs
BLUMERR - B Luminosity errors in ADUs
VDAYVAL - V Observation times in CTI dayno × 10^5
VLUM - V Luminosities in ADUs
VLUMERR - V Luminosity errors in ADUs

Note: older versions of this database using the **.MAS** and **.HIS** databases used 42 number arrays for BDAYVAL, BLUM, BLUMERR, VDAYVAL, VLUM, and VLUMERR and have the **.OBV** extension.

Database: .CAT Version: (93/11/22|08:02:56)
Description: Catalog

Header attributes...

NRECS	type: INTEGER	(scalar)
DATE	type: STRING* 8	(scalar)
PROGNAME	type: STRING*12	(scalar)
ORIGIN	type: STRING*44	(scalar)
PARM	type: REAL	(23)

Record attributes...

CATID	type: INTEGER	(scalar)
RA_HOUR	type: SHORT	(scalar)
RA_MIN	type: SHORT	(scalar)
RA_SEC	type: REAL	(scalar)
DEC_DEG	type: SHORT	(scalar)
DEC_MIN	type: SHORT	(scalar)
DEC_SEC	type: REAL	(scalar)
EPOCH	type: REAL	(scalar)
V	type: REAL	(scalar)
CATCODE	type: INTEGER	(scalar)

CATID - Identification of object in catalog (SAO number, Zwicky number, etc..)
RA_HOUR - Hour of right ascension
RA_MIN - Minute of right ascension
RA_SEC - Second of right ascension
DEC_DEG - Degree of declination
DEC_MIN - Arcminute of declination
DEC_SEC - Arcsecond of declination
EPOCH - Epoch of right ascension and declination
V - Magnitude
CATCODE - Identification of catalog (unique integer)

Database: .HST Version: (94/02/04|07:54:16)
Description: Histogram Result

Header attributes...

NRECS	type: INTEGER	(scalar)
DATE	type: STRING* 8	(scalar)
PROGNAME	type: STRING*12	(scalar)
ORIGIN	type: STRING*44	(scalar)
PARM	type: REAL	(23)

Record attributes...

BINID	type: REAL	(scalar)
BINTOTAL	type: INTEGER	(scalar)
BINSHADED	type: INTEGER	(scalar)

```
BINID   - Center of bin in histogram
BINTOTAL- Total number of records in bin
BINSHADED Total number of records shaded in bin
```

Database: .NPL Version:
Description: Normal Point List

```
Header attributes...
NRECS       type: INTEGER              (scalar)
DATE        type: STRING* 8            (scalar)
PROGNAME    type: STRING*12            (scalar)
ORIGIN      type: STRING*44            (scalar)
PARM        type: REAL                 (23)

Record attributes...
RYCTI       type: DOUBLE               (scalar)
RXCTI       type: DOUBLE               (scalar)
RYCTIERR    type: DOUBLE               (scalar)
RXCTIERR    type: DOUBLE               (scalar)
LUM         type: REAL map: LOG        (scalar)
LUMERR      type: REAL map: LOG        (scalar)
DAY         type: REAL                 (scalar)
RANGE       type: INTEGER              (scalar)
V_NDET      ext: INTEGER int: SHORT    (scalar)

RYCTI    - Right ascension in centipixels
RXCTI    - Declination in centipixels
RYCTIERR- Error in right ascension in centipixels
RXCTIERR- Error in declination in centipixels
LUM      - Luminosity in ADUs
LUMERR   - Error in luminosity in ADUs
DAY      - Mean CTI dayno of position measurement
RANGE    - Range of days going into position measurement
V_NDET   - Number of days going into position measurement
```

Database: .NPT Version: (95/02/16|12:59:03)
Description: Normal Point Table

```
Header attributes...
NRECS       type: INTEGER              (scalar)
DATE        type: STRING* 8            (scalar)
PROGNAME    type: STRING*12            (scalar)
ORIGIN      type: STRING*44            (scalar)
PARM        type: REAL                 (23)

Record attributes...
SET         type: REAL                 (scalar)
ITEM        type: REAL                 (scalar)
```

```
RYCTI      type: DOUBLE              (scalar)
RXCTI      type: DOUBLE              (scalar)
LUM        type: REAL map: LOG       (scalar)
MAG        type: REAL                (scalar)
RYCTIERR   type: DOUBLE              (scalar)
RXCTIERR   type: DOUBLE              (scalar)
YEAR       type: REAL                (scalar)

SET      - Number to distinguish between plates used in
           astrometry.
ITEM     - Number to distinguish between stars on all plates
           used in astrometry.
RYCTI    - Right ascension in centipixels
RXCTI    - Declination in centipixels
LUM      - Luminosity in ADUs
MAG      - Magnitude
RYCTIERR- Error in right ascension in centipixels
RXCTIERR- Error in declination in centipixels
YEAR     - Mean year of plate observation
```

Database: .NPP Version: (95/02/18|08:01:41)
Description: Normal Point POSS positions

```
Header attributes...
NRECS      type: INTEGER             (scalar)
DATE       type: STRING* 8           (scalar)
PROGNAME   type: STRING*12           (scalar)
ORIGIN     type: STRING*44           (scalar)
PARM       type: REAL                (23)

Record attributes...
E_X        type: REAL                (scalar)
E_Y        type: REAL                (scalar)
EX_ERR     type: REAL                (scalar)
EY_ERR     type: REAL                (scalar)
E_SIGMA    type: REAL                (scalar)
O_X        type: REAL                (scalar)
O_Y        type: REAL                (scalar)
OX_ERR     type: REAL                (scalar)
OY_ERR     type: REAL                (scalar)
O_SIGMA    type: REAL                (scalar)

E_X      - Right ascension in 20-μm pixels for POSS E plate
E_Y      - Declination in 20-μm pixels for POSS E plate
EX_ERR   - Error in E_X
EY_ERR   - Error in E_Y
E_SIGMA  - Related to luminosity for POSS E plate
O_X      - Right ascension in 20-μm pixels for POSS O plate
O_Y      - Declination in 20-μm pixels for POSS O plate
OX_ERR   - Error in O_X
```

```
OY_ERR  - Error in O_Y
O_SIGMA - Related to luminosity for POSS O plate
```

Database: .R01 Version: (93/12/01|14:55:11)

```
Header attributes...
NRECS      type: INTEGER            (scalar)
DATE       type: STRING* 8          (scalar)
PROGNAME   type: STRING*12          (scalar)
ORIGIN     type: STRING*44          (scalar)
PARM       type: REAL               (23)

Record attributes...
RNUM       type: REAL               (scalar)

RNUM     - Real number (used for sorting a list of real
           numbers to be used in an application).
```

Database: .R03 Version: (94/11/07|13:56:08)

```
Header attributes...
NRECS      type: INTEGER            (scalar)
DATE       type: STRING* 8          (scalar)
PROGNAME   type: STRING*12          (scalar)
ORIGIN     type: STRING*44          (scalar)
PARM       type: REAL               (23)

Record attributes...
RNUM       type: REAL               (3)

RNUM     - Array of three real number (used for creating data
           files of real numbers in preparation for printing a
           data table).
```

Database: .R06 Version: (95/02/06|11:33:33)
Description: Six real numbers

```
Header attributes...
NRECS      type: INTEGER            (scalar)
DATE       type: STRING* 8          (scalar)
PROGNAME   type: STRING*12          (scalar)
ORIGIN     type: STRING*44          (scalar)
PARM       type: REAL               (23)

Record attributes...
RNUM       type: REAL               ( 6)

RNUM     - Array of six real number
```

Database: .RRL Version: (94/09/01|08:41:37)
Description: RR Lyrae List

Header attributes...

NRECS	type: INTEGER	(scalar)
DATE	type: STRING* 8	(scalar)
PROGNAME	type: STRING*12	(scalar)
ORIGIN	type: STRING*44	(scalar)
PARM	type: REAL	(23)

Record attributes...

RA1987_HOUR	type: SHORT	(scalar)
RA1987_MIN	type: SHORT	(scalar)
RA1987_SEC	type: REAL	(scalar)
DEC1987_DEG	type: SHORT	(scalar)
DEC1987_MIN	type: SHORT	(scalar)
DEC1987_SEC	type: REAL	(scalar)
RA1950_HOUR	type: SHORT	(scalar)
RA1950_MIN	type: SHORT	(scalar)
RA1950_SEC	type: REAL	(scalar)
DEC1950_DEG	type: SHORT	(scalar)
DEC1950_MIN	type: SHORT	(scalar)
DEC1950_SEC	type: REAL	(scalar)

RA1987_HOUR - Hour of right ascension (1987.5 epoch)
RA1987_MIN - Minute of right ascension (1987.5 epoch)
RA1987_SEC - Second of right ascension (1987.5 epoch)
DEC1987_DEG - Degrees of declination (1987.5 epoch)
DEC1987_MIN - Arcminute of declination (1987.5 epoch)
DEC1987_SEC - Arcsecond of declination (1987.5 epoch)
RA1950_HOUR - Hour of right ascension (1950 epoch)
RA1950_MIN - Minute of right ascension (1950 epoch)
RA1950_SEC - Second of right ascension (1950 epoch)
DEC1950_DEG - Degrees of declination (1950 epoch)
DEC1950_MIN - Arcminute of declination (1950 epoch)
DEC1950_SEC - Arcsecond of declination (1950 epoch)

Database: .RRM Version: (94/08/04|13:50:31)
Description: RR Lyrae Magnitudes

Header attributes...

NRECS	type: INTEGER	(scalar)
DATE	type: STRING* 8	(scalar)
PROGNAME	type: STRING*12	(scalar)
ORIGIN	type: STRING*44	(scalar)
PARM	type: REAL	(23)

Record attributes...

DAY	type: REAL	(scalar)

```
PHASE      type: REAL                (scalar)
MAG        type: REAL                (scalar)
MAGERR     type: REAL                (scalar)

DAY      - CTI dayno of observation
PHASE    - Phase of observation given period and epoch
MAG      - Magnitude of observation
MAGERR   - Error in magnitude of observation
```

```
Database: .RRP    Version:   (94/08/03|16:50:28)
Description: RR Lyrae Space Densities

Header attributes...
NRECS      type: INTEGER             (scalar)
DATE       type: STRING* 8           (scalar)
PROGNAME   type: STRING*12           (scalar)
ORIGIN     type: STRING*44           (scalar)
PARM       type: REAL                (23)

Record attributes...
RR_SD      type: REAL                (scalar)
RR_DIST    type: REAL                (scalar)
SURVEY     type: INTEGER             (scalar)
DRR_SD     type: REAL                (scalar)
DRR_DIST   type: REAL                (scalar)

RR_SD    - RR Lyrae space density in number per cubic kpc
RR_DIST  - RR Lyrae Galactocentric distance in pc
SURVEY   - Identification of survey
DRR_SD   - Error in RR Lyrae space density
DRR_DIST- Error in RR Lyrae Galactocentric distance
```

```
Database: .RRT    Version:   (94/08/03|16:56:05)
Description: RR Lyrae Tables

Header attributes...
NRECS      type: INTEGER             (scalar)
DATE       type: STRING* 8           (scalar)
PROGNAME   type: STRING*12           (scalar)
ORIGIN     type: STRING*44           (scalar)
PARM       type: REAL                (23)

Record attributes...
RA1987_HOUR     type: SHORT              (scalar)
RA1987_MIN      type: SHORT              (scalar)
RA1987_SEC      type: REAL               (scalar)
DEC1987_DEG     type: SHORT              (scalar)
DEC1987_MIN     type: SHORT              (scalar)
```

```
DEC1987_SEC     type: REAL                  (scalar)
NDET            type: INTEGER               ( 2)
MAG_MAX         type: REAL                  (scalar)
MAG_MIN         type: REAL                  (scalar)
MAG_MEAN        type: REAL                  (scalar)
MAG_MEANERR     type: REAL                  (scalar)
AMP             type: REAL                  (scalar)
SKEW            type: REAL                  (scalar)
B_V             type: REAL                  (scalar)
EBV             type: REAL                  (scalar)
RDIST           type: REAL                  (scalar)
GLONG           type: REAL                  (scalar)
GLAT            type: REAL                  (scalar)
XDIST           type: REAL                  (scalar)
YDIST           type: REAL                  (scalar)
ZDIST           type: REAL                  (scalar)
RCENT           type: REAL                  (scalar)
RCENTERR        type: REAL                  (scalar)
TCENT           type: REAL                  (scalar)
PCENT           type: REAL                  (scalar)
VARPERIOD       type: DOUBLE                (scalar)
VAREPOCH        type: DOUBLE                (scalar)
EBV             type: REAL                  (scalar)
MLINK           ext: POINT int: INTEGER     (scalar)

RA1987_HOUR   - Hour of right ascension (1987.5 epoch)
RA1987_MIN    - Minute of right ascension
RA1987_SEC    - Second of right ascension
DEC1987_DEG   - Degree of declination (1987.5 epoch)
DEC1987_MIN   - Arcminute of declination
DEC1987_SEC   - Second of declination
NDET          - Number of V observations with CTI and at
                Capilla Peak observatory
MAG_MAX       - Magnitude of star at maximum light
MAG_MIN       - Magnitude of star at minimum light
MAG_MEAN      - Average magnitude of star
MAG_MEANERR   - Error in MAG_MEAN
AMP           - Amplitude of Variability
SKEW          - (M-m)/P of star.  Skewness of light curve
B_V           - B-V color of star
EBV           - Galactic reddening of star
RDIST         - Heliocentric distance in parsecs
GLONG         - Galactic Longitude
GLAT          - Galactic Latitude
XDIST         - Galactocentric x distance in parsecs
YDIST         - Galactocentric y distance in parsecs
ZDIST         - Galactocentric z distance in parsecs
RCENT         - Galactocentric radial distance in parsecs
RCENTERR      - Error in RCENT
TCENT         - Galactic polar angle θ in degrees
PCENT         - Galactic azimuthal angle ϕ in degrees
VARPERIOD     - Period of variable star in days
```

VAREPOCH - Epoch of variable star at maximum light
EBV - E(B-V) of star. Reddening.
MLINK - Pointer to **.MAS** and **.NML** databases

Database: .VNX Version: (94/11/27|16:08:54)
Description: Variable Star Index file

Header attributes...

NRECS	type: INTEGER	(scalar)
DATE	type: STRING* 8	(scalar)
PROGNAME	type: STRING*12	(scalar)
ORIGIN	type: STRING*44	(scalar)
PARM	type: REAL	(23)

Record attributes...

MLINK	ext: POINT int: INTEGER	(scalar)
HLINK	ext: POINT int: INTEGER	(2)
YCTI	ext: DOUBLE int: INTEGER map: LINEAR	(scalar)
XCTI	ext: DOUBLE int: INTEGER map: LINEAR	(scalar)
NDET	type: INTEGER	(scalar)
V	type: REAL	(scalar)
AMP	type: REAL	(scalar)
FLAG	ext: INTEGER int: SHORT	(4)

MLINK - Pointer to master list (.NML database)
HLINK - Pointer to history lists (B and V .NHL databases)
YCTI - Right Ascension in centipixels
XCTI - Declination in centipixels
NDET - Number of V observations
V - Mean instrumental V magnitude
AMP - Amplitude of variation in V magnitude
FLAG - Results of variability testing. 1st number: 0 = never variable, 100 = only variable with no prescreening, 110 = variable with prescreening but no additional error, and 111 = variable with prescreening and additional error. 2nd number: 0 = not masked by nearby bright star, 1 = masked by nearby bright star. 3rd number: V_COMB. 4th number: 0 = not correlated with nearest variable neighbor, 1 = correlated with nearest variable neighbor.

Appendix 3 - Photometry, Light Curves, and Finder Charts for CTI RR Lyrae Survey Stars

In the first part of this appendix, the combined CTI and Capilla Peak photometry is given for each candidate RR Lyrae variable star. The dayval (dayval = 1.0 corresponds to 85 Jan 01 0:00 UT), phase (using period and epoch listed in Table 5.3), instrumental V magnitude and error in this magnitude are listed. Stars identified with number from Table 5.1 and RR+right ascension (e.g. RR002101) or GCVS variable star name when applicable. All data after dayval = 3000 is from Capilla Peak Observatory.

In the second part of this appendix, a finder chart for each candidate RR Lyrae variable star is given along with the combined CTI and Capilla Peak light curve. Finder charts are CTI images, 8.25 arcminutes square with north towards the top of the page. For three stars blended with other stars, a 1' x 1' schematic finder chart with increased resolution is also given. CTI and Capilla Peak data are plotted as open and closed circles respectively in the light curve. Zero phase refers to maximum light for the pulsational variables, and primary minimum light for the eclipsing variables. The magnitudes listed are instrumental magnitudes.

1. RR002101

	Dayval	Phase	Vint	Vinterr
1	1020.25500	0.259	16.718	0.038
2	1023.24670	0.072	16.982	0.048
3	1055.15784	0.407	16.915	0.044
4	1354.34302	0.739	16.694	0.040
5	1355.34033	0.343	16.859	0.043
6	1377.27783	0.631	16.816	0.047
7	1378.27502	0.235	16.771	0.046
8	1379.27307	0.843	16.810	0.053
9	1401.21143	0.133	16.905	0.052
10	1403.20605	0.342	16.846	0.049
11	1404.20325	0.947	17.016	0.059
12	1405.20032	0.550	17.011	0.053
13	1410.18616	0.571	16.937	0.050
14	1411.18384	0.176	16.835	0.049
15	1413.17786	0.383	16.888	0.053
16	1414.17542	0.989	17.087	0.065
17	1416.16968	0.196	16.783	0.067
18	1417.16711	0.801	16.753	0.079
19	1418.16406	0.405	17.017	0.175
20	1432.12549	0.865	16.736	0.050
21	1435.11731	0.678	16.794	0.046
22	1436.11450	0.282	16.755	0.049
23	1442.09802	0.908	16.867	0.054
24	1768.20618	0.547	17.018	0.062
25	2061.40869	0.256	16.694	0.054
26	2063.40210	0.461	16.848	0.065
27	2094.31543	0.190	16.669	0.059
28	2095.30981	0.784	16.750	0.064
29	2110.27100	0.857	16.775	0.071
30	2113.26270	0.670	16.585	0.063
31	2121.24048	0.504	16.874	0.084
32	2123.23462	0.711	16.649	0.065
33	2124.23193	0.316	16.744	0.069
34	2125.22925	0.920	16.998	0.090
35	2147.16821	0.214	16.680	0.083
36	2170.10498	0.113	16.721	0.078
37	2171.10229	0.717	16.626	0.070
38	2178.08301	0.947	16.920	0.081
39	2499.20215	0.554	16.696	0.086
40	3539.13892	0.154	16.797	0.020
41	3539.14990	0.193	16.756	0.020
42	3539.23486	0.500	17.070	0.022
43	3539.24512	0.538	17.053	0.021
44	3539.32153	0.814	16.726	0.018
45	3539.33154	0.850	16.757	0.018
46	3539.38818	0.055	17.020	0.022
47	3539.39844	0.092	16.917	0.021
48	3539.44360	0.255	16.703	0.019
49	3539.45361	0.292	16.708	0.020

2. RR011358

	Dayval	Phase	Vint	Vinterr
1	1020.29187	0.360	16.368	0.031
2	1023.28363	0.161	16.343	0.032
3	1055.19482	0.378	16.444	0.031
4	1056.19165	0.977	16.716	0.121
5	1352.38440	0.375	16.406	0.035
6	1354.37988	0.578	16.520	0.031
7	1355.37720	0.179	16.312	0.031
8	1377.31482	0.387	16.459	0.036
9	1378.31189	0.987	16.600	0.040
10	1379.30994	0.590	16.494	0.041
11	1401.24829	0.800	16.356	0.030
12	1403.24292	0.001	16.686	0.041
13	1404.24011	0.602	16.432	0.036
14	1405.23718	0.202	16.296	0.031
15	1410.22290	0.203	16.304	0.030
16	1411.22070	0.805	16.400	0.034
17	1413.21472	0.005	16.686	0.051
18	1414.21179	0.605	16.414	0.038
19	1416.20654	0.807	16.355	0.043
20	1417.20398	0.408	16.552	0.062
21	1418.20093	0.008	16.731	0.130
22	1432.16235	0.416	16.474	0.039
23	1435.15430	0.218	16.297	0.029
24	1436.15137	0.818	16.343	0.036
25	1442.13501	0.422	16.533	0.039
26	1742.31604	0.220	16.241	0.033
27	1744.30969	0.419	16.488	0.061
28	1758.27124	0.827	16.353	0.039
29	1768.24304	0.831	16.357	0.040
30	2061.44556	0.430	16.509	0.043
31	2063.43896	0.629	16.314	0.044
32	2094.35229	0.243	16.232	0.048
33	2095.34668	0.837	16.520	0.056
34	2110.30786	0.851	16.334	0.059
35	2113.29956	0.653	16.303	0.046
36	2121.27734	0.457	16.530	0.064
37	2123.27148	0.658	16.247	0.046
38	2124.26587	0.250	16.358	0.049
39	2126.26294	0.458	16.546	0.175
40	2147.20508	0.070	16.436	0.057
41	2169.14160	0.275	16.440	0.054
42	2171.13916	0.484	16.570	0.064
43	2178.11987	0.688	16.272	0.045
44	2500.23853	0.694	16.228	0.058
45	2532.15063	0.913	16.406	0.076
46	3539.16724	0.963	16.616	0.020
47	3539.17798	0.991	16.634	0.020
48	3539.25732	0.197	16.335	0.016
49	3539.26733	0.224	16.296	0.017
50	3539.35547	0.454	16.619	0.019
51	3539.36475	0.478	16.677	0.019
52	3539.41016	0.597	16.490	0.019
53	3539.41968	0.621	16.426	0.018
54	3539.46582	0.741	16.275	0.017
55	3539.47534	0.766	16.251	0.018
56	3546.15967	0.197	16.284	0.023
57	3546.16919	0.222	16.266	0.021
58	3546.20410	0.313	16.332	0.018
59	3546.21338	0.337	16.313	0.020
60	3546.25146	0.437	16.588	0.023
61	3546.26074	0.461	16.641	0.021

3. RR012659

	Dayval	Phase	Vint	Vinterr
1	1020.30090	0.038	16.678	0.039
2	1023.29266	0.607	16.627	0.034
3	1055.20386	0.012	16.671	0.038
4	1056.20068	0.867	16.542	0.090
5	1352.39343	0.265	16.481	0.037
6	1354.38892	0.981	16.669	0.036
7	1355.38623	0.838	16.536	0.034
8	1377.32385	0.675	16.554	0.036
9	1378.32092	0.531	16.684	0.039
10	1379.31897	0.389	16.532	0.044
11	1401.25732	0.228	16.528	0.035
12	1403.25195	0.942	16.640	0.042
13	1404.24927	0.798	16.460	0.041
14	1405.24622	0.654	16.602	0.034
15	1410.23206	0.935	16.614	0.042
16	1411.22974	0.793	16.536	0.037
17	1413.22388	0.505	16.671	0.055
18	1414.22083	0.360	16.544	0.053
19	1416.21558	0.074	16.665	0.053
20	1417.21301	0.931	16.598	0.066
21	1418.21008	0.787	16.435	0.098
22	1432.17151	0.777	16.517	0.033
23	1435.16333	0.347	16.525	0.041
24	1436.16040	0.203	16.522	0.039
25	1442.14404	0.342	16.515	0.041
26	1742.32507	0.164	16.562	0.040
27	1744.31860	0.874	16.542	0.062
28	1758.28027	0.865	16.523	0.043
29	1768.25220	0.428	16.631	0.046
30	2061.45337	0.257	16.488	0.049
31	2063.44800	0.971	16.654	0.055
32	2095.35596	0.366	16.461	0.050
33	2110.31689	0.220	16.525	0.067
34	2113.30859	0.788	16.535	0.055
35	2121.28638	0.640	16.563	0.065
36	2123.28052	0.352	16.434	0.059
37	2124.27734	0.207	16.506	0.059
38	2126.27197	0.920	16.570	0.182

39	2147.21411	0.906	16.611	0.062
40	2171.14819	0.461	16.644	0.063
41	2178.12891	0.456	16.602	0.058
42	2500.24756	0.115	16.586	0.080
43	2532.15967	0.522	16.646	0.086
44	3540.20020	0.898	16.632	0.043
45	3540.20947	0.925	16.735	0.037
46	3540.28882	0.152	16.587	0.026
47	3540.29834	0.179	16.536	0.026
48	3546.18213	0.032	16.707	0.026
49	3546.19165	0.059	16.718	0.026
50	3546.23145	0.174	16.558	0.024
51	3546.24097	0.201	16.504	0.027
52	3546.33960	0.483	16.676	0.026
53	3546.34937	0.511	16.684	0.025

4. RR015856

	Dayval	Phase	Vint	Vinterr
1	1020.32318	0.612	17.145	0.052
2	1050.23987	0.703	17.264	0.059
3	1054.22852	0.715	17.281	0.078
4	1055.22607	0.718	17.283	0.060
5	1056.22302	0.721	17.547	0.199
6	1086.13916	0.811	17.303	0.063
7	1352.41565	0.660	17.281	0.062
8	1354.41125	0.668	17.219	0.050
9	1355.40710	0.668	17.236	0.059
10	1377.34607	0.735	17.351	0.065
11	1378.34314	0.738	17.375	0.068
12	1379.34131	0.743	17.378	0.085
13	1401.27954	0.809	17.246	0.076
14	1403.27417	0.815	17.432	0.064
15	1404.27148	0.818	17.348	0.080
16	1405.26843	0.821	17.331	0.070
17	1410.25427	0.835	17.409	0.069
18	1411.25195	0.839	17.466	0.095
19	1412.24866	0.841	17.442	0.541
20	1413.24573	0.844	17.375	0.074
21	1414.24316	0.847	17.244	0.076
22	1416.23779	0.854	17.367	0.093
23	1417.23535	0.858	17.160	0.106
24	1418.23230	0.860	17.590	0.251
25	1432.19373	0.903	17.130	0.057
26	1435.18555	0.913	16.988	0.061
27	1436.18262	0.916	17.077	0.056
28	1442.16626	0.934	16.682	0.045
29	1742.34741	0.885	17.376	0.067
30	1744.34094	0.889	17.426	0.092
31	1758.30261	0.932	17.531	0.080
32	1768.27441	0.962	16.833	0.048
33	2061.47559	0.892	17.334	0.088
34	2063.47021	0.899	17.537	0.095
35	2096.37769	0.997	16.365	0.042
36	2110.33911	0.041	16.747	0.080
37	2113.33081	0.050	16.720	0.065
38	2121.30811	0.073	16.697	0.072
39	2123.30298	0.080	16.789	0.062
40	2124.29980	0.082	16.716	0.075
41	2126.29419	0.088	16.819	0.203
42	2147.23608	0.152	17.007	0.079
43	2148.23315	0.155	17.117	0.068
44	2170.17285	0.224	17.147	0.095
45	2178.15112	0.249	17.407	0.105
46	2199.09375	0.315	17.245	0.103
47	2500.26978	0.263	17.437	0.123
48	2532.18188	0.363	17.382	0.129
49	3641.08423	0.728	17.401	0.026
50	3641.09863	0.756	17.427	0.025
51	3641.11279	0.785	17.424	0.025
52	3641.12720	0.813	17.372	0.025
53	3641.14258	0.844	17.230	0.023
54	3641.15967	0.879	17.066	0.021
55	3641.17383	0.907	16.894	0.018
56	3641.18823	0.936	16.661	0.016
57	3641.20239	0.965	16.381	0.014
58	3641.21655	0.993	16.331	0.014
59	3641.23071	0.022	16.451	0.015
60	3641.24487	0.050	16.518	0.015
61	3641.25928	0.079	16.682	0.018
62	3660.08008	0.883	17.187	0.021
63	3660.09082	0.904	16.917	0.022
64	3660.13818	0.999	16.454	0.038
65	3660.15234	0.028	16.487	0.067
66	3666.12524	0.025	16.597	0.015
67	3666.13965	0.054	16.684	0.017
68	3666.18774	0.151	16.943	0.020
69	3666.20825	0.192	16.971	0.024
70	3666.25342	0.282	17.142	0.028
71	3666.26758	0.311	17.255	0.030
72	3685.06470	0.067	16.882	0.022
73	3685.07886	0.096	16.970	0.017
74	3685.13965	0.218	17.124	0.019
75	3685.15405	0.247	17.149	0.020
76	3685.19995	0.339	17.237	0.021
77	3685.21411	0.368	17.233	0.022

5. RR020150

	Dayval	Phase	Vint	Vinterr
1	1020.32520	0.763	17.878	0.091
2	1023.31696	0.249	17.434	0.061
3	1050.24194	0.618	17.902	0.087
4	1054.23047	0.264	17.615	0.098
5	1055.22815	0.427	17.939	0.081
6	1056.22498	0.588	18.187	0.327
7	1086.14111	0.441	17.764	0.080
8	1352.41772	0.683	17.900	0.106
9	1354.41321	0.009	17.039	0.049
10	1355.40918	0.168	17.332	0.064
11	1377.34814	0.728	17.902	0.094
12	1378.34521	0.890	18.151	0.123
13	1379.34326	0.053	16.797	0.063
14	1401.28162	0.612	18.072	0.115
15	1403.27625	0.936	17.957	0.102
16	1404.27344	0.098	16.815	0.050
17	1405.27051	0.259	17.375	0.070
18	1410.25623	0.067	16.710	0.043
19	1411.25403	0.230	17.315	0.067
20	1413.24768	0.552	17.964	0.114
21	1414.24512	0.715	17.961	0.109
22	1416.23987	0.039	16.726	0.051
23	1417.23730	0.201	17.202	0.097
24	1432.19568	0.628	17.877	0.095
25	1435.18762	0.114	17.186	0.059
26	1436.18469	0.276	17.645	0.084
27	1442.16833	0.247	17.605	0.081
28	1742.34937	0.988	17.124	0.056
29	1744.34290	0.310	17.704	0.113
30	1758.30457	0.576	17.807	0.099
31	1768.27649	0.194	17.299	0.072
32	2061.47754	0.804	17.952	0.131
33	2063.47241	0.128	16.940	0.065
34	2096.37964	0.466	17.755	0.129
35	2113.33276	0.217	17.537	0.110
36	2121.31006	0.510	17.769	0.164
37	2123.30493	0.835	17.300	0.110
38	2124.30176	0.996	17.058	0.092
39	2126.29614	0.319	17.590	0.373
40	2147.23804	0.718	17.852	0.146
41	2148.23511	0.879	17.671	0.121
42	2170.17505	0.441	17.661	0.141
43	2178.15332	0.737	17.833	0.143
44	2199.09570	0.136	16.799	0.088
45	2500.27173	0.035	17.199	0.107
46	2532.18384	0.214	17.502	0.161
47	3175.26636	0.307	17.706	0.033
48	3175.28052	0.338	17.743	0.044
49	3175.32812	0.441	17.793	0.045
50	3175.34570	0.479	17.516	0.037
51	3181.28955	0.365	17.742	0.032
52	3181.30444	0.397	17.765	0.035
53	3181.37085	0.541	17.758	0.042
54	3181.38501	0.572	17.814	0.039
55	3181.43237	0.674	17.891	0.037
56	3181.44678	0.705	17.901	0.033
57	3181.46118	0.737	17.804	0.034
58	3186.25195	0.122	17.419	0.025

59	3186.26636	0.154	17.481	0.025
60	3186.28076	0.184	17.508	0.028
61	3186.29565	0.217	17.544	0.030
62	3186.30981	0.248	17.543	0.033
63	3186.32397	0.278	17.618	0.033
64	3187.28662	0.365	17.741	0.028
65	3187.30151	0.397	17.673	0.033
66	3189.23584	0.591	17.859	0.052
67	3189.25146	0.625	17.851	0.032
68	3189.26611	0.656	17.735	0.041
69	3189.28442	0.696	17.838	0.026
70	3189.30322	0.737	17.823	0.030
71	3189.32251	0.778	17.716	0.027
72	3189.34180	0.821	17.530	0.039
73	3189.39209	0.930	17.137	0.072
74	3232.27197	0.886	18.072	0.041
75	3232.28638	0.917	17.819	0.048
76	3234.07812	0.801	17.966	0.041
77	3234.09229	0.832	17.970	0.049
78	3234.13940	0.934	17.703	0.031
79	3234.15356	0.965	17.277	0.023
80	3234.20166	0.069	16.831	0.019
81	3234.21606	0.100	16.931	0.022
82	3234.27173	0.221	17.270	0.028
83	3234.28589	0.252	17.439	0.028
84	3234.31836	0.322	17.539	0.032
85	3234.33252	0.353	17.564	0.040
86	3234.38989	0.477	17.790	0.046
87	3234.40430	0.508	17.739	0.046
88	3234.42700	0.558	17.854	0.040
89	3546.30371	0.653	17.889	0.046
90	3546.36108	0.777	17.850	0.042
91	3546.37207	0.801	17.689	0.035
92	3559.28125	0.786	17.689	0.028
93	3559.29199	0.809	17.391	0.025
94	3559.36499	0.968	17.055	0.023
95	3559.37573	0.991	17.093	0.022
96	3559.44727	0.146	17.505	0.027
97	3559.45801	0.169	17.489	0.027

6. RR023140

	Dayval	Phase	Vint	Vinterr
1	1020.34595	0.534	14.003	0.007
2	1023.33771	0.804	13.871	0.006
3	1050.26270	0.232	13.828	0.006
4	1054.25134	0.257	13.836	0.007
5	1055.24890	0.015	14.028	0.007
6	1086.16199	0.465	14.011	0.006
7	1352.43848	0.538	14.044	0.007
8	1354.43396	0.055	14.049	0.006
9	1355.42993	0.806	13.871	0.006
10	1377.36890	0.451	14.020	0.007
11	1378.36597	0.207	13.898	0.007
12	1379.36401	0.967	14.043	0.009
13	1401.30237	0.609	13.960	0.008
14	1403.29700	0.123	13.958	0.007
15	1404.29431	0.880	13.978	0.007
16	1405.29126	0.636	13.922	0.007
17	1410.27710	0.417	13.997	0.007
18	1412.27148	0.930	13.957	0.011
19	1413.26843	0.686	13.887	0.007
20	1414.26587	0.443	13.990	0.008
21	1416.26013	0.955	14.041	0.008
22	1417.25806	0.715	13.860	0.008
23	1418.25513	0.471	13.888	0.023
24	1432.21655	0.064	14.014	0.007
25	1435.20837	0.334	13.900	0.007
26	1436.20544	0.090	13.978	0.008
27	1442.18909	0.631	13.922	0.007
28	1742.37024	0.422	13.967	0.007
29	1744.36365	0.932	14.009	0.008
30	1758.32434	0.522	13.992	0.008
31	1768.29724	0.090	13.957	0.008
32	2096.40039	0.066	14.042	0.009
33	2113.35352	0.929	14.025	0.010
34	2121.33081	0.979	14.008	0.005
35	2123.32568	0.494	14.034	0.011
36	2124.32251	0.249	13.872	0.010
37	2147.25879	0.651	13.904	0.011
38	2148.25586	0.407	14.000	0.009
39	2170.19580	0.055	14.029	0.011
40	2171.19263	0.810	13.922	0.010
41	2178.17407	0.109	13.980	0.009
42	2199.11646	0.000	14.025	0.012
43	2500.29248	0.540	14.009	0.011
44	2532.20459	0.754	13.869	0.011
45	3539.21875	0.208	13.901	0.008
46	3539.22412	0.228	13.877	0.008
47	3539.27612	0.425	13.985	0.009
48	3539.28076	0.441	14.003	0.009
49	3539.37402	0.793	13.855	0.008
50	3539.37842	0.810	13.860	0.008
51	3539.42969	0.003	14.062	0.009
52	3539.43433	0.020	14.058	0.009
53	3539.48438	0.209	13.889	0.009
54	3539.48877	0.226	13.889	0.008

7. RR034622

	Dayval	Phase	Vint	Vinterr
1	1020.39801	0.573	18.101	0.117
2	1023.38971	0.897	18.185	0.104
3	1050.31458	0.816	18.152	0.119
4	1054.30334	0.915	17.983	0.138
5	1055.30090	0.690	18.040	0.115
6	1056.29785	0.464	18.061	0.271
7	1086.21362	0.705	18.262	0.115
8	1120.12292	0.054	17.435	0.136
9	1352.49048	0.600	18.179	0.119
10	1377.42090	0.968	17.532	0.077
11	1378.41797	0.743	18.100	0.121
12	1379.41614	0.519	18.196	0.161
13	1401.35327	0.561	18.133	0.188
14	1403.34790	0.111	17.611	0.085
15	1404.34631	0.888	18.080	0.129
16	1405.34326	0.662	18.213	0.129
17	1410.32910	0.535	17.991	0.124
18	1411.32593	0.309	17.914	0.118
19	1412.32349	0.085	17.606	0.088
20	1413.32043	0.859	18.228	0.159
21	1414.31750	0.633	18.412	0.166
22	1416.31213	0.183	17.589	0.104
23	1417.31018	0.959	17.647	0.085
24	1432.26855	0.581	18.030	0.118
25	1436.25745	0.680	18.125	0.132
26	1442.24109	0.329	17.919	0.121
27	1742.42224	0.563	18.412	0.139
28	1744.41565	0.111	17.641	0.091
29	1758.37634	0.957	17.638	0.103
30	1768.34924	0.705	18.117	0.146
31	1816.21643	0.895	18.140	0.133
32	2096.45239	0.632	18.166	0.151
33	2121.38281	0.001	17.295	0.066
34	2123.37769	0.551	17.941	0.194
35	2124.37451	0.325	17.917	0.162
36	2125.37134	0.099	17.670	0.128
37	2126.36890	0.874	18.142	0.515
38	2147.31055	0.144	17.688	0.134
39	2148.30786	0.919	17.768	0.155
40	2170.24731	0.965	17.445	0.124
41	2171.24438	0.740	18.046	0.201
42	2178.22534	0.164	17.797	0.157
43	2199.16846	0.436	17.877	0.231
44	2206.14917	0.860	18.153	0.203
45	2500.34448	0.441	18.206	0.194
46	2532.25659	0.235	18.070	0.198
47	3666.16357	0.254	17.744	0.037
48	3666.17090	0.267	17.888	0.042
49	3666.28296	0.467	18.125	0.050
50	3666.29736	0.492	18.106	0.073
51	3666.33032	0.551	18.099	0.066
52	3666.34448	0.576	18.145	0.066
53	3681.09570	0.829	18.279	0.037
54	3681.11035	0.855	18.289	0.039
55	3681.17871	0.977	17.534	0.027
56	3681.19312	0.002	17.449	0.030
57	3681.22900	0.066	17.599	0.063

58	3685.09399	0.945	17.660	0.027
59	3685.10840	0.970	17.573	0.023
60	3685.12256	0.996	17.449	0.023
61	3685.16870	0.078	17.600	0.025
62	3685.18311	0.103	17.642	0.025
63	3685.22900	0.185	17.777	0.028
64	3685.24316	0.210	17.812	0.029
65	3685.28198	0.279	17.965	0.035
66	3685.29614	0.305	17.905	0.031

8. RR040258

	Dayval	Phase	Vint	Vinterr
1	1020.40955	0.279	17.635	0.074
2	1023.40131	0.646	17.795	0.078
3	1050.32593	0.943	17.829	0.085
4	1054.31482	0.432	17.957	0.106
5	1055.31250	0.556	18.003	0.117
6	1056.30933	0.677	17.741	0.209
7	1086.22510	0.339	17.619	0.071
8	1120.13452	0.505	17.925	0.177
9	1377.43250	0.072	18.002	0.111
10	1378.42957	0.193	17.655	0.079
11	1379.42761	0.318	17.659	0.104
12	1401.36475	0.001	18.054	0.167
13	1403.35950	0.246	17.732	0.097
14	1404.35779	0.371	17.513	0.079
15	1405.35486	0.493	17.994	0.108
16	1410.34070	0.103	17.708	0.088
17	1411.33740	0.224	17.585	0.097
18	1412.33508	0.347	17.436	0.089
19	1413.33203	0.469	17.775	0.111
20	1414.32910	0.590	17.814	0.096
21	1416.32373	0.835	17.443	0.094
22	1417.32166	0.960	17.812	0.098
23	1432.28003	0.792	17.477	0.078
24	1435.27197	0.159	17.591	0.178
25	1436.26904	0.281	17.543	0.084
26	1442.25269	0.015	18.052	0.125
27	1496.10547	0.621	17.764	0.112
28	1742.43213	0.838	17.606	0.086
29	1744.42725	0.085	17.962	0.114
30	1758.38757	0.793	17.593	0.088
31	1768.36084	0.018	18.112	0.137
32	1816.22803	0.883	17.555	0.097
33	2121.39453	0.320	17.657	0.153
34	2123.38843	0.563	17.799	0.174
35	2124.38599	0.687	17.468	0.127
36	2125.38281	0.807	17.628	0.124
37	2126.38013	0.929	17.799	0.396
38	2147.32202	0.496	17.974	0.214
39	2148.31934	0.618	17.664	0.129
40	2170.25903	0.308	17.618	0.126
41	2171.25586	0.430	17.758	0.155
42	2178.23706	0.287	17.250	0.115
43	2199.18018	0.857	17.522	0.147
44	2206.16089	0.713	17.543	0.131
45	2500.35620	0.800	17.617	0.148
46	2532.26831	0.713	17.610	0.139
47	3540.31470	0.776	17.621	0.037
48	3540.32544	0.809	17.573	0.035
49	3545.29443	0.366	17.408	0.040
50	3545.30542	0.401	17.632	0.046
51	3545.35010	0.541	17.886	0.055
52	3545.35962	0.571	17.829	0.049
53	3545.43408	0.803	17.547	0.036
54	3545.44409	0.835	17.544	0.033
55	3546.27515	0.437	17.780	0.043
56	3546.28613	0.471	18.100	0.051
57	3546.38501	0.781	17.411	0.070
58	3622.13574	0.947	17.913	0.035
59	3622.14990	0.991	18.132	0.038
60	3622.19751	0.140	17.635	0.029
61	3622.21143	0.184	17.589	0.027
62	3622.26880	0.363	17.622	0.029
63	3622.28174	0.404	17.810	0.032
64	3622.39844	0.769	17.607	0.026
65	3622.41284	0.814	17.623	0.027

9. CN Tau

	Dayval	Phase	Vint	Vinterr
1	1020.48920	0.903	12.617	0.003
2	1023.48096	0.571	12.900	0.004
3	1050.40503	0.585	12.937	0.003
4	1054.39453	0.810	12.593	0.004
5	1056.38818	0.922	12.545	0.005
6	1086.30481	0.605	12.899	0.004
7	1120.21375	0.514	12.908	0.004
8	1121.21118	0.070	12.553	0.004
9	1142.15466	0.749	12.863	0.003
10	1144.14929	0.862	12.683	0.003
11	1401.44434	0.341	12.781	0.006
12	1403.43909	0.454	12.891	0.004
13	1404.43750	0.010	12.568	0.003
14	1405.43457	0.566	12.922	0.004
15	1410.41919	0.346	12.777	0.004
16	1411.41711	0.903	12.619	0.003
17	1412.41467	0.459	12.879	0.004
18	1413.41089	0.014	12.553	0.003
19	1414.40869	0.571	12.798	0.004
20	1416.40259	0.683	12.892	0.004
21	1417.40137	0.240	12.710	0.003
22	1419.39429	0.351	12.803	0.004
23	1432.35974	0.581	12.914	0.004
24	1436.34875	0.806	12.771	0.004
25	1442.33228	0.142	12.622	0.003
26	1496.18506	0.173	12.621	0.003
27	1504.16333	0.622	12.899	0.005
28	1758.46729	0.434	12.864	0.004
29	1768.43933	0.995	12.569	0.003
30	1816.30762	0.688	12.904	0.004
31	1818.30188	0.801	12.787	0.004
32	1832.26367	0.586	12.875	0.006
33	1874.15063	0.944	12.576	0.003
34	1875.14795	0.501	12.873	0.004
35	2124.46484	0.531	12.892	0.005
36	2125.46265	0.088	12.557	0.004
37	2126.45947	0.644	12.895	0.012
38	2147.40161	0.322	12.774	0.005
39	2148.39868	0.878	12.656	0.004
40	2170.33813	0.112	12.599	0.004
41	2171.33545	0.669	12.901	0.006
42	2178.31641	0.561	12.864	0.005
43	2199.25977	0.240	12.777	0.009
44	2202.25098	0.908	12.559	0.006
45	2207.23755	0.689	12.885	0.005
46	2230.17554	0.481	12.843	0.005
47	2237.15674	0.374	12.828	0.005
48	2500.43530	0.190	12.637	0.005
49	2532.34692	0.985	12.522	0.005
50	2569.24634	0.562	12.881	0.059
51	3231.36523	0.791	12.813	0.007
52	3231.36768	0.792	12.813	0.007
53	3231.45020	0.838	12.722	0.007
54	3231.45264	0.839	12.716	0.007
55	3231.50244	0.867	12.668	0.007
56	3231.50488	0.869	12.666	0.007
57	3234.25928	0.405	12.841	0.007
58	3234.26172	0.406	12.849	0.007
59	3234.29810	0.426	12.864	0.007
60	3234.30054	0.428	12.855	0.007
61	3234.34302	0.451	12.868	0.007
62	3234.34546	0.453	12.875	0.007
63	3234.41431	0.491	12.898	0.007
64	3234.41675	0.492	12.895	0.007
65	3234.46777	0.521	12.903	0.007
66	3234.47021	0.522	12.901	0.007
67	3234.51611	0.548	12.902	0.007
68	3234.51880	0.549	12.912	0.007
69	3298.05249	0.979	12.552	0.007
70	3298.05518	0.980	12.553	0.007
71	3298.10889	0.010	12.563	0.006
72	3298.11133	0.011	12.551	0.006
73	3298.14014	0.028	12.561	0.006
74	3298.14282	0.029	12.560	0.006
75	3298.22412	0.074	12.573	0.006
76	3298.22656	0.076	12.570	0.006

77	3298.30469	0.119	12.602	0.006
78	3298.30737	0.121	12.593	0.006
79	3298.38428	0.164	12.642	0.007
80	3298.38672	0.165	12.642	0.007
81	3298.43921	0.194	12.662	0.007
82	3298.44165	0.196	12.669	0.007

10. RR064946

	Dayval	Phase	Vint	Vinterr
1	1050.44299	0.347	18.206	0.127
2	1054.43274	0.157	18.403	0.179
3	1055.42883	0.854	18.216	0.119
4	1056.42627	0.557	18.736	0.465
5	1086.34167	0.605	18.088	0.122
6	1119.25159	0.769	18.059	0.100
7	1120.24915	0.472	18.472	0.161
8	1121.24658	0.174	18.094	0.193
9	1142.18909	0.914	18.685	0.150
10	1144.18372	0.318	18.110	0.123
11	1403.47766	0.834	18.238	0.150
12	1404.47400	0.532	18.463	0.184
13	1405.47302	0.241	18.048	0.108
14	1410.45764	0.744	18.066	0.104
15	1412.45312	0.151	18.110	0.131
16	1413.44922	0.849	18.170	0.149
17	1414.44702	0.553	18.377	0.181
18	1416.44080	0.954	18.659	0.173
19	1417.43958	0.661	18.061	0.142
20	1419.43237	0.058	18.228	0.135
21	1442.36951	0.203	18.089	0.111
22	1496.22009	0.099	18.468	0.208
23	1504.19812	0.714	18.147	0.156
24	1527.13574	0.860	18.169	0.140
25	1528.13306	0.562	18.259	0.149
26	1529.13025	0.264	18.055	0.118
27	1530.12756	0.966	18.561	0.185
28	1758.50549	0.719	17.959	0.146
29	1768.47791	0.737	18.193	0.150
30	1816.34448	0.421	18.507	0.200
31	1818.33862	0.823	18.146	0.176
32	1832.29968	0.648	18.246	0.252
33	1850.25024	0.281	17.963	0.133
34	1851.24744	0.983	18.685	0.239
35	1854.23926	0.089	18.153	0.157
36	1855.23657	0.791	18.042	0.127
37	1874.18506	0.129	17.961	0.129
38	1875.18250	0.832	18.185	0.145
39	1880.16870	0.341	18.111	0.144
40	2125.50122	0.031	18.818	0.302
41	2126.49805	0.731	18.006	0.482
42	2147.43994	0.468	18.459	0.254
43	2171.37256	0.308	18.322	0.205
44	2178.35327	0.220	18.438	0.235
45	2199.29492	0.957	18.765	0.280
46	2202.28662	0.063	18.140	0.245
47	2207.27319	0.573	18.142	0.201
48	2230.21045	0.717	17.919	0.182
49	2237.19116	0.630	18.075	0.223
50	2500.47314	0.950	18.439	0.313
51	2532.38403	0.405	18.728	0.256
52	3331.11255	0.335	18.140	0.033
53	3331.13062	0.402	18.410	0.039
54	3331.21558	0.718	18.014	0.032
55	3331.23340	0.784	18.043	0.028
56	3331.29663	0.018	18.542	0.041
57	3331.34644	0.204	18.116	0.036
58	3331.36426	0.269	18.098	0.036
59	3342.08936	0.082	18.460	0.072
60	3342.10010	0.122	18.204	0.064
61	3342.11084	0.162	18.184	0.053
62	3342.12476	0.213	18.258	0.058
63	3342.13550	0.253	18.092	0.045
64	3342.14624	0.293	18.108	0.054
65	3622.30273	0.252	17.994	0.036
66	3622.31763	0.307	18.104	0.031
67	3622.36890	0.497	18.670	0.052
68	3622.38306	0.550	18.555	0.047

11. RR075350

	Dayval	Phase	Vint	Vinterr
1	1050.48743	0.539	16.229	0.029
2	1054.47607	0.845	16.118	0.033
3	1055.47339	0.422	16.179	0.027
4	1086.38538	0.291	16.065	0.027
5	1119.29626	0.321	16.094	0.027
6	1120.29382	0.899	15.940	0.029
7	1121.29114	0.475	16.184	0.042
8	1142.23376	0.584	16.174	0.028
9	1144.22827	0.738	16.301	0.029
10	1173.14978	0.460	16.206	0.027
11	1174.14709	0.037	15.876	0.024
12	1405.51770	0.820	16.245	0.031
13	1410.50220	0.700	16.222	0.037
14	1412.49768	0.855	16.068	0.037
15	1413.49390	0.430	16.187	0.031
16	1414.49158	0.007	15.797	0.031
17	1416.48547	0.159	15.984	0.025
18	1417.48413	0.738	16.252	0.032
19	1419.47693	0.888	15.977	0.029
20	1436.43079	0.691	16.289	0.029
21	1442.41418	0.151	15.981	0.027
22	1496.26465	0.285	16.008	0.035
23	1504.24268	0.898	15.981	0.031
24	1527.18030	0.161	15.970	0.029
25	1528.17761	0.737	16.305	0.036
26	1529.17480	0.314	16.100	0.031
27	1530.17224	0.891	15.988	0.027
28	1816.38904	0.382	16.149	0.036
29	1818.38269	0.534	16.201	0.034
30	1832.34436	0.606	16.211	0.056
31	1851.29211	0.561	16.225	0.043
32	1854.28394	0.291	16.112	0.067
33	1855.28125	0.868	16.008	0.026
34	1874.22974	0.824	16.138	0.034
35	1875.22717	0.401	16.174	0.033
36	1880.21313	0.284	16.094	0.032
37	1902.15405	0.971	15.897	0.027
38	1904.14868	0.124	15.957	0.028
39	2148.48071	0.398	16.183	0.039
40	2178.39746	0.694	16.199	0.051
41	2199.33911	0.802	16.256	0.074
42	2202.33105	0.532	16.264	0.053
43	2207.31787	0.416	16.236	0.044
44	2230.25464	0.677	16.335	0.050
45	2237.23560	0.714	16.262	0.059
46	2262.16821	0.131	15.950	0.056
47	2532.42847	0.396	16.225	0.049
48	2569.32642	0.729	16.293	0.537
49	3298.12085	0.907	15.904	0.025
50	3298.13184	0.925	15.904	0.022
51	3298.20288	0.037	15.845	0.021
52	3298.21338	0.054	15.837	0.021
53	3298.28369	0.165	16.011	0.024
54	3298.29443	0.182	16.045	0.024
55	3298.36401	0.292	16.094	0.021
56	3298.37476	0.309	16.074	0.021
57	3298.45630	0.438	16.169	0.022
58	3298.46704	0.455	16.179	0.021
59	3298.50366	0.512	16.185	0.025
60	3298.51440	0.530	16.180	0.027
61	3308.11060	0.700	16.274	0.028
62	3308.12134	0.717	16.276	0.026
63	3308.20459	0.849	16.089	0.023
64	3308.21533	0.866	16.016	0.023
65	3308.29883	0.998	15.877	0.023
66	3308.30933	0.015	15.802	0.022
67	3308.39404	0.149	15.946	0.022
68	3308.40503	0.166	15.992	0.022

12. RR084652

	Dayval	Phase	Vint	Vinterr
1	1054.51318	0.027	15.550	0.022
2	1055.51062	0.831	16.698	0.037
3	1086.42249	0.760	16.704	0.038
4	1119.33313	0.304	16.366	0.029
5	1121.32800	0.914	16.306	0.040

6	1142.27026	0.804	16.579	0.035
7	1144.26501	0.413	16.489	0.034
8	1172.18896	0.936	15.899	0.026
9	1173.18640	0.740	16.688	0.041
10	1174.18372	0.545	16.685	0.041
11	1175.18091	0.349	16.455	0.046
12	1417.52136	0.812	16.586	0.044
13	1419.51416	0.418	16.453	0.042
14	1435.47083	0.288	16.361	0.039
15	1436.46802	0.092	15.900	0.024
16	1442.45129	0.918	16.056	0.030
17	1496.30151	0.348	16.441	0.047
18	1504.27869	0.781	16.681	0.046
19	1527.21692	0.283	16.375	0.038
20	1528.21423	0.088	16.190	0.034
21	1529.21143	0.892	16.232	0.033
22	1530.20886	0.696	16.603	0.042
23	1552.14941	0.393	16.572	0.046
24	1816.42615	0.546	16.680	0.055
25	1818.41980	0.153	16.323	0.035
26	1832.38135	0.413	16.585	0.067
27	1850.33154	0.890	16.238	0.035
28	1851.32898	0.695	16.659	0.063
29	1854.32080	0.108	16.236	0.055
30	1855.31799	0.912	15.781	0.022
31	1874.26648	0.195	16.428	0.037
32	1875.26379	1.000	16.048	0.034
33	1880.24988	0.021	16.112	0.030
34	1886.23340	0.847	16.513	0.047
35	1902.19067	0.718	16.698	0.054
36	1904.18530	0.327	16.590	0.038
37	2148.51782	0.395	16.543	0.053
38	2202.36792	0.825	16.045	0.043
39	2207.35474	0.847	15.769	0.041
40	2230.29150	0.347	16.513	0.068
41	2237.27222	0.977	16.102	0.052
42	2262.20483	0.087	16.355	0.055
43	2263.20190	0.891	16.088	0.048
44	2532.46558	0.066	16.233	0.052
45	2569.36328	0.825	15.865	0.450
46	3234.36548	0.004	15.792	0.026
47	3234.37622	0.024	15.771	0.023
48	3234.44409	0.147	16.058	0.024
49	3234.45483	0.166	16.101	0.020
50	3234.49829	0.245	16.240	0.023
51	3234.50903	0.264	16.277	0.023
52	3298.15479	0.418	16.517	0.026
53	3298.16577	0.437	16.503	0.028
54	3298.23584	0.564	16.658	0.026
55	3298.24658	0.584	16.705	0.024
56	3298.31616	0.710	16.697	0.024
57	3298.32690	0.729	16.676	0.024
58	3298.39551	0.853	16.741	0.025
59	3298.40649	0.873	16.735	0.025
60	3298.47949	0.005	15.598	0.020
61	3298.52686	0.091	15.873	0.024
62	3307.14551	0.684	16.616	0.028
63	3307.15625	0.704	16.621	0.027
64	3307.19971	0.782	16.598	0.024
65	3307.21045	0.802	16.599	0.026
66	3307.25049	0.874	16.679	0.034
67	3307.25781	0.887	16.695	0.027
68	3307.31763	0.996	15.645	0.020
69	3307.32837	0.015	15.603	0.020
70	3307.38892	0.125	15.968	0.022
71	3307.39966	0.144	15.994	0.022
72	3307.47119	0.273	16.323	0.024
73	3307.48169	0.293	16.310	0.023

13. RR090118

	Dayval	Phase	Vint	Vinterr
1	1055.52075	0.778	16.529	0.036
2	1086.43250	0.967	15.680	0.018
3	1119.34314	0.048	16.026	0.024
4	1121.33813	0.932	15.855	0.029
5	1142.28027	0.709	16.612	0.032
6	1172.19897	0.964	15.984	0.025
7	1173.19641	0.906	15.864	0.021
8	1174.19373	0.848	16.155	0.028
9	1175.19092	0.790	16.507	0.039
10	1435.48096	0.604	16.698	0.045
11	1436.47803	0.545	16.732	0.042
12	1442.46143	0.195	16.226	0.029
13	1496.31152	0.048	15.957	0.035
14	1504.28870	0.580	16.549	0.038
15	1526.22913	0.301	16.398	0.035
16	1527.22693	0.243	16.327	0.031
17	1528.22424	0.185	16.242	0.030
18	1529.22144	0.127	16.131	0.029
19	1530.21887	0.069	15.977	0.029
20	1531.21570	0.010	15.859	0.025
21	1550.16467	0.906	15.866	0.028
22	1552.15942	0.790	16.641	0.042
23	1816.43616	0.366	16.397	0.044
24	1818.42981	0.248	16.289	0.034
25	1832.39136	0.433	16.603	0.056
26	1850.34155	0.384	16.433	0.042
27	1851.33899	0.326	16.388	0.046
28	1854.33081	0.151	16.122	0.048
29	1855.32800	0.093	16.111	0.030
30	1856.32483	0.034	16.122	0.028
31	1874.27649	0.988	15.777	0.023
32	1875.27380	0.930	15.530	0.021
33	1880.25989	0.638	16.690	0.048
34	1886.24341	0.289	16.351	0.040
35	1902.20068	0.359	16.388	0.042
36	1904.19519	0.243	16.220	0.032
37	1910.17883	0.894	16.085	0.033
38	2202.37769	0.838	16.294	0.056
39	2207.36475	0.548	16.498	0.056
40	2230.30151	0.209	16.271	0.053
41	2237.28223	0.801	16.599	0.083
42	2262.21484	0.348	16.317	0.060
43	2263.21191	0.289	16.427	0.095
44	2289.14209	0.778	16.615	0.069
45	2569.37329	0.420	16.517	0.626
46	3298.17896	0.486	16.396	0.028
47	3298.18970	0.507	16.358	0.027
48	3298.26001	0.644	16.427	0.026
49	3298.27075	0.665	16.455	0.025
50	3298.34033	0.800	16.377	0.025
51	3298.35107	0.821	16.360	0.025
52	3298.41895	0.954	15.868	0.022
53	3298.42969	0.975	15.877	0.020
54	3298.49121	0.094	16.026	0.023
55	3298.53882	0.187	16.137	0.028
56	3308.18140	0.962	15.842	0.026
57	3308.19214	0.983	15.874	0.024
58	3308.22778	0.053	15.985	0.025
59	3308.23877	0.074	16.051	0.024
60	3308.32227	0.236	16.120	0.025
61	3308.33301	0.257	16.110	0.023
62	3308.41797	0.423	16.311	0.023
63	3308.42871	0.444	16.314	0.025
64	3331.15259	0.690	16.609	0.026
65	3331.16333	0.711	16.561	0.026
66	3331.25293	0.885	16.233	0.023
67	3331.26367	0.906	15.884	0.022
68	3331.31421	0.004	15.442	0.023

14. RR095659

	Dayval	Phase	Vint	Vinterr
1	1086.47302	0.774	16.648	0.034
2	1119.38208	0.515	16.819	0.041
3	1121.37671	0.469	16.756	0.049
4	1142.31836	0.484	16.802	0.041
5	1172.23608	0.795	16.618	0.037
6	1173.23340	0.272	16.579	0.038
7	1174.23071	0.750	16.689	0.042
8	1175.22791	0.226	16.519	0.041
9	1179.21667	0.134	16.414	0.048
10	1435.52185	0.765	16.750	0.045
11	1436.51892	0.242	16.482	0.038
12	1442.50208	0.103	16.318	0.034
13	1496.34900	0.845	16.408	0.054
14	1504.32715	0.661	16.796	0.049

15	1526.26660	0.155	16.440	0.039
16	1527.26440	0.634	16.859	0.041
17	1528.26111	0.109	16.370	0.036
18	1529.25879	0.588	16.876	0.048
19	1530.25610	0.065	16.348	0.037
20	1531.25293	0.540	16.790	0.051
21	1550.20142	0.606	16.800	0.052
22	1552.19604	0.561	16.826	0.055
23	1816.47668	0.999	16.346	0.043
24	1818.47021	0.950	16.365	0.037
25	1832.43127	0.627	16.800	0.055
26	1850.38074	0.209	16.487	0.043
27	1851.37805	0.686	16.812	0.069
28	1854.36926	0.115	16.405	0.043
29	1855.36694	0.594	16.850	0.044
30	1856.36365	0.069	16.374	0.035
31	1874.31458	0.656	16.737	0.051
32	1875.31189	0.134	16.409	0.044
33	1880.29773	0.517	16.789	0.050
34	1886.28101	0.379	16.666	0.050
35	1902.23767	0.013	16.375	0.036
36	1904.23218	0.967	16.407	0.034
37	1932.15625	0.327	16.591	0.053
38	1935.14819	0.759	16.790	0.052
39	1910.21558	0.829	16.574	0.046
40	2202.41699	0.616	16.875	0.078
41	2207.40430	0.004	16.418	0.048
42	2230.33984	0.972	16.366	0.051
43	2237.32031	0.310	16.612	0.104
44	2262.25195	0.236	16.549	0.055
45	2263.24902	0.713	16.763	0.108
46	2289.17871	0.118	16.444	0.068
47	2290.17578	0.595	16.752	0.103
48	2295.16235	0.981	16.385	0.061
49	2569.41284	0.181	16.454	0.644
50	3331.18237	0.161	16.386	0.015
51	3331.19751	0.214	16.427	0.015
52	3331.27954	0.499	16.806	0.018
53	3331.32983	0.675	16.808	0.018
54	3331.41357	0.967	16.382	0.014
55	3331.47876	0.194	16.435	0.015
56	3331.49292	0.244	16.504	0.015
57	3342.23535	0.698	16.761	0.032
58	3342.24609	0.735	16.756	0.029
59	3342.25684	0.773	16.719	0.027
60	3342.26807	0.812	16.614	0.026
61	3342.29858	0.918	16.363	0.020
62	3342.30908	0.955	16.363	0.020
63	3342.31982	0.993	16.349	0.021
64	3342.33057	0.030	16.339	0.020

15. RR102605

	Dayval	Phase	Vint	Vinterr
1	1086.49329	0.959	17.951	0.091
2	1119.40234	0.491	18.299	0.145
3	1121.39685	0.099	17.791	0.107
4	1142.33862	0.982	17.785	0.093
5	1144.33252	0.589	18.527	0.148
6	1172.25635	0.102	17.947	0.106
7	1173.25366	0.906	18.165	0.132
8	1174.25098	0.710	18.559	0.164
9	1175.24817	0.514	18.593	0.176
10	1179.23694	0.730	18.372	0.200
11	1442.52234	0.005	17.861	0.104
12	1496.36926	0.412	18.216	0.159
13	1504.34729	0.845	18.591	0.183
14	1526.28687	0.533	18.512	0.156
15	1527.28381	0.336	18.319	0.141
16	1528.28137	0.140	18.042	0.126
17	1529.27905	0.945	17.918	0.122
18	1530.27637	0.749	18.626	0.181
19	1531.27319	0.553	18.328	0.164
20	1550.22168	0.830	18.617	0.180
21	1552.21631	0.438	18.357	0.167
22	1818.49048	0.120	17.996	0.138
23	1832.45154	0.375	18.446	0.197
24	1850.40088	0.845	18.392	0.176
25	1851.39832	0.649	18.487	0.223
26	1854.38953	0.060	17.956	0.125
27	1855.38721	0.865	18.319	0.161
28	1856.38391	0.668	18.395	0.168
29	1874.33484	0.140	17.924	0.154
30	1875.33215	0.945	17.905	0.131
31	1880.31799	0.964	17.951	0.122
32	1886.30127	0.787	18.564	0.210
33	1902.25793	0.653	18.525	0.211
34	1904.25244	0.261	18.315	0.136
35	1932.17651	0.774	18.605	0.243
36	1935.16846	0.187	18.165	0.179
37	1936.16577	0.991	17.941	0.140
38	1910.23584	0.084	18.126	0.137
39	2202.43726	0.668	18.476	0.277
40	2230.36011	0.179	18.083	0.175
41	2262.27222	0.907	17.953	0.154
42	2263.26904	0.710	18.541	0.293
43	2290.19604	0.421	18.504	0.299
44	2295.18262	0.441	18.438	0.235
45	3357.18628	0.573	18.700	0.061
46	3357.20435	0.606	18.401	0.066
47	3363.09302	0.258	18.254	0.042
48	3363.11084	0.290	18.315	0.044
49	3363.16431	0.387	18.492	0.041
50	3363.18213	0.419	18.395	0.051
51	3363.23438	0.514	18.397	0.051
52	3363.25195	0.546	18.442	0.045
53	3363.31860	0.666	18.502	0.043
54	3363.33618	0.698	18.491	0.044
55	3363.38794	0.792	18.335	0.052
56	3363.40576	0.824	18.349	0.043
57	3622.33789	0.224	18.190	0.039
58	3622.35059	0.247	18.229	0.035
59	3622.46680	0.457	18.423	0.040
60	3622.48096	0.483	18.477	0.038
61	3666.21948	0.605	18.866	0.112
62	3666.23389	0.631	18.689	0.088
63	3666.31396	0.776	18.671	0.048
64	3666.36133	0.861	18.395	0.042
65	3666.37549	0.887	18.086	0.049
66	3666.38965	0.913	17.986	0.042
67	3666.40381	0.938	17.911	0.030
68	3666.42065	0.969	17.798	0.030
69	3666.43506	0.995	17.746	0.035
70	3685.31177	0.142	17.925	0.040
71	3685.34009	0.193	18.123	0.036
72	3685.35425	0.219	18.159	0.037

16. RR103617

	Dayval	Phase	Vint	Vinterr
1	1086.50037	0.840	18.282	0.105
2	1119.40942	0.381	18.103	0.107
3	1121.40405	0.202	17.895	0.102
4	1142.34570	0.818	18.325	0.122
5	1144.33960	0.638	18.239	0.127
6	1172.26343	0.129	17.851	0.094
7	1173.26074	0.539	18.107	0.132
8	1174.25806	0.950	17.894	0.106
9	1175.25525	0.360	18.156	0.153
10	1179.24402	0.001	17.502	0.113
11	1528.28845	0.633	18.129	0.136
12	1530.28345	0.454	18.120	0.126
13	1578.15332	0.153	17.780	0.107
14	3342.20093	0.935	18.052	0.066
15	3351.13062	0.564	18.326	0.041
16	3351.20728	0.672	18.216	0.038
17	3351.33057	0.847	18.430	0.036
18	3351.34839	0.872	18.360	0.040
19	3352.09473	0.927	17.873	0.054
20	3352.11255	0.952	17.765	0.088
21	3356.10938	0.605	18.307	0.044
22	3356.12744	0.631	18.279	0.042
23	3356.19385	0.724	18.217	0.045
24	3356.23877	0.788	18.351	0.044
25	3356.28687	0.856	18.444	0.047
26	3356.33301	0.921	18.009	0.032
27	3356.38599	0.996	17.564	0.029
28	3356.40381	0.021	17.590	0.030

29	3622.43628	0.254	17.916	0.035
30	3622.45093	0.275	18.029	0.035
31	3622.49731	0.341	18.029	0.037
32	3622.51196	0.361	18.113	0.036
33	3622.52612	0.381	18.191	0.038
34	3622.54028	0.401	18.176	0.060
35	3641.28809	0.915	18.237	0.072
36	3641.30249	0.936	17.960	0.054
37	3641.31665	0.956	17.807	0.044
38	3641.33081	0.976	17.726	0.045
39	3641.37109	0.032	17.578	0.040
40	3641.38525	0.053	17.704	0.043
41	3641.41968	0.101	17.738	0.039
42	3641.43408	0.122	17.913	0.036
43	3641.47070	0.173	17.871	0.042
44	3641.48486	0.194	17.951	0.045
45	3641.53833	0.269	17.988	0.047

17. RR105742

	Dayval	Phase	Vint	Vinterr
1	1086.51526	0.944	16.622	0.030
2	1119.42432	0.387	16.701	0.035
3	1121.41895	0.474	16.649	0.034
4	1142.36060	0.391	16.742	0.036
5	1144.35449	0.477	16.823	0.041
6	1172.27832	0.704	16.971	0.049
7	1173.27563	0.748	16.982	0.047
8	1174.27295	0.792	16.928	0.049
9	1175.27014	0.835	16.956	0.056
10	1179.25903	0.010	16.501	0.046
11	1496.39124	0.939	16.514	0.037
12	1504.36938	0.289	16.722	0.042
13	1526.30896	0.251	16.677	0.044
14	1527.30579	0.294	16.689	0.043
15	1528.30334	0.339	16.773	0.039
16	1529.30103	0.384	16.797	0.048
17	1530.29846	0.428	16.888	0.045
18	1531.29517	0.470	16.908	0.050
19	1550.24329	0.302	16.762	0.043
20	1552.23828	0.391	16.847	0.051
21	1578.16821	0.533	16.999	0.048
22	1818.51245	0.095	16.481	0.046
23	1832.47351	0.706	16.943	0.062
24	1854.41150	0.663	17.041	0.057
25	1855.40930	0.709	16.924	0.048
26	1856.40601	0.751	16.815	0.046
27	1874.35681	0.539	16.958	0.069
28	1875.35413	0.583	16.971	0.067
29	1880.33923	0.798	16.638	0.040
30	1886.32324	0.062	16.517	0.046
31	1902.27991	0.764	16.729	0.052
32	1904.27441	0.852	16.499	0.038
33	1935.19043	0.211	16.669	0.047
34	1936.18774	0.255	16.791	0.050
35	1910.25745	0.112	16.646	0.042
36	2202.45923	0.950	16.564	0.052
37	2207.44531	0.168	16.618	0.052
38	2216.42017	0.561	17.005	0.074
39	2230.38208	0.175	16.650	0.056
40	2237.36206	0.479	16.932	0.079
41	2243.34546	0.740	16.898	0.068
42	2262.29419	0.575	16.972	0.083
43	2263.29102	0.617	16.921	0.090
44	2289.22070	0.758	16.753	0.081
45	2290.21802	0.802	16.687	0.071
46	2295.20459	0.021	16.541	0.058
47	2569.45435	0.067	16.467	0.584
48	3351.17480	0.980	16.566	0.016
49	3351.22803	0.143	16.501	0.014
50	3351.37451	0.590	17.016	0.018
51	3351.38892	0.634	16.997	0.018
52	3357.24829	0.517	17.018	0.055
53	3357.26245	0.560	17.019	0.045
54	3363.13086	0.471	16.924	0.017
55	3363.14502	0.515	16.991	0.018
56	3363.20093	0.686	17.023	0.020
57	3363.21533	0.729	16.975	0.019
58	3363.27100	0.899	16.579	0.014
59	3363.28516	0.943	16.526	0.014
60	3363.35498	0.156	16.559	0.015
61	3363.36938	0.199	16.613	0.015
62	3363.42456	0.368	16.796	0.017
63	3363.43872	0.411	16.841	0.017

18. RR114832

	Dayval	Phase	Vint	Vinterr
1	1119.46143	0.426	15.436	0.017
2	1121.45605	0.762	15.675	0.018
3	1142.39673	0.791	15.677	0.019
4	1172.31335	0.834	15.675	0.022
5	1173.31067	0.502	15.557	0.019
6	1174.30798	0.170	14.987	0.013
7	1175.30505	0.838	15.699	0.027
8	1179.29370	0.510	15.558	0.024
9	1496.42761	0.993	15.127	0.016
10	1504.40576	0.338	15.318	0.017
11	1527.34106	0.703	15.661	0.022
12	1528.33875	0.372	15.373	0.018
13	1529.33630	0.041	14.638	0.012
14	1530.33374	0.709	15.684	0.023
15	1531.33044	0.376	15.381	0.018
16	1550.27771	0.070	14.694	0.012
17	1552.27271	0.407	15.423	0.022
18	1578.20166	0.780	15.668	0.020
19	1590.16919	0.798	15.652	0.024
20	1851.45654	0.864	15.750	0.027
21	1854.44849	0.869	15.746	0.027
22	1855.44617	0.538	15.584	0.022
23	1856.44287	0.205	15.062	0.015
24	1874.39294	0.231	15.129	0.020
25	1875.39026	0.900	15.798	0.028
26	1880.37512	0.238	15.119	0.016
27	1886.35840	0.246	15.175	0.019
28	1932.23230	0.981	15.121	0.024
29	1935.22412	0.986	15.087	0.016
30	1936.22131	0.654	15.629	0.025
31	1910.29199	0.281	15.238	0.018
32	2202.49634	0.064	14.690	0.019
33	2207.48218	0.404	15.458	0.027
34	2216.45703	0.416	15.449	0.029
35	2237.39795	0.445	15.501	0.030
36	2243.38135	0.453	15.495	0.031
37	2262.32935	0.149	14.977	0.020
38	2289.25464	0.188	15.055	0.024
39	2290.25146	0.855	15.732	0.040
40	2295.23828	0.197	15.075	0.023
41	2318.17603	0.565	15.619	0.027
42	2323.16260	0.907	15.790	0.029
43	2569.49170	0.952	15.654	0.390
44	3342.21509	0.518	15.495	0.018
45	3342.22241	0.530	15.561	0.019
46	3342.28027	0.627	15.571	0.016
47	3342.28760	0.639	15.606	0.015
48	3342.34302	0.732	15.582	0.017
49	3342.35010	0.744	15.580	0.016
50	3356.14600	0.821	15.686	0.016
51	3356.15405	0.834	15.674	0.016
52	3356.20679	0.923	15.525	0.016
53	3356.25342	0.001	14.557	0.012
54	3356.30151	0.081	14.738	0.013
55	3356.30908	0.094	14.792	0.013
56	3356.31665	0.107	14.825	0.012
57	3356.34741	0.158	14.985	0.012
58	3356.35498	0.171	15.000	0.013
59	3356.36255	0.183	15.035	0.013

19. GR Com

	Dayval	Phase	Vint	Vinterr
1	1119.47278	0.198	16.203	0.027
2	1121.46729	0.020	15.851	0.022
3	1142.40796	0.150	16.140	0.026
4	1172.32458	0.481	16.628	0.041
5	1173.32190	0.392	16.473	0.037
6	1174.31921	0.303	16.349	0.033
7	1175.31628	0.214	16.220	0.033
8	1179.30493	0.858	16.615	0.043

9	1496.43884	0.600	16.650	0.054
10	1504.41699	0.889	16.688	0.039
11	1526.35486	0.930	16.314	0.032
12	1527.35229	0.842	16.762	0.049
13	1528.34998	0.753	16.658	0.049
14	1529.34753	0.665	16.678	0.041
15	1530.34497	0.577	16.656	0.042
16	1531.34167	0.487	16.655	0.042
17	1550.28894	0.796	16.748	0.045
18	1552.28394	0.619	16.701	0.048
19	1578.21289	0.309	16.414	0.034
20	1590.18042	0.243	16.303	0.037
21	1832.52112	0.654	16.652	0.051
22	1851.46777	0.963	16.025	0.031
23	1854.45972	0.697	16.695	0.044
24	1855.45740	0.609	16.624	0.043
25	1856.45410	0.519	16.632	0.036
26	1875.40149	0.829	16.769	0.059
27	1880.38635	0.381	16.488	0.040
28	1886.36963	0.848	16.616	0.050
29	1902.32617	0.426	16.552	0.077
30	1919.27832	0.912	16.453	0.082
31	1932.24353	0.758	16.757	0.065
32	1934.23755	0.580	16.657	0.056
33	1935.23535	0.492	16.674	0.047
34	1936.23254	0.403	16.607	0.044
35	1942.21594	0.869	16.690	0.150
36	1910.30322	0.713	16.666	0.050
37	2202.50757	0.681	16.741	0.074
38	2207.49341	0.236	16.242	0.047
39	2216.46826	0.435	16.568	0.056
40	2237.40918	0.565	16.756	0.068
41	2243.39258	0.032	15.966	0.038
42	2262.34058	0.343	16.457	0.055
43	2263.33667	0.252	16.306	0.054
44	2289.26587	0.941	16.084	0.047
45	2290.26270	0.852	16.820	0.087
46	2318.18726	0.365	16.414	0.048
47	2323.17383	0.921	16.169	0.038
48	2569.50293	0.976	16.005	0.498
49	3351.29761	0.175	16.062	0.018
50	3351.30908	0.197	16.105	0.018
51	3361.11035	0.980	15.852	0.018
52	3361.12109	0.000	15.614	0.016
53	3361.19629	0.144	15.982	0.018
54	3361.20703	0.165	16.029	0.018
55	3361.27588	0.297	16.307	0.020
56	3361.28662	0.317	16.346	0.021
57	3361.35840	0.455	16.535	0.023
58	3361.36914	0.475	16.562	0.023
59	3361.43872	0.609	16.674	0.024
60	3361.44946	0.630	16.682	0.024

20. RR120525

	Dayval	Phase	Vint	Vinterr
1	1119.47327	0.918	16.097	0.026
2	1121.46777	0.839	16.129	0.025
3	1142.40845	0.004	15.013	0.014
4	1172.32507	0.814	16.082	0.030
5	1173.32239	0.774	16.020	0.028
6	1174.31970	0.735	16.070	0.027
7	1175.31677	0.695	16.111	0.035
8	1179.30542	0.535	16.054	0.033
9	1496.43933	0.953	15.456	0.022
10	1504.41760	0.637	16.078	0.030
11	1526.35547	0.762	16.072	0.029
12	1527.35291	0.723	16.078	0.030
13	1528.35046	0.684	16.046	0.032
14	1529.34814	0.645	16.080	0.029
15	1530.34546	0.606	16.105	0.031
16	1531.34216	0.565	16.083	0.030
17	1550.28943	0.811	16.122	0.030
18	1552.28442	0.733	16.074	0.033
19	1578.21338	0.704	16.080	0.027
20	1590.18091	0.229	15.646	0.024
21	1832.52161	0.620	16.085	0.033
22	1851.46826	0.865	16.187	0.037
23	1854.46021	0.746	16.092	0.031
24	1855.45789	0.708	16.080	0.031
25	1856.45459	0.667	16.092	0.027
26	1875.40210	0.913	16.058	0.036
27	1880.38684	0.712	16.091	0.030
28	1886.37012	0.474	16.019	0.034
29	1902.32666	0.841	16.104	0.051
30	1919.27893	0.166	15.551	0.038
31	1932.24402	0.653	16.070	0.039
32	1934.23804	0.573	16.103	0.037
33	1935.23584	0.534	16.067	0.034
34	1936.23315	0.494	16.024	0.034
35	1942.21643	0.256	15.775	0.085
36	1910.30383	0.523	16.076	0.033
37	2202.50806	0.934	15.868	0.043
38	2207.49414	0.736	16.117	0.044
39	2216.46875	0.378	15.874	0.036
40	2237.40991	0.544	16.104	0.043
41	2243.39307	0.306	15.779	0.035
42	2262.34106	0.554	16.070	0.049
43	2263.33716	0.512	16.078	0.046
44	2289.26636	0.483	16.057	0.051
45	2290.26318	0.442	15.954	0.050
46	2318.18774	0.336	15.826	0.032
47	2323.17432	0.138	15.465	0.022
48	3641.35059	0.393	15.839	0.019
49	3641.35913	0.410	15.849	0.019
50	3641.39990	0.490	16.001	0.018
51	3641.40869	0.507	16.001	0.018
52	3641.45093	0.590	16.026	0.017
53	3641.45972	0.607	16.045	0.017
54	3641.50879	0.704	16.099	0.019
55	3641.51758	0.721	16.075	0.019
56	3641.52710	0.740	16.064	0.018
57	3641.55444	0.794	15.991	0.021
58	3683.36133	0.977	15.025	0.010
59	3683.37012	0.994	14.966	0.015
60	3683.37866	0.011	15.028	0.012
61	3683.38721	0.028	15.061	0.015
62	3683.39600	0.045	15.124	0.027
63	3683.40454	0.062	15.152	0.070

21. GS Com

	Dayval	Phase	Vint	Vinterr
1	1119.48645	0.821	16.900	0.042
2	1121.48096	0.589	16.757	0.038
3	1142.42163	0.141	16.189	0.029
4	1172.33826	0.646	16.789	0.045
5	1173.33557	0.529	16.700	0.044
6	1174.33289	0.413	16.625	0.040
7	1175.32996	0.296	16.461	0.038
8	1179.31860	0.830	16.846	0.053
9	1496.45251	0.818	16.852	0.053
10	1504.43066	0.887	16.801	0.046
11	1526.36853	0.323	16.527	0.044
12	1527.36597	0.207	16.308	0.036
13	1528.36365	0.091	16.082	0.029
14	1529.36121	0.975	15.989	0.027
15	1530.35864	0.859	16.911	0.047
16	1531.35461	0.740	16.772	0.049
17	1550.30237	0.528	16.765	0.048
18	1552.29761	0.296	16.518	0.044
19	1578.22656	0.270	16.420	0.035
20	1590.19409	0.873	16.819	0.065
21	1593.18579	0.524	16.795	0.091
22	1832.53479	0.596	16.754	0.066
23	1851.48145	0.381	16.585	0.051
24	1854.47339	0.033	15.801	0.024
25	1855.47107	0.917	16.790	0.048
26	1856.46777	0.799	16.742	0.045
27	1875.41516	0.587	16.836	0.065
28	1879.40259	0.118	16.144	0.045
29	1880.40002	0.002	15.759	0.025
30	1886.38330	0.303	16.459	0.049
31	1902.33984	0.441	16.699	0.068
32	1919.29199	0.459	16.773	0.087
33	1932.25720	0.947	16.207	0.047
34	1934.25122	0.713	16.820	0.063
35	1935.24902	0.598	16.759	0.055

36	1936.24622	0.482	16.729	0.062
37	1942.22961	0.783	16.814	0.062
38	1910.31689	0.507	16.825	0.051
39	2202.52124	0.410	16.599	0.079
40	2207.50708	0.827	16.812	0.069
41	2216.48193	0.778	16.782	0.076
42	2237.42285	0.331	16.543	0.077
43	2243.40625	0.632	16.857	0.074
44	2262.35425	0.420	16.671	0.067
45	2263.35034	0.302	16.717	0.111
46	2289.27954	0.275	16.416	0.063
47	2290.27637	0.158	16.196	0.054
48	2295.26294	0.576	16.839	0.081
49	2318.20093	0.901	16.948	0.066
50	2323.18750	0.319	16.499	0.053
51	3361.13428	0.748	16.759	0.031
52	3361.14526	0.768	16.748	0.027
53	3361.21851	0.907	16.775	0.023
54	3361.22949	0.927	16.629	0.022
55	3361.29883	0.058	15.981	0.016
56	3361.30957	0.078	16.016	0.017
57	3361.38110	0.214	16.278	0.017
58	3361.39185	0.234	16.291	0.017
59	3361.46143	0.365	16.537	0.019
60	3361.47217	0.386	16.567	0.020

22. DV Com

	Dayval	Phase	Vint	Vinterr
1	1119.49963	0.856	15.229	0.015
2	1121.49414	0.544	15.116	0.013
3	1142.43494	0.263	14.794	0.011
4	1172.35144	0.578	15.115	0.015
5	1173.34875	0.422	15.019	0.012
6	1174.34607	0.266	14.789	0.011
7	1175.34314	0.110	14.504	0.009
8	1179.33179	0.485	15.068	0.015
9	1496.46570	0.861	15.244	0.016
10	1504.44397	0.612	15.140	0.014
11	1526.38184	0.175	14.652	0.011
12	1527.37927	0.019	14.250	0.009
13	1528.37683	0.864	15.237	0.015
14	1529.37451	0.709	15.126	0.015
15	1530.37183	0.553	15.104	0.016
16	1531.36780	0.394	15.006	0.014
17	1550.31555	0.428	15.026	0.015
18	1552.31079	0.118	14.510	0.011
19	1578.23975	0.060	14.348	0.009
20	1590.20728	0.188	14.649	0.013
21	1851.49463	0.304	14.842	0.014
22	1854.48657	0.836	15.242	0.018
23	1855.48425	0.681	15.134	0.014
24	1856.48096	0.524	15.118	0.014
25	1875.42847	0.557	15.117	0.020
26	1879.41589	0.930	14.763	0.014
27	1880.41321	0.774	15.108	0.016
28	1886.39661	0.837	15.206	0.020
29	1919.30518	0.685	15.119	0.025
30	1932.27039	0.657	15.125	0.024
31	1934.26453	0.344	14.931	0.015
32	1935.26221	0.189	14.662	0.013
33	1936.25952	0.033	14.271	0.010
34	1942.24280	0.096	14.473	0.012
35	1910.33020	0.090	14.456	0.010
36	2202.53442	0.372	14.943	0.022
37	2216.49512	0.185	14.640	0.017
38	2243.41943	0.968	14.395	0.014
39	2262.36743	0.002	14.225	0.013
40	2263.36353	0.844	15.107	0.028
41	2289.29224	0.786	15.165	0.024
42	2290.28955	0.630	15.123	0.025
43	2295.27612	0.850	15.236	0.026
44	2318.21411	0.262	14.797	0.016
45	2323.20068	0.482	15.062	0.019
46	3361.16040	0.655	15.067	0.014
47	3361.16772	0.669	15.088	0.013
48	3361.24121	0.804	15.153	0.011
49	3361.24854	0.818	15.149	0.011
50	3361.32349	0.956	14.382	0.008
51	3361.33081	0.970	14.237	0.008
52	3361.40381	0.105	14.446	0.009
53	3361.41113	0.118	14.470	0.009
54	3361.48389	0.253	14.735	0.009
55	3361.49097	0.266	14.740	0.009

23. RR131403

	Dayval	Phase	Vint	Vinterr
1	1119.52100	0.656	13.975	0.006
2	1121.51562	0.996	13.674	0.005
3	1142.45630	0.550	13.986	0.006
4	1172.37292	0.633	13.996	0.007
5	1173.37024	0.802	13.833	0.006
6	1174.36743	0.972	13.672	0.006
7	1175.36462	0.141	13.719	0.006
8	1179.35327	0.818	13.796	0.006
9	1212.26257	0.412	13.929	0.012
10	1496.48682	0.746	13.895	0.007
11	1504.46448	0.101	13.681	0.006
12	1526.40308	0.828	13.763	0.006
13	1527.40063	0.998	13.669	0.006
14	1528.39832	0.169	13.731	0.006
15	1529.39587	0.339	13.856	0.007
16	1530.39319	0.509	13.989	0.007
17	1531.38904	0.674	13.959	0.009
18	1550.33704	0.895	13.681	0.006
19	1552.33130	0.234	13.770	0.007
20	1578.26111	0.645	13.983	0.007
21	1593.22046	0.189	13.765	0.009
22	1851.51611	0.116	13.702	0.006
23	1854.50806	0.626	13.985	0.007
24	1856.50244	0.964	13.683	0.006
25	1879.43726	0.857	13.739	0.007
26	1880.43469	0.027	13.667	0.006
27	1886.41760	0.042	13.666	0.007
28	1919.32666	0.635	13.978	0.010
29	1932.29187	0.842	13.775	0.007
30	1934.28589	0.179	13.730	0.007
31	1935.28308	0.348	13.868	0.007
32	1936.28088	0.520	13.982	0.008
33	1942.26416	0.536	13.986	0.008
34	1910.35156	0.110	13.703	0.006
35	3361.17725	0.190	13.754	0.007
36	3361.18457	0.213	13.766	0.007
37	3361.25684	0.443	13.955	0.006
38	3361.26392	0.466	13.982	0.006
39	3361.33936	0.705	13.964	0.006
40	3361.34644	0.728	13.947	0.006
41	3361.41992	0.961	13.698	0.006
42	3361.42700	0.984	13.691	0.006
43	3361.49976	0.215	13.756	0.006
44	3361.50708	0.239	13.796	0.007

24. EZ Com

	Dayval	Phase	Vint	Vinterr
1	1119.52344	0.694	16.881	0.046
2	1121.51807	0.203	16.631	0.036
3	1142.45850	0.045	16.488	0.032
4	1172.37537	0.679	16.930	0.051
5	1173.37268	0.434	16.855	0.045
6	1174.36987	0.188	16.634	0.042
7	1175.36707	0.942	16.549	0.043
8	1179.35571	0.960	16.611	0.038
9	1212.26489	0.859	17.088	0.138
10	1496.48926	0.911	16.895	0.058
11	1504.46692	0.947	16.489	0.036
12	1526.40552	0.545	16.898	0.057
13	1527.40308	0.300	16.788	0.043
14	1528.40076	0.055	16.501	0.037
15	1529.39832	0.810	17.089	0.054
16	1530.39563	0.565	16.850	0.052
17	1531.39148	0.317	16.729	0.053
18	1550.33948	0.653	16.963	0.059
19	1552.33374	0.162	16.517	0.044
20	1578.26355	0.782	16.935	0.058
21	1590.23108	0.837	16.892	0.069
22	1593.22278	0.101	16.552	0.068
23	1613.16943	0.194	16.562	0.035

24	1851.51843	0.535	17.048	0.070
25	1854.51050	0.799	17.016	0.057
26	1856.50488	0.308	16.844	0.047
27	1879.43970	0.659	16.937	0.061
28	1880.43701	0.413	16.845	0.054
29	1886.42004	0.939	16.435	0.043
30	1919.32910	0.838	16.720	0.067
31	1932.29419	0.649	17.020	0.068
32	1934.28833	0.157	16.625	0.054
33	1935.28552	0.911	16.512	0.044
34	1936.28333	0.667	16.975	0.058
35	1942.26660	0.194	16.687	0.052
36	1910.35400	0.048	16.512	0.038
37	2216.51904	0.702	16.834	0.078
38	2243.44336	0.072	16.484	0.058
39	2262.39136	0.408	16.933	0.080
40	2263.38721	0.160	16.741	0.071
41	2289.31592	0.778	16.882	0.082
42	2290.31348	0.533	16.984	0.087
43	2295.29980	0.306	16.796	0.071
44	2318.23804	0.662	16.979	0.066
45	2323.22437	0.435	16.858	0.077
46	3453.18506	0.441	16.925	0.019
47	3453.19946	0.466	16.939	0.018
48	3453.24146	0.540	16.999	0.020
49	3453.26245	0.577	16.994	0.020
50	3453.31104	0.662	16.967	0.023
51	3453.32520	0.687	16.932	0.028
52	3468.15088	0.771	16.893	0.019
53	3468.16504	0.796	16.900	0.019
54	3468.20898	0.873	16.835	0.019
55	3468.22339	0.899	16.792	0.020
56	3468.26587	0.973	16.545	0.023
57	3468.28003	0.998	16.525	0.022

25. RR132347

	Dayval	Phase	Vint	Vinterr
1	1119.52783	0.048	16.771	0.047
2	1121.52234	0.049	16.880	0.047
3	1142.46289	0.057	16.753	0.052
4	1496.49353	0.199	16.954	0.070
5	1504.47119	0.202	16.941	0.067
6	1526.40979	0.211	16.964	0.076
7	1527.40747	0.211	17.029	0.071
8	1528.40503	0.211	17.102	0.072
9	1529.40271	0.212	17.052	0.071
10	1530.40002	0.212	17.031	0.067
11	1531.39587	0.213	17.028	0.078
12	1550.34375	0.220	17.070	0.068
13	1552.33813	0.221	17.033	0.082
14	1578.26794	0.231	17.094	0.072
15	1593.22717	0.237	16.984	0.113
16	1614.17114	0.246	17.074	0.078
17	1851.52283	0.341	17.170	0.083
18	1854.51477	0.342	17.148	0.080
19	1856.50916	0.343	17.147	0.069
20	1879.44397	0.352	17.118	0.091
21	1880.44141	0.352	17.093	0.074
22	1886.42432	0.355	17.146	0.086
23	1919.33337	0.368	17.188	0.114
24	1932.29858	0.373	17.164	0.094
25	1934.29260	0.374	17.103	0.087
26	1935.28979	0.374	17.193	0.083
27	1942.27100	0.377	17.075	0.079
28	1910.35840	0.364	17.207	0.082
29	2216.52319	0.487	16.949	0.094
30	2243.44775	0.497	17.021	0.094
31	2262.39575	0.505	17.113	0.108
32	2289.32031	0.516	16.964	0.119
33	2290.31787	0.516	17.138	0.115
34	2295.30420	0.518	17.039	0.100
35	2318.24219	0.527	17.027	0.085
36	2323.22876	0.529	16.936	0.078
37	3453.15161	0.981	17.378	0.033
38	3453.16577	0.981	17.335	0.029
39	3453.21704	0.981	17.369	0.030
40	3453.23120	0.981	17.292	0.028
41	3453.27979	0.981	17.328	0.030
42	3453.29395	0.981	17.287	0.030
43	3454.14966	0.982	17.377	0.033
44	3454.16431	0.982	17.361	0.031
45	3454.22144	0.982	17.349	0.031
46	3454.29224	0.982	17.299	0.029
47	3454.30640	0.982	17.411	0.033

26. RR143313

	Dayval	Phase	Vint	Vinterr
1	1142.51270	0.972	17.640	0.075
2	1172.42871	0.346	18.064	0.112
3	1173.42590	0.625	18.205	0.116
4	1174.42322	0.904	17.828	0.108
5	1175.42029	0.183	17.858	0.093
6	1179.40881	0.299	18.024	0.111
7	1212.31702	0.511	18.200	0.202
8	1228.27344	0.980	17.669	0.088
9	1254.20361	0.244	17.783	0.104
10	1255.20093	0.524	18.191	0.564
11	1258.19287	0.362	18.232	0.219
12	1504.52100	0.351	18.085	0.123
13	1526.45886	0.491	18.335	0.145
14	1527.45667	0.771	18.103	0.122
15	1528.45435	0.051	17.776	0.083
16	1529.45190	0.331	18.018	0.112
17	1530.44922	0.611	18.261	0.113
18	1531.44507	0.887	17.796	0.100
19	1550.39233	0.191	18.043	0.133
20	1552.38660	0.749	18.199	0.131
21	1578.31567	0.011	17.738	0.092
22	1593.27429	0.199	17.904	0.151
23	1612.22314	0.507	18.278	0.116
24	1613.22058	0.787	18.121	0.107
25	1614.21790	0.066	17.718	0.109
26	1615.21521	0.346	18.161	0.124
27	1616.21252	0.625	18.241	0.155
28	1617.20984	0.904	17.663	0.434
29	1620.20166	0.742	18.162	0.139
30	1621.19910	0.022	17.695	0.112
31	1623.19373	0.581	18.307	0.216
32	1879.49316	0.360	18.045	0.135
33	1886.47375	0.314	18.100	0.127
34	1904.42297	0.338	18.053	0.141
35	1919.38184	0.527	18.164	0.147
36	1932.34668	0.158	17.980	0.295
37	1934.34058	0.715	18.186	0.134
38	1935.33777	0.994	17.683	0.103
39	1936.33484	0.273	17.977	0.114
40	1942.31873	0.949	17.684	0.092
41	1910.40710	0.014	17.844	0.094
42	2243.49731	0.301	18.012	0.164
43	2262.44482	0.606	18.179	0.201
44	2263.44067	0.882	17.700	0.315
45	2289.36841	0.141	18.180	0.174
46	2290.36572	0.420	18.188	0.199
47	2318.28979	0.241	18.041	0.156
48	2323.27588	0.637	17.952	0.141
49	2326.26758	0.474	18.178	0.147
50	3454.18286	0.355	18.262	0.035
51	3454.20068	0.395	18.232	0.038
52	3454.25366	0.516	18.298	0.035
53	3454.27148	0.557	18.211	0.034
54	3454.32324	0.675	18.211	0.037
55	3454.34106	0.716	18.241	0.038
56	3469.17651	0.623	18.069	0.061
57	3469.19458	0.664	18.153	0.048
58	3469.23901	0.766	18.243	0.068
59	3469.25684	0.807	18.119	0.093
60	3474.19043	0.082	17.827	0.027
61	3474.20825	0.123	17.917	0.027
62	3474.26758	0.258	18.049	0.028
63	3474.28516	0.299	18.005	0.034
64	3481.14404	0.975	17.866	0.095
65	3481.16211	0.016	17.631	0.059
66	3481.20776	0.120	17.809	0.029
67	3481.22534	0.161	17.873	0.028
68	3481.26855	0.260	17.960	0.031
69	3481.28638	0.300	17.903	0.035

27. RR145439

	Dayval	Phase	Vint	Vinterr
1	1142.52759	0.006	14.517	0.009
2	1172.44360	0.093	14.595	0.011
3	1173.44092	0.695	15.006	0.013
4	1174.43811	0.298	14.816	0.013
5	1175.43518	0.901	14.698	0.010
6	1179.42371	0.312	14.823	0.012
7	1205.35071	0.986	14.558	0.011
8	1212.33203	0.208	14.723	0.017
9	1228.28833	0.856	14.846	0.013
10	1254.21851	0.535	14.941	0.014
11	1255.21582	0.138	14.683	0.048
12	1257.21045	0.344	14.845	0.013
13	1258.20789	0.947	14.583	0.014
14	1526.47375	0.149	14.702	0.012
15	1527.47168	0.753	15.036	0.014
16	1528.46924	0.357	14.871	0.013
17	1529.46680	0.960	14.612	0.011
18	1530.46411	0.563	14.955	0.014
19	1531.45996	0.164	14.699	0.012
20	1550.40662	0.618	14.967	0.016
21	1552.40149	0.825	14.980	0.016
22	1578.33057	0.502	14.935	0.016
23	1593.28918	0.546	14.994	0.017
24	1612.23804	0.004	14.546	0.010
25	1613.23547	0.607	14.962	0.013
26	1614.23279	0.210	14.759	0.013
27	1615.22998	0.813	14.983	0.014
28	1616.22742	0.416	14.900	0.015
29	1620.21667	0.829	14.943	0.015
30	1621.21399	0.432	14.893	0.015
31	1623.20862	0.638	14.933	0.021
32	1879.50806	0.605	14.941	0.017
33	1886.48865	0.826	14.987	0.015
34	1919.39673	0.721	14.999	0.016
35	1932.36157	0.560	15.005	0.074
36	1934.35559	0.765	15.055	0.017
37	1935.35266	0.368	14.870	0.015
38	1936.34973	0.971	14.527	0.011
39	1942.33362	0.589	14.978	0.014
40	1910.42200	0.295	14.811	0.013
41	1997.18542	0.756	15.013	0.015
42	2243.51147	0.693	15.027	0.021
43	2262.45972	0.150	14.713	0.017
44	2263.45532	0.750	14.960	0.030
45	2289.38330	0.426	14.875	0.022
46	2290.38062	0.029	14.596	0.016
47	2295.36670	0.043	14.574	0.015
48	2318.30469	0.913	14.556	0.013
49	2323.29077	0.928	14.598	0.013
50	2326.28247	0.736	15.021	0.019
51	3093.14233	0.363	14.891	0.019
52	3093.15186	0.378	14.881	0.018
53	3097.15088	0.806	15.022	0.019
54	3097.16162	0.823	14.983	0.012
55	3109.18384	0.147	14.672	0.017
56	3109.19409	0.163	14.704	0.014
57	3109.20703	0.184	14.734	0.014
58	3109.22925	0.220	14.764	0.014
59	3109.24023	0.238	14.784	0.014
60	3109.25098	0.255	14.805	0.014
61	3109.27319	0.291	14.843	0.016
62	3109.28931	0.317	14.864	0.017
63	3109.29980	0.334	14.860	0.016
64	3112.19360	0.985	14.535	0.013
65	3112.20459	0.002	14.521	0.013
66	3385.22778	0.851	14.857	0.027
67	3385.23511	0.863	14.781	0.031

28. RR151628

	Dayval	Phase	Vint	Vinterr
1	1172.46069	0.630	17.920	0.132
2	1173.45789	0.374	17.883	0.098
3	1174.45508	0.117	17.689	0.095
4	1175.45215	0.861	18.131	0.122
5	1179.44055	0.835	18.151	0.123
6	1205.36658	0.168	17.847	0.101
7	1212.34753	0.374	17.834	0.139
8	1228.30322	0.274	17.919	0.099
9	1254.23230	0.612	17.918	0.137
10	1255.22961	0.356	17.832	0.529
11	1257.22424	0.844	18.139	0.137
12	1258.22156	0.588	18.047	0.159
13	1526.49109	0.672	18.074	0.122
14	1527.48889	0.417	18.022	0.125
15	1528.48645	0.162	17.729	0.102
16	1529.48242	0.903	17.968	0.100
17	1530.48132	0.650	18.148	0.109
18	1531.47717	0.391	18.014	0.121
19	1550.42322	0.519	17.836	0.151
20	1552.41760	0.007	17.520	0.095
21	1578.34607	0.344	18.005	0.148
22	1593.30408	0.499	18.129	0.175
23	1612.25208	0.631	18.041	0.110
24	1613.24951	0.375	17.952	0.101
25	1614.24683	0.118	17.633	0.102
26	1615.24390	0.862	17.937	0.143
27	1616.24133	0.606	17.964	0.122
28	1617.23865	0.350	17.728	0.241
29	1620.23022	0.581	17.937	0.134
30	1621.22778	0.325	17.871	0.130
31	1623.22229	0.813	17.991	0.192
32	1879.52563	0.974	17.683	0.097
33	1886.50610	0.179	17.748	0.103
34	1910.43872	0.027	17.673	0.085
35	1919.41321	0.719	18.116	0.133
36	1934.37134	0.875	17.940	0.132
37	1935.36853	0.618	18.104	0.140
38	1936.36548	0.361	17.914	0.136
39	1942.34912	0.824	18.235	0.141
40	1997.19873	0.732	18.211	0.130
41	2263.47241	0.326	17.976	0.265
42	2290.39648	0.405	18.149	0.200
43	2295.38257	0.123	17.551	0.138
44	2318.31958	0.230	17.907	0.134
45	2323.30566	0.948	17.657	0.116
46	2326.29688	0.179	17.611	0.117
47	3685.38184	0.617	18.097	0.040
48	3685.39624	0.642	18.132	0.043
49	3685.41040	0.667	18.240	0.044
50	3685.44971	0.736	18.055	0.038
51	3685.46411	0.761	18.076	0.040
52	3685.51807	0.855	18.207	0.037
53	3685.53247	0.880	17.945	0.037

29. RR162318

	Dayval	Phase	Vint	Vinterr
1	1173.50452	0.797	15.151	0.013
2	1174.49976	0.693	15.138	0.014
3	1175.49878	0.600	15.242	0.015
4	1179.48718	0.205	15.157	0.014
5	1205.41321	0.644	15.154	0.015
6	1212.39417	0.957	15.333	0.015
7	1228.34973	0.384	15.262	0.017
8	1237.32471	0.499	15.322	0.017
9	1254.27881	0.832	15.205	0.015
10	1255.27576	0.733	15.133	0.062
11	1257.27051	0.537	15.339	0.019
12	1258.26794	0.440	15.359	0.017
13	1263.25427	0.949	15.361	0.019
14	3685.42676	0.930	15.295	0.018
15	3685.43555	0.955	15.346	0.018
16	3685.49536	0.129	15.216	0.018
17	3685.50415	0.154	15.175	0.018

30. RR165009

	Dayval	Phase	Vint	Vinterr
1	1205.43384	0.899	15.614	0.020
2	1228.36951	0.078	14.979	0.014
3	1237.34399	0.800	15.760	0.021
4	1254.29736	0.499	15.649	0.022
5	1255.29419	0.246	15.367	0.079
6	1257.28894	0.740	15.693	0.025
7	1258.28589	0.486	15.613	0.023
8	1263.27246	0.222	15.305	0.020

9	1550.49097	0.381	15.537	0.026
10	1552.48511	0.874	15.603	0.025
11	1578.41187	0.293	15.376	0.025
12	1593.36987	0.497	15.645	0.023
13	1612.31750	0.690	15.687	0.021
14	1613.31482	0.437	15.573	0.019
15	1614.31165	0.184	15.221	0.017
16	1615.30908	0.931	15.257	0.018
17	1616.30652	0.678	15.689	0.024
18	1620.29492	0.665	15.667	0.023
19	1621.29272	0.413	15.561	0.024
20	1623.28711	0.907	15.221	0.025
21	1919.48010	0.788	15.718	0.022
22	1935.43567	0.739	15.697	0.025
23	1936.43262	0.486	15.608	0.022
24	1942.41602	0.967	14.927	0.016
25	1997.26306	0.050	14.925	0.013
26	2295.44946	0.423	15.606	0.028
27	2323.37183	0.338	15.408	0.022
28	2326.36304	0.578	15.639	0.027
29	3112.21753	0.263	15.221	0.026
30	3112.22974	0.284	15.321	0.013
31	3112.24292	0.307	15.350	0.011
32	3112.36768	0.526	15.606	0.013
33	3112.37866	0.545	15.603	0.014
34	3113.16455	0.922	15.382	0.014
35	3113.17529	0.941	15.197	0.012
36	3113.21851	0.017	14.765	0.009
37	3113.22925	0.035	14.821	0.009
38	3113.26660	0.101	14.976	0.010
39	3113.27734	0.120	15.016	0.010
40	3113.31470	0.185	15.148	0.010
41	3113.31934	0.193	15.194	0.011
42	3113.36401	0.272	15.292	0.011
43	3113.37500	0.291	15.327	0.012
44	3097.17529	0.912	15.146	0.036
45	3385.25513	0.579	15.677	0.034
46	3385.26270	0.592	15.698	0.030
47	3385.34668	0.740	15.565	0.031
48	3385.35425	0.753	15.629	0.025

31. RR165831

	Dayval	Phase	Vint	Vinterr
1	1205.43970	0.560	15.115	0.015
2	1552.49097	0.157	14.875	0.016
3	1578.41760	0.227	14.977	0.021
4	1593.37573	0.077	14.772	0.013
5	1612.32324	0.555	15.129	0.014
6	1613.32068	0.213	14.967	0.013
7	1614.31738	0.868	14.689	0.012
8	1615.31494	0.525	15.131	0.018
9	1616.31226	0.183	14.945	0.015
10	1617.30957	0.840	14.735	0.044
11	1620.30078	0.808	14.691	0.013
12	1621.29846	0.467	15.133	0.017
13	1623.29297	0.780	14.720	0.015
14	1919.48596	0.886	14.676	0.012
15	1936.43848	0.049	14.707	0.013
16	1942.42188	0.989	14.636	0.012
17	1997.26892	0.107	14.761	0.012
18	2295.45532	0.522	15.152	0.023
19	2323.37769	0.910	14.705	0.015
20	2326.36890	0.879	14.711	0.016
21	3685.48096	0.587	15.080	0.010
22	3685.48828	0.614	15.053	0.010
23	3685.54736	0.831	14.714	0.010
24	3685.55469	0.858	14.725	0.011
25	3685.56201	0.885	14.686	0.018

32. V375 Her

	Dayval	Phase	Vint	Vinterr
1	1205.44995	0.740	16.501	0.037
2	1228.38562	0.898	16.384	0.035
3	1237.36011	0.786	16.546	0.039
4	1254.31287	0.686	16.538	0.038
5	1255.31030	0.563	16.492	0.191
6	1257.30469	0.316	16.314	0.037
7	1258.30200	0.192	16.045	0.031
8	1263.28833	0.575	16.557	0.043
9	1269.27173	0.834	16.624	0.054
10	1578.42786	0.575	16.498	0.057
11	1593.38599	0.721	16.517	0.043
12	1612.33350	0.375	16.361	0.032
13	1613.33081	0.252	16.190	0.027
14	1614.32764	0.128	15.946	0.027
15	1615.32520	0.005	15.594	0.024
16	1616.32251	0.881	16.534	0.044
17	1617.31982	0.758	16.462	0.106
18	1620.31104	0.386	16.343	0.035
19	1621.30872	0.264	16.212	0.037
20	1623.30310	0.017	15.607	0.026
21	1935.45068	0.386	16.391	0.038
22	1936.44788	0.263	16.207	0.038
23	1942.43213	0.523	16.513	0.039
24	1997.27905	0.729	16.525	0.036
25	2305.43726	0.592	16.465	0.054
26	2323.38672	0.368	16.271	0.046
27	2326.37866	0.997	15.540	0.024
28	3097.19580	0.447	16.444	0.021
29	3097.20605	0.467	16.347	0.033
30	3126.14429	0.920	16.054	0.019
31	3126.15503	0.940	15.777	0.018
32	3126.36157	0.329	16.305	0.028
33	3129.15210	0.580	16.524	0.022
34	3129.16284	0.600	16.506	0.026
35	3129.23804	0.742	16.506	0.027
36	3129.24902	0.762	16.524	0.032
37	3129.30981	0.877	16.613	0.049
38	3129.32056	0.897	16.401	0.039
39	3385.28467	0.546	16.357	0.059
40	3385.29565	0.566	16.568	0.042
41	3385.38062	0.726	16.531	0.026
42	3385.39160	0.747	16.516	0.021
43	3481.17505	0.983	15.649	0.054
44	3481.18604	0.004	15.565	0.016
45	3481.23657	0.099	15.857	0.015
46	3481.24731	0.119	15.908	0.015

33. RR171524

	Dayval	Phase	Vint	Vinterr
1	1205.45142	0.407	17.985	0.120
2	1228.38708	0.835	18.299	0.143
3	1237.36157	0.219	17.834	0.094
4	1254.31445	0.057	17.310	0.069
5	1255.31177	0.989	17.582	0.374
6	1257.30615	0.852	18.136	0.155
7	1258.30347	0.784	18.130	0.142
8	1263.28979	0.443	18.243	0.133
9	1269.27332	0.033	17.284	0.081
10	1578.42944	0.883	18.461	0.230
11	1593.38757	0.857	18.396	0.158
12	1612.33508	0.559	18.369	0.129
13	1613.33240	0.491	18.219	0.119
14	1614.32922	0.422	18.083	0.133
15	1615.32666	0.354	17.971	0.126
16	1616.32410	0.286	17.912	0.119
17	1617.32129	0.218	17.651	0.221
18	1620.31250	0.012	17.305	0.077
19	1621.31030	0.945	18.532	0.189
20	1623.30469	0.808	18.291	0.157
21	1935.45227	0.452	18.626	0.222
22	1936.44946	0.384	18.090	0.136
23	1942.43359	0.976	17.861	0.092
24	1997.28064	0.217	17.790	0.091
25	2295.46704	0.817	18.246	0.240
26	2305.43872	0.133	17.709	0.125
27	2323.38843	0.902	18.446	0.209
28	3126.17261	0.932	18.415	0.094
29	3126.18359	0.954	18.448	0.237
30	3126.37524	0.325	18.185	0.088
31	3129.19385	0.785	18.340	0.045
32	3129.26782	0.928	18.207	0.089
33	3129.33789	0.064	17.427	0.057
34	3453.34180	0.674	18.272	0.034
35	3453.35986	0.709	18.331	0.036
36	3453.38062	0.749	18.251	0.040

37	3453.39844	0.784	18.296	0.039
38	3453.41626	0.819	18.463	0.043
39	3453.43408	0.853	18.301	0.045
40	3474.14722	0.975	17.345	0.023
41	3474.16528	0.010	17.328	0.022
42	3474.22485	0.125	17.619	0.027
43	3474.24268	0.160	17.717	0.027
44	3474.31982	0.309	18.000	0.030
45	3474.33740	0.344	18.049	0.034
46	3474.39746	0.460	18.210	0.036
47	3474.41504	0.494	18.304	0.041

34. V385 Her

	Dayval	Phase	Vint	Vinterr
1	1578.43030	0.014	14.674	0.015
2	1593.38831	0.336	15.175	0.017
3	1612.33569	0.211	15.019	0.013
4	1613.33301	0.099	14.895	0.012
5	1614.32983	0.987	14.749	0.013
6	1615.32727	0.875	14.948	0.016
7	1616.32471	0.764	15.351	0.021
8	1623.30518	0.981	14.766	0.014
9	1935.45325	0.008	14.791	0.016
10	1936.45044	0.896	14.801	0.015
11	1942.43457	0.227	15.008	0.016
12	1997.28101	0.074	14.787	0.013
13	2295.46802	0.667	15.312	0.028
14	2305.43970	0.548	15.415	0.026
15	2323.38916	0.534	15.351	0.024
16	3097.22217	0.724	15.421	0.017
17	3099.38257	0.814	15.178	0.014
18	3099.39380	0.836	15.061	0.013
19	3099.42529	0.895	14.900	0.015
20	3126.38818	0.948	14.807	0.015
21	3128.13574	0.256	15.102	0.013
22	3128.14795	0.279	15.123	0.012
23	3128.15918	0.301	15.160	0.013
24	3128.22778	0.430	15.247	0.012
25	3128.23853	0.451	15.243	0.012
26	3128.30933	0.585	15.316	0.013
27	3128.32007	0.605	15.330	0.013
28	3385.30786	0.191	15.025	0.019
29	3385.31519	0.205	15.013	0.019
30	3385.40283	0.371	15.221	0.028
31	3385.41040	0.385	15.286	0.034

35. RR171907

	Dayval	Phase	Vint	Vinterr
1	1578.43250	0.705	17.853	0.171
2	1593.39050	0.356	17.845	0.117
3	1612.33789	0.449	17.876	0.104
4	1613.33521	0.559	17.819	0.106
5	1614.33203	0.668	17.839	0.121
6	1615.32947	0.779	17.927	0.136
7	1616.32690	0.889	17.987	0.134
8	1620.31531	0.329	17.830	0.125
9	1621.31299	0.440	17.720	0.144
10	1623.30737	0.660	17.826	0.123
11	1935.45544	0.165	17.404	0.106
12	1936.45264	0.275	17.564	0.106
13	1942.43677	0.938	17.337	0.087
14	1997.28320	0.993	17.260	0.084
15	2295.47021	0.956	17.219	0.113
16	2305.44189	0.056	17.236	0.110
17	2323.39136	0.037	17.266	0.097

36. RR172059

	Dayval	Phase	Vint	Vinterr
1	1205.45532	0.862	14.713	0.012
2	1228.39099	0.503	14.901	0.013
3	1237.36548	0.884	14.679	0.011
4	1254.31836	0.272	14.774	0.013
5	1255.31567	0.649	14.888	0.055
6	1257.31006	0.400	14.886	0.014
7	1258.30737	0.776	14.760	0.012
8	1269.27722	0.911	14.689	0.014
9	1578.43335	0.461	14.885	0.018
10	1593.39136	0.097	14.681	0.012
11	1612.33887	0.238	14.761	0.011
12	1613.33630	0.614	14.901	0.012
13	1614.33313	0.988	14.675	0.012
14	1615.33057	0.365	14.841	0.014
15	1616.32800	0.741	14.826	0.013
16	1620.31641	0.243	14.670	0.012
17	1621.31409	0.620	14.804	0.015
18	1623.30859	0.372	14.841	0.014
19	1935.45605	0.048	14.659	0.014
20	1936.45325	0.424	14.870	0.015
21	1942.43750	0.682	14.886	0.014
22	1997.28455	0.349	14.846	0.012
23	2295.47095	0.764	14.833	0.019
24	2305.44263	0.520	14.911	0.017
25	2323.39233	0.283	14.783	0.016
26	2326.38379	0.410	14.864	0.016
27	3454.35938	0.814	14.698	0.010
28	3454.37402	0.864	14.657	0.010
29	3454.39746	0.943	14.638	0.009
30	3454.41211	0.992	14.623	0.009
31	3454.43457	0.068	14.636	0.009
32	3454.44995	0.120	14.600	0.014
33	3469.14136	0.853	14.691	0.036
34	3469.15649	0.905	14.683	0.015
35	3469.20630	0.074	14.673	0.015
36	3469.22998	0.154	14.660	0.016
37	3469.26880	0.285	14.857	0.021
38	3469.28369	0.335	14.765	0.021
39	3469.32520	0.476	14.924	0.024
40	3469.34009	0.526	14.941	0.042
41	3473.25293	0.772	14.701	0.021
42	3473.26807	0.823	14.722	0.010
43	3540.12109	0.133	14.657	0.011
44	3540.12622	0.151	14.670	0.011
45	3540.13159	0.169	14.665	0.011
46	3540.13867	0.193	14.672	0.011
47	3540.14404	0.210	14.699	0.011
48	3540.14917	0.228	14.747	0.011
49	3540.15430	0.245	14.729	0.011
50	3540.15942	0.263	14.733	0.011
51	3540.16455	0.280	14.742	0.011

37. RR173043

	Dayval	Phase	Vint	Vinterr
1	1205.46216	0.837	15.774	0.025
2	1228.39783	0.976	15.286	0.018
3	1237.37231	0.720	15.896	0.025
4	1254.32520	0.699	15.886	0.026
5	1255.32251	0.230	15.727	0.098
6	1257.31689	0.284	15.798	0.027
7	1258.31421	0.814	15.630	0.022
8	1263.30042	0.458	15.860	0.026
9	1269.28394	0.630	15.879	0.029
10	1292.22168	0.804	15.807	0.028
11	1578.43970	0.643	15.903	0.039
12	1593.39819	0.568	15.880	0.027
13	1612.34570	0.608	15.907	0.023
14	1613.34302	0.138	15.607	0.020
15	1614.33984	0.659	15.885	0.026
16	1615.33740	0.192	15.694	0.023
17	1616.33472	0.723	15.848	0.027
18	1617.33203	0.252	15.643	0.032
19	1620.32324	0.828	15.763	0.024
20	1621.32092	0.365	15.789	0.033
21	1623.31531	0.421	15.868	0.027
22	1935.46289	0.022	15.299	0.021
23	1936.46008	0.549	15.898	0.032
24	1942.44434	0.734	15.899	0.027
25	1980.33728	0.777	15.773	0.036
26	1997.29126	0.777	15.839	0.023
27	2295.47754	0.982	15.577	0.030
28	2305.44946	0.256	15.705	0.030
29	2323.39893	0.755	15.877	0.032
30	2326.39062	0.338	15.807	0.031
31	3097.23804	0.483	15.841	0.017
32	3099.28662	0.490	15.803	0.019
33	3099.31250	0.944	15.486	0.012
34	3099.32520	0.170	15.605	0.014

35	3099.33936	0.416	15.814	0.013
36	3099.41113	0.679	15.833	0.015
37	3112.25635	0.460	15.867	0.016
38	3112.26733	0.652	15.847	0.027
39	3112.35498	0.193	15.588	0.016
40	3112.39185	0.839	15.616	0.013
41	3112.40234	0.026	15.330	0.013
42	3112.41357	0.220	15.675	0.014
43	3112.42432	0.411	15.812	0.016
44	3130.33960	0.309	15.698	0.028
45	3130.34351	0.376	15.815	0.028
46	3130.34717	0.442	15.795	0.035
47	3130.35107	0.509	15.792	0.034
48	3130.35498	0.576	15.918	0.034
49	3130.35913	0.651	15.878	0.031
50	3130.36328	0.725	15.847	0.036
51	3130.36768	0.802	15.823	0.035
52	3130.37207	0.876	15.633	0.035
53	3130.37646	0.954	15.472	0.031
54	3385.42041	0.851	15.790	0.027
55	3385.42456	0.921	15.624	0.028
56	3385.42847	0.989	15.332	0.021
57	3385.43213	0.056	15.282	0.025

38. RR174152

	Dayval	Phase	Vint	Vinterr
1	1205.46985	0.205	15.661	0.022
2	1228.40552	0.659	16.093	0.029
3	1237.38000	0.488	16.053	0.029
4	1254.33276	0.389	15.934	0.028
5	1255.33020	0.148	15.545	0.101
6	1257.32458	0.665	16.082	0.035
7	1258.32190	0.424	15.992	0.030
8	1263.30823	0.219	15.670	0.025
9	1269.29175	0.773	16.102	0.030
10	1292.22937	0.230	15.692	0.027
11	1578.44739	0.054	15.290	0.024
12	1593.40588	0.437	15.977	0.030
13	1612.35352	0.856	16.229	0.030
14	1613.35083	0.615	16.112	0.028
15	1614.34766	0.373	15.897	0.030
16	1615.34509	0.133	15.511	0.022
17	1616.34253	0.892	16.178	0.034
18	1617.33972	0.651	16.074	0.039
19	1620.33093	0.927	15.812	0.027
20	1621.32861	0.686	16.070	0.033
21	1623.32312	0.204	15.669	0.023
22	1935.47070	0.762	16.064	0.039
23	1936.46777	0.521	16.074	0.037
24	1942.45203	0.076	15.372	0.020
25	1980.34509	0.910	16.076	0.040
26	1997.29907	0.813	16.180	0.030
27	2035.19604	0.655	16.099	0.038
28	2305.45728	0.335	15.867	0.036
29	2323.40674	0.994	15.195	0.020
30	2326.39844	0.270	15.764	0.034
31	3097.27417	0.921	15.795	0.015
32	3113.19458	0.001	15.180	0.011
33	3113.20532	0.020	15.226	0.011
34	3113.24243	0.085	15.420	0.011
35	3113.25317	0.104	15.447	0.013
36	3113.29053	0.170	15.612	0.012
37	3113.30151	0.190	15.627	0.018
38	3113.33960	0.257	15.754	0.013
39	3113.35059	0.276	15.801	0.013
40	3113.38818	0.342	15.880	0.015
41	3113.39917	0.362	15.828	0.031
42	3385.44385	0.187	15.602	0.015
43	3385.45483	0.207	15.644	0.036

39. RR174240

	Dayval	Phase	Vint	Vinterr
1	1205.47046	0.060	16.226	0.033
2	1228.40613	0.635	16.883	0.054
3	1237.38062	0.685	16.896	0.048
4	1254.33337	0.893	16.974	0.056
5	1255.33081	0.788	17.018	0.244
6	1257.32520	0.577	16.881	0.062
7	1258.32251	0.472	16.816	0.050
8	1263.30872	0.945	16.629	0.050
9	1269.29236	0.313	16.639	0.047
10	1292.22998	0.891	16.634	0.051
11	1578.44800	0.666	16.941	0.081
12	1593.40649	0.085	16.244	0.032
13	1612.35400	0.083	16.302	0.029
14	1613.35132	0.977	16.218	0.029
15	1614.34814	0.871	16.757	0.052
16	1615.34570	0.766	16.884	0.062
17	1616.34302	0.661	16.879	0.056
18	1617.34033	0.556	16.894	0.065
19	1620.33154	0.239	16.592	0.051
20	1621.32922	0.134	16.489	0.053
21	1623.32361	0.923	16.502	0.046
22	1935.47119	0.961	16.348	0.046
23	1936.46838	0.855	16.962	0.067
24	1942.45264	0.224	16.541	0.041
25	1980.34558	0.216	16.582	0.061
26	1997.29968	0.426	16.824	0.046
27	2035.19666	0.425	16.773	0.067
28	2305.45776	0.884	16.791	0.063
29	2323.40747	0.986	16.086	0.038
30	2326.39893	0.669	16.931	0.073
31	3129.21362	0.907	16.493	0.024
32	3129.22461	0.928	16.461	0.026
33	3129.28589	0.044	16.292	0.024
34	3129.29663	0.064	16.376	0.033
35	3129.36060	0.186	16.556	0.032
36	3129.37158	0.207	16.539	0.025
37	3175.11230	0.108	16.323	0.016
38	3175.12329	0.129	16.340	0.017
39	3175.16992	0.217	16.482	0.021
40	3175.18115	0.239	16.546	0.019
41	3181.09253	0.469	16.891	0.024
42	3181.10327	0.490	16.842	0.023
43	3181.11401	0.510	16.833	0.025
44	3181.12476	0.531	16.800	0.021
45	3181.20288	0.679	16.871	0.026
46	3181.21558	0.703	16.933	0.024
47	3181.22656	0.724	16.930	0.028
48	3181.23730	0.744	16.868	0.026
49	3186.08960	0.963	16.278	0.017
50	3186.10059	0.984	16.229	0.016
51	3186.11133	0.005	16.226	0.015
52	3186.12231	0.025	16.200	0.017
53	3186.13354	0.047	16.254	0.017
54	3186.14453	0.067	16.284	0.015
55	3186.15527	0.088	16.316	0.018
56	3186.18091	0.136	16.408	0.019
57	3186.19214	0.158	16.434	0.020
58	3186.20288	0.178	16.485	0.020
59	3186.21362	0.199	16.532	0.027
60	3186.22437	0.219	16.559	0.030
61	3186.23535	0.240	16.502	0.022
62	3385.47046	0.759	16.854	0.057
63	3385.48486	0.787	16.888	0.027

40. RR174420

	Dayval	Phase	Vint	Vinterr
1	1205.47156	0.488	15.842	0.025
2	1228.40723	0.315	15.715	0.022
3	1237.38171	0.115	15.529	0.022
4	1254.33459	0.075	15.519	0.022
5	1255.33191	0.720	15.726	0.097
6	1257.32629	0.009	15.538	0.023
7	1258.32361	0.654	15.819	0.025
8	1263.30994	0.878	15.584	0.022
9	1269.29346	0.746	15.666	0.024
10	1292.23108	0.578	15.869	0.028
11	1578.44910	0.638	15.799	0.036
12	1593.40771	0.308	15.729	0.024
13	1612.35522	0.558	15.860	0.023
14	1613.35254	0.203	15.615	0.021
15	1614.34937	0.846	15.602	0.021
16	1615.34680	0.492	15.837	0.027
17	1616.34424	0.137	15.574	0.022
18	1617.34143	0.782	15.649	0.026

19	1620.33264	0.714	15.727	0.025
20	1621.33044	0.360	15.742	0.027
21	1623.32483	0.650	15.800	0.025
22	1935.47241	0.476	15.599	0.024
23	1936.46960	0.120	15.692	0.026
24	1942.45374	0.991	15.820	0.026
25	1980.34680	0.484	15.569	0.028
26	1997.30078	0.447	15.573	0.021
27	2035.19775	0.951	15.816	0.029
28	2305.45898	0.693	15.609	0.030
29	2323.40845	0.296	15.846	0.031
30	2326.40015	0.229	15.794	0.030
31	3464.37500	0.178	15.546	0.021
32	3464.38257	0.198	15.562	0.021
33	3468.17700	0.261	15.642	0.015
34	3468.18799	0.290	15.662	0.016
35	3468.23340	0.411	15.776	0.016
36	3468.24414	0.440	15.814	0.016
37	3468.28833	0.556	15.836	0.017
38	3468.29907	0.585	15.861	0.016
39	3468.34814	0.715	15.710	0.022
40	3468.35913	0.744	15.663	0.024
41	3468.42163	0.910	15.522	0.017
42	3468.43237	0.939	15.543	0.016
43	3487.28369	0.933	15.530	0.016
44	3487.29517	0.963	15.499	0.016
45	3487.30566	0.991	15.465	0.016
46	3487.31641	0.020	15.542	0.017

41. RR175017

	Dayval	Phase	Vint	Vinterr
1	1228.41284	0.666	13.204	0.005
2	1237.38721	0.579	13.282	0.005
3	1254.33948	0.970	13.362	0.006
4	1255.33679	0.406	13.267	0.018
5	1257.33118	0.275	13.174	0.005
6	1258.32837	0.710	13.176	0.005
7	1263.31458	0.884	13.248	0.005
8	1292.23474	0.496	13.352	0.006
9	1593.41333	0.846	13.210	0.005
10	1612.36023	0.108	13.261	0.005
11	1613.35754	0.543	13.339	0.005
12	1614.35437	0.977	13.378	0.005
13	1615.35181	0.413	13.277	0.005
14	1616.34924	0.848	13.212	0.005
15	1617.34644	0.283	13.075	0.008
16	1620.33752	0.586	13.276	0.005
17	1621.33521	0.022	13.376	0.005
18	1623.32959	0.891	13.262	0.005
19	1942.45972	0.072	13.321	0.005
20	1980.35181	0.592	13.267	0.006
21	1997.30518	0.986	13.378	0.006
22	2035.20093	0.512	13.363	0.006
23	2305.46484	0.381	13.217	0.006
24	2323.41406	0.207	13.151	0.006
25	2326.40552	0.512	13.324	0.006
26	3463.32422	0.366	13.222	0.009
27	3463.33667	0.384	13.242	0.009
28	3463.38770	0.457	13.345	0.009
29	3463.40039	0.475	13.354	0.009
30	3464.39209	0.902	13.263	0.009
31	3464.40430	0.920	13.291	0.009
32	3473.30249	0.723	13.176	0.010
33	3473.31299	0.738	13.163	0.010
34	3473.43896	0.919	13.297	0.011
35	3473.44971	0.935	13.312	0.011
36	3546.08276	0.443	13.304	0.012
37	3546.08594	0.447	13.312	0.011
38	3546.11694	0.492	13.352	0.011
39	3546.11328	0.487	13.331	0.011
40	3546.11987	0.496	13.320	0.011
41	3546.12305	0.501	13.325	0.011
42	3546.12598	0.505	13.320	0.011
43	3546.12915	0.510	13.340	0.011
44	3546.13232	0.514	13.356	0.011
45	3546.14990	0.540	13.342	0.011

42. RR181101

	Dayval	Phase	Vint	Vinterr
1	1228.42737	0.697	17.475	0.066
2	1237.40161	0.456	17.306	0.065
3	1254.35388	0.781	17.292	0.083
4	1255.35132	0.977	16.639	0.190
5	1257.34558	0.368	17.123	0.074
6	1258.34290	0.563	17.391	0.068
7	1263.32874	0.541	17.369	0.080
8	1269.31213	0.715	17.349	0.072
9	1292.24915	0.217	16.822	0.051
10	1317.18164	0.112	16.516	0.055
11	1593.42773	0.337	17.259	0.066
12	1612.37476	0.053	16.552	0.038
13	1613.37207	0.249	17.106	0.057
14	1614.36877	0.444	17.367	0.077
15	1615.36621	0.640	17.431	0.082
16	1617.36084	0.032	16.853	0.171
17	1620.35193	0.617	17.449	0.084
18	1621.34875	0.812	17.420	0.086
19	1623.34399	0.205	17.056	0.065
20	1980.36621	0.279	17.252	0.071
21	1997.31958	0.606	17.507	0.068
22	2035.21533	0.043	16.683	0.055
23	2036.21265	0.239	17.253	0.083
24	2057.15625	0.352	17.195	0.105
25	2323.42847	0.617	17.487	0.098
26	2326.41992	0.203	17.070	0.074
27	3128.17358	0.465	17.384	0.032
28	3128.18555	0.491	17.429	0.033
29	3128.25659	0.648	17.419	0.023
30	3128.33984	0.831	17.228	0.019
31	3128.41333	0.993	16.365	0.030
32	3169.12036	0.619	17.425	0.032
33	3169.13452	0.651	17.425	0.027
34	3169.20850	0.813	17.492	0.025
35	3169.22290	0.845	17.305	0.025
36	3169.29614	0.007	16.367	0.024
37	3180.09839	0.790	17.463	0.029
38	3180.11279	0.822	17.386	0.026
39	3180.19482	0.003	16.358	0.017
40	3180.20923	0.034	16.508	0.018
41	3180.25708	0.139	16.803	0.022
42	3180.27051	0.169	16.892	0.023
43	3187.10742	0.222	17.036	0.022
44	3187.12207	0.255	17.130	0.020
45	3187.13672	0.287	17.196	0.022
46	3187.15161	0.320	17.178	0.025
47	3187.16650	0.353	17.225	0.025
48	3187.18091	0.384	17.280	0.024
49	3187.19580	0.417	17.326	0.028
50	3187.21021	0.449	17.335	0.030
51	3187.22437	0.480	17.419	0.029
52	3187.23853	0.511	17.429	0.025
53	3187.25269	0.542	17.406	0.026

43. V532 Her

	Dayval	Phase	Vint	Vinterr
1	1228.42761	0.852	16.000	0.027
2	1237.40186	0.426	15.735	0.023
3	1254.35413	0.734	15.872	0.029
4	1255.35156	0.576	15.814	0.103
5	1257.34583	0.259	15.559	0.023
6	1258.34314	0.101	15.252	0.016
7	1263.32898	0.309	15.598	0.023
8	1269.31250	0.360	15.665	0.023
9	1292.24951	0.720	15.856	0.025
10	1317.18188	0.767	15.861	0.036
11	1593.42798	0.948	15.312	0.017
12	1612.37500	0.940	15.345	0.016
13	1613.37231	0.782	15.944	0.025
14	1614.36914	0.623	15.835	0.025
15	1617.36108	0.149	15.421	0.052
16	1620.35229	0.673	15.843	0.026
17	1621.34912	0.514	15.795	0.032
18	1623.34424	0.199	15.453	0.021
19	1980.36646	0.561	15.805	0.032

20	1997.31995	0.871	15.914	0.027
21	2035.21570	0.859	15.976	0.032
22	2036.21289	0.700	15.851	0.031
23	2057.15674	0.380	15.647	0.038
24	2323.42871	0.142	15.360	0.023
25	2326.42017	0.666	15.885	0.031
26	3128.20020	0.424	15.730	0.018
27	3128.21191	0.446	15.747	0.018
28	3128.27515	0.563	15.800	0.018
29	3128.29443	0.598	15.814	0.019
30	3128.35864	0.717	15.845	0.019
31	3128.36963	0.737	15.873	0.019
32	3128.42603	0.841	15.940	0.020
33	3097.28540	0.329	15.693	0.020
34	3169.15405	0.059	15.195	0.016
35	3169.16504	0.079	15.248	0.017
36	3169.24487	0.227	15.516	0.018
37	3169.25562	0.247	15.532	0.018
38	3175.13623	0.107	15.304	0.016
39	3175.14697	0.127	15.344	0.017
40	3175.19189	0.210	15.487	0.017
41	3175.20264	0.230	15.512	0.017

44. RR183606

	Dayval	Phase	Vint	Vinterr
1	1228.44482	0.734	17.000	0.050
2	1237.41907	0.271	16.608	0.038
3	1254.37134	0.289	16.673	0.044
4	1255.36877	0.349	16.734	0.264
5	1257.36267	0.468	16.926	0.057
6	1258.36035	0.528	16.956	0.050
7	1263.34619	0.827	16.904	0.059
8	1269.32959	0.187	16.447	0.035
9	1292.26660	0.566	16.992	0.057
10	1317.19910	0.067	16.070	0.041
11	1593.44519	0.689	16.958	0.050
12	1612.39136	0.825	17.053	0.050
13	1613.38953	0.887	17.018	0.058
14	1615.38293	0.005	15.836	0.028
15	1616.38013	0.064	16.051	0.029
16	1617.37720	0.124	16.278	0.039
17	1620.36951	0.305	16.646	0.051
18	1621.36621	0.364	16.729	0.047
19	1623.36145	0.485	16.876	0.061
20	1980.38354	0.960	16.548	0.046
21	1997.33716	0.980	15.955	0.027
22	2035.23291	0.259	16.605	0.045
23	2057.17383	0.581	17.075	0.083
24	2323.44604	0.600	16.923	0.072
25	2326.43750	0.780	16.977	0.069
26	3126.40332	0.212	16.456	0.023
27	3126.41406	0.235	16.560	0.029
28	3126.42505	0.257	16.610	0.028
29	3129.38916	0.380	16.719	0.034
30	3129.40308	0.409	16.703	0.075
31	3130.38794	0.443	16.813	0.023
32	3130.39868	0.465	16.881	0.027
33	3130.40942	0.487	16.907	0.028
34	3130.42017	0.510	16.917	0.027
35	3169.18066	0.574	16.995	0.024
36	3169.19165	0.597	16.984	0.028
37	3169.27026	0.760	16.965	0.028
38	3169.28125	0.782	16.990	0.029
39	3174.09814	0.732	16.926	0.025
40	3174.11133	0.759	17.009	0.025
41	3174.12231	0.782	17.041	0.023
42	3174.18677	0.915	16.882	0.023
43	3174.19775	0.938	16.597	0.020
44	3174.24658	0.039	15.990	0.016
45	3174.25757	0.061	16.028	0.016
46	3454.38599	0.703	16.992	0.021
47	3454.42285	0.779	16.947	0.021

45. RR183918

	Dayval	Phase	Vint	Vinterr
1	1228.44702	0.313	16.668	0.041
2	1237.42126	0.954	16.541	0.036
3	1254.37354	0.834	17.068	0.063
4	1255.37097	0.239	16.611	0.168
5	1257.36487	0.047	16.316	0.035
6	1258.36255	0.453	16.792	0.043
7	1263.34839	0.476	16.817	0.049
8	1269.33191	0.904	16.918	0.051
9	1292.26892	0.213	16.533	0.039
10	1317.20129	0.333	16.673	0.052
11	1593.44739	0.456	16.741	0.048
12	1612.39355	0.143	16.429	0.034
13	1613.39172	0.549	16.834	0.049
14	1615.38513	0.357	16.685	0.048
15	1616.38232	0.762	17.024	0.056
16	1617.37939	0.166	16.477	0.043
17	1620.37170	0.381	16.707	0.046
18	1621.36841	0.785	17.013	0.059
19	1623.36365	0.596	16.856	0.052
20	1980.38574	0.500	16.868	0.051
21	1997.33936	0.381	16.785	0.042
22	2035.23511	0.761	16.993	0.066
23	2057.17603	0.667	16.867	0.068
24	2323.44824	0.740	16.968	0.064
25	2326.43970	0.954	16.590	0.047
26	3473.34888	0.499	16.814	0.022
27	3473.35962	0.514	16.868	0.022
28	3473.39526	0.564	16.848	0.023
29	3473.40649	0.580	16.893	0.023
30	3478.25171	0.405	16.763	0.018
31	3478.30493	0.480	16.830	0.019
32	3478.31909	0.500	16.855	0.019
33	3478.35645	0.552	16.892	0.020
34	3478.37061	0.572	16.892	0.020
35	3478.40698	0.624	16.881	0.020
36	3478.42114	0.644	16.886	0.020
37	3516.15967	0.802	17.031	0.021
38	3516.19824	0.856	17.048	0.023
39	3516.21094	0.875	17.012	0.023
40	3516.25439	0.936	16.588	0.019
41	3516.26733	0.954	16.536	0.019
42	3516.28027	0.972	16.446	0.019
43	3516.32471	0.035	16.305	0.019
44	3516.33789	0.053	16.321	0.017

46. RR184019

	Dayval	Phase	Vint	Vinterr
1	1228.44775	0.437	14.679	0.011
2	1237.42200	0.896	14.482	0.010
3	1254.37427	0.098	14.439	0.012
4	1255.37170	0.817	14.303	0.038
5	1257.36560	0.251	14.279	0.010
6	1258.36328	0.970	14.754	0.012
7	1263.34912	0.559	14.566	0.011
8	1269.33252	0.866	14.403	0.010
9	1292.26953	0.380	14.453	0.011
10	1317.20203	0.332	14.351	0.012
11	1593.44812	0.227	14.276	0.009
12	1612.39429	0.864	14.398	0.009
13	1613.39246	0.584	14.519	0.010
14	1615.38586	0.017	14.729	0.013
15	1616.38306	0.735	14.278	0.010
16	1617.38013	0.452	14.726	0.014
17	1620.37244	0.607	14.371	0.011
18	1621.36914	0.324	14.368	0.010
19	1623.36438	0.762	14.264	0.009
20	1980.38647	0.808	14.289	0.010
21	1997.34009	0.014	14.745	0.012
22	2035.23584	0.297	14.305	0.011
23	2057.17676	0.096	14.486	0.013
24	2323.44897	0.807	14.251	0.010
25	2326.44043	0.960	14.614	0.013
26	3463.34912	0.547	14.590	0.009
27	3463.36597	0.593	14.413	0.008
28	3463.41113	0.716	14.231	0.007
29	3463.42651	0.758	14.220	0.007
30	3473.27734	0.606	14.381	0.007
31	3473.29224	0.646	14.307	0.007
32	3473.32007	0.722	14.220	0.007
33	3473.33447	0.762	14.207	0.007
34	3473.36963	0.857	14.306	0.008

35	3473.38379	0.896	14.416	0.008
36	3473.41626	0.984	14.670	0.009
37	3473.43042	0.023	14.650	0.009

47. RR184315

	Dayval	Phase	Vint	Vinterr
1	1228.44971	0.786	16.214	0.030
2	1237.42407	0.460	16.453	0.034
3	1254.37634	0.291	16.194	0.037
4	1255.37378	0.811	16.263	0.150
5	1257.36768	0.849	16.313	0.036
6	1258.36523	0.370	16.284	0.032
7	1263.35120	0.967	16.600	0.043
8	1269.33459	0.084	16.486	0.039
9	1292.27161	0.034	16.549	0.038
10	1317.20410	0.025	16.564	0.048
11	1593.45020	0.953	16.540	0.038
12	1612.39636	0.822	16.221	0.028
13	1613.39453	0.343	16.243	0.030
14	1616.38513	0.900	16.326	0.035
15	1617.38220	0.419	16.507	0.059
16	1620.37439	0.979	16.519	0.042
17	1621.37122	0.498	16.493	0.036
18	1623.36646	0.538	16.568	0.040
19	1980.38855	0.548	16.554	0.039
20	1997.34204	0.381	16.355	0.031
21	2035.23779	0.125	16.376	0.039
22	2057.17871	0.557	16.516	0.041
23	2323.45093	0.288	16.205	0.037
24	2326.44238	0.846	16.249	0.036

48. RR184421

	Dayval	Phase	Vint	Vinterr
1	1228.45056	0.242	16.949	0.046
2	1237.42480	0.184	16.948	0.043
3	1254.37708	0.189	16.941	0.054
4	1255.37451	0.072	17.099	0.243
5	1257.36841	0.836	17.097	0.060
6	1258.36609	0.720	16.982	0.048
7	1263.35193	0.133	17.035	0.051
8	1269.33545	0.430	17.308	0.059
9	1292.27234	0.735	17.077	0.056
10	1317.20483	0.809	17.139	0.067
11	1593.45093	0.370	17.199	0.059
12	1612.39709	0.138	17.077	0.050
13	1613.39526	0.024	17.380	0.059
14	1616.38586	0.669	17.017	0.056
15	1617.38293	0.551	17.237	0.081
16	1620.37512	0.201	16.973	0.055
17	1621.37195	0.083	17.045	0.054
18	1623.36719	0.850	17.218	0.060
19	1980.38928	0.915	17.271	0.060
20	1997.34290	0.924	17.325	0.066
21	2035.23865	0.471	17.140	0.065
22	2057.17944	0.897	17.205	0.072
23	2323.45166	0.626	16.990	0.067
24	2326.44312	0.273	16.942	0.056
25	3468.31860	0.159	16.911	0.019
26	3468.33325	0.201	16.930	0.023
27	3468.37451	0.320	16.904	0.019
28	3468.40698	0.414	17.106	0.022
29	3481.30103	0.688	16.975	0.020
30	3481.31519	0.729	16.968	0.023
31	3481.35547	0.845	17.107	0.024
32	3481.36743	0.880	17.157	0.025
33	3481.40283	0.982	17.374	0.025
34	3481.41724	0.023	17.282	0.024

49. RR184747

	Dayval	Phase	Vint	Vinterr
1	1228.45288	0.921	16.965	0.052
2	1237.42725	0.660	17.326	0.060
3	1254.37952	0.836	17.167	0.068
4	1255.37683	0.141	17.111	0.241
5	1257.37085	0.749	17.367	0.082
6	1258.36841	0.054	17.067	0.052
7	1263.35425	0.576	17.305	0.071
8	1269.33777	0.403	17.295	0.063
9	1292.27478	0.407	17.218	0.067
10	1317.20728	0.022	17.120	0.067
11	1593.45337	0.382	17.169	0.067
12	1612.39941	0.166	17.071	0.050
13	1613.39758	0.472	17.365	0.063
14	1616.38831	0.384	17.292	0.068
15	1617.38525	0.688	17.497	0.123
16	1620.37756	0.602	17.517	0.086
17	1621.37439	0.906	17.087	0.057
18	1623.36963	0.516	17.436	0.089
19	1980.39160	0.541	17.263	0.069
20	1997.34521	0.718	17.378	0.064
21	2035.24097	0.290	17.184	0.068
22	2036.23816	0.594	17.268	0.081
23	2057.18188	0.991	17.030	0.065
24	2326.44556	0.218	17.181	0.071
25	3474.35864	0.816	17.226	0.019
26	3474.37646	0.839	17.131	0.019
27	3480.26538	0.542	17.258	0.019
28	3480.28345	0.566	17.254	0.019
29	3480.32031	0.614	17.299	0.019
30	3480.33789	0.637	17.298	0.018
31	3480.37158	0.681	17.283	0.020
32	3480.38940	0.704	17.326	0.020
33	3480.42358	0.749	17.346	0.021
34	3480.44141	0.772	17.307	0.023
35	3488.25293	0.991	17.076	0.023
36	3488.27051	0.014	17.083	0.021
37	3488.28833	0.037	17.096	0.022
38	3488.35083	0.119	17.104	0.022
39	3488.36841	0.142	17.081	0.020
40	3488.42798	0.220	17.108	0.019
41	3539.10425	0.510	17.294	0.020
42	3539.11841	0.528	17.314	0.018
43	3539.19141	0.624	17.360	0.026
44	3539.20337	0.640	17.377	0.024
45	3539.28882	0.751	17.402	0.026
46	3539.29956	0.765	17.389	0.027
47	3563.07349	0.864	17.111	0.020
48	3563.08545	0.880	17.042	0.018
49	3563.12256	0.929	16.946	0.020
50	3563.13477	0.945	16.914	0.017
51	3563.14844	0.962	16.883	0.018
52	3563.16089	0.979	16.852	0.019
53	3563.17407	0.996	16.850	0.019
54	3563.18652	0.012	16.858	0.034
55	3606.05566	0.090	16.992	0.020
56	3606.07007	0.109	17.038	0.019
57	3607.05078	0.391	17.292	0.031
58	3607.06519	0.410	17.281	0.026
59	3607.07983	0.429	17.305	0.027
60	3607.09692	0.452	17.386	0.032
61	3607.11108	0.471	17.337	0.034
62	3607.12573	0.489	17.358	0.041
63	3607.13989	0.508	17.504	0.041
64	3607.15405	0.527	17.392	0.042
65	3622.05103	0.013	16.894	0.015
66	3622.06519	0.032	16.919	0.016
67	3622.07935	0.051	16.935	0.017
68	3622.09375	0.069	16.973	0.017

50. GS Lyr

	Dayval	Phase	Vint	Vinterr
1	1237.43896	0.095	12.528	0.003
2	1254.39075	0.102	12.651	0.004
3	1255.38855	0.102	12.646	0.010
4	1257.38245	0.103	12.713	0.004
5	1258.38000	0.103	12.744	0.003
6	1263.36572	0.105	12.822	0.004
7	1269.34888	0.108	12.897	0.004
8	1292.28589	0.117	12.749	0.004
9	1317.21802	0.127	12.793	0.004
10	1612.41113	0.245	12.904	0.004
11	1613.40930	0.245	12.895	0.004
12	1615.40247	0.246	12.886	0.004
13	1616.39990	0.247	12.957	0.004
14	1617.39697	0.247	12.963	0.004
15	1620.38916	0.248	12.960	0.004

16	1621.38599	0.249	12.939	0.004
17	1623.38123	0.249	13.011	0.004
18	1997.35669	0.399	13.003	0.004
19	2035.25195	0.414	12.472	0.003
20	2036.24902	0.414	12.511	0.003
21	2057.19263	0.423	12.956	0.005
22	2061.18188	0.424	12.993	0.005
23	2062.17920	0.425	12.976	0.005
24	3097.30200	0.839	12.799	0.008
25	3126.43628	0.851	13.017	0.010
26	3126.44214	0.851	13.000	0.008
27	3126.44971	0.851	13.010	0.008
28	3128.39478	0.851	13.044	0.008
29	3128.40088	0.851	13.041	0.008
30	3128.43628	0.851	13.022	0.009
31	3128.44263	0.851	13.017	0.009
32	3128.44849	0.851	13.018	0.008
33	3174.13818	0.870	12.673	0.010
34	3174.14160	0.870	12.688	0.013
35	3174.20532	0.870	12.688	0.013
36	3174.20776	0.870	12.689	0.013
37	3174.26562	0.870	12.688	0.013
38	3174.26807	0.870	12.685	0.011
39	3175.15649	0.870	12.693	0.013
40	3175.15918	0.870	12.697	0.013
41	3175.21045	0.870	12.688	0.013
42	3175.21387	0.870	12.683	0.011
43	3181.13501	0.872	12.762	0.013
44	3181.13794	0.872	12.757	0.013
45	3187.26660	0.875	12.847	0.011
46	3187.27075	0.875	12.839	0.011
47	3194.10986	0.878	12.971	0.010
48	3194.11401	0.878	12.960	0.010
49	3195.08643	0.878	12.980	0.010
50	3195.09058	0.878	12.979	0.010
51	3201.11133	0.880	13.000	0.012
52	3201.11450	0.880	12.983	0.012
53	3203.13745	0.881	12.964	0.012
54	3204.08447	0.882	12.938	0.012
55	3204.08765	0.882	12.943	0.012
56	3205.11963	0.882	12.913	0.012
57	3205.12305	0.882	12.912	0.012
58	3206.08105	0.882	12.921	0.012
59	3206.08350	0.882	12.905	0.012
60	3209.20923	0.884	12.874	0.008
61	3209.21753	0.884	12.879	0.013
62	3211.06836	0.884	12.846	0.013
63	3211.07861	0.884	12.880	0.012
64	3217.07349	0.887	12.862	0.012
65	3217.07617	0.887	12.834	0.010
66	3223.07373	0.889	12.870	0.012
67	3223.07666	0.889	12.865	0.012
68	3231.04224	0.892	12.834	0.012
69	3231.04468	0.892	12.818	0.012
70	3245.05640	0.898	12.776	0.013
71	3245.05884	0.898	12.779	0.013
72	3262.05078	0.905	12.790	0.013
73	3262.05371	0.905	12.806	0.012
74	3453.45239	0.981	12.908	0.012
75	3453.45508	0.981	12.931	0.013
76	3463.44629	0.985	13.039	0.012
77	3463.44897	0.985	13.012	0.012
78	3464.41504	0.986	13.022	0.014
79	3464.41748	0.986	13.013	0.014
80	3465.43262	0.986	13.040	0.012
81	3465.43506	0.986	13.036	0.012
82	3468.44287	0.987	13.040	0.012
83	3468.44531	0.987	13.043	0.012
84	3469.35059	0.988	13.111	0.044
85	3469.35327	0.988	13.043	0.027
86	3473.45630	0.989	13.063	0.014
87	3473.45898	0.989	13.074	0.015
88	3474.45288	0.990	13.054	0.012
89	3474.45801	0.990	13.044	0.014
90	3480.45312	0.992	13.128	0.012
91	3480.45776	0.992	13.129	0.013
92	3481.45068	0.993	13.196	0.013
93	3481.45557	0.993	13.202	0.014
94	3487.45532	0.995	13.362	0.012
95	3487.46069	0.995	13.358	0.013
96	3488.43945	0.995	13.382	0.012
97	3488.44482	0.995	13.368	0.012
98	3516.34741	0.007	13.314	0.012
99	3516.35376	0.007	13.312	0.012
100	3539.30786	0.016	13.362	0.011
101	3539.31079	0.016	13.326	0.011
102	3540.25122	0.016	13.314	0.013
103	3540.25366	0.016	13.333	0.012
104	3545.25317	0.018	13.360	0.012
105	3545.25562	0.018	13.365	0.011
106	3546.10229	0.018	13.408	0.011
107	3546.13843	0.018	13.371	0.011
108	3563.09497	0.025	13.347	0.011
109	3563.10059	0.025	13.344	0.011
110	3569.06152	0.028	13.384	0.011
111	3569.06738	0.028	13.399	0.011
112	3606.03784	0.042	13.231	0.012
113	3606.04321	0.042	13.220	0.011
114	3607.03271	0.043	13.245	0.015
115	3607.03857	0.043	13.204	0.012
116	3622.03247	0.049	12.828	0.014
117	3622.03955	0.049	12.835	0.012

51. V427 Lyr

	Dayval	Phase	Vint	Vinterr
1	1237.44556	0.529	16.664	0.040
2	1254.39734	0.453	16.645	0.053
3	1255.39502	0.803	16.744	0.193
4	1257.38892	0.499	16.632	0.051
5	1258.38611	0.848	16.742	0.044
6	1269.35547	0.682	16.691	0.046
7	1292.29248	0.703	16.713	0.050
8	1317.22461	0.422	16.608	0.050
9	1355.12305	0.679	16.753	0.038
10	1612.41772	0.650	16.699	0.043
11	1613.41589	0.001	15.767	0.023
12	1615.40906	0.695	16.779	0.056
13	1616.40649	0.044	15.913	0.025
14	1617.40344	0.392	16.590	0.041
15	1620.39575	0.439	16.668	0.047
16	1621.39246	0.787	16.832	0.054
17	1623.38770	0.486	16.632	0.046
18	1980.40979	0.331	16.587	0.043
19	1997.36328	0.259	16.477	0.037
20	2036.25562	0.857	16.617	0.046
21	2057.19922	0.183	16.378	0.045
22	2061.18823	0.578	16.671	0.050
23	2062.18555	0.927	15.756	0.025
24	2082.13257	0.905	16.157	0.035
25	3097.31470	0.825	16.599	0.029
26	3129.42432	0.448	16.643	0.056
27	3129.43579	0.475	16.742	0.088
28	3194.12744	0.834	16.654	0.026
29	3194.13867	0.861	16.572	0.026
30	3194.17822	0.954	15.861	0.019
31	3194.18896	0.980	15.799	0.017
32	3194.21875	0.049	15.903	0.018
33	3194.22949	0.075	15.974	0.022
34	3194.26001	0.147	16.147	0.025
35	3194.27075	0.172	16.177	0.026
36	3195.10498	0.137	16.117	0.019
37	3195.11572	0.162	16.171	0.020
38	3195.14551	0.232	16.294	0.021
39	3195.15625	0.258	16.332	0.023
40	3195.18579	0.327	16.341	0.025
41	3195.19653	0.352	16.460	0.025
42	3195.22656	0.423	16.551	0.027
43	3195.23730	0.448	16.623	0.032
44	3474.43408	0.003	15.744	0.015
45	3474.44482	0.028	15.803	0.017

52. V926 Cyg

	Dayval	Phase	Vint	Vinterr
1	1255.41357	0.610	15.334	0.053
2	1257.40747	0.105	15.032	0.014
3	1258.40454	0.353	15.222	0.014

4	1263.39038	0.593	15.162	0.021
5	1269.37366	0.083	14.995	0.013
6	1292.31018	0.795	15.009	0.016
7	1317.24158	0.005	14.932	0.016
8	1354.14185	0.202	15.144	0.011
9	1355.13928	0.451	15.313	0.013
10	1612.43628	0.554	15.264	0.017
11	1613.43323	0.802	15.024	0.014
12	1615.42761	0.298	15.100	0.015
13	1616.42468	0.546	15.300	0.017
14	1617.42200	0.795	14.990	0.016
15	1620.41418	0.541	15.232	0.018
16	1621.41101	0.788	15.052	0.016
17	1623.40613	0.287	15.070	0.017
18	1980.42834	0.229	15.177	0.015
19	1997.38147	0.452	15.354	0.016
20	2035.27551	0.885	15.036	0.016
21	2036.27283	0.134	15.052	0.016
22	2061.20508	0.346	15.288	0.018
23	2062.20215	0.595	15.374	0.018
24	2063.19946	0.843	15.126	0.016
25	2082.14868	0.567	15.434	0.022
26	3097.36401	0.468	15.279	0.029
27	3194.15088	0.736	15.134	0.017
28	3194.15820	0.760	15.075	0.017
29	3194.16553	0.784	15.065	0.017
30	3194.19873	0.892	14.967	0.017
31	3194.20605	0.916	14.965	0.015
32	3194.24023	0.027	14.974	0.017
33	3194.24756	0.051	14.997	0.019
34	3195.12549	0.910	14.976	0.017
35	3195.13281	0.934	14.959	0.016
36	3195.16602	0.042	14.983	0.017
37	3195.17334	0.066	14.980	0.016
38	3195.20654	0.175	15.084	0.018
39	3195.21387	0.198	15.098	0.019
40	3195.24707	0.307	15.247	0.021
41	3195.25439	0.330	15.250	0.022
42	3474.29834	0.271	15.143	0.012
43	3474.30591	0.296	15.162	0.013
44	3488.30420	0.893	15.018	0.013
45	3488.31128	0.917	14.986	0.012
46	3488.38232	0.148	15.032	0.014
47	3488.38965	0.172	15.045	0.013

53. RR210716

	Dayval	Phase	Vint	Vinterr
1	1269.43628	0.541	13.063	0.004
2	1292.37280	0.805	12.767	0.004
3	1317.30371	0.615	12.841	0.005
4	1354.20337	0.696	12.755	0.003
5	1355.20068	0.969	13.170	0.004
6	1359.18982	0.059	13.009	0.005
7	1378.13916	0.238	12.733	0.004
8	1379.13660	0.511	13.129	0.004
9	1742.14258	0.679	12.771	0.005
10	2035.33765	0.771	12.743	0.004
11	2036.33472	0.043	13.088	0.005
12	2061.26685	0.855	12.842	0.004
13	2062.26416	0.128	12.835	0.004
14	2063.26099	0.399	12.934	0.005
15	2094.17798	0.848	12.691	0.005
16	2110.13525	0.210	12.750	0.005
17	2113.12744	0.028	13.167	0.006
18	2121.10620	0.209	12.736	0.005
19	3465.32153	0.221	12.761	0.012
20	3465.32959	0.240	12.729	0.012
21	3465.35718	0.303	12.786	0.011
22	3465.36133	0.312	12.784	0.011
23	3465.36938	0.330	12.816	0.011
24	3465.39307	0.384	12.895	0.011
25	3465.40088	0.402	12.919	0.011
26	3517.14795	0.316	12.765	0.015
27	3517.15161	0.325	12.795	0.013
28	3517.21948	0.479	13.128	0.010
29	3517.22339	0.488	13.143	0.010
30	3517.29492	0.651	12.837	0.011
31	3517.29858	0.660	12.810	0.011
32	3517.36816	0.818	12.782	0.011
33	3517.37207	0.827	12.798	0.011
34	3517.47339	0.058	13.045	0.020
35	3517.47705	0.066	13.019	0.015

54. RR212011

	Dayval	Phase	Vint	Vinterr
1	1354.21448	0.779	16.628	0.034
2	1355.21167	0.001	16.408	0.032
3	1359.20044	0.891	16.663	0.050
4	1378.14771	0.121	16.425	0.034
5	1379.14502	0.344	16.439	0.043
6	2035.35254	0.885	16.595	0.046
7	2061.28003	0.672	16.605	0.048
8	2062.27710	0.895	16.617	0.047
9	2063.27393	0.116	16.386	0.049
10	2094.18774	0.017	16.398	0.050
11	2110.14355	0.578	16.549	0.050
12	2113.13525	0.246	16.391	0.053
13	2121.11328	0.027	16.335	0.053

55. RR212110

	Dayval	Phase	Vint	Vinterr
1	1354.21509	0.986	15.182	0.014
2	1355.21240	0.053	15.207	0.014
3	1359.20105	0.320	15.473	0.025
4	1378.14844	0.591	15.601	0.019
5	1379.14575	0.658	15.743	0.029
6	2035.35315	0.762	15.524	0.023
7	2061.28076	0.500	15.576	0.022
8	2062.27783	0.567	15.583	0.023
9	2063.27466	0.632	15.609	0.024
10	2094.18848	0.705	15.585	0.026
11	2110.14429	0.775	15.505	0.025
12	2113.13599	0.976	15.204	0.019
13	2121.11401	0.512	15.572	0.028

56. RR213430

	Dayval	Phase	Vint	Vinterr
1	1292.39307	0.371	16.841	0.055
2	1317.32349	0.181	16.724	0.056
3	1354.22192	0.905	16.943	0.046
4	1355.21924	0.898	16.870	0.047
5	1359.20825	0.868	16.791	0.063
6	1378.15698	0.729	16.693	0.042
7	1404.08752	0.541	17.064	0.066
8	1405.08496	0.534	17.184	0.056
9	1742.16040	0.022	17.115	0.091
10	1758.11755	0.906	16.882	0.062
11	2035.35767	0.842	16.769	0.054
12	2061.28613	0.647	16.793	0.054
13	2062.28320	0.640	16.814	0.051
14	2063.28003	0.631	16.804	0.061
15	2094.19604	0.403	17.009	0.066
16	2110.15308	0.287	16.770	0.066
17	2113.14502	0.265	16.737	0.063
18	2121.12378	0.207	16.768	0.069
19	3487.36841	0.003	17.268	0.022
20	3487.38281	0.046	17.128	0.021
21	3487.43115	0.191	16.795	0.018
22	3487.44556	0.234	16.746	0.018
23	3516.18115	0.463	17.184	0.028
24	3516.22485	0.594	16.847	0.023
25	3516.23779	0.633	16.859	0.022
26	3516.29517	0.806	16.788	0.021
27	3516.30811	0.844	16.891	0.022
28	3516.36230	0.007	17.225	0.024
29	3516.37524	0.046	17.103	0.022
30	3516.43677	0.230	16.804	0.021
31	3516.44971	0.269	16.735	0.020
32	3545.19043	0.513	17.161	0.028
33	3545.20044	0.544	17.025	0.026
34	3545.21045	0.574	16.939	0.025
35	3545.22046	0.604	16.836	0.025

57. RR214612

	Dayval	Phase	Vint	Vinterr
1	1292.40125	0.970	15.108	0.018

2	1317.33167	0.025	14.920	0.017
3	1354.22998	0.268	15.167	0.014
4	1355.22742	0.951	15.182	0.014
5	1359.21631	0.680	15.446	0.022
6	1378.16516	0.644	15.437	0.017
7	1379.16260	0.327	15.162	0.022
8	1403.09839	0.704	15.453	0.024
9	1404.09570	0.386	15.277	0.017
10	1405.09302	0.069	14.793	0.012
11	1742.16858	0.679	15.438	0.025
12	1758.12573	0.597	15.425	0.022
13	2035.36572	0.271	15.216	0.018
14	2061.29419	0.010	14.833	0.015
15	2062.29150	0.692	15.465	0.023
16	2063.28833	0.373	15.305	0.019
17	2094.20435	0.525	15.432	0.023
18	2110.16138	0.443	15.355	0.025
19	2113.15332	0.490	15.396	0.023
20	2121.13184	0.949	15.318	0.025
21	3465.34204	0.488	15.347	0.016
22	3465.34961	0.500	15.333	0.016
23	3465.37842	0.549	15.399	0.015
24	3465.38623	0.562	15.384	0.015
25	3465.40967	0.601	15.405	0.016
26	3465.41699	0.614	15.422	0.016
27	3503.29224	0.506	15.435	0.056
28	3503.30591	0.529	15.390	0.014
29	3517.13110	0.850	15.404	0.019
30	3517.13843	0.863	15.379	0.028
31	3517.20532	0.975	14.966	0.017
32	3517.21265	0.988	14.906	0.018
33	3517.28101	0.103	14.989	0.014
34	3517.28833	0.115	15.020	0.013
35	3517.35376	0.226	15.135	0.014
36	3517.36108	0.238	15.150	0.014
37	3517.43604	0.364	15.288	0.019
38	3517.44336	0.377	15.300	0.016

58. RR215735

	Dayval	Phase	Vint	Vinterr
1	1292.40918	0.661	17.581	0.096
2	1317.33960	0.318	17.266	0.077
3	1354.23792	0.733	17.647	0.069
4	1355.23523	0.879	17.772	0.085
5	1359.22424	0.465	17.476	0.090
6	1378.17310	0.247	17.113	0.055
7	1379.17053	0.394	17.002	0.082
8	1403.10632	0.910	17.544	0.140
9	1404.10364	0.057	16.471	0.040
10	1405.10095	0.203	16.980	0.047
11	1411.08508	0.083	16.634	0.037
12	1742.17651	0.679	17.555	0.123
13	1758.13367	0.023	16.408	0.040
14	2035.37366	0.717	17.659	0.095
15	2061.30225	0.522	17.559	0.092
16	2062.29932	0.668	17.681	0.089
17	2063.29614	0.813	17.773	0.107
18	2094.21216	0.353	17.421	0.089
19	2113.16113	0.136	16.800	0.059
20	2121.13989	0.308	17.169	0.092
21	3231.05518	0.139	16.802	0.019
22	3231.06934	0.170	16.894	0.017
23	3231.12793	0.295	17.244	0.022
24	3231.14258	0.327	17.281	0.024
25	3231.20898	0.470	17.508	0.031
26	3231.22339	0.501	17.527	0.026
27	3231.28174	0.627	17.560	0.039
28	3231.29590	0.657	17.607	0.045
29	3234.04712	0.578	17.534	0.035
30	3234.06152	0.609	17.555	0.029
31	3234.11035	0.715	17.549	0.031
32	3234.12476	0.745	17.549	0.031
33	3234.17236	0.848	17.773	0.028
34	3234.18701	0.879	17.710	0.028
35	3234.23389	0.980	16.329	0.015
36	3234.24829	0.011	16.332	0.015
37	3245.06543	0.293	17.219	0.024
38	3245.07959	0.323	17.265	0.027
39	3245.15088	0.476	17.494	0.028
40	3245.16504	0.507	17.448	0.041
41	3246.16040	0.649	17.526	0.036
42	3246.17456	0.680	17.470	0.035
43	3246.22290	0.784	17.598	0.030
44	3246.23706	0.814	17.742	0.036
45	3247.07837	0.625	17.607	0.054
46	3247.08643	0.642	17.697	0.053

59. RR215817

	Dayval	Phase	Vint	Vinterr
1	1292.40967	0.289	15.321	0.019
2	1317.33997	0.743	15.614	0.025
3	1354.23840	0.977	14.791	0.011
4	1355.23572	0.875	15.227	0.014
5	1359.22473	0.468	15.485	0.022
6	1378.17358	0.536	15.409	0.017
7	1379.17102	0.435	15.497	0.027
8	1403.10669	0.995	14.695	0.021
9	1404.10413	0.894	15.385	0.018
10	1405.10144	0.792	15.569	0.018
11	1411.08545	0.183	14.900	0.012
12	1742.17700	0.400	15.466	0.023
13	1758.13416	0.773	15.544	0.022
14	2035.37415	0.487	15.432	0.020
15	2061.30273	0.840	15.515	0.023
16	2062.29980	0.739	15.629	0.023
17	2063.29663	0.636	15.588	0.025
18	2094.21265	0.483	15.518	0.025
19	2110.16943	0.856	15.470	0.018
20	2113.16162	0.552	15.482	0.025
21	2121.14038	0.739	15.481	0.024
22	3641.03833	0.793	15.485	0.016
23	3641.04712	0.810	15.384	0.017
24	3660.05054	0.982	14.719	0.023
25	3660.05786	0.996	14.621	0.020
26	3660.10718	0.090	14.706	0.029
27	3660.11450	0.104	14.748	0.022
28	3666.05713	0.415	15.391	0.022
29	3666.06421	0.429	15.420	0.012
30	3666.09302	0.483	15.489	0.029
31	3667.04614	0.298	15.244	0.063
32	3667.05347	0.312	15.213	0.029
33	3667.08008	0.362	15.282	0.039
34	3667.08740	0.376	15.387	0.060

60. RR220055

	Dayval	Phase	Vint	Vinterr
1	1292.41150	0.980	15.057	0.017
2	1317.34180	0.079	15.224	0.017
3	1354.24023	0.790	15.912	0.021
4	1355.23755	0.674	15.956	0.021
5	1359.22656	0.210	15.505	0.024
6	1378.17542	0.010	15.016	0.013
7	1379.17285	0.894	15.864	0.027
8	1403.10864	0.115	15.243	0.024
9	1404.10596	0.999	15.050	0.013
10	1405.10327	0.883	15.950	0.026
11	1411.08728	0.189	15.442	0.018
12	1742.17883	0.705	15.873	0.036
13	1758.13599	0.852	15.986	0.029
14	2035.37598	0.630	15.930	0.027
15	2061.30444	0.615	15.903	0.030
16	2062.30176	0.499	15.931	0.028
17	2063.29858	0.382	15.804	0.026
18	2094.21460	0.791	16.002	0.031
19	2110.17139	0.937	15.758	0.023
20	2113.16357	0.590	15.961	0.033
21	2121.14209	0.664	15.968	0.034
22	3481.33228	0.410	15.768	0.014
23	3481.34302	0.431	15.782	0.041
24	3481.38306	0.507	15.858	0.024
25	3481.39185	0.523	15.871	0.024
26	3481.43311	0.601	15.902	0.015
27	3481.44385	0.621	15.904	0.014
28	3503.26978	0.856	15.954	0.021
29	3503.28052	0.876	16.021	0.016
30	3503.31714	0.945	15.452	0.011

31	3503.32861	0.967	15.205	0.014
32	3503.39355	0.090	15.212	0.018
33	3503.40576	0.113	15.256	0.054
34	3517.10303	0.990	15.020	0.019
35	3517.11133	0.006	15.011	0.014
36	3517.12036	0.023	15.065	0.014
37	3517.19141	0.158	15.378	0.016
38	3517.19580	0.166	15.417	0.017
39	3517.25635	0.280	15.597	0.012
40	3517.26807	0.302	15.637	0.012
41	3517.33252	0.424	15.782	0.013
42	3517.34326	0.444	15.820	0.013
43	3517.41235	0.575	15.892	0.013
44	3517.42334	0.596	15.890	0.016
45	3563.20288	0.085	15.223	0.021
46	3563.21313	0.105	15.269	0.020
47	3563.22339	0.124	15.317	0.043
48	3563.25049	0.175	15.408	0.018
49	3563.25928	0.191	15.477	0.025
50	3563.26978	0.211	15.423	0.016

61. RR220245

	Dayval	Phase	Vint	Vinterr
1	1292.41284	0.138	13.885	0.008
2	1317.34314	0.448	14.027	0.009
3	1354.24158	0.632	13.913	0.006
4	1355.23889	0.205	13.811	0.006
5	1359.22791	0.495	14.057	0.009
6	1378.17676	0.377	13.951	0.007
7	1379.17407	0.950	13.841	0.007
8	1403.10986	0.697	13.816	0.007
9	1404.10730	0.270	13.844	0.007
10	1405.10461	0.843	13.840	0.006
11	1411.08862	0.280	13.864	0.007
12	1414.08069	0.998	13.981	0.008
13	1742.18005	0.375	13.971	0.010
14	1758.13721	0.540	14.016	0.008
15	2035.37732	0.719	13.866	0.008
16	2061.30566	0.605	13.974	0.008
17	2062.30298	0.177	13.843	0.008
18	2063.29980	0.748	13.861	0.008
19	2094.21582	0.501	14.068	0.010
20	2113.16479	0.384	13.983	0.009
21	2121.14355	0.966	14.030	0.010
22	3478.28223	0.753	13.840	0.008
23	3478.29419	0.797	13.879	0.008
24	3478.33350	0.937	14.047	0.008
25	3478.34521	0.980	14.072	0.008
26	3478.38452	0.120	13.933	0.008
27	3478.39624	0.162	13.899	0.008
28	3478.43506	0.302	13.904	0.008
29	3478.44702	0.344	13.937	0.008

62. RR221023

	Dayval	Phase	Vint	Vinterr
1	1292.41809	0.768	16.792	0.060
2	1317.34851	0.695	16.765	0.059
3	1354.24683	0.190	16.328	0.028
4	1355.24414	0.987	16.474	0.037
5	1359.23315	0.175	16.271	0.042
6	1378.18201	0.323	16.454	0.041
7	1379.17944	0.121	16.153	0.049
8	1403.11523	0.255	16.402	0.041
9	1404.11255	0.053	16.356	0.037
10	1405.10986	0.850	16.709	0.043
11	1411.09399	0.634	16.739	0.043
12	1414.08594	0.026	15.919	0.029
13	1742.18542	0.295	16.505	0.048
14	1758.14258	0.052	15.934	0.032
15	2035.38257	0.667	16.794	0.060
16	2061.31104	0.393	16.592	0.054
17	2062.30835	0.190	16.313	0.041
18	2063.30518	0.986	16.268	0.044
19	2094.22119	0.700	16.781	0.066
20	2121.14868	0.226	16.471	0.057
21	3641.05664	0.258	16.562	0.020
22	3641.06567	0.275	16.541	0.020
23	3660.06665	0.516	16.794	0.023
24	3660.07520	0.532	16.773	0.025
25	3660.12354	0.619	16.848	0.039
26	3660.13232	0.634	16.760	0.055
27	3666.07471	0.343	16.700	0.025
28	3666.08325	0.359	16.676	0.027
29	3666.10938	0.406	16.704	0.028
30	3667.06274	0.124	16.413	0.032
31	3667.07153	0.140	16.414	0.027
32	3673.10205	0.007	16.145	0.064
33	3673.11060	0.023	16.165	0.060
34	3681.06152	0.351	16.630	0.027
35	3681.07031	0.367	16.670	0.025
36	3681.07935	0.383	16.668	0.024
37	3681.08813	0.399	16.713	0.029
38	3683.06567	0.963	16.591	0.055
39	3683.07446	0.979	16.424	0.030

63. RR222036

	Dayval	Phase	Vint	Vinterr
1	1023.16327	0.324	15.075	0.012
2	1292.43213	0.277	15.070	0.018
3	1317.36292	0.788	15.078	0.017
4	1354.25940	0.381	15.098	0.013
5	1355.25671	0.721	15.095	0.013
6	1359.24536	0.083	15.269	0.018
7	1378.19214	0.549	15.306	0.016
8	1379.18945	0.890	15.148	0.015
9	1401.12769	0.377	15.134	0.015
10	1403.12231	0.058	15.307	0.016
11	1404.11963	0.399	15.181	0.015
12	1405.11682	0.739	15.084	0.013
13	1411.10010	0.782	15.059	0.013
14	1414.09167	0.803	15.064	0.015
15	1742.19556	0.837	15.114	0.018
16	1758.15088	0.283	15.077	0.017
17	2035.39697	0.958	15.297	0.020
18	2061.32495	0.809	15.091	0.017
19	2062.32227	0.149	15.169	0.018
20	2063.31885	0.488	15.355	0.020
21	2094.23267	0.040	15.343	0.022
22	2113.17920	0.507	15.347	0.023
23	2121.15723	0.230	15.101	0.021
24	3488.33154	0.882	15.135	0.012
25	3488.34253	0.908	15.190	0.012
26	3488.41040	0.067	15.280	0.012
27	3488.42114	0.092	15.225	0.012
28	3485.41040	0.026	15.341	0.016
29	3485.44556	0.108	15.216	0.016
30	3485.45630	0.134	15.196	0.021
31	3517.17017	0.564	15.242	0.016
32	3517.18140	0.590	15.250	0.015
33	3517.23901	0.726	15.096	0.013
34	3517.25000	0.751	15.074	0.012
35	3517.31470	0.903	15.220	0.012
36	3517.32568	0.929	15.258	0.012
37	3517.38843	0.076	15.260	0.012
38	3517.39917	0.101	15.219	0.012
39	3517.46094	0.246	15.062	0.014
40	3517.47168	0.271	15.080	0.014

64. RR223619

	Dayval	Phase	Vint	Vinterr
1	1023.17419	0.441	16.778	0.042
2	1292.44312	0.494	16.811	0.058
3	1317.37378	0.237	16.620	0.057
4	1354.27039	0.535	16.737	0.040
5	1355.26758	0.165	16.555	0.040
6	1359.25623	0.683	16.688	0.051
7	1378.20312	0.647	16.726	0.047
8	1379.20044	0.277	16.707	0.046
9	1401.13867	0.130	16.635	0.044
10	1403.13330	0.389	16.727	0.051
11	1404.13049	0.019	16.511	0.040
12	1405.12769	0.649	16.792	0.044
13	1411.11108	0.427	16.747	0.046
14	1412.10815	0.056	16.548	0.045
15	1414.10266	0.316	16.738	0.051
16	1417.09436	0.205	16.744	0.087

17	1742.20654	0.520	16.794	0.064
18	2035.40796	0.685	16.778	0.061
19	2061.33594	0.058	16.559	0.053
20	2062.33325	0.688	16.750	0.056
21	2063.32983	0.316	16.752	0.054
22	2094.24365	0.837	16.709	0.064
23	2113.19019	0.801	16.827	0.069
24	2121.16821	0.839	16.563	0.069
25	3516.40991	0.014	16.538	0.015
26	3516.42310	0.036	16.505	0.016
27	3516.47266	0.117	16.589	0.018
28	3516.48560	0.138	16.730	0.044
29	3540.22534	0.935	16.579	0.041
30	3540.23486	0.950	16.524	0.043
31	3545.12061	0.935	16.554	0.022
32	3545.13013	0.951	16.495	0.021
33	3545.13989	0.966	16.495	0.019
34	3545.14917	0.981	16.492	0.020
35	3545.15845	0.997	16.492	0.020
36	3569.08057	0.092	16.579	0.019
37	3569.09009	0.107	16.592	0.019
38	3569.11353	0.145	16.592	0.020
39	3569.12305	0.161	16.594	0.019
40	3569.14502	0.197	16.666	0.020
41	3569.15430	0.212	16.676	0.020
42	3569.17285	0.242	16.696	0.020
43	3569.18237	0.258	16.704	0.019
44	3569.20068	0.288	16.710	0.020
45	3569.21021	0.303	16.721	0.020
46	3569.22803	0.332	16.729	0.020
47	3569.23730	0.348	16.717	0.021
48	3622.10132	0.741	16.818	0.021
49	3622.11084	0.756	16.855	0.020
50	3622.16479	0.844	16.866	0.022
51	3622.17407	0.860	16.877	0.020
52	3622.18359	0.875	16.777	0.028
53	3622.22632	0.945	16.551	0.018
54	3622.23560	0.960	16.491	0.017
55	3622.24512	0.976	16.480	0.018
56	3622.25391	0.990	16.440	0.017

65. RR224735

	Dayval	Phase	Vint	Vinterr
1	1023.18201	0.233	13.424	0.005
2	1292.45093	0.993	13.626	0.007
3	1317.38159	0.708	13.451	0.006
4	1354.27820	0.962	13.607	0.005
5	1355.27551	0.591	13.605	0.005
6	1359.26404	0.105	13.570	0.006
7	1378.21094	0.046	13.664	0.006
8	1379.20825	0.675	13.474	0.005
9	1401.14648	0.501	13.658	0.006
10	1403.14111	0.759	13.406	0.005
11	1404.13831	0.388	13.509	0.005
12	1405.13562	0.016	13.679	0.006
13	1411.11890	0.788	13.400	0.005
14	1412.11597	0.416	13.512	0.007
15	1414.11047	0.673	13.487	0.006
16	1417.10217	0.559	13.679	0.009
17	1742.21436	0.515	13.666	0.007
18	1758.16943	0.571	13.608	0.006
19	2035.41577	0.359	13.476	0.006
20	2061.34375	0.702	13.463	0.006
21	2062.34106	0.331	13.447	0.006
22	2094.25146	0.443	13.616	0.007
23	2113.19800	0.384	13.535	0.007
24	2147.10352	0.754	13.421	0.007
25	3480.30835	0.922	13.556	0.011
26	3480.31421	0.937	13.613	0.016
27	3480.36035	0.059	13.627	0.010
28	3480.36621	0.074	13.601	0.010
29	3480.41211	0.195	13.433	0.010
30	3480.41821	0.211	13.420	0.010
31	3480.47241	0.354	13.454	0.012
32	3480.47827	0.369	13.445	0.015

66. RR230520

	Dayval	Phase	Vint	Vinterr
1	1023.19440	0.297	17.089	0.052
2	1055.10547	0.396	17.296	0.051
3	1354.29053	0.236	17.009	0.043
4	1355.28784	0.145	16.773	0.040
5	1359.27649	0.782	17.422	0.096
6	1378.22327	0.059	16.508	0.033
7	1379.22058	0.969	16.500	0.042
8	1401.15881	0.973	16.475	0.037
9	1403.15344	0.792	17.497	0.070
10	1404.15076	0.702	17.420	0.078
11	1411.13123	0.067	16.497	0.037
12	1412.12830	0.976	16.420	0.039
13	1414.12292	0.795	17.452	0.087
14	1417.11450	0.523	17.671	0.162
15	2035.42822	0.388	17.240	0.075
16	2061.35620	0.031	16.374	0.041
17	2062.35327	0.941	17.211	0.068
18	2094.26367	0.038	16.445	0.046
19	2113.21045	0.315	17.090	0.075
20	2121.18799	0.589	17.493	0.124
21	2147.11572	0.232	17.022	0.097
22	3174.15967	0.679	17.394	0.031
23	3174.17480	0.709	17.392	0.031
24	3174.22119	0.797	17.401	0.029
25	3174.23535	0.825	17.505	0.030
26	3174.31836	0.983	16.343	0.020
27	3174.33276	0.011	16.337	0.019
28	3174.40259	0.145	16.746	0.024
29	3174.42969	0.197	16.868	0.025
30	3174.46411	0.263	17.001	0.028
31	3174.47852	0.290	17.127	0.030
32	3180.13379	0.118	16.718	0.022
33	3180.14819	0.146	16.795	0.020
34	3180.22754	0.297	17.112	0.023
35	3180.29053	0.418	17.292	0.027
36	3180.30493	0.446	17.298	0.027
37	3180.35522	0.542	17.349	0.027
38	3180.36938	0.569	17.433	0.028
39	3180.42285	0.672	17.410	0.031
40	3180.43726	0.699	17.460	0.031
41	3503.36011	0.989	16.373	0.027
42	3503.37427	0.016	16.281	0.033

67. RR232138

	Dayval	Phase	Vint	Vinterr
1	1023.20575	0.170	16.356	0.029
2	1055.11682	0.083	16.469	0.033
3	1317.40417	0.134	16.388	0.041
4	1354.30188	0.691	16.335	0.031
5	1355.29919	0.220	16.300	0.032
6	1359.28784	0.333	16.412	0.048
7	1378.23462	0.374	16.475	0.033
8	1379.23193	0.903	16.542	0.038
9	1401.17017	0.529	16.614	0.039
10	1403.16479	0.587	16.434	0.037
11	1405.15906	0.643	16.411	0.035
12	1411.14258	0.815	16.371	0.035
13	1412.13965	0.343	16.391	0.043
14	1413.13672	0.871	16.495	0.034
15	1417.12585	0.986	16.719	0.082
16	1435.07605	0.500	16.630	0.041
17	1742.23804	0.334	16.346	0.047
18	1758.19324	0.790	16.337	0.037
19	2035.43958	0.770	16.293	0.036
20	2061.36743	0.513	16.600	0.045
21	2062.36475	0.041	16.542	0.047
22	2094.27515	0.953	16.517	0.053
23	2096.26880	0.008	16.553	0.055
24	2110.22998	0.407	16.421	0.056
25	2113.22192	0.993	16.559	0.053
26	2121.19922	0.221	16.363	0.054
27	2147.12720	0.963	16.614	0.063
28	3540.10059	0.959	16.510	0.024
29	3540.11035	0.984	16.546	0.023
30	3540.17529	0.149	16.380	0.019
31	3540.18506	0.173	16.279	0.021

32	3540.26782	0.384	16.242	0.032
33	3540.27734	0.407	16.474	0.028
34	3545.09814	0.631	16.366	0.023
35	3545.10767	0.655	16.384	0.021
36	3545.17261	0.820	16.273	0.021
37	3545.18213	0.844	16.307	0.020
38	3545.23828	0.986	16.595	0.019
39	3545.24756	0.010	16.587	0.021
40	3569.27148	0.924	16.439	0.018
41	3569.28101	0.949	16.473	0.019
42	3569.30298	0.004	16.528	0.019
43	3569.31226	0.028	16.507	0.020
44	3569.33105	0.076	16.443	0.019
45	3569.34058	0.100	16.381	0.019
46	3569.35864	0.146	16.349	0.018
47	3569.36816	0.169	16.332	0.019
48	3569.38159	0.204	16.261	0.017
49	3569.39087	0.227	16.241	0.018
50	3569.40039	0.251	16.249	0.018
51	3569.41602	0.291	16.289	0.019

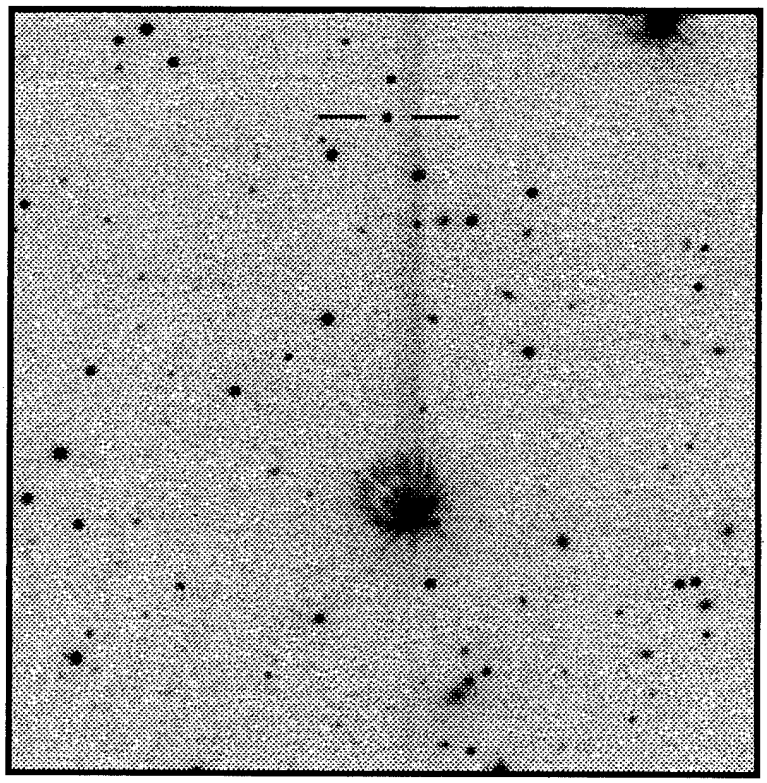
68. RR233207

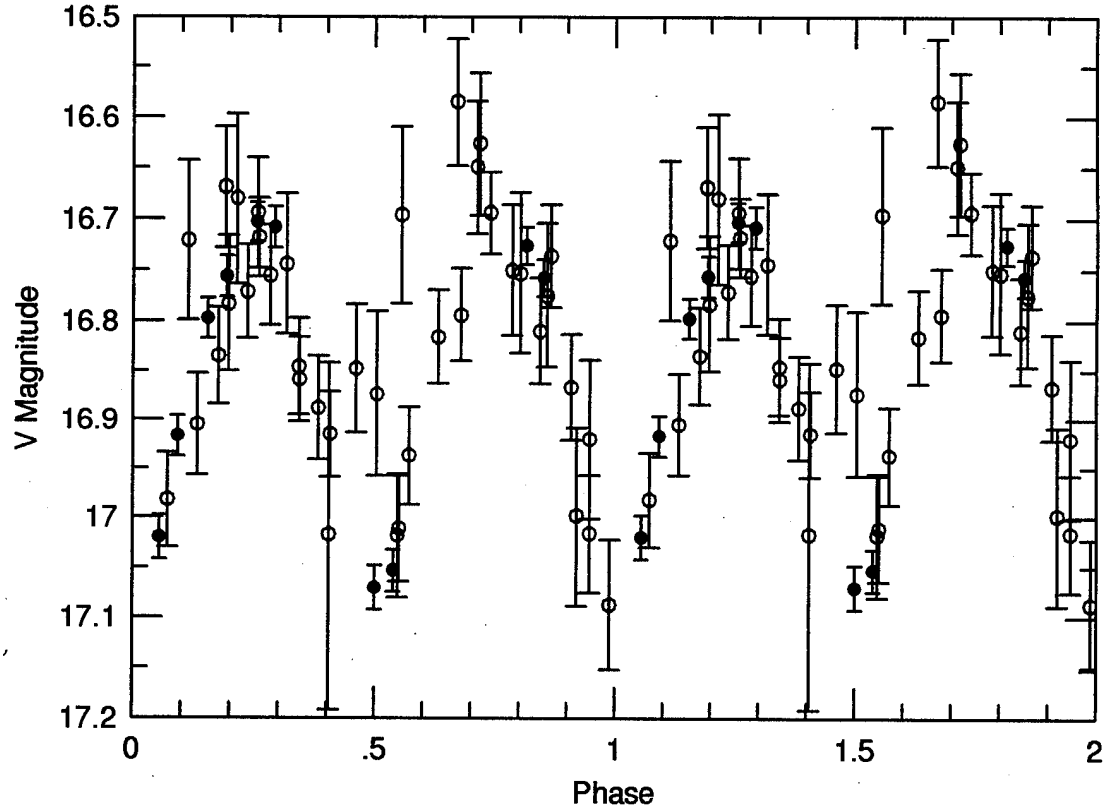
	Dayval	Phase	Vint	Vinterr
1	1023.21289	0.542	17.509	0.068
2	1055.12390	0.599	17.531	0.065
3	1317.41150	0.157	17.069	0.066
4	1354.30920	0.412	17.458	0.059
5	1355.30652	0.851	17.628	0.084
6	1359.29517	0.608	17.614	0.085
7	1377.24402	0.513	17.549	0.069
8	1378.24194	0.954	16.841	0.042
9	1379.23926	0.393	17.410	0.072
10	1401.17749	0.056	16.861	0.049
11	1403.17212	0.935	17.027	0.053
12	1404.16943	0.374	17.337	0.076
13	1405.16638	0.813	17.667	0.084
14	1410.15234	0.010	16.770	0.046
15	1411.14990	0.449	17.431	0.067
16	1412.14697	0.888	17.469	0.094
17	1413.14404	0.328	17.297	0.063
18	1414.14148	0.767	17.629	0.092
19	1416.13574	0.645	17.463	0.114
20	1417.13318	0.085	16.922	0.102
21	1418.13013	0.524	17.543	0.254
22	1435.08337	0.992	16.744	0.043
23	1742.24536	0.318	17.297	0.080
24	1758.20044	0.346	17.351	0.078
25	2035.44678	0.494	17.402	0.084
26	2061.37476	0.916	17.263	0.077
27	2062.37207	0.355	17.227	0.082
28	2094.28247	0.411	17.476	0.100
29	2096.27612	0.289	17.294	0.084
30	2110.23730	0.439	17.352	0.106
31	2113.22900	0.757	17.658	0.116
32	2121.20654	0.271	17.212	0.106
33	2123.20093	0.149	17.083	0.073
34	2124.19800	0.588	17.493	0.119
35	2125.19531	0.028	16.770	0.084
36	2147.13452	0.692	17.474	0.167
37	2500.16821	0.224	17.162	0.109
38	3174.28735	0.177	17.114	0.021
39	3174.30151	0.198	17.168	0.021
40	3174.37012	0.297	17.304	0.022
41	3174.38501	0.318	17.303	0.023
42	3174.44604	0.406	17.437	0.027
43	3174.49463	0.476	17.460	0.053
44	3175.23169	0.540	17.520	0.028
45	3157.24707	0.583	17.462	0.028
46	3175.29736	0.635	17.501	0.028
47	3175.31177	0.656	17.518	0.031
48	3180.16553	0.661	17.540	0.033
49	3180.17993	0.682	17.530	0.029
50	3180.24316	0.773	17.636	0.027
51	3180.32397	0.890	17.541	0.028
52	3180.33838	0.910	17.387	0.027
53	3180.39185	0.988	16.741	0.018
54	3180.40625	0.009	16.719	0.017
55	3180.45435	0.078	16.846	0.021
56	3180.46851	0.098	16.941	0.024
57	3180.48291	0.119	16.981	0.023
58	3487.34204	0.007	16.688	0.019
59	3487.35620	0.028	16.743	0.017
60	3487.40723	0.101	16.918	0.018
61	3487.42139	0.122	16.947	0.019

69. RR235226

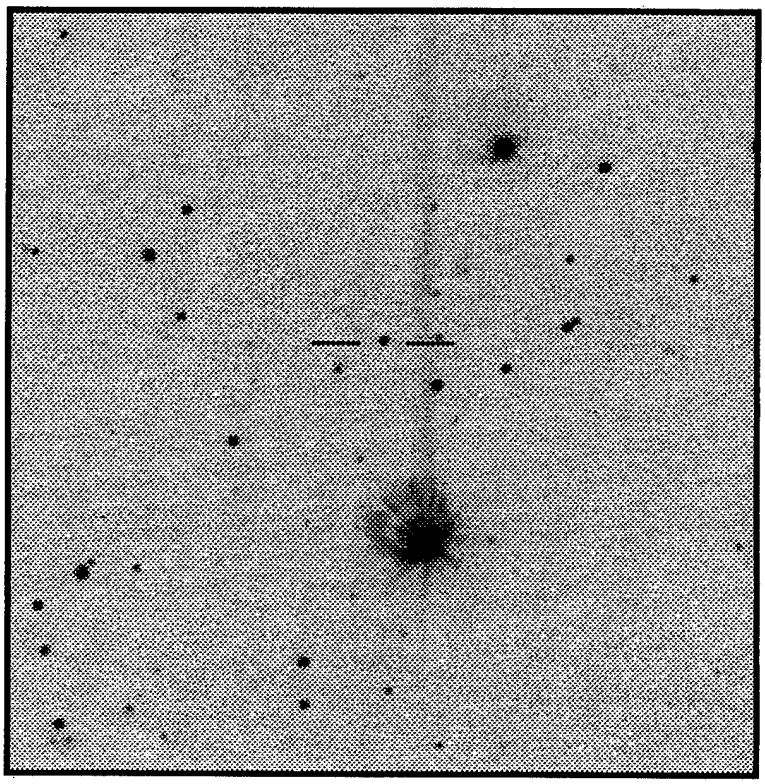
	Dayval	Phase	Vint	Vinterr
1	1023.22705	0.316	17.569	0.065
2	1055.13806	0.476	17.699	0.077
3	1317.42566	0.641	17.810	0.104
4	1354.32336	0.265	17.493	0.061
5	1355.32068	0.958	17.298	0.058
6	1377.25818	0.191	17.436	0.061
7	1378.25610	0.885	17.667	0.085
8	1379.25342	0.578	17.738	0.099
9	1401.19165	0.812	17.834	0.110
10	1403.18628	0.198	17.392	0.075
11	1404.18359	0.890	17.645	0.090
12	1405.18054	0.582	17.629	0.084
13	1410.16650	0.045	17.239	0.052
14	1411.16406	0.738	17.735	0.084
15	1412.16113	0.430	17.710	0.135
16	1413.15808	0.122	17.345	0.056
17	1414.15564	0.815	17.921	0.114
18	1416.14978	0.200	17.365	0.103
19	1417.14734	0.893	17.684	0.176
20	1418.14429	0.585	17.926	0.290
21	1432.10571	0.281	17.592	0.085
22	1435.09753	0.359	17.623	0.077
23	1442.07812	0.206	17.422	0.077
24	1742.25952	0.686	17.710	0.098
25	1758.21460	0.766	17.874	0.101
26	1768.18652	0.690	17.763	0.112
27	2035.46094	0.319	17.583	0.094
28	2061.38892	0.325	17.631	0.092
29	2062.38623	0.018	17.147	0.075
30	2063.38232	0.709	17.908	0.096
31	2094.29590	0.176	17.412	0.092
32	2096.29028	0.561	17.768	0.132
33	2110.25122	0.256	17.526	0.112
34	2113.24292	0.334	17.578	0.114
35	2121.22070	0.874	17.844	0.152
36	2123.21509	0.259	17.479	0.111
37	2124.21216	0.951	17.216	0.110
38	2125.20947	0.644	17.804	0.145
39	2170.08496	0.809	17.966	0.143
40	2500.18237	0.063	17.224	0.116
41	3232.19482	0.463	17.897	0.039
42	3232.21021	0.489	17.696	0.043
43	3232.23462	0.531	17.678	0.042
44	3232.24927	0.556	17.788	0.040
45	3245.10107	0.368	17.629	0.032
46	3245.11597	0.393	17.691	0.032
47	3245.17920	0.501	17.700	0.043
48	3245.19336	0.525	17.794	0.066
49	3246.18994	0.216	17.471	0.030
50	3246.20410	0.240	17.490	0.027
51	3246.25073	0.320	17.588	0.031
52	3246.26514	0.344	17.537	0.029
53	3247.10278	0.765	17.859	0.051
54	3247.11060	0.779	17.810	0.057
55	3273.05127	0.807	17.606	0.099
56	3273.06616	0.832	17.881	0.042
57	3273.15356	0.980	17.131	0.060
58	3273.18384	0.031	17.199	0.030
59	3273.23096	0.111	17.314	0.038
60	3273.24512	0.136	17.283	0.054
61	3485.36694	0.157	17.381	0.046
62	3485.38135	0.181	17.459	0.043
63	3545.26953	0.826	17.882	0.037
64	3545.28027	0.844	17.794	0.035
65	3545.37231	0.001	17.101	0.027
66	3545.38330	0.019	17.183	0.025
67	3545.45752	0.145	17.371	0.030
68	3545.46826	0.163	17.423	0.028

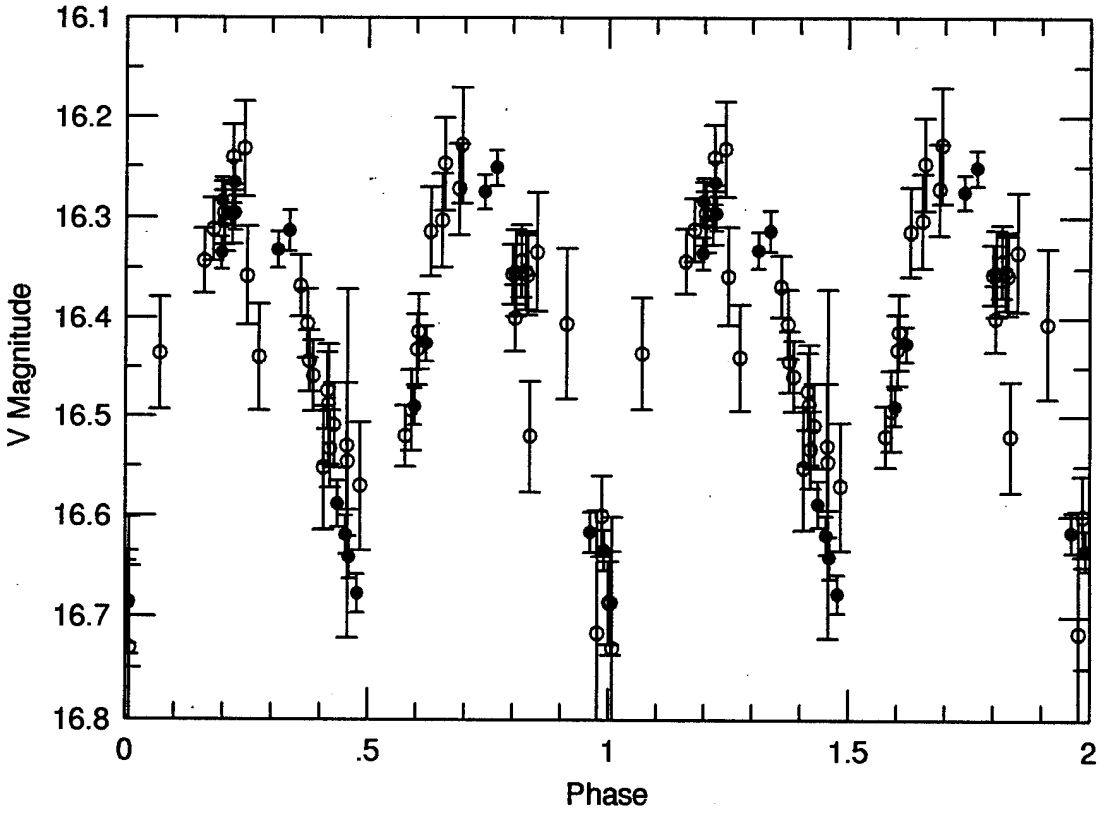
RA : 00 21 01.3
Dec: 28 05 18.0
<V> = 16.837
<B-V> = 0.60
P = 0.276682 days
Epoch = 3539.373
Type: W UMa





RA : 01 13 58.1
Dec: 28 02 47.1
<V> = 16.415
<B-V> = 0.47
P = 0.383472 days
Epoch = 3539.565
Type: W UMa





RA : 01 26 59.2

Dec: 28 03 54.3

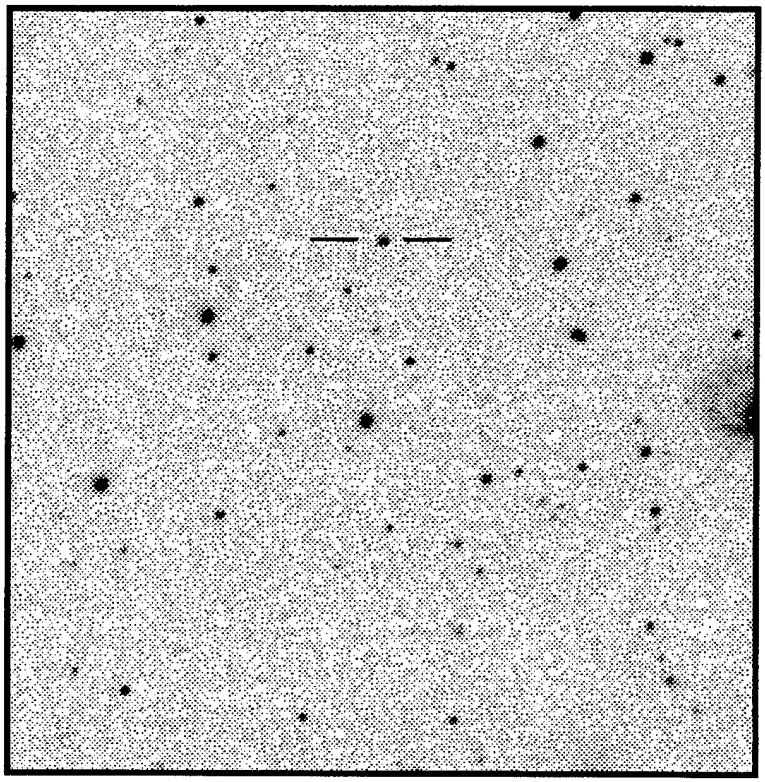
<V> = 16.580

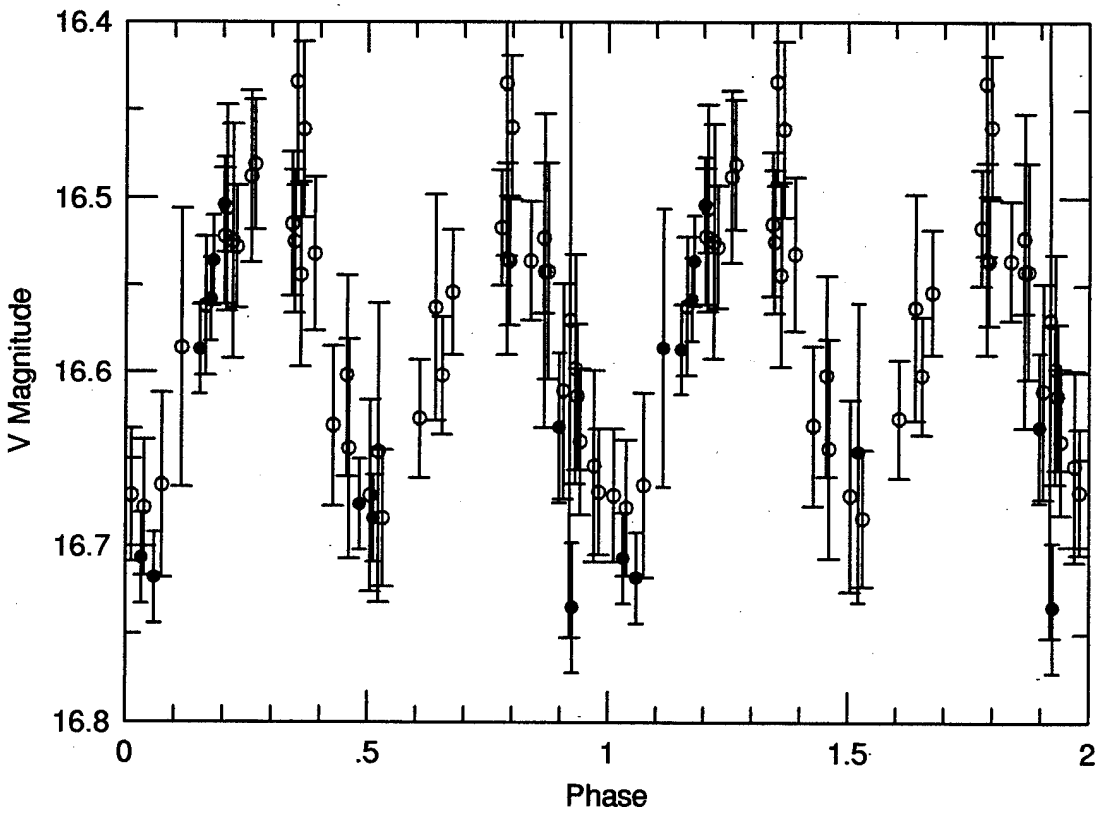
<B-V> = 0.80

P = 0.349120 days

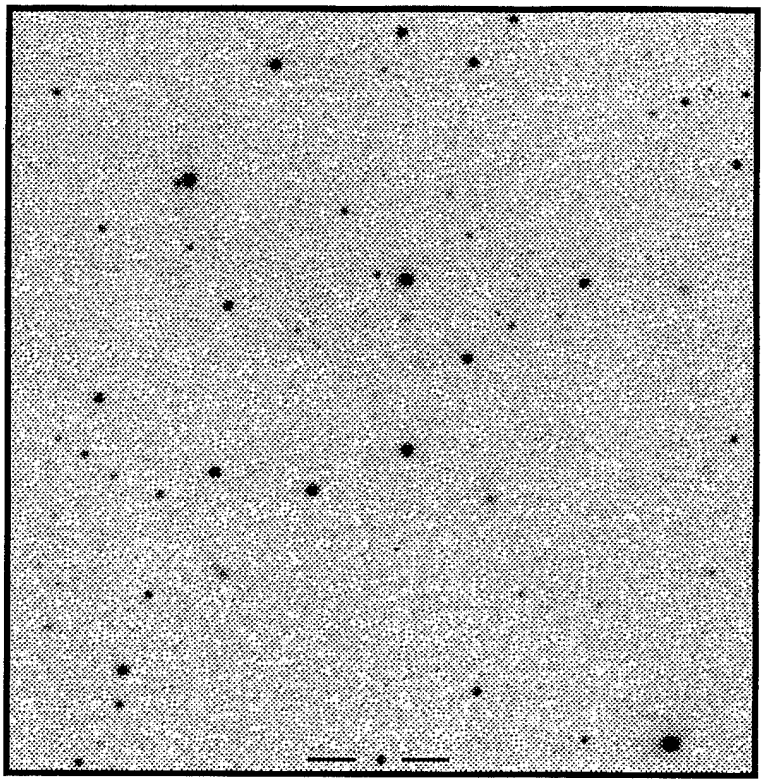
Epoch = 3546.52

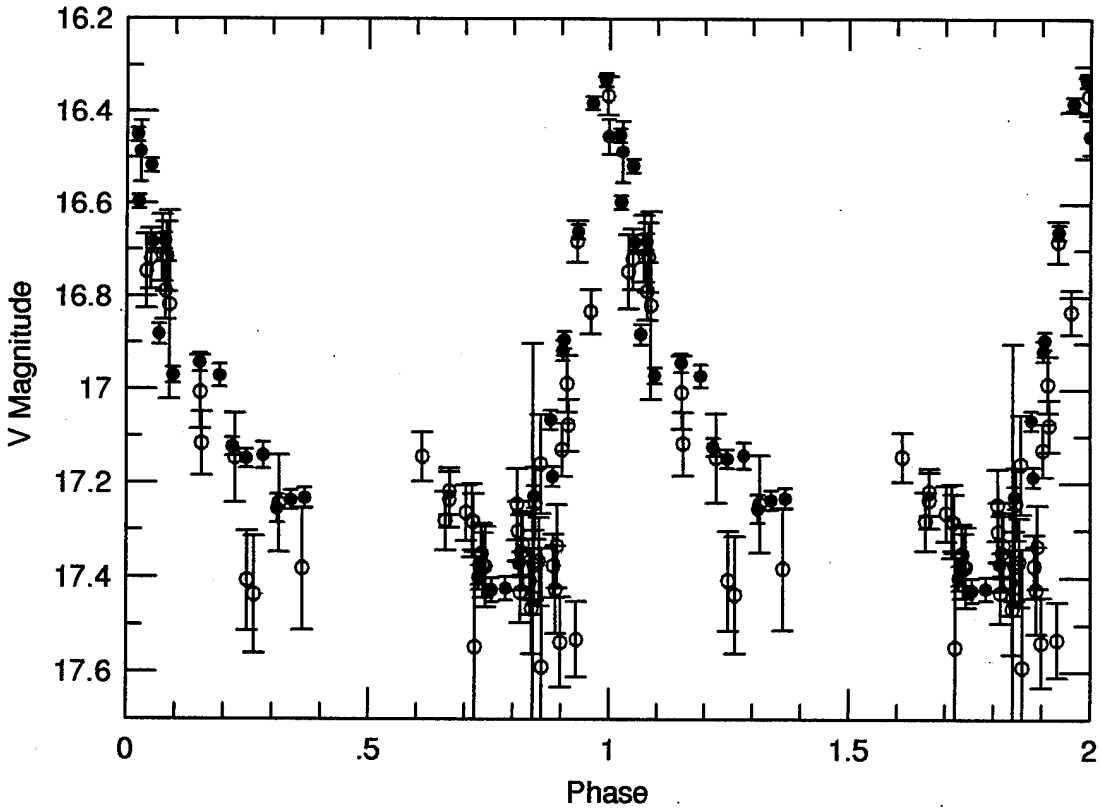
Type: W UMa



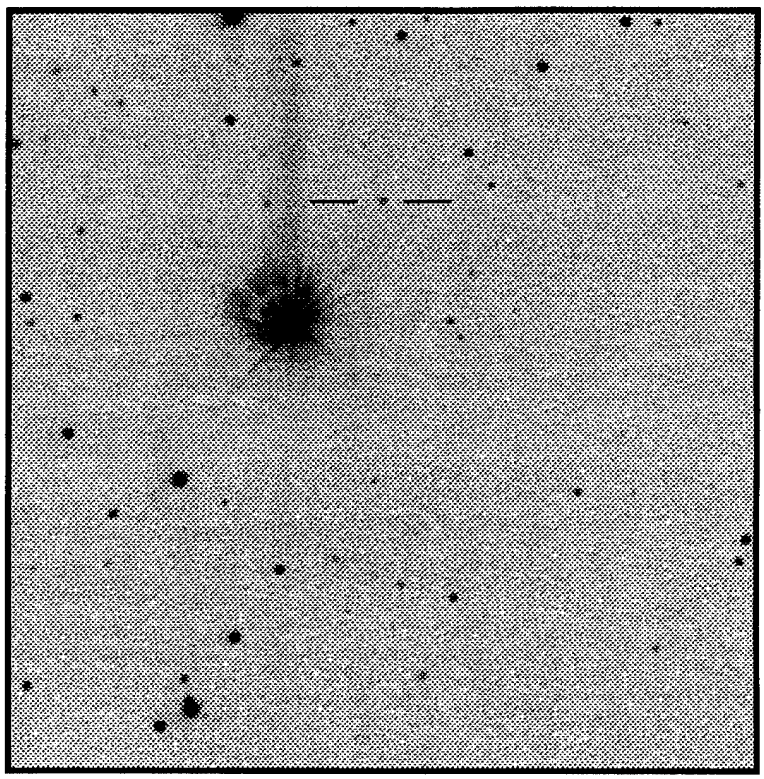


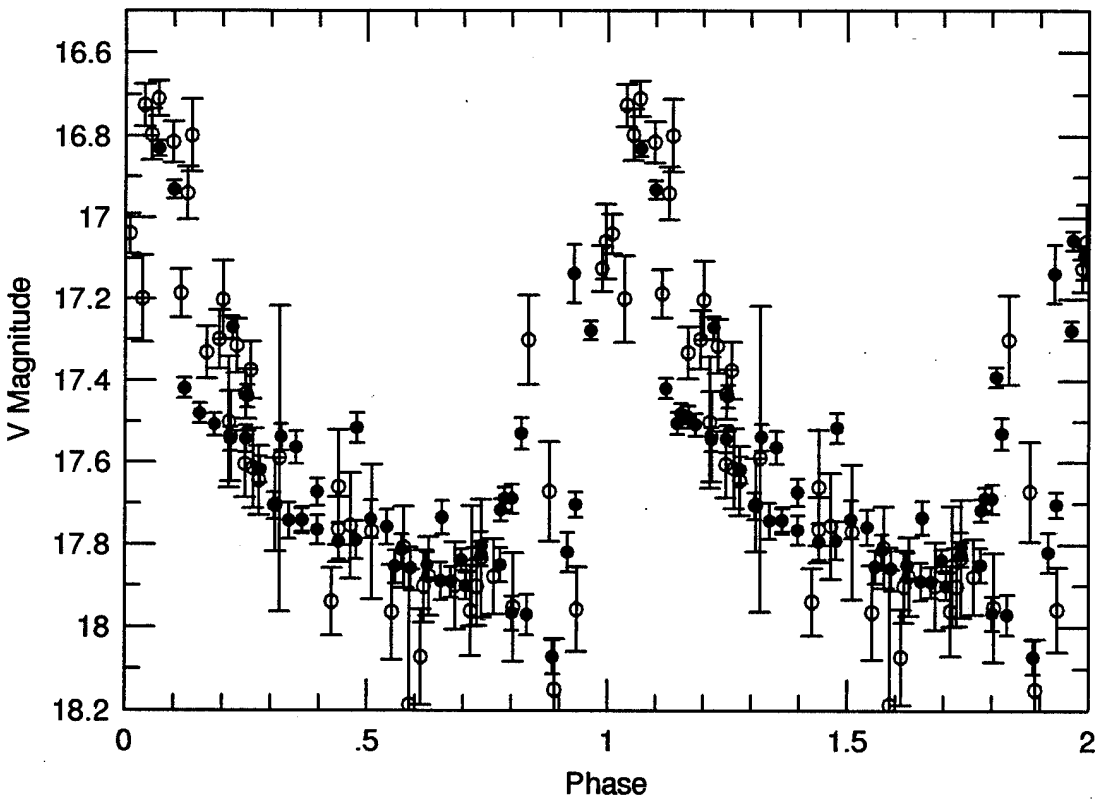
RA : 01 58 55.9
Dec: 27 58 09.5
<V> = 17.081
<B-V> = 0.20
P = 0.497854 days
Epoch = 3641.220
Type: RRab



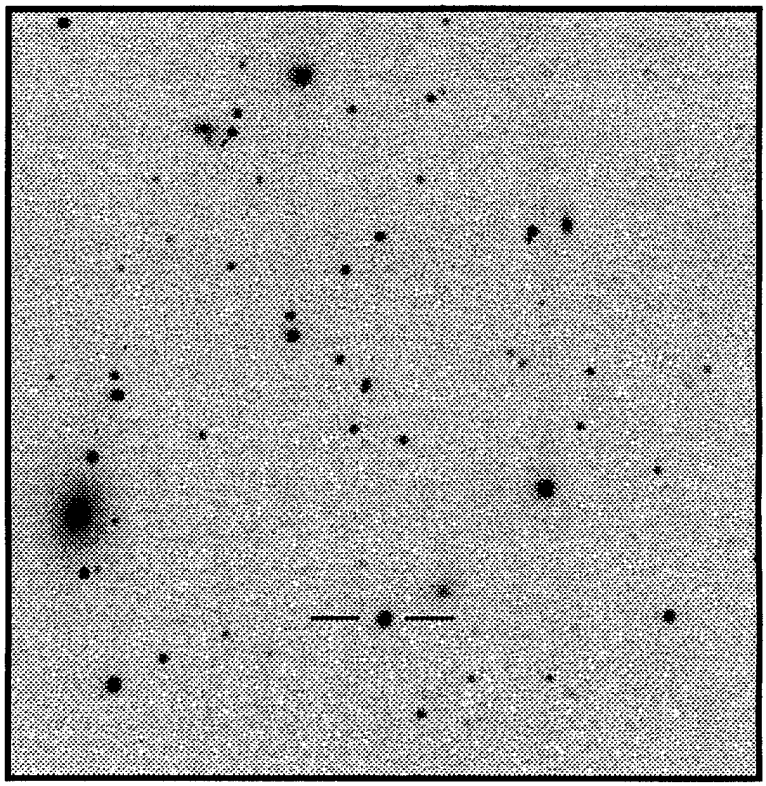


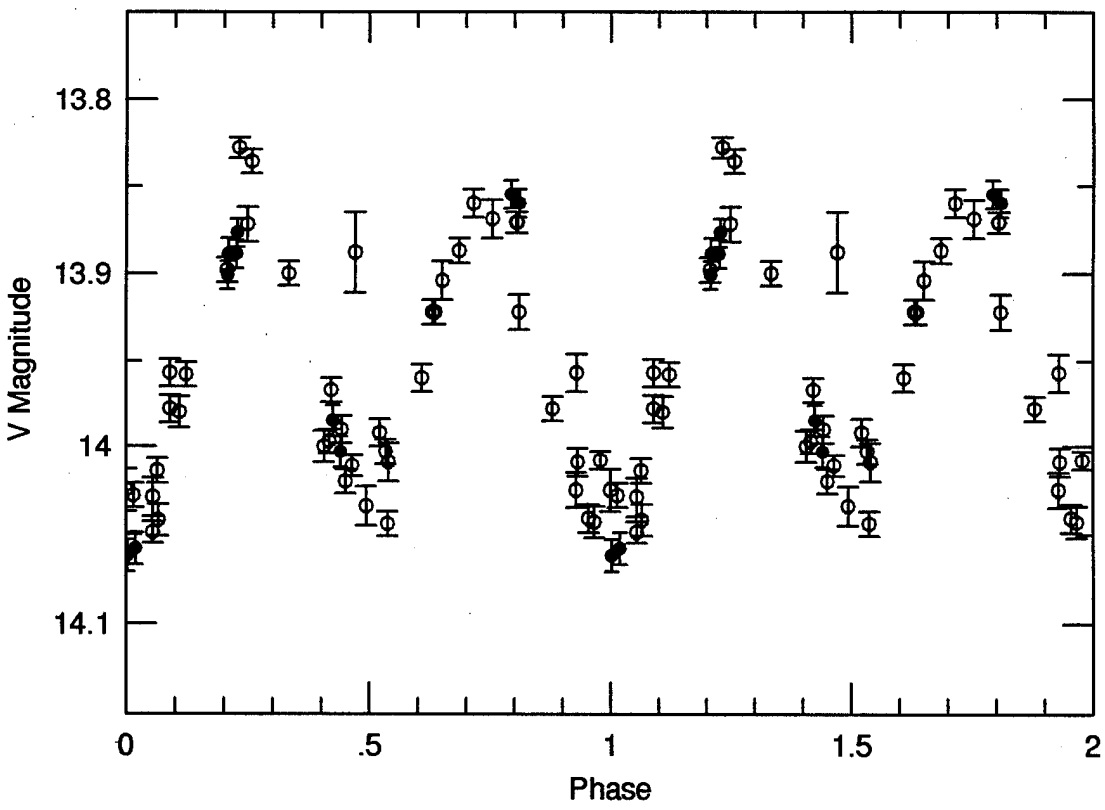
RA : 02 01 50.4
Dec: 28 04 22.6
<V> = 17.517
<B-V> = 0.40
P = 0.461291 days
Epoch = 3559.380
Type: RRab B



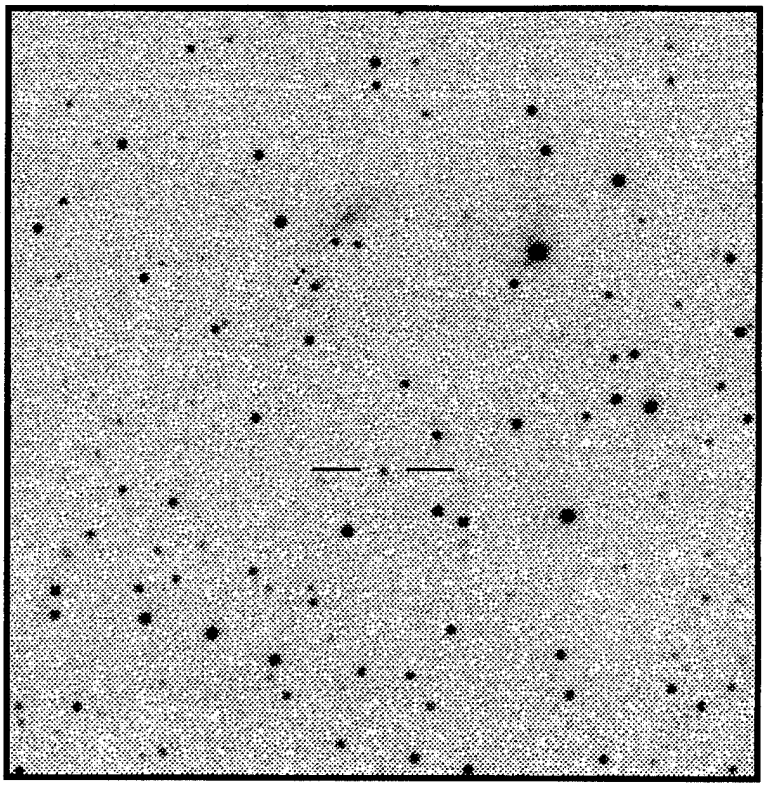


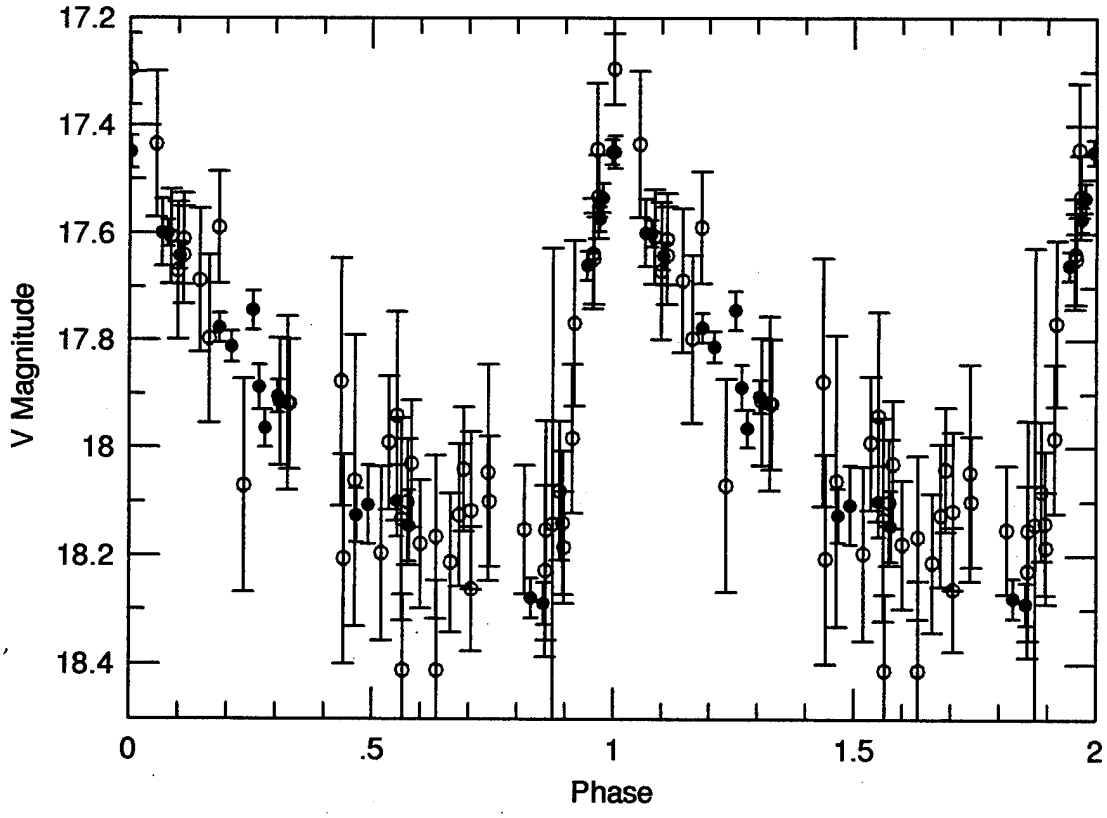
RA : 02 31 40.3
Dec: 27 59 47.3
<V> = 13.947
<B-V> = 0.78
P = 0.265461 days
Epoch = 3539.429
Type: W UMa



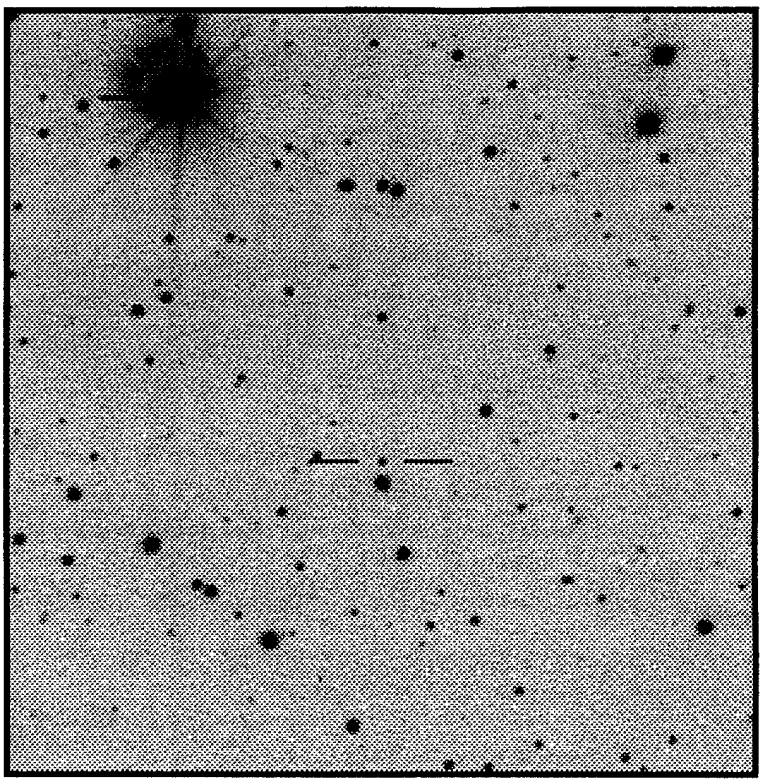


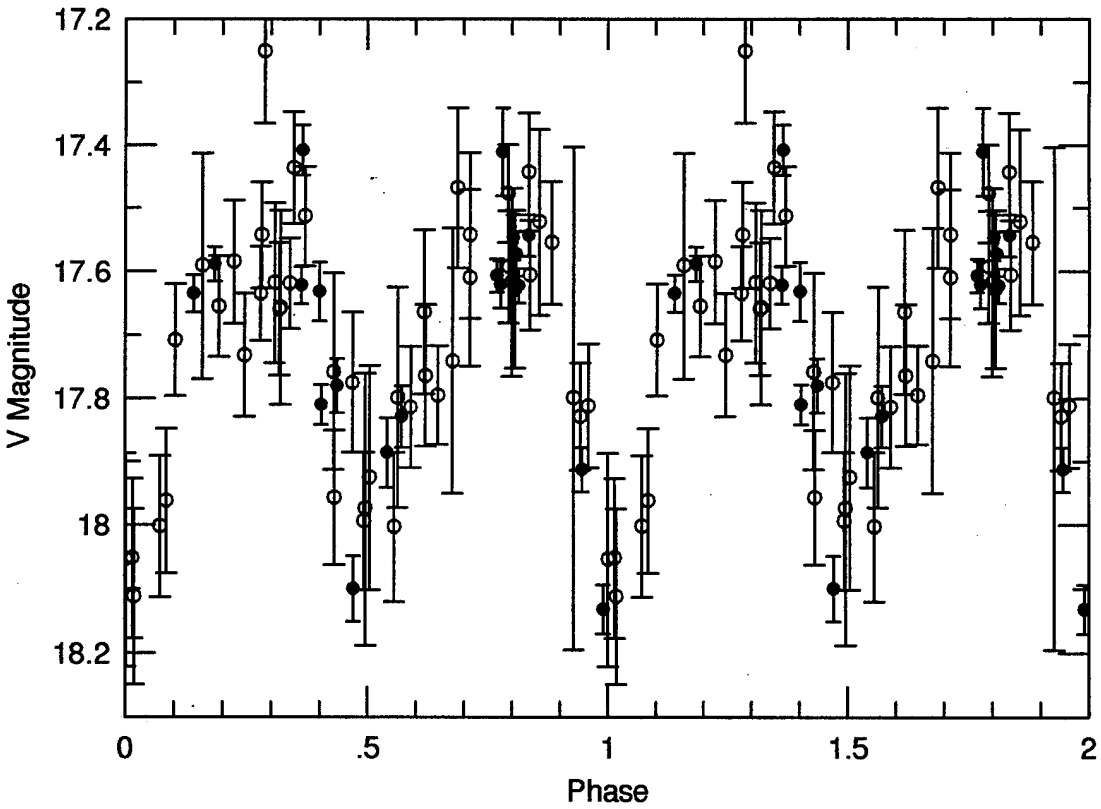
RA : 03 46 21.7
Dec: 28 01 24.7
<V> = 17.905
<B-V> = 0.45
P = 0.561891 days
Epoch = 3685.125
Type: RRab





RA : 04 02 57.9
Dec: 28 01 30.5
<V> = 17.711
<B-V> = 0.60
P = 0.319400 days
Epoch = 3546.455
Type: W UMa





RA : 05 57 22.1

Dec: 28 02 31.0

<V> = 12.739

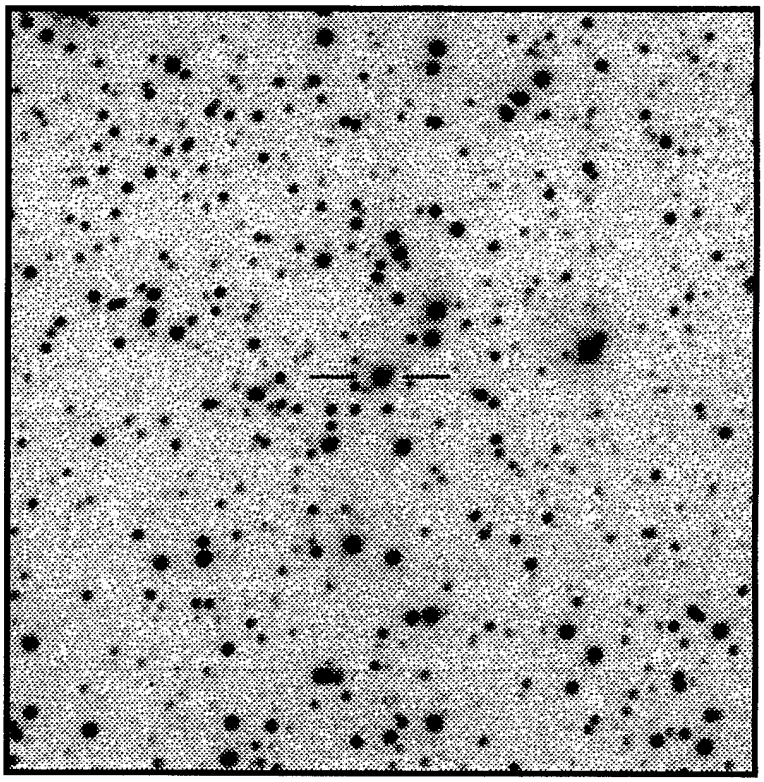
<B-V> = 0.80

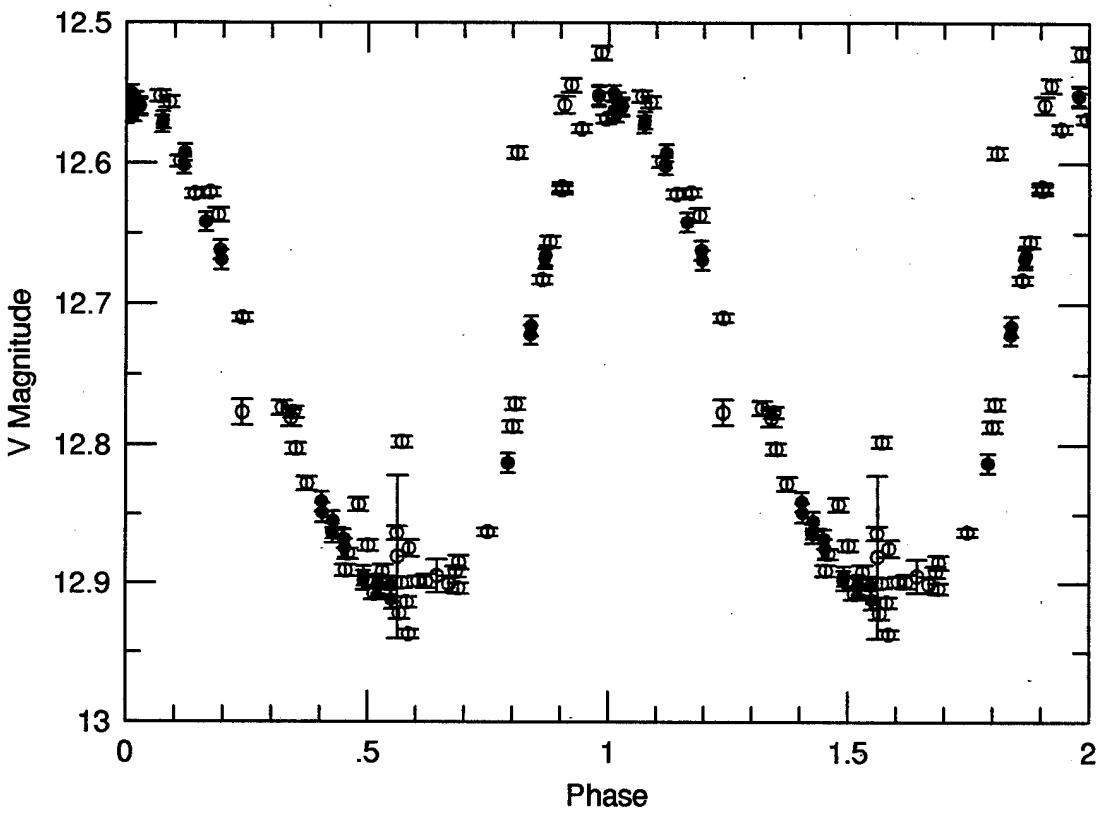
P = 1.79325 days

Epoch = 3299.884

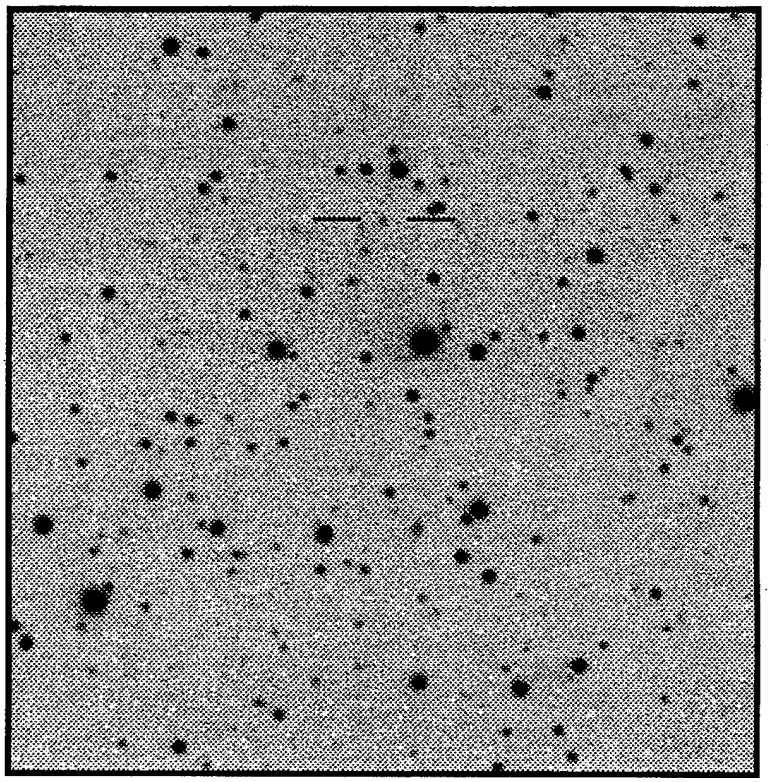
Type: Cepheid

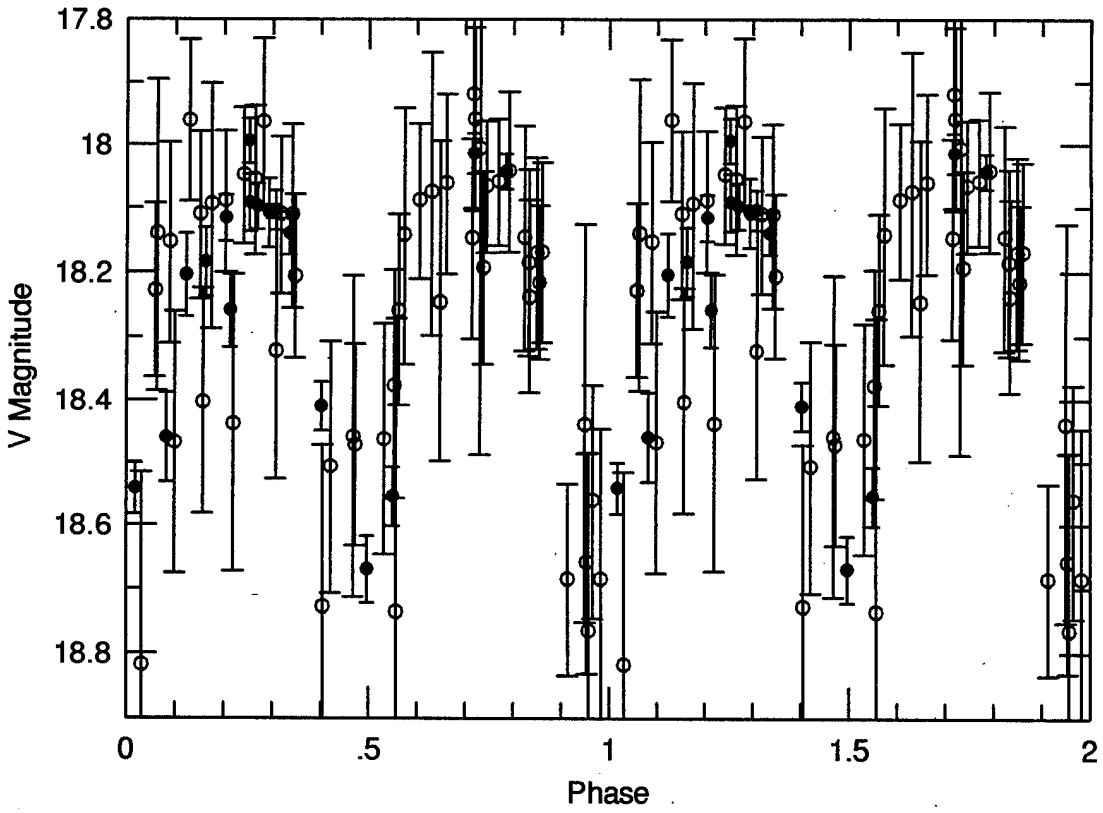
CN Tau





RA : 06 49 46.1
Dec: 28 04 59.5
<V> = 18.267
<B-V> = 0.75
P = 0.269392 days
Epoch = 3622.235
Type: W UMa





RA : 07 53 50.3

Dec: 28 01 58.2

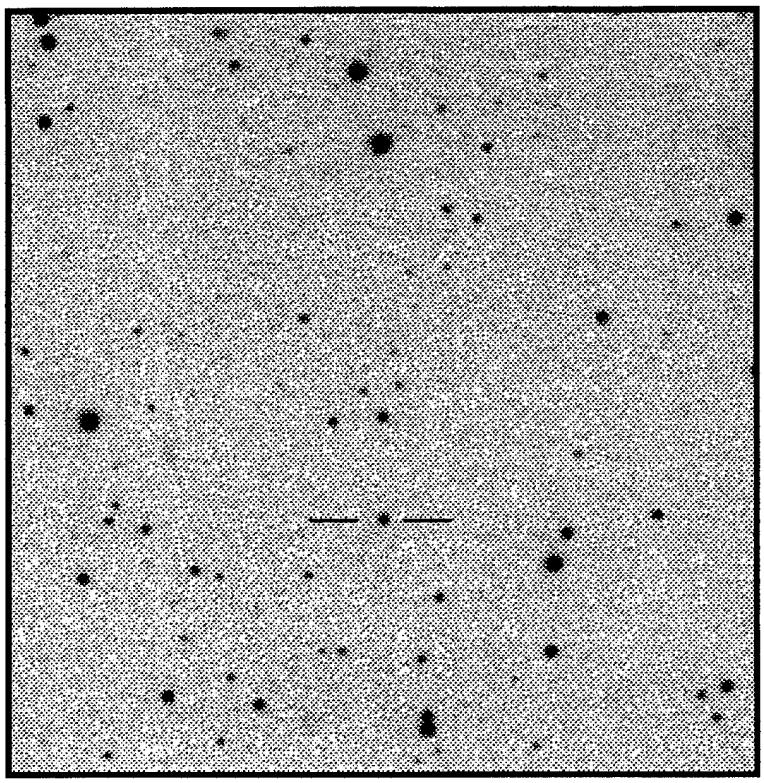
<V> = 16.085

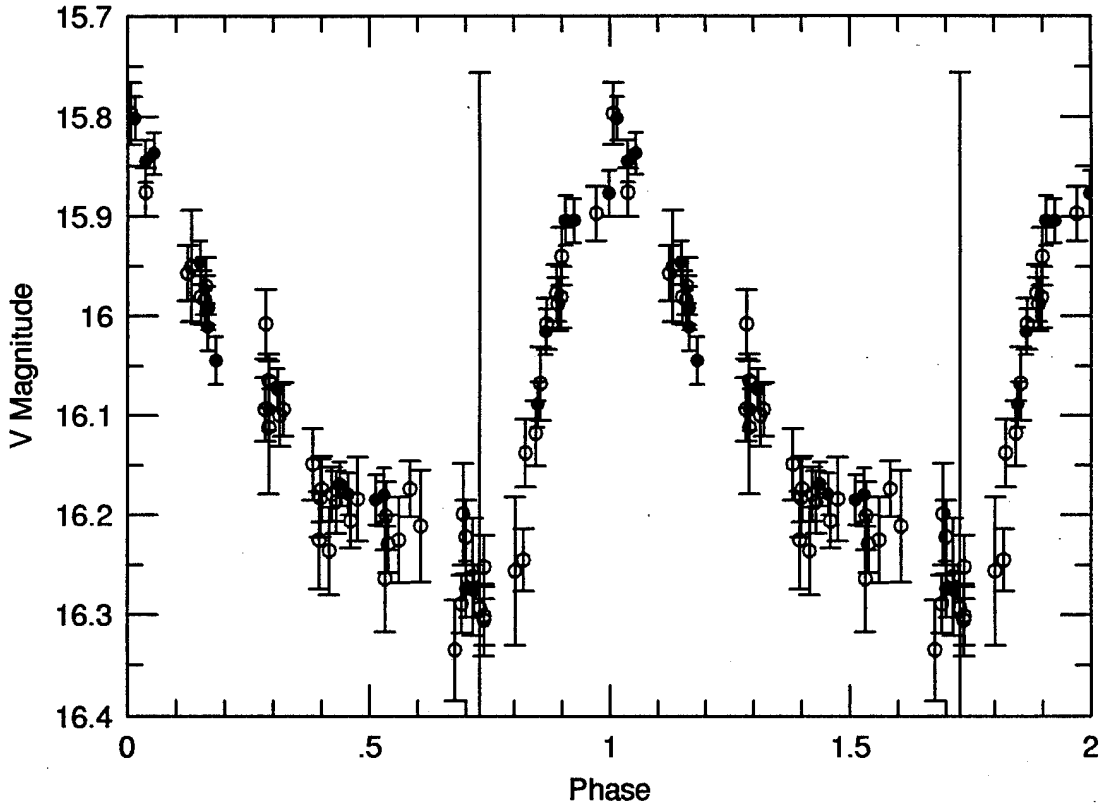
<B-V> = 0.33

P = 0.632536 days

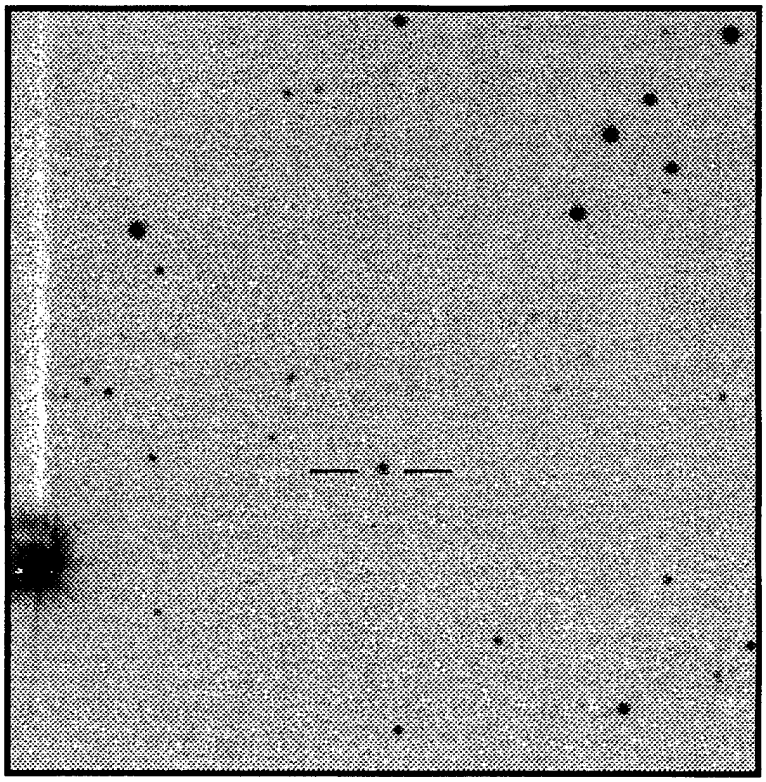
Epoch = 3308.3

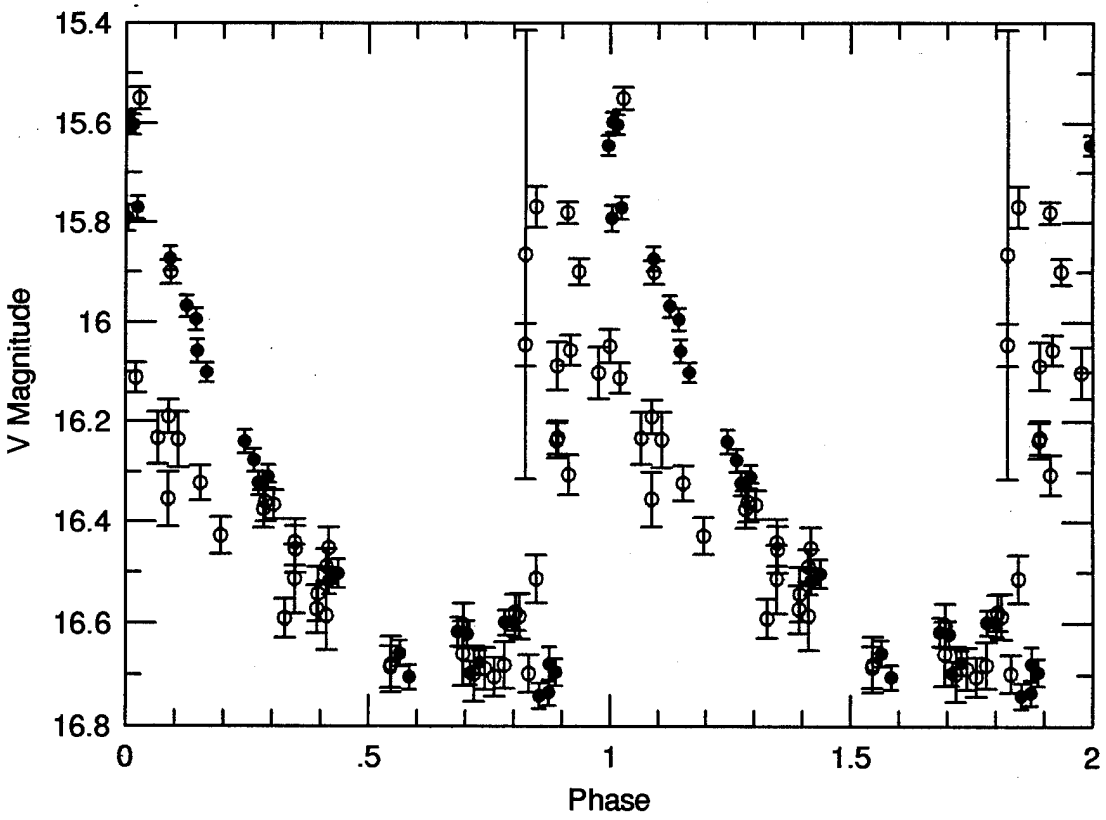
Type: RRab



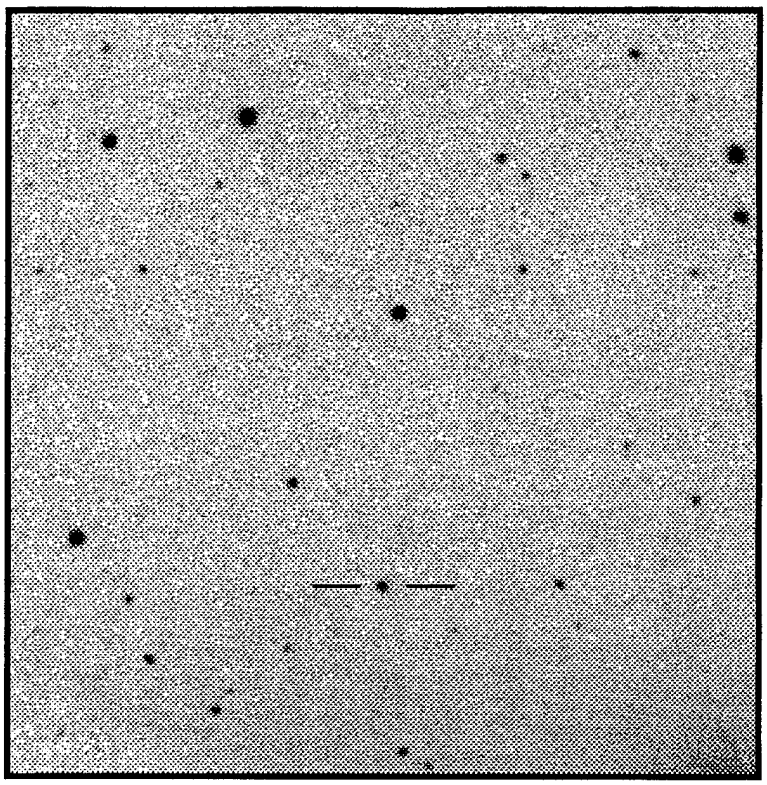


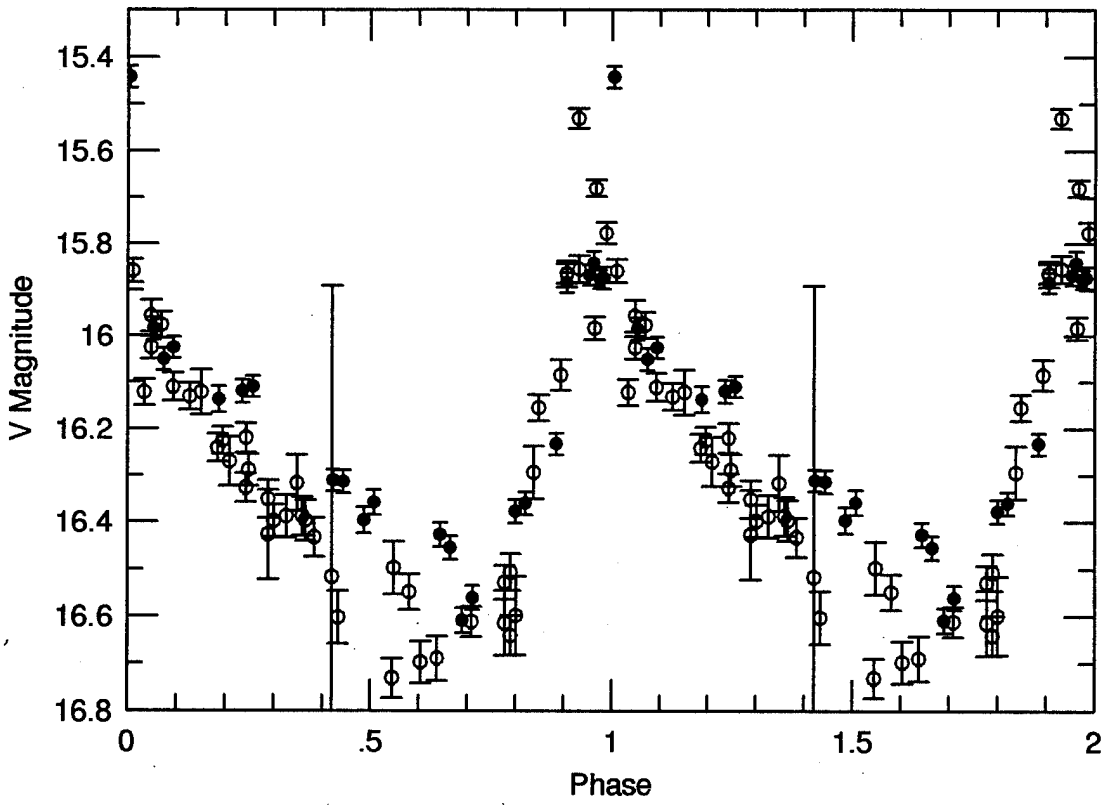
RA : 08 46 51.7
Dec: 28 02 45.3
<V> = 16.344
<B-V> = 0.21
P = 0.552704 days
Epoch = 3307.320
Type: RRab B



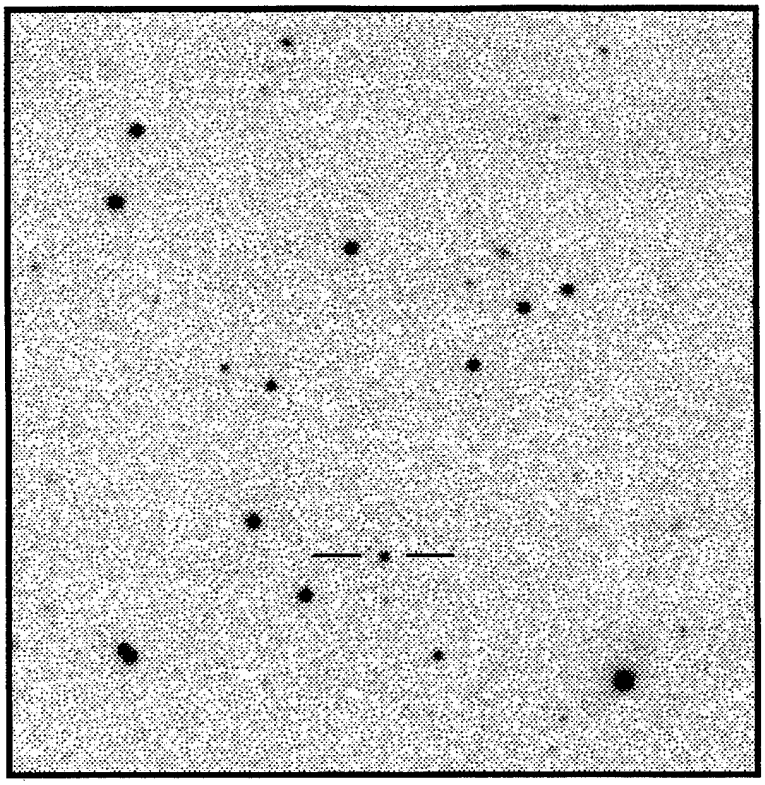


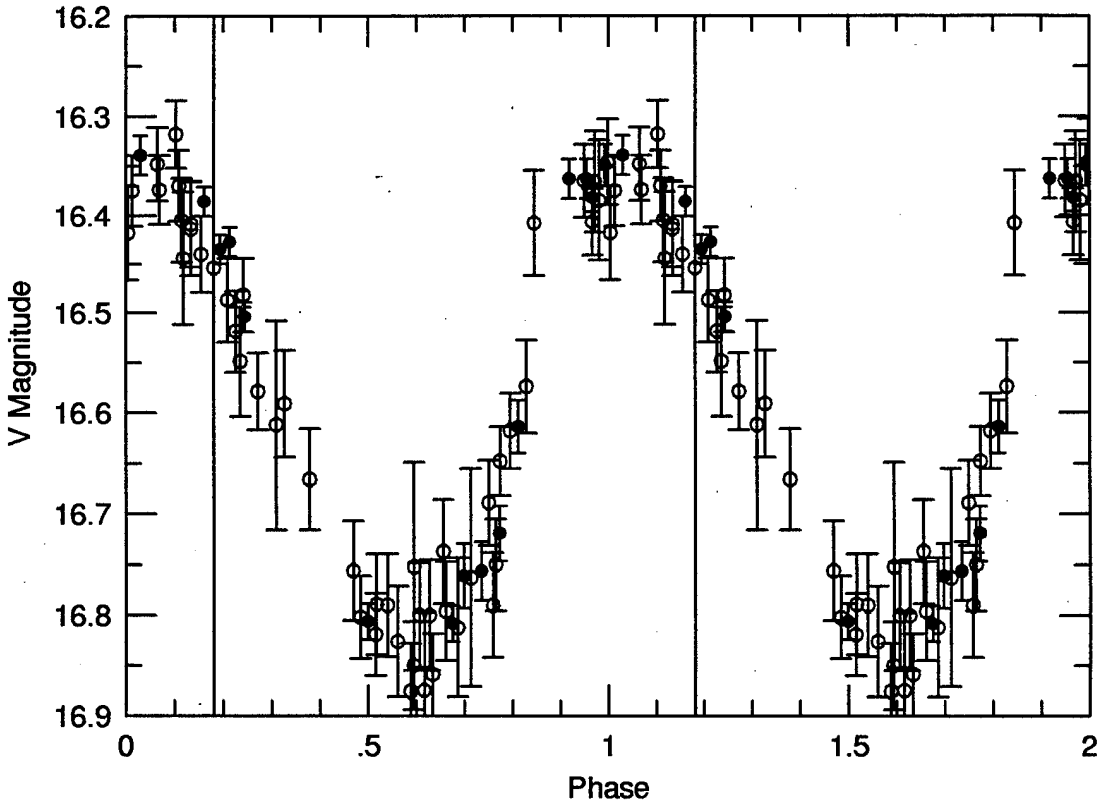
RA : 09 01 17.7
Dec: 28 01 31.3
<V> = 16.255
<B-V> = 0.30
P = 0.513581 days
Epoch = 3331.312
Type: RRab B



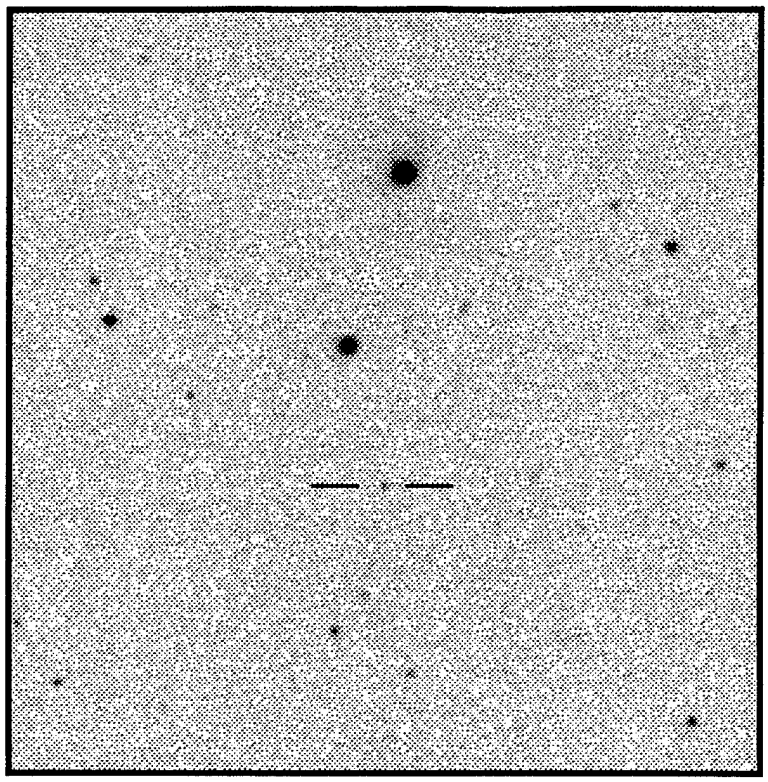


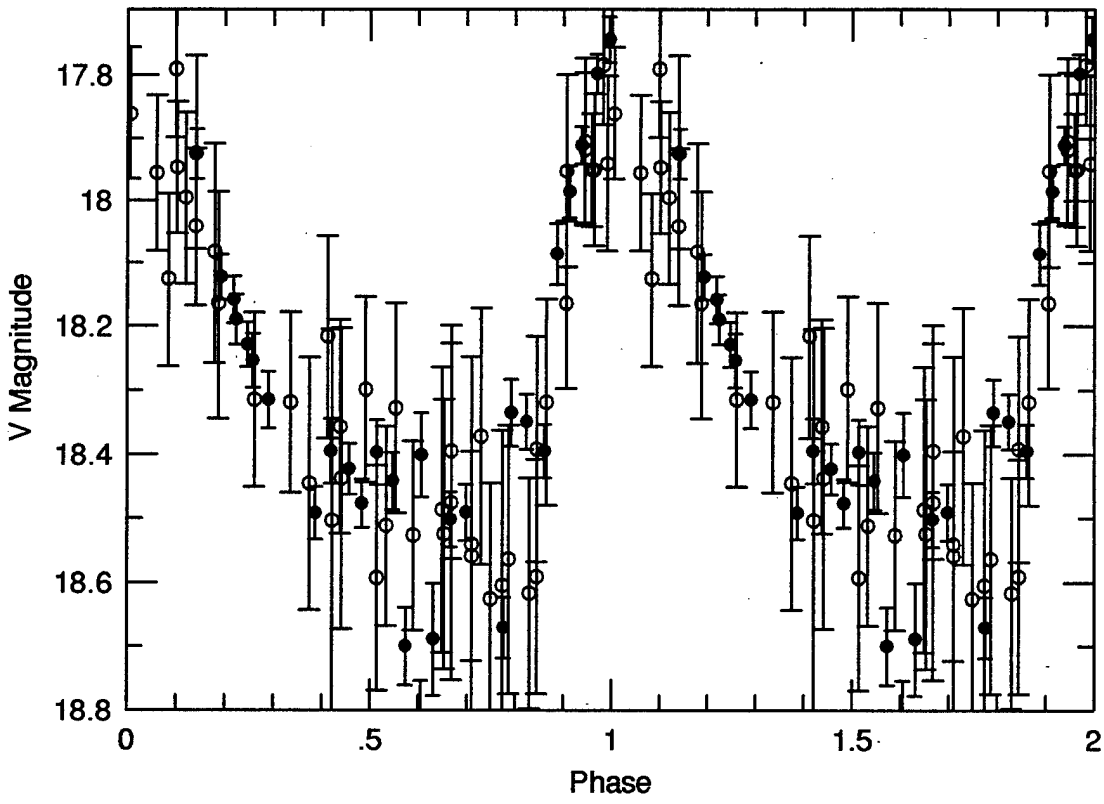
RA : 09 56 59.1
Dec: 28 02 02.6
<V> = 16.571
<B-V> = 0.07
P = 0.286813 days
Epoch = 3342.322
Type: RRc



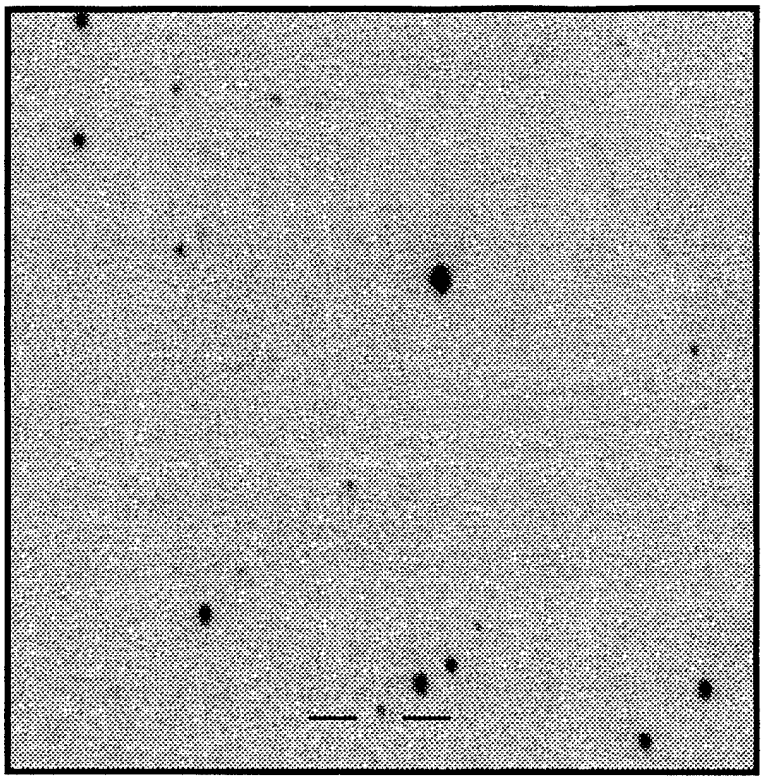


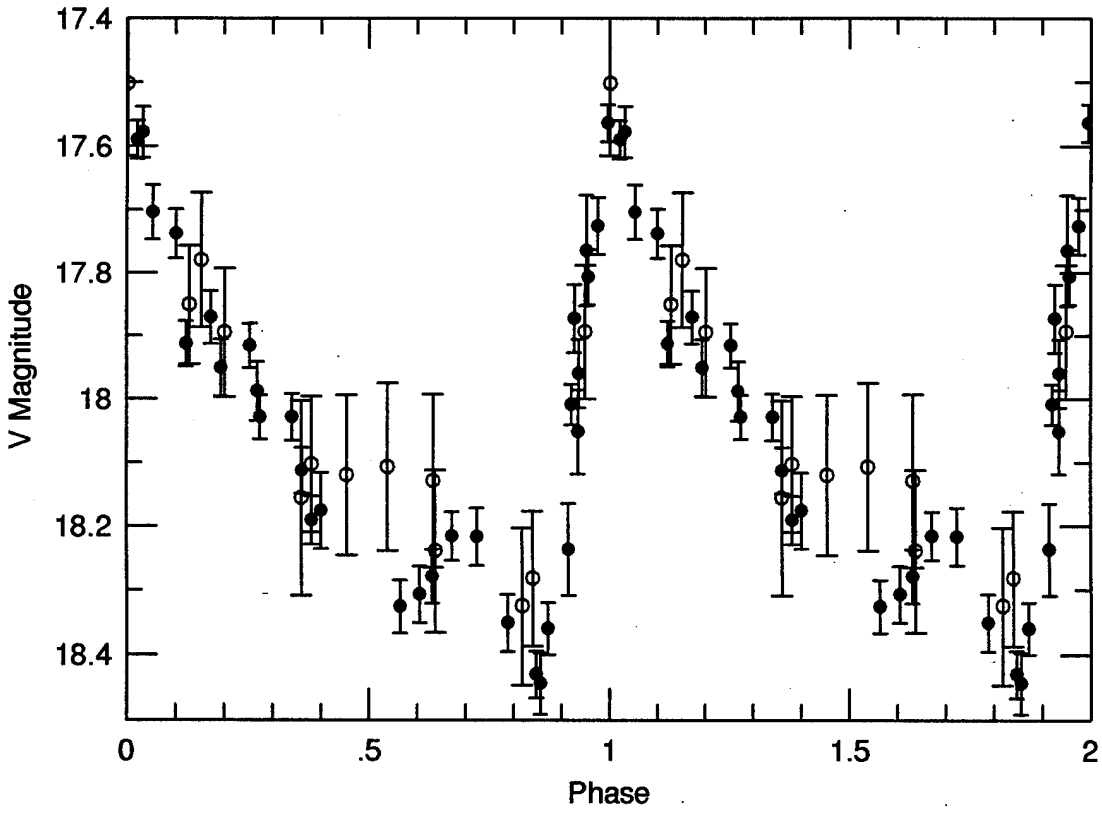
RA : 10 26 04.7
Dec: 28 02 51.5
<V> = 18.250
<B-V> = 0.32
P = 0.552801 days
Epoch = 3666.438
Type: RRab



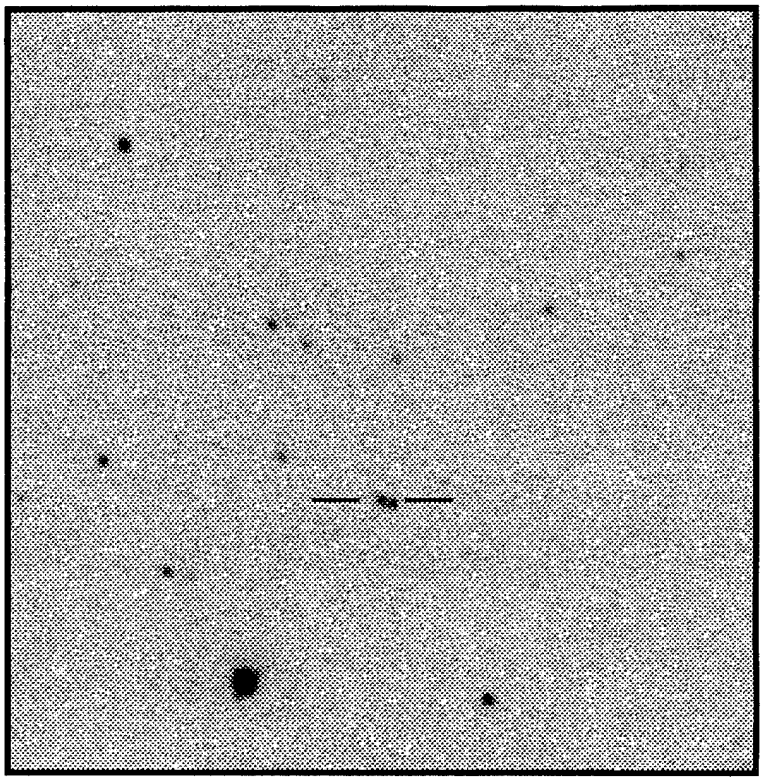


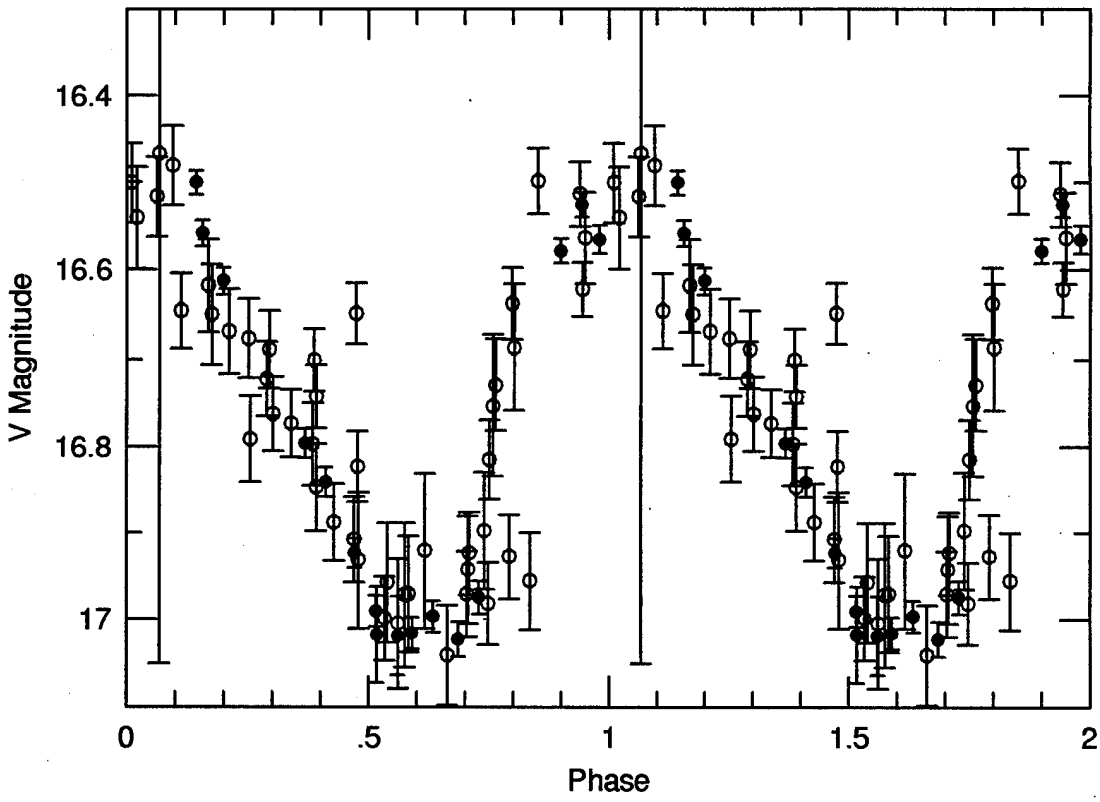
RA : 10 36 17.2
Dec: 27 59 07.7
<V> = 18.037
<B-V> = 0.24
P = 0.707095 days
Epoch = 3461.348
Type: RRab





RA : 10 57 41.6
Dec: 28 02 46.0
<V> = 16.740
<B-V> = 0.12
P = 0.327640 days
Epoch = 3363.304
Type: RRc





RA : 11 48 32.1

Dec: 28 04 36.1

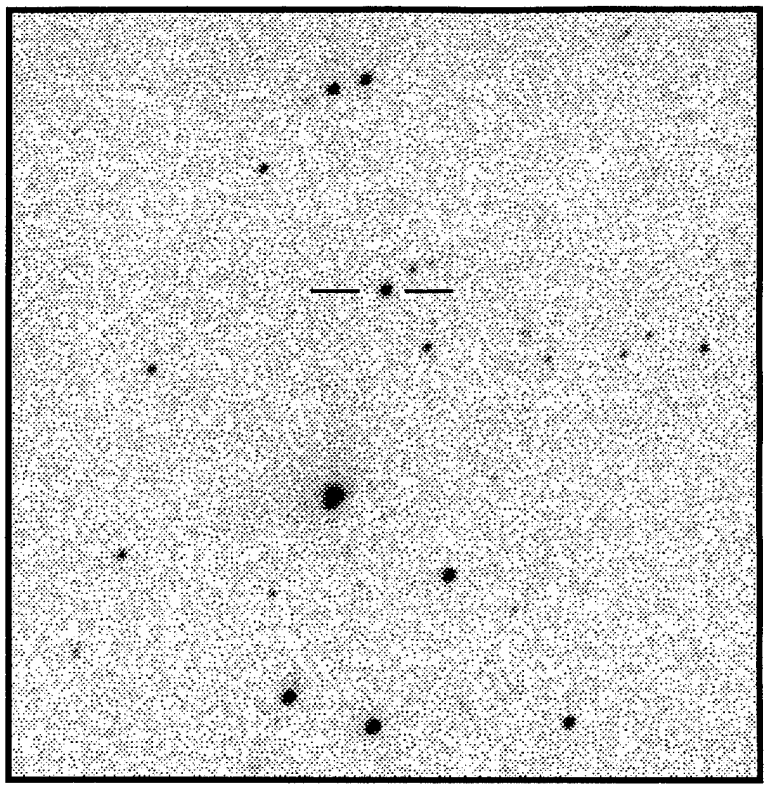
<V> = 15.305

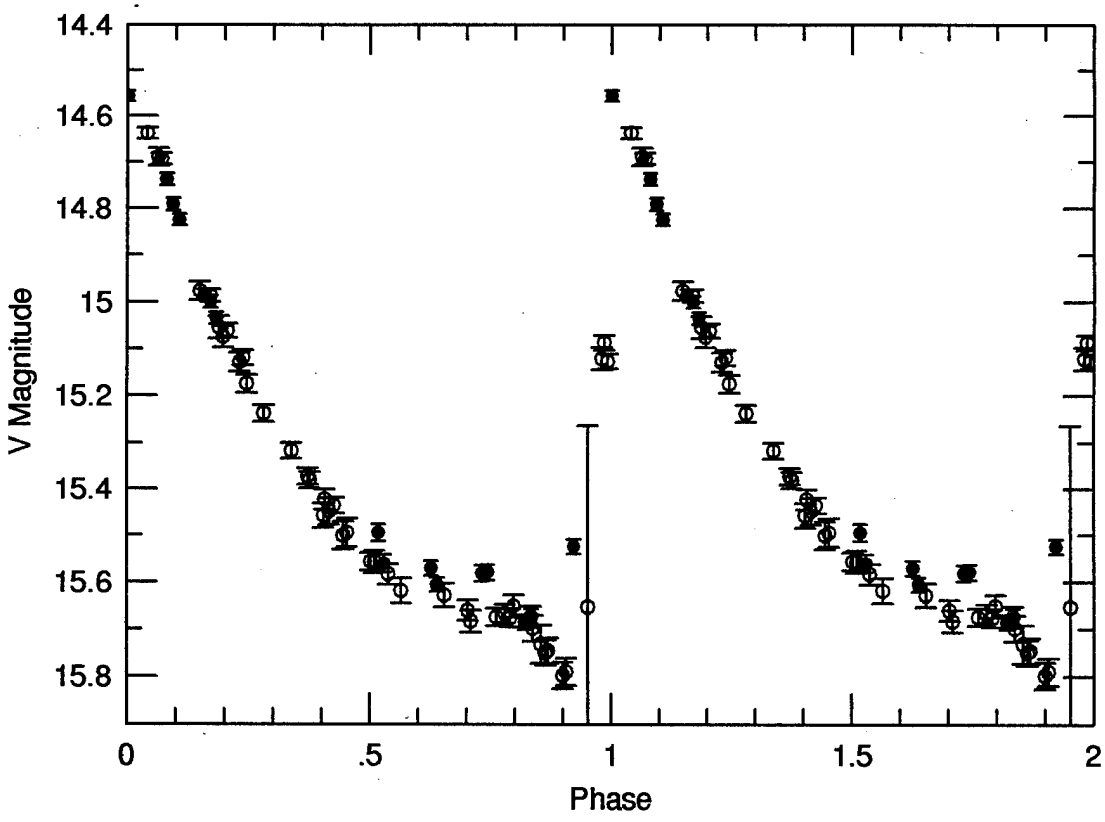
<B-V> = 0.36

P = 0.597821 days

Epoch = 3356.253

Type: RRab





RA : 12 04 40.4

Dec: 28 01 08.5

<V> = 16.364

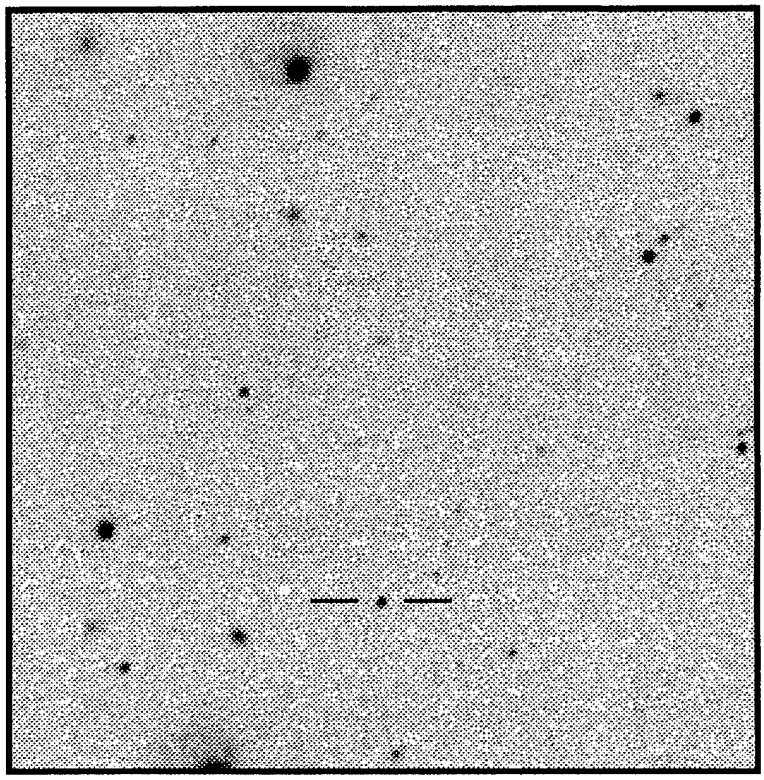
<B-V> = 0.20

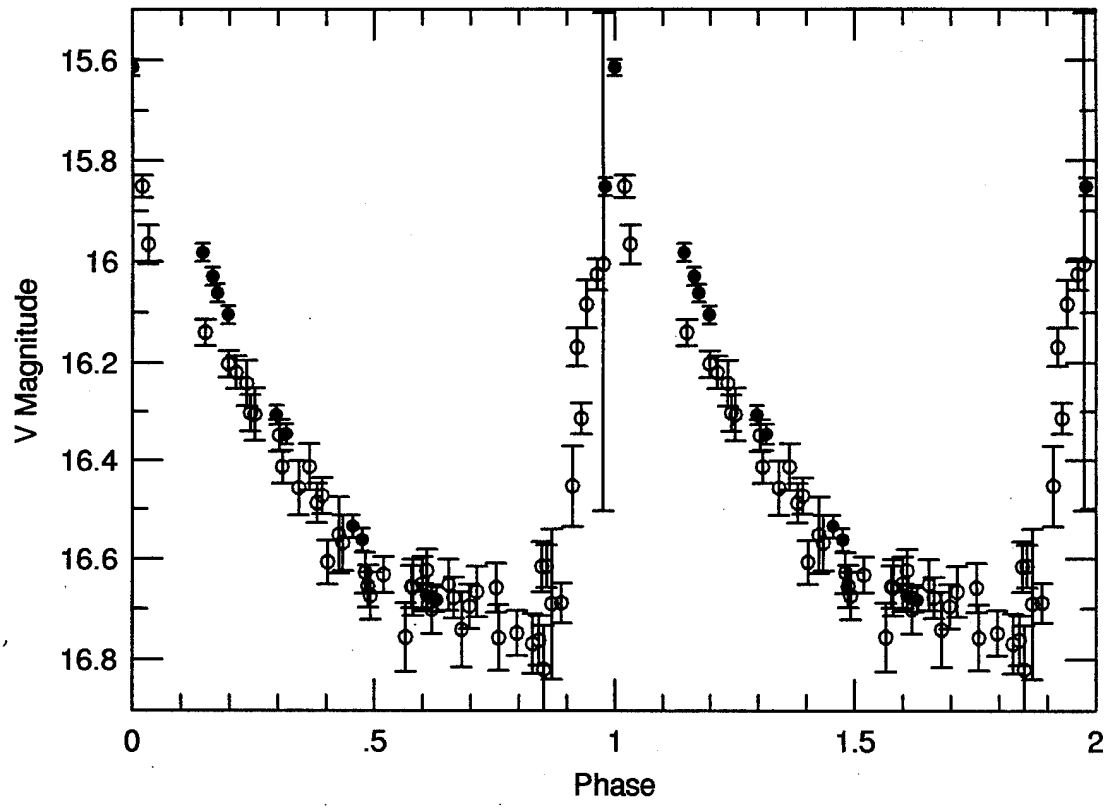
P = 0.521823 days

Epoch = 3361.121

Type: RRab

GR Com





RA : 12 05 25.4

Dec: 28 03 28.8

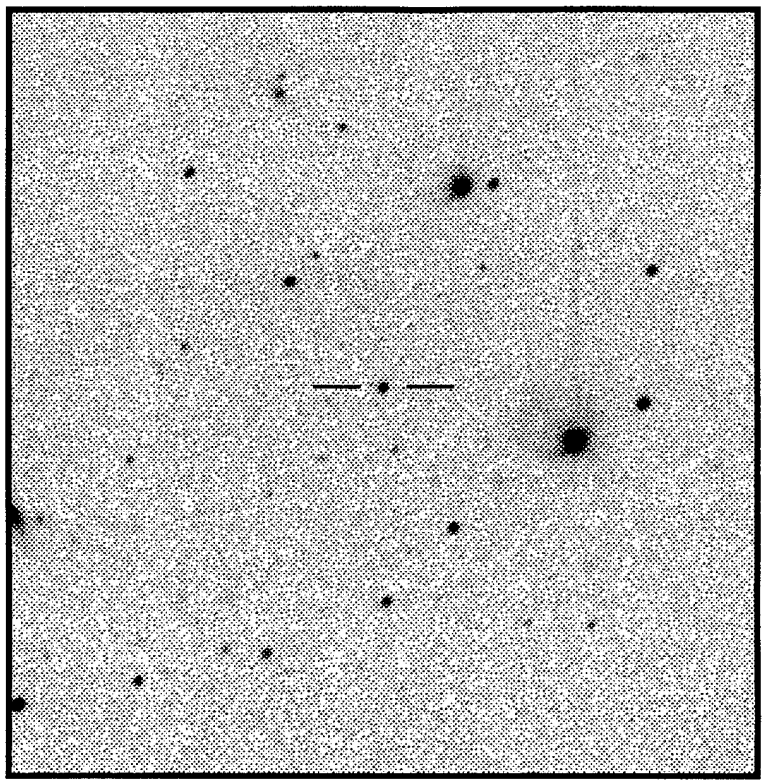
<V> = 15.737

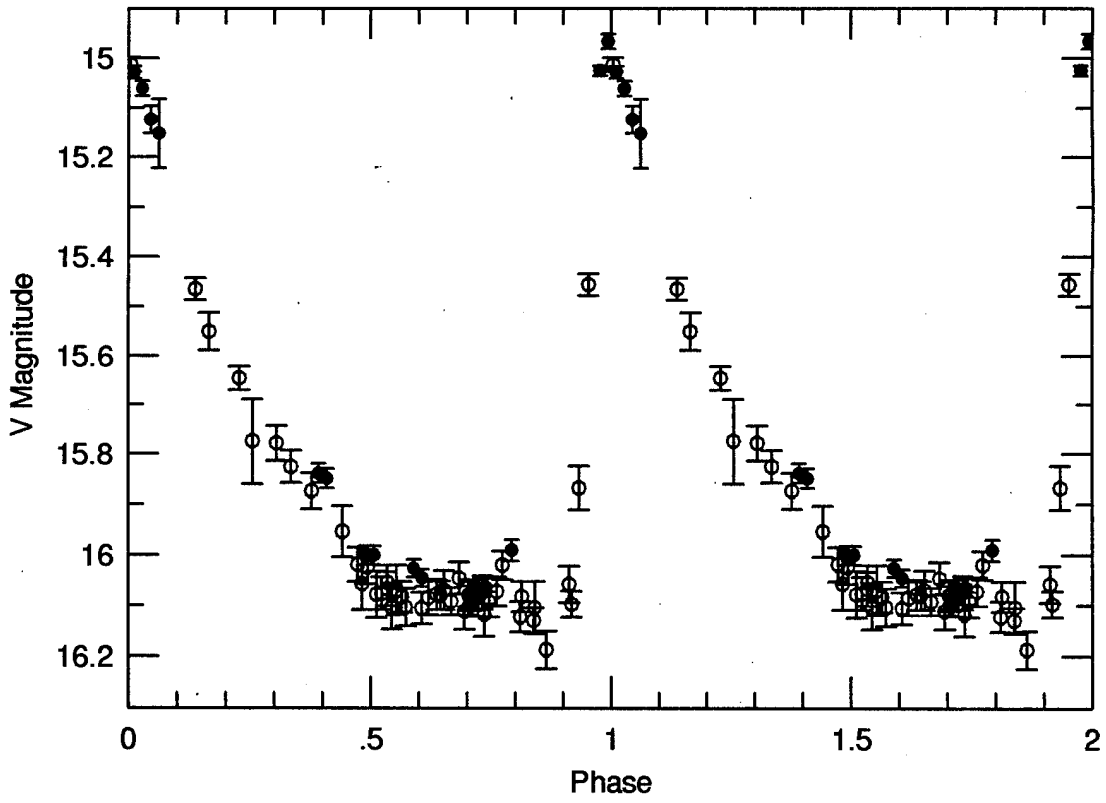
<B-V> = 0.32

P = 0.508702 days

Epoch = 3683.373

Type: RRab





RA : 12 24 18.6

Dec: 28 03 17.4

<V> = 16.470

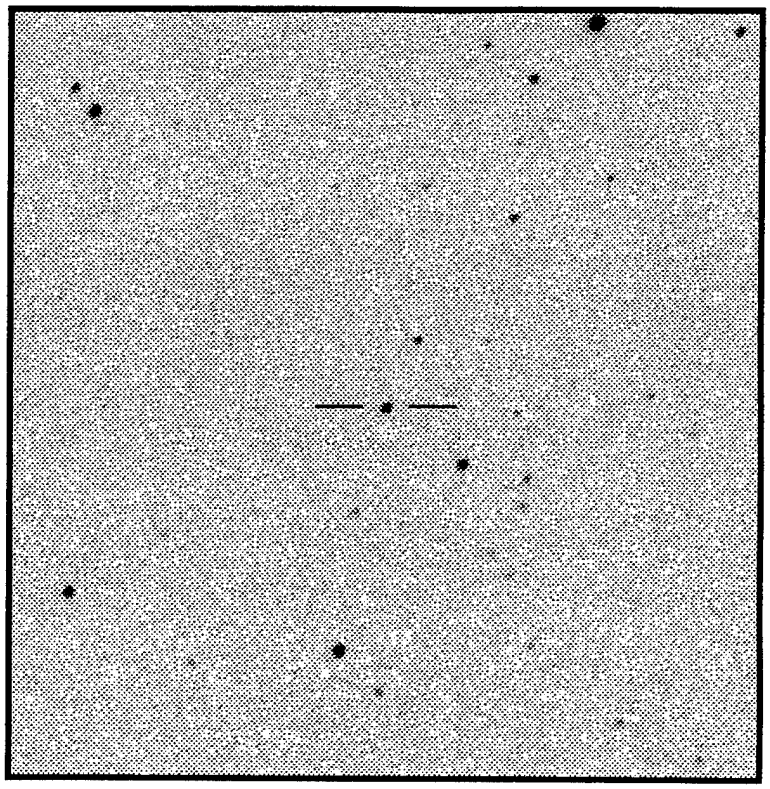
<B-V> = 0.33

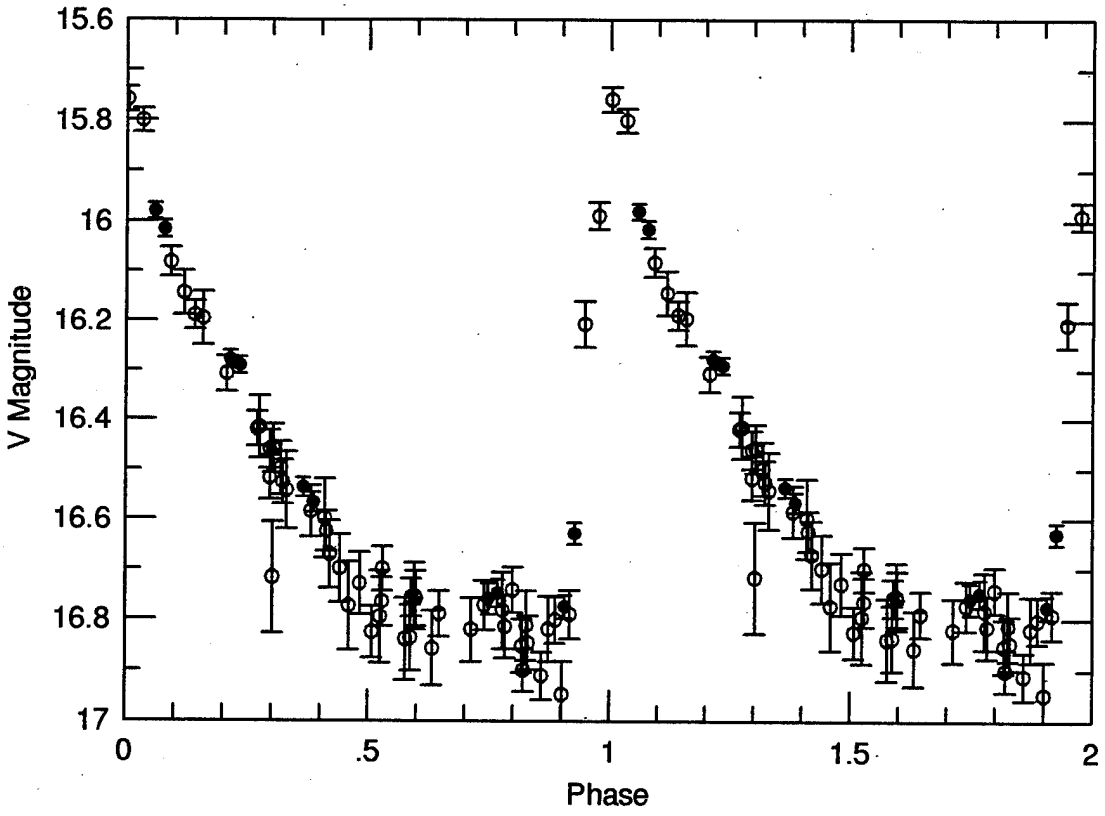
P = 0.529449 days

Epoch = 3361.268

Type: RRab

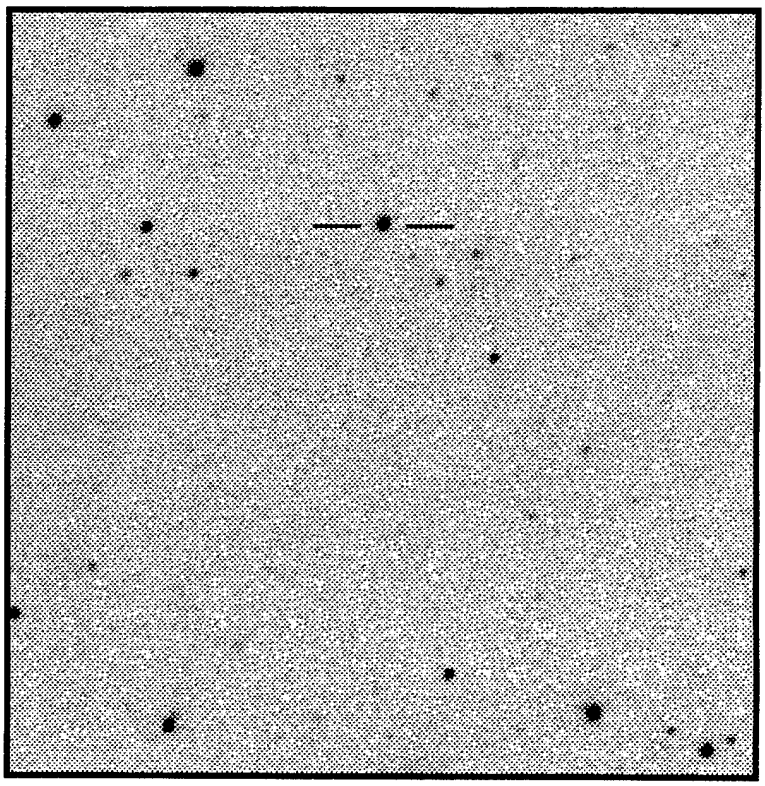
GS Com

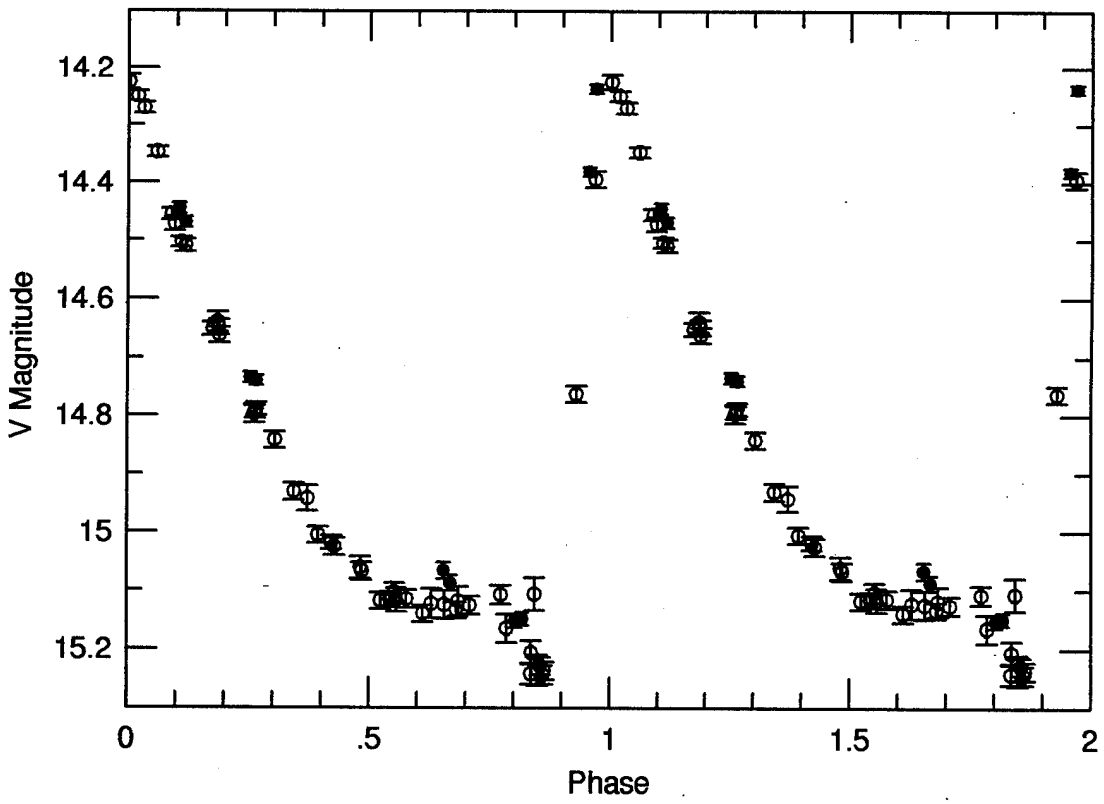




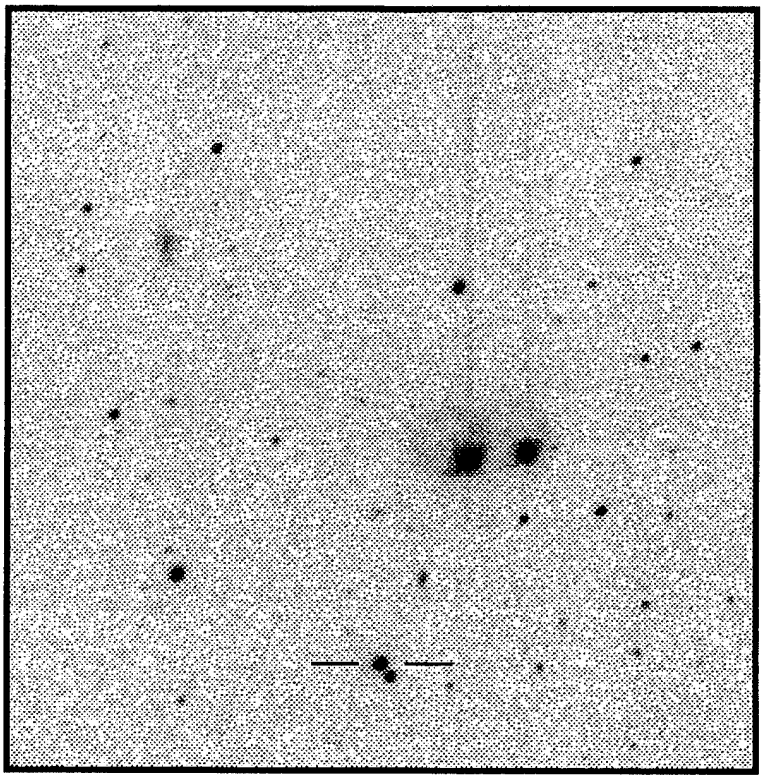
RA : 12 43 17.6
Dec: 28 05 21.7
<V> = 14.820
<B-V> = 0.35
P = 0.540837 days
Epoch = 3361.347
Type: RRab

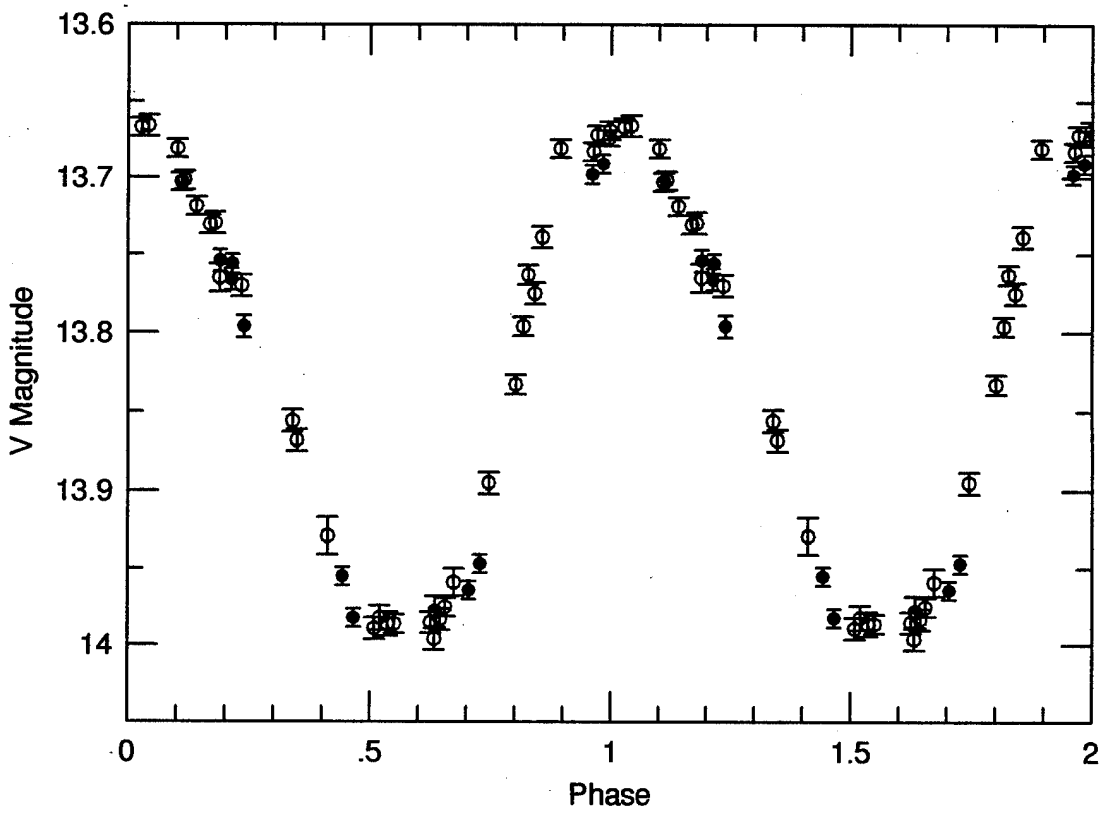
DV Com





RA : 13 14 03.3
Dec: 28 00 26.7
<V> = 13.825
<B-V> = 0.05
P = 0.314639 days
Epoch = 3361.432
Type: RRc





RA : 13 17 32.5

Dec: 28 01 39.4

<V> = 16.770

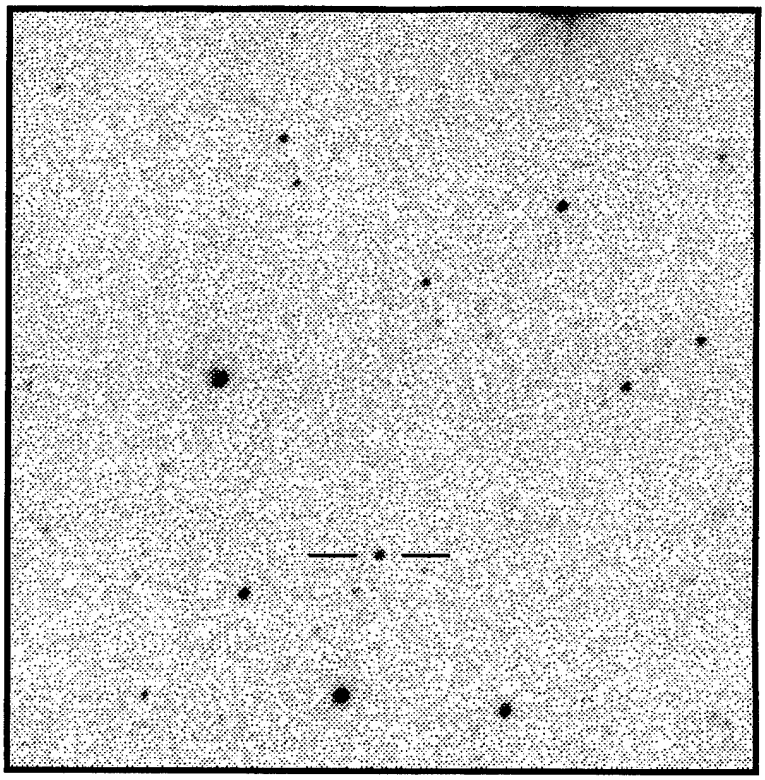
<B-V> = 0.35

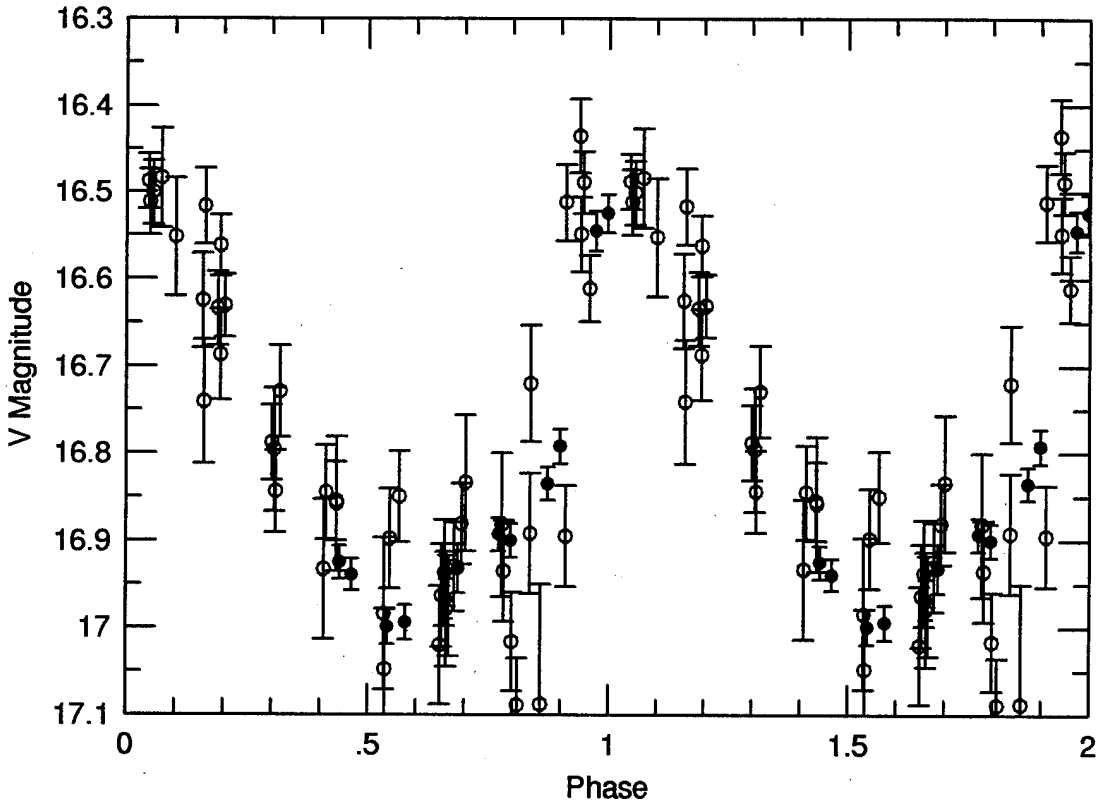
P = 0.568389 days

Epoch = 3468.281

Type: RRab B

EZ Com





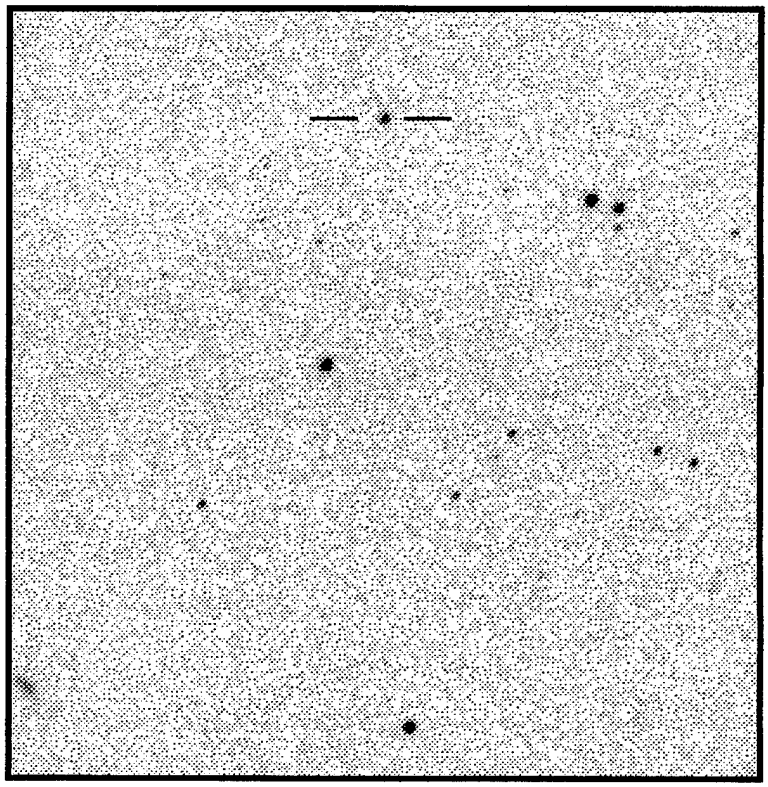
RA : 13 23 46.7

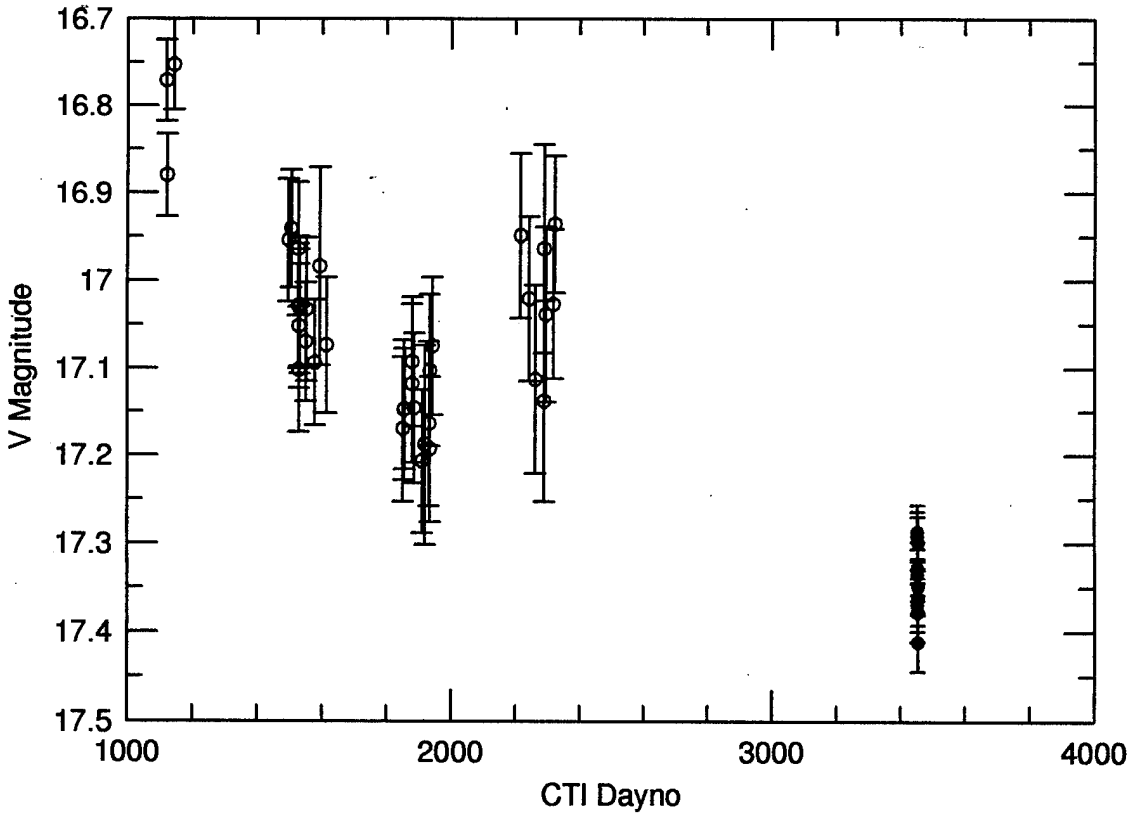
Dec: 28 06 32.5

<V> = 17.056

<B-V> = 0.60

Type: AGN/QSO





RA : 14 33 13.2

Dec: 28 01 17.0

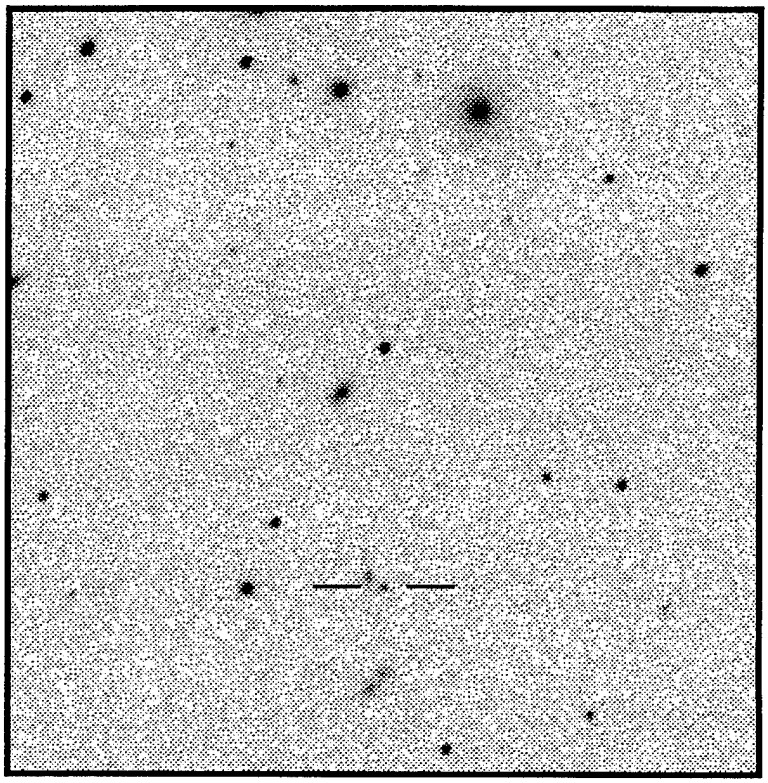
<V> = 17.995

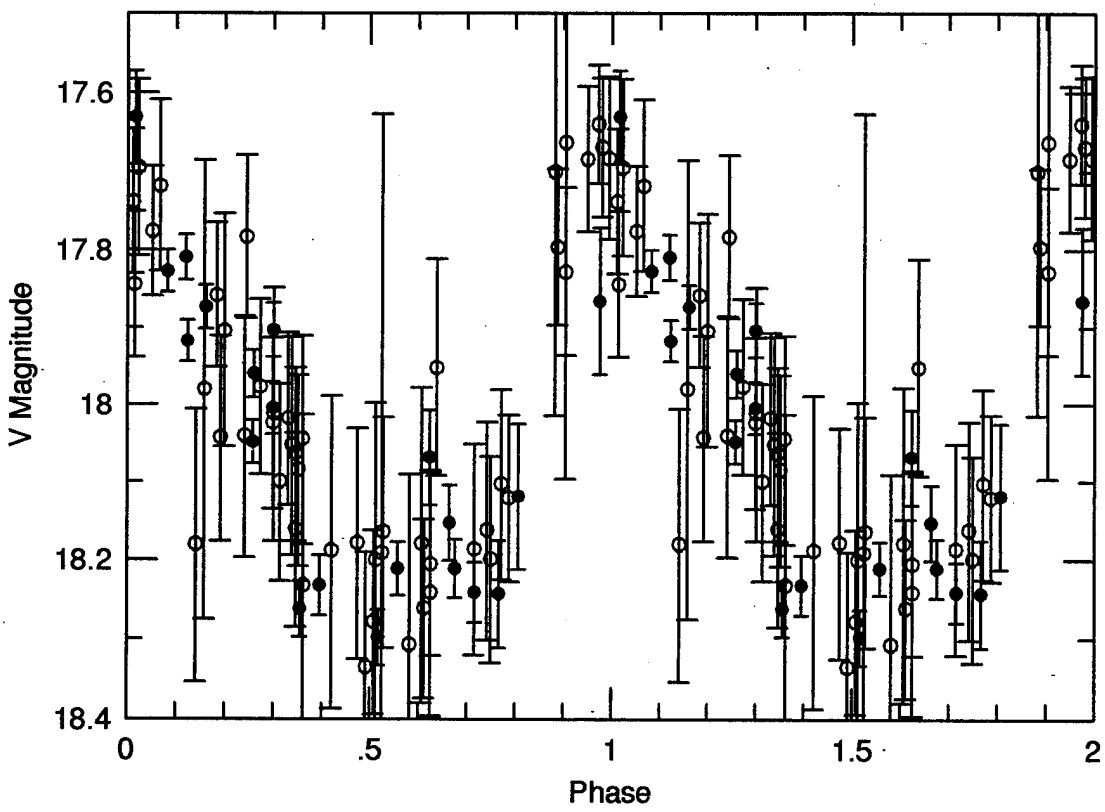
<B-V> = 0.40

P = 0.437536 days

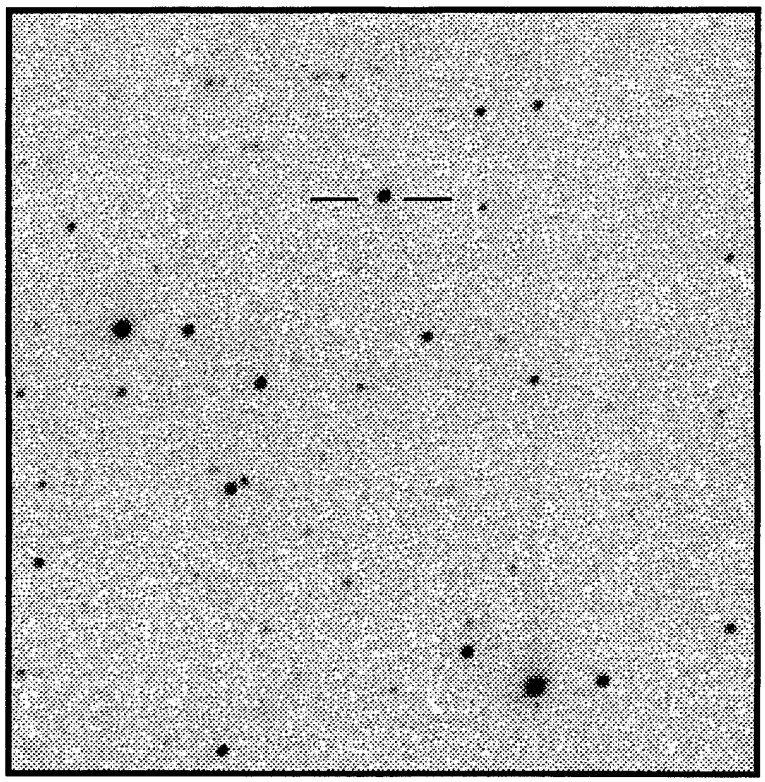
Epoch = 3481.155

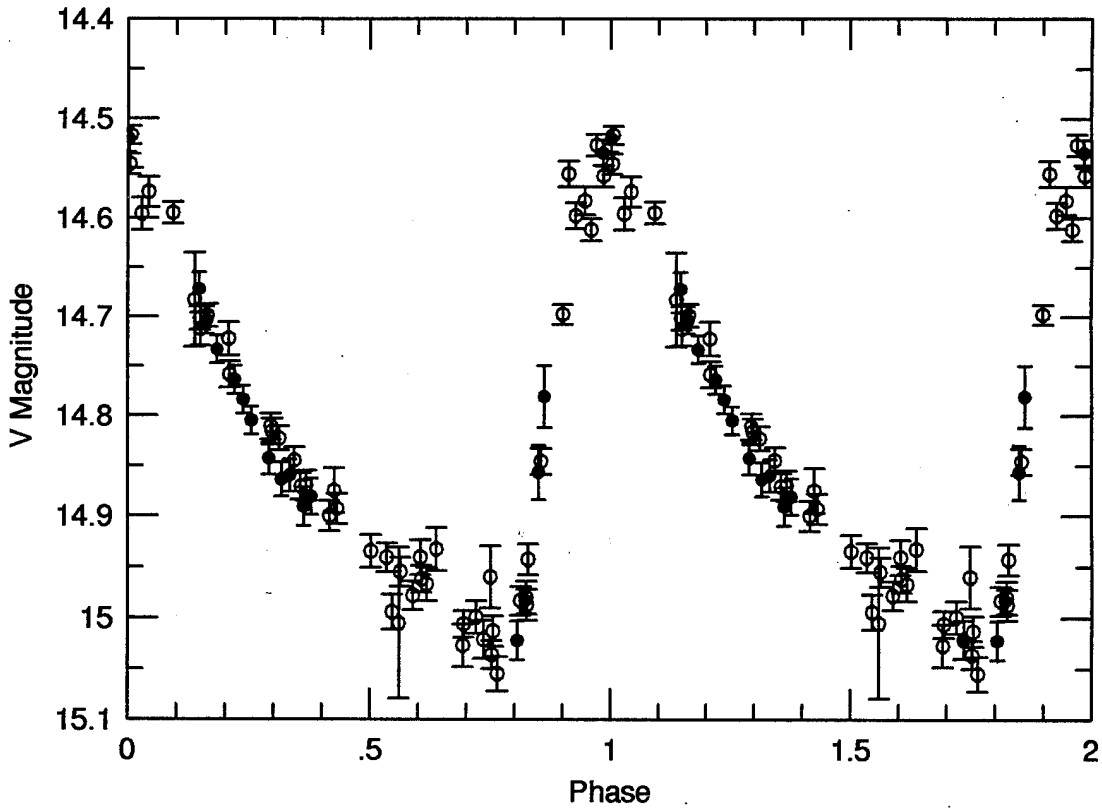
Type: RRab





RA : 14 54 39.0
Dec: 28 05 32.8
<V> = 14.810
<B-V> = 0.36
P = 0.622135 days
Epoch = 3112.203
Type: RRab





RA : 15 16 28.1

Dec: 28 00 41.6

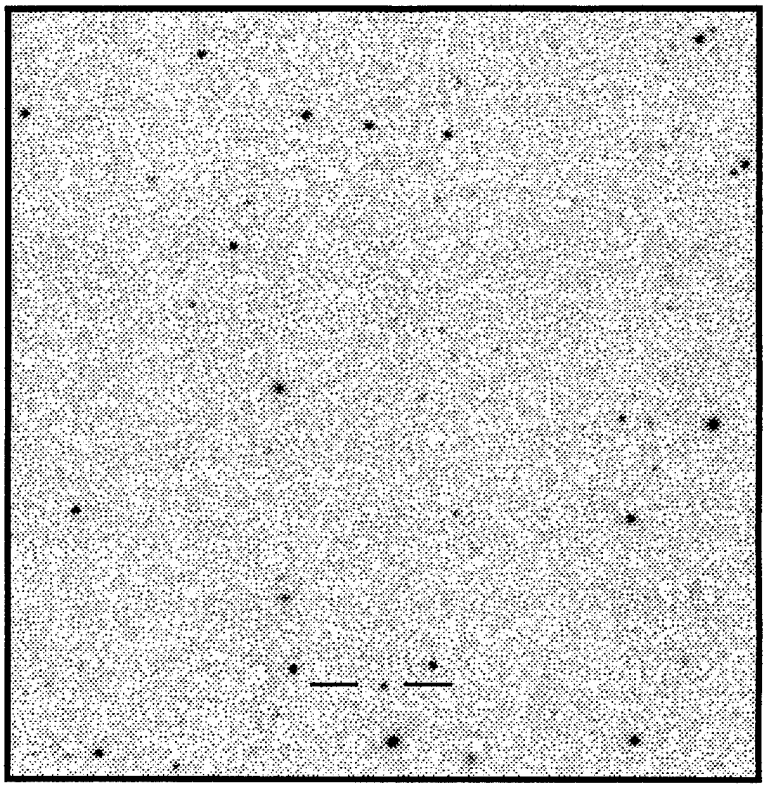
<V> = 17.897

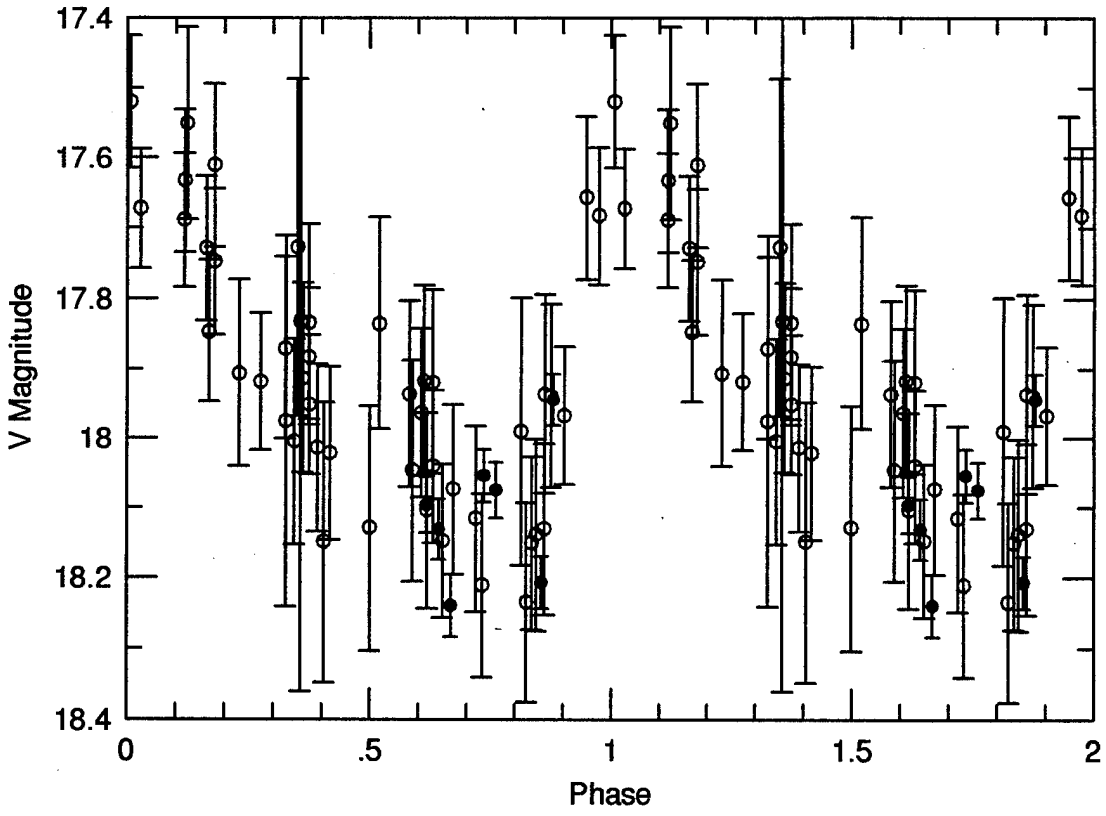
<B-V> = 0.30

P = 0.571900 days

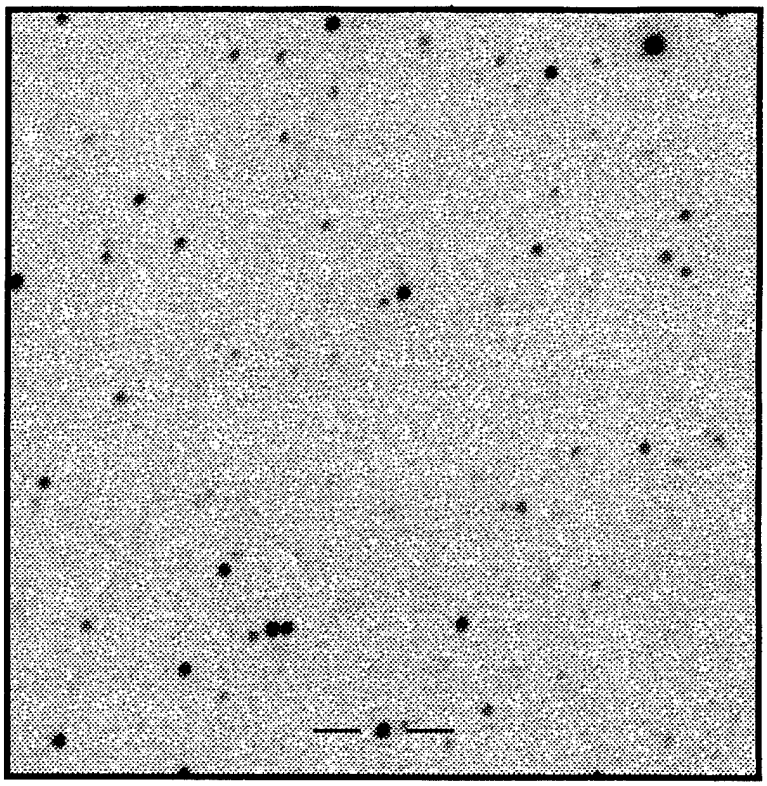
Epoch = 3685.029

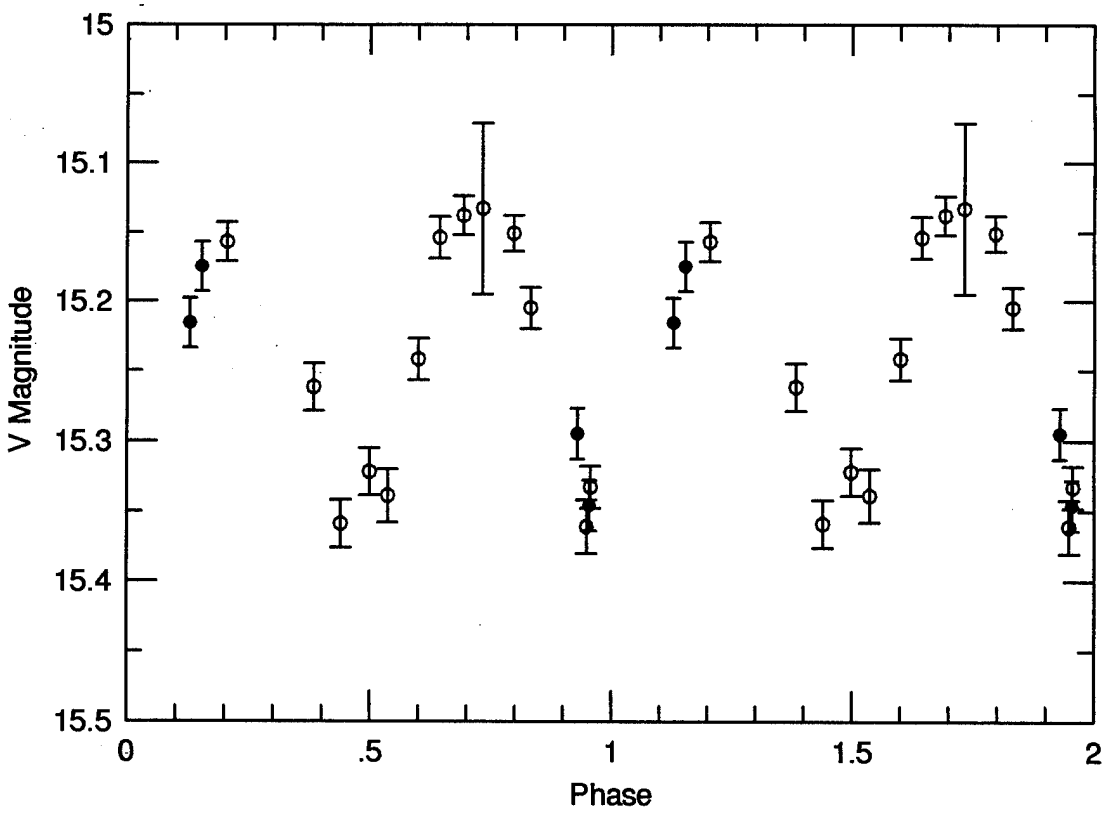
Type: RRab



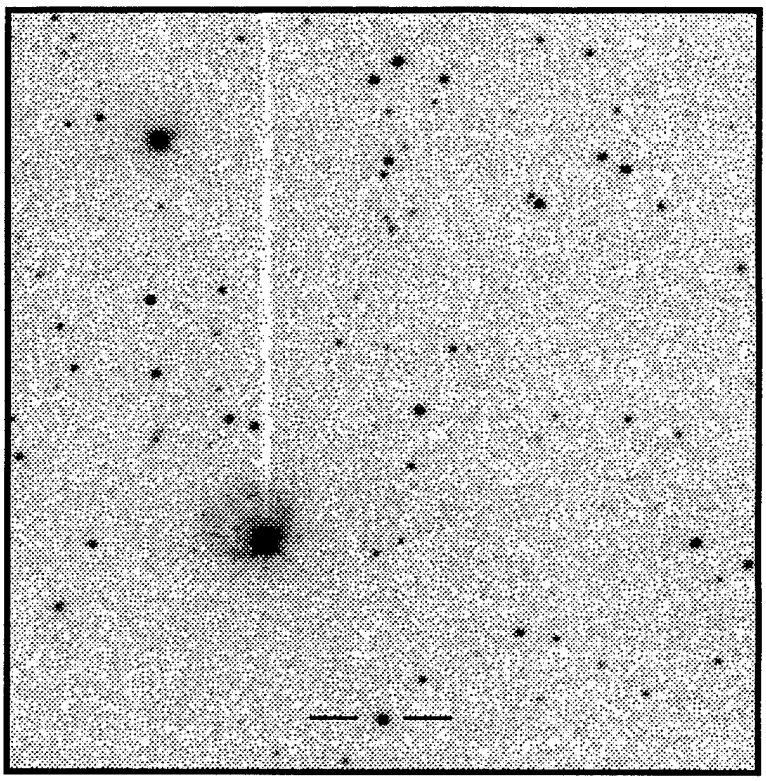


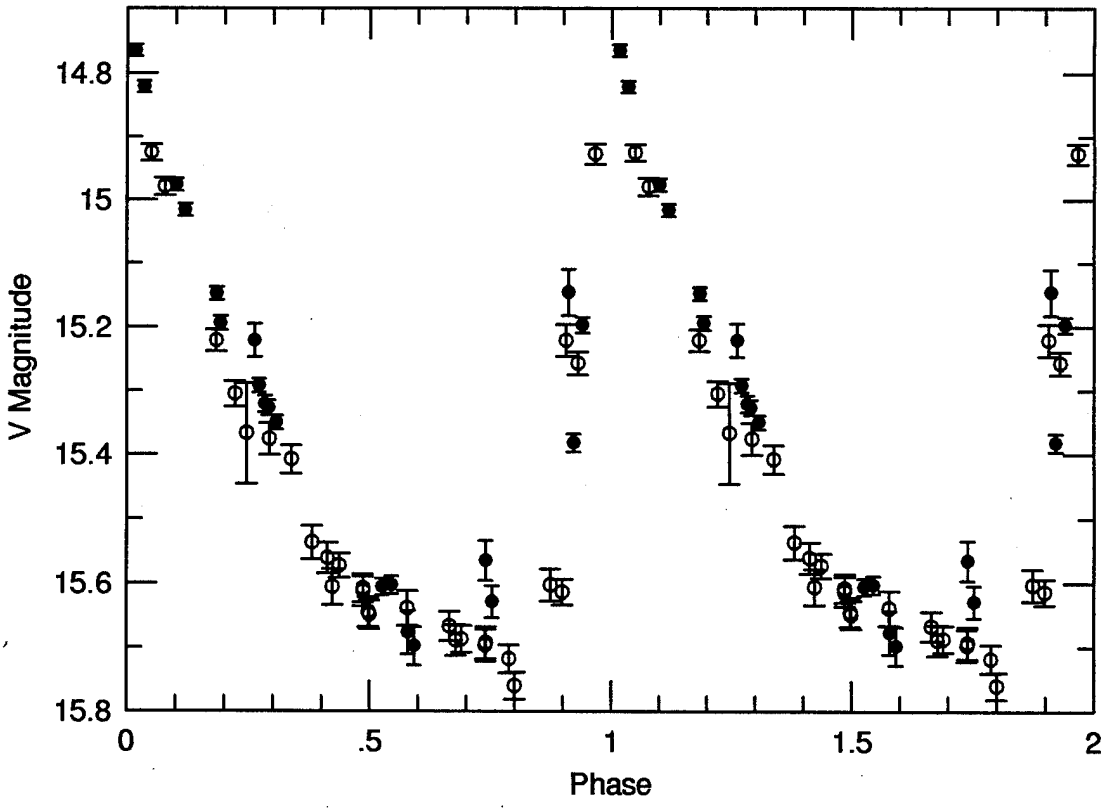
RA : 16 23 17.6
Dec: 27 58 28.9
<V> = 15.234
<B-V> = 0.47
P = 0.343669 days
Epoch = 3685.451
Type: W UMa



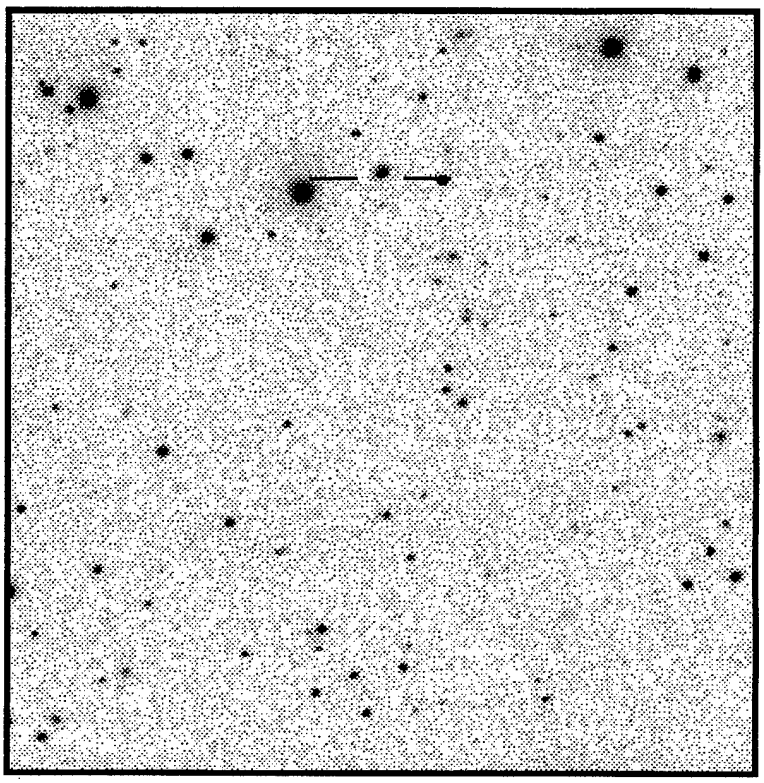


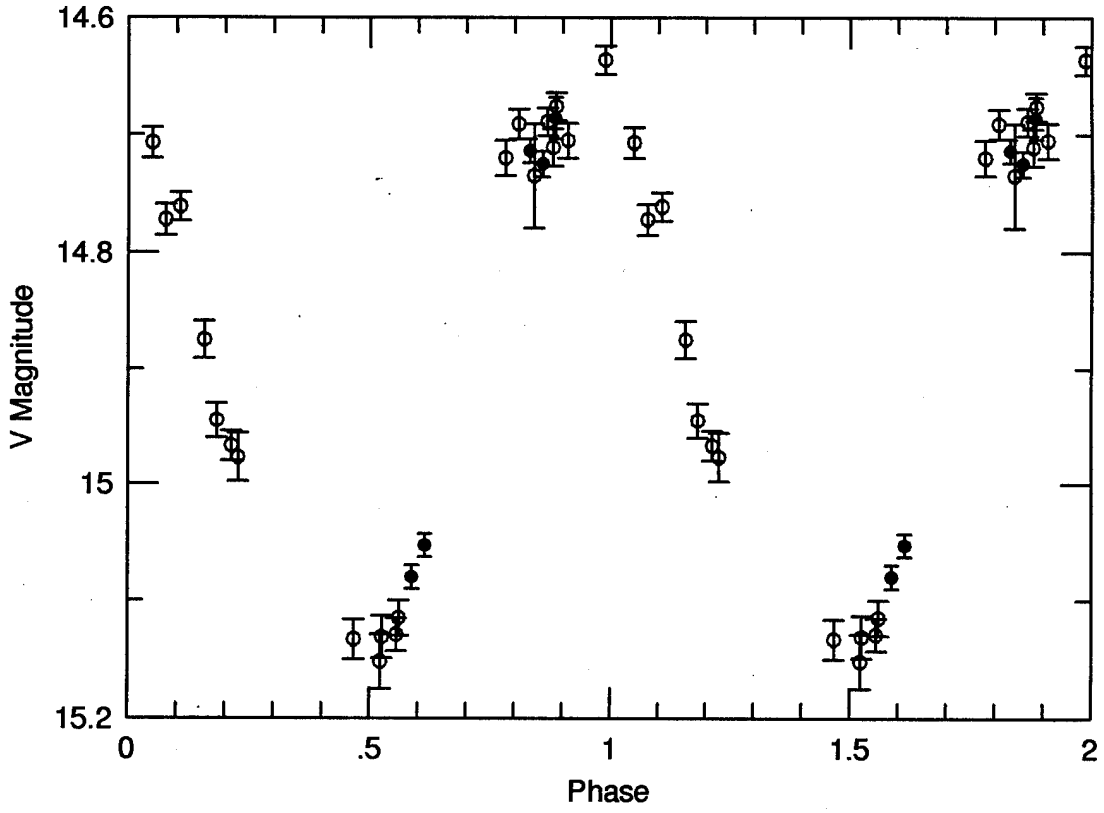
RA : 16 50 08.8
Dec: 27 59 55.0
<V> = 15.368
<B-V> = 0.33
P = 0.570831 days
Epoch = 3113.209
Type: RRab





RA : 16 58 30.7
Dec: 28 06 00.7
<V> = 14.884
<B-V> = 0.30
P = 0.272711 days
Epoch = 3685.586
Type: RRc?





RA : 17 13 10.9

Dec: 28 00 10.3

<V> = 16.202

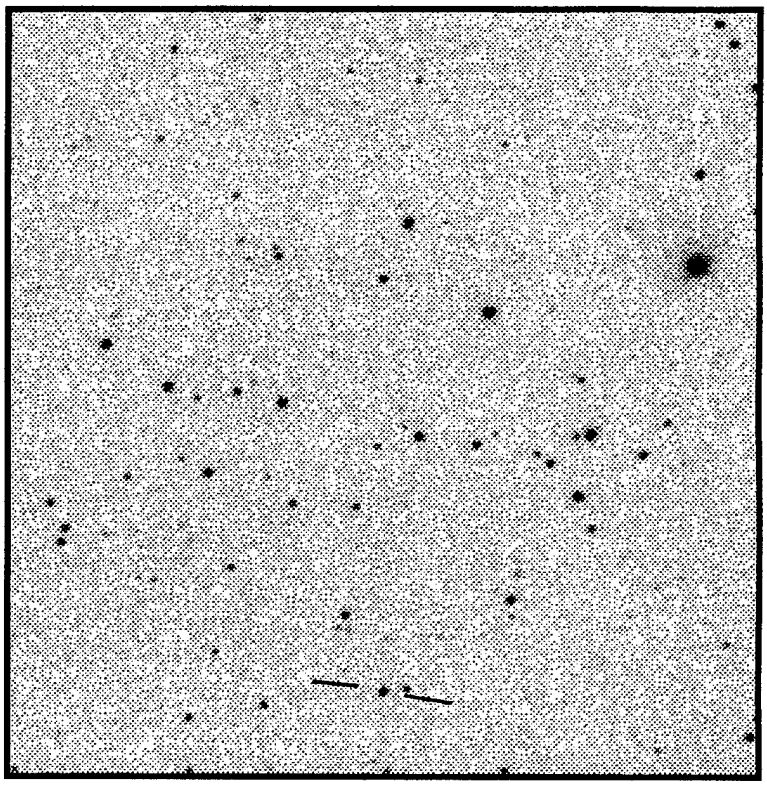
<B-V> = 0.30

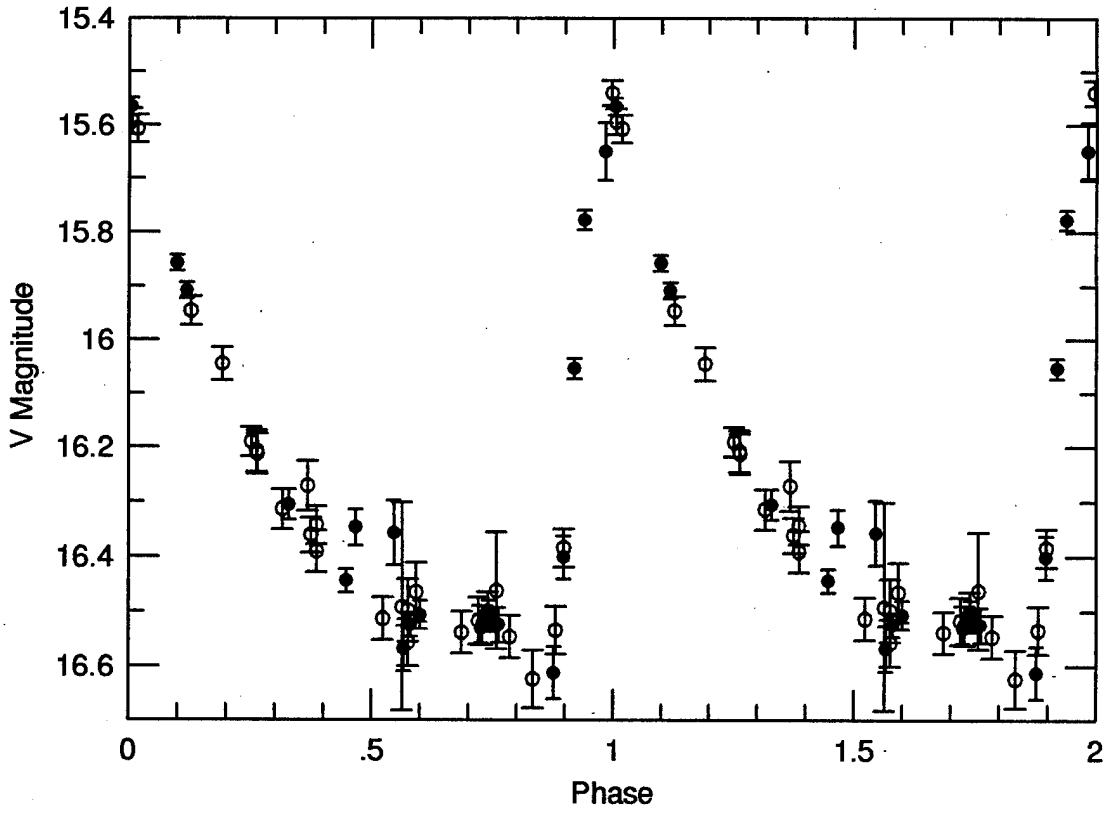
P = 0.531433 days

Epoch = 3481.184

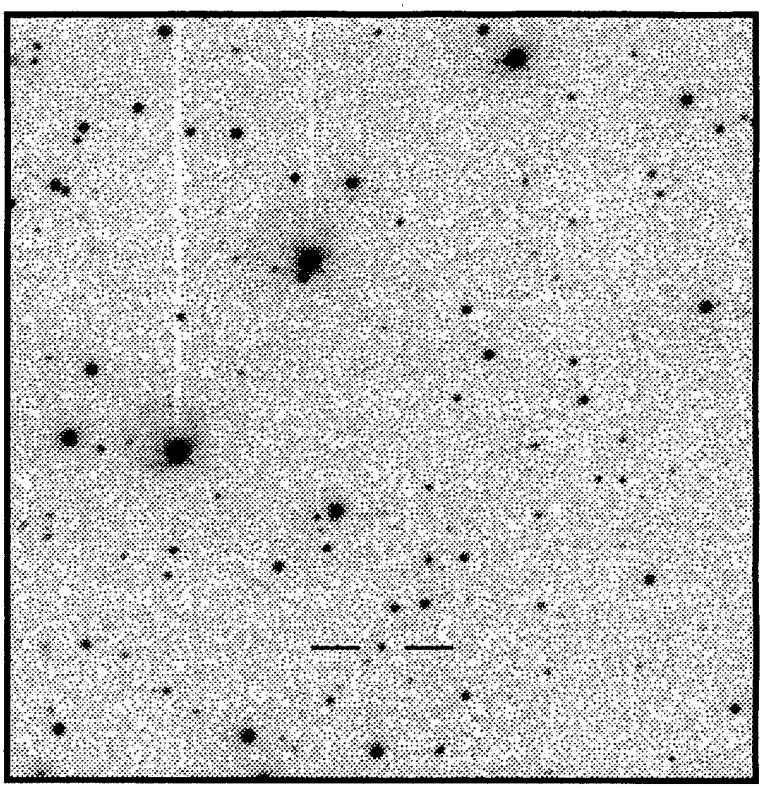
Type: RRab

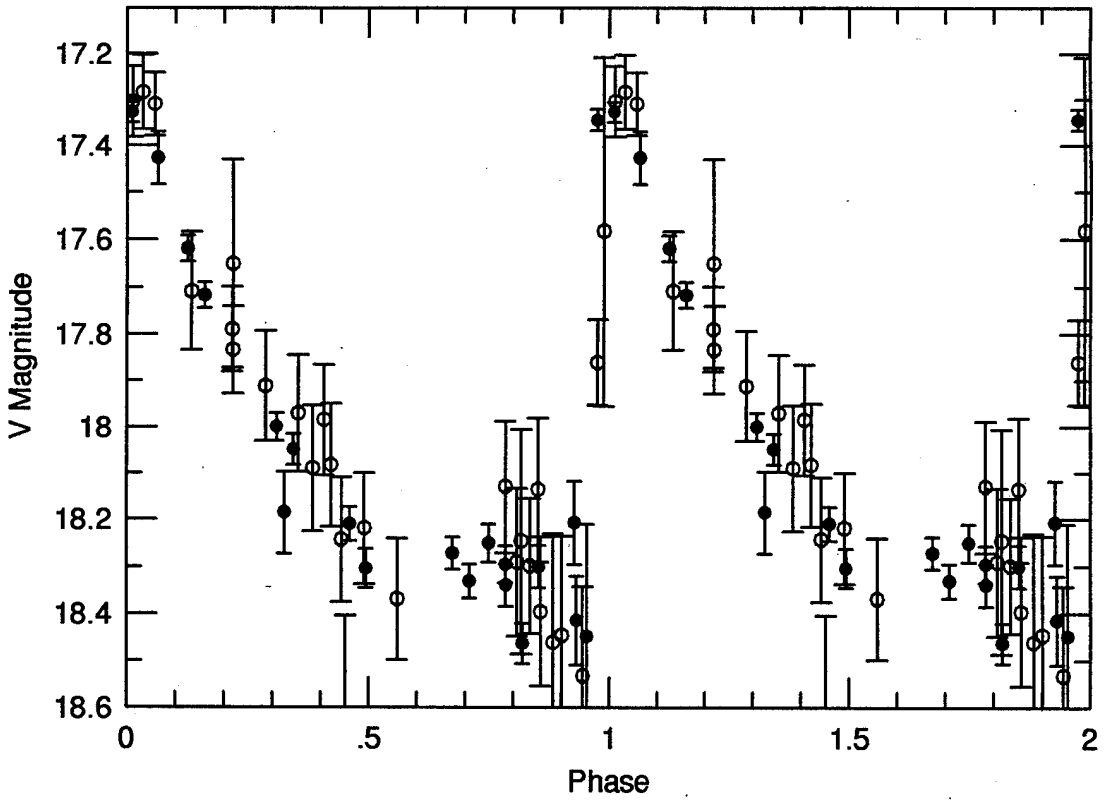
V375 Her





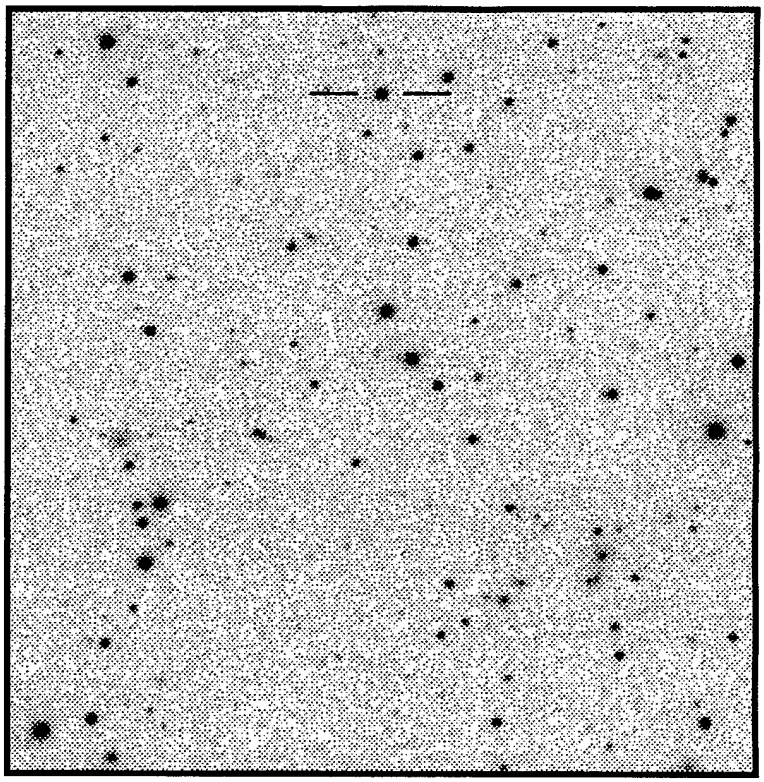
RA : 17 15 23.9
Dec: 28 00 43.0
<V> = 17.998
<B-V> = 0.35
P = 0.516250 days
Epoch = 3474.160
Type: RRab

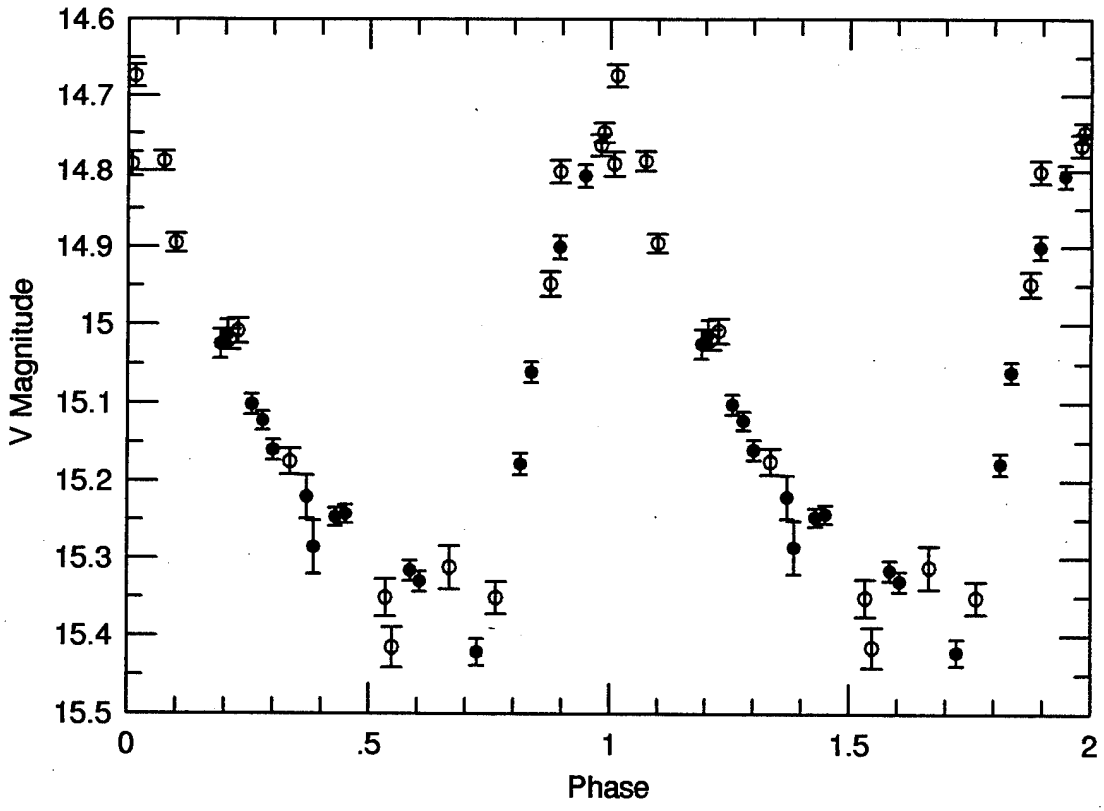




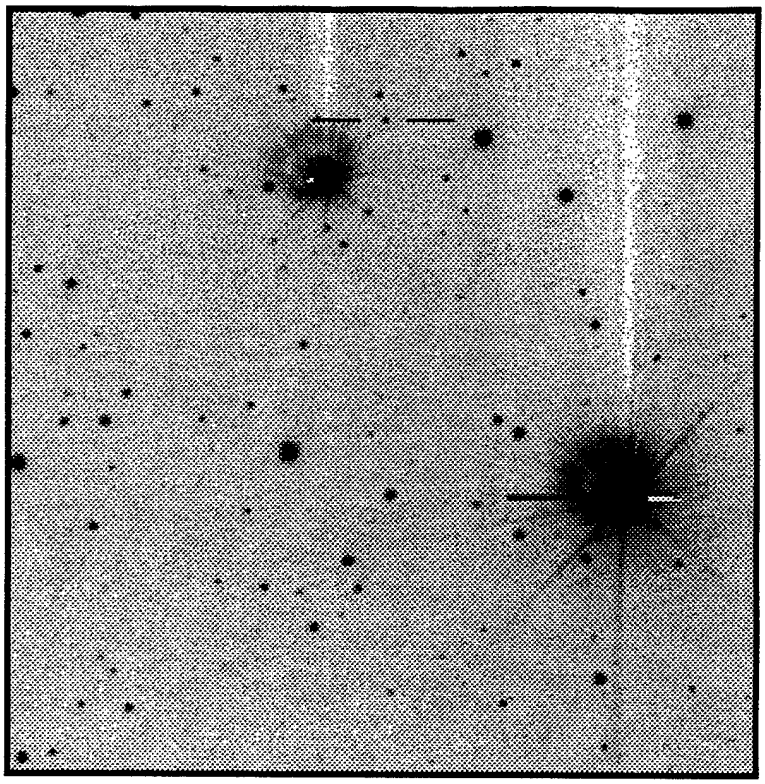
RA : 17 15 57.0
Dec: 28 06 44.6
<V> = 15.090
<B-V> = 0.45
P = 0.528145 days
Epoch = 3385.207
Type: RRab

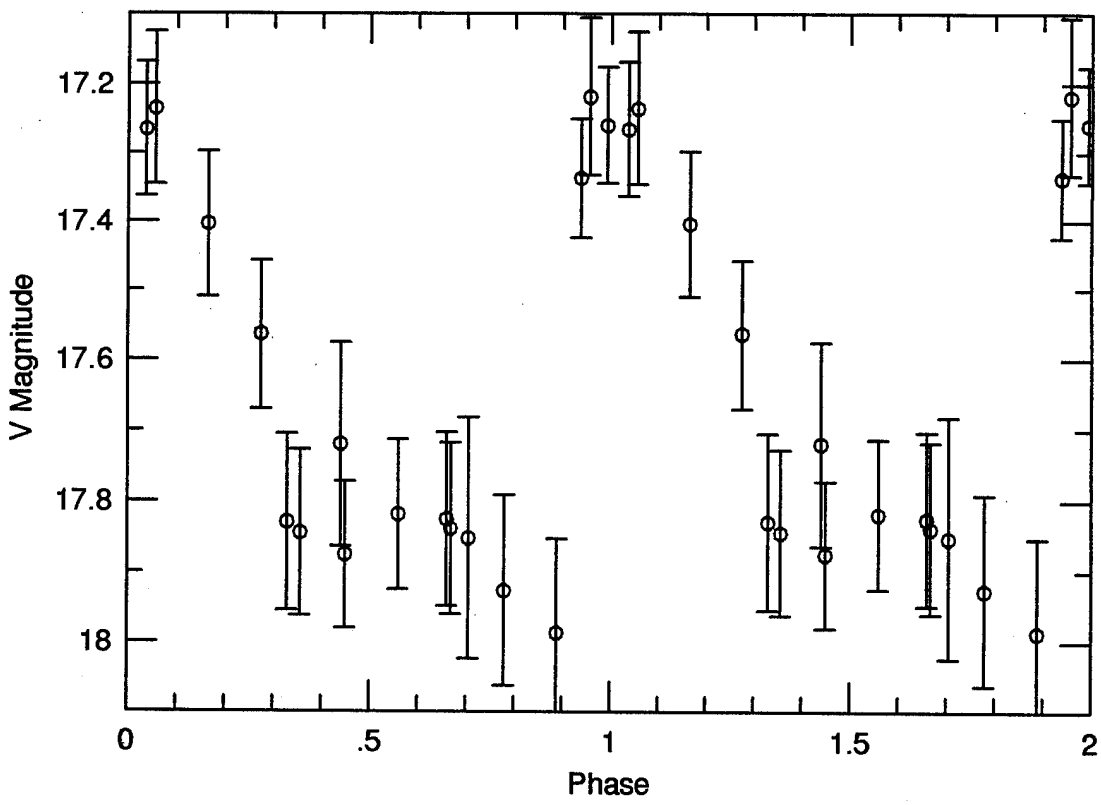
V385 Her



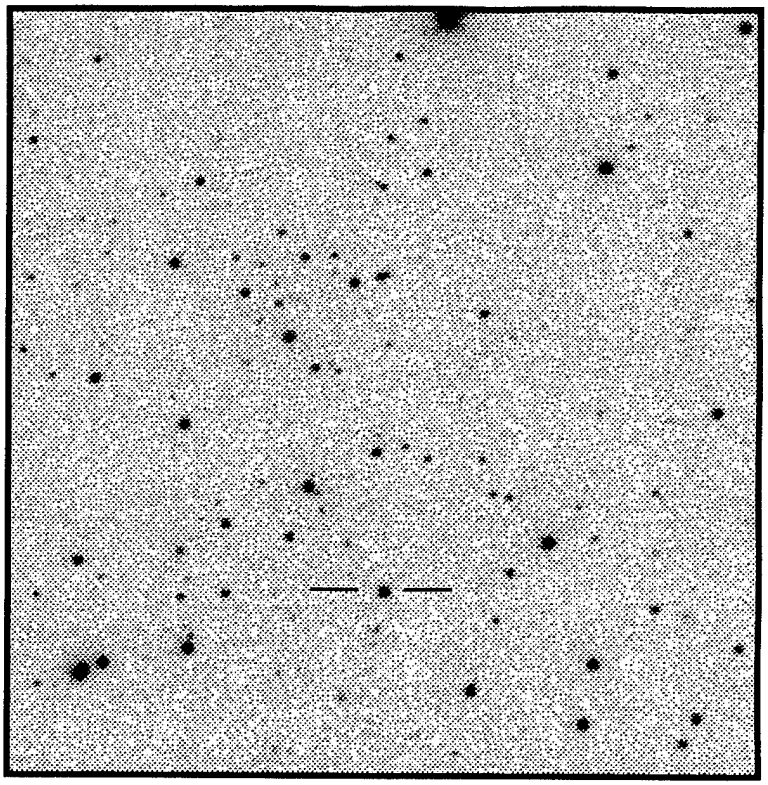


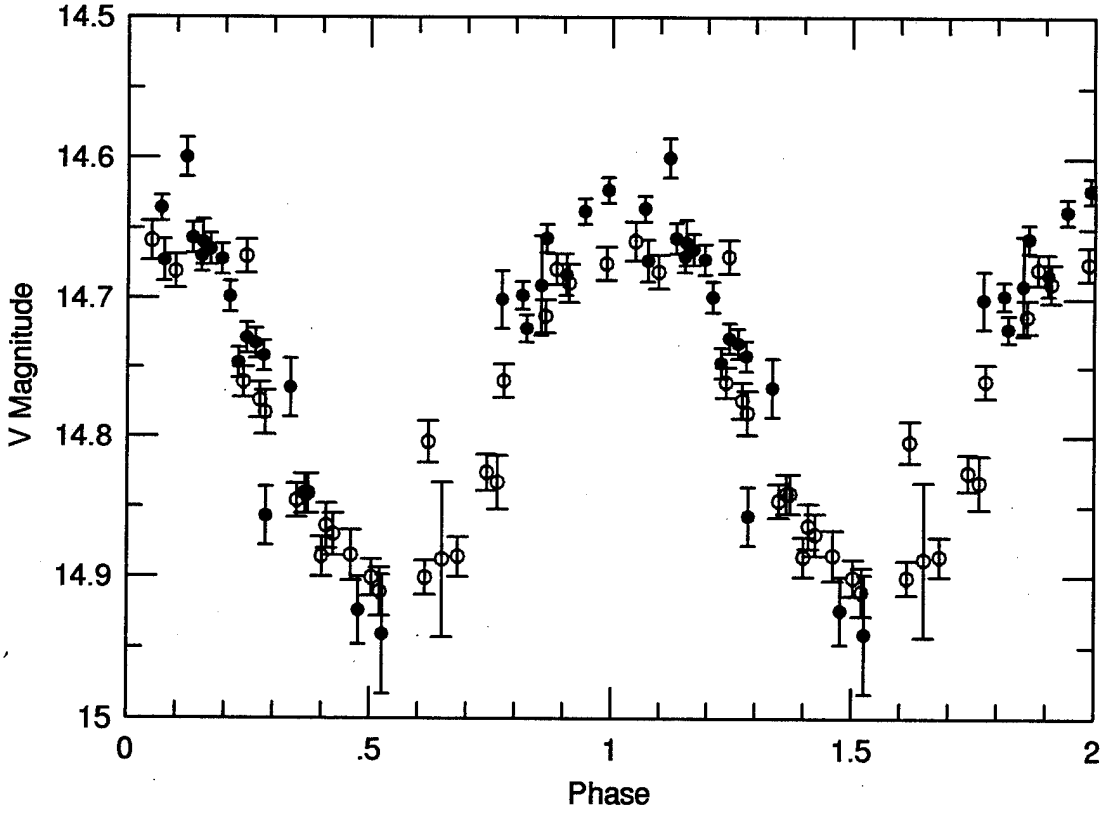
RA : 17 19 06.6
Dec: 28 06 28.2
<V> = 17.637
<B-V> = 0.6
P = 0.47259 days
Epoch = 3385.248
Type: RRab?



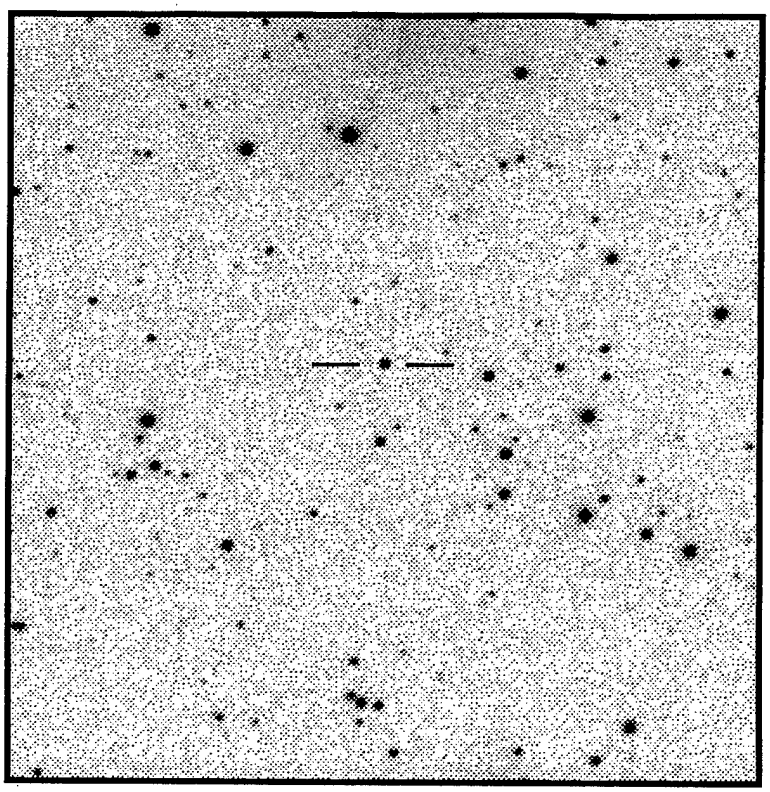


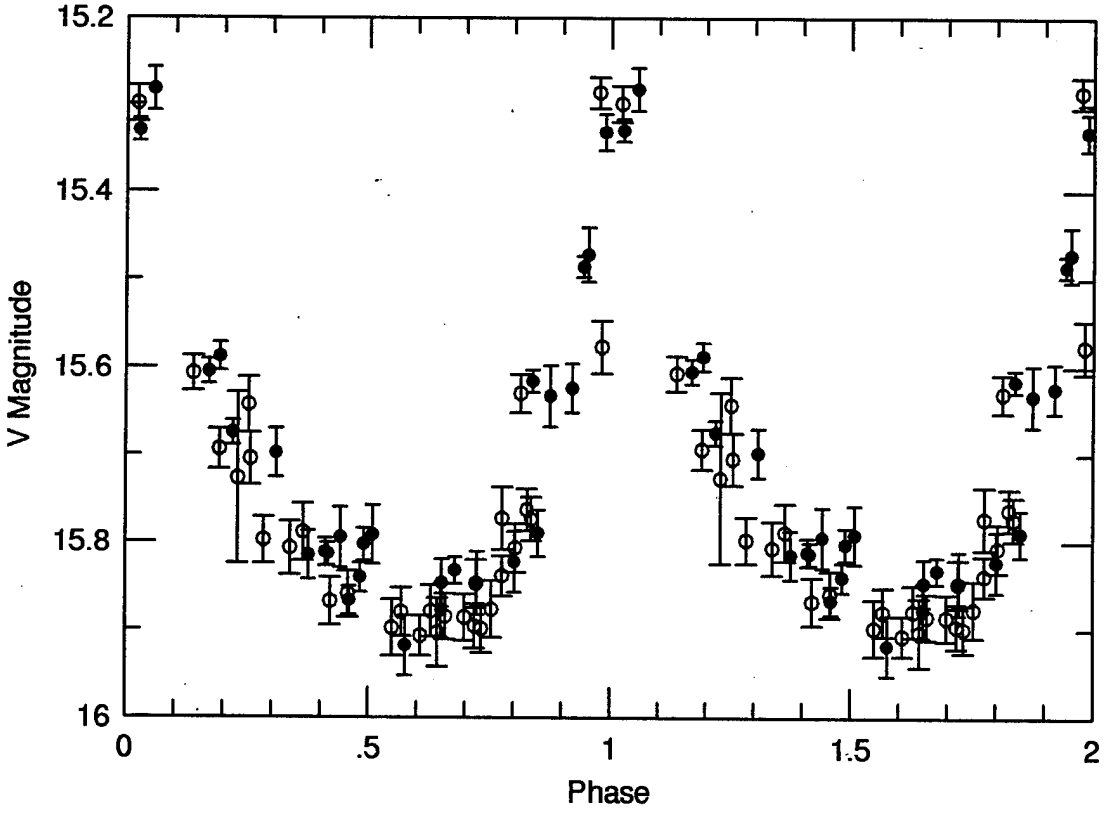
RA : 17 20 58.6
Dec: 28 01 15.2
<V> = 14.768
<B-V> = 0.15
P = 0.295405 days
Epoch = 3469.480
Type: RRc





RA : 17 30 43.1
Dec: 28 03 48.3
<V> = 15.686
<B-V> = 0.15
P = 0.0568927 days
Epoch = 3385.429
Type: SX Phe





RA : 17 41 51.5

Dec: 28 03 53.2

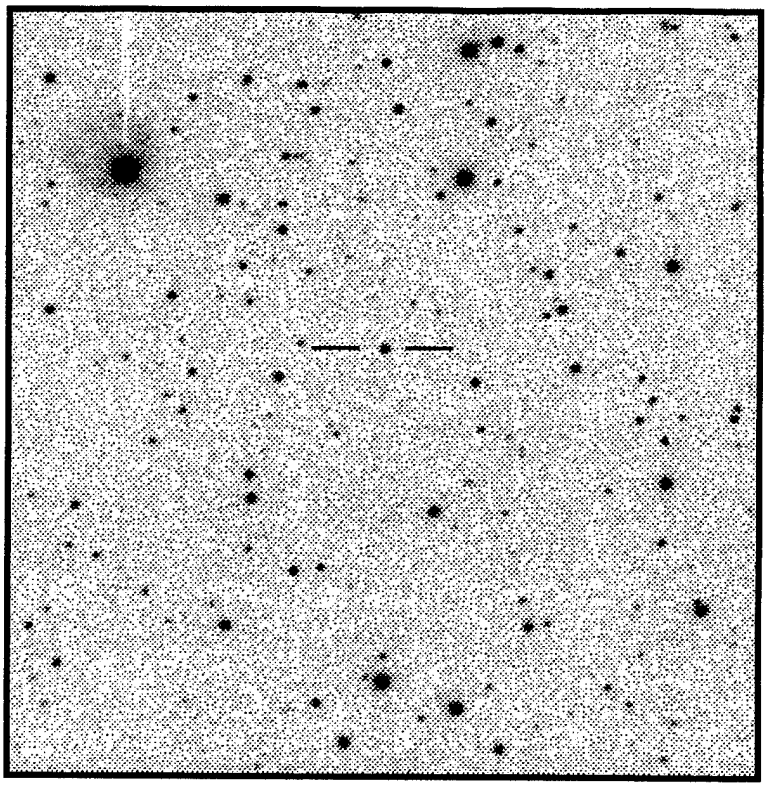
<V> = 15.807

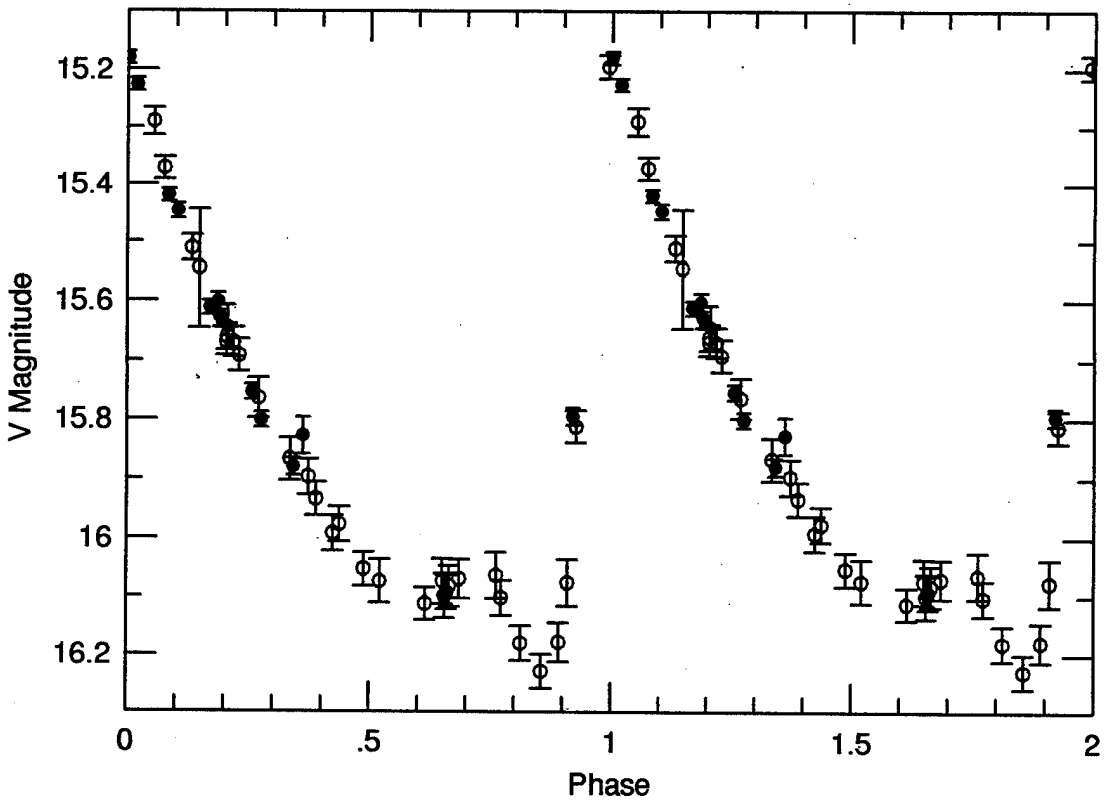
<B-V> = 0.30

P = 0.566966 days

Epoch = 3113.194

Type: RRab





RA : 17 42 40.2

Dec: 28 04 44.7

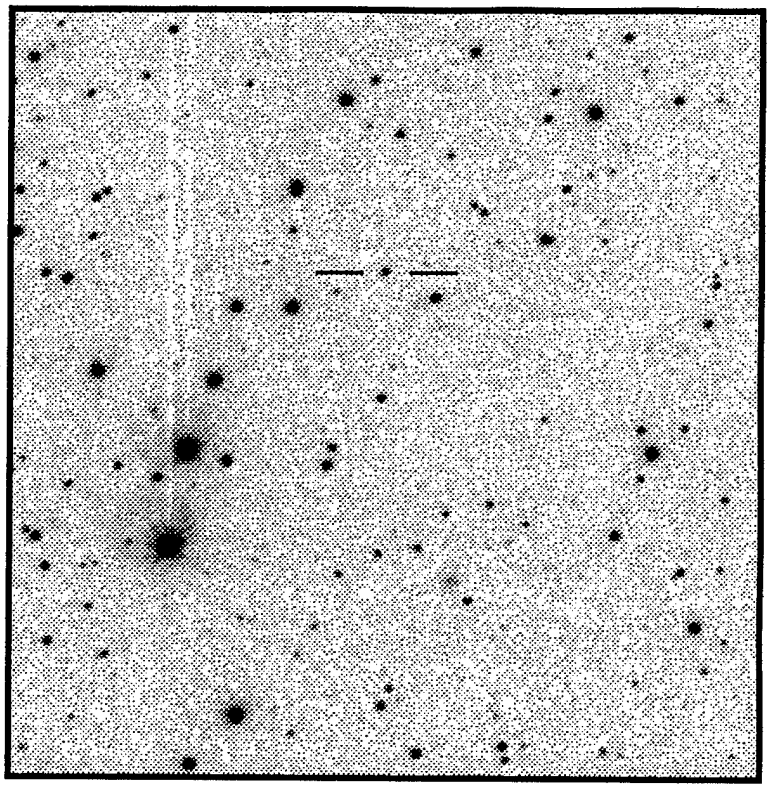
<V> = 16.642

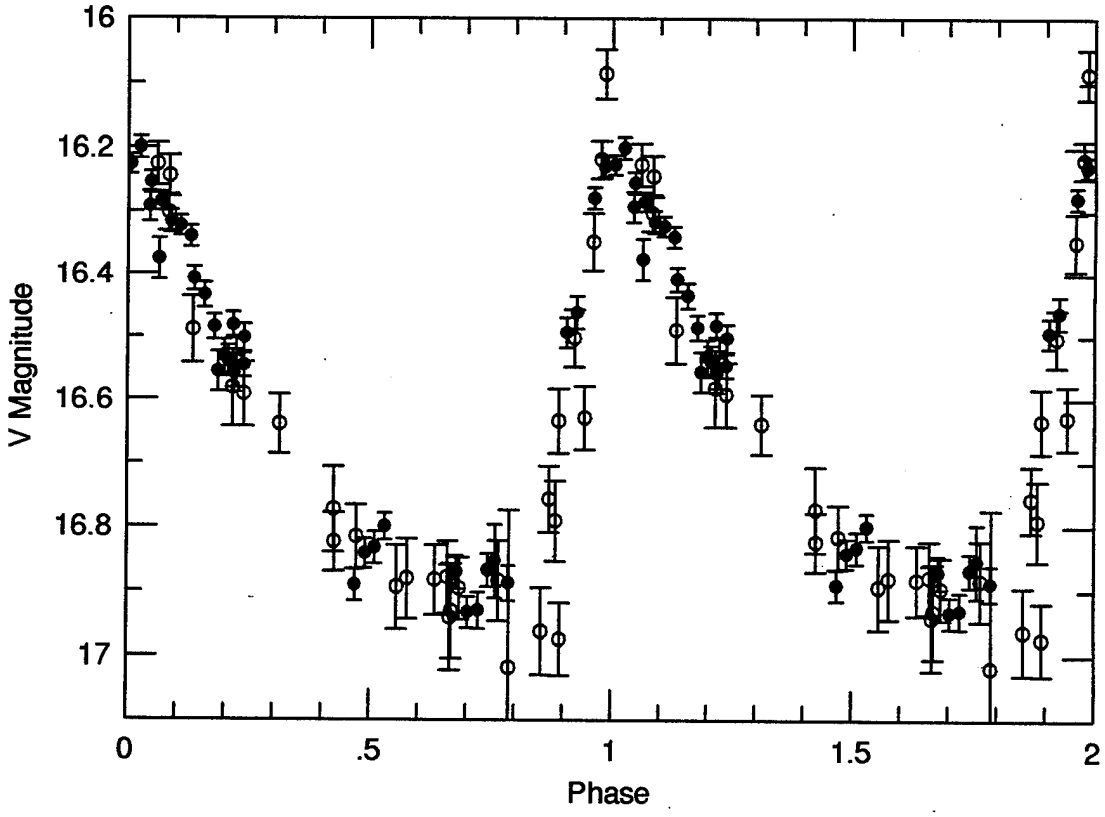
<B-V> = 0.30

P = 0.526354 days

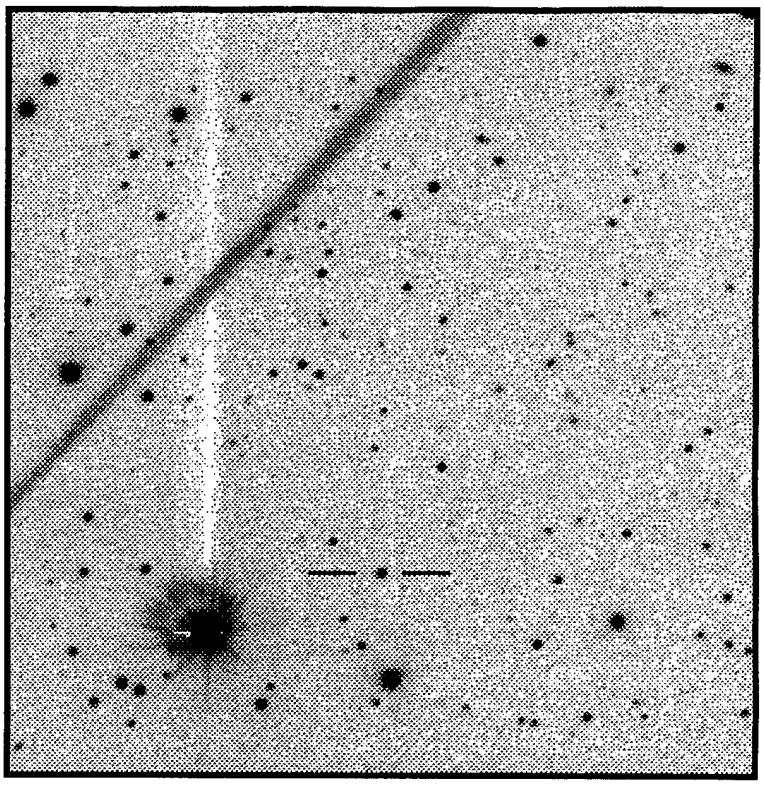
Epoch = 3186.109

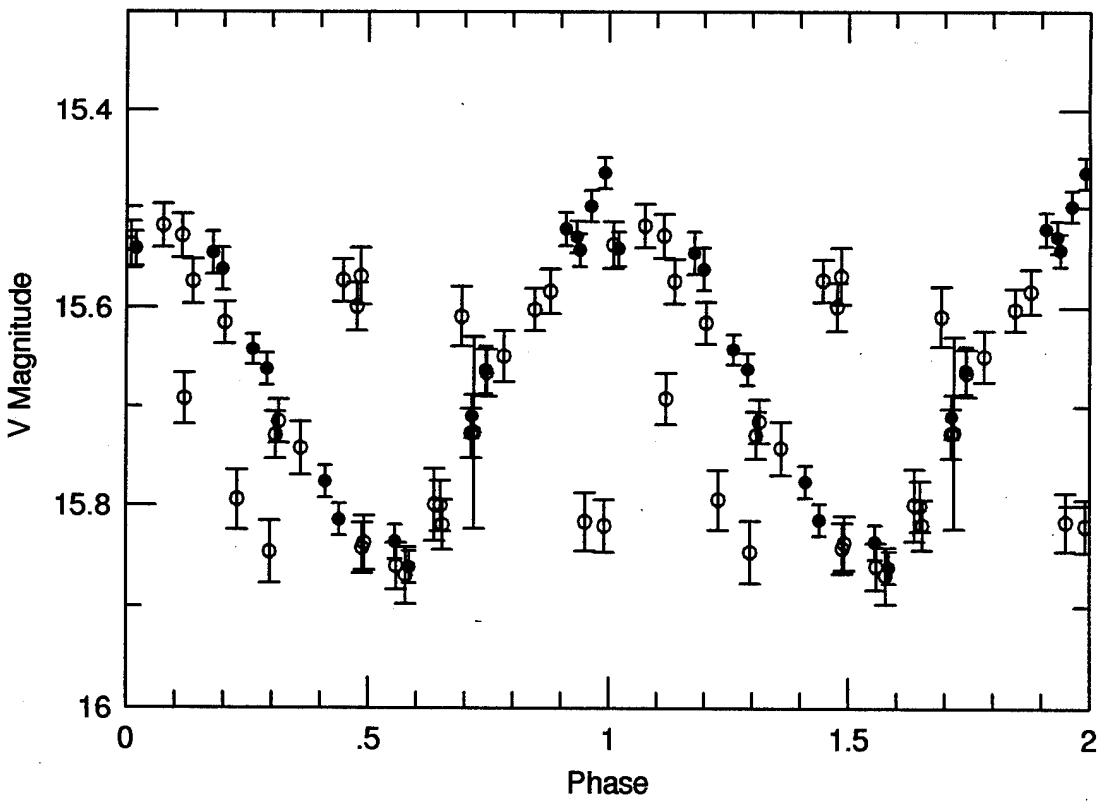
Type: RRab



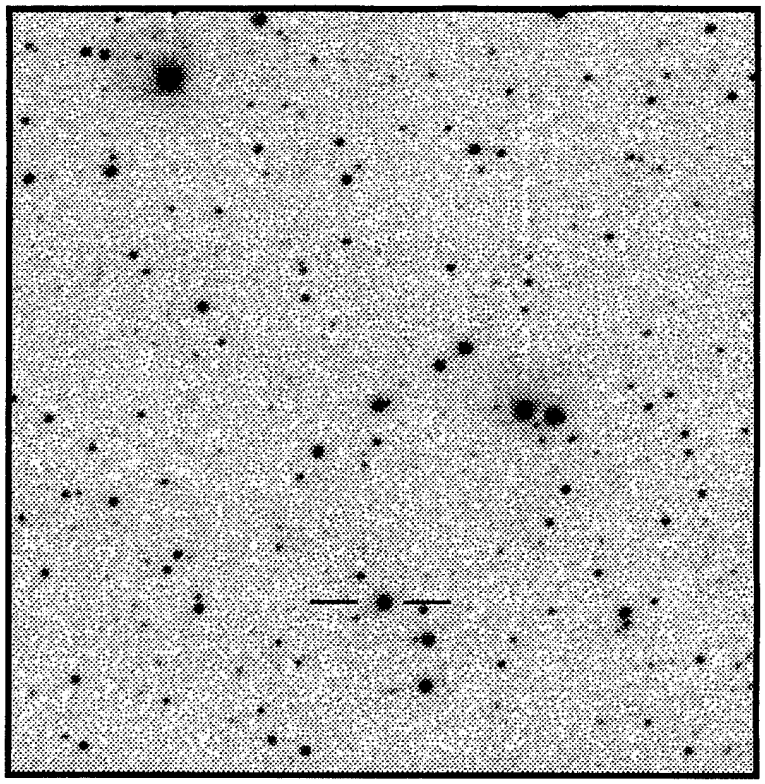


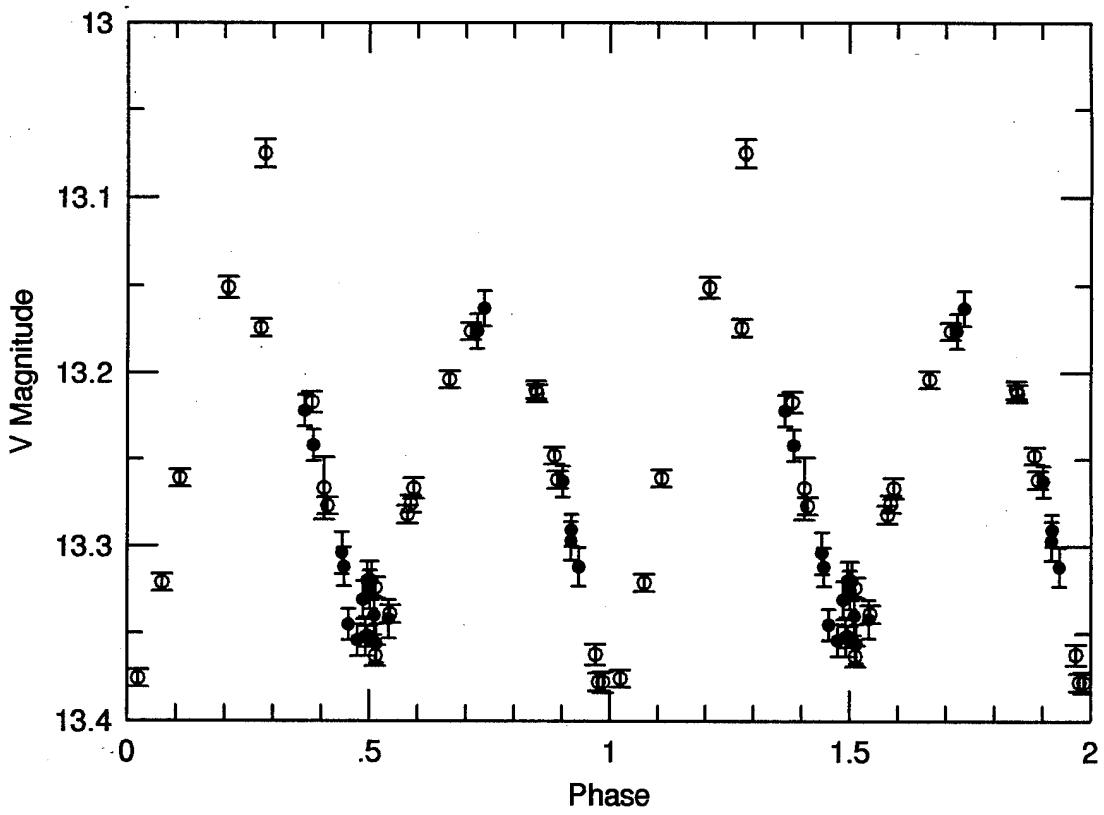
RA : 17 44 19.7
Dec: 28 01 21.6
<V> = 15.666
<B-V> = 0.22
P = 0.377069 days
Epoch = 3487.309
Type: RRc



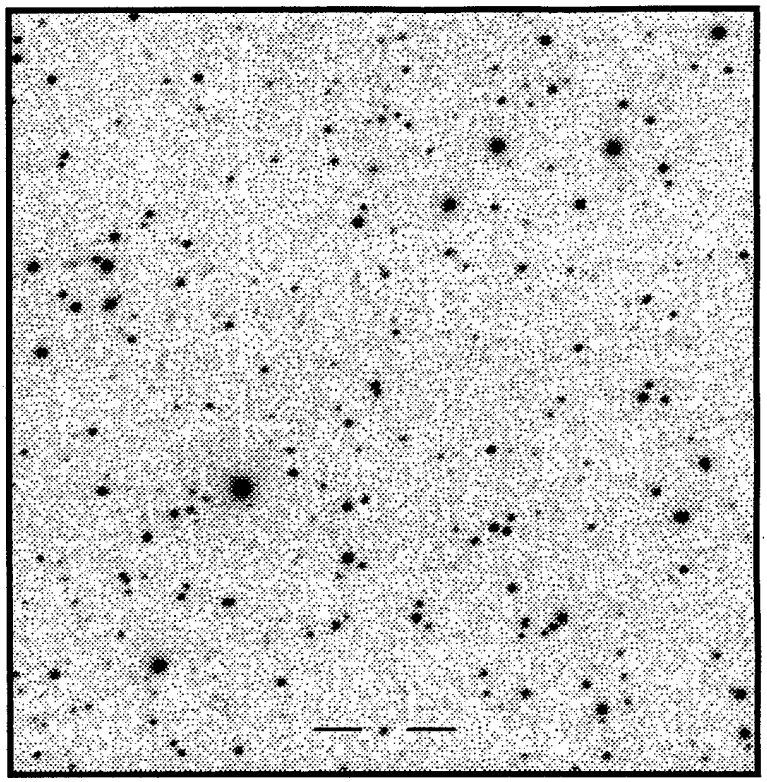


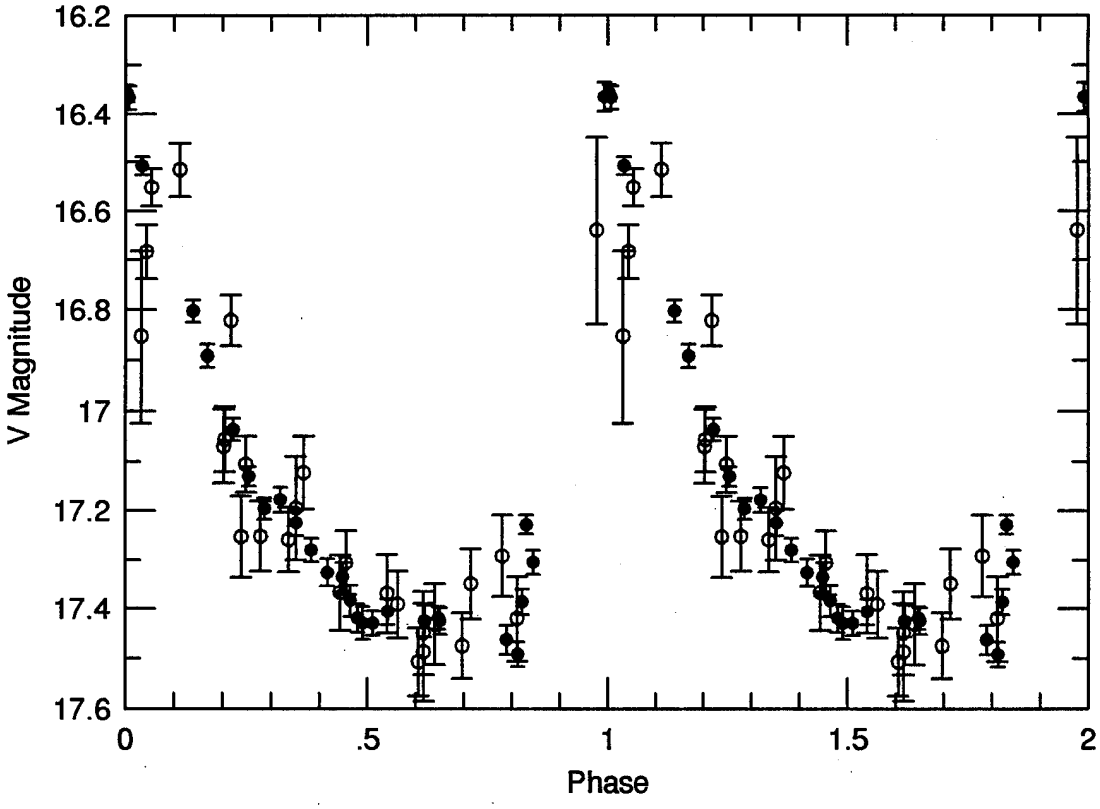
RA : 17 50 17.0
Dec: 28 01 00.0
<V> = 13.244
<B-V> = 0.28
P = 0.695000 days
Epoch = 3474.19
Type: W UMa





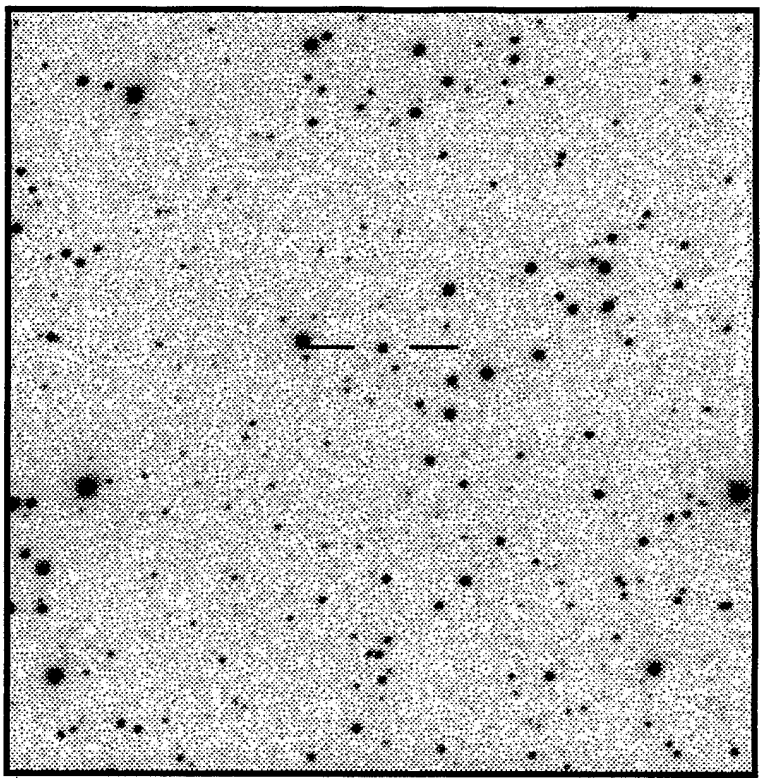
RA : 18 11 01.2
Dec: 27 59 27.4
<V> = 17.072
<B-V> = 0.38
P = 0.454185 days
Epoch = 3181.102
Type: RRab

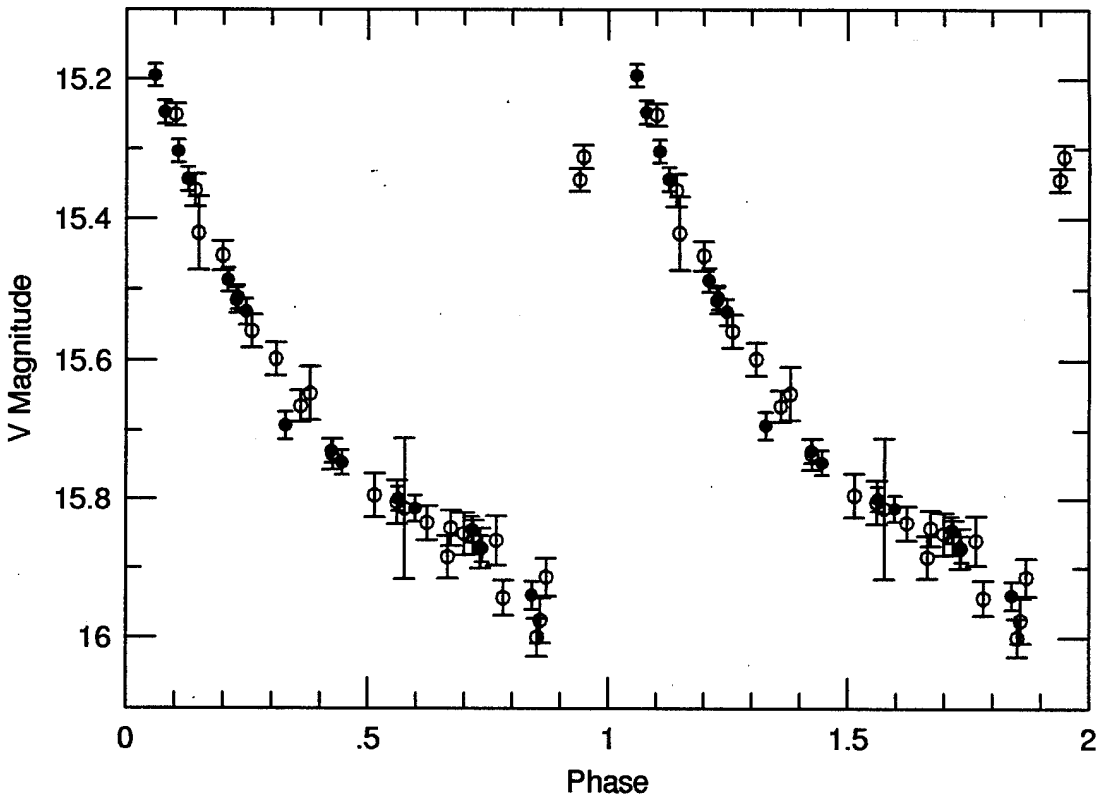




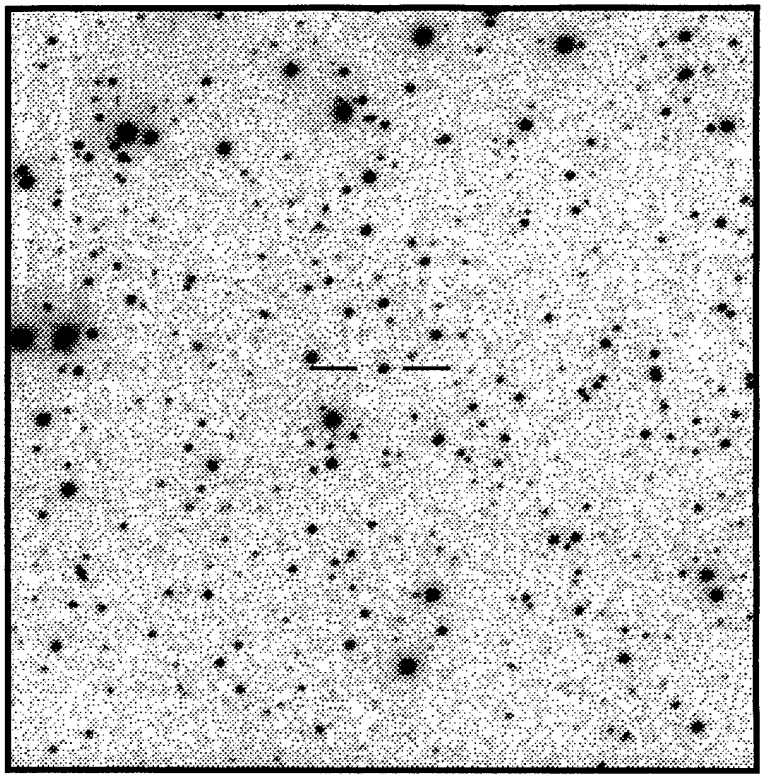
RA : 18 11 26.7
Dec: 28 03 45.4
<V> = 15.610
<B-V> = 0.43
P = 0.541466 days
Epoch = 3169.122
Type: RRab

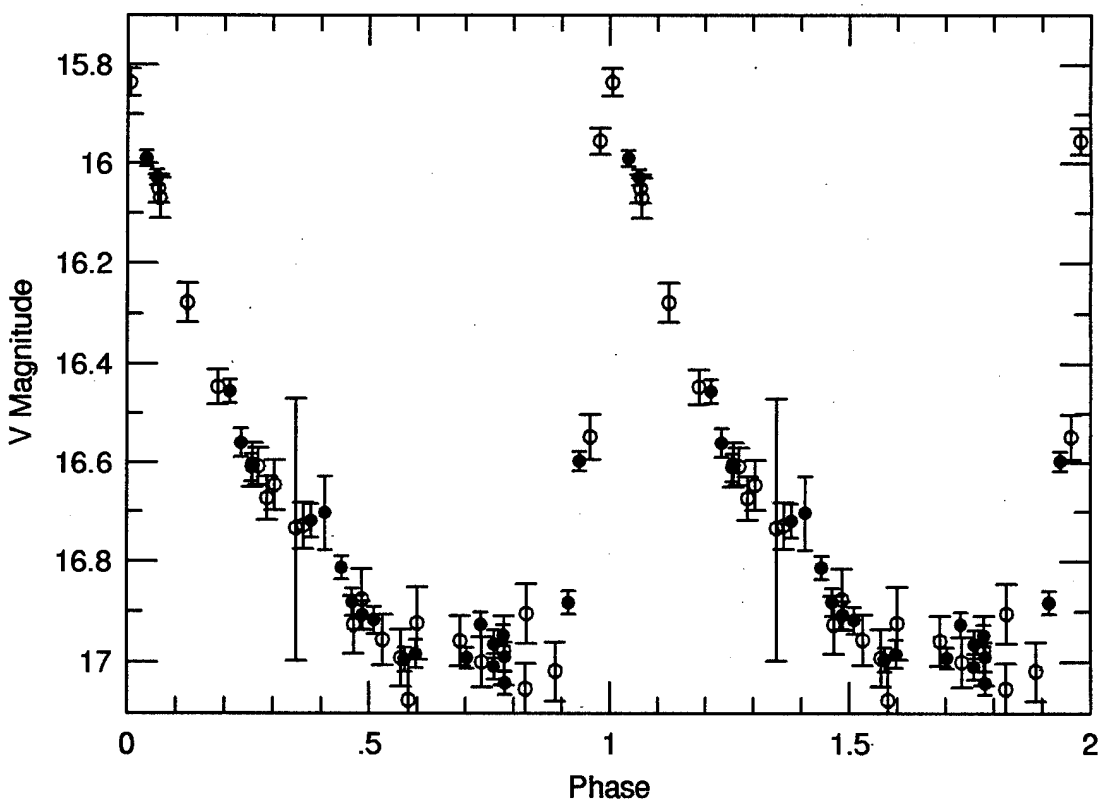
V532 Her



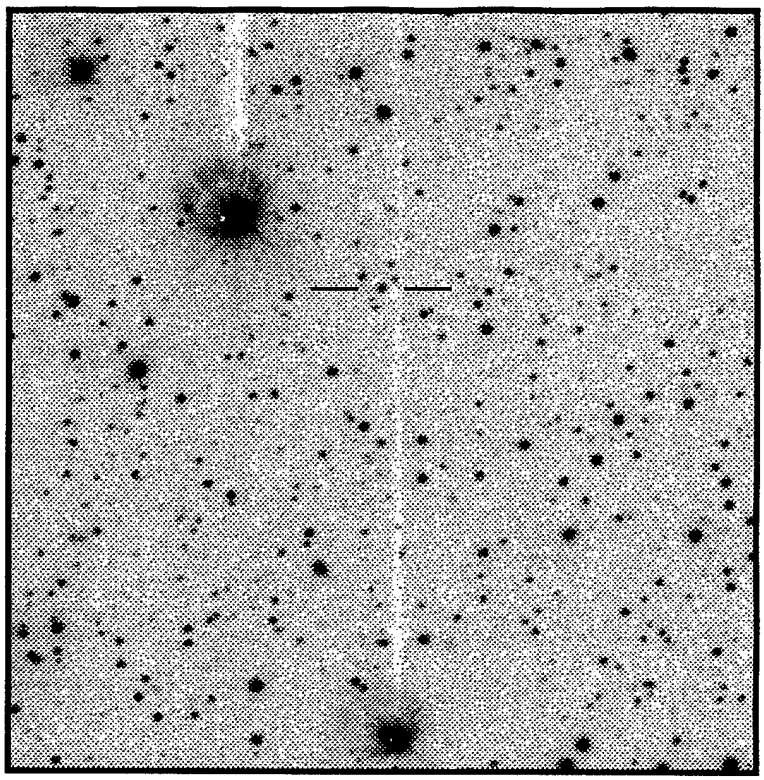


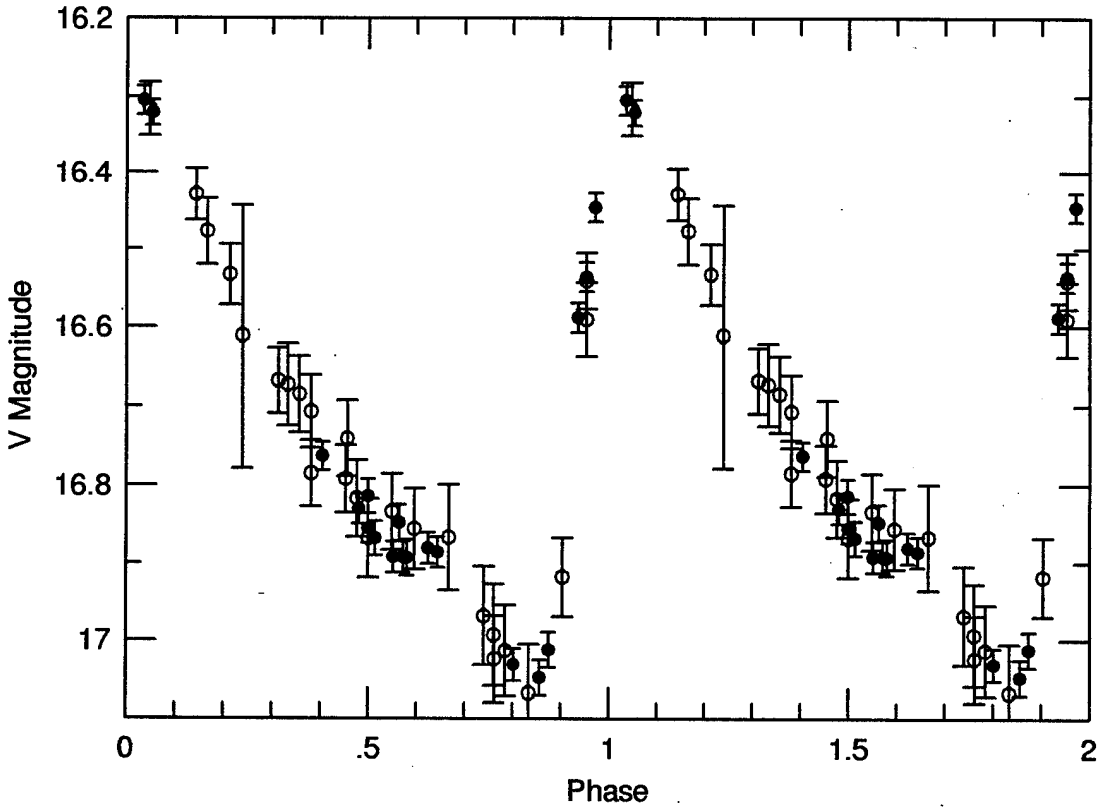
RA : 18 36 06.3
Dec: 28 03 21.6
<V> = 16.621
<B-V> = 0.49
P = 0.484114 days
Epoch = 3175.196
Type: RRab



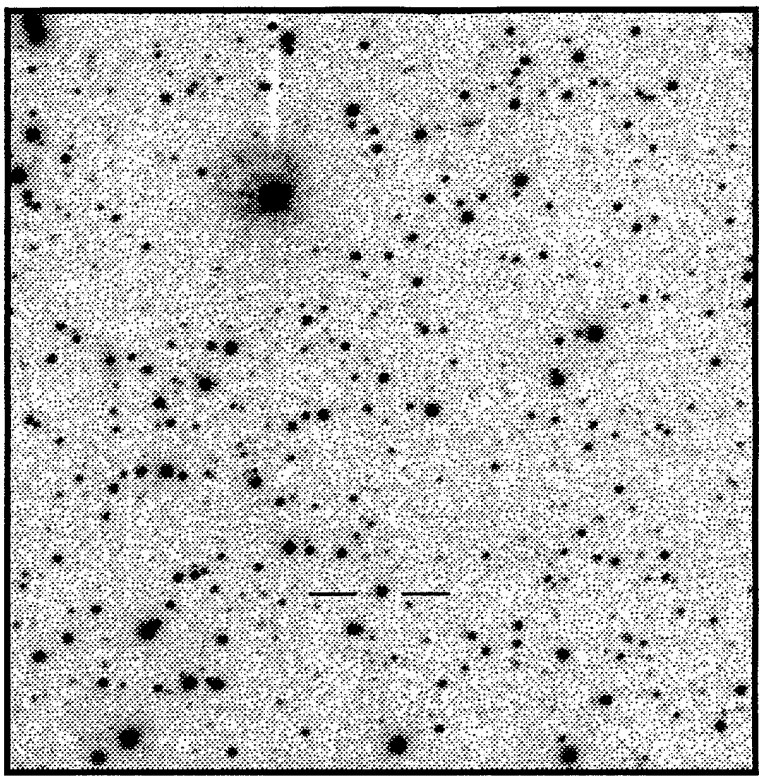


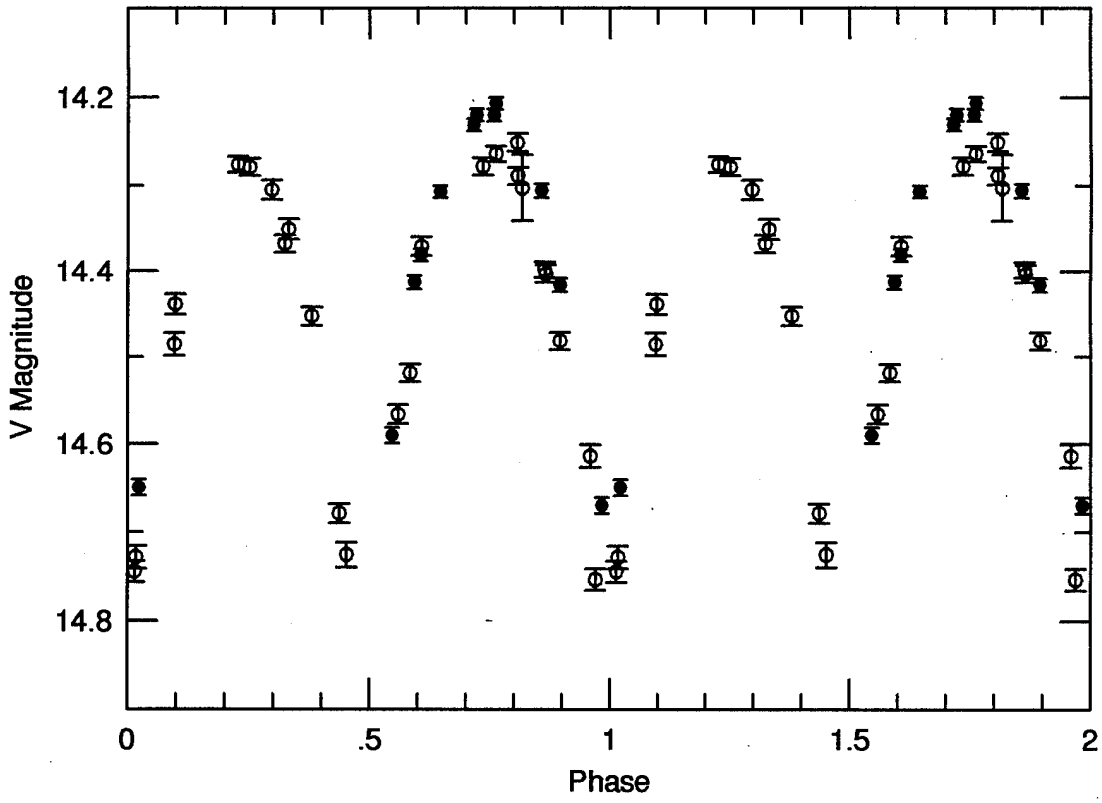
RA : 18 39 18.3
Dec: 28 04 16.6
<V> = 16.698
<B-V> = 0.55
P = 0.709921 days
Epoch = 3516.300
Type: RRab



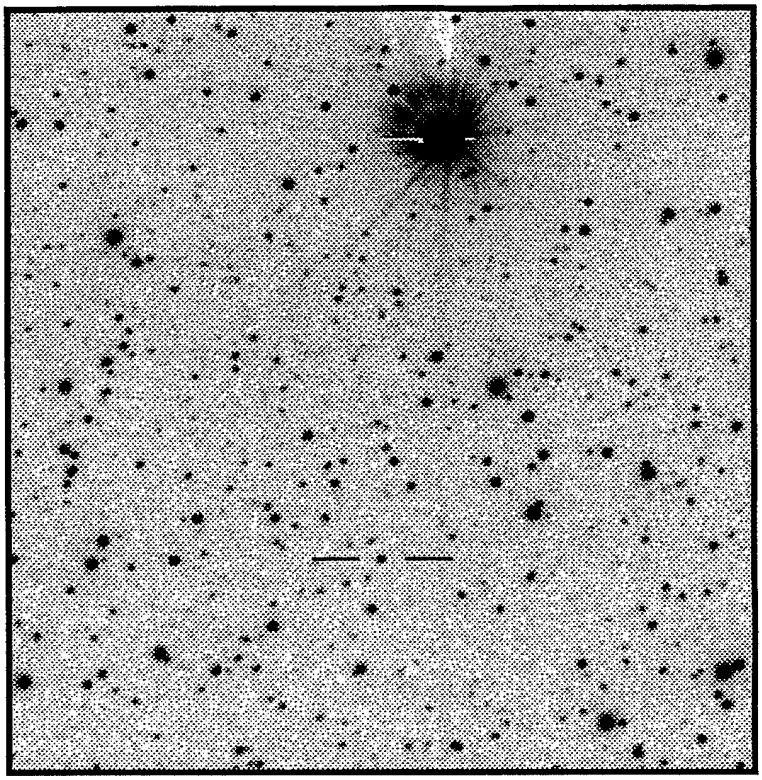


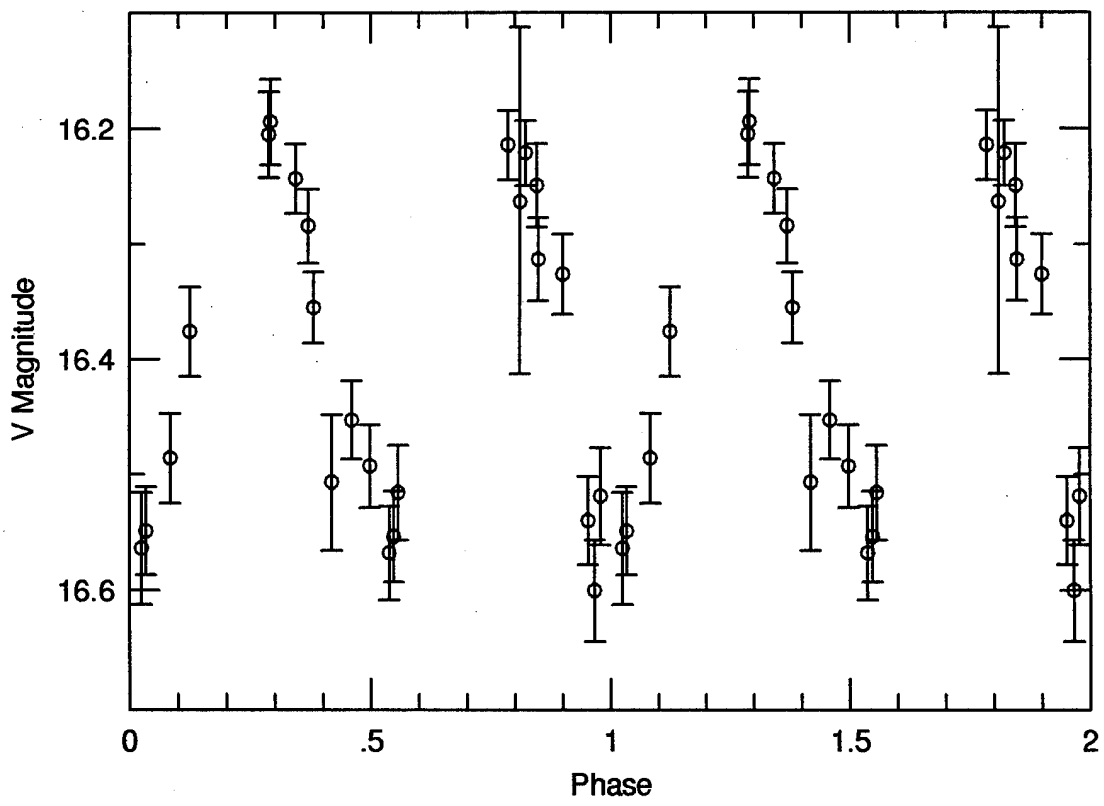
RA : 18 40 18.8
Dec: 28 00 54.1
<V> = 14.427
<B-V> = 0.52
P = 0.366912 days
Epoch = 3473.422
Type: W UMa



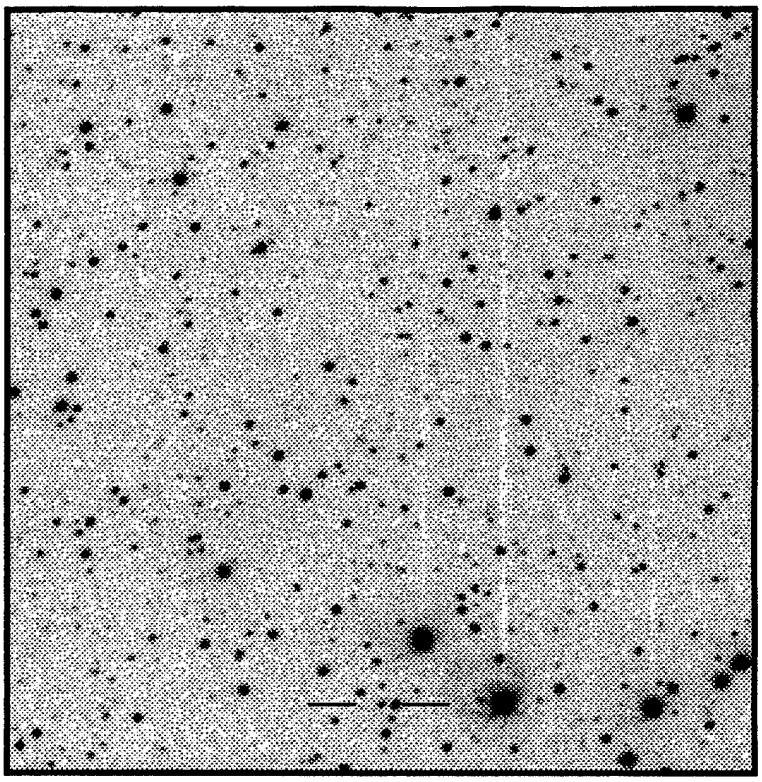


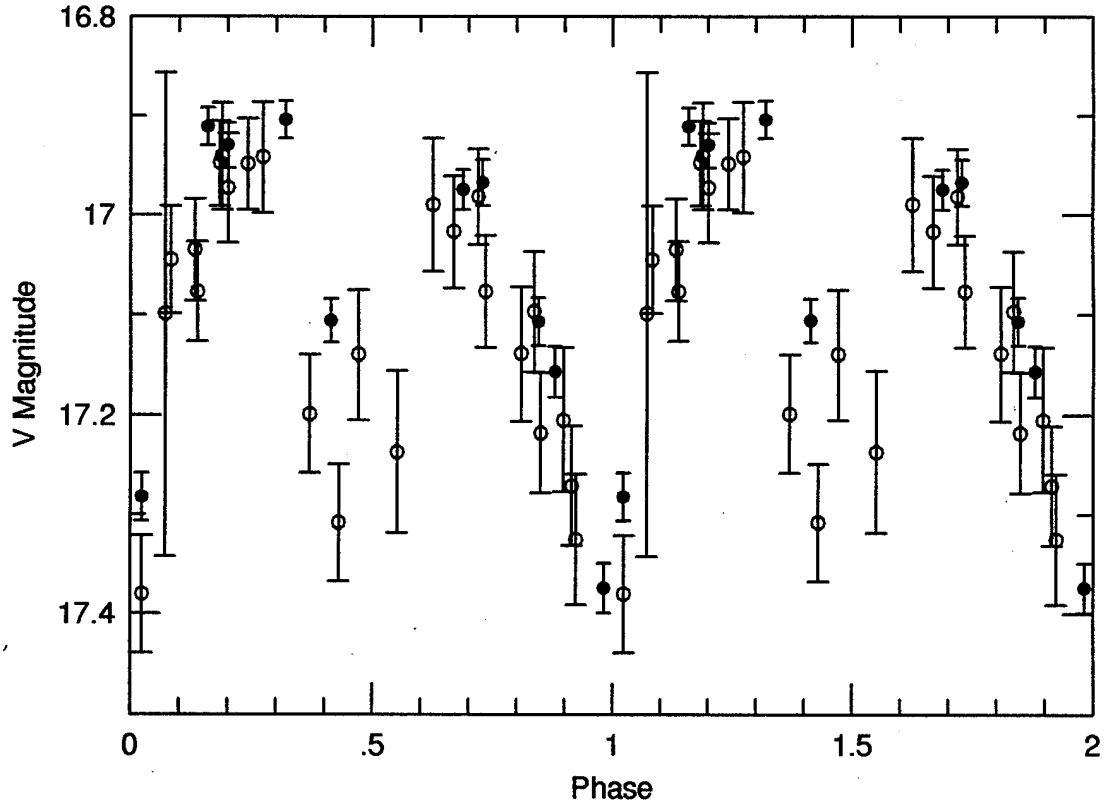
RA : 18 43 15.3
Dec: 28 01 14.7
<V> = 16.373
<B-V> = 0.66
P = 0.656278 days
Epoch = 3473.717
Type: W UMa



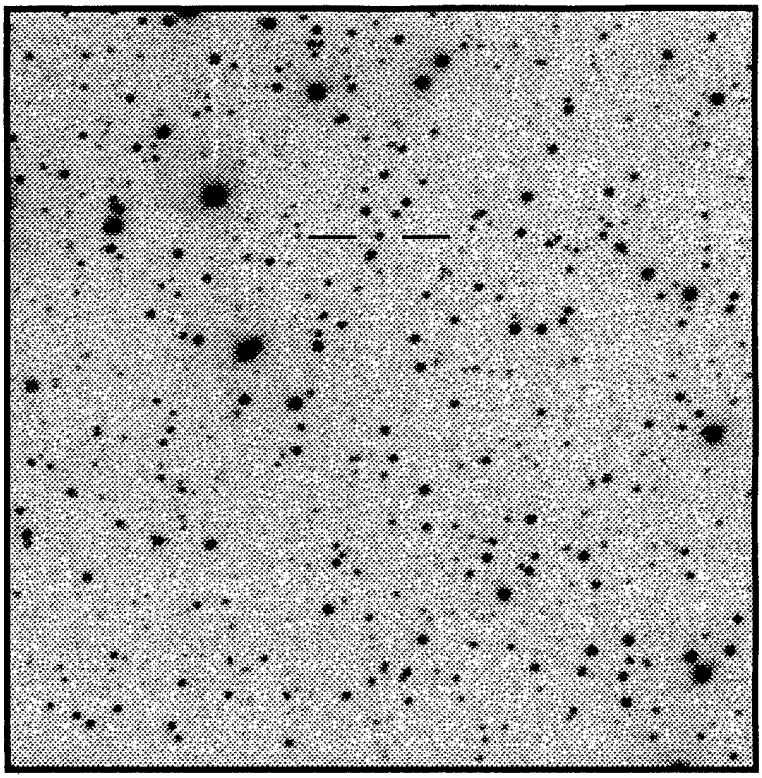


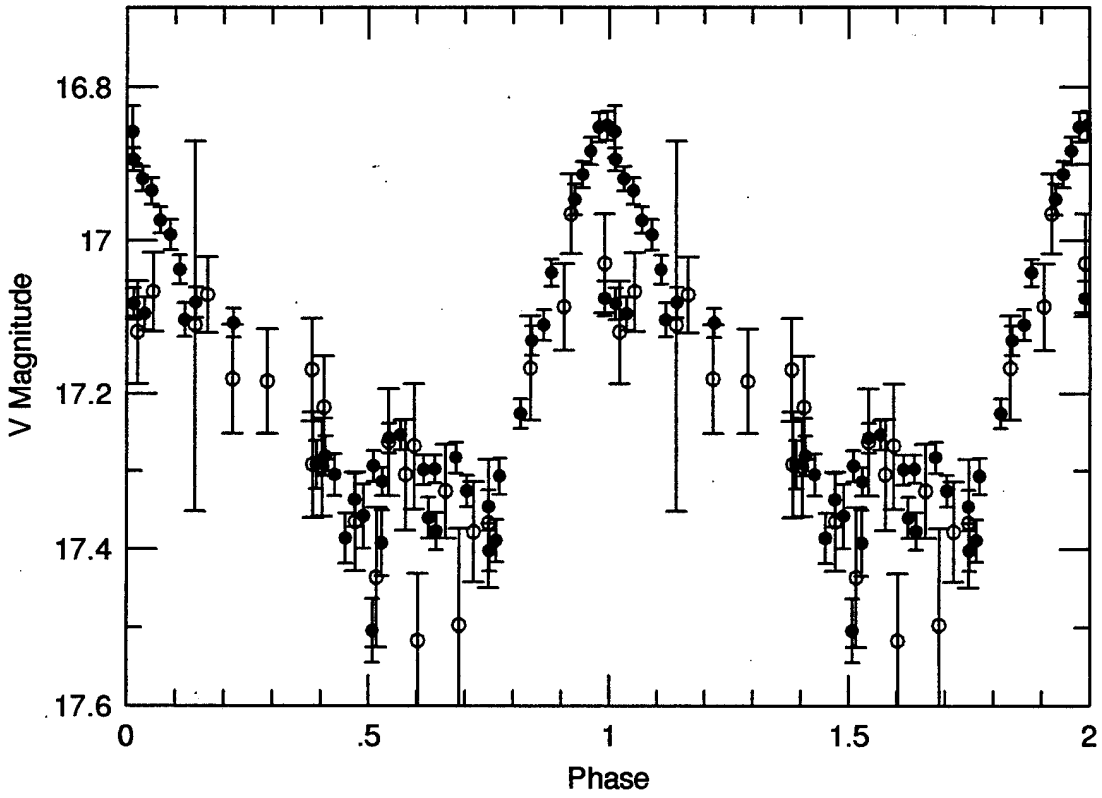
RA : 18 44 20.6
Dec: 27 59 36.6
<V> = 17.103
<B-V> = 0.45
P = 0.345930 days
Epoch = 3481.409
Type: W UMa





RA : 18 47 46.9
Dec: 28 04 47.0
<V> = 17.175
<B-V> = 0.65
P = 0.764461 days
Epoch = 3488.260
Type: RRab B





RA : 19 03 50.4

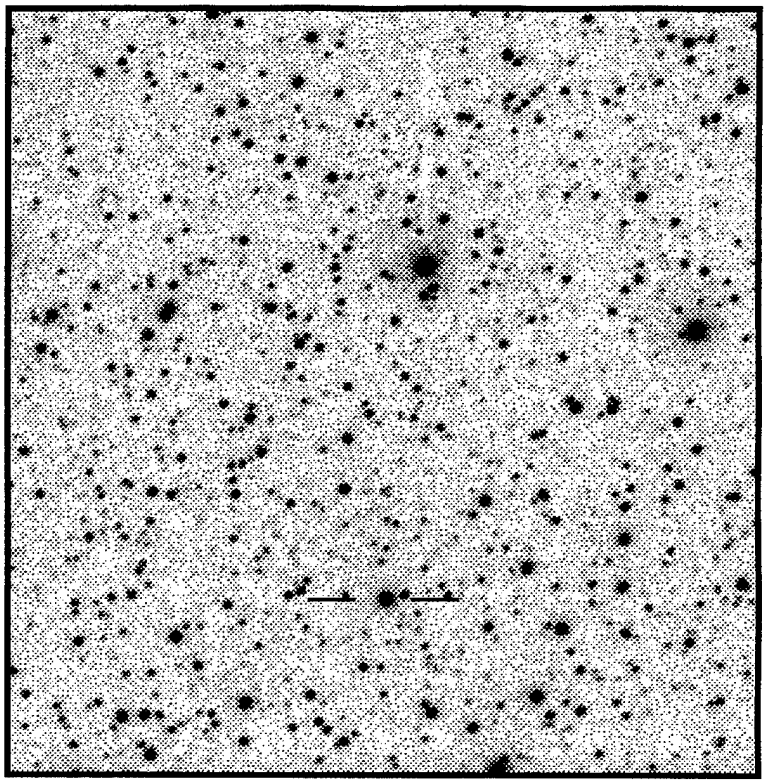
Dec: 28 00 44.9

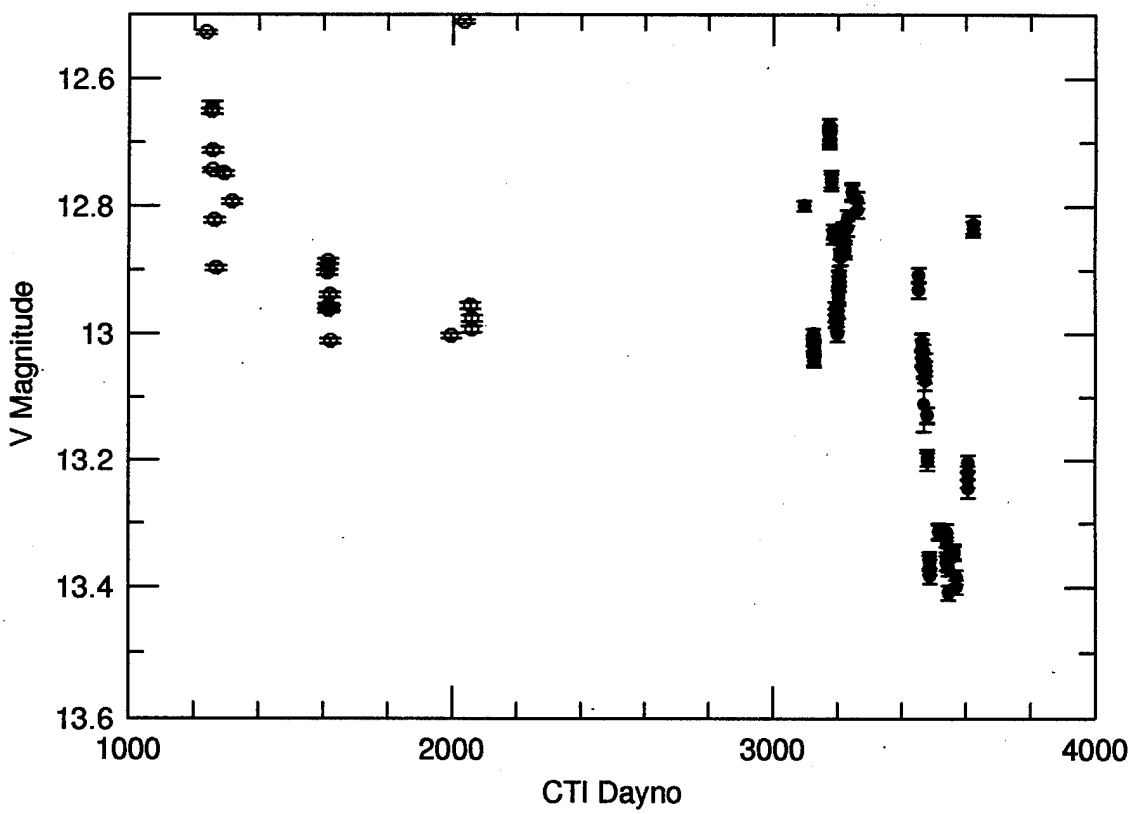
<V> = 12.976

<B-V> = 1.75

Type: Irregular

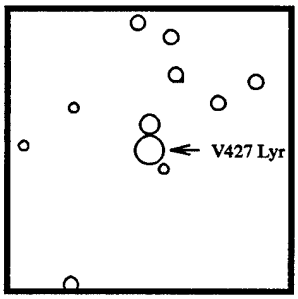
GS Lyr

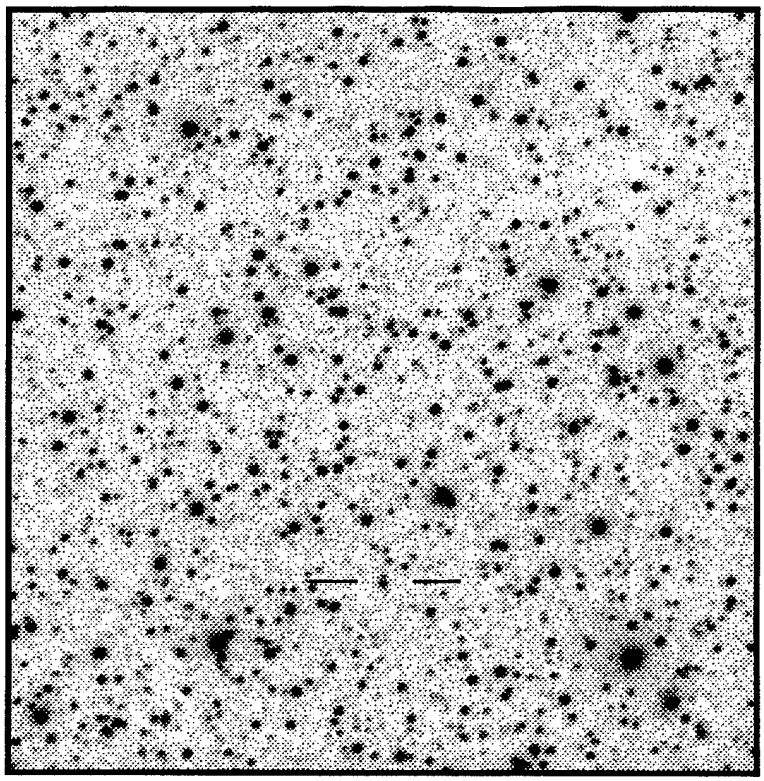


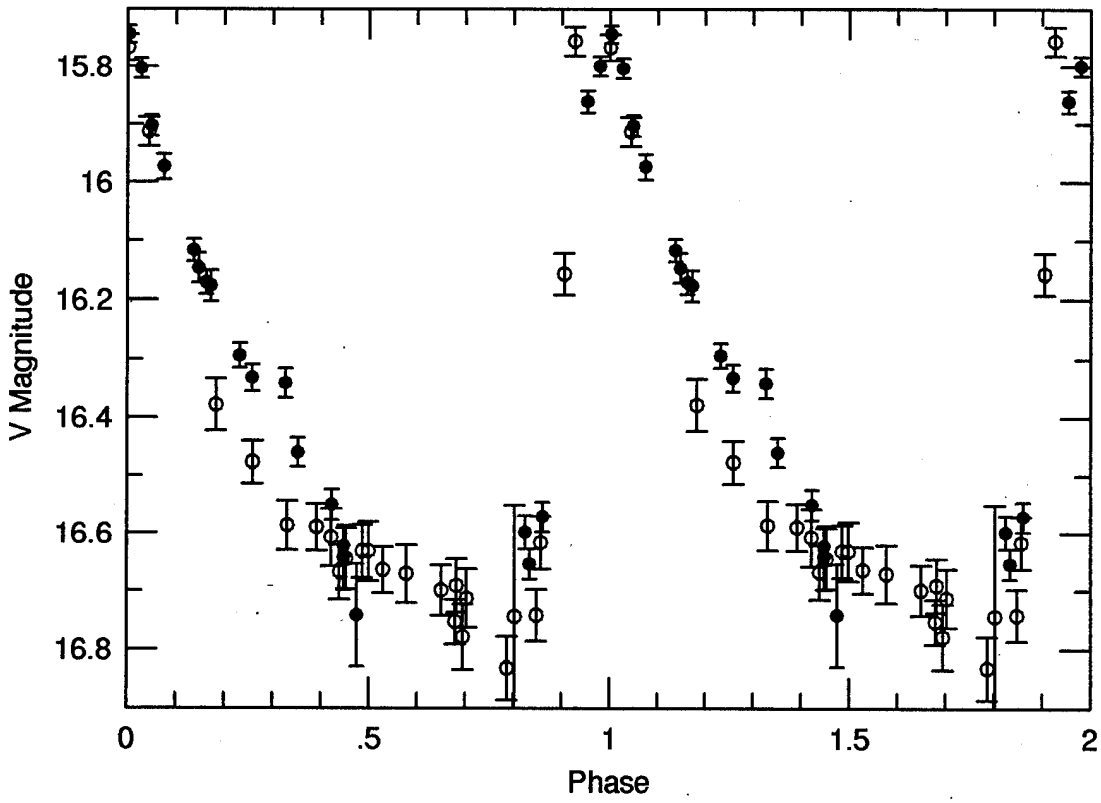


RA : 19 13 11.8
Dec: 28 00 51.5
<V> = 16.359
<B-V> = 0.60
P = 0.424599 days
Epoch = 3474.433
Type: RRab

V427 Lyr

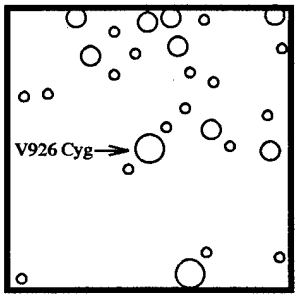


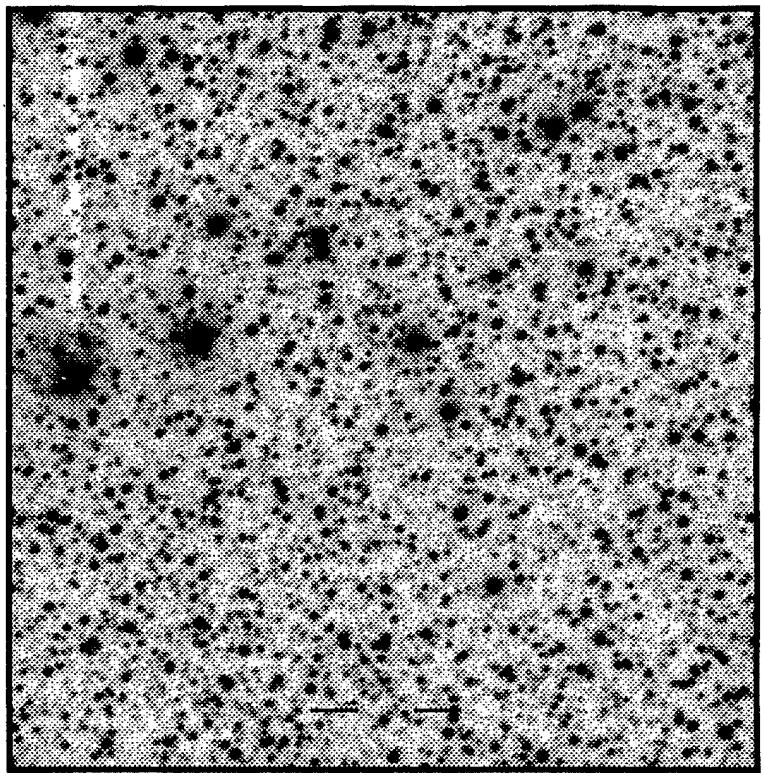


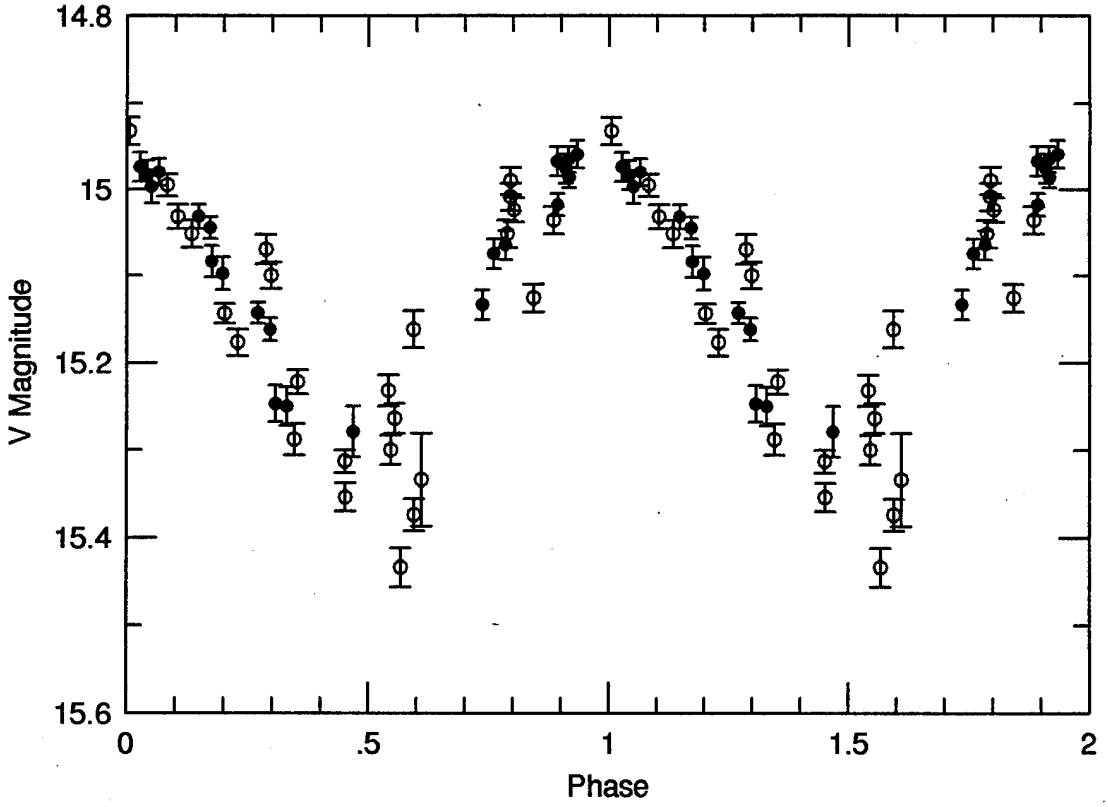


RA : 19 38 06.6
Dec: 27 59 09.9
<V> = 15.131
<B-V> = 0.60
P = 0.306999 days
Epoch = 3488.337
Type: RRc

V926 Cyg







RA : 21 07 16.1

Dec: 28 02 29.2

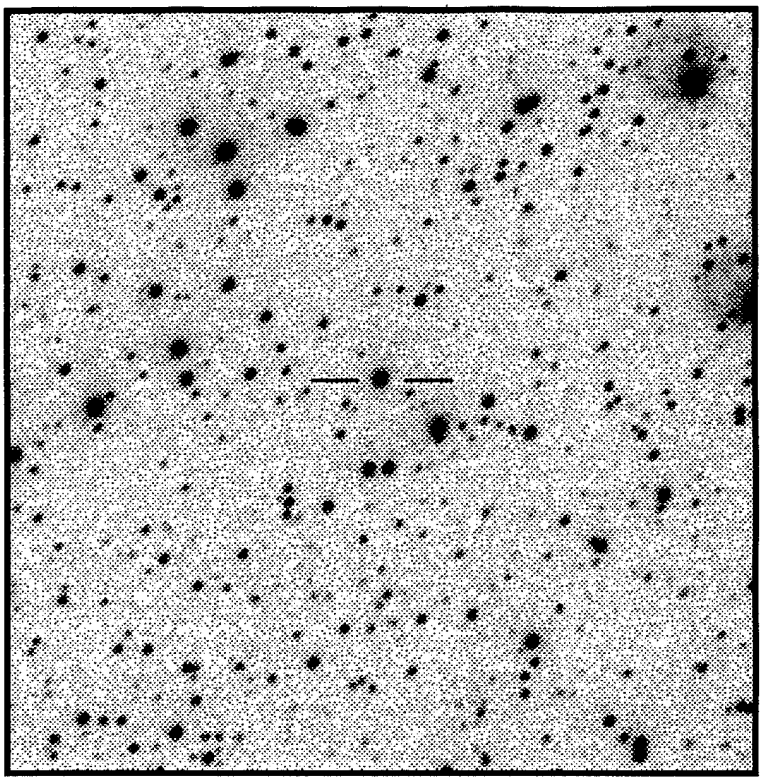
<V> = 12.894

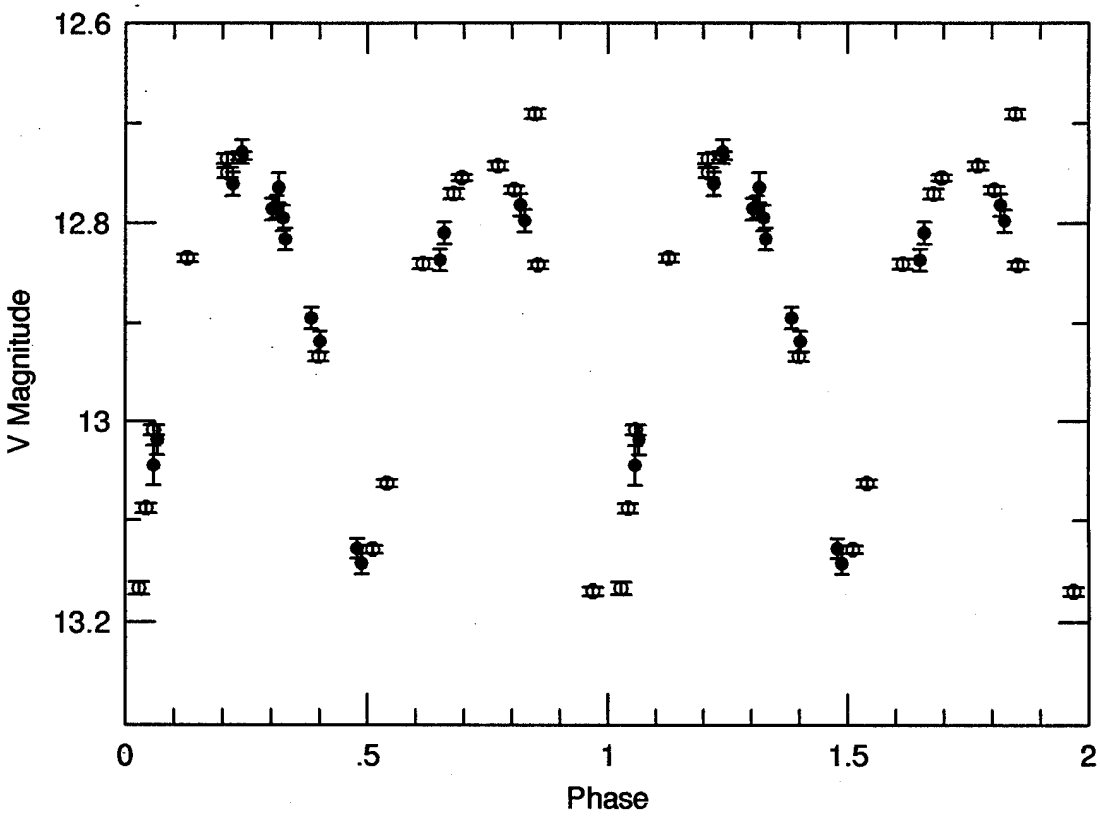
<B-V> = 0.42

P = 0.438854 days

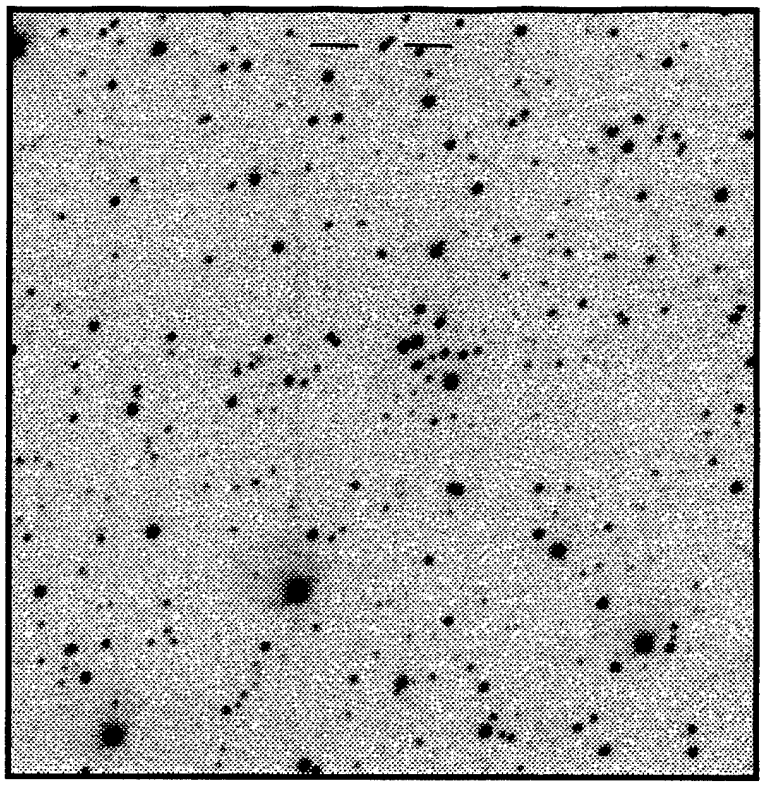
Epoch = 3517.448

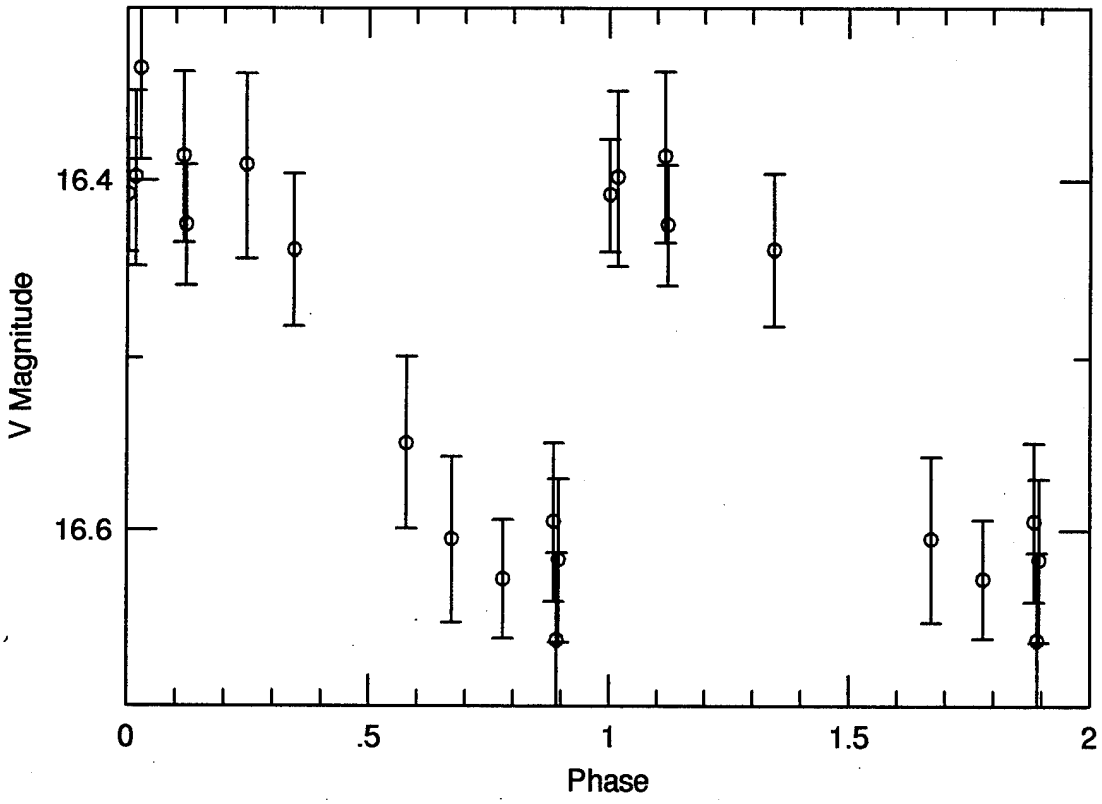
Type: W UMa



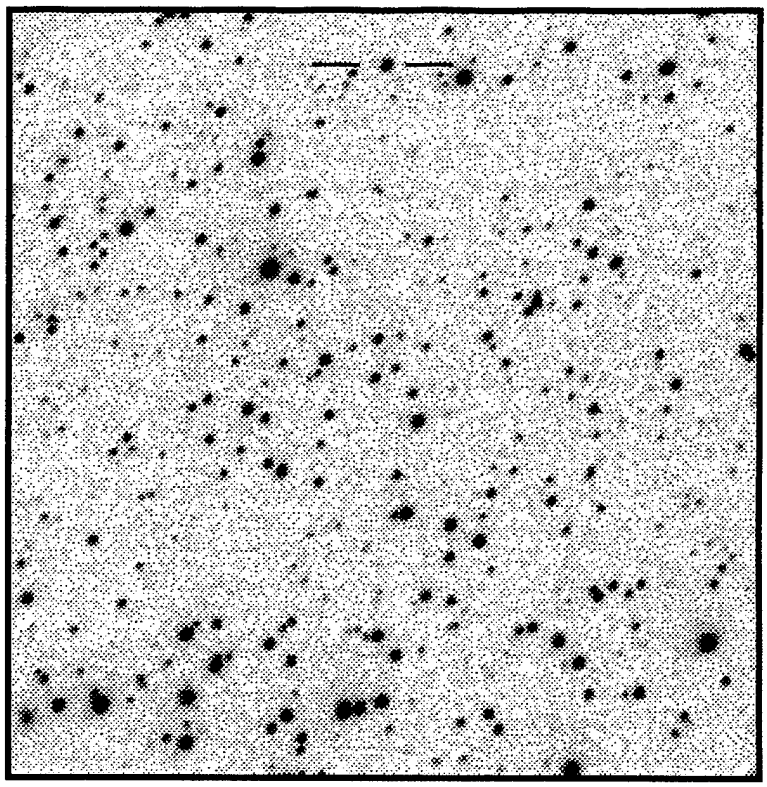


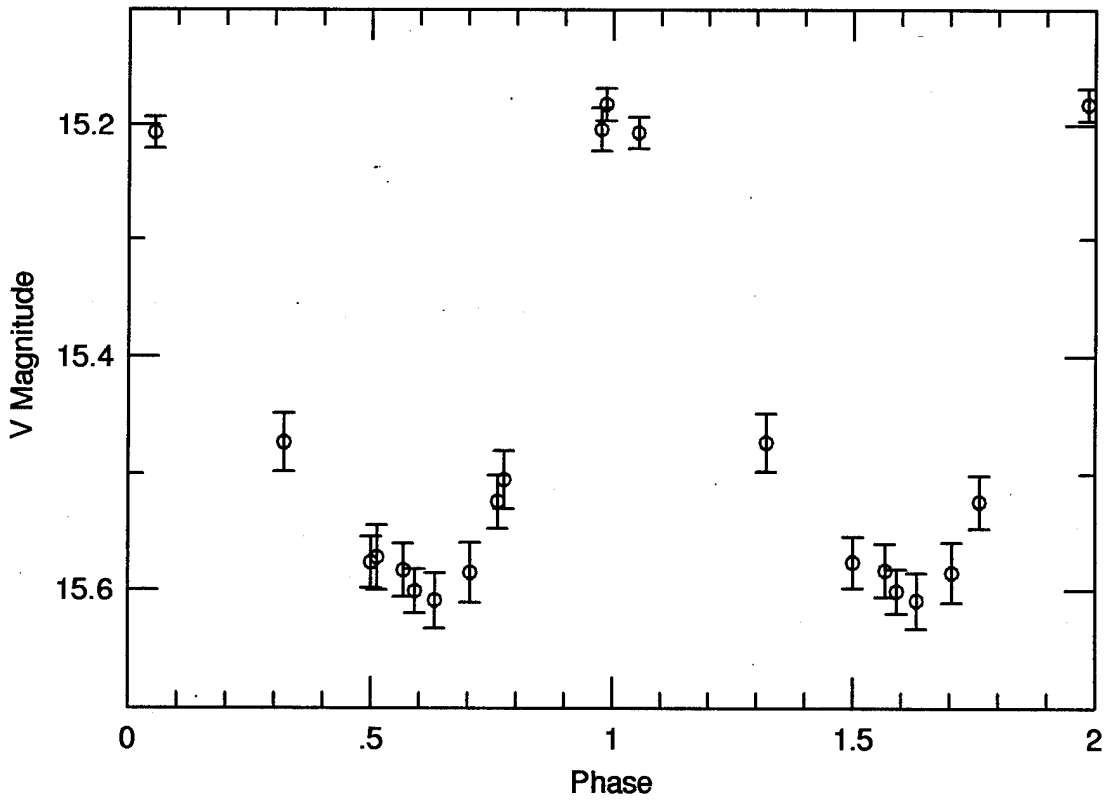
RA : 21 20 11.2
Dec: 28 06 09.3
<V> = 16.493
<B-V> = 0.43
P = 0.448676 days
Epoch = 3517.381
Type: RR



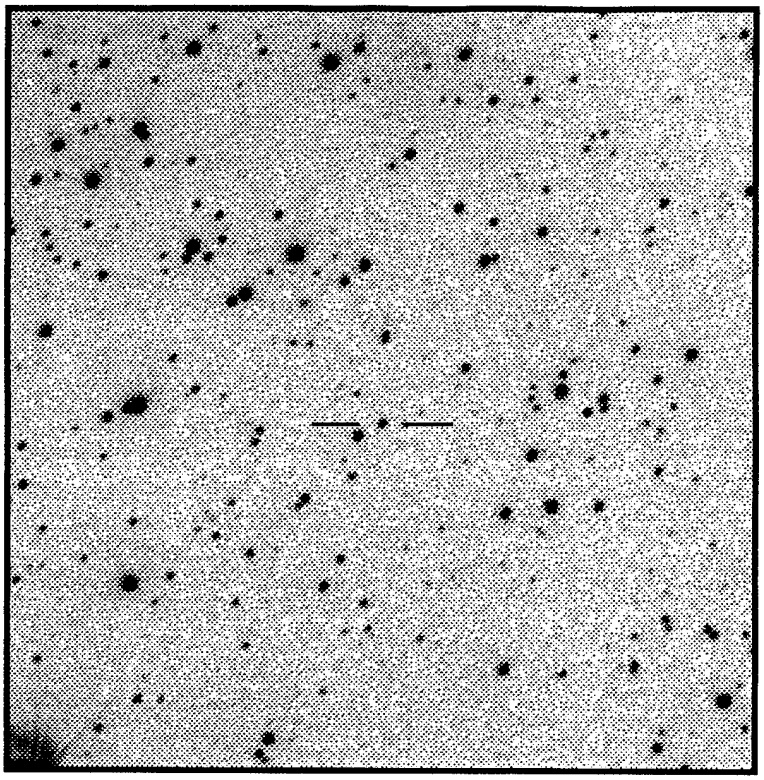


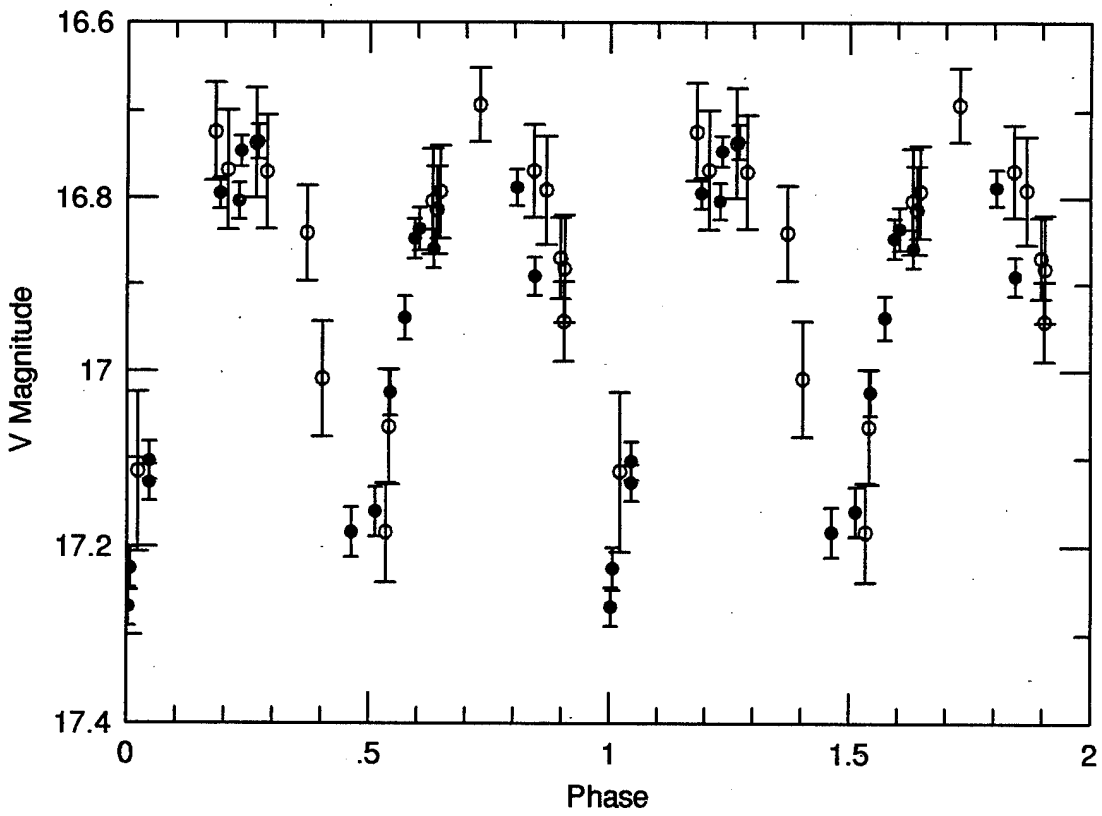
RA : 21 21 10.2
Dec: 28 05 56.5
<V> = 15.423
<B-V> = 0.25
P = 0.325160 days
Epoch = 3517.511
Type: RRc





RA : 21 34 29.8
Dec: 28 01 56.9
<V> = 16.892
<B-V> = 0.70
P = 0.333247 days
Epoch = 3516.360
Type: W UMa





RA : 21 46 11.6

Dec: 28 00 57.2

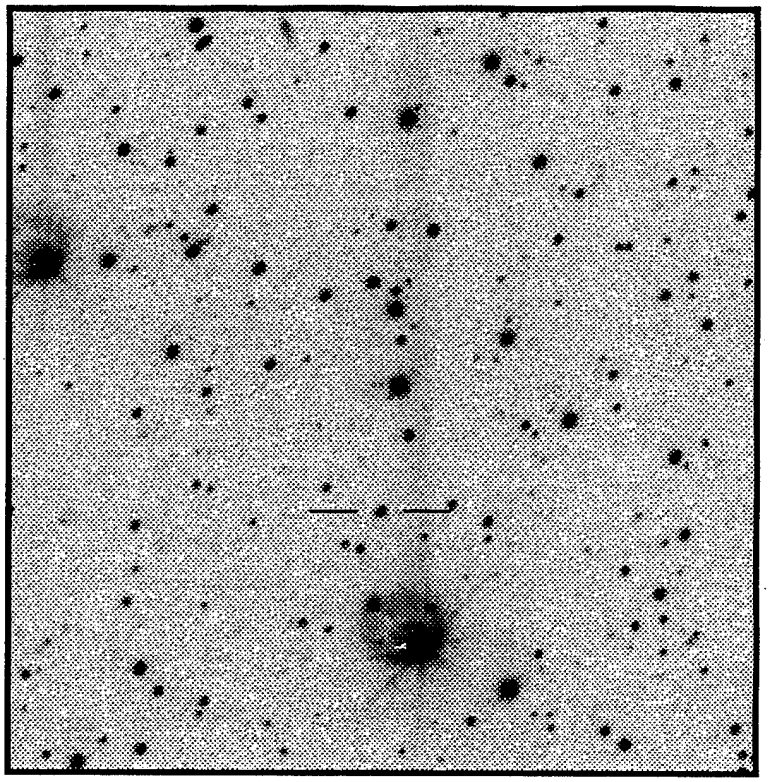
<V> = 15.233

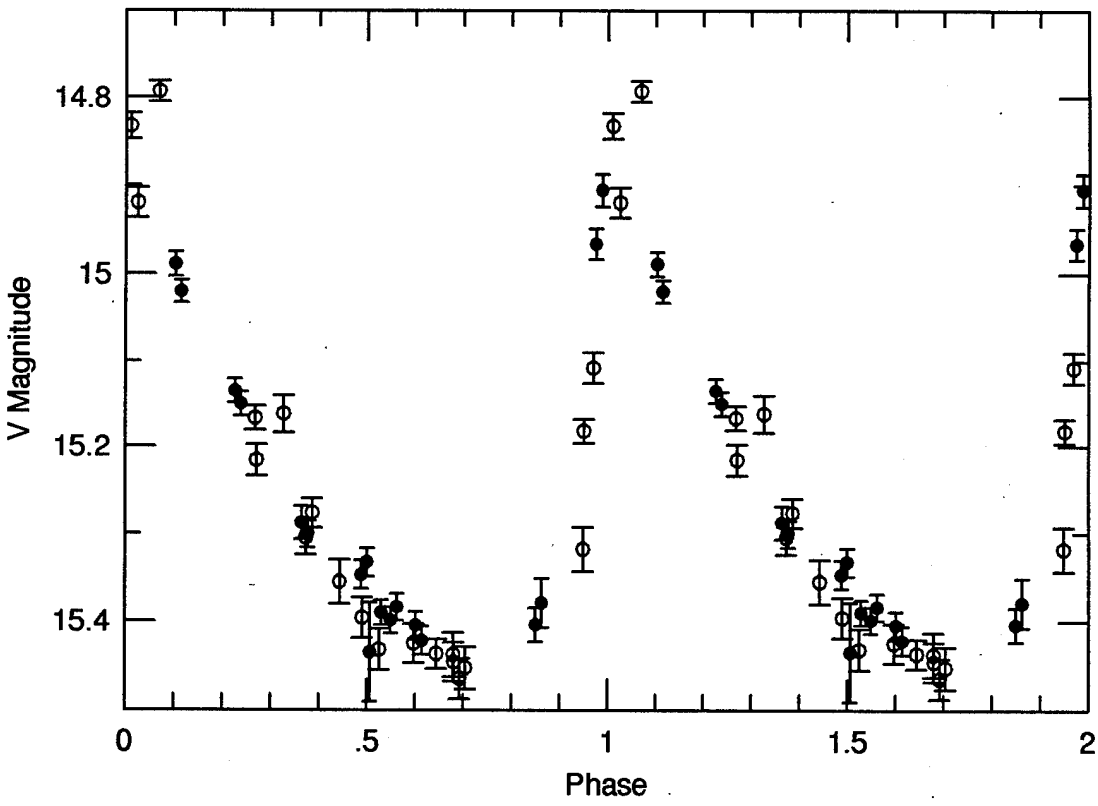
<B-V> = 0.45

P = 0.592806 days

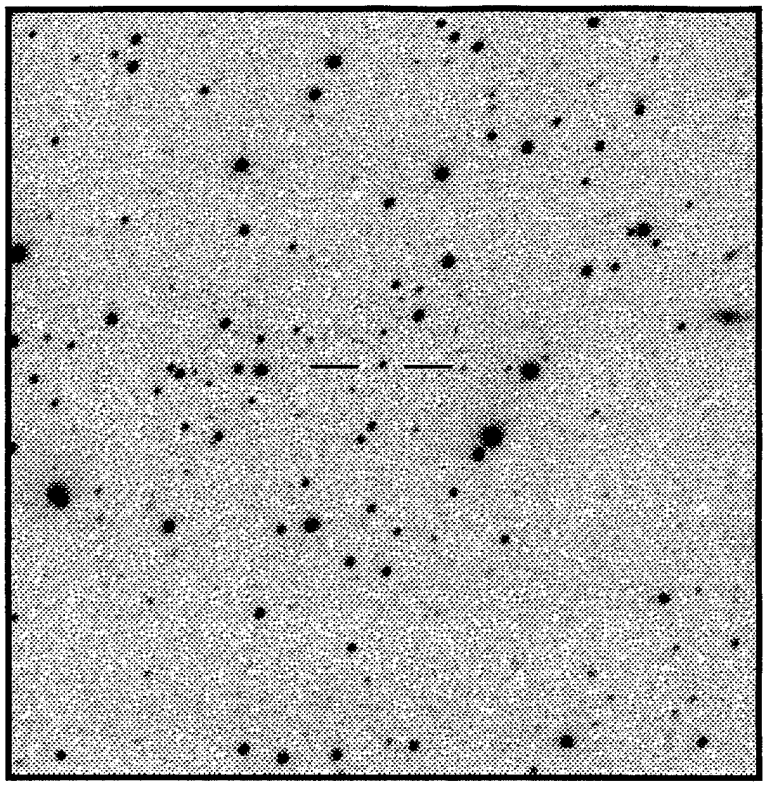
Epoch = 3517.220

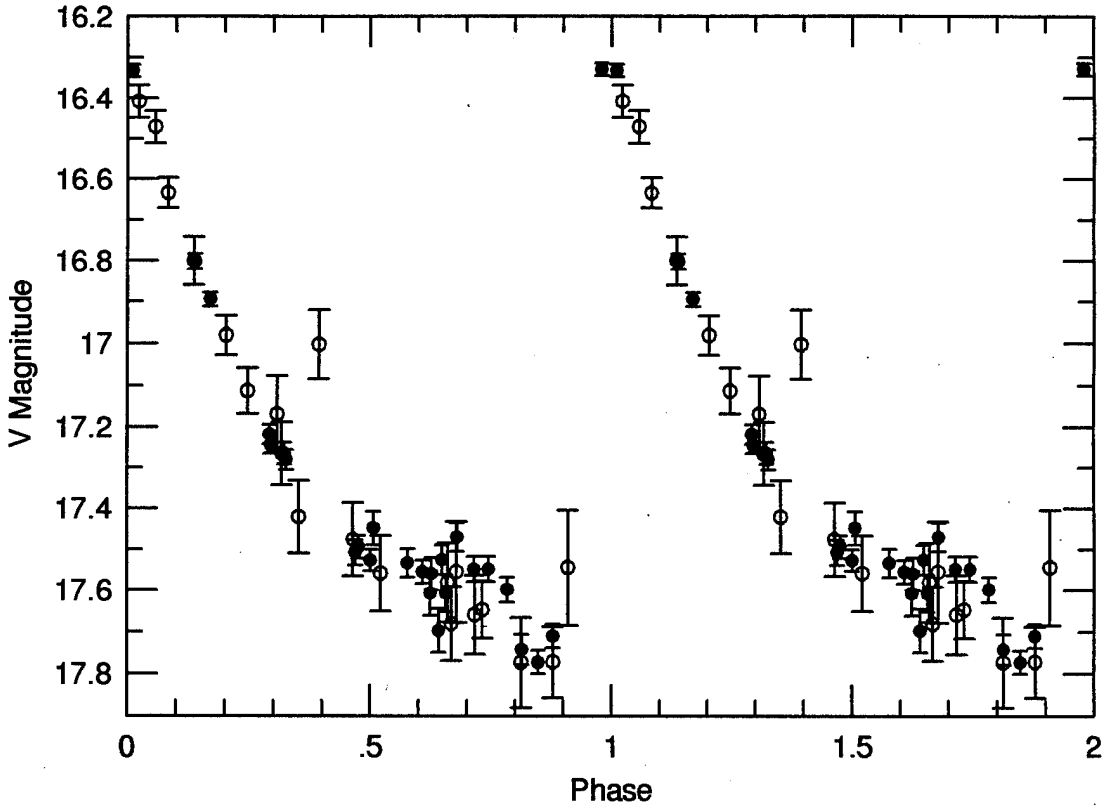
Type: RRab



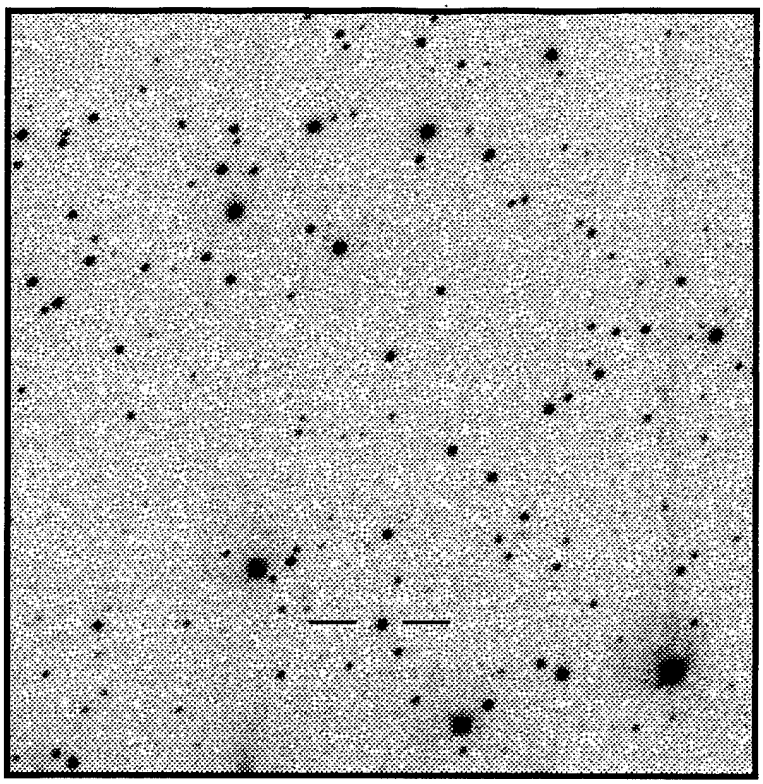


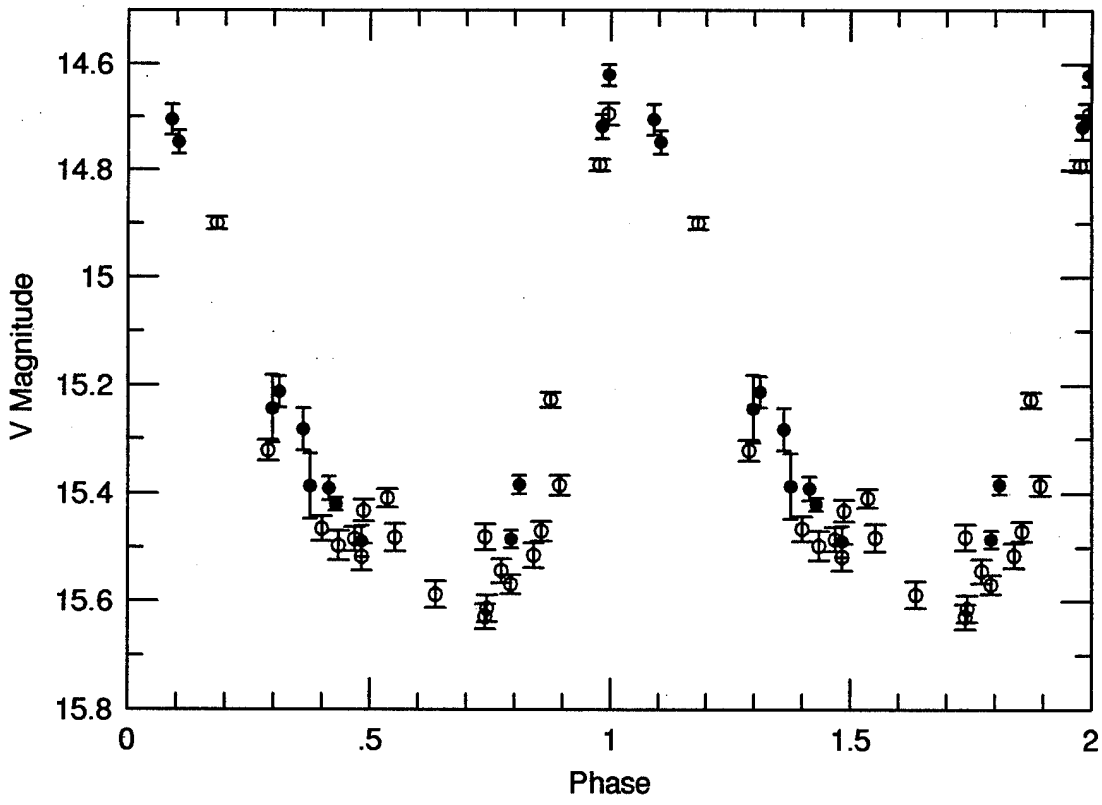
RA : 21 57 35.4
Dec: 28 02 37.5
<V> = 17.137
<B-V> = 0.38
P = 0.464627 days
Epoch = 3234.243
Type: RRab





RA : 21 58 16.5
Dec: 27 58 09.5
<V> = 15.192
<B-V> = 0.35
P = 0.525361 days
Epoch = 3660.060
Type: RRab





RA : 22 00 54.8

Dec: 28 00 20.1

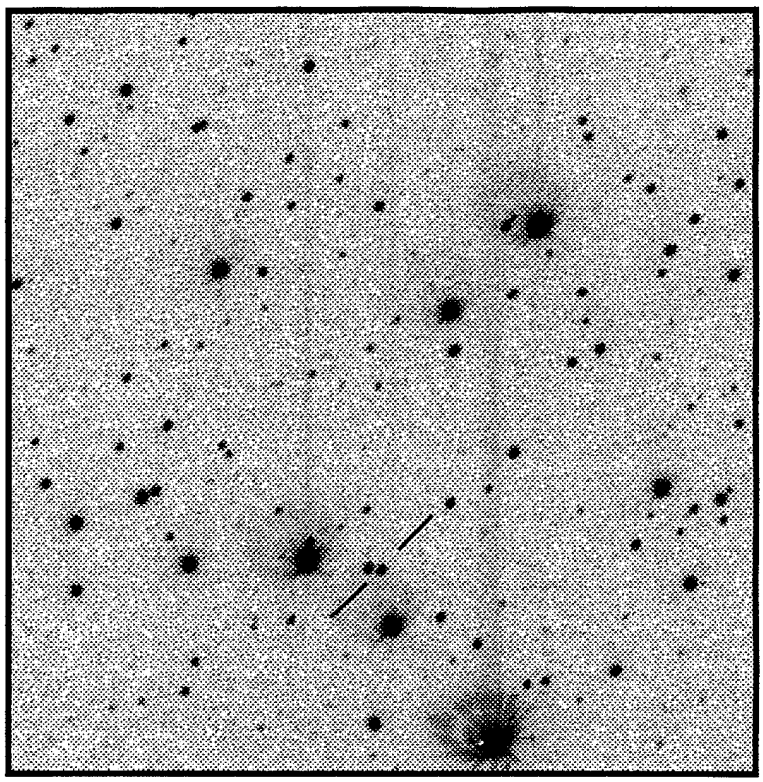
<V> = 15.630

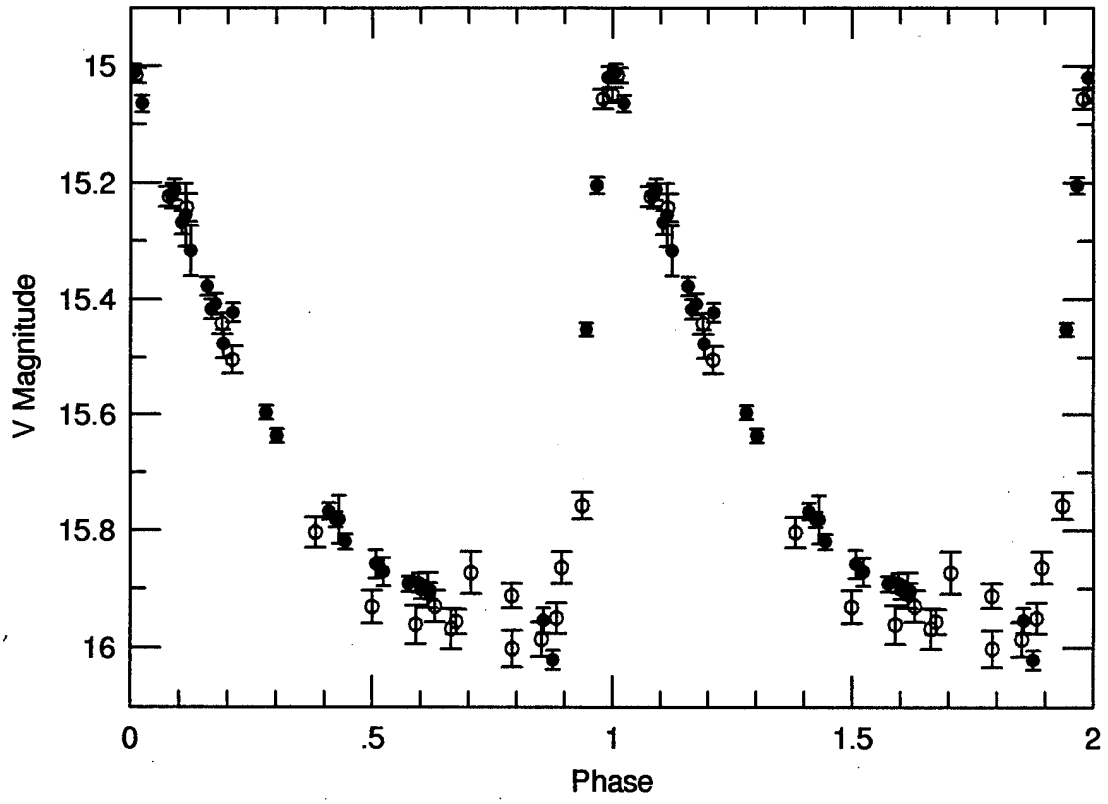
<B-V> = 0.38

P = 0.529309 days

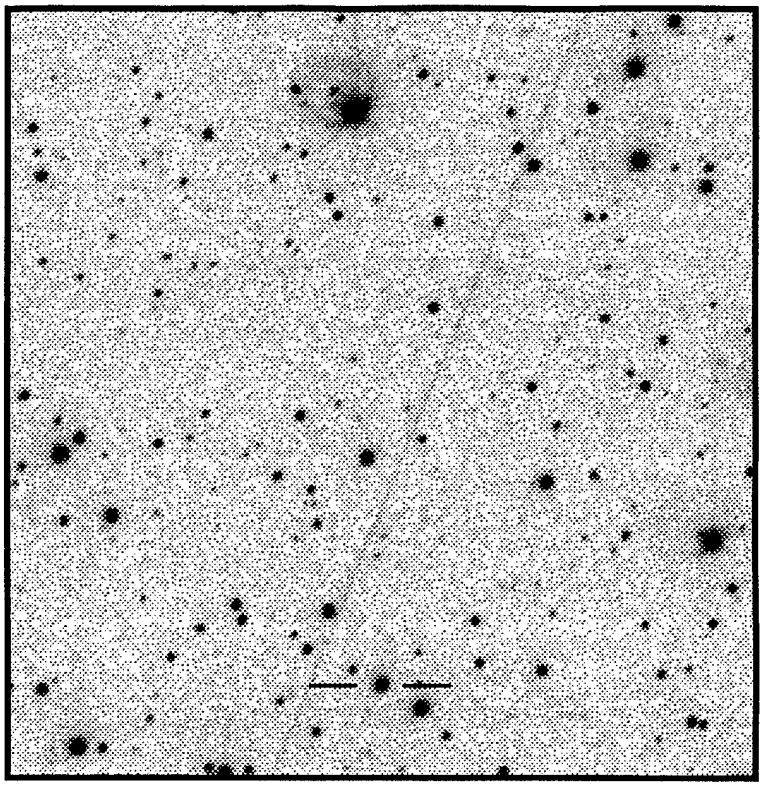
Epoch = 3517.108

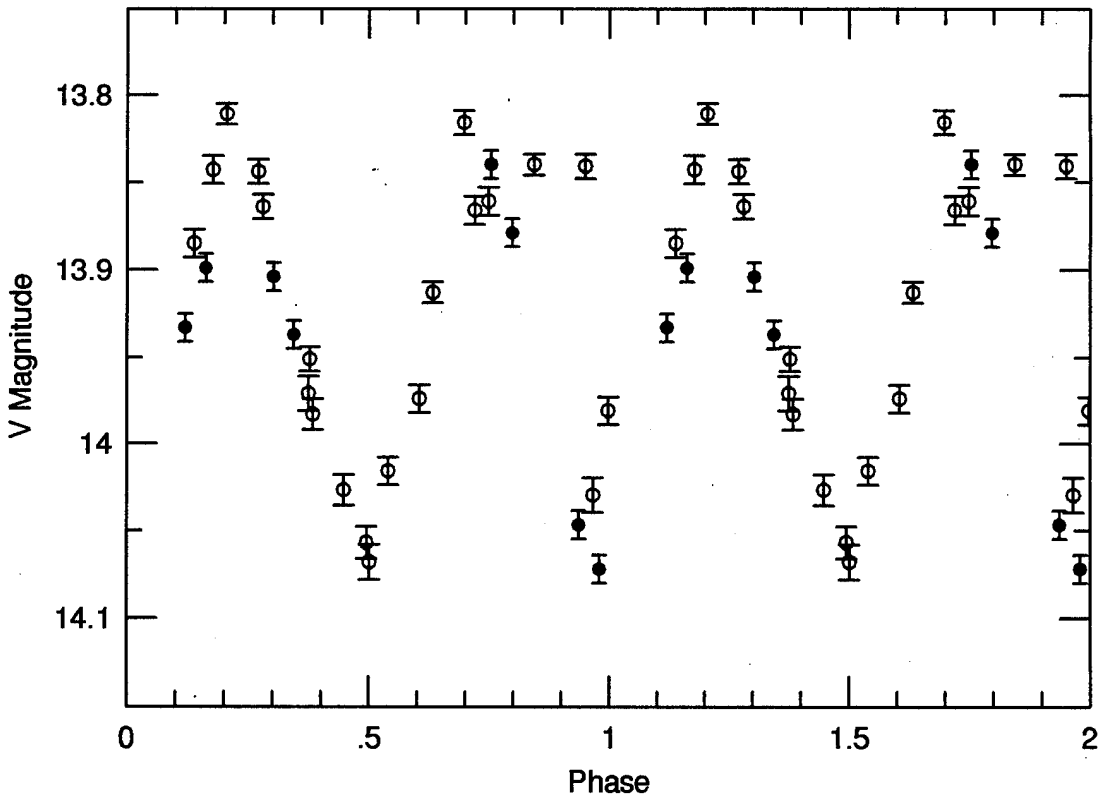
Type: RRab



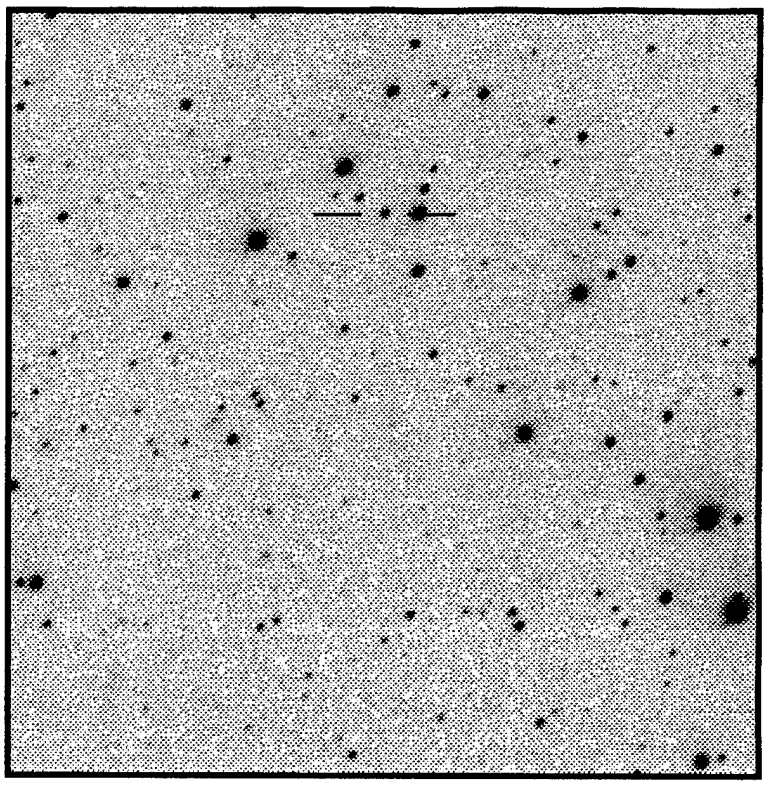


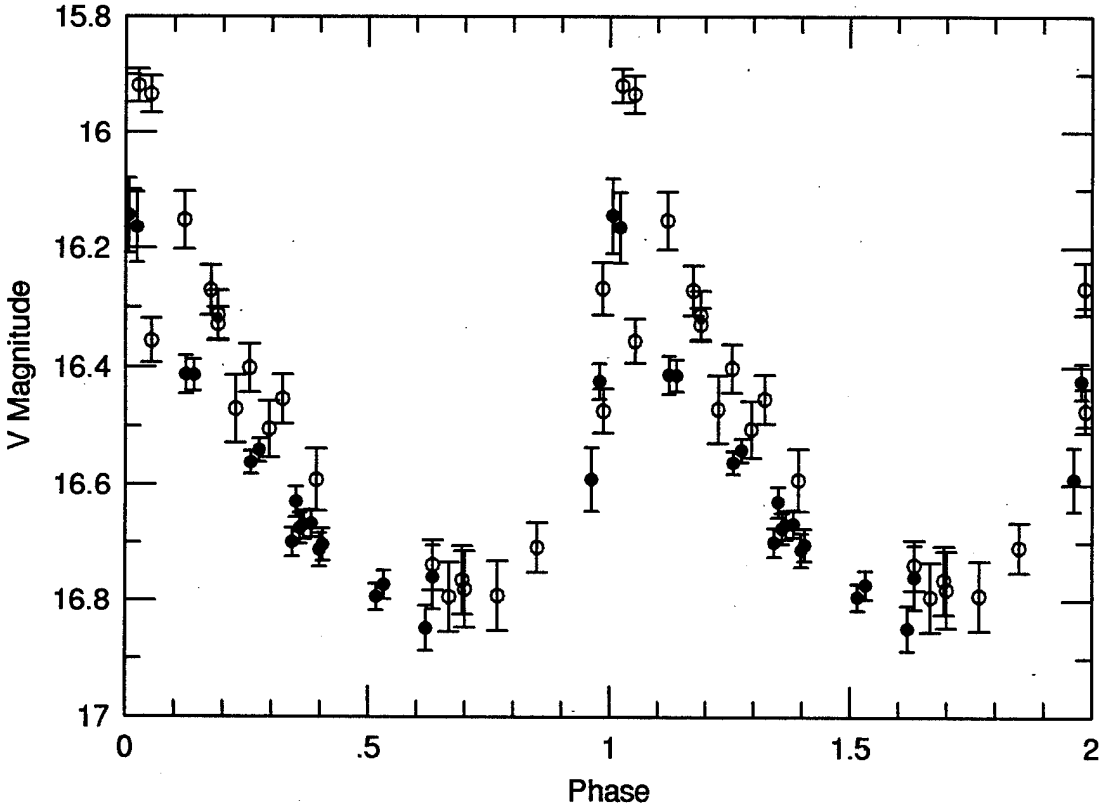
RA : 22 02 44.8
Dec: 27 59 04.0
<V> = 13.927
<B-V> = 0.79
P = 0.279144 days
Epoch = 3478.351
Type: W UMa





RA : 22 10 22.8
Dec: 28 04 16.2
<V> = 16.566
<B-V> = 0.30
P = 0.554907 days
Epoch = 3673.098
Type: RRab B





RA : 22 20 36.4

Dec: 27 59 39.2

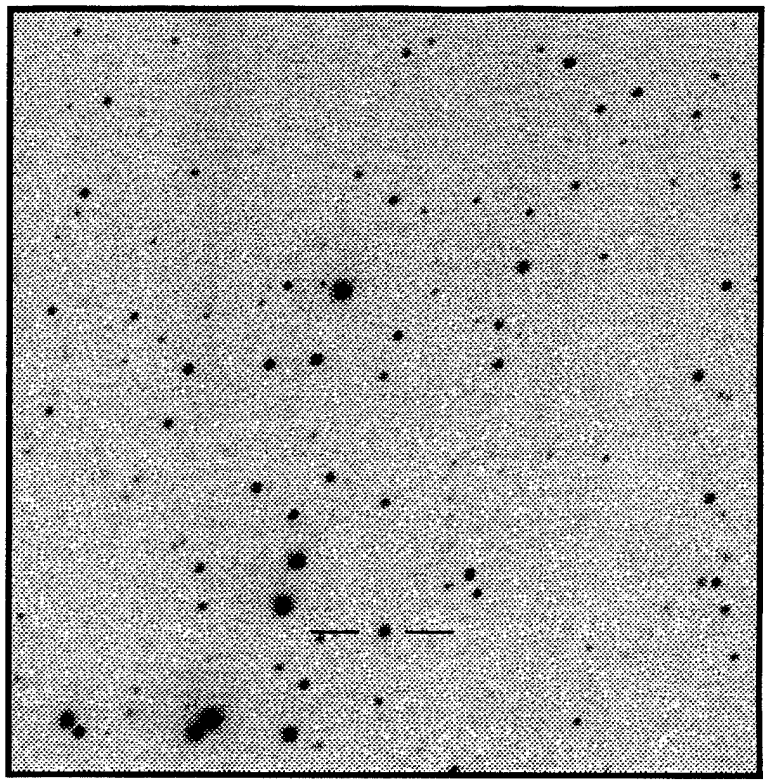
<V> = 15.185

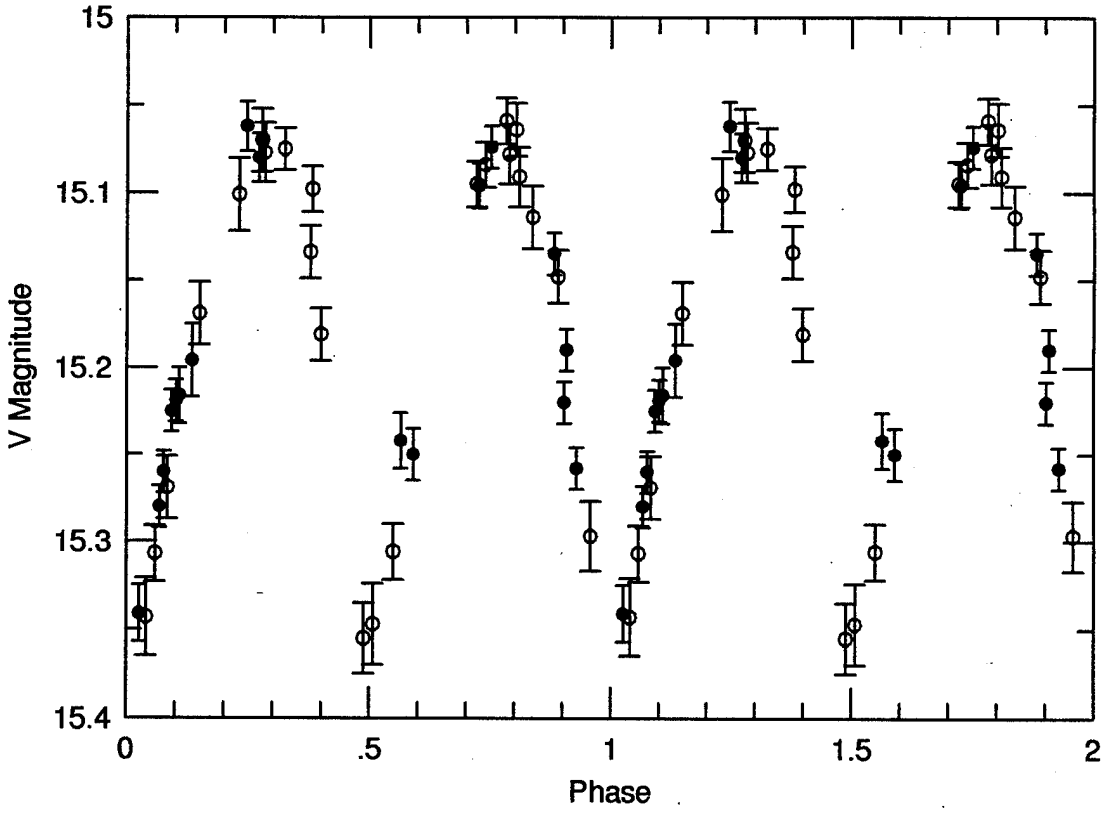
<B-V> = 0.35

P = 0.426090 days

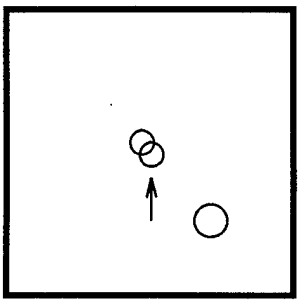
Epoch = 3517.356

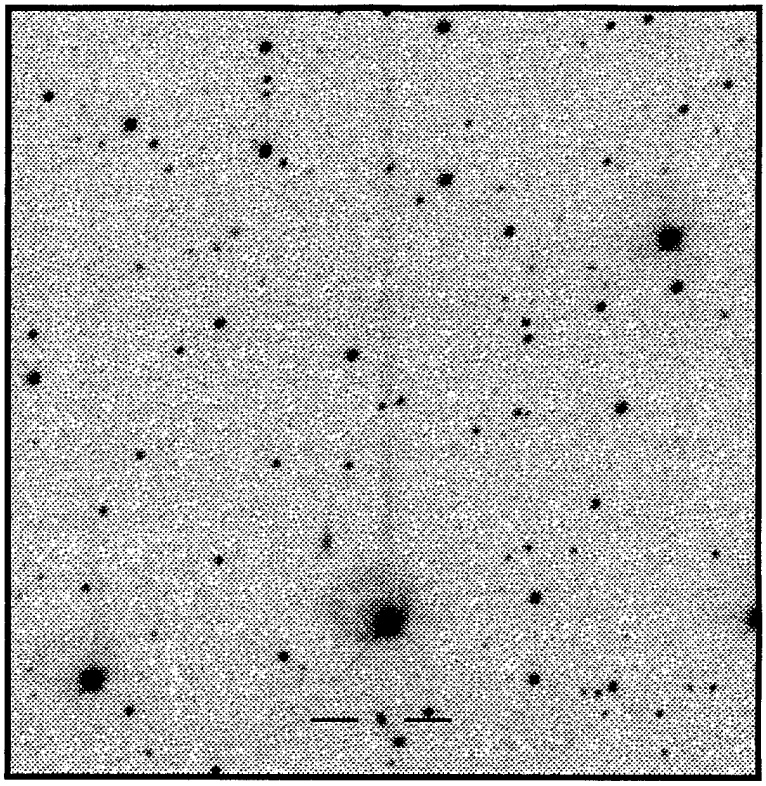
Type: W UMa

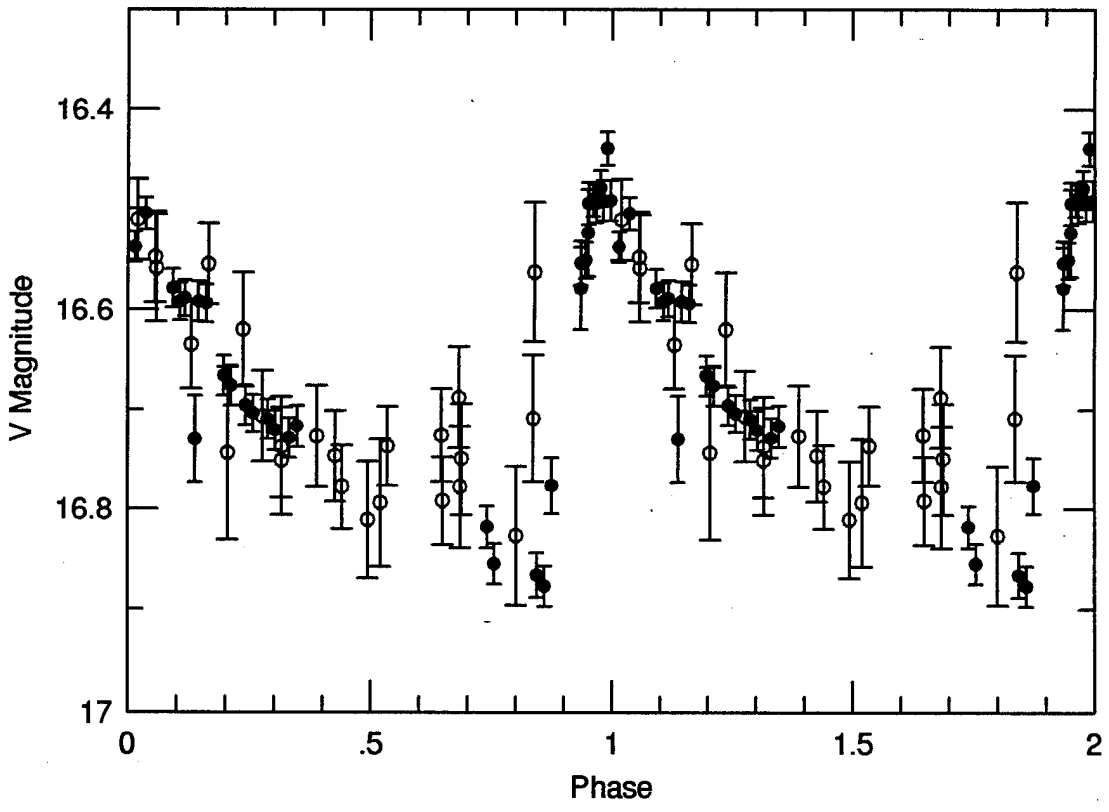




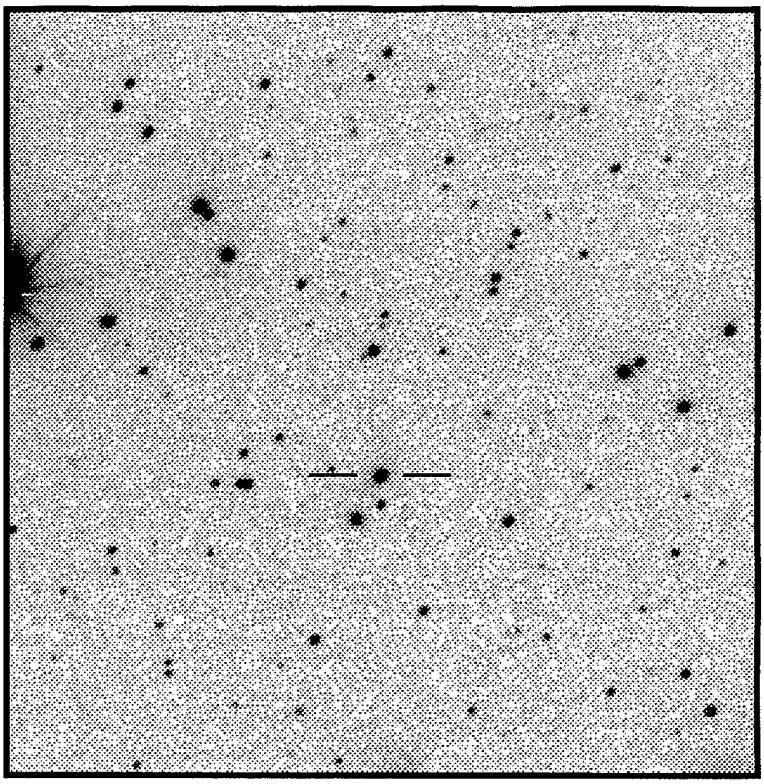
RA : 22 36 18.9
Dec: 27 58 38.4
<V> = 16.693
<B-V> = 0.45
P = 0.611901 days
Epoch = 3622.260
Type: RRab

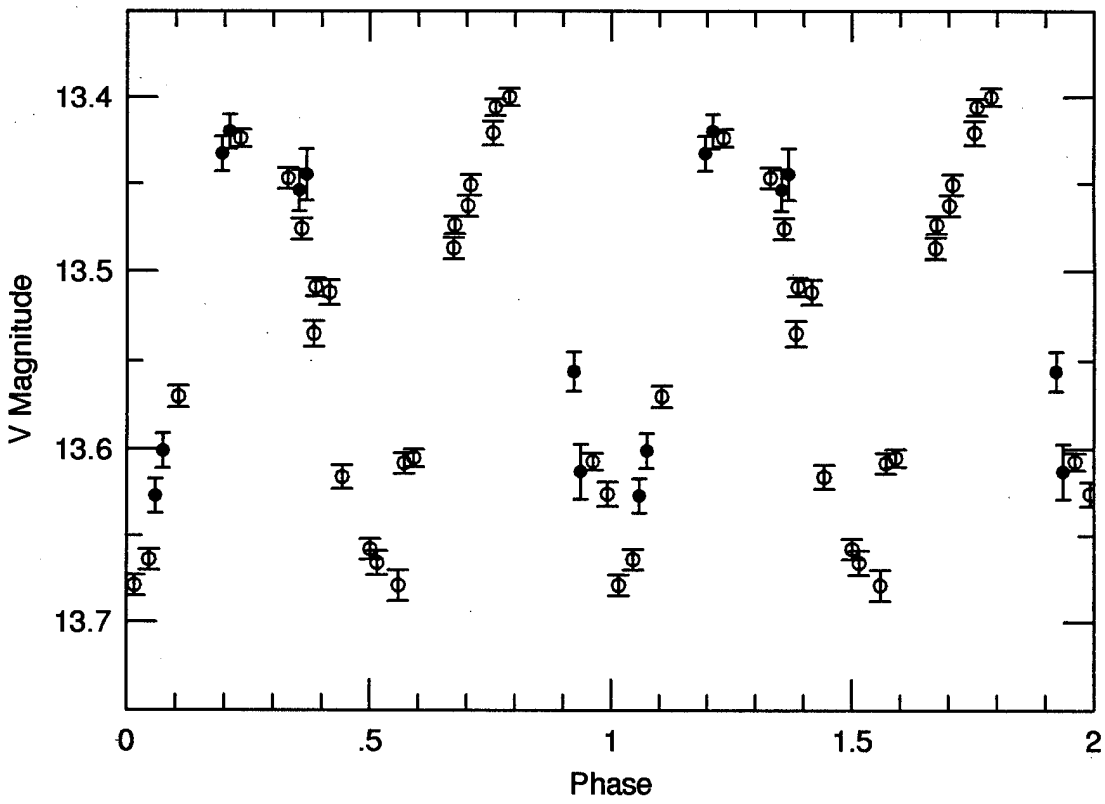




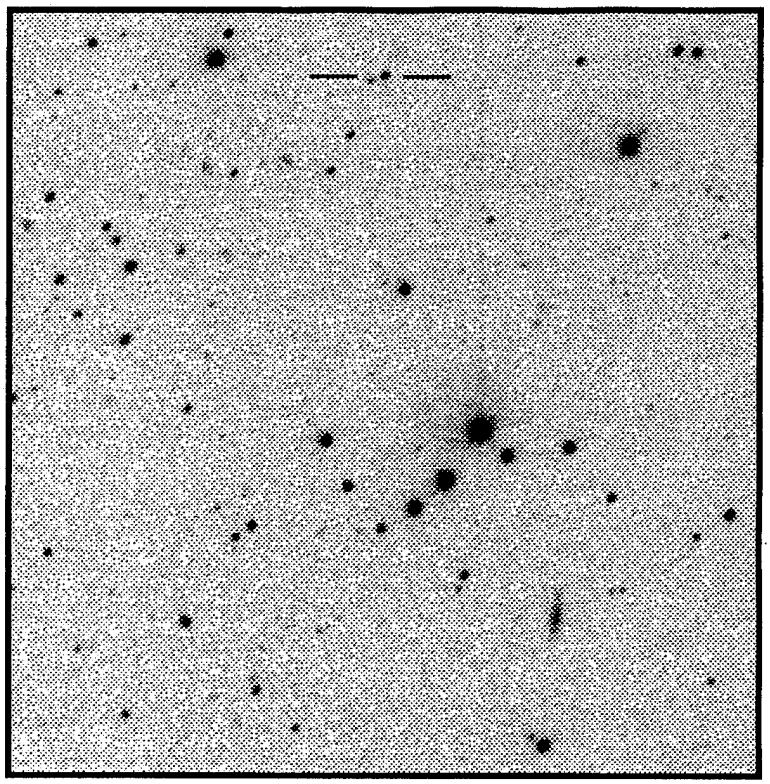


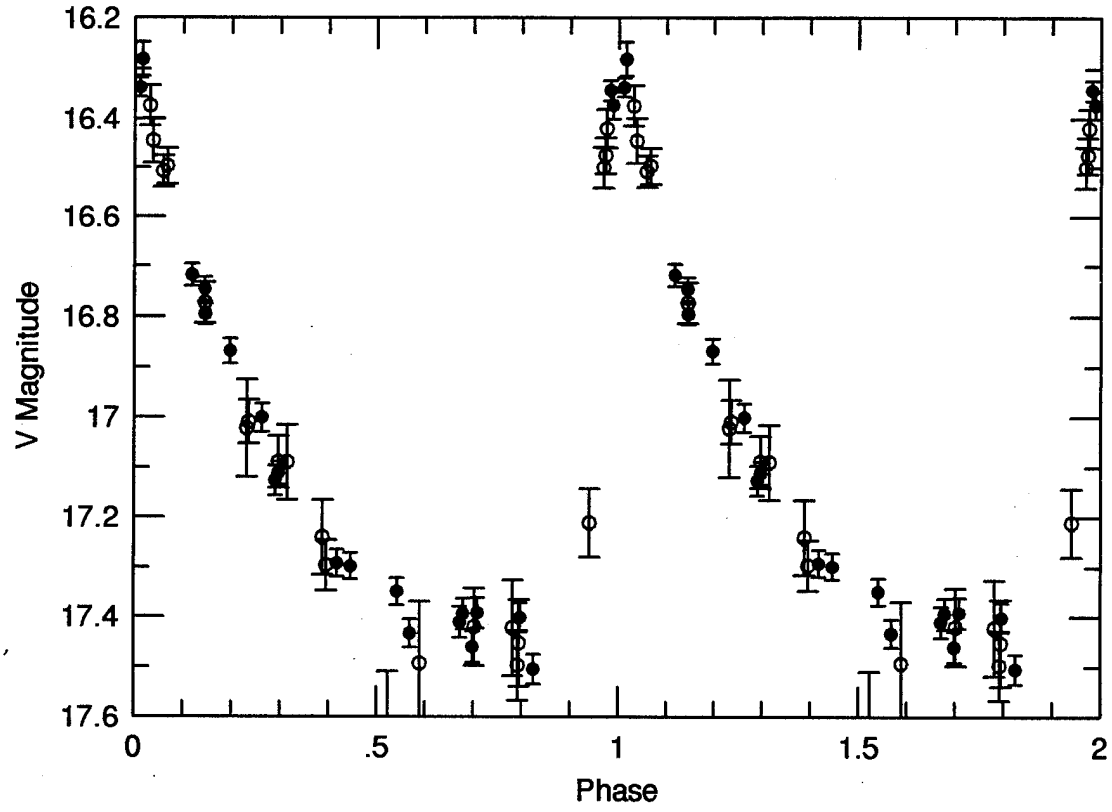
RA : 22 47 34.7
Dec: 28 01 20.8
<V> = 13.525
<B-V> = 0.40
P = 0.379380 days
Epoch = 3480.338
Type: W UMa



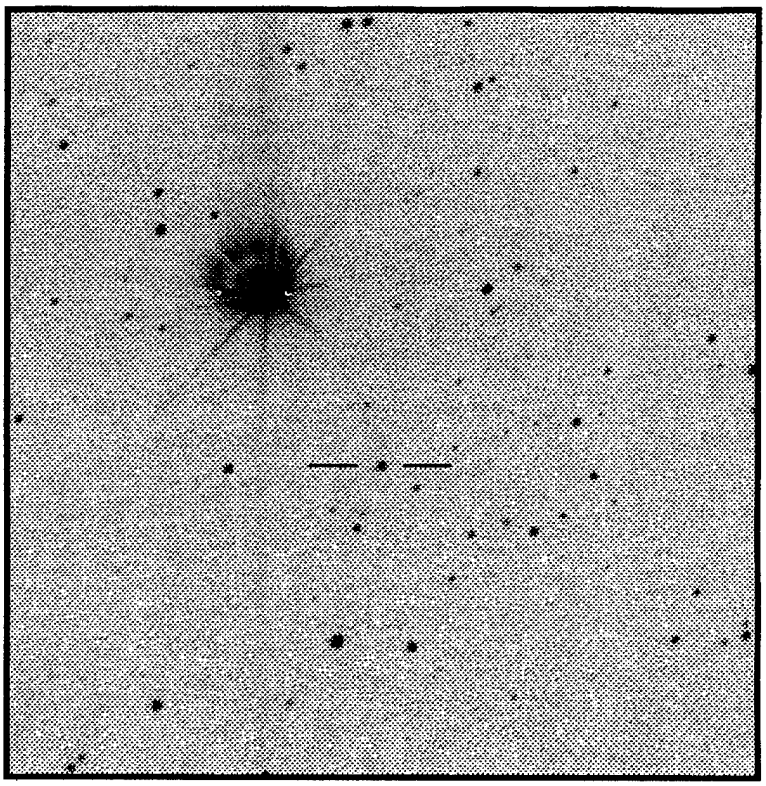


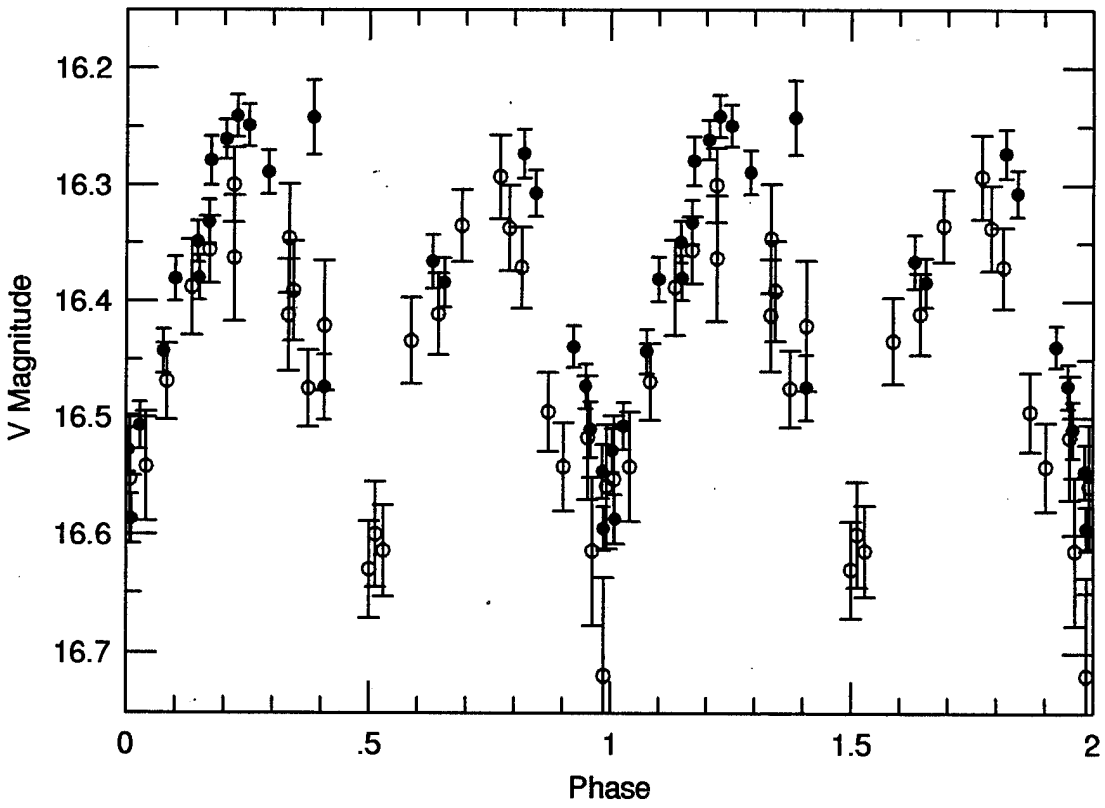
RA : 23 05 19.7
Dec: 28 05 44.1
<V> = 17.064
<B-V> = 0.30
P = 0.522284 days
Epoch = 3174.327
Type: RRab



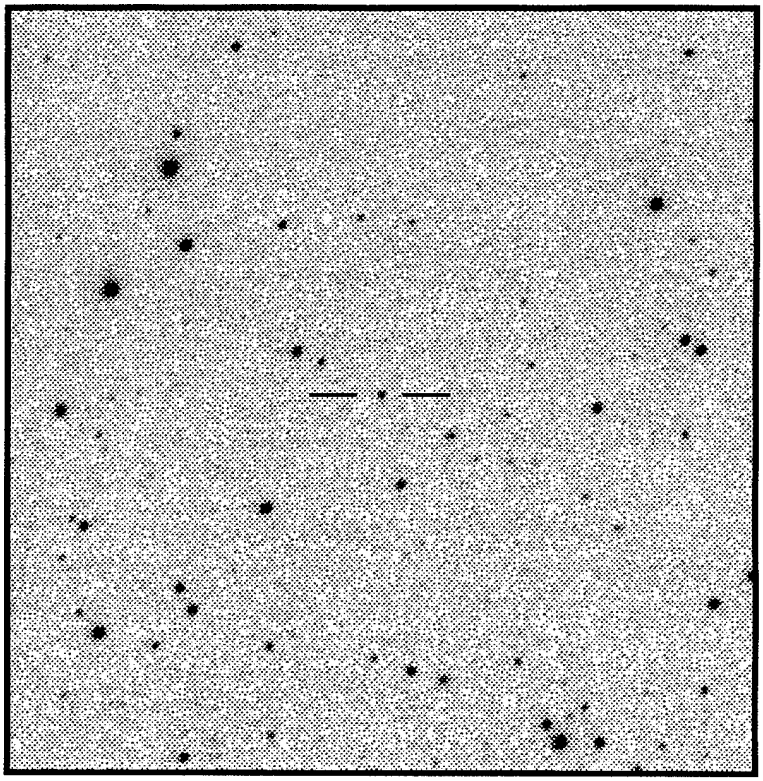


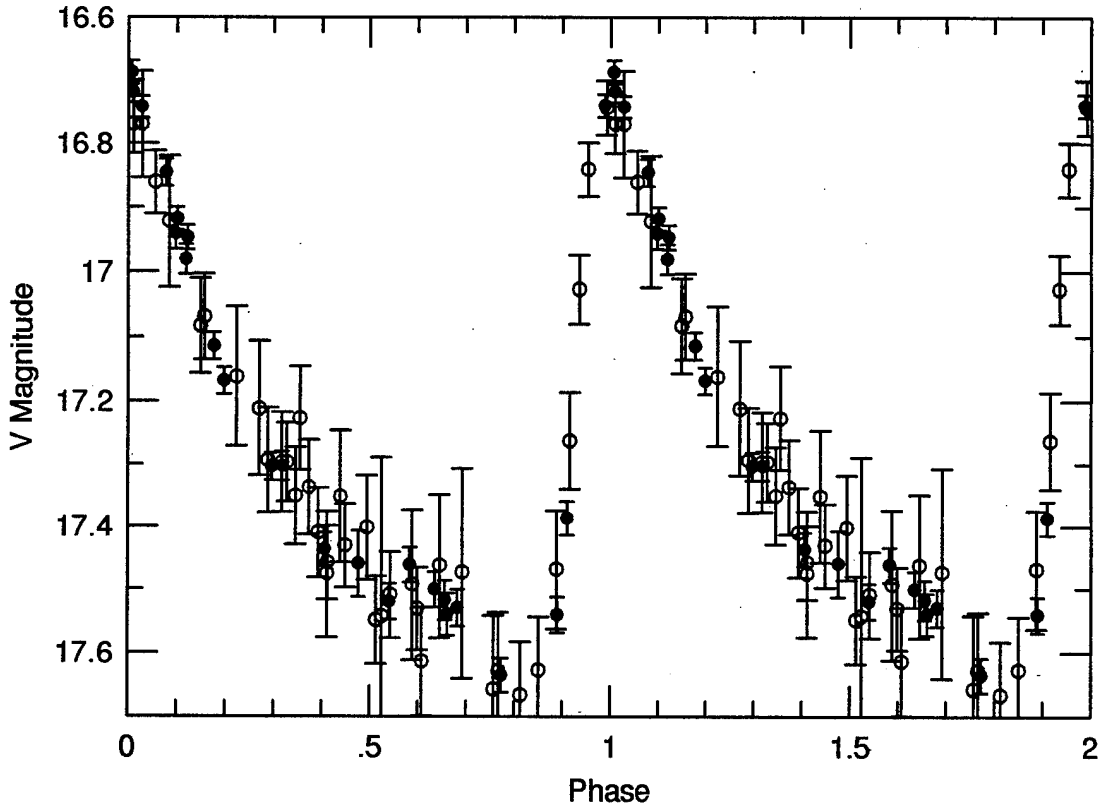
RA : 23 21 38.0
Dec: 28 01 25.6
<V> = 16.411
<B-V> = 0.40
P = 0.394387 days
Epoch = 3545.638
Type: W UMa



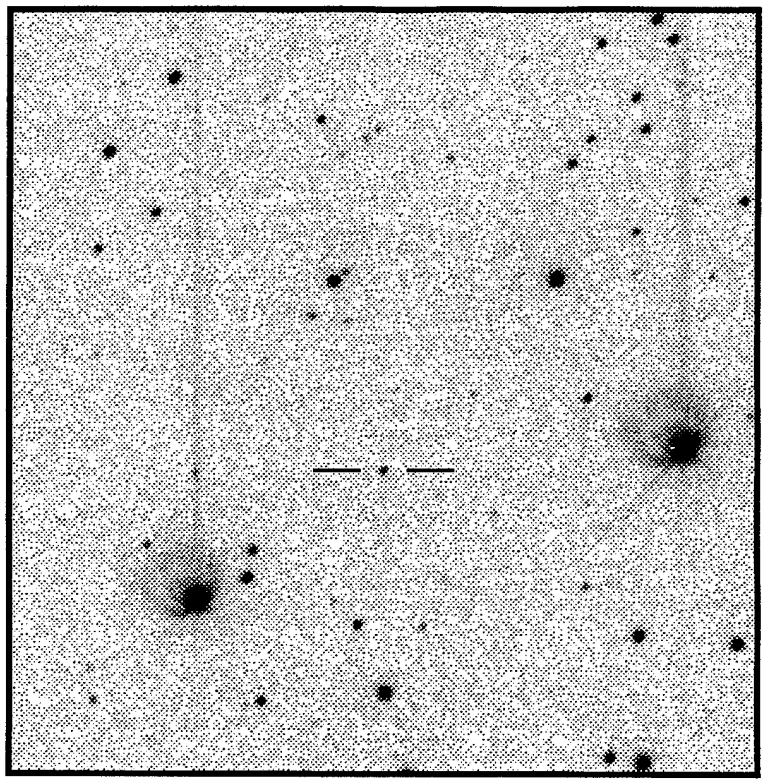


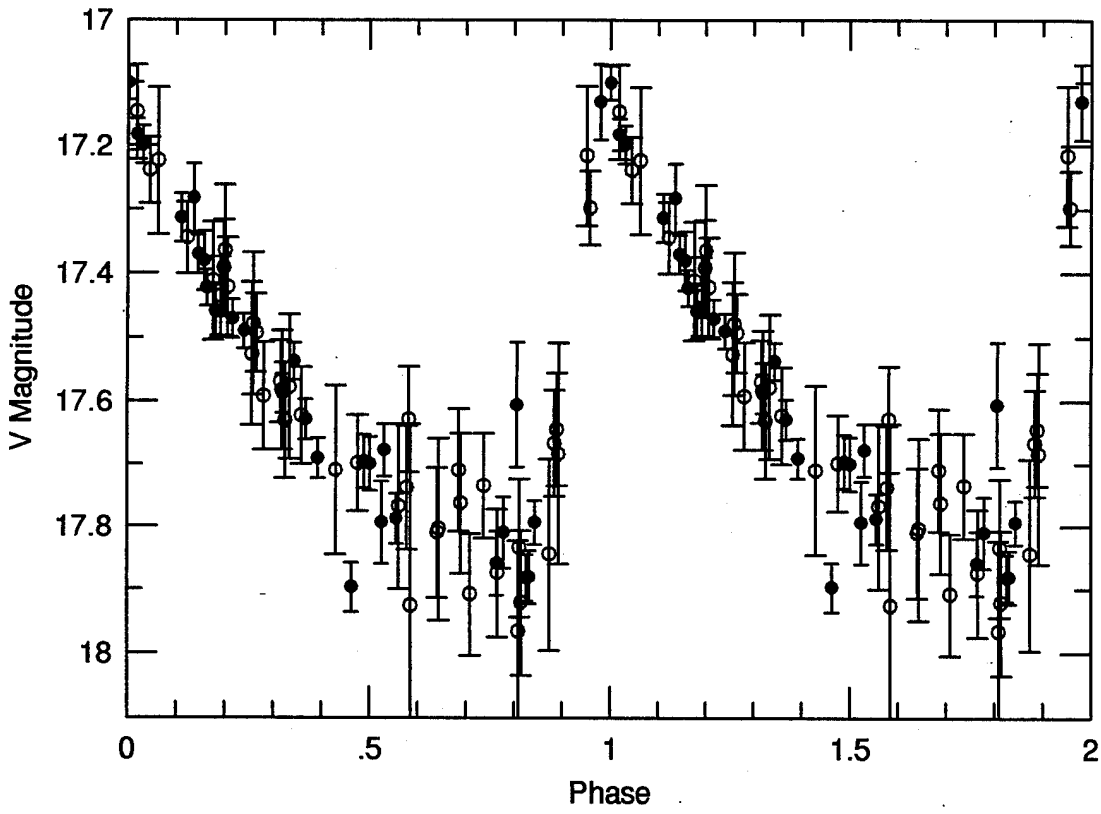
RA : 23 32 06.7
Dec: 28 02 10.9
<V> = 17.265
<B-V> = 0.44
P = 0.692859 days
Epoch = 3187.329
Type: RRab





RA : 23 52 26.0
Dec: 28 01 18.9
<V> = 17.565
<B-V> = 0.48
P = 0.589192 days
Epoch = 3545.372
Type: RRab





References

Chapter 1

Chapter 2

Baker, J.G., "On Improving the Effectiveness of Large Telescopes," IEEE Trans. on Aerospace and Electronic Systems Vol. AES-5, No. 2, p. 261, 1969.

Benedict, G.F., McGraw, J.T., Hess, T.R., Cawson, M.G.M., Keane, M.J., "Relative Astrometry with the Steward Observatory CCD/Transit Instrument," Bulletin of the American Astonomical Society Vol. 21, No. 4, p. 1109, 1989.

Benedict, G.F., McGraw, J.T., Hess, T.R., Cawson, M.G.M., Keane, M.J., "Relative Astrometry with the Steward Observatory CCD/Transit Instrument," Astronomical Journal **101**, p. 279, 1991.

Borra, E.F., Content, R., Drinkwater, M.J., Szapiel, S., "A Deffraction Limited f/2 1.5 meter Diameter Liquid Mirror," Astrophysical Journal Letters **346**, p. L41, 1989.

Borra, E.F., Content, R., Girard, L., Szapiel, S., Tremblay, L.M., "Liquid Mirrors: Optical Shop Tests and Contributions to the Technology," Astrophysical Journal **393**, p. 829, 1992.

Cawson, M.G.M., McGraw, J.T., Keane, M.J., "A Relational Database Approach to Astronomical Research," SPIE Proc. Vol. 627, p. 70, 1986.

Cawson, M.G.M., McGraw, J.T., Keane, M.J., "The CCD/Transit Instrument (CTI) Data-Analysis System," SPIE Proc. Vol. 627, p. 79, 1986.

Content, R., Borra, E.F., Drinkwater, M.J., Poirier, S., Poisson, E., Beauchemin, M., Boily, E., Gauthier, A., Tremblay, L.M., "A Search for Optical Flares and Flashes with a Liquid Mirror Telescope," Astronomical Journal **97** (3), p. 917, 1989.

Delporte, E., Délimitation Scientifique des Constellations (Tables et Cartes), (Cambridge, At the University Press, 1930).

Dixon, R.S., Gearhart, M.R., and Schmidtke, P.C., Atlas of Sky Overlay Maps (for the Palomar Sky Survey), (The Ohio State Radio Observatory, 1981).

Hoffleit, D., Bright Star Catalogue, 5th revised edition (Yale University Observatory, 1982).

Jones, K.G. (editor), Webb Society Deep-Sky Observer's Handbook Volume 5: Clusters of Galaxies, (Enslow Publishing, 1981).

Kent, S.M., Ramella, M., Nonino, M., "A Small Drift Scan Survey for Galaxies in the Northern Sky," Astronomical Journal **105** (2), p. 393, 1993.

Kent, S.M., Stoughton, C., Newberg, H., Loveday, J., Petravick, D., Gurbani, V., Berman, E., Sergey, G., Lupton, R., Sloan Digital Sky Survey, Report #FNAL/C-94/084, (Batavia, Ill.: Fermi National Accelerator Laboratory, 1994).

Kholopov, P.N., Samus, N.N., Frolov, M.S., Goranskij, V.P., Gorynya, N.A., Kireeva, N.N., Kukarkina, N.P., Kurochkin, N.E., Medvedeva, G.I., Perova, N.B., and Shugarov, S.Y., General Catalogue of Variable Stars, 4th edition (Moscow: Nauka Publishing House, 1985-88).

Kirkpatrick, J.D., McGraw, J.T., "The CCD/Transit Instrument (CTI) Blue Object Survey," IAU Colloquium #114 (White Dwarfs), p. 167, 1988.

Kirkpatrick, J.D., Henry, T.J., McCarthy, D.W., McGraw, J.T., "Constraining the Faint End of the Stellar Luminosity Function Through a Systematic Search for M Dwarfs," Bulletin of the American Astronomical Society, Vol. 22, No. 4, p. 1204, 1990.

Kirkpatrick, J.D., Spectroscopic and Photometric Studies of Main Sequence M Stars and a Search for Late Type Dwarfs in the Solar Vicinity, Phd dissertation, (Department of Astronomy, The University of Arizona, 1992).

Kirkpatrick, J.D., "The Luminosity Function of Field M Dwarfs: Evidence for a Population of Substellar Objects," Bulletin of the American Astronomical Society Vol. 26, No. 2, p. 944, 1994.

Kirkpatrick, J.D., "The Luminosity Function at the End of the Main Sequence: Results of a Deep, Large-Area, CCD Survey for Cool Dwarfs," Astrophysical Journal Supplement Series **94**, p. 749, 1994.

Kron, R., "Digital Optical Sky Surveys," Bulletin of the American Astronomical Society Vol. 26, No. 2, p. 915, 1994.

McGraw, J.T., Angel, J.R.P., and Sargent, T.A., "A CCD Transit-telescope Survey for Galactic and Extragalactic Variability and Polarization," SPIE Proc. Vol. 264, p. 20,

1980.

McGraw, J.T., Stockman, H.S., Angel, J.R.P., Epps, H., and Williams, J.T., "The CCD/transit instrument (CTI) deep photometric and polarimetric survey - a progress report," SPIE Proc. Vol. 331, p. 137, 1983.

McGraw, J.T., Cawson, M.G.M., Keane, M.J., "Operation of the CCD/Transit Instrument (CTI)," SPIE Proc. Vol. 627, p. 60, 1986.

McGraw, J.T., Cawson, M.G.M., Kirkpatrick, J.D., Haemmerle, V., "A Strip Search for Quasars: The CCD/Transit Instrument (CTI) Quasar Survey," Proceedings of a Workshop on Optical Surveys for Quasars, p. 163, 1988.

McGraw, J.T., Hess, T.R., Green, E.M., Bridges, C.T., Benedict, G.F., "Photometric and Positional Calibration of the CCD/Transit Instrument (CTI) Strip of the Sky," Bulletin of the American Astronomical Society Vol. 21, No. 3, p. 1021, 1989.

McGraw, J.T., "A Strip Search of the Universe," Variable Stars and Galaxies, ASP Conference Series, Vol. 30, p. 77 (San Francisco: Astronomical Society of the Pacific, 1992).

McGraw, J.T., "The Lunar Transit Telescope (LTT): An Early Lunar Based Science and Engineering Mission," Engineering, Construction and Operations in Space III, p. 1865, 1992.

McGraw, J.T. (editor), Proceedings of the Lunar Ultraviolet Telescope Experiment (LUTE) Science Workshop, (Institute for Astrophysics, The University of New Mexico, 1993).

McGraw, J.T., Wetterer, C.J., Hess, T.R., Green, E.M., "Photometric Standard Stars in the CCD/Transit Instrument (CTI) Survey," Bulletin of the American Astronomical Society Vol. 26, No. 2, p. 899, 1994.

Paul, M., "Corrective Systems for Astronomical Reflectors," Rev. d'Optique Vol. 14, p. 169, 1935.

Stoughton, C., Annis, J., Kent, S., Kron, R., Loveday, J., McKay, T., Newberg, H., "First Data from the Fermilab Drift Scan Camera," Bulletin of the American Astronomical Society Vol. 26, No. 2, p. 897, 1994.

Sulentic, J.W. and Tifft, W.G., The Revised New General Catalogue of Nonstellar Astronomical Objects, (Tucson: The University of Arizona Press, 1973).

Veron-Cetty, M.P., and Veron, P., "A Catalogue of Quasars and

Active Galactic Nuclei, 4th edition," E.S.O. Sci. Rep. 7, 1989.

Wetterer, C.J., McGraw, J.T., Hess, T.R., Grashuis, R., "Variable Stars in the CCD/Transit Instrument (CTI) Survey," Bulletin of the American Astronomical Society Vol. 26, No. 2, p. 899, 1994.

Wetterer, C.J., The CCD/Transit Instrument Atlas and Database Guide, Supplement to PhD Dissertation, (Department of Physics and Astronomy, University of New Mexico, 1995).

Zwicky, F., Herzog, E., Wild, P., Karpowicz, M., Kowal, C.T., The Catalogue of Galaxies and Clusters of Galaxies, (California Institute of Technology, 1961-68).

, The National Geographic Society - Palomar Observatory Sky Survey, (California Institute of Technology, 1954).

, Smithsonian Astrophysical Observatory Star Catalog, (Washington, Smithsonian Institution, 1966-1990).

(variable star original finder chart references)

Bond, H.E., Kron, R.G. and Spinrad, H., "GQ Comae and V396 Herculis: Two Low-Redshift Optically Variable QSOs," Astrophysical Journal **213** (1), p. 1, 1977. (GQ Com)

Erleksova, G.E., "EQ Vulpeculae," Переменные звезды, Прцложенце **2** №10, p. 248, 1975. (EQ Vul)

Hoffmeister, C., "Untersuchung der Schtaube des Positions-Fadenmikrometers *Heyde 3013*," Mitteilungen der Sternwarte zu Sonneberg Nr. 6, 1924. (UU Lyr)

Hoffmeister, C., "Relative Koordinaten, Örter und Karten neuer Veränderlicher," Mitteilungen der Sternwarte zu Sonneberg Nr. 17, 1930. (CE Lyr and CV Lyr)

Hoffmeister, C., "Relative Koordinaten, Örter und Karten neuer Veränderlicher," Mitteilungen der Sternwarte zu Sonneberg Nr. 22, 1933. (GS Lyr)

Hoffmeister, C., "89 neue veränderliche Sterne," Astronomische Nachrichten **284**, p. 275, 1959. (V375 Her and V385 Her)

Hoffmeister, C., "Mitteilungen über neuentdeckte Veränderliche Sterne (S9727-S10152)," Astronomische Nachrichten **290** H1-2, p. 43, 1967. (KW Vul)

Pinto, G. and Romano, G., "Researches with the Schmidt Telescope VI - The Variable Stars around Gamma Comae," Memorie della Società Astronomica Italiana **44** №1, p. 53, 1973. (GR Com and GS Com)

Kurochkin, N.E., "New Variable Stars in the Region of M56," Переменные звезды **17** №128, p. 186, 1970. (V427 Lyr)

Kinman, T., Wirtanen, C.A. and Janes, K.A., "An RR Lyrae Star Survey with the Lick 20 inch Astrograph. IV. A Survey of Three Fields Near the North Galactic Pole," Astrophysical Journal Supplement **119**, p. 379, 1966 (DV Com and EZ Com)

Meinunger, L., "Über Veränderliche in einigen T-Assoziationen," Mitteilungen über Veränderliche Sterne **3** H5, p. 137, 1966. (CN Tau)

Miller, W.J. and Wachmann, A.A., "Six New Variable Stars in the Cygnus Cloud, VV 125-130," Ricerche Astronomiche **6** №22, p. 497, 1964. (V926 Cyg)

Miller, W.J., "Eleven Variable Stars in the Cygnus Cloud, VV 151-161," Ricerche Astronomiche **7** №4, p. 197, 1965. (V911 Cyg)

Miller, W.J., "Ten New Variable Stars in the Cygnus Cloud, VV 191-200," Ricerche Astronomiche **7** №10, p. , 1967. (V1140 Cyg)

Rügemer, H., "Neue Veränderliche Sterne," Astronomische Nachrichten **248**, p. 409, 1933. (EP Tau)

Shaganian, B.L. and Shaganian, V.B., "On Three Longperiod Variable Stars in the Region of M56," Переменные звезды, Прцложенце **3** №18, p. 748, 1979. (TY Lyr)

Vogt, N. and Bateson, F.M., "An Atlas of Southern and Equitorial Dwarf Novae," Astronomy and Astrophysics Supplement **48** (3), p. 383, 1982. (IR Gem)

Wachmann, A.A., "Die Veränderlichen im Südteil der Cygnuswolke - Teil II," Astronomische Abhandlungen der Hamburger Sternwarte, Band VI Nr. 2, 1963. (PP Lyr)

Wachmann, A.A., "Die Veränderlichen im Südteil der Cygnuswolke - Teil III," Astronomische Abhandlungen der Hamburger Sternwarte, Band VI Nr. 3, 1964. (EH Cyg and AI Cyg)

, Mitteilungen über Veränderliche Sterne №299, 1957. (V532 Her)

Chapter 3

Cawson, M.G.M., McGraw, J.T., Keane, M.J., "A Relational Database Approach to Astronomical Research," SPIE Proc. Vol. 627, p. 70, 1986.

Cawson, M.G.M., McGraw, J.T., Keane, M.J., "The CCD/Transit Instrument (CTI) Data-Analysis System," SPIE Proc. Vol. 627, p. 79, 1986.

Dieckvoss, W., Kox, H., Gunther, A., and Brosterhus, E., AGK3 Star Catalog of Positions and Proper Motions North of -2.5 degree Declination (Hamburg-Bergedorf, 1975).

Lasker, B.M., Sturch, C.R., McLean, B.J., Russell, J.L., Jenkner, H., Shara, M.M., "The Guide Star Catalog I. Astronomical Foundations and Image Processing," Astronomical Journal **99**(6), p. 2019, 1990.

McGraw, J.T., Hess, T.R., Green, E.M., Bridges, C.T., Benedict, G.F., "Photometric and Positional Calibration of the CCD/Transit Instrument (CTI) Strip of the Sky," Bulletin of the American Astronomical Society Vol. 21, No. 3, p. 1021, 1989.

McGraw, J.T., "A Strip Search of the Universe," Variable Stars and Galaxies, ASP Conference Series, Vol. 30, p. 77 (San Francisco: Astronomical Society of the Pacific, 1992).

Wetterer, C.J., The CCD/Transit Instrument Atlas and Database Guide, Supplement to PhD Dissertation, (Department of Physics and Astronomy, University of New Mexico, 1995).

Chapter 4

Allen, R.H., Star Names: Their Lore and Meaning (New York: Dover Publications, 1963).

Bevington, P.R., Data Reduction and Error Analysis for the Physical Sciences (New York: McGraw-Hill Book Company, 1969).

Campbell, L. and Jacchia, L., The Story of Variable Stars (Philidelphia: The Blakiston Company, 1941).

Cox, J.P., Theory of Stellar Pulsation (Princeton: Princeton University Press, 1980).

Hawkins, M.R.S., "A Study of the Galactic halo from a complete sample of RR Lyrae variables to B = 21," Monthly Notices for the Royal Astronomical Society **206**, p.433, 1984.

Jacoby, G.H., Branch, D., Ciardullo, R., Davies, R.L., Harris, W.E., Pierce, M.J., Pritchet, C.J., Tonry, J.L., Welch, D.L., "A Critical Review of Selected Techniques for Measuring Extragalactic Distances," Publications of the Astronomical Society of the Pacific **104**, p. 599, 1992.

Kholopov, P.N., Samus, N.N., Frolov, M.S., Goranskij, V.P., Gorynya, N.A., Kireeva, N.N., Kukarkina, N.P., Kurochkin, N.E., Medvedeva, G.I., Perova, N.B., and Shugarov, S.Y., General Catalogue of Variable Stars, 4th edition (Moscow: Nauka Publishing House, 1985-88).

Madore, B.F., Freedman, W.L., " The Cepheid Distance Scale," Publications of the Astronomical Society of the Pacific **103**, p. 933, 1991.

Petit, M., Variable Stars (English translation, New York: John Wiley & Sons Ltd., 1987).

Saha, A. and Hoessel, J.G., "RR Lyrae stars in Local Group galaxies I: NGC 185," Astronomical Journal **99** (1), p. 97, 1990.

Stobie, R.S., Bishop, I.S., King, D.L., "Variable Stars in the South Galactic Cap," Monthly Notices of the Royal Astronomical Society **222**, p. 473, 1986.

Chapter 5

Barnes III, T.G., Hawley, S.L., "On Absolute Magnitues of RR Lyrae Stars," Astrophysical Journal **307**, p. L9, 1986.

Beckert, D.C. and Newberry M.V., "The Design and Testing of Filter-Detector Systems using Synthetic Photometry," Publications of the Astronomical Society of the Pacific **101**, p. 849, 1989.

Burstein, D., and Heiles, C., "Reddenings Derived form HI and Galaxy Counts: Accuracy and Maps," Astronomical Journal **87** (8), p. 1165, 1982.

Carney, B.W., Storm, J., Jones , R.V., "The Baade-Wesselink Method and the Distances to RR Lyrae Stars. VIII. Comparisons with Other Techniques and Implications for Globular Cluster Distances and Ages," Astrophysical Journal **386**, p. 663, 1992.

Cox, J.P., Theory of Stellar Pulsation (Princeton: Princeton University Press, 1980).

Hawley, S.L., Jeffreys, W.H., Barnes III, T.G., "Absolute Magnitudes and Kinematic Properties of RR Lyrae Stars,"

Astrophysical Journal **302**, p. 626, 1986.

Kholopov, P.N., Samus, N.N., Frolov, M.S., Goranskij, V.P., Gorynya, N.A., Kireeva, N.N., Kukarkina, N.P., Kurochkin, N.E., Medvedeva, G.I., Perova, N.B., and Shugarov, S.Y., General Catalogue of Variable Stars, 4th edition (Moscow: Nauka Publishing House, 1985-88).

Kukarkin, B.V., Kholopov, P.N., Artiukhina, N.M., Fedorovich, V.P., Frolov, M.S., Goranskij, V.P., Gorynya, N.A., Karitskaya, E.A., Kirreeva, N.N., Kukarkina, N.P., Kurochkin, N.E., Medvedeva, G.I., Perova, N.B., Ponomareva, G.A., Samus, N.N., and Shugarov, S.Y., New Catalogue of Suspected Variable Stars (Moscow: Nauka Publishing Office, 1982).

Lafler, J., and Kinman, T.D., "An RR Lyrae Star Survey with the Lick 20-inch Astrograph II. The Calculation of RR Lyrae Periods by Electronic Computer," Astrophysical Journal Supplement **11** p. 216, 1965.

Laubscher, B., Gregory, S., Bauer, T., Zeilik, M., Burns, J., "A CCD Camera System at Capilla Peak Observatory, New Mexico," Publications of the Astronomical Society of the Pacific **100**, p. 131, 1988.

Layden, A.C., Hanson, R.B., Hawley, S.L., "Absolute Magnitudes and Kinematics of RR Lyrae Stars via Statistical Parallax," Bulletin of the American Astronomical Society Vol. 26, No. 2, p. 911, 1994.

Lee, Y-W, "Evidence for an Old Galactic Bulge from RR Lyrae Stars in Baade's Window: Implications for the Formation of the Galaxy and the Age of the Universe," Astronomical Journal **104** (5), p. 1780, 1992.

Mihalas, D. and Binney, J., Galactic Astronomy: Structure and Kinematics, second edition (New York: W.H. Freeman and Company, 1981).

Nemec, J.M., Linnell Nemec, A.F., Lutz, T.E., "Period-Luminosity-Metallicity Relations, Pulsation Modes, Absolute Magnitudes, and Distances for Population II Variable Stars," Astronomical Journal **108**, p. 222, 1994.

Newberry, M.V., "Signal-to-Noise Considerations for Sky-Subtracted CCD Data," Publications of the Astronomical Society of the Pacific **103**, p. 122, 1991.

Saha, A. and Hoessel, J.G., "RR Lyrae stars in Local Group galaxies I: NGC 185," Astronomical Journal **99** (1), p. 97, 1990.

Sandage, A., "Evidence for a Period-Luminosity-Amplitude Relation for RR Lyrae Stars," Astrophysical Journal **244**, p. L23, 1981.

Sandage, A., Katem, B., Sandage, M., "The Oosterhoff Period Groups and the Age of Globular Clusters. I. Photometry of Cluster Variables in M15," Astrophysical Jouranl Supplement **46**, p. L41, 1981.

Sandage, A., "The Oosterhoff Period Groups and the Age of Globular Clusters. II. Properties of RR Lyrae Stars in Six Clusters: The P-L-A Realation," Astrophysical Jouranl **248**, p. 161, 1981.

Sandage, A., "The Oosterhoff Period Groups and the Age of Globular Clusters. III. The Age of the Globular Cluster System," Astrophysical Jouranl **252**, p. 553, 1982.

Sandage, A., Katem, B., Sandage, M., "The Oosterhoff Period Groups and the Age of Globular Clusters. IV. Field RR Lyrae Stars: Age of the Galactic Disk," Astrophysical Jouranl Supplement **252**, p. 574, 1982.

Stellingwerf, R.F., "Period Determination using Phase Dispersion Minimization," Astrophysical Journal **224**, p. 953, 1978.

Szeidl, B. "Multiple Periodic Variable Stars," IAU Colloquium No. 29, edited by W.S. Fitch (Reidel, Dordrecht), p. 133, 1976.

Tsesevich, V.P. "RR Lyrae Stars," in Pulsating Stars (edited by B.V. Kukarkin), English translation (New York: Halsted Press, 1975).

Tyson, J.A., "The Shift-and-Stare Technique and a Large Area CCD Mosaic," CCDs in Astronomy, ASP Conference series, Vol. 8, p. 1, (San Francisco: Astronomical Society of the Pacific, 1990).

, The Astronomical Almanac for the year 1993 (Washington D.C.: United States Government Printing, 1992).

(Capilla Peak research references)

Beckert, D.C., Cox, D., Gordon, S., Jaderlund, E., Mann, E., Zeilik, M., "1989 BVR photometry of CG Cygni", IBVS #3398, 1989.

Beckert, D.C. and Newberry M.V., "The Design and Testing of Filter-Detector Systems using Synthetic Photometry,"

Publications of the Astronomical Society of the Pacific **101**, p. 849, 1989.

Beckert, D.C., Gordon, S., Jaderlund, E., Mann, E., Zeilik, M., "CG Cygni redux : more 1989 BVR data", IBVS #3556, 1991.

Bryja, C., Lawrence, G., "Photometry of Suspected Low Mass Hyades Cluster Members," Bulletin of the American Astronomical Society, Vol. 23, No. 2, p. 908, 1991.

Bryja, C., Jones, T.J., Humphreys, R.M., Lawrence, G., Pennington, R.L., Zumach, W., "Candidate Brown Dwarfs in the Hyades," Astrophysical Journal **388**, p. L23, 1992.

Deeg, H-J., Brinks, E., Duric, N., Klein, U., Skillman, E., "New 325 MHz Observations of HII Galaxies: The Mechanisms That Shape the Unusual Radio Spectra," Astrophysical Journal **410**, p. 626, 1993.

Gordon, S., Hall, S., Ledlow, M., Mann, E., Zeilik, M., "1989 BVR light curves of RT And," IBVS #3469, 1990.

Gisler, G., Laubscher, B., Chabot, N., Boudreaux, K., Grashuis, R., "Multi-filter Optical Observations of SL9 Impact Spots on Jupiter," Bulletin of the American Astronomical Society Vol. 26, No. 4, p. 1374, 1994.

Gregory, S.A., Deeg, H.-J., Morrison, G., Crane, M., Grashuis, R., Lacey, C., "Galaxian Nuclear Spectral Types as a Function of Environment," Bulletin of the American Astronomical Society Vol. 22 No. 2, p. 881, 1990.

Hayes, J.J.E., Sadun, A.C., and R. Grashuis, "Narrow-band images of Arp 213," Bulletin of the American Astronomical Society Vol. 25 No. 4, p. 1248, 1993.

Kidger, M., et al., "Multiband Monitoring of OJ287 in 1993/94," Bulletin of the American Astronomical Society Vol. 26, No. 4, p. 1506, 1994.

Laubscher, B., Gregory, S., Bauer, T., Zeilik, M., Burns, J., "A CCD Camera System at Capilla Peak Observatory, New Mexico," Publications of the Astronomical Society of the Pacific **100**, p. 131, 1988.

Laubscher, B., Gregory, S., "Galaxy alignments in the Perseus supercluster," Bulletin of the American Astronomical Society Vol. 25, No. 2, p. 913, 1993.

Laubscher, B., "Problems with Galaxy Position Angles," Bulletin of the American Astronomical Society Vol. 26, No. 2, p. 963, 1994.

Odewahn, S.C., "Properties of the Magellanic-type spirals. I - Surface photometry of NGC 4618 and NGC 4625," Astronomical Journal **101**, p. 829, 1991.

Odewahn, S.C., Bryja, C., Humphreys ,R.M., "Improved CCD Standard Fields," Publications of the Astronomical Society of the Pacific **104**, p. 553, 1992.

Sadun, A., "Optical Variability of the Blazar OJ 287," Bulletin of the American Astronomical Society Vol. 26, No. 4, p. 1467, 1994.

Schmidt, B.P., Kirshner, R.P., Eastman, R.G., Grashuis, R., Dell'Antonio, I., Caldwell, N., Foltz, C., Huchra, J.P., Milone, A.A.E., "The Unusual Supernoa SN 1993J in M81," Nature **364**, p. 600, 1993.

Schmidt, B.P., Kirshner, R.P., Eastman, R.G., Phillips, M.M., Suntzeff, N.B., Hamuy, M., Aviles, R., Filippenko, A.V., Ho, L., Matheson, T., Grashuis, R., Maza, J., Kirkpatrick, J.D., Kuijken, K. Zucker, D., Bolte, M., Tyson, N., "The Expanding Photosphere Method Applied to SN 1992am at cz = 14600 km s^{-1}," Astronomical Journal **107**, p. 1444, 1994.

Summers, D.L., Zeilik, M., "Starspot activity on the RS CVn candidate 1E 1919+0427," Bulletin of the American Astronomical Society, Vol. 22, No. 4, p. 1295, 1990.

Summers, D.L., Zeilik, M., Jaderlund, E., Hoeppe, G., Collins, A., "1991 V-band photometry of an eclipsing binary: 1E 1919+0427," IBVS #3708, 1992.

Takalo, L.O., Pursimo, T., Sillanpää, A., Lehto, H., Nilsson, K., Kidger, M., deDiego, J.A., Gonzales-Perez, J.N., Rodriguez-Espinoza, J-M., Mahoney, T., Boltwood, P., Dultzin-Hacyan, D., Benitez, E., Turner, G.W., Robertson, J.W., Honeycutt, R.K., Efimov, T.S., Shakhovskoy, N., Charles, P.A., Schramm, K.J., Borgeest, U., Linde, J.V., Sadun, A., Grashuis, R., "The Light Curve of Blazar 3C 66A," Bulletin of the American Astronomical Society Vol. 26, No. 4, p. 1507, 1994.

Taylor, C., Brinks, E., Grashuis, R., Skillman, E., "An Optical and Radio Atlas of Companions to Dwarf Galaxies," to be published in Astrophysical Journal Supplement Series, 1995.

Wetterer, C.J., McGraw, J.T., Hess, T.R., Grashuis, R., "Variable Stars in the CCD/Transit Instrument (CTI) Survey," Bulletin of the American Astronomical Society Vol. 26, No. 2, p. 899, 1994.

Zeilik, M., DeBlasi, D., Rhodes, M., Budding, E., "A Half-Century of Starspot Activity on SV Camelopardalis," Bulletin

of the American Astronomical Society Vol. 19., No. 4, p. 1086, 1987.

Zeilik, M., Beckert, D., DeBlasi, C., Ledlow, M., Rhodes, M., Williams, T., "1987 BVRI Photometry of RT And," IBVS #3173, 1988.

Zeilik, M., Cox, D., DeBlasi, D., Ledlow, M., Rhodes, M., Williams, T., "1988 BVRI Photometry of XY UMa," IBVS #3200, 1988.

Zeilik, M., DeBlasi, D., Rhodes, M., Budding, E., "A Half-Century of Starspot Activity on SV Camelopardalis," The Astrophysical Journal **332**, p. 293, 1988.

Zeilik, M., Beckert, D., Cox, D., Dolby, J., Ledlow, M., Newberry, M., Rhodes, M., "1989 V-band light curve of RT And," IBVS #3301, 1989.

Zeilik, M., Cox, D.A., DeBlasi, C., Rhodes, M., Budding, E., "Long-Term Starspot Activity of Short-Period RS CVn Stars, Part II, RT Andromedae," The Astrophysical Journal **345**, p.991, 1989.

Zeilik, M., DeBlasi, C.B., Gordon, S., Ledlow, M., "1990 BVR photometry of XY UMa," IBVS #3535, 1990.

Zeilik, M., Gordon, S., Cox, D., Beckert, D., "Long-term starspot activity of short-period RS CVn stars : CG Cygni," Bulletin of the American Astronomical Society, Vol. 22, No. 2, p. 830, 1990.

Zeilik, M., Ledlow, M., Rhodes, M., Arevardo, M.J., Budding, E., "Long-Term Starspot Activity of Short-Period RS CVn Stars, Part III, BH Virginis," The Astrophysical Journal **354**, p.352, 1990.

Zeilik, M., Cox, D.A., De Blasi, C., Rhodes, M., Budding, E., "Long-Term Starspot Activity of Short-Period RS CVn Stars, Part IV, WY Cancri," The Astrophysical Journal **363**, p.467, 1990.

Zeilik, M., Heckert, P., Ledlow, M., Summers, D.L., Jaderlund, E., Boudreau, K., M., "1991 BVR photometry of CG Cygni," IBVS #3663, 1991.

Zeilik, M., Deeg, H.J., "Long-term starspot activity of short-period RS CVn stars : XY UMa," Bulletin of the American Astronomical Society, Vol. 23, No. 2, p. 880, 1991.

Zeilik, M., Gordon, S., Jaderlund, E., Ledlow, M., Summers, D.L., Heckert, P.A., Budding, E., Banks, T.S., "Long-term

Starspot Activity of Short-Period RS Canum Venaticorum Stars. V. CG Cygni," Astrophysical Journal **421**, p. 303, 1994.

Chapter 6

Blanco, B.M., "RR Lyrae Variables in Baade's Window," Astronomical Journal **89**, p. 1836, 1984.

Blanco, B.M., "RR Lyare Variables in a Galactic Bulge Window," Astronomical Journal **103**, p. 1872, 1992.

Hartwick, F.D.A., Barlow, D.J., Hesser, J.E., "Variable Stars in the Bulge of the Galaxy in a Field Around NGC 6304," Astronomical Journal **86**, p. 1044, 1981.

Hawkins, M.R.S., "A Study of the Galactic halo from a complete sample of RR Lyrae variables to B = 21," Monthly Notices for the Royal Astronomical Society **206**, p.433, 1984.

Kinman, T.D., "An RR Lyrae Star Survey with the Lick 20-inch Astrograph I. Methods of Observation and Reduction," Astrophysical Journal Supplement Series **11**, p. 199, 1965.

Kinman, T.D., Wirtanen, C.A., and Janes, K.A. "An RR Lyrae Star Survey with the Lick 20-inch Astrograph III. A Survey of Part of the Variable Star Field MWF 361," Astrophysical Journal Supplement Series **11**, p. 223, 1965.

Kinman, T.D., Wirtanen, C.A., and Janes, K.A. "An RR Lyrae Star Survey with the Lick 20-inch Astrograph IV. A Survey of Three Fields Near the North Galactic Pole," Astrophysical Journal Supplement Series **13**, p. 379, 1966.

Kinman, T.D., Mahaffey, C.T., and Wirtanen, C.A. "An RR Lyrae Star Survey with the Lick 20-inch Astrograph V. A Survey of Three Fields at Intermediate Latitudes Towards the Galactic Anti-Center," Astronomcal Journal **87**, p. 314, 1982.

Kinman, T.D., Wong-Swanson, B., Wenz, M., Harlan, E.A., "An RR Lyrae Star Survey with the Lick Astrograph VI. New Photometric Observations and Ephemerides for the Variables in the Field RR I (MWF 361A)," Astronomcal Journal **89**, p. 1200, 1984.

Lafler, J., and Kinman, T.D., "An RR Lyrae Star Survey with the Lick 20-inch Astrograph II. The Calculation of RR Lyrae Periods by Electronic Computer," Astrophysical Journal Supplement Series **11**, p. 216, 1965.

Layden, A.C., Hanson, R.B., Hawley, S.L., "Absolute Magnitudes and Kinematics of RR Lyrae Stars via Statistical Parallax," Bulletin of the American Astronomical Society Vol. 26, No. 2,

p. 911, 1994.

Merrifield, M.R., "The Rotation Curve of the Milky Way to $2.5R_0$ from the Thickness of the HI Layer," Astronomical Journal **103**, p. 1552, 1992.

Oort, J.H., and Plaut, L., "The Distance to the Galactic Centre Derived form RR Lyrae Variables, the Distribution of these Variables in the Galaxy's Inner Region and Halo, and a Redicussion of the Galactic Rotation Constants," Astronomy and Astrophysics **41**, p. 71, 1975.

Plaut, L., "Variable Stars in a Field Centered at l = 0°, b = +29° (Field 1 of the Palomar-Groningen Variable-Star Survey)," Bulletin of the Astronomical Institute of the Netherlands Supplement **1**, p. 105, 1966.

Plaut, L., "Variable Stars in a Field Centered at l = 4°, b = +12° (Field 2 of the Palomar-Groningen Variable-Star Survey) Part 1: Introduction and RR Lyrae-Type Variables," Bulletin of the Astronomical Institute of the Netherlands Supplement **2**, p. 293, 1968.

Plaut, L., "Variable Stars in a Field Centered at l = 4°, b = +12° (Field 2 of the Palomar-Groningen Variable-Star Survey)," Bulletin of the Astronomical Institute of the Netherlands Supplement **3**, p. 1, 1968.

Plaut, L., "Variable Stars in a Field Centered at l = 0°, b = -10° (Field 3 of the Palomar-Groningen Variable-Star Survey $\alpha_{1950} = 18^h24^m04^s$, $\delta_{1950} = -33°\ 58.6'$)," Astronomy and Astrophysics **8**, p. 341, 1970.

Plaut, L., "Variable Stars in a Field Centered at l = 0°, b = -10° (Field 3 of the Palomar-Groningen Variable-Star Survey)," Astronomy and Astrophysics Supplement **4**, p. 73, 1971.

Plaut, L., "Palomar-Groningen Variable Star Survey. VI. B and V Observations of Twenty RR Lryae Variables and Some Related Problems," Astronomy and Astrophysics Supplement **12**, p. 351, 1973.

Preston, G.W., Shectman, S.A., and Beers, T.C., "Detection of a Galactic Color Gradient for Blue Horizontal-Branch Stars of the Halo Field and Implications for the Halo Age and Denisty Distrubutions," Astrophysical Journal **375**, p. 121, 1991.

Reid, M.J., in The Center of the Galaxy, IAU Symposium No. 136, (Kluwer, Dordrecht, 1989).

Saha, A., "A Search for Distant Halo RR Lyrae Stars," Astrophysical Journal **283**, p. 580, 1984.

Saha, A., and Oke, J.B., "Spectroscopy and Spectrophotometry of Distant Halo RR Lyrae Stars," Astrophysical Journal **285**, p. 688, 1984.

Saha, A., "RR Lyrae Stars and the Distant Galactic Halo: Distribution, Chemical Composition, Kinematics, and Dynamics," Astrophysical Journal **289**, p. 310, 1985.

Stobie, R.S., Bishop, I.S., King, D.L., "Variable Stars in the South Galactic Cap," Monthly Notices of the Royal Astronomical Society **222**, p. 473, 1986.

Suntzeff, N.B., Kinman, T.D., Kraft, R.P., "Metal Abundances of RR Lyrae Variables in Selected Galactic Star Fields. V. The Lick Astrographic Fields at Intermediate Galactic Latitudes," Astrophysical Journal **367**, p. 528, 1991.

van den Bergh, S., "UBV Photometry in the Nuclear Bulge of the Galaxy," Astronomical Journal **76**, p. 1082, 1971.

Zinn, R., "The Globular Cluster System of the Galaxy. IV. The Halo and Disk Subsystems," Astrophysical Journal **293**, p. 424, 1985.

Chapter 7

Armandroff, T.E., DaCosta, G.S., "The Radial Velocity, Velocity Dispersion, and Mass-to-Light Ratio of the Sculptor Dwarf Galaxy," Astronomical Journal **92**, p. 777, 1986.

Benedict, G.F., and Shelus, P.J., "Applications of Automated Invenotry Techniques to Astrometry," Proceedings of I.A.U. Colloquium No. 48 on Modern Astronomy (Institute of Astronomy, Vienna, 1978).

Benedict, G.F., McGraw, J.T., Hess, T.R., Cawson, M.G.M., Keane, M.J., "Relative Astrometry with the Steward Observatory CCD/Transit Insturment," Astronomical Journal **101**, p. 279, 1991.

Frenk, C.S., White, S.D.M., "The kinematics and dynamics of the Galactic globular cluster system," Monthly Notices of the Royal Astronomical Society **193**, p. 295, 1980.

Harris, W.E., "Spatial structure of the globular cluster system and the distance to the Galactic center," Astronomical Journal **81**, p. 1095, 1976.

Hartwick, F.D.A., Sargent, W.L.W., "Radial Velocities for Outlying Satellites and their Implications for the Mass of the Galaxy," Astrophysical Journal **221**, p. 512, 1978.

Hawkins, M.R.S., "Direct evidence for a massive Galactic halo," Nature **303**, p. 406, 1983.

Hawkins, M.R.S., "A Study of the Galactic halo from a complete sample of RR Lyrae variables to B = 21," Monthly Notices for the Royal Astronomical Society **206**, p.433, 1984.

Hesser, J.E., Shawl, S.J., Meyer, J.E., "Systematic Reinvestigation of the Radial Velocities of the Galactic Globular Clusters: Image-Tube Results," Publications of the Astronomical Society of the Pacific **98**, p.403, 1986.

Jeffreys, W.H., Fitzpatrick, M.J., McArthur, B.E., Gaussfit - A System for Least Squares and Robust Estimation: User's Manual (Department of Astronomy, University of Texas, Austin, 1989).

Kulessa, A.S., Lynden-Bell, D., "The mass of the Milky Way Galaxy," Monthly Notices for the Royal Astronomical Society **255**, p. 105, 1992.

Layden, A.C., "The Metallicities and Kinematics of RR Lyrae Variables. I. New Observations of Local Stars," Astronomical Journal **108**, p. 1016, 1994.

Little, B., Tremaine, S., "Distant Satellites as Probes of our Galaxy's Mass Distribution," Astrophysical Journal **320**, p. 493, 1987.

Liu, T., and Janes, K.A., "The Luminosity Scale of RR Lyrae Stars with the Baade-Wesselink Method. I. Photometry and Radial Velocities," Astrophysical Journal Supplement Series **69**, p. 593, 1989.

Lynden-Bell, D., Cannon, R.D., Godwin, P.J., "Slippery evidence on the Galaxy's invisible heavy halo," Monthly Notices of the Royal Astronomical Society **204**, p. 87P, 1983.

Merrifield, M.R., "The Rotation Curve of the Milky Way to $2.5R_0$ from the Thickness of the HI Layer," Astronomical Journal **103**, p. 1552, 1992.

Mihalas, D. and Binney, J., Galactic Astronomy: Structure and Kinematics, second edition (New York: W.H. Freeman and Company, 1981).

Oke, J.B., Giver, L.P., and Searle, L., "An Analysis of the Absolute Energy Distribution in the Spectrum of SU Draconis," Astrophysical Journal **136**, p. 393, 1962.

Oke, J.B., "A Spectrophotometric Study of X Arietis," Astrophysical Journal **145**, p. 468, 1966.

Olszewski, E.W., Peterson, R.C., Aaronson, M., "High-Precision Radial Velocities for Faint Giants: Radial Velocities of Extreme Halo Systems and the Mass of the Galaxy," Astrophysical Journal **302**, p. L45, 1986.

Peterson, R.C., "Radial Velocities of Remote Globular Clusters: Stalking the Missing Mass," Astrophysical Journal **297**, p. 309, 1985.

Peterson, R.C., Latham, D.W., "The Radial Velocity and Velocity Dispersion of the Remote Globular Cluster Palomar 15: Constraints on the Mass of the Galaxy," Astrophysical Journal **336**, p. 178, 1989.

Saha, A., and Oke, J.B., "Spectroscopy and Spectrophotometry of Distant Halo RR Lyrae Stars," Astrophysical Journal **285**, p. 688, 1984.

Saha, A., "RR Lyrae Stars and the Distant Galactic Halo: Distribution, Chemical Composition, Kinematics, and Dynamics," Astrophysical Journal **289**, p. 310, 1985.

Webbink, R.F., "A Catalog of Radial Velocities in Galactic Globular Clusters," Astrophysical Journal Supplement **45**, p. 259, 1981.

Zaritsky, D., Olszewski, E.W., Schommer, R.A., Peterson, R.C., Aaronson, M., "Velocities of Stars in Remote Galactic Satellites and the Mass of the Galaxy," Astrophysical Journal **345**, p. 769, 1989.

Appendix 1

Appendix 2

Wetterer, C.J., The CCD/Transit Instrument Atlas and Database Guide, Supplement to PhD Dissertation, (Department of Physics and Astronomy, University of New Mexico, 1995).

Appendix 3

RR LYRAE VARIABLE STARS IN THE CCD/TRANSIT INSTRUMENT SURVEY

by

Charles J. Wetterer

Captain, US Air Force

343 pages

PhD, Physics, University of New Mexico, 1995

ABSTRACT

RR Lyrae variable stars have long been recognized as important tools in probing the mass, chemical distribution and kinematics of the Galaxy from the inner recesses of the nuclear bulge to the outer environs of the distant Galactic halo. This dissertation chronicles an RR Lyrae variable star survey from a thorough description of the initial observations with the CCD/Transit Instrument (CTI), to an examination of RR Lyrae space density and the Galactic mass using the discovered RR Lyrae stars.

The RR Lyrae space density as a function of Galactocentric distance is shown to be a power-law function ($R^{-3 \text{ to } -3.5}$) and consistant with an ellipsoidal distribution in the nuclear bulge and more spherically symmetric distribution in the Galactic halo. The unique area of the CTI survey and comparison to other RR Lyrae surveys verifies this function is valid throughout the Galactic halo and over the range of Galactocentric distances sampled ($0.6 < R < 40$ kpc). Local underdensities and overdensities of RR Lyrae stars are

discussed, including a possible resonance with the Magallenic Clouds ($R \approx 50$ kpc).

The Galactic mass estimated using radial velocities of RR Lyrae stars discovered in the CTI survey does not support the existence of a massive dark Galactic halo. This result is compared to the mass as determined from the radial velocities of other halo objects. Depending on the type of orbits assumed, the radial velocities of RR Lyrae stars, globular clusters, and dwarf elliptical galaxies can be used to support the notion that a massive dark halo exists (i.e. the mass-to-light ratio increases for increasing Galactocentric distance), or that no excessive dark matter exists in the Galactic halo (i.e. the mass-to-light ratio remains constant for increasing Galactocentric distance).

References (primary)

Chapter 2

Cawson, M.G.M., McGraw, J.T., Keane, M.J., "A Relational Database Approach to Astronomical Research," SPIE Proc. Vol. 627, p. 70, 1986.

Cawson, M.G.M., McGraw, J.T., Keane, M.J., "The CCD/Transit Instrument (CTI) Data-Analysis System," SPIE Proc. Vol. 627, p. 79, 1986.

Delporte, E., Délimitation Scientifique des Constellations (Tables et Cartes), (Cambridge, At the University Press, 1930).

Dixon, R.S., Gearhart, M.R., and Schmidtke, P.C., Atlas of Sky Overlay Maps (for the Palomar Sky Survey), (The Ohio State Radio Observatory, 1981).

Hoffleit, D., Bright Star Catalogue, 5th revised edition (Yale University Observatory, 1982).

Jones, K.G. (editor), Webb Society Deep-Sky Observer's Handbook Volume 5: Clusters of Galaxies, (Enslow Publishing, 1981).

Kholopov, P.N., Samus, N.N., Frolov, M.S., Goranskij, V.P., Gorynya, N.A., Kireeva, N.N., Kukarkina, N.P., Kurochkin, N.E., Medvedeva, G.I., Perova, N.B., and Shugarov, S.Y., General Catalogue of Variable Stars, 4th edition (Moscow: Nauka Publishing House, 1985-88).

McGraw, J.T., Angel, J.R.P., and Sargent, T.A., "A CCD Transit-telescope Survey for Galactic and Extragalactic Variability and Polarization," SPIE Proc. Vol. 264, p. 20, 1980.

McGraw, J.T., Stockman, H.S., Angel, J.R.P., Epps, H., and Williams, J.T., "The CCD/transit instrument (CTI) deep photometric and polarimetric survey - a progress report," SPIE Proc. Vol. 331, p. 137, 1983.

McGraw, J.T., Cawson, M.G.M., Keane, M.J., "Operation of the CCD/Transit Instrument (CTI)," SPIE Proc. Vol. 627, p. 60, 1986.

McGraw, J.T., Hess, T.R., Green, E.M., Bridges, C.T., Benedict, G.F., "Photometric and Positional Calibration of the CCD/Transit Instrument (CTI) Strip of the Sky," Bulletin of the American Astronomical Society Vol. 21, No. 3, p. 1021, 1989.

McGraw, J.T., "A Strip Search of the Universe," Variable Stars and Galaxies, ASP Conference Series, Vol. 30, p. 77 (San Francisco: Astronomical Society of the Pacific, 1992).

McGraw, J.T., Wetterer, C.J., Hess, T.R., Green, E.M., "Photometric Standard Stars in the CCD/Transit Instrument (CTI) Survey," Bulletin of the American Astronomical Society Vol. 26, No. 2, p. 899, 1994.

Paul, M., "Corrective Systems for Astronomical Reflectors," Rev. d'Optique Vol. 14, p. 169, 1935.

Sulentic, J.W. and Tifft, W.G., The Revised New General Catalogue of Nonstellar Astronomical Objects, (Tucson: The University of Arizona Press, 1973).

Veron-Cetty, M.P., and Veron, P., "A Catalogue of Quasars and Active Galactic Nuclei, 4th edition," E.S.O. Sci. Rep. 7, 1989.

Wetterer, C.J., McGraw, J.T., Hess, T.R., Grashuis, R., "Variable Stars in the CCD/Transit Instrument (CTI) Survey," Bulletin of the American Astronomical Society Vol. 26, No. 2, p. 899, 1994.

Wetterer, C.J., The CCD/Transit Instrument Atlas and Database Guide, Supplement to PhD Dissertation, (Department of Physics and Astronomy, University of New Mexico, 1995).

Zwicky, F., Herzog, E., Wild, P., Karpowicz, M., Kowal, C.T., The Catalogue of Galaxies and Clusters of Galaxies, (California Institute of Technology, 1961-68).

, The National Geographic Society - Palomar Observatory Sky Survey, (California Institute of Technology, 1954).

, Smithsonian Astrophysical Observatory Star Catalog, (Washington, Smithsonian Institution, 1966-1990).

Chapter 3

Cawson, M.G.M., McGraw, J.T., Keane, M.J., "A Relational Database Approach to Astronomical Research," SPIE Proc. Vol. 627, p. 70, 1986.

Cawson, M.G.M., McGraw, J.T., Keane, M.J., "The CCD/Transit Instrument (CTI) Data-Analysis System," SPIE Proc. Vol. 627, p. 79, 1986.

Dieckvoss, W., Kox, H., Gunther, A., and Brosterhus, E., AGK3 Star Catalog of Positions and Proper Motions North of -2.5 degree Declination (Hamburg-Bergedorf, 1975).

Lasker, B.M., Sturch, C.R., McLean, B.J., Russell, J.L., Jenkner, H., Shara, M.M., "The Guide Star Catalog I. Astronomical Foundations and Image Processing," Astronomical Journal **99**(6), p. 2019, 1990.

McGraw, J.T., Hess, T.R., Green, E.M., Bridges, C.T., Benedict, G.F., "Photometric and Positional Calibration of the CCD/Transit Instrument (CTI) Strip of the Sky," Bulletin of the American Astronomical Society Vol. 21, No. 3, p. 1021, 1989.

McGraw, J.T., "A Strip Search of the Universe," Variable Stars and Galaxies, ASP Conference Series, Vol. 30, p. 77 (San Francisco: Astronomical Society of the Pacific, 1992).

Wetterer, C.J., The CCD/Transit Instrument Atlas and Database Guide, Supplement to PhD Dissertation, (Department of Physics and Astronomy, University of New Mexico, 1995).

Chapter 4

Allen, R.H., Star Names: Their Lore and Meaning (New York: Dover Publications, 1963).

Bevington, P.R., Data Reduction and Error Analysis for the Physical Sciences (New York: McGraw-Hill Book Company, 1969).

Campbell, L. and Jacchia, L., The Story of Variable Stars (Philidelphia: The Blakiston Company, 1941).

Cox, J.P., Theory of Stellar Pulsation (Princeton: Princeton University Press, 1980).

Hawkins, M.R.S., "A Study of the Galactic halo from a complete sample of RR Lyrae variables to B = 21," Monthly Notices for the Royal Astronomical Society **206**, p.433, 1984.

Kholopov, P.N., Samus, N.N., Frolov, M.S., Goranskij, V.P., Gorynya, N.A., Kireeva, N.N., Kukarkina, N.P., Kurochkin, N.E., Medvedeva, G.I., Perova, N.B., and Shugarov, S.Y., General Catalogue of Variable Stars, 4th edition (Moscow: Nauka Publishing House, 1985-88).

Petit, M., Variable Stars (English translation, New York: John Wiley & Sons Ltd., 1987).

Saha, A. and Hoessel, J.G., "RR Lyrae stars in Local Group galaxies I: NGC 185," Astronomical Journal **99** (1), p. 97, 1990.

Stobie, R.S., Bishop, I.S., King, D.L., "Variable Stars in the South Galactic Cap," Monthly Notices of the Royal Astronomical Society **222**, p. 473, 1986.

Chapter 5

Barnes III, T.G., Hawley, S.L., "On Absolute Magnitues of RR Lyrae Stars," Astrophysical Journal **307**, p. L9, 1986.

Beckert, D.C. and Newberry M.V., "The Design and Testing of Filter-Detector Systems using Synthetic Photometry," Publications of the Astronomical Society of the Pacific **101**, p. 849, 1989.

Burstein, D., and Heiles, C., "Reddenings Derived form HI and Galaxy Counts: Accuracy and Maps," Astronomical Journal **87** (8), p. 1165, 1982.

Carney, B.W., Storm, J., Jones , R.V., "The Baade-Wesselink Method and the Distances to RR Lyrae Stars. VIII. Comparisons with Other Techniques and Implications for Globular Cluster Distances and Ages," Astrophysical Journal **386**, p. 663, 1992.

Cox, J.P., Theory of Stellar Pulsation (Princeton: Princeton University Press, 1980).

Hawley, S.L., Jeffreys, W.H., Barnes III, T.G., "Absolute Magnitudes and Kinematic Properties of RR Lyrae Stars," Astrophysical Journal **302**, p. 626, 1986.

Kholopov, P.N., Samus, N.N., Frolov, M.S., Goranskij, V.P., Gorynya, N.A., Kireeva, N.N., Kukarkina, N.P., Kurochkin, N.E., Medvedeva, G.I., Perova, N.B., and Shugarov, S.Y., General Catalogue of Variable Stars, 4th edition (Moscow: Nauka Publishing House, 1985-88).

Kukarkin, B.V., Kholopov, P.N., Artiukhina, N.M., Fedorovich, V.P., Frolov, M.S., Goranskij, V.P., Gorynya, N.A., Karitskaya, E.A., Kirreeva, N.N., Kukarkina, N.P., Kurochkin, N.E., Medvedeva, G.I., Perova, N.B., Ponomareva, G.A., Samus, N.N., and Shugarov, S.Y., New Catalogue of Suspected Variable Stars (Moscow: Nauka Publishing Office, 1982).

Lafler, J., and Kinman, T.D., "An RR Lyrae Star Survey with the Lick 20-inch Astrograph II. The Calculation of RR Lyrae Periods by Electronic Computer," Astrophysical Journal Supplement **11** p. 216, 1965.

Laubscher, B., Gregory, S., Bauer, T., Zeilik, M., Burns, J., "A CCD Camera System at Capilla Peak Observatory, New Mexico," Publications of the Astronomical Society of the Pacific **100**, p. 131, 1988.

Layden, A.C., Hanson, R.B., Hawley, S.L., "Absolute Magnitudes and Kinematics of RR Lyrae Stars via Statistical Parallax," Bulletin of the American Astronomical Society Vol. 26, No. 2, p. 911, 1994.

Lee, Y-W, "Evidence for an Old Galactic Bulge from RR Lyrae Stars in Baade's Window: Implications for the Formation of the Galaxy and the Age of the Universe," Astronomical Journal **104** (5), p. 1780, 1992.

Mihalas, D. and Binney, J., Galactic Astronomy: Structure and Kinematics, second edition (New York: W.H. Freeman and Company, 1981).

Nemec, J.M., Linnell Nemec, A.F., Lutz, T.E., "Period-Luminosity-Metallicity Relations, Pulsation Modes, Absolute Magnitudes, and Distances for Population II Variable Stars," Astronomical Journal **108**, p. 222, 1994.

Newberry, M.V., "Signal-to-Noise Considerations for Sky-Subtracted CCD Data," Publications of the Astronomical Society of the Pacific **103**, p. 122, 1991.

Saha, A. and Hoessel, J.G., "RR Lyrae stars in Local Group galaxies I: NGC 185," Astronomical Journal **99** (1), p. 97, 1990.

Sandage, A., "Evidence for a Period-Luminosity-Amplitude Relation for RR Lyrae Stars," Astrophysical Journal **244**, p. L23, 1981.

Sandage, A., Katem, B., Sandage, M., "The Oosterhoff Period Groups and the Age of Globular Clusters. I. Photometry of Cluster Variables in M15," Astrophysical Jouranl Supplement **46**, p. L41, 1981.

Sandage, A., "The Oosterhoff Period Groups and the Age of Globular Clusters. II. Properties of RR Lyrae Stars in Six Clusters: The P-L-A Realation," Astrophysical Jouranl **248**, p. 161, 1981.

Sandage, A., "The Oosterhoff Period Groups and the Age of Globular Clusters. III. The Age of the Globular Cluster System," Astrophysical Jouranl **252**, p. 553, 1982.

Sandage, A., Katem, B., Sandage, M., "The Oosterhoff Period Groups and the Age of Globular Clusters. IV. Field RR Lyrae Stars: Age of the Galactic Disk," Astrophysical Jouranl Supplement **252**, p. 574, 1982.

Stellingwerf, R.F., "Period Determination using Phase Dispersion Minimization," Astrophysical Journal **224**, p. 953, 1978.

Szeidl, B. "Multiple Periodic Variable Stars," IAU Colloquium No. 29, edited by W.S. Fitch (Reidel, Dordrecht), p. 133, 1976.

Tsesevich, V.P. "RR Lyrae Stars," in Pulsating Stars (edited

by B.V. Kukarkin), English translation (New York: Halsted Press, 1975).

Tyson, J.A., "The Shift-and-Stare Technique and a Large Area CCD Mosaic," CCDs in Astronomy, ASP Conference series, Vol. 8, p. 1, (San Francisco: Astronomical Society of the Pacific, 1990).

, The Astronomical Almanac for the year 1993 (Washington D.C.: United States Government Printing, 1992).

Chapter 6

Blanco, B.M., "RR Lyrae Variables in Baade's Window," Astronomical Journal **89**, p. 1836, 1984.

Blanco, B.M., "RR Lyare Variables in a Galactic Bulge Window," Astronomical Journal **103**, p. 1872, 1992.

Hartwick, F.D.A., Barlow, D.J., Hesser, J.E., "Variable Stars in the Bulge of the Galaxy in a Field Around NGC 6304," Astronomical Journal **86**, p. 1044, 1981.

Hawkins, M.R.S., "A Study of the Galactic halo from a complete sample of RR Lyrae variables to B = 21," Monthly Notices for the Royal Astronomical Society **206**, p.433, 1984.

Kinman, T.D., "An RR Lyrae Star Survey with the Lick 20-inch Astrograph I. Methods of Observation and Reduction," Astrophysical Journal Supplement Series **11**, p. 199, 1965.

Kinman, T.D., Wirtanen, C.A., and Janes, K.A. "An RR Lyrae Star Survey with the Lick 20-inch Astrograph III. A Survey of Part of the Variable Star Field MWF 361," Astrophysical Journal Supplement Series **11**, p. 223, 1965.

Kinman, T.D., Wirtanen, C.A., and Janes, K.A. "An RR Lyrae Star Survey with the Lick 20-inch Astrograph IV. A Survey of Three Fields Near the North Galactic Pole," Astrophysical Journal Supplement Series **13**, p. 379, 1966.

Kinman, T.D., Mahaffey, C.T., and Wirtanen, C.A. "An RR Lyrae Star Survey with the Lick 20-inch Astrograph V. A Survey of Three Fields at Intermediate Latitudes Towards the Galactic Anti-Center," Astronomcal Journal **87**, p. 314, 1982.

Kinman, T.D., Wong-Swanson, B., Wenz, M., Harlan, E.A., "An RR Lyrae Star Survey with the Lick Astrograph VI. New Photometric Observations and Ephemerides for the Variables in the Field RR I (MWF 361A)," Astronomcal Journal **89**, p. 1200, 1984.

Lafler, J., and Kinman, T.D., "An RR Lyrae Star Survey with

the Lick 20-inch Astrograph II. The Calculation of RR Lyrae Periods by Electronic Computer," Astrophysical Journal Supplement Series **11**, p. 216, 1965.

Layden, A.C., Hanson, R.B., Hawley, S.L., "Absolute Magnitudes and Kinematics of RR Lyrae Stars via Statistical Parallax," Bulletin of the American Astronomical Society Vol. 26, No. 2, p. 911, 1994.

Merrifield, M.R., "The Rotation Curve of the Milky Way to $2.5R_0$ from the Thickness of the HI Layer," Astronomical Journal **103**, p. 1552, 1992.

Oort, J.H., and Plaut, L., "The Distance to the Galactic Centre Derived form RR Lyrae Variables, the Distribution of these Variables in the Galaxy's Inner Region and Halo, and a Redicussion of the Galactic Rotation Constants," Astronomy and Astrophysics **41**, p. 71, 1975.

Plaut, L., "Variable Stars in a Field Centered at l = 0°, b = +29° (Field 1 of the Palomar-Groningen Variable-Star Survey)," Bulletin of the Astronomical Institute of the Netherlands Supplement **1**, p. 105, 1966.

Plaut, L., "Variable Stars in a Field Centered at l = 4°, b = +12° (Field 2 of the Palomar-Groningen Variable-Star Survey) Part 1: Introduction and RR Lyrae-Type Variables," Bulletin of the Astronomical Institute of the Netherlands Supplement **2**, p. 293, 1968.

Plaut, L., "Variable Stars in a Field Centered at l = 4°, b = +12° (Field 2 of the Palomar-Groningen Variable-Star Survey)," Bulletin of the Astronomical Institute of the Netherlands Supplement **3**, p. 1, 1968.

Plaut, L., "Variable Stars in a Field Centered at l = 0°, b = -10° (Field 3 of the Palomar-Groningen Variable-Star Survey $\alpha_{1950} = 18^h24^m04^s$, $\delta_{1950} = -33°\ 58.6'$)," Astronomy and Astrophysics **8**, p. 341, 1970.

Plaut, L., "Variable Stars in a Field Centered at l = 0°, b = -10° (Field 3 of the Palomar-Groningen Variable-Star Survey)," Astronomy and Astrophysics Supplement **4**, p. 73, 1971.

Plaut, L., "Palomar-Groningen Variable Star Survey. VI. B and V Observations of Twenty RR Lryae Variables and Some Related Problems," Astronomy and Astrophysics Supplement **12**, p. 351, 1973.

Preston, G.W., Shectman, S.A., and Beers, T.C., "Detection of a Galactic Color Gradient for Blue Horizontal-Branch Stars of the Halo Field and Implications for the Halo Age and Denisty Distrubutions," Astrophysical Journal **375**, p. 121, 1991.

Reid, M.J., in The Center of the Galaxy, IAU Symposium No. 136, (Kluwer, Dordrecht, 1989).

Saha, A., "A Search for Distant Halo RR Lyrae Stars," Astrophysical Journal **283**, p. 580, 1984.

Saha, A., and Oke, J.B., "Spectroscopy and Spectrophotometry of Distant Halo RR Lyrae Stars," Astrophysical Journal **285**, p. 688, 1984.

Saha, A., "RR Lyrae Stars and the Distant Galactic Halo: Distribution, Chemical Composition, Kinematics, and Dynamics," Astrophysical Journal **289**, p. 310, 1985.

Stobie, R.S., Bishop, I.S., King, D.L., "Variable Stars in the South Galactic Cap," Monthly Notices of the Royal Astronomical Society **222**, p. 473, 1986.

Suntzeff, N.B., Kinman, T.D., Kraft, R.P., "Metal Abundances of RR Lyrae Variables in Selected Galactic Star Fields. V. The Lick Astrographic Fields at Intermediate Galactic Latitudes," Astrophysical Journal **367**, p. 528, 1991.

van den Bergh, S., "UBV Photometry in the Nuclear Bulge of the Galaxy," Astronomical Journal **76**, p. 1082, 1971.

Zinn, R., "The Globular Cluster System of the Galaxy. IV. The Halo and Disk Subsystems," Astrophysical Journal **293**, p. 424, 1985.

Chapter 7

Armandroff, T.E., DaCosta, G.S., "The Radial Velocity, Velocity Dispersion, and Mass-to-Light Ratio of the Sculptor Dwarf Galaxy," Astronomical Journal **92**, p. 777, 1986.

Benedict, G.F., and Shelus, P.J., "Applications of Automated Invenotry Techniques to Astrometry," Proceedings of I.A.U. Colloquium No. 48 on Modern Astronomy (Institute of Astronomy, Vienna, 1978).

Benedict, G.F., McGraw, J.T., Hess, T.R., Cawson, M.G.M., Keane, M.J., "Relative Astrometry with the Steward Observatory CCD/Transit Insturment," Astronomical Journal **101**, p. 279, 1991.

Frenk, C.S., White, S.D.M., "The kinematics and dynamics of the Galactic globular cluster system," Monthly Notices of the Royal Astronomical Society **193**, p. 295, 1980.

Harris, W.E., "Spatial structure of the globular cluster system and the distance to the Galactic center," Astronomical Journal **81**, p. 1095, 1976.

Hartwick, F.D.A., Sargent, W.L.W., "Radial Velocities for Outlying Satellites and their Implications for the Mass of the Galaxy," Astrophysical Journal **221**, p. 512, 1978.

Hawkins, M.R.S., "Direct evidence for a massive Galactic halo," Nature **303**, p. 406, 1983.

Hawkins, M.R.S., "A Study of the Galactic halo from a complete sample of RR Lyrae variables to B = 21," Monthly Notices for the Royal Astronomical Society **206**, p.433, 1984.

Hesser, J.E., Shawl, S.J., Meyer, J.E., "Systematic Reinvestigation of the Radial Velocities of the Galactic Globular Clusters: Image-Tube Results," Publications of the Astronomical Society of the Pacific **98**, p.403, 1986.

Jeffreys, W.H., Fitzpatrick, M.J., McArthur, B.E., Gaussfit - A System for Least Squares and Robust Estimation: User's Manual (Department of Astronomy, University of Texas, Austin, 1989).

Kulessa, A.S., Lynden-Bell, D., "The mass of the Milky Way Galaxy," Monthly Notices for the Royal Astronomical Society **255**, p. 105, 1992.

Layden, A.C., "The Metallicities and Kinematics of RR Lyrae Variables. I. New Observations of Local Stars," Astronomical Journal **108**, p. 1016, 1994.

Little, B., Tremaine, S., "Distant Satellites as Probes of our Galaxy's Mass Distribution," Astrophysical Journal **320**, p. 493, 1987.

Liu, T., and Janes, K.A., "The Luminosity Scale of RR Lyrae Stars with the Baade-Wesselink Method. I. Photometry and Radial Velocities," Astrophysical Journal Supplement Series **69**, p. 593, 1989.

Lynden-Bell, D., Cannon, R.D., Godwin, P.J., "Slippery evidence on the Galaxy's invisible heavy halo," Monthly Notices of the Royal Astronomical Society **204**, p. 87P, 1983.

Merrifield, M.R., "The Rotation Curve of the Milky Way to $2.5R_0$ from the Thickness of the HI Layer," Astronomical Journal **103**, p. 1552, 1992.

Mihalas, D. and Binney, J., Galactic Astronomy: Structure and Kinematics, second edition (New York: W.H. Freeman and Company, 1981).

Oke, J.B., Giver, L.P., and Searle, L., "An Analysis of the Absolute Energy Distribution in the Spectrum of SU Draconis," Astrophysical Journal **136**, p. 393, 1962.

Oke, J.B., "A Spectrophotometric Study of X Arietis," Astrophysical Journal **145**, p. 468, 1966.

Olszewski, E.W., Peterson, R.C., Aaronson, M., "High-Precision Radial Velocities for Faint Giants: Radial Velocities of Extreme Halo Systems and the Mass of the Galaxy," Astrophysical Journal **302**, p. L45, 1986.

Peterson, R.C., "Radial Velocities of Remote Globular Clusters: Stalking the Missing Mass," Astrophysical Journal **297**, p. 309, 1985.

Peterson, R.C., Latham, D.W., "The Radial Velocity and Velocity Dispersion of the Remote Globular Cluster Palomar 15: Constraints on the Mass of the Galaxy," Astrophysical Journal **336**, p. 178, 1989.

Saha, A., and Oke, J.B., "Spectroscopy and Spectrophotometry of Distant Halo RR Lyrae Stars," Astrophysical Journal **285**, p. 688, 1984.

Saha, A., "RR Lyrae Stars and the Distant Galactic Halo: Distribution, Chemical Composition, Kinematics, and Dynamics," Astrophysical Journal **289**, p. 310, 1985.

Webbink, R.F., "A Catalog of Radial Velocities in Galactic Globular Clusters," Astrophysical Journal Supplement **45**, p. 259, 1981.

Zaritsky, D., Olszewski, E.W., Schommer, R.A., Peterson, R.C., Aaronson, M., "Velocities of Stars in Remote Galactic Satellites and the Mass of the Galaxy," Astrophysical Journal **345**, p. 769, 1989.

References (secondary)

Chapter 2

Baker, J.G., "On Improving the Effectiveness of Large Telescopes," IEEE Trans. on Aerospace and Electronic Systems Vol. AES-5, No. 2, p. 261, 1969.

Benedict, G.F., McGraw, J.T., Hess, T.R., Cawson, M.G.M., Keane, M.J., "Relative Astrometry with the Steward Observatory CCD/Transit Instrument," Bulletin of the American Astonomical Society Vol. 21, No. 4, p. 1109, 1989.

Benedict, G.F., McGraw, J.T., Hess, T.R., Cawson, M.G.M., Keane, M.J., "Relative Astrometry with the Steward Observatory CCD/Transit Instrument," Astronomical Journal **101**, p. 279, 1991.

Bond, H.E., Kron, R.G. and Spinrad, H., "GQ Comae and V396 Herculis: Two Low-Redshift Optically Variable QSOs," Astrophysical Journal **213** (1), p. 1, 1977.

Borra, E.F., Content, R., Drinkwater, M.J., Szapiel, S., "A Deffraction Limited f/2 1.5 meter Diameter Liquid Mirror," Astrophysical Journal Letters **346**, p. L41, 1989.

Borra, E.F., Content, R., Girard, L., Szapiel, S., Tremblay, L.M., "Liquid Mirrors: Optical Shop Tests and Contributions to the Technology," Astrophysical Journal **393**, p. 829, 1992.

Content, R., Borra, E.F., Drinkwater, M.J., Poirier, S., Poisson, E., Beauchemin, M., Boily, E., Gauthier, A., Tremblay, L.M., "A Search for Optical Flares and Flashes with a Liquid Mirror Telescope," Astronomical Journal **97** (3), p. 917, 1989.

Erleksova, G.E., "EQ Vulpeculae," Переменные звезды, Прцложенце **2** №10, p. 248, 1975.

Hoffmeister, C., "Untersuchung der Schtaube des Positions-Fadenmikrometers *Heyde 3013*," Mitteilungen der Sternwarte zu Sonneberg Nr. 6, 1924.

Hoffmeister, C., "Relative Koordinaten, Örter und Karten neuer Veränderlicher," Mitteilungen der Sternwarte zu Sonneberg Nr. 17, 1930.

Hoffmeister, C., "Relative Koordinaten, Örter und Karten neuer Veränderlicher," Mitteilungen der Sternwarte zu Sonneberg Nr. 22, 1933.

Hoffmeister, C., "89 neue veränderliche Sterne," Astronomische Nachrichten **284**, p. 275, 1959.

Hoffmeister, C., "Mitteilungen über neuentdeckte Veränderliche Sterne (S9727-S10152)," Astronomische Nachrichten **290** H1-2, p. 43, 1967.

Kent, S.M., Ramella, M., Nonino, M., "A Small Drift Scan Survey for Galaxies in the Northern Sky," Astronomical Journal **105** (2), p. 393, 1993.

Kent, S.M., Stoughton, C., Newberg, H., Loveday, J., Petravick, D., Gurbani, V., Berman, E., Sergey, G., Lupton, R., Sloan Digital Sky Survey, Report #FNAL/C-94/084, (Batavia, Ill.: Fermi National Accelerator Laboratory, 1994).

Kron, R., "Digital Optical Sky Surveys," Bulletin of the American Astronomical Society Vol. 26, No. 2, p. 915, 1994.

Kurochkin, N.E., "New Variable Stars in the Region of M56," Переменные звезды **17** №128, p. 186, 1970.

Kinman, T., Wirtanen, C.A. and Janes, K.A., "An RR Lyrae Star Survey with the Lick 20 inch Astrograph. IV. A Survey of Three Fields Near the North Galactic Pole," Astrophysical Journal Supplement **119**, p. 379, 1966.

Kirkpatrick, J.D., McGraw, J.T., "The CCD/Transit Instrument (CTI) Blue Object Survey," IAU Colloquium #114 (White Dwarfs), p. 167, 1988.

Kirkpatrick, J.D., Henry, T.J., McCarthy, D.W., McGraw, J.T., "Constraining the Faint End of the Stellar Luminosity Function Through a Systematic Search for M Dwarfs," Bulletin of the American Astronomical Society, Vol. 22, No. 4, p. 1204, 1990.

Kirkpatrick, J.D., Spectroscopic and Photometric Studies of Main Sequence M Stars and a Search for Late Type Dwarfs in the Solar Vicinity, Phd dissertation, (Department of Astronomy, The University of Arizona, 1992).

Kirkpatrick, J.D., "The Luminosity Function of Field M Dwarfs: Evidence for a Population of Substellar Objects," Bulletin of the American Astronomical Society Vol. 26, No. 2, p. 944, 1994.

Kirkpatrick, J.D., "The Luminosity Function at the End of the Main Sequence: Results of a Deep, Large-Area, CCD Survey for Cool Dwarfs," Astrophysical Journal Supplement Series **94**, p. 749, 1994.

McGraw, J.T., Cawson, M.G.M., Kirkpatrick, J.D., Haemmerle, V., "A Strip Search for Quasars: The CCD/Transit Instrument (CTI) Quasar Survey," Proceedings of a Workshop on Optical Surveys for Quasars, p. 163, 1988.

McGraw, J.T., "The Lunar Transit Telescope (LTT): An Early Lunar Based Science and Engineering Mission," Engineering, Construction and Operations in Space III, p. 1865, 1992.

McGraw, J.T. (editor), Proceedings of the Lunar Ultraviolet Telescope Experiment (LUTE) Science Workshop, (Institute for Astrophysics, The University of New Mexico, 1993).

Meinunger, L., "Über Veränderliche in einigen T-Assoziationen," Mitteilungen über Veränderliche Sterne **3** H5, p. 137, 1966.

Miller, W.J. and Wachmann, A.A., "Six New Variable Stars in the Cygnus Cloud, VV 125-130," Ricerche Astronomiche **6** №22, p. 497, 1964.

Miller, W.J., "Eleven Variable Stars in the Cygnus Cloud, VV 151-161," Ricerche Astronomiche **7** №4, p. 197, 1965.

Miller, W.J., "Ten New Variable Stars in the Cygnus Cloud, VV

191-200," Ricerche Astronomiche 7 №10, p. , 1967.

Pinto, G. and Romano, G., "Researches with the Schmidt Telescope VI - The Variable Stars around Gamma Comae," Memorie della Società Astronomica Italiana **44** №1, p. 53, 1973.

Rügemer, H., "Neue Veränderliche Sterne," Astronomische Nachrichten **248**, p. 409, 1933.

Shaganian, B.L. and Shaganian, V.B., "On Three Longperiod Variable Stars in the Region of M56," Переменные звезды, Прцложенце **3** №18, p. 748, 1979.

Stoughton, C., Annis, J., Kent, S., Kron, R., Loveday, J., McKay, T., Newberg, H., "First Data from the Fermilab Drift Scan Camera," Bulletin of the American Astronomical Society Vol. 26, No. 2, p. 897, 1994.

Vogt, N. and Bateson, F.M., "An Atlas of Southern and Equitorial Dwarf Novae," Astronomy and Astrophysics Supplement **48** (3), p. 383, 1982.

Wachmann, A.A., "Die Veränderlichen im Südteil der Cygnuswolke - Teil II," Astronomische Abhandlungen der Hamburger Sternwarte, Band VI Nr. 2, 1963.

Wachmann, A.A., "Die Veränderlichen im Südteil der Cygnuswolke - Teil III," Astronomische Abhandlungen der Hamburger Sternwarte, Band VI Nr. 3, 1964.

, Mitteilungen über Veränderliche Sterne №299, 1957.

Chapter 4

Jacoby, G.H., Branch, D., Ciardullo, R., Davies, R.L., Harris, W.E., Pierce, M.J., Pritchet, C.J., Tonry, J.L., Welch, D.L., "A Critical Review of Selected Techniques for Measuring Extragalactic Distances," Publications of the Astronomical Society of the Pacific **104**, p. 599, 1992.

Madore, B.F., Freedman, W.L., " The Cepheid Distance Scale," Publications of the Astronomical Society of the Pacific **103**, p. 933, 1991.

Chapter 5

Beckert, D.C., Cox, D., Gordon, S., Jaderlund, E., Mann, E., Zeilik, M., "1989 BVR photometry of CG Cygni", IBVS #3398, 1989.

Beckert, D.C. and Newberry M.V., "The Design and Testing of Filter-Detector Systems using Synthetic Photometry,"

Publications of the Astronomical Society of the Pacific **101**, p. 849, 1989.

Beckert, D.C., Gordon, S., Jaderlund, E., Mann, E., Zeilik, M., "CG Cygni redux : more 1989 BVR data", IBVS #3556, 1991.

Bryja, C., Lawrence, G., "Photometry of Suspected Low Mass Hyades Cluster Members," Bulletin of the American Astronomical Society, Vol. 23, No. 2, p. 908, 1991.

Bryja, C., Jones, T.J., Humphreys, R.M., Lawrence, G., Pennington, R.L., Zumach, W., "Candidate Brown Dwarfs in the Hyades," Astrophysical Journal **388**, p. L23, 1992.

Deeg, H-J., Brinks, E., Duric, N., Klein, U., Skillman, E., "New 325 MHz Observations of HII Galaxies: The Mechanisms That Shape the Unusual Radio Spectra," Astrophysical Journal **410**, p. 626, 1993.

Gordon, S., Hall, S., Ledlow, M., Mann, E., Zeilik, M., "1989 BVR light curves of RT And," IBVS #3469, 1990.

Gisler, G., Laubscher, B., Chabot, N., Boudreaux, K., Grashuis, R., "Multi-filter Optical Observations of SL9 Impact Spots on Jupiter," Bulletin of the American Astronomical Society Vol. 26, No. 4, p. 1374, 1994.

Gregory, S.A., Deeg, H.-J., Morrison, G., Crane, M., Grashuis, R., Lacey, C., "Galaxian Nuclear Spectral Types as a Function of Environment," Bulletin of the American Astronomical Society Vol. 22 No. 2, p. 881, 1990.

Hayes, J.J.E., Sadun, A.C., and R. Grashuis, "Narrow-band images of Arp 213," Bulletin of the American Astronomical Society Vol. 25 No. 4, p. 1248, 1993.

Kidger, M., et al., "Multiband Monitoring of OJ287 in 1993/94," Bulletin of the American Astronomical Society Vol. 26, No. 4, p. 1506, 1994.

Laubscher, B., Gregory, S., Bauer, T., Zeilik, M., Burns, J., "A CCD Camera System at Capilla Peak Observatory, New Mexico," Publications of the Astronomical Society of the Pacific **100**, p. 131, 1988.

Laubscher, B., Gregory, S., "Galaxy alignments in the Perseus supercluster," Bulletin of the American Astronomical Society Vol. 25, No. 2, p. 913, 1993.

Laubscher, B., "Problems with Galaxy Position Angles," Bulletin of the American Astronomical Society Vol. 26, No. 2, p. 963, 1994.

Odewahn, S.C., "Properties of the Magellanic-type spirals. I -

Surface photometry of NGC 4618 and NGC 4625," Astronomical Journal **101**, p. 829, 1991.

Odewahn, S.C., Bryja, C., Humphreys ,R.M., "Improved CCD Standard Fields," Publications of the Astronomical Society of the Pacific **104**, p. 553, 1992.

Sadun, A., "Optical Variability of the Blazar OJ 287," Bulletin of the American Astronomical Society Vol. 26, No. 4, p. 1467, 1994.

Schmidt, B.P., Kirshner, R.P., Eastman, R.G., Grashuis, R., Dell'Antonio, I., Caldwell, N., Foltz, C., Huchra, J.P., Milone, A.A.E., "The Unusual Supernoa SN 1993J in M81," Nature **364**, p. 600, 1993.

Schmidt, B.P., Kirshner, R.P., Eastman, R.G., Phillips, M.M., Suntzeff, N.B., Hamuy, M., Aviles, R., Filippenko, A.V., Ho, L., Matheson, T., Grashuis, R., Maza, J., Kirkpatrick, J.D., Kuijken, K. Zucker, D., Bolte, M., Tyson, N., "The Expanding Photosphere Method Applied to SN 1992am at cz = 14600 km s^{-1}," Astronomical Journal **107**, p. 1444, 1994.

Summers, D.L., Zeilik, M., "Starspot activity on the RS CVn candidate 1E 1919+0427," Bulletin of the American Astronomical Society, Vol. 22, No. 4, p. 1295, 1990.

Summers, D.L., Zeilik, M., Jaderlund, E., Hoeppe, G., Collins, A., "1991 V-band photometry of an eclipsing binary: 1E 1919+0427," IBVS #3708, 1992.

Takalo, L.O., Pursimo, T., Sillanpää, A., Lehto, H., Nilsson, K., Kidger, M., deDiego, J.A., Gonzales-Perez, J.N., Rodriguez-Espinoza, J-M., Mahoney, T., Boltwood, P., Dultzin-Hacyan, D., Benitez, E., Turner, G.W., Robertson, J.W., Honeycutt, R.K., Efimov, T.S., Shakhovskoy, N., Charles, P.A., Schramm, K.J., Borgeest, U., Linde, J.V., Sadun, A., Grashuis, R., "The Light Curve of Blazar 3C 66A," Bulletin of the American Astronomical Society Vol. 26, No. 4, p. 1507, 1994.

Taylor, C., Brinks, E., Grashuis, R., Skillman, E., "An Optical and Radio Atlas of Companions to Dwarf Galaxies," to be published in Astrophysical Journal Supplement Series, 1995.

Wetterer, C.J., McGraw, J.T., Hess, T.R., Grashuis, R., "Variable Stars in the CCD/Transit Instrument (CTI) Survey," Bulletin of the American Astronomical Society Vol. 26, No. 2, p. 899, 1994.

Zeilik, M., DeBlasi, D., Rhodes, M., Budding, E., "A Half-Century of Starspot Activity on SV Camelopardalis," Bulletin of the American Astronomical Society Vol. 19., No. 4, p. 1086, 1987.

Zeilik, M., Beckert, D., DeBlasi, C., Ledlow, M., Rhodes, M., Williams, T., "1987 BVRI Photometry of RT And," IBVS #3173, 1988.

Zeilik, M., Cox, D., DeBlasi, D., Ledlow, M., Rhodes, M., Williams, T., "1988 BVRI Photometry of XY UMa," IBVS #3200, 1988.

Zeilik, M., DeBlasi, D., Rhodes, M., Budding, E., "A Half-Century of Starspot Activity on SV Camelopardalis," The Astrophysical Journal **332**, p. 293, 1988.

Zeilik, M., Beckert, D., Cox, D., Dolby, J., Ledlow, M., Newberry, M., Rhodes, M., "1989 V-band light curve of RT And," IBVS #3301, 1989.

Zeilik, M., Cox, D.A., DeBlasi, C., Rhodes, M., Budding, E., "Long-Term Starspot Activity of Short-Period RS CVn Stars, Part II, RT Andromedae," The Astrophysical Journal **345**, p.991, 1989.

Zeilik, M., DeBlasi, C.B., Gordon, S., Ledlow, M., "1990 BVR photometry of XY UMa," IBVS #3535, 1990.

Zeilik, M., Gordon, S., Cox, D., Beckert, D., "Long-term starspot activity of short-period RS CVn stars : CG Cygni," Bulletin of the American Astronomical Society, Vol. 22, No. 2, p. 830, 1990.

Zeilik, M., Ledlow, M., Rhodes, M., Arevardo, M.J., Budding, E., "Long-Term Starspot Activity of Short-Period RS CVn Stars, Part III, BH Virginis," The Astrophysical Journal **354**, p.352, 1990.

Zeilik, M., Cox, D.A., De Blasi, C., Rhodes, M., Budding, E., "Long-Term Starspot Activity of Short-Period RS CVn Stars, Part IV, WY Cancri," The Astrophysical Journal **363**, p.467, 1990.

Zeilik, M., Heckert, P., Ledlow, M., Summers, D.L., Jaderlund, E., Boudreau, K., M., "1991 BVR photometry of CG Cygni," IBVS #3663, 1991.

Zeilik, M., Deeg, H.J., "Long-term starspot activity of short-period RS CVn stars : XY UMa," Bulletin of the American Astronomical Society, Vol. 23, No. 2, p. 880, 1991.

Zeilik, M., Gordon, S., Jaderlund, E., Ledlow, M., Summers, D.L., Heckert, P.A., Budding, E., Banks, T.S., "Long-term Starspot Activity of Short-Period RS Canum Venaticorum Stars. V. CG Cygni," Astrophysical Journal **421**, p. 303, 1994.